Coupling of geological processes in the Earth's crust and mantle

Dissertation

zur Erlangung des Doktorgrades

der Naturwissenschaften

vorgelegt beim Fachbereich Geowissenschaften / Geographie

der Johann Wolfgang Goethe - Universität

in Frankfurt am Main

Von

Timo Luchs

aus Paderborn

Frankfurt (2012)

(D30)

vom Fachbereich Geowissenschaften / Geographie der

Johann Wolfgang Goethe - Universität als Dissertation angenommen.

Dekan: Prof. Dr. A. Junge

Gutachter: Prof. Dr. G. P. Brey
Prof. Dr. S. Weyer

Datum der Disputation: 14.12.2012

Table of contents

Zusammenfassung

In dieser Arbeit werden neue geochemische Daten zur Entwicklung von Krusten- und Mantelkomponenten im Hinblick auf ihre geochronologische Geschichte, sowie deren Randbedingungen, vorgestellt.

Zu diesem Zweck wurden zwei Lokalitäten ausgewählt. Das Rehoboth Terrane in Namibia, mit besonderen Bezug auf das Gibeon Kimberlit Feld, sowie die südöstliche vulkanische Provinz in Spanien (SEVP), mit besonderem Hinblick auf die Region um die Ortschaft von Casas de Tallante.

Das Rehoboth Terrane stellt eine tektonische Einheit im Süd Afrikanischen Gebiet dar. Aufgrund mächtiger Überlagerungen durch Sedimente ist das Wissen über den Aufbau und das Alter der darunterliegenden Kruste und Mantel nur sehr lückenhaft. Eine detaillierte Beschreibung der regionalen Geologie rund um das Rehoboth Terrane befindet sich in Kapitel 3.3.

Die SEVP ist geprägt durch verschiedene Stadien Neogener vulkanischer Aktivität. Informationen über die tiefere Kruste und den oberen Mantel, mit besonderem Bezug auf die zeitlichen Abfolgen, sind sehr spärlich. Ein detaillierterer geologischer Überblick über die SEVP befindet sich in Kapitel 5.3.

Charakteristisch für beide Arbeitsgebiete ist rezente vulkanische Aktivität, bei der Xenolithe von Kruste und Mantel an die Oberfläche befördert wurden.

Diese Xenolithe waren Gegenstand der hier vorliegenden Arbeit. Die Untersuchungen dieser Proben sollten einen Einblick in die Entwicklung der tieferen Kruste und des oberen Mantels der entsprechenden Region ermöglichen.

Ausgewählte Minerale der Xenolithe des Erdmantels beider Regionen wurden auf ihre Haupt- und Spurenelementkonzentrationen hin untersucht. Dies geschah mithilfe einer Elektronenstrahlmikrosonde und eines Laser ablations inductively coupled plasma Massenspektrometers (LA-ICPMS). Damit sollten geochemische Charakteristika, Anreicherungs- und Verarmungsprozesse, sowie Druck und Temperatur Randbedingungen ermittelt werden. Zusätzlich wurden Lu-Hf (Namibia und Spanien), Sm-Nd (Namibia und Spanien) und Sr (Spanien) Isotopien mithilfe eines Multicollector ICP Massenspektrometers

ermittelt, mit dem Ziel den Zeitpunkt von Mantelverarmungs- und der Anreicherungsprozesse zu datieren.

Bei den krustalen Proben wurden Zirkone von den krustalen Xenolithen und aus Ablagerungen von Tufflagen separiert. U-Th-Pb Isotopien wurden mithilfe von Laser Ablations ICPMS bestimmt mit dem Ziel das Alter der Kristallisation zu datieren. Darüber hinaus sollte die Bestimmung der Hf Isotopien derselben Zirkonkörner in denselben Wachstumszonen Informationen liefern über das geochemische Reservoir aus denen die Zirkone stammen. Die Kombination mit den zuvor bestimmten U-Th-Pb Isotopen erlaubt eine Aussage darüber zu treffen ob die Zirkone juvenil gebildet wurden, ob sie das Produkt eines krustalen Recyclings sind oder ob Krustenbereiche mit verschiedenen Isotopien miteinander vermischt wurden („crustal mixing“).

Schlussendlich bietet der Vergleich der neu gewonnenen Daten über Mantel und Kruste die Möglichkeit eine Hypothese zu erstellen inwiefern Mantel- und Krustenprozesse miteinander im Zusammenhang standen und ob Prozesse, die sich ein einem Kompartiment abgespielt haben, in dem anderen widergespiegelt werden.

Entwicklung der unteren Kruste und des oberen Mantels des Rehoboth Terranes

Mantel

Insgesamt wurden 19 Mantelxenolithe (Granat Peridotite) aus den Kimberlit Diatremen Gibeon Townlands und Hanaus untersucht. Diese wurden vor etwa 72.5 Ma bei kimberlitischen Eruptionen an die Oberfläche befördert (Davies et al., 2001). Hauptelemente wurden bestimmt für Klinopyroxen, Granat, Olivin und Orthopyroxen, sowie Spurenelemente in Klinopyroxen und Granat.

Der Großteil der Proben fällt entlang eines geothermischen Gradienten von etwa 40 mW/m², wohingegen sich eine kleinere Anzahl an Proben versetzt bei höheren Temperaturen und gleichbleibenden Drücken befindet. Alle Proben befinden sich im Graphit Stabilitätsfeld.

Die Muster der seltene Erdelemente (SEE) von Granaten und Klinopyroxenen zeigen, dass der Mantel unterhalb des Gibeon Kimberlit Feldes aus mindestens zwei verschiedenen Komponenten besteht (siehe Fig.0.1).

Der erste Typ (Typ „N“), dem 14 Proben entsprechen, zeigt normale SEE Muster und Grt/(Grt+CPX) Verhältnisse der modalen Gemengteile von etwa 0.5 bis etwa 0.8. Dem zweiten Typ (Typ „σ“) entsprechen 5 Proben. Charakteristisch sind die sigmoidalen SEE Muster mit Grt/(Grt+CPX) Verhältnissen von etwa 0.99.

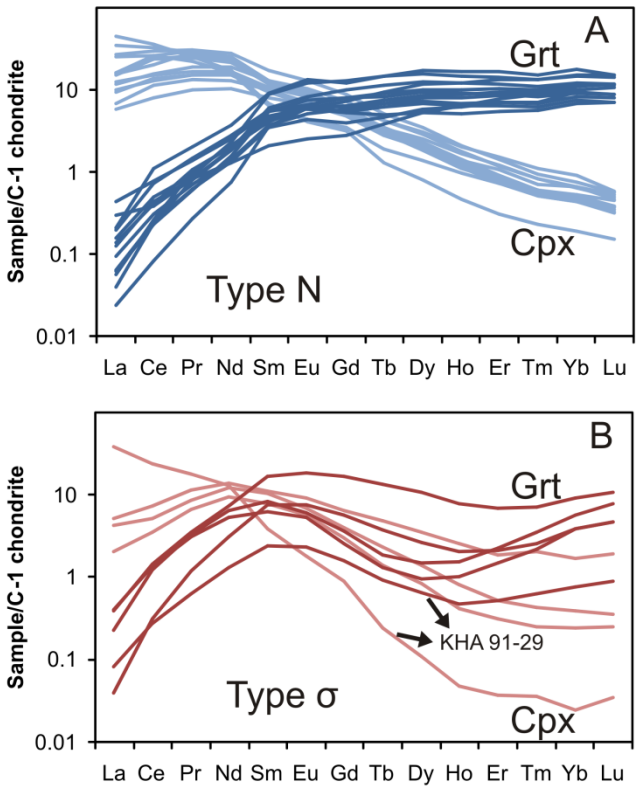

Fig.0.1 Typ „N“ (A; Blau) und Typ „σ“ (B; Rot) Proben, entsprechend ihrer SEE Muster von einander entsprechenden Klinopyroxenen und Granaten. Konzentrationen sind normiert auf C1 (McDonough and Sun, 1995)

Lu-Hf Isotopien beider Typen wurden mittels multicollector ICPMS bestimmt mit dem Ziel den Zeitpunkt der Verarmung der entsprechenden Mantelquelle zu bestimmen. Sm-Nd Isotopien derselben Proben wurden in einem zweiten Schritt bestimmt mit dem Ziel den Zeitpunkt der Anreicherung des entsprechenden Mantels durch Metasomatose zu bestimmen.

Die Normierung der Spurenelementkonzentrationen von Klinopyroxen und Granat auf eine primitive Probe aus Vitim (Sibirien) (Ionov et al., 2005) vor der Isotopenanalytik hat ergeben, dass beide Isotopensysteme metasomatisch überprägt worden sind. Aufgrund dessen entsprechen Alter, die auf Basis der beiden Isotopensysteme berechnet werden, Zeitpunkten der Anreicherung.

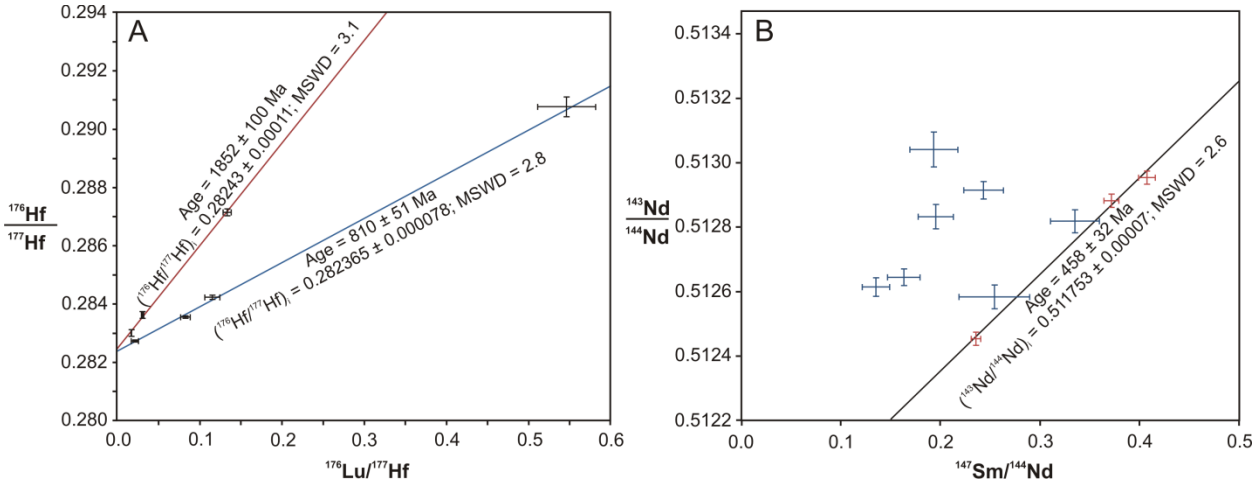

Fig.0.2 Lu-Hf (A) und Sm-Nd (B) Isotopien der Gesamtgesteine für typ „N“ (blau) und typ „σ“ (rot) Peridotite. Gezeigt ist die metasomatische Überprägung um einen Zeitpunkt von etwa 0.85 Ga für den erstgenannten und etwa 1.9 Ga für die zuletztgenannten Typ. Sm-Nd Isotopien der σ Peridotite deuten auf eine späte Anreicherung im Rahmen der Pan Afrikanischen Orogenese hin.

Die Korrelation der Lu-Hf Isotopie von vier Proben der „N“ Peridotite ergeben ein proterozoisches Anreicherungsalter von etwa 850 Ma, mit dem Ursprung aus einer leicht verarmten Mantelquelle ($\varepsilon Hf_{initial}$ = +3.3).

Drei Proben mit sigmoidalen Granatmuster entsprechen einer Isochrone mit einem Alter von etwa 1.9 Ga. Der Initialwert von $\varepsilon Hf_{initial}$ = +29.4 deutet auf eine stark verarmte Mantelquelle hin (Fig.0.2).

Die Ergebnisse der Sm-Nd Isotopien streuen. Dennnoch fallen 3 Proben der σ Peridotite entlang einer Isochrone mit einem Alter von etwa 450 Ma, was einer metasomatischen Überprägung während der Pan Afrikanischen Orogenese entsprechen könnte.

Zusätzlich zu den eigenen Ergebnisse, präsentieren wir unsere Neuinterpretation eines zuvor publizierten Re-Os Datensatzes von Granat Peridotiten des Louwrensia Kimberlit Diatrems im

Gibeon Kimberlit Feld (Pearson et al., 2004), mit einer Isochrone die einem Alter von etwa 2.9 Ga entspricht. Die Vorstellung, dass Archaische Komponenten Bestandteil des Rehoboth Terranes sind, wurde bereits zuvor in verschiedenen anderen Studien vorgeschlagen (Hoal et al., 1995; Franz et al., 1996). Diese Vermutung wird zudem gestützt von Zirkonaltern im Bereich von 2.7 bis 2.9 Ga von Cornell et al. (2011) und Van Schijndel et al. (2011), sowie durch eigene Arbeiten (siehe Kapitel 4). Wir interpretieren dieses Alter als den Zeitpunkt der Verarmung der σ Peridotite.

Die Neuerkentnisse, die durch diese Arbeit im Hinblick auf die Entwicklung des Mantels unterhalb des Gibeon Kimberlit Feldes gewonnen wurden, ermöglichen eine neue Interpretation der tektonischen Vorgänge, die das südliche Afrika geprägt haben.

Während des Zusammenschlusses des Ost- und Westblocks des Kaapvaalkratons wurden erste Mantelkomponenten des Rehoboth Terranes im Spinel Stabilitätsfeld gebildet, die im Anschluss unter bereits existierende Kruste subduziert und zu Granatperidotit umgewandelt wurde. Die Kollision des Rehoboth Terranes mit dem Kaapvaal Kraton um etwa 1.9 Ga führte zu einer Anreicherung dieses Mantels durch Metasomatose.

Während der Namaqua Orogenese zwischen 0.9 und 1.3 Ga, wurde neues Mantelmaterial unter das Rehoboth Terrane subduziert und in einem späten Stadium vor etwa 850 Ma, metasomatisch angereichert. Eine letzte Anreicherung hat eventuell bei der Pan Afrikanischen Orogenese vor etwa 450 Ma stattgefunden.

Kruste

Die Bestimmung von Kristallisationsereignissen der tieferen Kruste unterhalb des Rehoboth Terranes, in Kombination mit den Ergebnissen der Anreicherungsvorgänge im Mantel ermöglicht ein besseres Verständnis der tektonischen Vorgänge die das Terrane geformt haben.

Zirkone aus sechs krustalen Xenolithen, die von Karbonatitischen Diatremen, nahe des Gross Brukkaros Berges stammen, sowie Zirkone eines aus einem krustalen Xenolith des Louwrensia Kimberlit Schlots und aus einer weiteren Probe aus der Matrix des Louwrensia Kimberlits wurden in diesem Teil der Arbeit analysiert.

Mit Ausnahme der Probe aus der Matrix des Kimberlits, handelt es sich bei allen Proben um hochgradig metamorphe Gesteine.

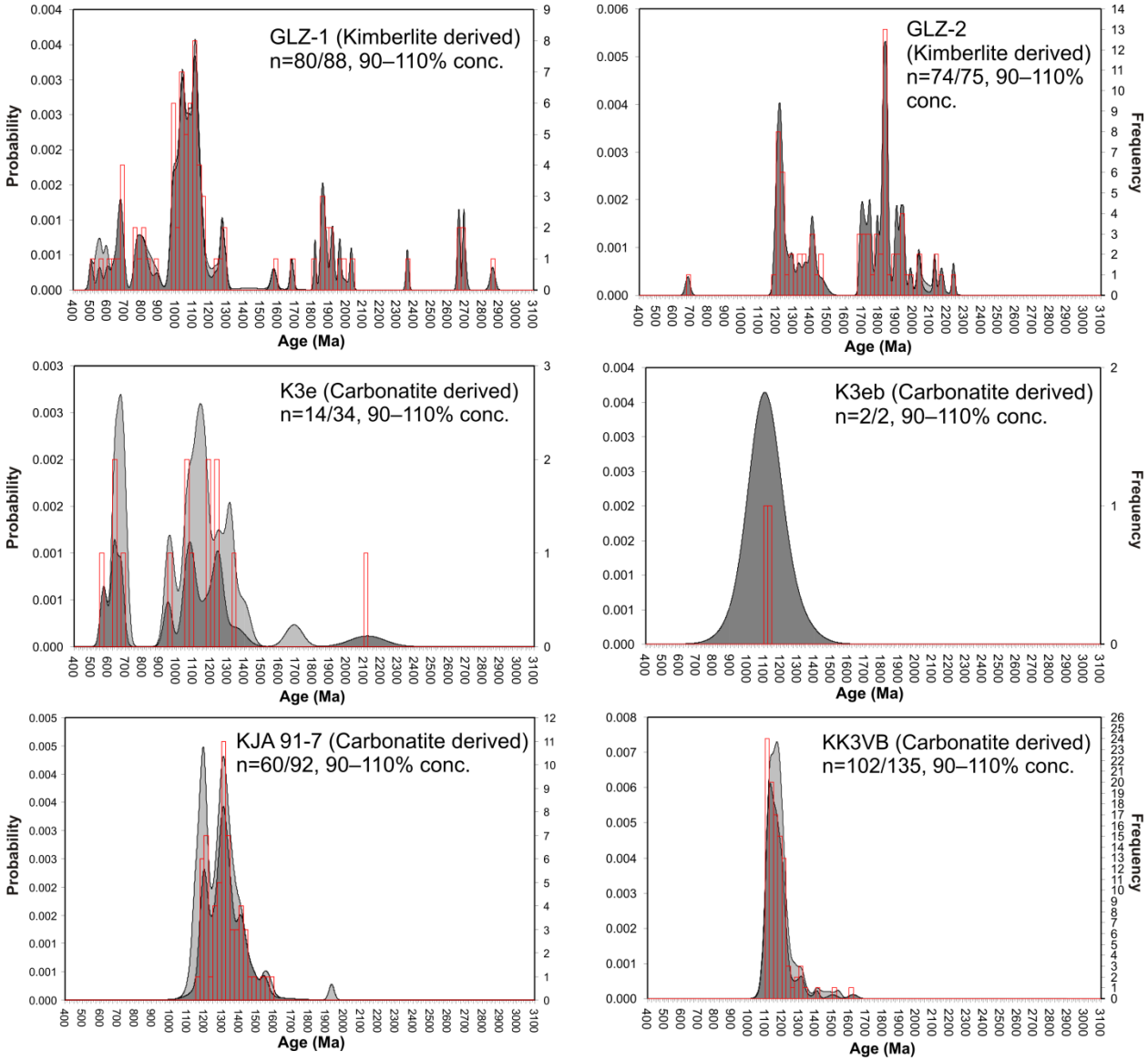

Fig.0.3 U-Pb Altersspektren für Zirkone aus Xenolithen, die aus kimberlitischen Diatremen innerhalb des Gibeon Kimberlit Feldes oder aus karbonatitischen Diatremen nahe des Gross Brukkaros Berges stammen.

Im Anschluss an die Mineralseparation, der Einbettung und Politur, wurden die Zirkone mithilfe der Laser ablations ICPMS analysiert. Zuvor angefertigte Kathodenlumineszenz Bilder der Zirkone ermöglichten eine präzise Altersbestimmung der verschiedenen Wachstumszonen

innerhalb der Kristalle. Abhängig davon ob die Probe aus einem karbonatitischen oder kimberlitischen Diatrem stammt, ergibt sich ein unterschiedliches Bild für die Altersverteilung (Fig.0.3).

Abgesehen von einer Probe, die jüngere Zirkone vom Karbonatit selbst enthält (K3e), haben karbonatitische Xenolithe Altersmaxima hauptsächlich zwischen 1.0 und 1.5 Ga, wohingegen Zirkone aus Kimberlitischen Xenolithen zwischen 0.6 und bis zu 2.9 Ga variieren mit Hauptverteilungen um 1.1 bis 1.2 und 1.8 – 1.9 Ga. Die Probe aus der Matrix des Kimberlits zeigt ein wesentlich breiteres Altersspektrum, von 0.5 bis 2.9 Ga, wobei es sich bei den jüngeren Altern vermutlich um Zirkone aus den Nama Shales handelt.

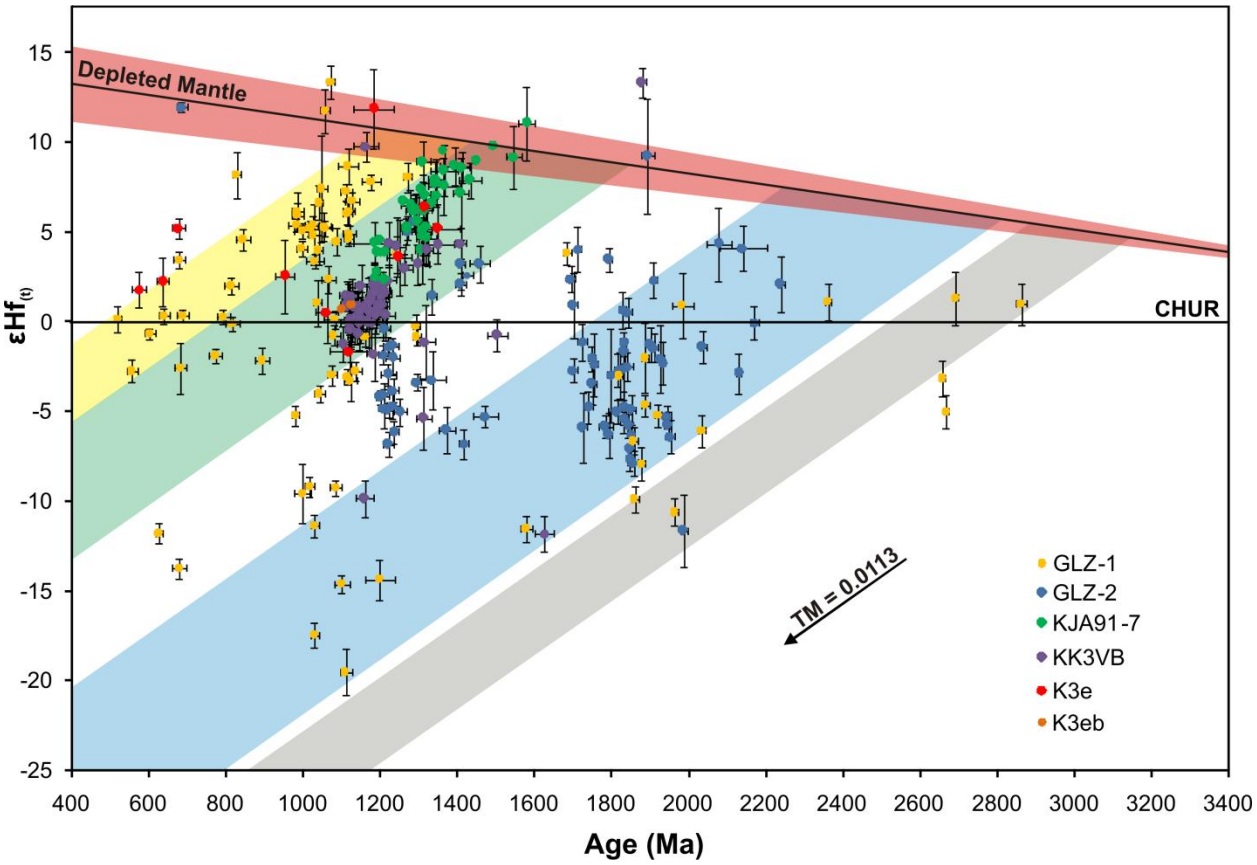

Fig.0.4 Hf Isotopien der Zirkone aus Gibeon und Umgebung in Kombination mit den entsprechenden U-Pb Altern. Vier Krustenwachstumstrends können mit Krustenrecycling und Krustenmischung können identifiziert werden. Trends wurden berechnet mit einem $^{176}Lu/^{177}Hf$ von 0.0113 (Rudnick and Gao, 2003). $^{176}Hf/^{177}Hf$ Werte für den verarmten Mantel stamen aus Chauvel and Blichert-Toft (2001) und Vervoort et al. (1999).

Zusätzlich wurde die Hafnium Isotopie derselben Zirkone in denselben Wachstumszonen, direkt auf oder neben den Laserspots von den U-Th-Pb Analysen, bestimmt. Diese sollte in Kombination mit den U-Th-Pb Isotopien, eine Aussage über die Quelle aus der die Kruste entstanden ist, sowie Informationen über Krustenentstehung, Recycling oder die Mischung von isotopisch verschienenden Krustenkompartimenten ermöglichen.

Vier Phasen krustalen Wachstums von einer verarmten Mantelquelle können basierend auf diesen Ergebnissen identifiziert werden (Fig.0.4).

Erstes Krustenwachstum von einer primitiven Mantelquelle fand im Archaikum in einem Zeitraum von 2.7 bis 2.9 Ga statt oder ausgehend von einer verarmten Mantelquelle mit Modellaltern zwischen 3.05 und 3.38 Ga.

Juvenile Kruste wurde gebildet zwischen 2.3 und 2.7 Ga von einer verarmten Mantelquelle mit anschließendem Recycling bis 1.0 und 1.2 Ga.

Der Zeitraum zwischen 1.5 und 1.6 Ga ist gekennzeichnet durch erneutes Krustenwachstum, ausgehend von einer verarmten Mantelquelle, sowie intensivem Krustenrecycling bis etwa 1.1 Ga und einem Krustenmischungstrend zwischen 1.3 und 1.1 Ga. Charakteristisch für diesen Zeitraum sind zudem die fast durchwegs positiven Werte für $\varepsilon Hf(t)$. Etwa 60% aller Datenpunkte liegen im Zeitraum zwischen 1 und 1.4 Ga.

Jüngste Krustenbildung fand zwischen 0.8 und 1.1 Ga statt mit anschließendem Krustenrecycling im Rahmen der Pan Afrikanischen Orogenese bei etwa 0.5 bis 0.6 Ga.

Die Bandbreite und Variation der Probe aus der Kimberlitmatrix des Louwrensia Kimberlit Diatrems ist im Vergleich zu den übrigen Proben deutlich größer. Dies ist vermutlich darauf zurückzuführen, dass Zirkone aus den Nama Schiefern einen Teil der Probe ausmachen.

Im Hinblick auf die Unterschiede zwischen Proben aus Kimberliten und Proben aus Karbonatiten, kann geschlussfolgert werden, dass verschiedene stratigraphische Einheiten beprobt worden sind.

Dieses Kapitel der Arbeit hat gezeigt, dass die Kruste unterhalb des Gibeon Kimberlit Feldes aus metamorphen Sedimenten aufgebaut wird. Unter Ausschluss der Zirkonalter der Nama Schiefer, liegen die jüngsten Alter der darunterliegenden Kruste bei etwa 0.9 Ga.

Die älteste Kruste ist vermutlich im Archaikum entstanden, gefolgt von einer Episode zwischen 1.8 und 1.9 Ga in der das Rehoboth Terrane mit dem Kaapvaal Kraton kollidiert ist.

Das zuletzt genannte Ereignis konnte zudem in den Erdmantelxenolithen der Gibeon Kimberlit Provinz in Form einer Anreicherung der σ Peridotite nachgewiesen werden (siehe Kapitel 3).

Subduktion unterhalb des Kalahari Kratons ist vermutlich der Grund für Krustenbildung, -recycling und -mischung in einem Zeitraum von 1.5 und 1.1 Ga, in dem sich etwa 60 % aller Datenpunkte dieser Studie befinden. Ein solches Szenario wurde bereits zuvor von Becker et al. (2006) vorgeschlagen.

Die Namaqua Orogenese hatte zudem auch einen Effekt auf die Kruste unterhalb des Gibeon Kimberlit Feldes in Form von juvenilem Krustenwachstum ausgehend von einer verarmten Mantelquelle und anschließendem Krustenrecycling während der Pan-Afrikanischen Orogenese. Während der Namaqua Orogenese wurden zudem neue Mantelkomponenten unterhalb des Gibeon Kimberlit Feldes hinzugefügt („N" Peridotite), die anschließend gegen Ende derselben angereichert wurden. Der Effekt einer späten Überprägung während der Pan Afrikanischen Orogenese ist zudem erkennbar anhand der Sm-Nd Isotopie der σ Peridotite (siehe Kapitel 3).

Die untere Kruste und der obere Mantel der Südöstlich vulkanischen Provinz in Spanien

Mantel

Spinell / Plagioklas Peridotite des Neogenen Alkali basaltischen Vulkans Cabezo Negro de Tallante wurden gesammelt und ausgewählte Minerale von 11 Proben in einem nächsten Schritt separiert, mit Plagioklasen in nur 5 Proben. Haupt- und Spurenelemente von Klinopyroxenen und Orthopyroxenen, sowie Hauptelemente von Olivinen und Plagioklasen (falls vorhanden) wurden mit der Elektronenstrahlmikrosonde und eines Laser Ablations ICPMS gemessen. Sieben Proben wurden ausgewählt für isotopengeochemische Analysen, im Hinblick auf die Lu-Hf, Sm-Nd und Rb-Sr Isotopensysteme.

Alle ausgewählten Proben stammen aus einem Druckbereich zwischen 7 und 20 kbar und einem Temperaturbereich zwischen 900 und 1000°C. Temperaturen wurden ermittelt mithilfe des zwei Pyroxen Thermomethers von Brey and Koehler (1990), der Druck mithilfe des Ca in Olivin Barometers von Koehler and Brey (1990).

Ausgehend von den Spurenelementkonzentrationen, konnten drei verschiedene Typen von Spurenelementmustern unterschieden werden. Typ eins ist charakterisiert durch eine leichte

Anreicherung der mittleren seltenen Erden (MSEE) und relativ dazu leicht verarmten leichten seltenen Erden (LSEE) (siehe Fig.0.5 – grün). Typ zwei ist genkennzeichnet durch fast flache seltene Erdelementmuster und insgesamt niedrigeren Gehalten an seltenen Erdelementen im Vergleich zu Typ 1 (siehe Fig.0.5 – rot). Typ drei ist vertreten durch lediglich eine Probe, die stark angereichert ist an LSEE, wohingegen die entsprechenden MSEE und schweren seltenen Erdelemente (HSEE) im Allgemeinen fast den Muster von Typ 1 entsprechen (siehe Fig.0.5 – blau).

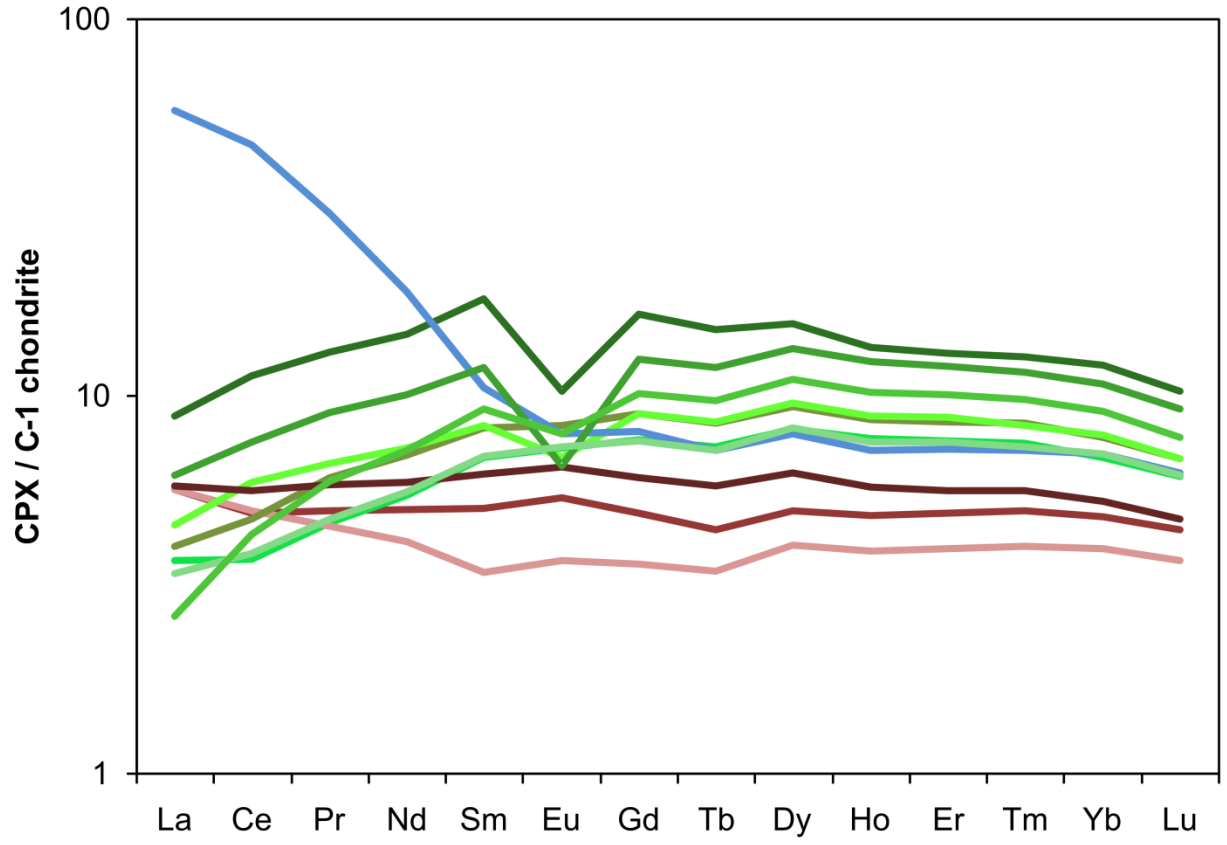

Fig.0.5 Drei Typen von Proben für Spinell / Plagioklas Peridotite von Cabezo Negro de Tallante werden unterschieden anhand der SEE Muster der entsprechenden Klinopyroxene, normiert auf C1 (McDonough and Sun, 1995). Typ 1 wird dargestellt durch die Farbe grün, Typ 2 durch die Farbe rot und Typ 3 durch die Farbe blau.

Die Normierung auf eine primitive Probe aus Vitim (Sibirien) (Ionov et al., 2005) zeigt, dass alle drei Typen eine Anreicherung der leichten seltenen Erden erfahren haben.

Die Lu-Hf Isotopien der gemessenen Proben zeigen keine eindeutige Korrelation aufgrund des kleinen Bereichs für $^{176}Lu/^{177}Hf$ und aufgrund von Streuung der Datenpunkte. Durch Hinzunahme eines weiteren Datenpunkts (TL16) derselben Lokalität aus einer früheren Publikation (Beccaluva et al., 2004; Bianchini et al., 2011), können vier Datenpunkte miteinander zu einem Alter von etwa 550 Ma korreliert werden (Fig.0.6). Da Hf offensichtlich keine Anreicherung widerfahren ist, könnte dieses Alter einem Verarmungsalter unterhalb der SEVP entsprechen.

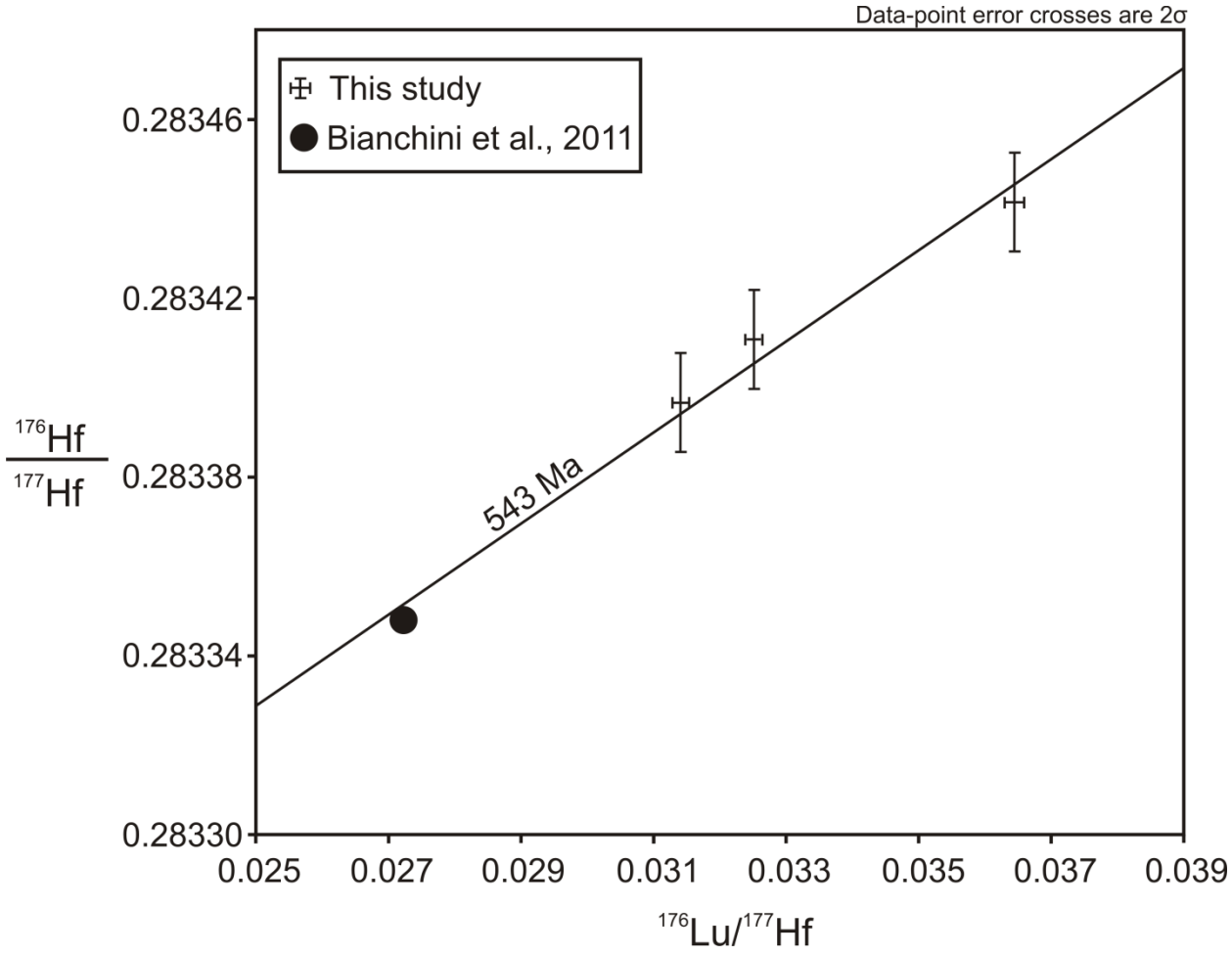

Fig.0.6: Eine mögliche Mantelverarmung zu einem Zeitpunkt von etwa 550 Ma könnte stattgefunden haben. Drei Datenpunkte dieser Studie und ein weiterer Datenpunkt, publiziert von Bianchini et al. (2011) und Beccaluva et al. (2004) fallen entlang einer entsprechenden Referenzisochrone.

Das Hf Modellalter zweier weitere Proben deuten auf die Präsenz von älteren Komponenten unterhalb der SEVP hin, im Einklang mit isotopischen Studien der Tallante Xenolithe von

Bianchini et al. (2011) und anderen Lokalitäten innerhalb Europas (Downes and Dupuy, 1987; Reisberg et al., 1989; Bodinier et al., 1991; Downes et al., 1991; Zangana et al., 1997; Beccaluva et al., 2001; Downes et al., 2002).

Isotopien für Sm-Nd entsprechen keiner einheitlichen Isochrone, sie streuen jedoch um eine Projektion von etwa 550 Ma.

Sr Isotopien der Klinopyroxene und Plagioklase weichen voneinander ab. $^{87}Sr/^{86}Sr$ Isotopenverhältnisse der Plagioklase sind höher im Vergleich zu denen der Klinopyroxene. Die erhöhten Isotopenverhältnisse der Plagioklase sind vermutlich zurückzuführen auf eine Interaktion mit den alkali basaltischen Schmelzen, die die Mantelxenolithe and die Oberfläche befördert haben. Die Klinopyroxene scheinen von diesem Ereignis keine Anreicherung widerfahren zu haben.

Kruste

Drei Proben von akali basaltischen Aufschlüssen innerhalb der SEVP wurden untersucht mit dem Ziel die Entwicklung der unteren Kruste dieses Gebiets zu entschlüsseln. Die Probennahme erfolgte entweder aus Tufflagen (CNTS-1 und ALCS-1) oder aus der Matrix der alkali Basalte (CG-Z1 – CG-Z3). In einem ersten Schritt wurden die Proben im Gelände gesiebt, gefolgt von Schweretrennung, Magnettrennung, einer Behandlung mit 6 M HCl, einer Siebung mit Einmal-Sieben und einer Separation mithilfe eines Stereomikroskops.

Wachstumszonen innerhalb der Zirkonkristalle wurden sichtbar gemacht mithilfe von Kathodenlumineszenz Bildern. U-Th-Pb Isotopien von homogenen Wachstumszonen wurden anschließend mittels laser Ablations ICPMS bestimmt. Anschließend wurde die Hf Isotopie der entsprechenden Wachstumszonen mittels Laser Ablation multicollector ICPMS ermittelt. Die Kombination beider Informationen ermöglichte einen besseren Einblick in die Entwicklungsgeschichte der Kruste unterhalb der SEVP im Hinblick auf juveniles Krustenwachstum, Krustenrecycling und Krustenmischungsprozessen.

Alle drei Proben zeigen sehr ähnliche Altersverteilungsmuster mit einer großen Alterspanne zwischen 2.6 Ma und 3 Ga. Hauptaltersverteilungsbereiche liegen zwischen 0.3 und 0.4, 0.5 und 0.6 bis 0.7 Ga. Geringere Alterspopulationen liegen zwischen 1 Ga bis 1.1 Ga, 1.8 bis 2.2 Ga, 2.4 bis 2.6 Ga und 2.9 bis 3 Ga (Fig.0.7).

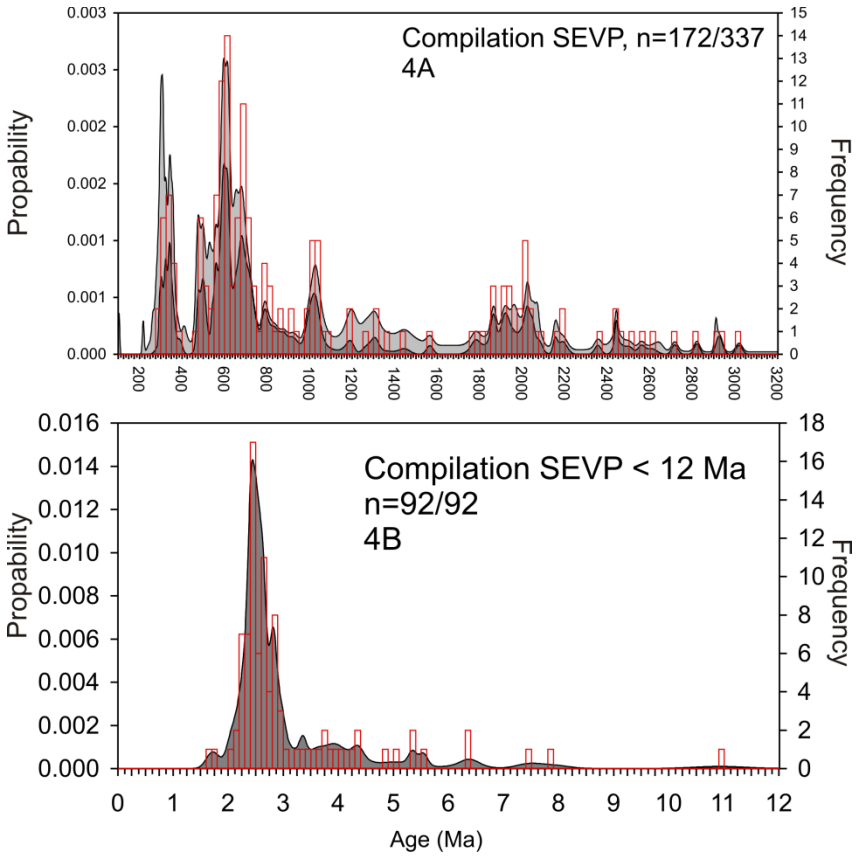

Fig.0.7: Zusammenstellung der U-Pb Daten aller drei Lokalitäten innerhalb der SEVP mit Altern > 100 Ma in (A) und Altern <12 Ma in (B).

Hf Isotopien in Kombination mit den entsprechenden U-Pb Altern zeigen 2 Krustenbildungstrends (Fig.0.8). Erste Krustenbildung fand im Archaikum statt und wurde anschließend recycled zwischen 2.5 und 1 Ga.

Der Zeitraum zwischen 1.0 und 1.5 Ga ist gekennzeichnet von juvenilem Krustenwachstum von einer verarmten Mantelquelle, die während der Kaledonischen und Variszischen Orogenese immer wieder recycelt wurde. Zusätzlich scheint während der Zeit der Variszischen Orogenese der Mantel unterhalb der SEVP verarmt worden zu sein (siehe Kapitel 5). Nahezu vertikal angeordnete Datenpunkte im Bereich von etwa 0.5 bis 0.6 Ga deuten auf ein Krustenmischungsereignis in diesem Zeitraum hin.

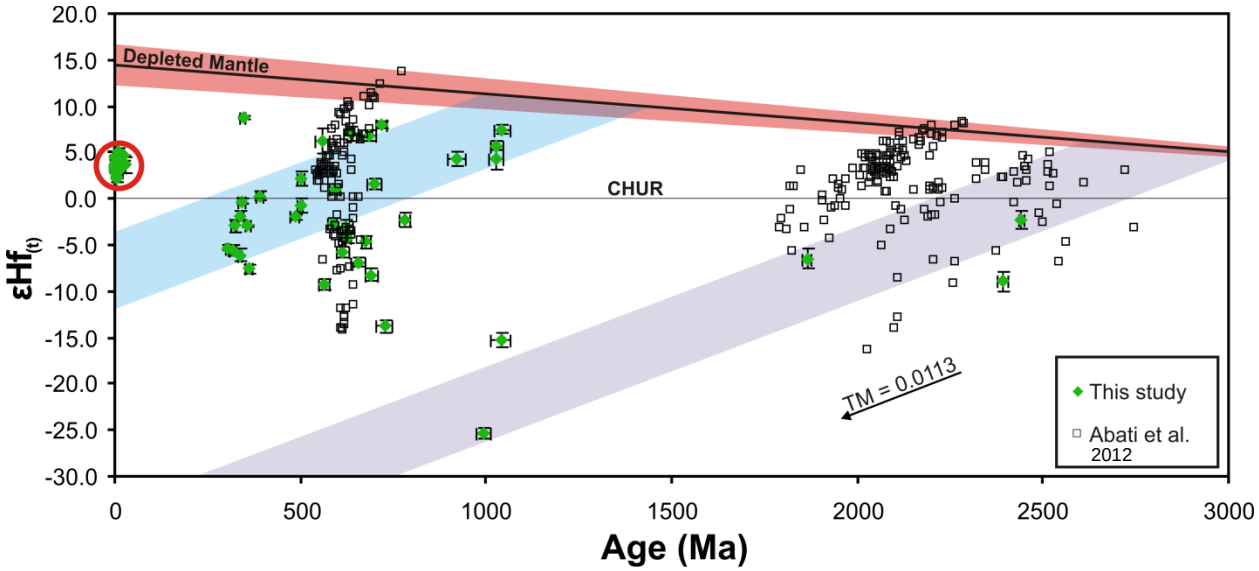

Fig.0.8: Kombination der U-Pb Alter mit ihren entsprechenden Werten für εHf(*t*) für Zirkone aus dieser Studie (grün) und Zirkone, publiziert von Abati et al. (2012) (schwarze Kästchen). Ein $^{176}Lu/^{177}Hf$ Verhältnis von 0.0113 (Rudnick and Gao, 2003) wurde für die Berechnung der Krustenwachstumszonen benutzt. Werte für den verarmeten Mantel stammen von Chauvel and Blichert-Toft (2001) und Vervoort et al. (1999).

Neogene Alter sind gekennzeichnet von fast chondritischen εHf(*t*) Werten, die auf einen leicht verarmente Mantel als Quelle hinweisen. Jüngste Alter liegen bei etwa 2.6 Ma, mit oszillierender Zonierung und abgerundeten Kristallgrenzen der entsprechenden Zirkonkristalle. Diese Zirkone datieren das Alter der Eruption der Alkali Basalte, welches bereits zuvor durch K-Ar Datierungen bestimmt wurde von Bellon et al. (1983). Geringere Altersverteilungen zwischen 5 und 8 Ma bezeugen, dass die Extrusion von kalk-alkalischen Magmen, die generell weiter südwestlich aufgeschlossen sind (Turner et al., 1999; Duggen et al., 2003; Duggen et al., 2004), auch die SEVP beeinflusst haben.

Der Vergleich zu Studien von restitischen Einschlüssen eines Dacits und eines graphitischen Schiefers von Zeck und Williams (2002) und Zeck und Williams (2001) aus der Lokalität Cerro del Hoyazo und einer dazu nahegelegenen Lokalität, beide etwa 150 km Südwestlich von der SEVP entfernt, zeigt, dass die Altersverteilungen insgesamt sehr ähnlich sind. Diese Ähnlichkeiten weisen auf intensive Krustenstapelung innerhalb der Betischen Kordillere hin, da die Proben von Cerro del Hoyazo vermutlich aus größeren Tiefen entstammen.

Weitere Vergleiche zu Studien aus dem West Afrikanischen Kraton und des Arabisch-Nubischen Schildes (Abati et al, 2012; Avigad et al., 2012) zeigen, dass ein Großteil der hier analysierten Zirkone von den zuvor genannten Blöcken entstammen und während des Zusammenschlusses von Gondwana auf die Iberische Platte transportiert wurden.

Summary

In this work we present new geochemical data about the evolution of mantle and crustal components in terms of their geochronological records and geochemical constraints. Two localities were chosen for this purpose. The Rehoboth Terrane in Namibia, with special regards to the Gibeon Kimberlite field and the south eastern volcanic province in Spain (SEVP), with special regards to the region around the small village of Casas de Tallante.

The Rehoboth Terrane is a tectonic domain of the southern African framework and due to its thick cover of sediments, not much is known about the composition, or the age of the underlying crust and mantle. A more detailed description of the regional geology can be found in chapter 3.3.

The SEVP is marked by different stadiums of volcanic activity from Neogene times. Knowledge about the deeper crust and the upper mantle with respect to time constraints is very rare. A broader overview about the geological setting is given in chapter 5.3.

Both areas are characterized by recent volcanic activity that has transported mantle and crustal xenoliths to the surface. These xenoliths and some other types of samples were subject for the work presented here. Samples collected in both areas were assumed to provide an insight into the evolution of the lower crust and upper mantle.

Regarding the mantle of both regions, major and trace elements of selected minerals (garnet, clinopyroxene, orthopyroxene, olivine) were measured by electron microprobe measurements and laser ablation ICPMS in order to determine the geochemical character, enrichment or depletion characteristics and pressure (P), temperature (T) relationships. Additionally, isotope systematics of the Lu-Hf (Namibia and Spain), Sm-Nd (Namibia and Spain) and Sr (Spain) isotope systems were determined by multicollector ICPMS in order to calculate the timing of mantle depletion and enrichment and to characterize mantle reservoirs.

For crustal samples, zircons were extracted from the crustal xenoliths (Namibia) and the debris of tuff layers (Namibia and Spain). The U-Th-Pb isotope systematics were determined by laser ablation ICPMS in order to get information about the age of crystallization. Additionally, Hf isotope analyses of the same zircon grains and the same growing domains were carried out by laser ablation multicollector ICPMS, providing information about the geochemical reservoir the zircons were derived from. Combining the ages as determined by U-Th-Pb isotope systematics

with Hf isotope systematics enabled us to see whether zircons are a product of juvenile crust formation and if the zircons analysed are related to each other in terms of crustal recycling or if crustal components with different isotopic characteristics were mixed (crustal mixing).

Finally, comparing the results about the makeup of the mantle and the crust provides the opportunity to make an assumption of how mantle and crustal processes were connected and if processes reflected in one domain can be seen in the other.

Evolution of the lower crust and the upper mantle of the Rehoboth Terrane

Mantle

We have investigated 19 mantle xenoliths (garnet peridotites) from the Gibeon Townlands and the Hanaus kimberlite pipes on the Gibeon kimberlite field that were transported to the surface by kimberlite eruptions 72.5 Ma ago (Davies et al., 2001). Major elements were determined for clinopyroxenes, garnets, olivine and orthopyroxenes and trace elements were analyzed in clinopyroxenes and garnets.

Most samples plot along a geothermal gradient of around 40 mW/m², whereas a smaller number of samples are displaced to higher temperatures at same pressures. All samples are in the graphite stability field.

Rare earth element compositions of the garnets and clinopyroxenes suggest that the mantle beneath the Gibeon kimberlite field is made up of at least two different components (see Fig.0.1). The first type (type ‘N’) with 14 samples, has normal garnet REE patterns and Grt/(Grt+CPX) ratios of their modal abundance from around 0.5 to around 0.8. The second type (type ‘σ’) with only 5 samples, has sigmoidal garnet REE patterns with Grt/(Grt+CPX) ratios mostly around 0.99.

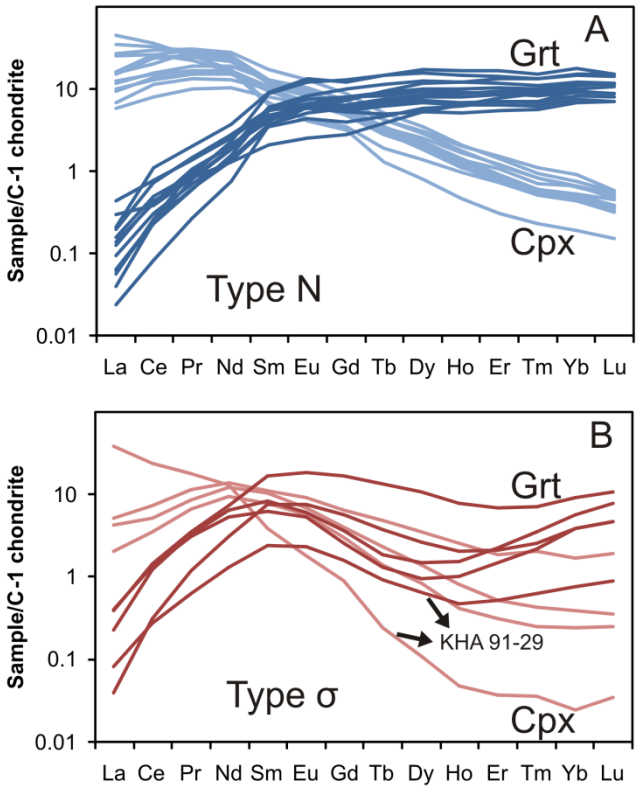

Fig.0.1 Type 'N' (A; blue) and type 'σ' (B; red) samples as determined by the REE patterns of corresponding clinopyroxenes and garnets. Concentrations are normalized to chondrite C1 (McDonough and Sun, 1995).

Lu-Hf isotope systematics of both types were determined by multicollector ICP-MS in order to calculate the timing of depletion from the corresponding mantle source. Sm-Nd isotope systematics of the same samples were obtained in a second step in order to determine the timing of enrichment by mantle metasomatism.

Trace element compositions of clinopyroxene and garnet normalized on a primitive sample from Vitim (Siberia) (Ionov et al., 2005), determined prior to isotope analyses, revealed that both isotope systems were affected by metasomatism for both types of samples. Therefore, ages calculated are regarded as to represent enrichment ages for both isotope systems.

Correlation of the Lu-Hf isotope systematics of four 'N' peridotites revealed a Proterozoic enrichment age of around 850 Ma from a slightly depleted mantle source ($\varepsilon Hf_{initial}$ = + 3.3). Three samples with sigmoidal garnet patterns plot along an isochron with an age of around 1.9

Ga. The initial value of $\varepsilon Hf_{initial}$ = + 29.4 points towards a highly depleted mantle source (Fig.0.2).

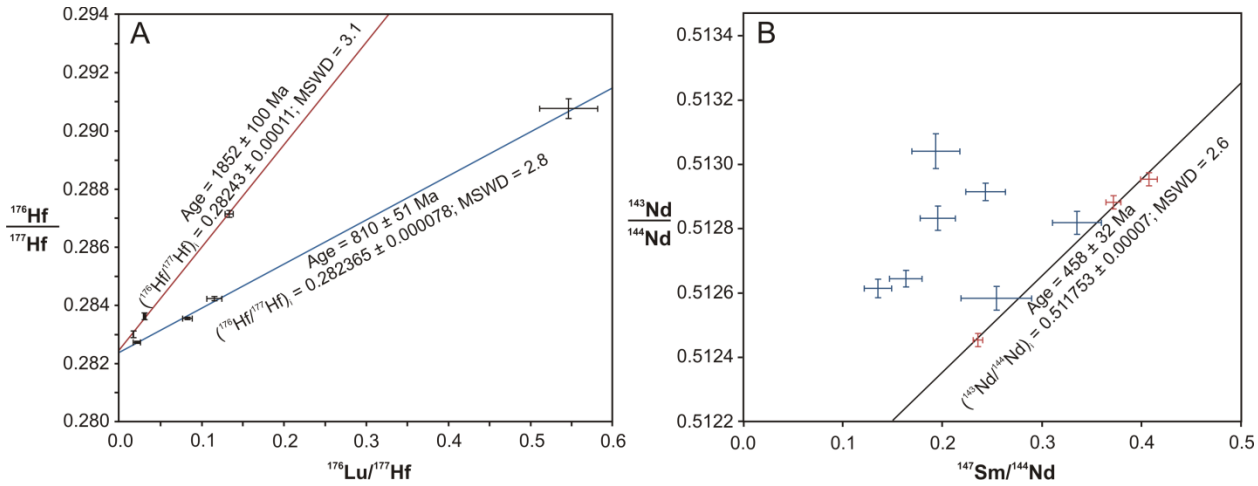

Fig.0.2 Lu-Hf (A) and Sm-Nd (B) whole rock isotope systematics of type 'N' (blue) and type 'σ' (red) samples, showing a metasomatic overprint around 0.85 for the first and around 1.9 Ga for the latter. Sm-Nd isotope systematics of σ peridotites might point towards a late enrichment during the Pan African Orogeny.

Isotope systematics of Sm and Nd are scattered but three σ peridotites plot along an isochron with an age of around 450 Ma, suggesting metasomatic overprint during the Pan African Orogeny.

In addition, we have reinterpreted a previously published Re-Os dataset of garnet peridotites from the Louwrensia kimberlite pipe (Pearson et al., 2004), located within the Gibeon Kimberlite field. We propose an isochron being hidden in this dataset with an Archean age of around 2.9 Ga. The idea of an Archean component underneath the Rehoboth Terrane been envisaged before by different other authors (e.g. Hoal et al., 1995; Franz et al., 1996) and is supported by zircon ages from 2.7 to 2.9 Ga from our own works (see chapter 4) and as published by Cornell et al. (2011) and Van Schijndel et al. (2011). We interpret this age as the timing of depletion of the σ peridotites.

Our new results regarding the mantle underneath the Gibeon kimberlite field allows us to propose a revised geotectonical model as follows. We propose that by the time of the assembly of Eastern- and Western-block of the Kaapvaal Craton, fist mantle components of the Rehoboth

Terrane were created in the spinel stability field which were subsequently subducted underneath already existing crustal components and transformed into garnet peridotite. Collision of the Rehoboth Terrane with the Kaapvaal craton at around 1.9 Ga led to reenrichment of this mantle due to mantle metasomatism.

By the time of the Namaquan orogeny from 0.9 to 1.3 Ga, new mantle material was subducted beneath the Rehoboth Terrane and reenriched by mantle metasomatism at the end of this period at around 850 Ma. Final reenrichment may have occurred during the Pan African Orogeny at around 450 Ma.

Crust

Additional determinations of the crystallization events in the lower crust beneath the Rehoboth Terrane in combination with the results of the enrichment events in the mantle should provide a better understanding about the tectonic events that have created the Terrane as is it nowadays.

We have analysed zircons of six carbonatite derived crustal xenoliths from the Gross Brukkaros Mountain as well as zircons from one crustal xenolith and from one sample of the kimberlite matrix of the Louwrensia Kimberlite pipe. Except for the matrix sample, all samples were high grade metamorphic rocks. After mineral separation, embedding and polishing, zircons were analyzed by Laser ablation ICPMS. Cathodoluminescence images of the zircons allowed precise age determinations of different growth domains within each zircon crystal. Depending on whether the zircons analysed stem from carbonatite or kimberlite derived crustal xenoliths, different age spectras are revealed (Fig.0.3).

Except for one sample, which contains younger zircons from the carbonatite itself, carbonatite derived xenoliths have age peaks mainly between 1.0 and 1.5 Ga, whereas zircons from kimberlite derived samples range from about 0.6 Ga up to 2.9 Ga, with major age peaks around 1.1 to 1.2 and 1.8 to 1.9 Ga. The matrix sample shows a much broader range of ages, from around 0.5 to 2.9 Ga, whereas younger ages can be the result of zircons derived from the Nama shales.

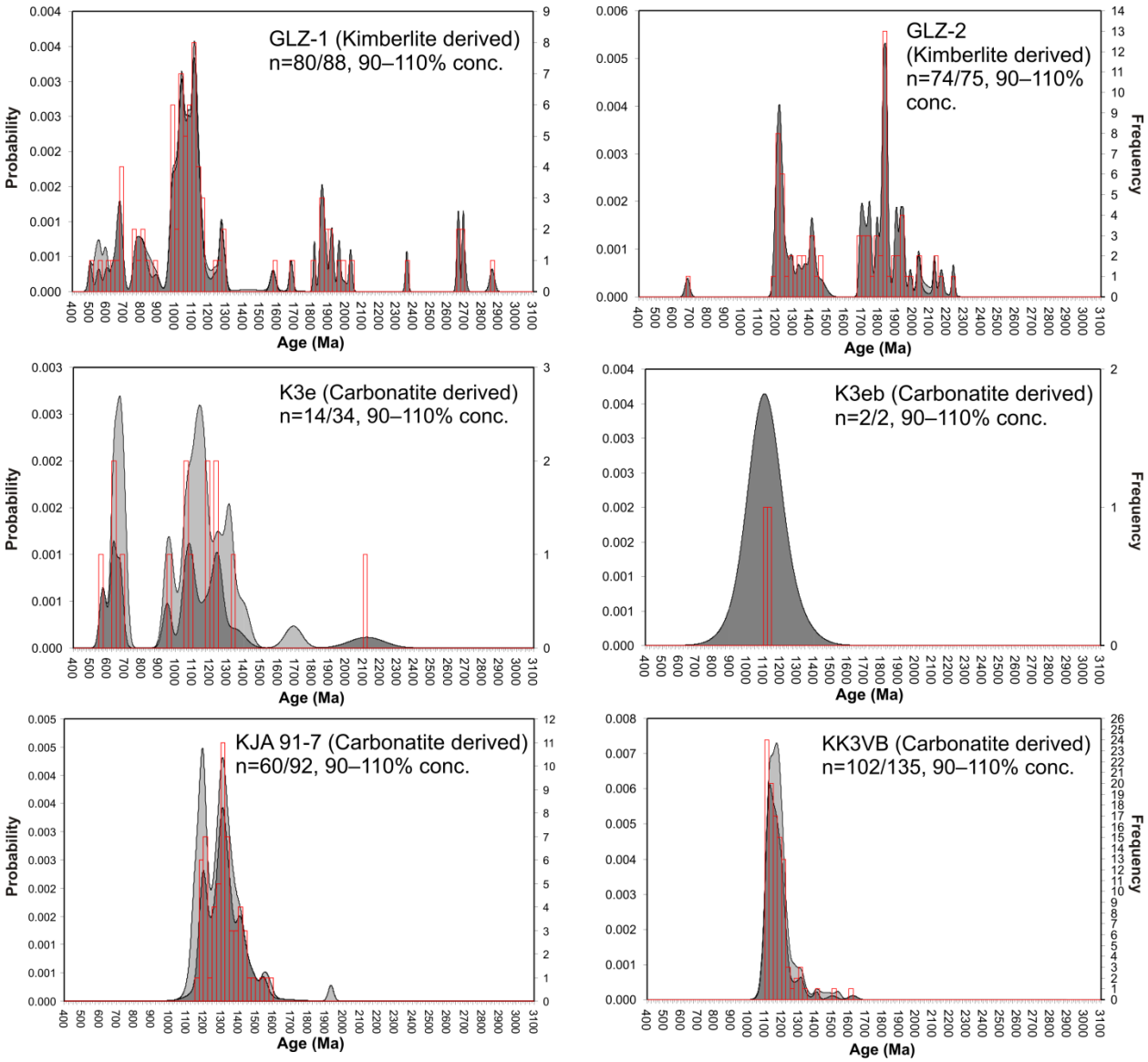

Fig.0.3 U-Pb age spectras for kimberlite and carbonatite derived samples from the Gibeon Kimberlite field and carbonatite vents close to the Gross Brukkaros Mountain.

Additional Hf isotope analyses of the same zircons on top or next to the U-Pb laserspots but in the same growing domain yielded more information about the source of the crust. Combined with the results of the U-Pb analyses, they can reveal crust formation, recycling or mixing events.

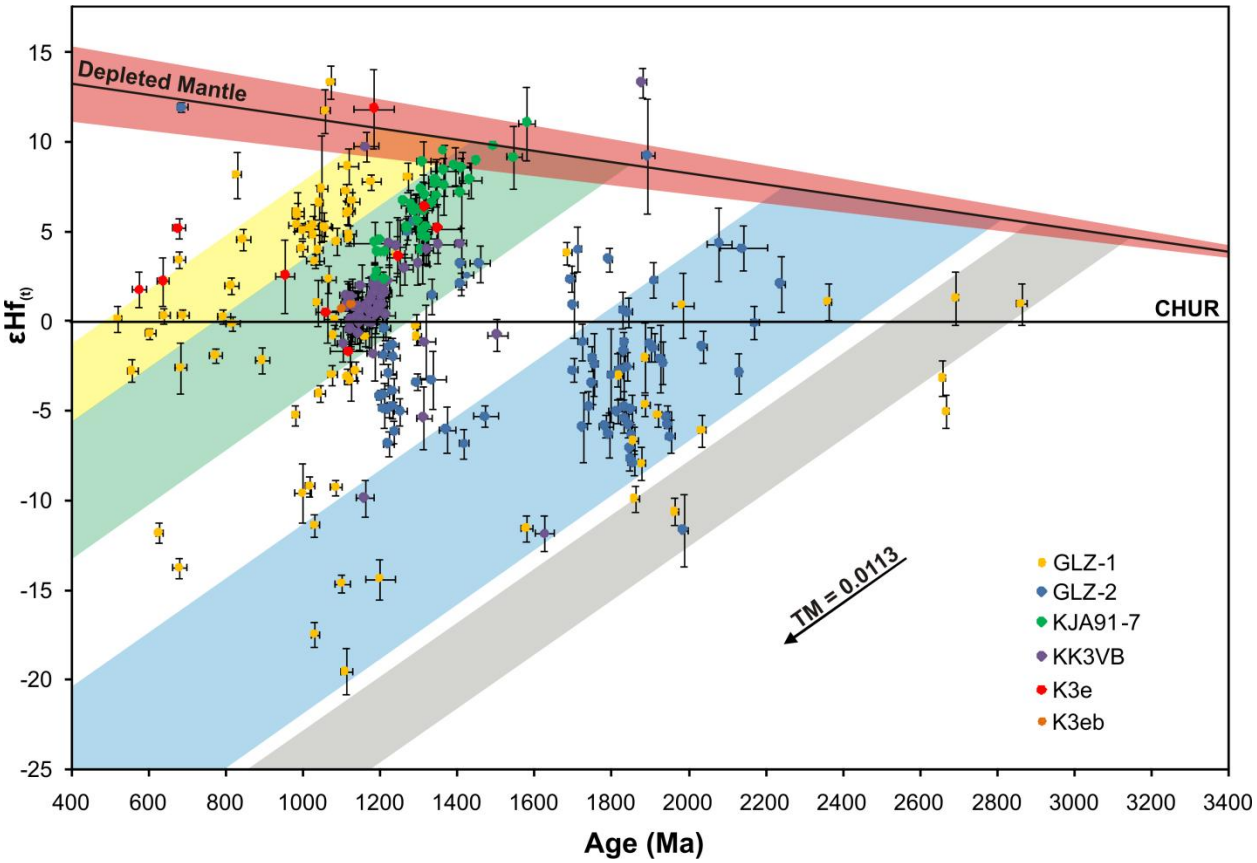

Fig.0.4 Hf isotope systematics of the zircons from Gibeon and around the Gross Brukkaros Mountain combined with the corresponding U-Pb ages, marking four episodes of juvenile crust generation, with subsequent crust recycling and crustal mixing trends. Trend were calculated with a $^{176}Lu/^{177}Hf$ of 0.0113 (Rudnick and Gao, 2003). $^{176}Hf/^{177}Hf$ values for the depleted mantle are taken from Chauvel and Blichert-Toft (2001) and Vervoort et al. (1999).

With respect to these events, there are four phases of crustal growth from a depleted mantle source within the dataset (Fig.0.4).

First crustal growth is recorded in the Archean at around 2.7 to 2.9 Ga from a primitive mantle source or from a depleted mantle source with model ages from 3.05 to 3.38 Ga.

Juvenile crust was formed between 2.3 and 2.7 Ga from a depleted mantle source with subsequent recycling until 1.0 to 1.2 Ga.

The timespan between 1.5 to 1.6 Ga marks the next time of juvenile crust formation from a depleted mantle source and intensive crustal recycling until around 1.1 Ga and crustal mixing between 1.3 and 1.1 Ga. Mostly positive εHf(*t*) values are characteristic for the timespan beween 1.3 to 1.5 Ga. About 60 % of all data point plot in the range between 1.0 to 1.4 Ga.

The youngest crust forming event ranges from 0.8 to 1.1 Ga with subsequent recycling during the Pan African Orogeny at around 0.5 to 0.6 Ga.

The sample, derived from the matrix of the louwrensia kimberlite pipe shows a much higher variation in ages and Hf isotope systematics than all other samples. This is probably related to the fact that zircons from the Nama shales are incorporated in this sample.

Considering the different age spectras of kimberlite and carbonatite derived samples, slightly different stratigraphic units must have been sampled.

This part of the study has shown that the crust beneath the Gibeon Kimberlite field is made up of metamorphosed sediments. Without considering the ages that probably stem from zircons from Nama shale sediments, youngest ages are in the range of about 0.9 Ga.

Oldest crust was probably generated in the Archean, followed by an episode between 1.8 and 1.9 Ga in which the Rehoboth Terrane has been attached to the Kaapvaal Craton. The latter event is also recorded in the geochronological record of the mantle xenoliths from Gibeon as an enrichment event of the σ peridotites (see chapter 3).

Subduction beneath the Kalahari plate is probably the cause for crust generation, recycling and mixing during a timespan between 1.5 and 1.1 Ga with around 60 % of all datapoints of this study lying in this range and has first been proposed by (Becker et al., 2006).

The Namaquan Orogeny also affected the crust beneath the Gibeon Kimberlite field by forming juvenile crust from a depleted mantle source that was subsequently recycled during the Pan African Orogeny. The Namaquan orogeny is reflected by the addition of new mantle components (‘N’ peridotites) and their subsequent enrichment. A late Pan African overprint is also reflected in the Sm-Nd isotope systematics of the σ peridotites (see chapter 3).

The lower crust and the upper mantle of the South eastern volcanic province in Spain

Mantle

Spinel / Plagioclase peridotites from the neogene alkaline basaltic volcano Cabezo Negro de Tallante were collected and selected minerals from 11 samples were separated. Plagioclase could

only be found in 5 samples. Major and trace elements of clinoyproxenes and orthopyroxenes, as well as major element for olivines and plagioclases (if available) were measured by the electron microprobe and laser ablation ICPMS. Seven samples were chosen for isotope analyses, specifically the Lu-Hf, Sm-Nd and Rb-Sr isotope systems.

All samples chosen stem from pressure ranges between 7 to 20 kbar and temperature ranges between 900 and 1000°C as determined by the two pyroxene thermometer of Brey and Koehler (1990) and the Ca in olivine barometer of Koehler and Brey (1990).

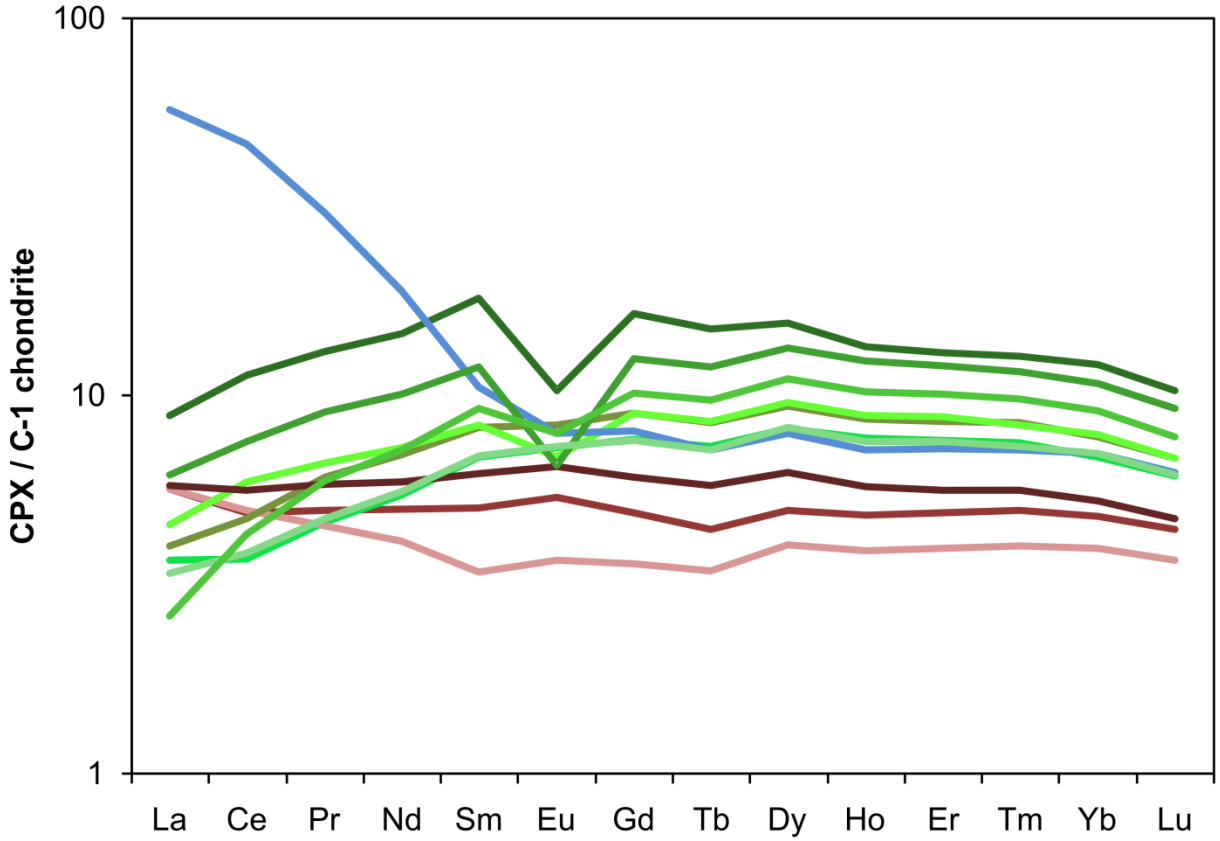

Fig.0.5 Three types of samples for the Spinel / Plagioclase peridotites from Cabezo Negro de Tallante as determined by the REE patterns of the corresponding clinopyroxenes, normalized to C1 (McDonough and Sun, 1995). Type 1 is marked in green, whereas type 2 is marked in red and type 3 is marked in blue.

Based on the trace element concentrations, three different types of patterns could be differentiated. Type one is characterized by slightly enriched middle rare earth elements (MREE), and slightly depleted light rare earth elements (LREE) relative to the MREE (see Fig.0.5 - green). Type two shows almost flat rare earth element patterns and lower contents of

REE in general compared to type one (see Fig.0.5 - red). Type three consists of only one sample that is highly enriched in LREE, whereas the corresponding MREE and heavy rare earth elements (HREE) are mostly following the patterns of type 1 (see Fig.0.5 - blue).

Normalization on a primitive sample from Vitim Siberia (Ionov et al., 2005) shows enrichment of LREE for all 3 types of samples.

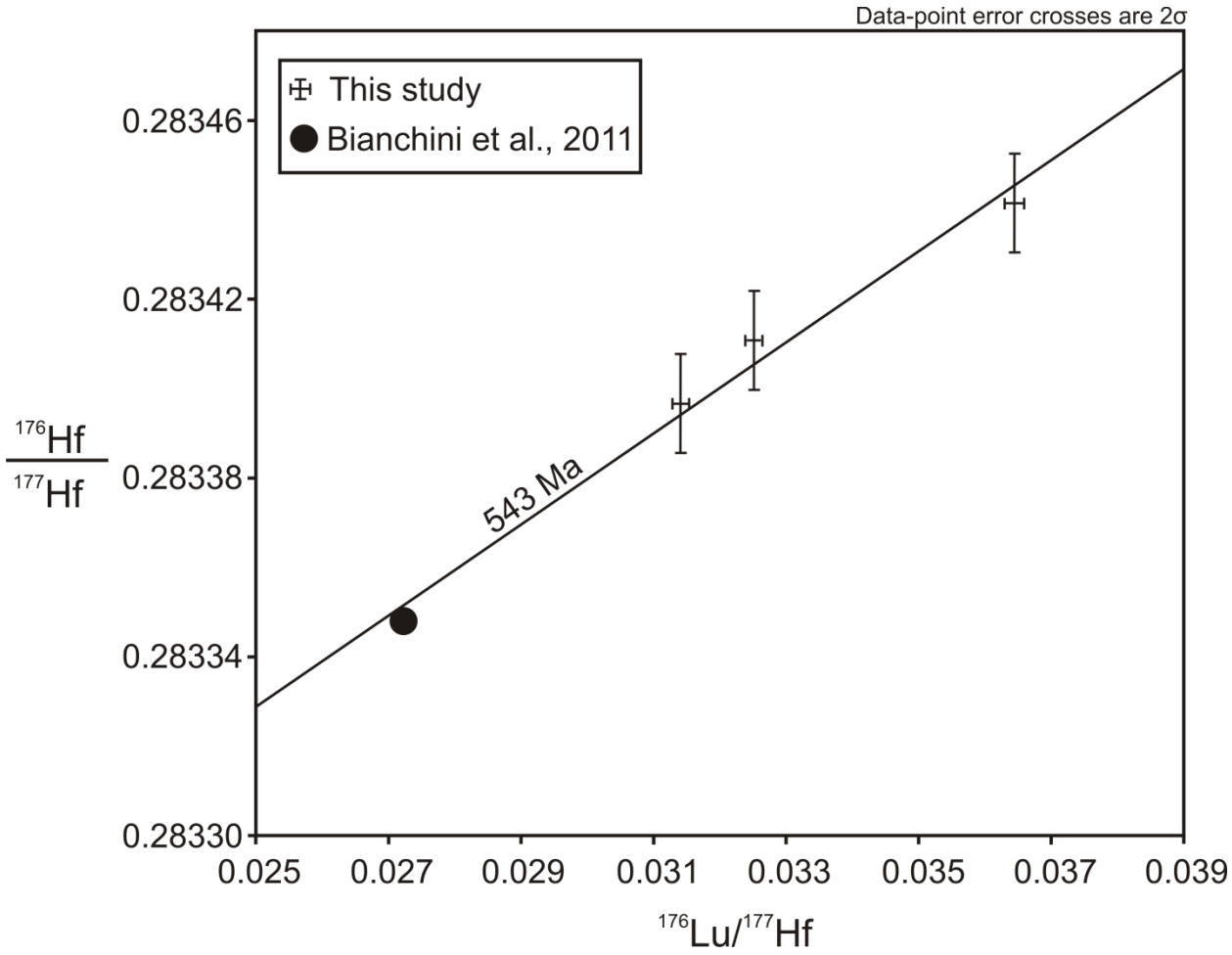

Fig.0.6 A possible depletion event might have occurred at a time around 550 Ma, as interpreted from Lu-Hf isotope systematics of three samples from this dataset and an additional sample as published by Bianchini et al. (2011) and Beccaluva et al. (2004).

Lu-Hf isotope systematics of all samples measured do not show a clear correlation due to a small $^{176}Lu/^{177}Hf$ range and some scatter. However, including one additional sample (TL16) from the same locality that was published earlier (Beccaluva et al., 2004; Bianchini et al., 2011), four datapoints can be correlated to an age at around 550 Ma (Fig.0.6). As Hf seems to be

untouched by enrichment events, this age could be a possible age of depletion for the mantle underneath the SEVP. Model ages of two additional samples point towards an older component being present underneath the SEVP, which is in accordance with the isotope studies of Tallante xenoliths by Bianchini et al. (2011) and the comparison to other localities in Europe (Downes and Dupuy, 1987; Reisberg et al., 1989; Bodinier et al., 1991; Downes et al., 1991; Zangana et al., 1997; Beccaluva et al., 2001; Downes et al., 2002).

Sm-Nd isotope systematics cannot be associated in an isochron, but the datapoints scatter around a projection of 550 Ma.

Sr isotope systematics of clinopyroxene and plagioclase mostly differ, with higher $^{87}Sr/^{86}Sr$ isotope ratios for the plagioclase in comparison to the clinopyroxenes. The first are probably the result of a metasomatic overprint while in contact with the alkaline basaltic melts, while the latter seem to have remained untouched by this event.

Crust

Three samples from alkali basaltic outcrops within the SEVP were collected in order to decipher the evolution of the corresponding lower crust. These samples were either taken from tuff layers (CNTS-1 and ALCS-1) or the matrix of the alkali basalts (CG-Z1 – CG-Z3).

Sieving of the samples in the field was followed by heavy liquid separation, magnetic separation, treatment with 6M HCl, sieving with one-time fabric sieves and handpicking with the use of a stereomicroscope.

Growing domains within the zircons crystals were revealed by cathodoluminescence images and U-Th-Pb isotope ratios of homogenous domains were determined by laser ablation ICPMS. In a later step, Hf isotope compositions were determined by laser ablation multicollector ICPMS. By combining the information obtained from both methods it was possible to obtain a better understanding of how the crust beneath the SEVP developed in terms of juvenile crust generation, crustal recycling and crustal mixing.

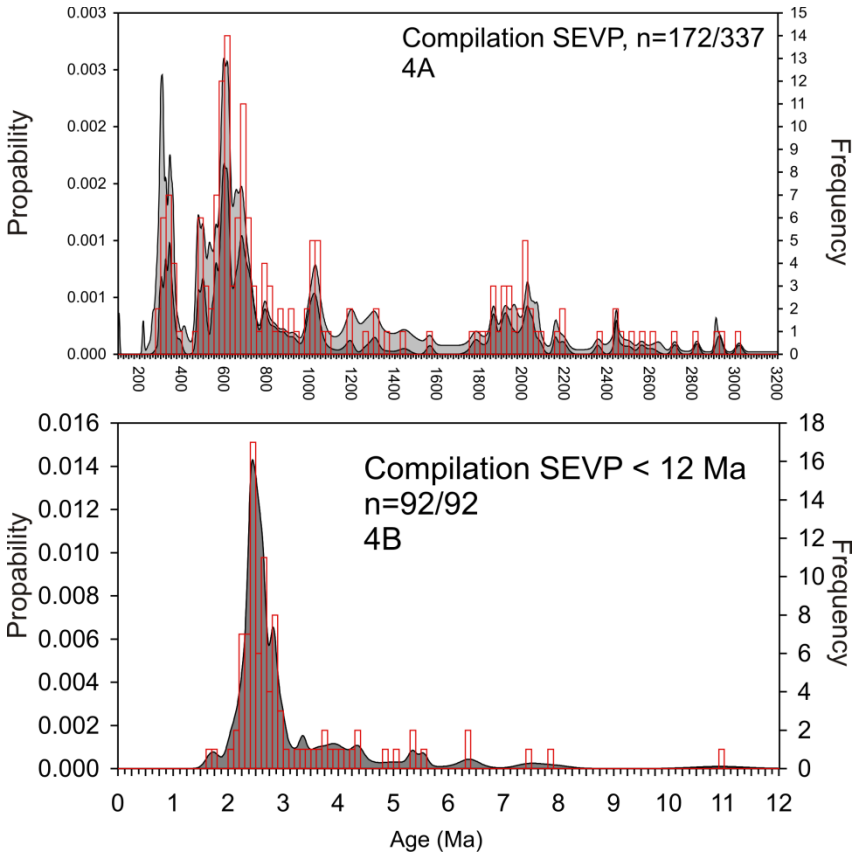

Fig.0.7 A compilation of the U-Pb data of all three localities within the SEVP with ages > 100 Ma shown in (A) and ages < 12 Ma as shown in (B).

All three samples show very similar age patterns, with a wide range from around 2.6 Ma up to 3 Ga. Main age distributions are between 0.3 to 0.4, 0.5 Ga and 0.6 to 0.7 Ga. Some minor age distributions are between 1 Ga to 1.1 Ga, 1.8 to 2.2 Ga, 2.4 to 2.6 Ga and 2.9 to 3 Ga (Fig.0.7).

Hf isotope systematics in combination with the U-Pb ages revealed two major crustal development trends (Fig.0.8). First crust was formed during the Archean and was subsequently recycled between 2.5 to 1 Ga. In a timespan between 1.0 to 1.5 Ga, new crust was generated from a depleted mantle source, which was constantly recycled during the Caledonian and Variscian orogenies. The latter might be reflected in a depletion event in the mantle (see chapter 5). Additionally, a vertical array of datapoints points to a crustal mixing event at a time around 0.5 to 0.6 Ga.

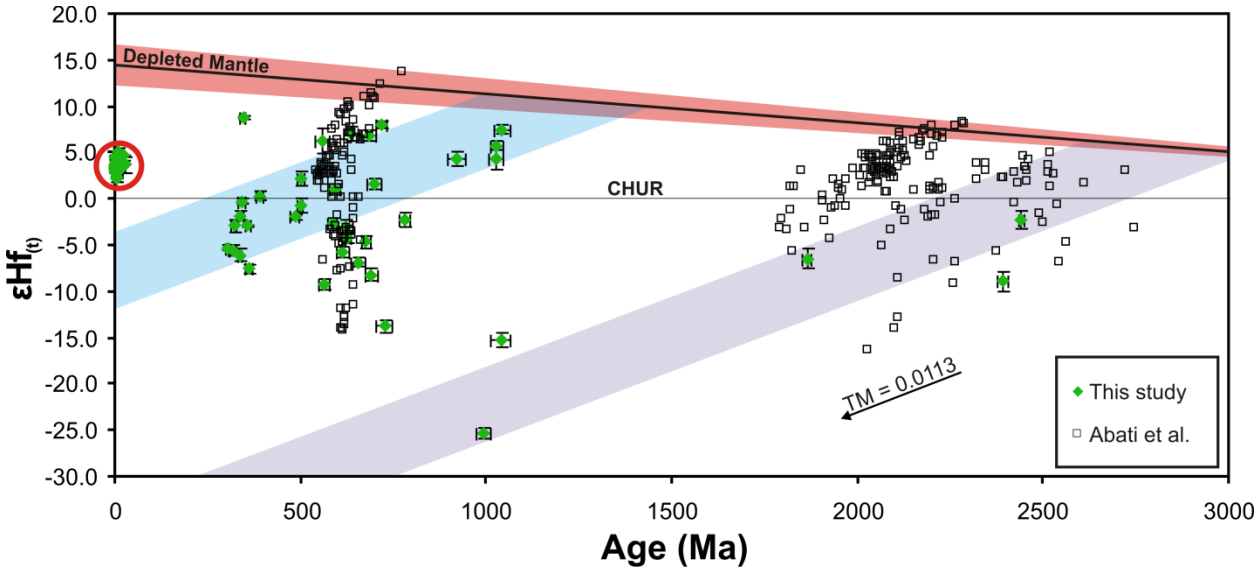

Fig.0.8 Combination of U-Pb and corresponding εHf(*t*) values for the zircons from this study (green) and from Abati et al. (2012), marked as black squares. A $^{176}Lu/^{177}Hf$ of 0.0113 (Rudnick and Gao, 2003) was used for the calculation of the fields of crustal growth. Values for the depleted mantle are from Chauvel and Blichert-Toft (2001) and Vervoort et al. (1999).

Neogene ages have εHf(*t*) values that are nearly chondritic, indicating a slightly depleted mantle as the source of melt extraction. The most recent ages amongst these are around 2.6 Ma with oscillary zoning and subrounded edges of the corresponding zircon crystals. They record the timing of when the alkali basalts erupted to the surface as determined previously by K-Ar (Bellon et al., 1983). Minor age distributions around 5 to 8 Ma, indicate that the extrusion of calc-alkaline magmas that are generally be found further southwest of the SEVP (Turner et al., 1999; Duggen et al., 2003; Duggen et al., 2004) have affected the SEVP as well.

The comparison to previously published data of restitic enclaves of a dacite and a graphitic schist from Zeck and Williams (2002) and Zeck and Williams (2001) of Cerro del Hoyazo and another nearby locality around 150 km further Southwest in the Betic Cordillera of Cabezo Negro de Tallante, show that the age patterns are very similar. These similiarties in ages suggest a stacking of nappes within the Betic cordillera as the samples from Cerro del Hoyazo are probably derived from greater depths.

Further comparisons to studies from the West African Craton and the Arabian-Nubian shield (Abati et al, 2012; Avigad et al., 2012) suggest that a major part of the zircons are derived from these blocks and were transported onto Iberia during the assembly of Gondwana.

References

Abati, J., Aghzer, A.M., Gerdes, A. and Ennih, N., 2012. Insights on the crustal evolution of the West African Craton from Hf isotopes in detrital zircons from the Anti-Atlas belt. Precambrian Research, 212 - 213: 263 - 274.

Avigad, D., Gerdes, A., Morag, N. and Bechstadt, T., 2012. Coupled U-Pb-Hf of detrital zircons of Cambrian sandstones from Morocco and Sardinia: Implications for provenance and Precambrian crustal evolution of North Africa. Gondwana Research, 21(2-3): 690-703.

Beccaluva, L., Bianchini, G., Bonadiman, C., Siena, F. and Vaccaro, C., 2004. Coexisting anorogenic and subduction-related metasomatism in mantle xenoliths from the Betic Cordillera (southern Spain). Lithos, 75(1-2): 67-87.

Beccaluva, L. et al., 2001. Multistage evolution of the European lithospheric mantle: new evidence from Sardinian peridotite xenoliths. Contributions to Mineralogy and Petrology, 142(3): 284-297.

Becker, T., Schreiber, U., Kampunzu, A.B. and Armstrong, R., 2006. Mesoproterozoic rocks of Namibia and their plate tectonic setting. Journal of African Earth Sciences, 46(1-2): 112-140.

Bellon, H., Bordet, P. and Montenat, C., 1983. Chronology of the Neogene Magmatism from Betic Ranges (Southern Spain). Bulletin De La Societe Geologique De France, 25(2): 205-217.

Bianchini, G., Beccaluva, L., Nowell, G.M., Pearson, D.G. and Siena, F., 2011. Mantle xenoliths from Tallante (Betic Cordillera): Insights into the multi-stage evolution of the south Iberian lithosphere. Lithos, 124(3-4): 308-318.

Bodinier, J.L., Menzies, M.A. and Thirlwall, M.F., 1991. Continental to Oceanic Mantle Transition-REE and Sr-Nd Isotopic Geochemistry of the Lanzo Lherzolite Massif. Journal of Petrology: 191-210.

Brey, G.P. and Koehler, T., 1990. Geothermobarometry in 4-Phase Lherzolites .2. New Thermobarometers, and Practical Assessment of Existing Thermobarometers. Journal of Petrology, 31(6): 1353-1378.

Chauvel, C. and Blichert-Toft, J., 2001. A hafnium isotope and trace element perspective on melting of the depleted mantle. Earth and Planetary Science Letters, 190(3-4): 137-151.

Cornell, D.H. et al., 2011. Evidence from Dwyka tillite cobbles of Archaean basement beneath the Kalahari sands of southern Africa. Lithos, 125(1-2): 482-502.

Davies, G.R., Spriggs, A.J. and Nixon, P.H., 2001. A non-cognate origin for the Gibeon kimberlite megacryst suite, Namibia: Implications for the origin of Namibian kimberlites. Journal of Petrology, 42(1): 159-172.

Downes, H., Bodinier, J.L., Thirlwall, M.F., Lorand, J.P. and Fabries, J., 1991. REE and Sr-Nd Isotopic Geochemistry of Eastern Pyrenean Peridotite Massifs: Sub-Continental Lithospheric Mantle Modified by Continental Magmatism. Journal of Petrology: 97-115.

Downes, H. and Dupuy, C., 1987. Textural, Isotopic and Ree Variations in Spinel Peridotite Xenoliths, Massif-Central, France. Earth and Planetary Science Letters, 82(1-2): 121-135.

Downes, H. et al., 2002. Geochemistry and Sr-Nd isotopic compositions of mantle xenoliths from the Monte Vulture carbonatite-melilitite volcano, central southern Italy. Contributions to Mineralogy and Petrology, 144(1): 78-92.

Duggen, S., Hoernle, K., van den Bogaard, P. and Harris, C., 2004. Magmatic evolution of the Alboran region: The role of subduction in forming the western Mediterranean and causing the Messinian Salinity Crisis. Earth and Planetary Science Letters, 218(1-2): 91-108.

Duggen, S., Hoernle, K., van den Bogaard, P., Rupke, L. and Morgan, J.P., 2003. Deep roots of the Messinian salinity crisis. Nature, 422(6932): 602-606.

Franz, L., Brey, G.P. and Okrusch, M., 1996. Steady state geotherm, thermal disturbances, and tectonic development of the lower lithosphere underneath the Gibeon Kimberlite Province, Namibia. Contributions to Mineralogy and Petrology, 126(1-2): 181-198.

Hoal, B.G., Hoal, K.E.O., Boyd, F.R. and Pearson, D.G., 1995. Age constraints on crustal and mantle lithosphere beneath the Gibeon kimberlite field, Namibia. South African Journal of Geology, 98(2): 112-118.

Ionov, D.A., Blichert-Toft, J. and Weis, D., 2005. Hf isotope compositions and HREE variations in off-craton garnet and spinel peridotite xenoliths from central Asia. Geochimica Et Cosmochimica Acta, 69(9): 2399-2418.

Koehler, T.P. and Brey, G.P., 1990. Calcium Exchange between Olivine and Clinopyroxene Calibrated as a Geothermobarometer for Natural Peridotites from 2 to 60 Kb with Applications. Geochimica Et Cosmochimica Acta, 54(9): 2375-2388.

McDonough, W.F. and Sun, S.S., 1995. The Composition of the Earth. Chemical Geology, 120(3-4): 223-253.

Pearson, D.G., Irvine, G.J., Ionov, D.A., Boyd, F.R. and Dreibus, G.E., 2004. Re-Os isotope systematics and platinum group element fractionation during mantle melt extraction: a study of massif and xenolith peridotite suites. Chemical Geology, 208(1-4): 29-59.

Reisberg, L., Zindler, A. and Jagoutz, E., 1989. Further Sr and Nd Isotopic Results from Peridotites of the Ronda Ultramafic Complex. Earth and Planetary Science Letters, 96(1-2): 161-180.

Rudnick, R.L. and Gao, S., 2003. Composition of the continental crust. In: Rudnick RL (ed) The crust. Treatise in Geochemistry 3: 1-64.

Turner, S.P. et al., 1999. Magmatism associated with orogenic collapse of the Betic-Alboran Domain, SE Spain. Journal of Petrology, 40(6): 1011-1036.

Van Schijndel, V., Cornell, D.H., Hoffmann, K.-H. and Frei, D., 2011. Three episodes of crustal developement in the Rehoboth Province, Namibia. In: Van Hinsbergen, D.J.J., Buiter, S.J.H., Torsvik, T.H., Gaina, C., Webb, S. (Eds.), The formation and evolution of Africa from the Archaean to Present. Geol. Soc. Spec. Pub.

Vervoort, J.D., Patchett, P.J., Blichert-Toft, J. and Albarede, F., 1999. Relationships between Lu-Hf and Sm-Nd isotopic systems in the global sedimentary system. Earth and Planetary Science Letters, 168(1-2): 79-99.

Zangana, N.A., Downes, H., Thirlwall, M.F. and Hegner, E., 1997. Relationship between deformation, equilibration temperatures, REE and radiogenic isotopes in mantle xenoliths (Ray Pic, Massif Central, France): An example of plume-lithosphere interaction? Contributions to Mineralogy and Petrology, 127(1-2): 187-203.

Zeck, H.P. and Williams, I.S., 2001. Hercynian metamorphism in nappe core complexes of the Alpine Betic-Rif belt, Western Mediterranean - a SHRIMP zircon study. Journal of Petrology, 42(7): 1373-1385.

Zeck, H.P. and Williams, I.S., 2002. Inherited and magmatic zircon from Neogene Hoyazo cordierite dacite, SE Spain - Anatectic source rock provenance and magmatic evolution. Journal of Petrology, 43(6): 1089-1104.

Chapter 1: Introduction

The formation of the continental crust and the lithospheric mantle is a topic of high significance in geo sciences and the geochronological aspects of this process are still unknown for larger areas of the earth. Despite years of research, there is no clear agreement of how the generation of crustal portions and its corresponding underlying mantle are associated with each other. The theory of pulsed growth is in direct contrast to the steady accumulaction of continental crust as summarized by Pearson et al. (2007).

In this work, we try to bring new light into the discussion through the investigation of crustal and mantle material with the comparison between two distinct localities in Namibia and the southeastern volcanic province in Spain. These localities were chosen as they enable direct access to sample material that was transported by the ascent of kimberlitic and carbonatitic (Namibia) or basaltic melts (Spain). Furthermore there is a lack of data regarding the crustal and mantle processes that happened in the past for both study areas. It is still unknown how the Rehoboth Terrane fits into the southern African framework with respect to its geochronological past. Despite numerous investigations of mantle xenoliths from Cabezo Negro de Tallante in the South eastern volcanic Province (SEVP), no information about depletion or enrichment processes is available from that area, as well as no information about the evolution of the deeper crust.

The comparison of the geochronological records from both study areas as well as major and trace element budgets should give direct information about the coherency between mantle and crustal development. The questions of when, how often and in what geothermobarometrical regime the mantle was depleted and enriched as well as the question of when crustal material crystallized from which sources are subject of this study.

Since the routine usage of laser ablation ICP mass spectrometry in the last years, the determination of geochronological records of crustal material has increased dramatically (e.g. Fryer et al., 1993; Hirata and Nesbitt, 1995; Scott and Gauthier, 1996; Gerdes and Zeh, 2006; Zeh and Gerdes, 2010; Avigad et al., 2012). The analysis of the accessory mineral zircon, which can be found in most crustal rocks, for U-Pb isotope systematic allows a precise determination of the age of crustal crystallization. Additionally, Hf isotope ratios of the same mineral grains give information about the source of melt extraction.

Age determination of mantle material, specifically of garnet and spinel peridotites, requires a much more extensive sample preparation. In this work, we have analyzed our samples for Lu-Hf (Namibia and Spain) and Sm-Nd (Namibia and Spain) and Sr (Spain) isotope systematics by isotope dilution multicollector ICP mass spectrometry. Lu-Hf can thereby provide information about the timing of mantle depletion, Sm-Nd and Sr isotope measurements, however, show great potential for giving information about the enrichment of mantle portions due to mantle metasomatism by the interaction with fluids.

1.1. Determination of mantle depletion ages

The conventional method of determining mantle depletion ages/the age of melt extraction, is Re-Os isotope measurements, of, in most cases, whole rock samples of peridotites (e.g. Hoal et al., 1995; Pearson et al., 2004; Rudnick and Walker, 2009). The basic assumption hereby is that during melt extraction, all Re is extracted into the melt and that Re/Os ratios in the residue are zero. This however is only the case for high degrees of partial melting which is true for most cratonic areas, such as the Kaapvaal craton, but has turned out to be much lower in the surrounding Proterozoic mobile belts, such as the Namaqua Natal belt in southern Africa. As the derivation of an isochron for Re-Os is very difficult, model ages are usually determined by calculating of Rhenium depletion (T_{RD}) or Rhenium model ages (T_{MA}). If during melt extraction all Re has been driven off into the melt, no radiogenic ^{187}Os can be formed in the residue since this event. If however some Re was still in the residue after melt extraction, the $^{187}Os/^{188}Os$ ratio increases and the T_{RD} age only represent a minimum age. In contrast, T_{MA} ages represent a maximum age. Due to the uncertainty of the concentration of Re in the residue after melt extraction and the uncertainty of the initial chrondritic $^{187}Os/^{188}Os$ isotope ratio, ages determined by the methods mentioned before are afflicted by a certain factor of uncertainty.

Another potential way of determining the timing of mantle depletion is the application of the Lu-Hf isotope system. In contrast to the Re-Os isotope system, during melt extraction, the daughter element Hf is extracted into the melt. It has become more and more popular in the last years as it appeared to be more robust to a metasomatic overprint compared to other isotopic systems (e.g. Schmidt et al., 2008; Lazarov et al., 2009). This means that the information about the age of mantle depletion is still preserved in the residue. In this study we analyze garnet and

clinopyroxenes as they carry the major amount of Hf in their crystal lattice with respect to all other coexisting phases in garnet, spinel, and plagioclase peridotites. The initial value of an isochron derived from clinopyroxenes in the spinel field or from bulk rocks calculated from the modal amounts of clinopyroxenes and garnets, gives additional information about the source of melt extraction, specifically if the source was the depleted or primitive mantle, i.e. if the source has experienced earlier melt extraction. We find, however, that Hf is commonly also reintroduced in small amounts and that it appears to date a first metasomatic overprint (which may also be the trigger of renewed partial melting) more accurately.

1.2. Determination of metasomatic overprint in the mantle

After melt extraction from a mantle source of whatever nature, trace elements carrying fluids with high concentrations of the more incompatible elements like the light rare earth elements can overprint the residue again. The age dating of such overprints should yield the most accurate results with the radiogenic Sm-Nd or the Rb-Sr isotope systems. After enrichment with the specific elements, the geochronological clock is reset and starts to tick again from the time of enrichment. Given enough time to reequilibrate, isochron ages can be determined, resulting in the age of enrichment. If, however, multiple enrichments occur at different times, the age of mantle metasomatism can no longer be deciphered for the individual events.

1.3. The age of crystallization of the continental crust

As mentioned earlier, the accessory mineral phase zircon is most suitable to determine crustal ages and crustal growth. Until the advent of SIMS (Secondary Ion Mass Spectrometry) and Laser Ablation Inductively Coupled Mass Spectrometry (LA ICPMS), this was carried out by dissolving individual or pooled zircons and measuring the U and Pb isotope systems by Thermo ionization mass spectrometry (TIMS). The introduction of LA ICPMS has dramatically simplified the analysis of zircons (at a cost of accuracy compared to TIMS). The huge advantage compared to TIMS is the possibility to analyse single domains in individual zircons (which were previously characterized by cathodoluminescence) and the much higher sample throughput compared to SIMS.

LA ICPMS has therefore become the most popular method to determine the age of crystallization in zircon grains since its beginning in the early 1990's (e.g. Fryer et al., 1993). U has a similar ionic radius as zirconium and can therefore easily replace the zirconium within the crystal lattice. In contrast, almost no Pb fits into the lattice due to its higher ionic radius. The Pb in the zircons is therefore almost exclusively radiogenic and general, only very small corrections have to be made for common lead (^{204}Pb). Much more information can be hidden in the zircon crystal, such as a later phase of metamorphism, during which zircon can have added another rim domain, surrounding the older core. The analysis of these domains can, for example, reveal the timing of metamorphism in connection with regional orogeny events.

The information about the age of crystallization alone does not necessarily allow the prediction of genetical relationships of different crustal components. Such relationships can be further explored from the combination with the analysis of Hafnium isotope composition by LA ICPMS on the same spots which will give further information on the nature of crustal melt extraction and crustal development trends. It shows, based on average ^{176}Lu/^{177}Hf contents of a hypothetical crust, if zircon ages are cogenetic on the same trend for crustal development or if crustal components have been mixed and were isotopically homogenized.

1.4. Goals of this study

A. Determination of mantle depletion and enrichment processes as well as geothermobarometrical constraints underneath the Gibeon Kimberlite Field / the Rehoboth Terrane using by major, trace element and isotope (Lu-Hf, Sm-Nd) data.
B. Determination of crustal forming or recrystallization events of the deeper crust of the Rehoboth Terrane by U-Pb isotope measurements of zircons that stem from crustal xenoliths. These results shall be compared to the results of 1.4.A..
C. Determination of mantle depletion and enrichment processes in the South Eastern Volcanic Province (SEVP) as well as the determination of the thermobaromatric regime of the spinel / plagioclase peridotites by major, trace element and isotope measurements of the constitutent minerals.

D. Deciphering the crust forming events beneath the SEVP by U-Pb and Hf isotope analyses of zircons from crustal debris available from tuff layers that are associated with Neogene alkaline basaltic volcanism of southeastern Spain. Comparison to the results of 1.4.C.

1.5. References

Avigad, D., Gerdes, A., Morag, N. and Bechstadt, T., 2012. Coupled U-Pb-Hf of detrital zircons of Cambrian sandstones from Morocco and Sardinia: Implications for provenance and Precambrian crustal evolution of North Africa. Gondwana Research, 21(2-3): 690-703.

Fryer, B.J., Jackson, S.E. and Longerich, H.P., 1993. The Application of Laser-Ablation Microprobe-Inductively Coupled Plasma-Mass Spectrometry (Lam-Icp-Ms) to in-Situ (U)-Pb Geochronology. Chemical Geology, 109(1-4): 1-8.

Gerdes, A. and Zeh, A., 2006. Combined U–Pb and Hf isotope LA-(MC-)ICP-MS analyses of detrital zircons: Comparison with SHRIMP and new constraints for the provenance and age of an Armorican metasediment in Central Germany. Earth and Planetary Science Letters, 249: 47-61.

Hirata, T. and Nesbitt, R.W., 1995. U-Pb Isotope Geochronology of Zircon - Evaluation of the Laser Probe-Inductively Coupled Plasma-Mass Spectrometry Technique. Geochimica Et Cosmochimica Acta, 59(12): 2491-2500.

Hoal, B.G., Hoal, K.E.O., Boyd, F.R. and Pearson, D.G., 1995. Age constraints on crustal and mantle lithosphere beneath the Gibeon kimberlite field, Namibia. South African Journal of Geology, 98(2): 112-118.

Lazarov, M., Brey, G.P. and Weyer, S., 2009. Time steps of depletion and enrichment in the Kaapvaal craton as recorded by subcalcic garnets from Finsch (SA). Earth and Planetary Science Letters, 279(1-2): 1-10.

Pearson, D.G., Irvine, G.J., Ionov, D.A., Boyd, F.R. and Dreibus, G.E., 2004. Re-Os isotope systematics and platinum group element fractionation during mantle melt extraction: a study of massif and xenolith peridotite suites. Chemical Geology, 208(1-4): 29-59.

Pearson, D.G., Parman, S.W. and Nowell, G.M., 2007. A link between large mantle melting events and continent growth seen in osmium isotopes. Nature, 449(7159): 202-205.

Rudnick, R.L. and Walker, R.J., 2009. Interpreting ages from Re-Os isotopes in peridotites. Lithos, 112: 1083-1095.

Schmidt, A. et al., 2008. Rapid eclogitisation of the Dabie-Sulu UHP terrane: Constraints from Lu-Hf garnet geochronology. Earth and Planetary Science Letters, 273(1-2): 203-213.

Scott, D.J. and Gauthier, G., 1996. Comparison of TIMS (U-Pb) and laser ablation microprobe ICP-MS (Pb) techniques for age determination of detrital zircons from Paleoproterozoic metasedimentary rocks from northeastern Laurentia, Canada, with tectonic implications. Chemical Geology, 131(1-4): 127-142.

Zeh, A. and Gerdes, A., 2010. Baltica- and Gondwana-derived sediments in the Mid-German Crystalline Rise (Central Europe): Implications for the closure of the Rheic ocean. Gondwana Research, 17(2-3): 254-263.

Chapter 2: Methodology

2.1. Sample crushing - SelFrag®

As a first separation step, hand specimens were crushed with a SelFrag® fragmentation system. Using this technique allows a clean separation of the samples along the grain boundaries with a highly reduced risk of cross contamination. In contrast to conventional techniques (e.g. jaw crusher), the sample is placed into a vessel filled with tap- or deionized water. Two electrodes are placed face to face, with the sample in between in the vessel. A built-in sieve with a mesh size of 1 mm separates two compartments within the vessel. The distance between these electrodes can be adjusted from 40 to 10 mm. The sample is processed by electrical pulses with high voltage currents, starting from 90 KV up to 200 KV and frequencies from 1 to 5 Hz. Thereby currents run through the sample, following grain boundaries. Electrical discharges within the sample crush the sample as they are converted into acoustical shockwaves.

Depending on the constitution of the sample, pulse rates for crushing a sample in hand specimen size range from 50 to 200 pulses.

As all parts of the machine and the vessel can be rinsed with water, and the risk of remaining particles is practically nil and cross contamination does not occur.

2.2. Major element analyses

Major elements were determined by wavelength dispersive analyses with a Jeol JXA 8900RL Superprobe with five spectrometers, each of which contains several crystals for quantitative analyses. In general, sample mounts or thick sections were polished and cleaned with benzine (p.a.) before drying in a vacuum oven at 50°C for several hours. After drying down, samples were carbon coated with a Jeol JEE4B coating system. Samples were built into the microprobe under high vacuum conditions (10^{-6} mbar). Acceleration voltage was adjusted to 15 kV and a 3 µm beam with a current of 20 nA was chosen. Measuring times for element peaks was adjusted from 20 to 30 s, while background measurement times were from 10 to 30 s.

For the determination of Ca in olivine (see Chapter 5), peak and background measurement times were increased to 120 s, in order to lower the detection limit of Ca.

Standards were either mineral standards, pure oxides or metals. For the determination of Ca in olivine, standard SCKA, as described in Koehler and Brey (1990), was used for calibration.

Where ever possible, multiple analyses on each grain were performed.

For all measurements, matrix corrections were carried out using the CITZAF© algorithm by John T. Armstrong.

2.3. Trace Element analyses

Trace element analyses were carried out with a Thermo-Finnigan® Element 2 inductivly coupled plasma mass spectrometer coupled to either a Resonetics M50 laser ablation system or a New Wave Research® UP213 ultraviolet Nd-YAG laser. Aluminum sample and skimmer cones were used throughout the analytical sessions. The same sample mounts or thick sections used for major element analyses were used here.

Before each session, the mass spectrometer was tuned to maximum signal yield and minimum oxide formation rate by line scans on standard Nist 612.

Samples were ablated with 40 µm spots, laser energies of around 0.6 mJ and a frequency of 10 Hz with several spots on each grain. External standardization was performed, using a Nist 612 glass standard, combined with CaO concentrations as determined earlier by electron microprobe measurements. Precision of the analyses as well as machine conditions were checked by analyzing USGS standard Bir-1G at the beginning and the end of a session as well as in between.

Raw data was processed with the Gemoc GLITTER© software, using reference values for CaO from Pearce et al. (1997).

2.4. Isotope analyses

2.4.1. Chromatographic separation

Low concentrations of Lu, Hf, Sm, Nd and Sr and high interference with isotopes of other elements makes a direct in-situ measurement by Laser Ablation ICP mass spectrometry not possible for our mantle derived samples. In order to increase the amount of the desired elements, chromatographic separation was a first step prior to analysis. This was performed in several laboratory sessions (‘batch’) in a PicoTrace clean laboratory at the Goethe University Frankfurt

am Main. After the separation of the garnet- or spinel xenoliths with SelFrag®, heavy liquid separation, magnetic separation, sieving, handpicking under a microscope and leaching with 6 M HCl on a hot plate, mineral separates of clinopyroxene and garnet were ultrasonicated in Milli-Q water for at least 1 hour and then rinsed with Milli-Q® water again. These steps were followed by weighing in each sample and spiking separately with a ^{176}Lu-^{180}Hf and ^{149}Sm-^{150}Nd spike solution. For each sample batch, standard BCR-1 and a blank were performed to assure that no isotope fractionation has occurred during separation as well as that no contamination came from performing the separation or the resin itself. Subsequent dissolution of the samples was carried out with either a 2:1 HF (24 M) HNO_3 (15 M) solution or a 3:1 HF (24 M) HNO_3 (15 M) acid mixture in closed Savillex® Teflon beakers at 120°C.

After a three day treatment with a 2:1 HF HNO_3 solution, samples were dried down with open lids at 120°C. From here, sample cakes were treated variantly with 6 M HCl and 6 M HNO_3 overnight and then fumed off. HNO_3 was used in order to break down fluorides. After these steps, full dissolution was achieved.

Another fraction of the samples was dissolved in a 3:1 HF HNO_3 acid solution for 24 hours at 120°C in closed Savillex® Teflon beakers. 150 µL of perchloric acid was added in each beaker before the evaporation of the acid mixture at 120°C with the lids removed from the beakers. Perchloric acid was added in order to prevent fluorides to be formed, which was subsequently evaporated at 180°C.

After drying down, the sample cake was redissolved in 3 M HCl, together with 0.1 M ascorbic acid ($C_6H_8O_6$) in order to reduce Fe^{3+} to Fe^{2+} as otherwise the resin in the column might be blocked (Muenker et al., 2001).

Before loading the columns, all samples were centrifuged in order to avoid loading the columns with possible inclusions that were remaining in the dissolved mineral grains.

Chromatographic separation of Lu and Hf followed the procedures of Muenker et al. (2001) using 1 mL Teflon columns, filled with Eichrom® Ln.Spec resin.The zirconium washing step was omitted as the concentrations of Hf in the individual samples were extremely low and a possible loss of Hf would have been crucial to the following measurements with the mass spectrometer. Hf was collected using 2 M HF instead of 6 M HCl with 0.2 M HF as proposed by Muenker et al. (2001).

The matrix collected in the first step was dried down at 120°C for each sample, redissolved in 2 M HCl and loaded on 1.5 mL Teflon columns, filled with Biorad 50Wx8 resin. The separation of LREE from the matrix with 6 M HCl and of Sm and Nd followed the procedures of Pin and Zalduegui (1997) and the separation of Sr with 2.2 M HCl as taken from ((Lazarov, Unpublished results) PhD thesis).

Using exactly the same columns as for the separation of Lu and Hf, Sm and Nd were eluted with 0.75 M HCl and 0.25 M HCl respectively in the Eichrom® Ln.Spec resin.

All elements to be measured with the mass spectrometer were dried down at 120°C and redissolved in 2% HNO_3.

2.4.1. Isotope analyses solution (Lu-Hf, Sm-Nd, Rb-Sr)

After calibration of the machine to highest level of sensitivity of the desired element, samples were measured, using a Thermo-Finnigan® Neptune multicollector ICPMS at the Goethe University in Frankfurt. Ni X cones were used and measurements were perfomed following the procedures of Schmidt et al. (2008). To increase the sensitivity for Lu and Hf measurements, a CETAC Aridus™ nebulization system (ca. 70 µL/min; e.g., Hf, 500-800 $Vppm^{-1}$) was used instead of a conventional glass spray chamber. For Sm-Nd and Rb-Sr, a conventional glass spray chamber was used for the introduction of the sample.

JMC 475, Merck, Ames, Mir a (Rankenburg et al., 2004) and inhouse standards were used for tuning the mass spectrometer and for checking measurement conditions. BCR-1 was measured during each analytical session in order to assure perfect conditions for the previous chromatographic separation.

Mass bias correction was performed with 0.7325 for $^{179}Hf/^{177}Hf$ and 0.7219 for $^{143}Nd/^{144}Nd$ (Blichert-Toft et al., 1997). Interference correction of ^{176}Lu and ^{176}Yb was monitored with a $^{173}Yb/^{171}Yb$ ratio of 1.1248. For samples with very low amounts of Hf, a blank correction was performed.

Data was evaluated using Excel® in-house spreadsheets and subsequent age calculations, using Isoplot 3.7 (Ludwig, 2008).

2.4.2. Isotope analyses laser ablation (U-Pb, Lu-Hf)

After the separation steps, zircons crystals were embedded onto round epoxy holders with a diameter of 1 inch, polished and coated with gold. Cathodoluminescence (CL) images of each grain were necessary as a preliminary work for the subsequent analyses with the mass spectrometer as they reveal the growing patterns of the crystals. Before starting isotope measurements, gold coating was removed and the sample mounts were cleaned with ultrapure Ethanol and low concentration (2 %) ultrapure nitric acid.

U-Pb and Hf analyses for crustal sample material from Spain were performed using a New Wave Research® UP213 ultraviolet Nd-YAG laser with spot sizes varying between 20 and 40 µm and Ni X skimmer and Al sample cones. Zircons from Namibia were analyzed for U-Th-Pb and Hf isotopes with the help of a Resonetics M-50 laser ablation system. Spot sizes hereby varied between 20 to 33 µm with laser energies around 90 to 100 mJ. Before starting the measurement, samples were preablated with three shots of the same laser energy as used for the subsequent measurement in order to remove possible surface contamination. Measurements were performed on a Thermo-Finnigan® Element 2 mass spectrometer that was tuned to maximum signal and low oxidation rate prior to analysis, ablating GJ1 reference standards in line scans.

Independent from the laser used, U-Pb analyses were performed following the procedures as described by Gerdes and Zeh (2006). Laser spots were placed on homogenous growth sections of each zircon crystal with the help of CL images. Standard GJ1 was measured repeatedly before, in between and at the end of each analytical session. Additionally, Plešovice (see Slama et al., 2008) was measured as a secondary external standard to assure ideal machine conditions.

Data was evaluated using Excel® in-house spreadsheets created by A. Gerdes. Concordia diagrams were created, using Isoplot 3.7 (Ludwig, 2008). Age propability-density diagrams were created, using the Excel® spreadsheet of Sircombe (2004).

Hf isotope analyses were performed using the laser systems mentioned before, connected to a Thermo-Finnigan® Neptune multicollector ICP mass spectrometer. Additional laser spots were placed on top of the craters remaining from the U-Pb measurements of the zircons grains. As for the Hf isotope solution measurements, a CETAC Aridus™ nebulization system was used instead of a conventional glass spray chamber for signal enhancement. Standard solution JMC 475 was

used to tune the mass spectrometer to maximum signal yield while standards GJ1 and Plešovice were used as secondary standards.

Analyses followed the procedures as described by Gerdes and Zeh (2006). Evaluation of the raw data was performed using Excel® in-house spreadsheets by A. Gerdes.

2.5. References

Blichert-Toft, J., Chauvel, C. and Albarede, F., 1997. Separation of Hf and Lu for high-precision isotope analysis of rock samples by magnetic sector multiple collector ICP-MS. Contributions to Mineralogy and Petrology, 127(3): 248-260.

Gerdes, A. and Zeh, A., 2006. Combined U–Pb and Hf isotope LA-(MC-)ICP-MS analyses of detrital zircons: Comparison with SHRIMP and new constraints for the provenance and age of an Armorican metasediment in Central Germany. Earth and Planetary Science Letters, 249: 47-61.

Koehler, T.P. and Brey, G.P., 1990. Calcium Exchange between Olivine and Clinopyroxene Calibrated as a Geothermobarometer for Natural Peridotites from 2 to 60 Kb with Applications. Geochimica Et Cosmochimica Acta, 54(9): 2375-2388.

Lazarov, M., Unpublished results. Archean to present day evolution of the lithospheric mantle beneath the Kaapvaal craton – Processes recorded in subcalcic garnets, peridotites and polymict breccia. PhD thesis, Goethe-Univ. Frankfurt, Germany: 213 pp.

Ludwig, K.R., 2008. Isoplot 3.7: A geochronological toolkit for Microsoft Excel. Berkley Geochronology Center, Spec. Pub. No. 4: 1-77.

Muenker, C., Weyer, S., Scherer, E. and Mezger, K., 2001. Separation of High field strength elements (Nb, Ta, Zr, Hf) and Lu from rock samples for MC-ICPMS measurements. Geochemistry Geophysics Geosystems, 2(10.1029/2001GC000183).

Pearce, N.J.G. et al., 1997. A compilation of new and published major and trace element data for NIST SRM 610 and NIST SRM 612 glass reference materials. Geostandards Newsletter - the Journal of Geostandards and Geoanalysis, 21(1): 115-144.

Pin, C. and Zalduegui, J.F.S., 1997. Sequential separation of light rare-earth elements, thorium and uranium by miniaturized extraction chromatography: Application to isotopic analyses of silicate rocks. Analytica Chimica Acta, 339(1-2): 79-89.

Rankenburg, K., Lassiter, J.C. and Brey, G., 2004. Origin of megacrysts in volcanic rocks of the Cameroon volcanic chain - constraints on magma genesis and crustal contamination. Contributions to Mineralogy and Petrology, 147(2): 129-144.

Schmidt, A. et al., 2008. Rapid eclogitisation of the Dabie-Sulu UHP terrane: Constraints from Lu-Hf garnet geochronology. Earth and Planetary Science Letters, 273(1-2): 203-213.

Sircombe, K.N., 2004. AGEDISPLAY: an EXCEL workbook to evaluate and display univariate geochronological data using binned frequency histograms and probability density distributions. Computers & Geosciences, 30(1): 21-31.

Slama, J. et al., 2008. Plesovice zircon - A new natural reference material for U-Pb and Hf isotopic microanalysis. Chemical Geology, 249(1-2): 1-35.

Chapter 3:

The lithospheric mantle underneath the Gibeon Kimberlite field (Namibia): a mix of old and young components - evidence from Lu-Hf and Sm-Nd isotope systematics

T. Luchs*, G. P. Brey, A. Gerdes, H.E.Hoefer

Institut für Geowissenschaften, J.W. Goethe-Universität, Altenhöferallee 1, D-60438 Frankfurt am Main, Germany

Submitted to Precambrian Research 18/04/2012

3.1. Abstract

We have determined major and trace elements and the Sm-Nd and Lu-Hf isotope systematics in minerals of 19 garnet peridotites from the Gibeon Townlands and Hanaus kimberlite pipes. These are situated within the mixed age Proterozoic to Archean (?) Rehoboth crustal province in Namibia. Our geothermobarometric results confirm the similarities of the conductive geothermal gradients underneath the Rehoboth province and the Kaapvaal craton and also that the Rehoboth mantle must have lost a significant proportion of its lithosphere. We distinguish peridotites with sigmoidal REEpatterns similar as they commonly occur in the Archean Kaapvaal subcratonic mantle and peridotites with LREE depleted patterns typical for the Proterozoic. Both types are reenriched restites with a kinship of processes in the sigmoidal (σ) peridotites with the Archean (higher degrees of partial melting, style of reenrichment). Time constraints for these processes can be found from the Sm-Nd and Lu-Hf isotope systems and from published Re-Os data. The Lu-Hf isotope systematics date an enrichment event of a highly depleted mantle (εHf = + 29.4) for the σ-peridotites of around 1.9 Ga ago. Enrichment for the N-peridotites occurred around 850 Ma ago in a slightly depleted mantle (εHf = + 3.3). The last enrichment event at around 458 Ma may be recorded by the Sm-Nd system in the σ-peridotites. published Re-Os isotope data set from the neighbouring Louwrensia pipe yields oldest, probably realistic Archean Rhenium model ages of 2.65 Ga (calculated for a Primitive Upper Mantle model). Archean mantle ages

underneath the Rehoboth crust are in accord with recently published zircon ages between 2.7 and 2.9 Ga from cobbles in tillites and from our own sampling of zircons in the Louwrensia pipe.

3.2. Introduction

Recent comparative work on mantle samples from on- and off-craton localities from Southern Africa (Bell et al., 2003; Janney et al., 2010; Mather et al., 2011) has shown that distinct differences but also strong similarities exist between mantle xenoliths from beneath the Kaapvaal craton and the Proterozoic terranes (for which most information comes from the Gibeon province in Namibia). Differences are expressed i) in higher average forsterite in olivine and lower Al_2O_3 and CaO whole rock concentrations of the Archean mantle indicating higher degrees of depletion, ii) in differing depletion ages with very unradiogenic $^{187}Os/^{188}Os$ indicating extensive melt depletion before 2.5 Ga in the 'Archean' mantle compared to a wider range and higher Os isotope ratios in the 'Proterozoic' mantle. The latter indicate lower degrees of partial melting possibly with incomplete removal of Re from the residue and give Re-depletion ages less than 2.2 Ga [Janney et al. (2010) and earlier work] and iii) in the lithosphere thickness which is thinner underneath the Proterozoic terranes by 30 – 40 km (see also Boyd et al. (2004) and Muller et al. (2009)). Similarities exist a) in the conductive limbs of the geothermal gradients indicating similar lithospheric thicknesses sometime in the past (see also Boyd et al. (2004), Franz et al. (1996a) and Mitchell (1984)), b) with respect to the overabundance of orthopyroxene in the mantle samples [less pronounced in the residual peridotites from Gibeon than from the Kaapvaal craton -see also Boyd et al. (2004) and Franz et al. (1996b), and c) in the existence of garnets with sigmoidal REE patterns. These are common amongst Kaapvaal peridotites but also occur as a minor proportion in the Gibeon (see below) and Rietfontein area [2 out 10 samples in the latter; see Hoal et al. (1994)].

Franz et al. (1996b) suggested that the orthopyroxene enriched peridotites from the Gibeon province represent pieces of the Kaapvaal lithosphere, which were rifted underneath the Rehoboth Terrane in the wake of the Atlantic ocean opening or that the Kaapvaal lithosphere extended underneath the Rehoboth Terrane. Both models were rendered unlikely by (Boyd et al., 2004; Pearson et al., 2004) because the oldest T_{RD} age from peridotites of the Gibeon province is

2.1 Ga. This argument is only valid if Re is completely removed from the residue at very high degrees of partial melting, so that T_{RD} ages date the depletion event. Otherwise, these ages are only minimum ages. Alternatively, depletion ages younger than the Archean may indicate that the thermal regime in a cooling Earth may have been still high enough in the Proterozoic to produce relatively high degrees of partial melting; orthopyroxene enrichment was produced by some process like it occurred in the Archean. These mantle portions were later juxtaposed to or injected by less depleted mantle material. We have set out to clarify these questions by creating and evaluating an extensive major and trace element and Sm-Nd and Lu-Hf isotope data set on minerals from peridotite xenoliths from the Hanaus and Gibeon Townlands kimberlite pipe in Namibia. These could give supplementary answers to the Re-Os isotope data from the neighbouring Louwrensia kimberlite pipe or enable a more comprehensive interpretation of these data. We assume in our approach that clinopyroxene and garnet carry almost the entire incompatible trace element inventory of the rock and that their analysis combined with the mineral proportions gives the bulk rock major, trace and Sm-Nd and Lu-Hf isotope composition.

3.3. Geological setting and previous work

The Gibeon Kimberlite Province is located in Namibia between Keetmanshoop and Mariental on the border of the mid Proterozoic to Archean (?) Rehoboth Terrane to the 0.9 to 1.3 Ga old Namaqua-Natal belt (Fig.3.1). The Rehoboth Terrane is bordered to the east by the Kheis-Magondi belt (1.7 to 2.0 Ga) and then to the Kaapvaal craton. The assembly of these geological units began at about 2.9 Ga with the collision of the two main Kaapvaal Craton building blocks (Schmitz et al., 2004). The Kheis-Maghondi belt accreted along its western border between 1.93 and 1.75 Ga (Tinker et al., 2004), followed by the collision of the Rehoboth Terrane (Jacobs et al., 2008). The Rehoboth Terrane is a mixed age province with a nucleus that is possibly Archean (e.g. Hoal et al., 1995) and with products of major magmatic events from the time between 1.7 and 2.1 Ga and again from 0.9 and 1.3 Ga, the time of the Namaquan orogeny between (taken from summaries by Janney et al. (2010) and Cornell et al. (2011)). The latter authors make a case where the Rehoboth Terrane had an early common history with the Kaapvaal Craton, was separated and reunited at around 1.2 Ga. Magnetotelluric measurements

along a SE-NW profile of southern Africa show that the present day lithosphere underneath the Rehoboth Terrane is significantly thinner than underneath the Kaapvaal Craton (Muller et al., 2009) in agreement with the latest geothermobarometric evaluation in combination with other geophysical constraints by Mather et al. (2011). Maximum depth of the eastern Kimberley block is believed to be approximately 220-250 km, compared to approximately 180 km of the Rehoboth Terrane (Muller et al., 2009). These results also support earlier work by Bell et al. (2003) which suggested a cratonic thermal regime and similar lithospheric thickness across the Proterozoic and Archean southern Africa into the Mesozoic. Thermal erosion then destroyed the lower part of the Rehoboth lithosphere and local thermal disturbances reached to shallower depths in Namibia than underneath the Kaapvaal craton.

The Gibeon Kimberlite field stretches 70 km from East to West and 110 km from North to South (Kurszlaukis et al., 1998). It consists of more than 75 non-diamondiferous kimberlite pipes and carbonatite diatremes. They intruded into sediments of the Kalahari, Karoo and Nama groups which cover the basement. Kimberlite volcanism occurred at around 71.5 Ma (Davies et al., 2001) and was possibly triggered by the drift of the African continent over the Vema plume (Spriggs, 1988). To the present knowledge, the basement is made up of 1.6 – 1.8 Ga proterozoic metamorphic rocks (Hartnady and LeRoex, 1985).

Previous work on the localities Louwrensia, Hanaus, Gibeon Townlands and Anis Kubub by Mitchell (1984), Franz et al. (1996a), Franz et al. (1996b) and Boyd et al. (2004) established the thermal structure underneath the Gibeon Province at the time of kimberlite eruption [Fig. 3.2 modified from Bell et al. (2003)]. This figure shows that the conductive geothermal gradients beneath the Gibeon Province and the Kaapvaal craton coincide, that it stops at shallower depth in Gibeon and that there is a distinct departure of high temperature peridotites in both mantle areas from the main array. This occurs at shallower depth in Gibeon than on the Kaapvaal craton. Franz et al. (1996a), Franz et al. (1996b), Mitchell (1984) and Boyd et al. (2004) all distinguished granular and deformed peridotites. Franz et al. (1996a) and Franz et al. (1996b) distinguished coarse equant peridotites which mostly plot on the conductive geotherm, highly deformed mosaic-porphyroclastic types which mainly belong to the high temperature peridotites and transitional porphyroclastic types. Hoal et al. (1995), Franz et al. (1996a), Franz et al. (1996b) and Boyd et al. (2004) established the orthopyroxene rich nature of a portion of the Gibeon peridotites which is a common feature of Kaapvaal peridotites. In consequence, Hoal et

al. (1995) and Franz et al. (1996b) advocated the idea of an Archean lithospheric component within the Gibeon subcontinental lithosphere and the latter suggested that this may be rifted material from underneath the Kaapvaal craton. Such an idea is not supported by the Re depletion ages from 20 peridotites which range from 0.5 to 2.1 Ga (Hoal et al., 1995; Pearson et al., 2004).

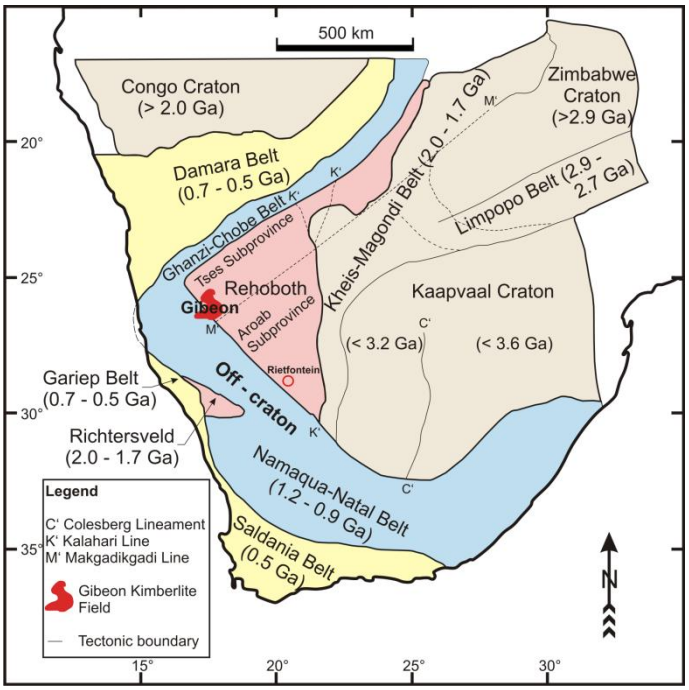

Fig 3.1: The ca. 75 Ma old Gibeon kimberlite field within the framework of major crustal units of Southern Africa (after Hoal et al., 1995; Boyd et al., 2004).

3.4. Materials and Methods

We wanted to unravel the history of the Gibeon subcontinental mantle in more detail and carried out a comprehensive study of major and trace elements and isotope ratios on minerals from variously altered xenoliths from Hanaus and from Gibeon Townlands. They were available to us from own sampling and partly from the collection of Franz et al. (1996b).

Nineteen samples from more than 40 garnet peridotites were selected according to the variation of their clinopyroxene and garnet modal amounts with the aim to obtain the largest possible range in $^{147}Sm/^{144}Nd$ and $^{176}Lu/^{177}Hf$ ratios. All samples are variously altered, but

clinopyroxene and garnet were preserved in all of them and fresh olivine and orthopyroxene could be found in eleven xenoliths. Alteration varied from pervasive with extreme samples where all olivin and orthopyroxene were replaced by SiO_2 and in others by unidentified sheet silicates and carbonates to alteration along cracks and grain boundaries by the same minerals. Structural types were difficult to establish but it could be seen that some of the samples belonged to the coarse granular and others to porphyroclastic types.

The xenolith sizes range from a few centimeters up to 10 cm. Five samples contained only very small amounts of clinopyroxene (KGG 91-20c, KGG 91-37, KGG 91-46, KHA 91-93, SKGGIVc); no clinopyroxene was found in one sample (SKGGIVb) and no garnet in another (SKGGIVd). Samples were prepared for major and trace element analysis either as polished thick sections (150 µm), or as mineral separates which were mounted in epoxy and polished.

Clean garnet and clinopyroxene separates were prepared for isotope analysis. In 14 samples, clinopyroxenes were surrounded by a thin rim (10 – 20 µm) of newly grown, sieve textured clinopyroxene (Table 3.1), probably as a result of reaction with the host kimberlite during ascent [already observed by Franz et al. (1996a)]. Great care was taken to avoid these portions during mineral separation. We achieved this by crushing the bulk samples with a SelFrag® fragmentation system using voltages of 90 - 120 kV and a built in sieve of 1 mm mesh size. In the SelFrag®, minerals are liberated along grain boundaries and fractures. Fresh, solid mineral pieces with grain sizes larger than 1 mm are retained by the sieve. Smaller pieces and the major proportion of the sieve textured clinopyroxene rims fell through the sieve. Only very minor amounts of sieve textured clinopyroxene still adhered to the large pieces which were removed by handpicking after the following procedure: The retained sample portion was dried and light and heavy fractions were separated using bromoform (density c. 2.9 g/cm³). The heavy mineral fraction contained mostly only clinopyroxene and garnet which were quantitatively separated using a Frantz® magnetic separator. Modal proportions of clinopyroxene and garnet were determined by weighing the two fractions and cpx/grt ratios of the bulk rock were calculated. The material left from the SelFrag® sieving and the various separation steps was combined and weighed together. These portions approximate the (former) olivine + orthopyroxene modal contents. The results are given in Table 3.1. The overall error of the modal contents determined this way is taken to be about 10% relative. Modal mineral contents of four samples used in this study have been determined previously by Franz et al. (1996b) by pointcounting of thin sections.

In comparison to our present results and those of Boyd et al. (2004) on samples from Louwrensia, the garnet and cpx abundances seem to be overestimated.

Table 3.1: Modal contents, geothermobarometrical data and Lu-Hf and Sm-Nd isotope characteristics of the analyzed samples.

Sample	Ol+OPX	Grt / (Grt + CPX)	T_{BKN} [°C]	P_{BKN} [Kbar]	$^{176}Lu/^{177}Hf$	$^{176}Hf/^{177}Hf$	$^{147}Sm/^{144}Nd$	$^{143}Nd/^{144}Nd$	Type
Gibeon Townsland									
Gibtown 93 1/1 WR*	0.91	0.59	1069	39.4	0.5356	0.293208	0.1938	0.513042	N
Grt[b]					0.7423	0.296108	0.4582	0.513568	
CPX[b]					0.0030	0.285734	0.0980	0.512851	
Gibtown 93-11 WR[d]*	0.93	0.48	1062	41.3	0.0222	0.282731	0.1357	0.512616	N
Grt[a]					0.0432	0.282837	0.4155	0.512728	
CPX[a]					0.0009	0.282624	0.0985	0.512601	
KGG 91-46 Grt[c,e]	0.93	0.99	1217	40.4	0.0315	0.283624	0.3712	0.512885	σ
SKGG IV WR[d]*		0.52	1076	45.6	0.0834	0.283543	0.2545	0.512585	N
Grt[b]					0.1023	0.283647	0.4856	0.512752	
CPX[a]					0.0015	0.283096	0.1034	0.512477	
SKGG IVa WR*	0.95	0.48	1072	37.7	0.0714	0.283943	0.1914	0.512823	σ
Grt[c]					0.2499	0.286258	0.2933	0.512880	
CPX[a]					0.0012	0.283046	0.1441	0.512797	
SKGG Ivb Grt[c,e]*	0.95	1.00	1081 [2]	32.9	0.1345	0.287136	0.2351	0.512456	σ
SKGG IVd CPX[c]*	0.95	0.00	837	42.7 [1]	0.0011	0.282929	0.0882	0.512604	N
SKGG IVe WR[d]*	0.90	0.54	1031	38.0	0.5458	0.290770	0.1958	0.512834	N
Grt[c]					0.6595	0.291866	0.2737	0.512889	
CPX[c]					0.0046	0.285553	0.0720	0.512746	
KGG 91-20c*	0.83	0.999	1256	42.5	n.d.	n.d.	n.d.	n.d.	N
KGG 91-37*	0.88	0.87 [3]	1167	42.1	n.d.	n.d.	n.d.	n.d.	N
KGG 91-60*	0.70	0.78 [3]	1074	44.0	n.d.	n.d.	n.d.	n.d.	N
KGG 91-62*	0.65	0.62 [3]	1056	42.6	n.d.	n.d.	n.d.	n.d.	N
KGG 91-65*	0.88	0.64 [3]	1020	38.7	n.d.	n.d.	n.d.	n.d.	N
SKGG IVc	0.95	0.90	1252	43.1	n.d.	n.d.	n.d.	n.d.	N
Hanaus									
KHA 91-93 Grt[c,e]*	0.93	0.999	1202	36.6	0.0178	0.282997	0.4067	0.512955	σ
KHA 91-94 WR	0.90	0.51	1074	43.2	0.0341	0.283144	0.1637	0.512646	N
Grt[b]					0.0822	0.283458	0.4872	0.512736	
CPX[b]					0.0008	0.282926	0.1164	0.512633	
KHA 91-100 WR[d]*	0.95	0.61	1090	37.2	0.1161	0.284228	0.3354	0.512820	N
Grt[c]					0.1525	0.284482	0.4537	0.512834	
CPX[c]					0.0010	0.283424	0.1322	0.512795	
HAN 93-20 WR	0.97	0.66	1299	41.5	0.0357	0.284142	0.2437	0.512916	N
Grt[b]					0.0465	0.284509	0.4768	0.513026	
CPX[b]					0.0037	0.283053	0.1536	0.512873	
KHA 91-29	0.81	0.49	805	21.6	n.d.	n.d.	n.d.	n.d.	σ

*sieve textured cpx [1]Nimis and Taylor (2000) [2]Brey and Köhler (1990) [3]from Franz et al. (1996b) [a]batch 1 [b]batch 2 [c]batch 3
[d]WR Isochron type N [e]WR isochron type σ

3.4.1. Major element analysis

Major elements were determined in olivine, orthopyroxene, clinopyroxene and garnet with a Jeol JXA 8900RL Superprobe with five spectrometers in WDS mode with a beam size of 3 µm, an acceleration voltage of 15 KV and a probe current of 20 nA. For each sample and each mineral, three grains were analysed, with three analyses from core to rim to test for homogeneity. Peak measuring times varied between 20 to 30 s, background measuring times were 10 to 30 s. Standards were a mix of natural minerals and pure oxides and metals. CITZAF© algorithm by John T. Armstrong was used for matrix correction.

3.4.2. Trace element analysis

Trace elements were analysed by Laser Ablation Inductively Coupled Plasma Mass Spectrometry (LA-ICPMS) using a New Wave Research® UP213 ultraviolet Nd–YAG laser coupled with a Thermo-Finnigan® Element 2 at the Goethe University of Frankfurt.

Only unaltered and clear grains were considered for trace element analyses. For each sample, three grains of clinopyroxene and garnet were analysed with three laserspots from core to rim.

Analyses were performed with a spot size of 40 µm, an energy density of c. 2 Jcm^{-1} and a frequency of 10 Hz. We used as external standard a Nist 612 glass and CaO from microprobe analyses as an internal standard. Reference values for Nist 612 were taken from Pearce et al. (1997). The data were processed with the Gemoc GLITTER© software. USGS standard Bir-1G was always measured several times during an analytical session as secondary standard to monitor the machine performance and estimate the analytical precision and accuracy of the method. The obtained accuracy and precision for all analysed elements lie in the range of 5 to 10 %.

3.4.3. Isotope analysis

Based on the relative amounts of clinopyroxene and garnet and their trace element abundances and the actual size, twelve samples appeared suitable for isotope analysis.

The garnets and clinopyroxenes were carefully handpicked under the binocular to avoid alterated grains and the little left-over sieved-textured clinopyroxenes removed. They were

subsequently leached for 10 min in 2 M HCl which does not fractionate Hafnium or Neodymium isotopes as demonstrated by previous studies with 6 M HCl (DeWolf et al., 1996; Wittig et al., 2007). After rinsing with Milli-Q® H_2O, samples were re-examined and then cleaned with Milli-Q® H_2O in an ultrasonic bath for at least 1 hour. Each sample was weighed in and spiked with a ^{176}Lu-^{180}Hf and ^{149}Sm-^{150}Nd spike. Chemical separation of the desired elements was performed in three sessions ('batch') with 8 to 12 samples per session, each including one column for a blank and one for standard BCR-1.

One of three sample batches (see Table 3.1 'batch c') was dissolved in 5 mL 3:1 HF (24 M): HNO_3 (15 M) solution in closed Savillex® teflon beakers at 120°C for 24 hours. Before fuming off, 150 µL of 11.6 M perchloric acid was added in order to prevent the formation of fluorides. After evaporation to dryness, the sample cake was re-dissolved in 6 M HCl and placed with the closed lid overnight on the hotplate at 120°C.

Two of the three samples batches (see Table 3.1 'batch a and b') were dissolved by using a 3 mL 2:1 HF (24 M) : HNO_3 (15 M) acid mixture in closed Savillex® teflon beakers for three days on a hot plate at 120°C. Samples were ultrasonicated for 10 minutes in between. After fuming off the acid mixture, 6 M HCl and 6 M HNO_3 was alternatively added, heated overnight (120°C) and then fumed off for cracking down fluorides and achieving full dissolution.

Samples were dried down and taken up in 3 M HCl in which 0.1 M ascorbic acid was added. Ascorbic acid is needed to reduce Fe^{3+} to Fe^{2+}, as Fe^{3+} may block the resin in the column (Muenker et al., 2001). Before loading the columns, each sample was centrifuged in order to remove any possible left over inclusions.

For the separation of Lu and Hf we followed the procedures of Muenker et al. (2001),using Eichrom® Ln.spec resin. The procedures of Muenker et al. (2001), were slightly modified by omitting the zirconium washing step and by using 2 M HF instead of 6 M HCl with 0.2 M HF for collecting Hf. Washing out the zirconium would result in a partial loss of Hf, which is not desirable considering the very low amounts of Hf down to 3 ng.

Following the procedures of Pin and Zalduegui (1997), light rare earth elements (LREE) were separated from the dissolved sample using Biorad 50Wx8 resin, while the separation of Sm and Nd were performed in Ln.Spec resin, using the same columns and digestion batch that were used for the Lu and Hf separation.

Because of the small amounts of samples, column sizes were reduced from conventional sizes to 1 mL resin volume for Ln.Spec columns and 1.5 mL in case of Biorad 50Wx8 columns.

Samples were measured using a Thermo-Finnigan® Neptune MC-ICPMS at the Goethe University Frankfurt with Ni x cones following the method described in Schmidt et al. (2008). In case of Lu and Hf isotope measurements a CETAC Aridus™ nebulization system (ca. 70 µL/min) was used to enhance sensitivity (e.g., Hf, 500-800 $Vppm^{-1}$). A conventional glass spray chamber was used as sample introduction system for Sm and Nd. Procedural blanks were generally below 25 pg for Hf, below 10 pg for Lu, below 35 pg for Nd, and around 15 pg for Sm. Mass bias was corrected using of 0.7325 for the $^{179}Hf/^{177}Hf$ and 0.7219 for $^{143}Nd/^{144}Nd$ (Blichert-Toft et al., 1997). The mass bias for Yb was monitored with $^{173}Yb/^{171}Yb = 1.1248$ and used for interference correction of ^{176}Lu and ^{176}Yb on mass 176. Blank correction was performed for samples that contained very low amounts of Hf.

JMC 475, Merck and Ames standards were measured during the analytical sessions to assure high quality isotope measurements of Hf and Nd isotopes. The comparison with published reference values (Blichert-Toft et al., 1997; Caro et al., 2006) shows that this was achieved since we obtained isotope ratios of 0.282149 ± 0.000016 for $^{176}Hf/^{177}Hf$ and 0.51173 ± 0.000021 for $^{143}Nd/^{144}Nd$ (Merck) and 0.51194 ± 0.000011 for $^{143}Nd/^{144}Nd$ (Ames).

Measurements of the standard BCR-1 yielded isotope ratios of 0.282865 ± 0.000017 for $^{176}Hf/^{177}Hf$ and 0.512627 ± 0.000021 for $^{143}Nd/^{144}Nd$. The measured ratios are in a good agreement with published data for Hf (see compilation Chu et al. (2002)) and Nd (see compilation Yang et al. (2010)). The data were processed using in-house Excel® spreadsheets. Age calculations, following isotope ratio calculations were performed using Isoplot 3.7 (Ludwig, 2008).

For single mineral analyses, errors for isotope ratios are based on an error propagation including the uncertainty of the spike calibration and the deviation from the reference value of the corresponding standard. For $^{176}Lu/^{177}Hf$, errors are in average around 0.8 % (1 sigma) and for $^{176}Hf/^{177}Hf$ around 0.003 % (1 sigma). $^{147}Sm/^{144}Nd$ ratios have an average error of around 0.2 % (1 sigma) and around 0.002 % for $^{143}Nd/^{144}Nd$ (1 sigma).

For whole rock analyses, the error increases up to several percent for $^{176}Lu/^{177}Hf$ and $^{147}Sm/^{144}Nd$ and for $^{176}Hf/^{177}Hf$ and $^{143}Nd/^{144}Nd$ up to 0.028 % 0.0027 % (1 sigma) respectivly,

depending on the isotopic characteristics and modal abundance of clinopyroxene and garnet of the individual sample.

3.5. Results

3.5.1. Major elements

Our new mineral data from Hanaus and Gibeon Townlands (representative analyses selected for thermobarometry are given in Table A3.1) lie within the compositional spread of previous work as summarized by Janney et al. (2010). This means e.g. that all garnets plot in a CaO-Cr_2O_3 diagram in the lherzolite field. Our garnets have 2 to 6 wt% Cr_2O_3 except for one which contains 9 wt % Cr_2O_3. Forsterite contents in olivine (fresh remnants in only 11 samples) range from 90 to 93 with a peak between 91 and 92. This is identical with the compositional range and peak as derived by Janney et al. (2010) for a much larger data set for the Gibeon field and other off-craton occurrences. It contrasts with a peak between 92 and 93 for the Kaapvaal craton which reflect a higher average degree of depletion there. It is important to note that those olivines coexisting with garnets with sigmoidal shaped REE patterns (see below) are Fo-richer and closer to olivines from the Kaapvaal craton. All minerals are generally unzoned except very near to the rims as described for a restricted number of samples by Franz et al. (1996b).

3.5.1.1. Geothermobarometry

Pressures and temperatures of equilibration were calculated with T_{BKN} and P_{BKN} of (Brey and Koehler, 1990) to be directly comparable with previous work, but the use of the thermobarometer versions recommended by Nimis and Grutter (2010) would not change the results to any significance. These are given in Table 3.1 and shown in Fig.3.2 (modified from Bell et al. (2003)) as blue (LREE depleted patterns in garnets) and red symbols (sigmoidal REE patterns –see below). They coincide with the PT-fields of coarse equant, porphyroblastic and highly deformed mosaic-porphyroclastic peridotites of the Gibeon kimberlite field. One sample

(KHA 91-29) yields 805°C at 21.6 kbar. All other samples plot either along a conductive geotherm or to higher temperatures at similar pressures.

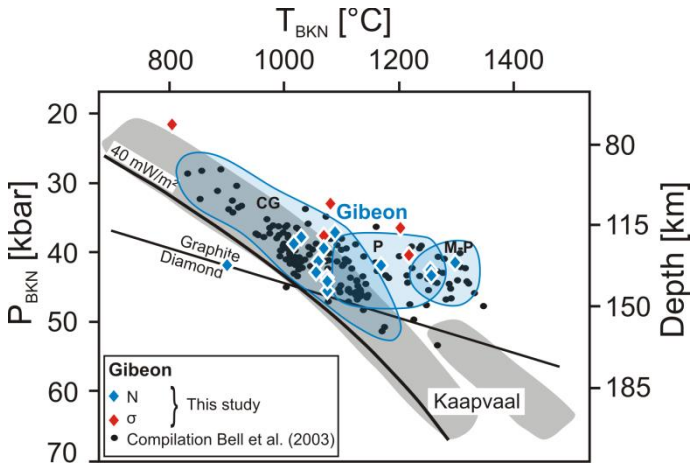

Fig.3.2: The thermal structure of the lithospheric mantle underneath Gibeon and the Kaapvaal craton (grey fields) after a compilation of mantle P/T conditions by Bell et al. (2003). Our new data for the Gibeon Townsland and Hanaus kimberlite pipes are shown as blue and red diamonds. Light blue shaded fields and abbreviations are textural classifications from Franz et al. (1996b): CG = Coarse Granular, P = Porphyroclastic, M-P = Mosaic-Porphyroclastic.

3.5.2. Trace elements

3.5.2.1. REE and extended trace element patterns in garnets and clinopyroxenes

Averaged trace element contents of garnets and clinopyroxenes for the nineteen analyzed samples are given in Table A3.2 and shown as chondrite normalized REE patterns (McDonough and Sun, 1995) in Fig.3.3 a-b. Two peridotite types can be distinguished from the REE patterns: 13 samples with normal, flat HREE garnet patterns (described furtheron as N-type – Fig.3.3a) and 5 samples with sigmoidal garnet REE patterns (type 'σ' – Fig.3.3b).

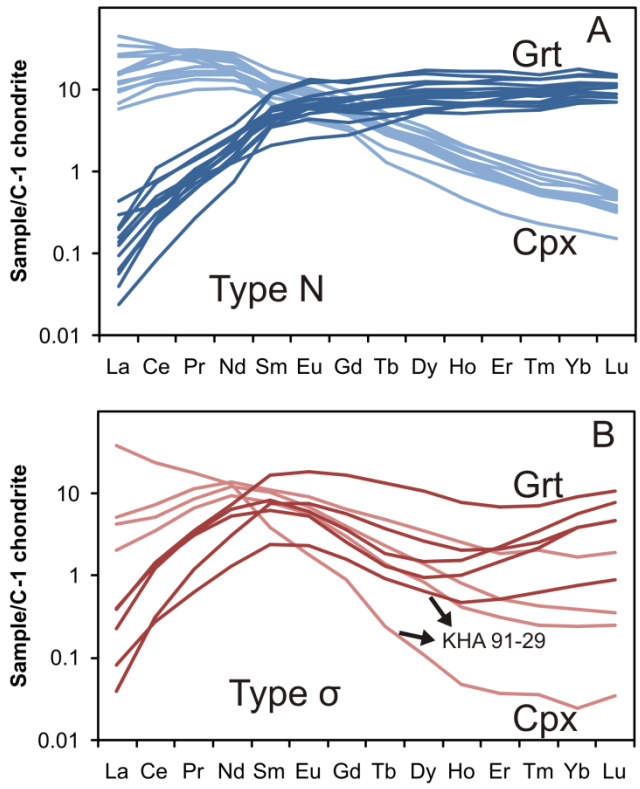

Fig.3.3: Averaged REE patterns of garnets and clinopyroxenes from peridotites from the Hanaus and Gibeon Townsland kimberlite pipes normalized to C1 (McDonough and Sun, 1995). Coexisting garnets and clinopyroxenes for samples with LREE depleted garnet patterns (type N) are shown in A as blue lines and for samples with sigmoidal garnet patterns (type σ) in B as reddish lines.

The clinopyroxenes have supplementary patterns to the garnets. Only sample SKGGIVa is different to all other samples with a sigmoidal garnet and a normal clinopyroxene REE pattern (Fig.3.3) which do not correspond to equilibrium partitioning (Fig.3.4).

The REE patterns of both N- and σ-type garnets and clinopyroxenes are composites of at least two components: i) The garnets of the N-peridotites have flat $(HREE)_N$ patterns and variable contents but the LREE of each sample are elevated relative to a smooth decrease to La as dictated by the ionic radii. ii) The σ-type peridotites have fractionated $(HREE)_N$ patterns and variable contents and the LREE and most MREE are elevated and bow-shaped compared to the HREE. Normalization of minerals to primitive chondrite only serves the purpose to visualize analytical results. Instead, we normalized in Fig. 3.5a and 3.5b the REE, Y, Sr and the LILE of garnets resp. clinopyroxenes to those from garnet peridotite 313-105 from, Vitim (Siberia; (Ionov et al., 2005)).

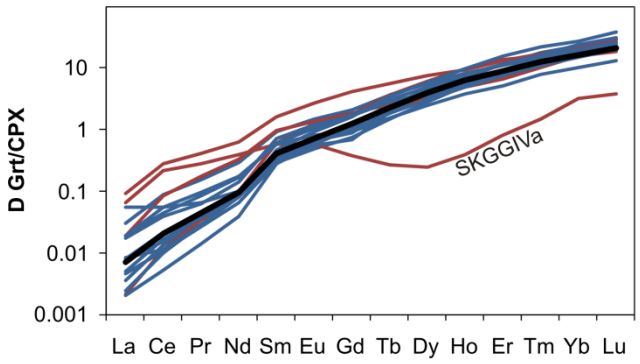

Fig.3.4: Garnet/clinopyroxene partition coefficients for N-peridotites (blue) and σ-peridotites (red) compared to the primitive peridotite from Vitim, Siberia (black line; (Ionov et al., 2005)). All samples are in inter mineral equilibrium except for sample SKGGIVa which is not considered any further.

This peridotite is very close to a primitive mantle composition and the garnet and clinopyroxene REE patterns correspond to those of an undepleted mantle (strictly speaking only to those at the P, T-conditions of this sample which are 21 kbar and 1034°C). The normalization of the Gibeon garnets and clinopyroxenes to those from Vitim show relative changes caused by depletion and reenrichment (Fig.3.5a,b). All HREE of our samples are lower than one; the blue band resp. the red band gives the range and a visual estimate of a smooth decrease according the ionic radii and the arrows visualize the degree of overabundance of the more incompatible elements.

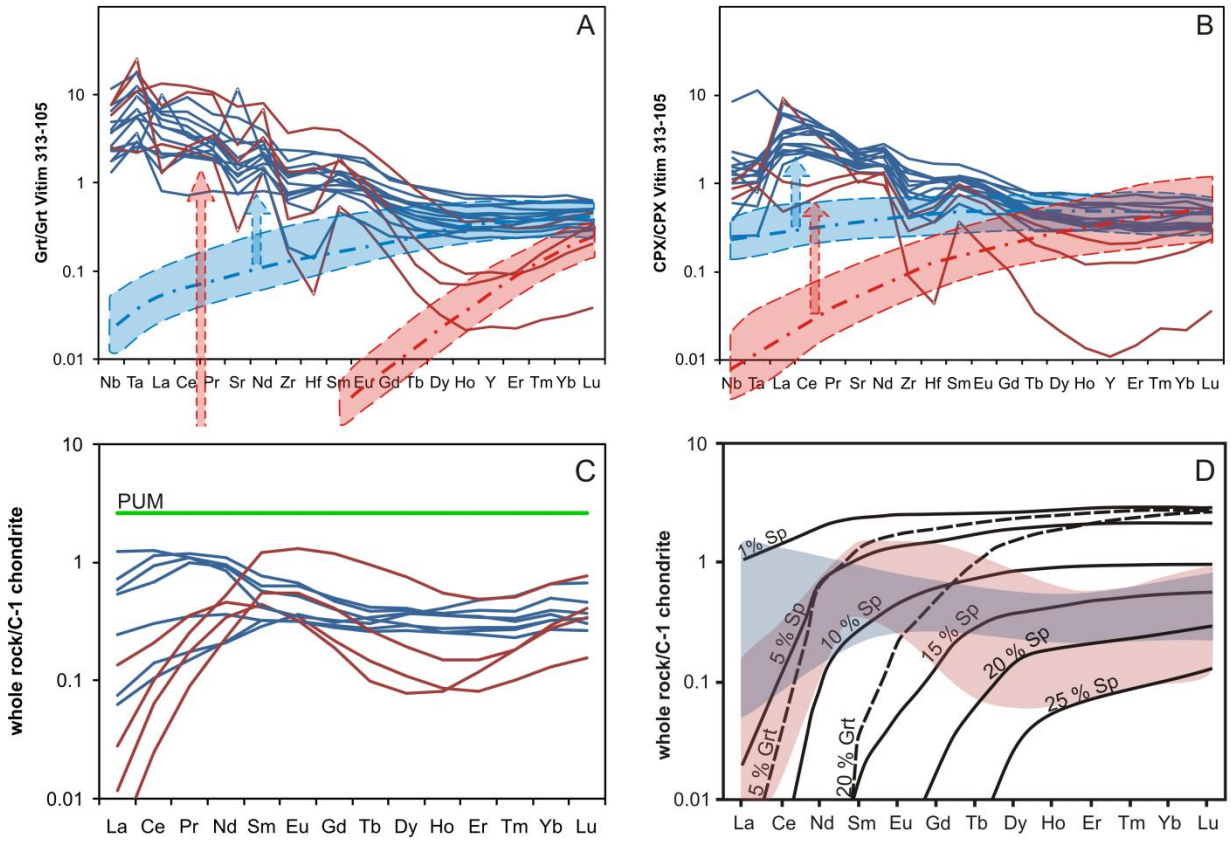

Fig.3.5: A and B: Extended trace element patterns of garnets and clinopyroxenes normalized to Vitim 313-105 garnet and clinopyroxene (Ionov et al, 2005). This sample is taken as a measure for the primitive Earth. A coincidence at one would indicate no change; deviation of incompatible elements to lower values indicate partial melting and to higher values reenrichment. HREE are lower than one and the blue (N) and red (σ) fields are estimates of the shape of the trace element patterns after partial melting. The blue and red arrows indicate subsequent enrichment. C: Calculated REE whole rock compositions based on the relative proportions of garnet and clinopyroxene and the combined modal amounts of olivine + orthopyroxene. PUM = Primitive upper mantle (McDonough and Sun, 1995). D: Non modal fractional melting curves (taken from Lazarov (unpublished results; PhD Thesis)) for the spinel (green) and the garnet stability field (red) in comparison to the calculated bulk rock compositions. These are indicated by the red and blue shaded areas.

3.5.2.2. Calculated REE bulk rock compositions

Another way to visualize depletion and enrichment effects is to calculate whole rock compositions from the modal amounts of the minerals and their composition and compare them

with the primitive mantle. Whole rock REE patterns were calculated based on the relative amounts of clinopyroxene and garnet and the amounts of olivine + orthopyroxene (see above under Materials and Methods and Table 3.1). Olivine and orthopyroxene were assumed to contain no REE.

3.5.2.3. Trace element partitioning between garnet and clinopyroxene

In the sample set from Hanaus and Gibeon Townlands we distinguish N-type peridotites with flat $(HREE)_N$ and σ-type peridotites with fractionated $(HREE)_N$. Despite the very different trace element patterns the garnet-clinopyroxene element partitioning must fulfill inter-mineral equilibrium criteria at the high mantle temperatures, if there was no selective disturbance of a mineral shortly before eruption through the kimberlite. This means that partition coefficients must be the same for the same P, T conditions and major element composition and must show systematic shifts with differing pressure, temperature and compositional parameters. Most of our N samples stem from PT-conditions between 35 to 45 kbar and 1000 – 1100°C and half of the σ types from similar pressures, but temperatures between 1200 – 1250°C. Fig.3.4 shows that the REE partitioning between garnet and clinopyroxene is very similar for the HREE for all samples but that the LREE partition coefficients are higher for the σ samples and lower for the N samples. Sample SKGGIVa is very different to all other samples and garnet and clinopyroxene apparently are in disequilibrium. Also shown in Fig.3.4 is the REE partitioning for the Vitim peridotite 313-105 which overlaps with the HREE partitioning and the lower range of the LREE. This sample equilibrated at 21 kbar and 1034°C. Its REE partitioning agrees with the experimental results of (Green et al., 2000) at similar P,T-conditions. A whole range of further trace elements were analyzed in this sample (Ionov et al., 2005) which enables us to test more elements for equilibrium (Fig.3.6). We normalized the garnet-clinopyroxene partition coefficients of Nb, Ta, Sr, Zr, Hf, Y and the REE from our samples to those of Vitim 313-105. The normalized partition coefficients of the HREE and Y plot at around one which is consistent with a temperature independent partitioning behaviour. The middle and light REE and Sr split into a fan whereby $D^{grt/cpx}_{sample}/^{grt/cpx}_{Vitim}$ for La are below 1 for the lower temperature xenoliths and up to 10x for the higher temperature xenoliths. Zr and Hf show a similar range of temperature dependency whereas Nb and Ta range between about 2 and 15. All but one of the

investigated samples from Hanaus and Gibeon Townlands appear to be in internal mineral equilibria - an important prerequisite for the study of the Sm-Nd and Lu-Hf isotope systems of garnet and clinopyroxene.

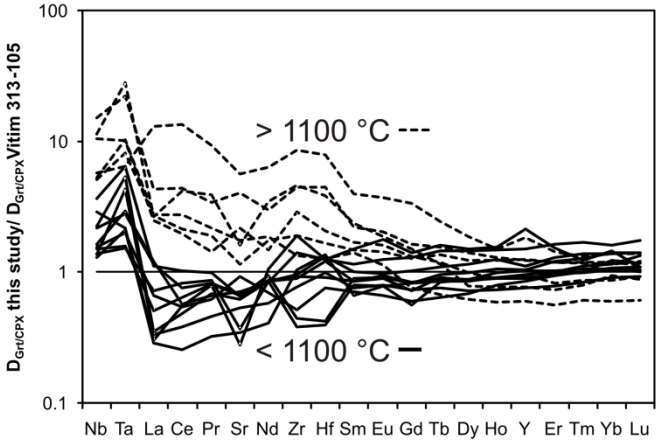

Fig.3.6: Garnet/clinopyroxene partition coefficients of our samples normalized to the partition coefficients of a primitive garnet peridotite 313-105 from Vitim, Siberia (Ionov et al., 2005). This sample was equilibrated at 2.1 GPa and 1034°C. Pressures of our samples are higher on average by about 2 GPa whereas temperatures are very similar for most of the samples. The partition coefficients plot at around one for the HREE whereas the more incompatible elements increasingly deviate to greater values for the higher temperature peridotites. Nb and Ta seem to be systematically offset.

3.5.3. Isotopic composition

3.5.3.1. Lutetium-Hafnium

The results for Lu-Hf isotope system of all samples are given in Table 3.1 and shown in Fig. 3.7a for the N samples. Coexisting garnets and clinopyroxenes are connected by tie-lines whose slopes yield ages ranging from 268 to 746 Ma. These ages are from samples with equilibration temperatures of around 1050°C, a temperature which may be below the closure temperature of the Lu-Hf system. One sample with an equilibration temperature of around 1300°C and which is in apparent mineral equilibrium gives a tie-line age of 1791 Ma (HAN 93-20). In the three samples with sigmoidal REE patterns the modal amount of clinopyroxene was too low (< 0.1%) and the sample size too small to obtain sufficient clean clinopyroxene separates and isotopes

could be measured only in garnet. One sample (SKGGIVa) contained sufficient clinopyroxene but is out of internal mineral equilibrium (see above) and is not considered any further.

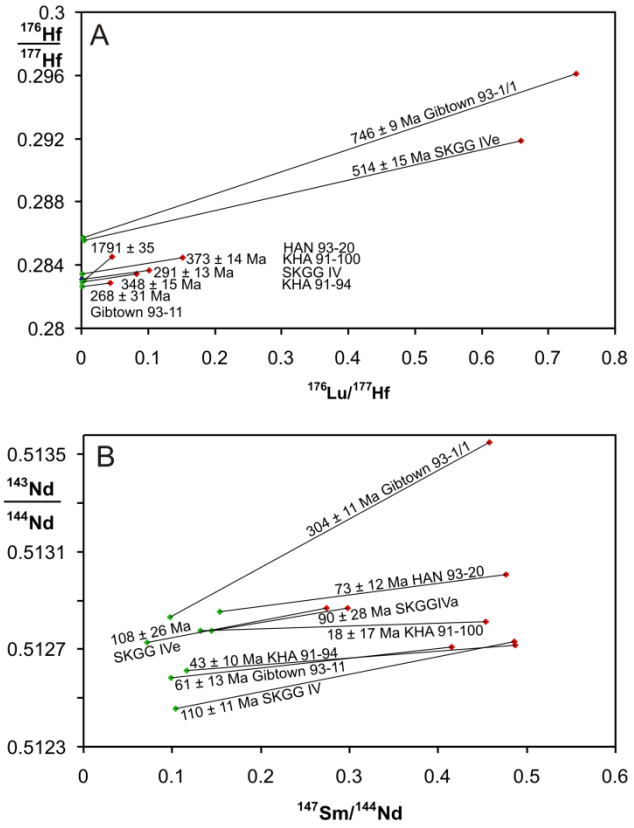

Fig.3.7: A and B: Lu-Hf and Sm-Nd tie line ages for clinopyroxene (green diamonds) and garnet (red diamond) pairs. The ages range from 746 to 268 Ma for the Lu-Hf system (except for one very much 'older' sample) and are similar to the kimberlite eruption age (except one) for the Sm-Nd system. Almost all samples stem from temperatures between 1050 and 1100°C. This temperature range seems to be below the closure temperature for Lu-Hf and above for Sm-Nd, i.e. this isotope system was in inter mineral equilibrium until the time of eruption.

Based on the relative proportions of garnet and clinopyroxene, whole rock $^{176}Lu/^{177}Hf$ and $^{176}Hf/^{177}Hf$ ratios were calculated for group N samples and plotted in an isochron diagram (Fig.3.8a). The error bars are a combination of the errors from the isotope and trace element measurements and the determination of the relative modal amounts of clinopyroxene and garnet. Four samples yield an age of 810 ± 51 Ma with an initial of 0.282365 (εHf_{CHUR} = + 3.3) and MWSD = 2.8. This is a minimum age because the possible effect of orthopyroxene. Lu and Hf

contents in orthopyroxenes are low and their ratio is about ¼ of that of coexisting garnet (judging from our previous work on peridotites from the Finsch diamond mine (Lazarov, Unpublished results; PhD Thesis). $^{176}Lu/^{177}Hf$ is therefore somewhat lower than that of the calculated bulk rocks. The 'real bulk' $^{176}Lu/^{177}Hf$ would be lower maximal by 5 % and $^{176}Hf/^{177}Hf$ by 0.5‰. This would add 38 Ma to the above number.

The three σ garnets yield an age of 1852 Ma ± 100 Ma and an initial of 0.28243 (εHf_{CHUR} = + 29.4) and MWSD = 3.1. The isotopic composition of clinopyroxene could not be measured and we estimate from its trace element composition and its abundance of less than 0.01 % that it will reduce the age by about 2 Ma at the most. The neglected orthopyroxene would add a maximum of 86 Ma to the age.

3.5.3.2. Samarium-Neodymium

The results for Sm-Nd of all samples are given in Table 3.1 and shown in Fig. 3.7b for the N samples. Coexisting garnets and clinopyroxenes are connected by tie-lines whose slopes yield ages from 18 to 110 Ma (one exception lies at 304 Ma) roughly around the eruption age of about 71.5 (Davies et al., 2001) Ma assumed for the kimberlite field. The Sm-Nd system was in inter mineral isotopic equilibrium up to the time of eruption in most samples. Temperatures of around 1050°C appear to be above the closure temperature for the Sm-Nd isotopic system in peridotites. Since only garnets could be measured from the σ samples, their isotope ratios are representative for the bulk rock. The results for the garnets are shown in Fig. 3.8b together with the whole rock isotopic compositions of the N samples. No correlation is discernible in the whole data set. The peridotites are a complex product of partial melting and metasomatic overprint which affects the LREE most strongly. The Sm and Nd isotope ratios for the N-type peridotites are a mixed signal which cannot be resolved. The three σ garnets yield an age of 458 ± 32 Ma which may be a realistic age because metasomatism probably did overprint Sm and Nd completely because of the low contents after high degrees of partial melting (see below).

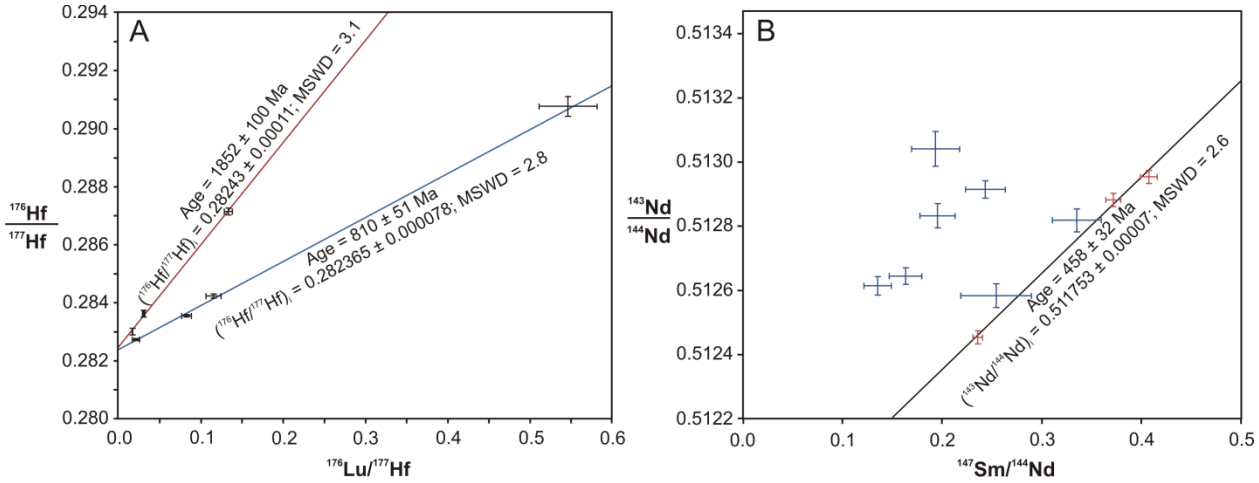

Fig.3.8: A: Calculated whole rock isochrons for the Lu-Hf system. This system yields an isochron age of 810 Ma for the N-peridotites and 1852 Ma for the σ-peridotites. Both isochrons are interpreted as enrichment ages because Hafnium was reintroduced into these mantle portions (compare Fig.3.5). B: The Sm-Nd isotope system yields a scatter for the N peridotites because of (mulitiple?) reenrichment processes which affected mostly the LREE. The correlation of the σ-peridotites may represent a further enrichment at around 458 Ma.

3.6. Discussion

We have established the Hanaus and Gibeon Townlands xenoliths as a diverse suite of depleted and reenriched peridotites which can be divided into two groups σ and N by their garnet REE patterns. A twofold division is also expressed in their modal mineral abundances (type σ have lower clinopyroxene contens), their major element composition (e.g. higher forsterite on average in σ-olivines) and in the Lu-Hf isotope systematics (type σ give a Lu-Hf age of 1852 Ma with εHf_{CHUR} = + 29.4 and type N an age of 810 Ma with εHf_{CHUR} = + 3.3). These differences are expressions of different melting regimes and of partial melting and reenrichment at different times.

Depletion and enrichment compared to a primitive Earth's mantle is visualized in Fig.3.5, where we normalize the HREE and the more incompatible trace elements of garnets and clinopyroxenes to those of the primitive Vitim sample 313-305. The blue and red bands indicate the hypothetical range of the more incompatible trace elements for the N- resp. σ-type peridotites as dictated for the HREE abundances for partial melting. The measured trace

elements are substantially higher and the red and blue arrows indicate the respective enrichments. This metasomatic 'overabundance' is seemingly higher in the σ than in the N peridotites. However, modal abundances of garnet and clinopyroxene are lower in σ than in N peridotites and the same amount of metasomatic agent affects the former much more than the latter. Nevertheless, the Sm and Nd contents of the σ minerals were very low after depletion and their present abundances must stem mostly from the metasomatic agent. The Sm-Nd system therefore provides age information on the timing of metasomatism of the σ□-peridotites (Fig.3.5a). The Sm-Nd contents of the N samples are a mix of residual and reintroduced components and their isotope systematics give a mixed signal. It can also be seen in this figure that Hf and Zr are elevated compared to a hypothetical residual peridotite and that they are reintroduced as well. It follows that the Lu-Hf Isochrons found for the N- and σ-type peridotites (Fig.3.8) also date enrichment events.

Measures of depletion and indicators of the melting regime in residual peridotites are HREE abundances, HREE fractionation and Cr-Al_2O_3 and Y-Al_2O_3 whole rock relationships. In the following, we use the HREE as the unmodified composition of the residual peridotites since the time of last partial melting. Their contents and relative abundances allow us to estimate degrees of partial melting and judge whether partial melting has occurred in either the spinel or garnet peridotite field or both. Fig. 3.5c shows the calculated REE patterns of the samples from Gibeon, for which modal data are given in Table 3.1 and Fig.3.5d shows the results for non-modal fractional melting calculations in the spinel and garnet stability field. The qualitative comparison of the range of M- to HREE abundances in the N peridotites indicates 15 to 20 % of partial melting in the spinel peridotite field. The σ-type peridotites appear to be the products of 15 – 25 % partial melting as judged from the HREE abundances. This is combined with mild to strong HREE fractionation. These two features together indicate partial melting in the spinel and garnet stability field. Our interpretation is that these peridotites suffered successive melting first at low pressures, followed by subduction and subsequent melting in the garnet stability field. Boyd et al. (2004) had used the Y-Al_2O_3 relationship to suggest that partial melting occurred at pressures less than 3 GPa for the xenolith suite from the neighbouring Louwrensia kimberlite pipe.

The timing of enrichment

The Sm-Nd isotope system a priori has the highest potential to date enrichment processes in the mantle. These two light rare earth elements are readily affected by the fractionated, LREE rich mantle metasomatic agents while the HREE and Hf will see the impact only at high to very high degrees of overprint. A clear enrichment age signal can be expected for Sm-Nd when the original peridotite was strongly depleted and when there is only one metasomatic overprint. This could be the case for the σ peridotites for which we obtained about 460 Ga as a possible enrichment age. The Lu-Hf system should then yield the same age. Yet we obtained ~1.9 Ga as an enrichment age. This difference could be reconciled if a first enrichment at 1.9 Ga was caused by an agent with a relatively flat REE pattern like a silicate melt and the second by a silicocarbonatitic or kimberlitic melt which did not affect Hf anymore. The age of 1.9 Ga lies in the middle of the 1.7 – 2.1 Ga crust forming period known from the Rehoboth province (e.g. Cornell et al. (2011)) and is older than the presently presumed basement age of 1.6 – 1.8 Ga (Hartnady and LeRoex, 1985). A 460 Ma enrichment may be connected with the accretion of the Damara orogen. The N-type peridotites gave an enrichment age of 810 Ma which may herald the final stages of the Namaqua orogeny. Both Lu-Hf isochrones have high, positive εHf initials which shows that Hf was reintroduced into an already depleted mantle. The εHf is substantially higher for the σ-type (+ 30) than for the N-type peridotites (+ 3). These differences further demonstrate, that the former are residues from higher degrees of partial melting (which partly occurred in the garnet stability field) than the N-type peridotites, that first melting of the σ-peridotites occurred before and for the N-peridotites later than 1.9 Ga.

Timing of partial melting

We could not find direct evidence from both isotopic systems for the timing of the first melting event(s) of these different mantle portions. The high εHf of the σ-peridotites requires that depletion occurred either shortly before 1.9 Ga for high Lu/Hf in the residue or earlier for low Lu/Hf ratios. Model calculations show that melting should have occurred at around 2.3 Ga for 20 % non-modal batch melting in the spinel stability field and at around 2.8 Ga for 10 %. Twenty percent non-modal fractional melting reduces the time span between partial melting and

reenrichment to less than 100 Ma for melting either in the spinel or garnet stability field. This range is extended to 2.5 Ga for 10 % melting in the spinel field but remains short for melting in the garnet field. The low positive εHf for the N-peridotites requires that partial melting occurred only several hundred million years before 810 Ga.

The Re-Os isotopic system has the greatest potential to date partial melting events in a peridotitc mantle. However, statistically significant isochrons have not been reported so far, because the isotopic system, and especially Re, can be altered subsequent to an event in various ways (see summary article by Rudnick and Walker (2009)). Model ages (Re model ages T_{MA} and Re depletion ages T_{RD}) as intersections with a model mantle evolution curve are in use instead, whereby T_{RD} comes close or corresponds to the true age of melt extraction for very high degrees of partial melting (Walker et al., 1989). If an isochron exists, the T_{MA}'s of each point along the isochron is identical with the isochron age, provided that a primitive mantle is melted and that the chosen Re-Os mantle evolution line is correct. Rhenium-Os isotope data are reported by Pearson et al. (2004) for 21 peridotites from Louwrensia in the Gibeon province and the platin group element (PGE) contents in six of them. The textural types, the occurrence of samples with normal and enhanced modal orthopyroxene contents and the range of calculated pressures and temperatures are very similar for xenoliths from the three localities Louwrensia, Hanaus and Gibeon Townlands (compare Boyd et al. (2004) and Franz et al. (1996b)). The Re-Os data from Louwrensia may therefore be representative for the Gibeon province. They are reproduced in Fig. 3.9 together with the six PGE patterns analyzed from there. Oldest Re depletion ages from Louwrensia (calculated for a chondritic Earth model; (Walker et al., 1989)) are 2.1 Ga, 2.0 ,1.98 and 1.94 Ga. These ages increase by about 200 Ma for the Primitive Upper Mantle (PUM) model of Meisel et al. (2001). Model ages (T_{MA}) calculated with PUM reach 2.65 Ga (Fig. 9, ignoring the 2.83 Ga from a Re-enriched sample). The PGE pattern of the 2.65 Ga and this age approaches the real age of partial melting. Discarding the two data points with the kinky PGE patterns on the left side of the diagram, six points form a limiting line with a slope corresponding to an age of 2.9 Ga. Four of these data points are highly colinear and give an age of 2885 ± 51 Ma, with $^{187}Os/^{188}Os_{initial}$ of 0.10984 ± 0.00014 and a MWSD = 0.16. The initial is slightly higher than the value for a chondritic Earth model ($\gamma Os = 2.44$) and less so for the PUM model of Meisel et al. (2001) ($\gamma Os = 1.21$) and T_{MA}'s slightly decrease from 2.67 to 2.49 Ga along this line. These results from the model calculations do not prove the reality of this isochron. PGE's

are measured only from one of the samples (see above). A proof for the reality of the isochron would be, if the other samples also showed that Re was not reintroduced. In that case partial melting occurred already in the Archean and would overlap with partial melting of the Kaapvaal subcratonic mantle.

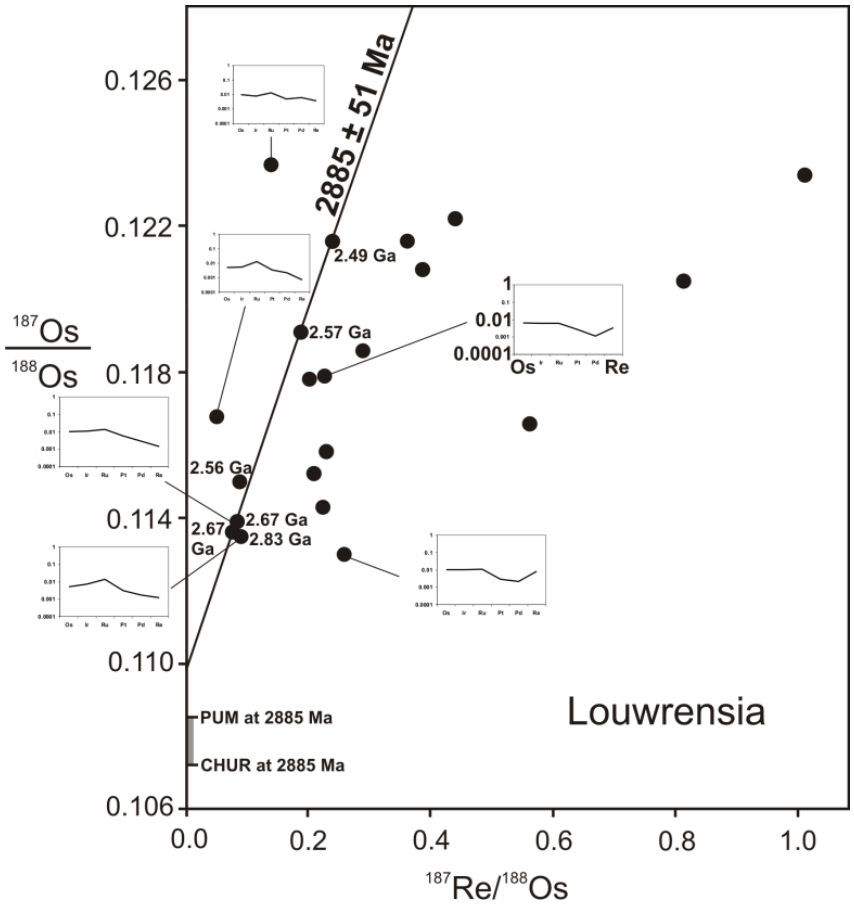

Fig.3.9: A tentative reinterpretation of the Re-Os data by Pearson et al. (2004) from Louwrensia. Oldest T_{MA} ages (PUM model) of 2.67 Ga indicate late Archean melting. A line through samples with a restricted range of Re model ages between 2.67 and 2.49 Ga gives an age of 2885 Ma. This isochron may be real because its initial is close to that of a primitive mantle at that time. It may record partial melting in the Archean.

Melting in the Archean within the circum cratonic mantle is supported by ten T_{RD} ages between 2.4 and 2.6 Ga (chondritic Earth model) resp. 2.6 to 2.8 Ga (PUM model) in other off-craton areas in southern Africa (Janney et al., 2010). Further support for an Archean component in the Rehoboth province comes from recent work by Cornell et al. (2011) who report zircon

ages between 2.7 and 2.9 Ga from trondhjemitic cobbles in Dwyka tillites of the Rietfontein area, which they consider as samples of the directly underlying crust. Furthermore, Van Schijndel et al. (2011) found detrital zircons in the Rehoboth Basement Inlier with ages between 2.7 and 2.9 Ga. We found 4 zircon grains with ages between 2.7 and 2.9 Ga (see Chapter 4) in a zircon separate from the Louwrensia kimberlite pipe.

3.7. Conclusions

Our new geochemical data, the age constraints from the Sm-Nd and Lu-Hf systems, the reinterpretation of the Re-Os system, age constraints from crustal rocks and the results from geothermobarometry and magnetotellurics (Muller et al., 2009) lead us to depict the following sequence of events in the assembly of the geological units of southern Africa:

The major part of the Kaapvaal craton assembled at about 2.9 Ga ago by the collision of East block and the West block along the Colesberg lineament (Schmitz et al., 2004). Oldest recorded T_{RD} and crustal ages from the W-block are around 3.1 Ga (Carlson and Moore, 2004; Schmitz et al., 2004) and from the E-block 3.2 resp. 3.6 Ga (Kroner et al., 1996; Carlson and Moore, 2004). T_{RD} ages have a maximum at around 2.88 Ga for both the E- and the W-block. Lu-Hf-ages for mantle samples from Finsch on the W-block give about 2.6 Ga. (Lazarov et al., 2009). The youngest major Archean crustal event on the Kaapvaal craton is represented by the 2.7 Ga old Ventersdoorp lavas.

At the time of collision of the Kaapvaal E- and W-blocks at 2.9 Ga the first mantle segments of the lithospheric mantle of the Rehoboth Terrane were created by partial melting at relatively shallow levels in the spinel stability field. Segments of the Rehoboth crust (probably independent of the Kaapvaal craton) existed at that time and residual spinel peridotite was placed underneath this crust by subduction or a similar process to be transformed into garnet peridotite. These are parallels to the generation of the Kaapvaal mantle as envisaged by a number of authors (e.g. Pearson and Nowell, 2002). The principal difference is the lower degree of partial melting on average. Attachment of the Rehoboth Terrane occurred somewhere around 2 Ga which is about the time of reenrichment at 1.9 Ga recorded in the σ-peridotites. Reenrichment may have occurred in a mantle wedge setting, may simoultaneously have triggered second stage partial melting and may have been ultimately responsible for magmatic activity in the overlying crust.

Ages of 1.7 to 2.1 Ga are reported in the overlying crust in the Aroab Subprovince and in granite boulders in the Dwyka tillites (Blignault et al., 1974; Hoal et al., 1995; Cornell et al., 2011).

The N-type peridotites originated as low pressure partial melting residues sometime in the middle to early Proterozoic and were subducted underneath the Rehoboth province in the course of the Namaquan orogenic cycle between 0.9 to 1.3 Ga. This mantle portion was reenriched at the end of this period at around 850 Ma years ago.

A common thermal history and lithosphere thickness was established across the block consisting of the Rehoboth province, the Kheis Magondi belt and the Kaapvaal craton until the Mesozoic (Bell et al., 2003) when first, the lower parts of Kaapvaal lithosphere between 170 and 200 km were thermally disturbed and partly eroded sometime around about 150 Ma and second, the part of the Rehoboth lithosphere below about 140 km was removed and the mantle section between 120 and 140 km thermally overprinted (Bell et al., 2003; Boyd et al., 2004; Janney et al., 2010; Mather et al., 2011). This happened in the realm and at the beginning of the break-up of Gondwana and the opening of the Atlantic.

3.8. Acknowledgements

The authors thank M. Lazarov and A. Neumann for support in the laboratory. Help during preparation by J.Heliosch and M. Krebs is gratefully acknowledged. Many thanks to L. Franz for providing additional samples. We thank S. Aulbach for helpful discussions. This project was supported by the Deutsche Forschungsgemeinschaft, grant BR 1012/37-1.

3.9. References

Bell, D.R., Schmitz, M.D. and Janney, P.E., 2003. Mesozoic thermal evolution of the southern African mantle lithosphere. Lithos, 71(2-4): 273-287.

Blichert-Toft, J., Chauvel, C. and Albarede, F., 1997. Separation of Hf and Lu for high-precision isotope analysis of rock samples by magnetic sector multiple collector ICP-MS. Contributions to Mineralogy and Petrology, 127(3): 248-260.

Blignault, H.J., Jackson, M.P.A., Beukes, G.J. and D.J., T., 1974. The Namaqua tectonic province in South West Africa. Precambrian Res. Unit, Univ. Cape Town, Geol. Dep. Bull., 15: 29-47.

Boyd, F.R. et al., 2004. Garnet lherzolites from Louwrensia, Namibia: bulk composition and P/T relations. Lithos, 77(1-4): 573-592.

Brey, G.P. and Koehler, T., 1990. Geothermobarometry in 4-Phase Lherzolites .2. New Thermobarometers, and Practical Assessment of Existing Thermobarometers. Journal of Petrology, 31(6): 1353-1378.

Carlson, R.W. and Moore, R.O., 2004. Age of the Eastern Kaapvaal mantle: Re-Os isotope data for peridotite xenoliths from the Monastery kimberlite. South African Journal of Geology, 107(1-2): 81-90.

Caro, G., Bourdon, B., Birck, J.L. and Moorbath, S., 2006. High-precision Nd-142/Nd-144 measurements in terrestrial rocks: Constraints on the early differentiation of the Earth's mantle. Geochimica Et Cosmochimica Acta, 70(1): 164-191.

Chu, N.C. et al., 2002. Hf isotope ratio analysis using multi-collector inductively coupled plasma mass spectrometry: an evaluation of isobaric interference corrections. Journal of Analytical Atomic Spectrometry, 17(12): 1567-1574.

Cornell, D.H. et al., 2011. Evidence from Dwyka tillite cobbles of Archaean basement beneath the Kalahari sands of southern Africa. Lithos, 125(1-2): 482-502.

Davies, G.R., Spriggs, A.J. and Nixon, P.H., 2001. A non-cognate origin for the Gibeon kimberlite megacryst suite, Namibia: Implications for the origin of Namibian kimberlites. Journal of Petrology, 42(1): 159-172.

DeWolf, C.P., Zeissler, C.J., Halliday, A.N., Mezger, K. and Essene, E.J., 1996. The role of inclusions in U-Pb and Sm-Nd garnet geochronology: Stepwise dissolution experiments

and trace uranium mapping by fission track analysis. Geochimica Et Cosmochimica Acta, 60(1): 121-134.

Franz, L., Brey, G.P. and Okrusch, M., 1996a. Reequilibration of ultramafic xenoliths from Namibia by metasomatic processes at the mantle boundary. Journal of Geology, 104(5): 599-615.

Franz, L., Brey, G.P. and Okrusch, M., 1996b. Steady state geotherm, thermal disturbances, and tectonic development of the lower lithosphere underneath the Gibeon Kimberlite Province, Namibia. Contributions to Mineralogy and Petrology, 126(1-2): 181-198.

Green, T.H., Blundy, J.D., Adam, J. and Yaxley, G.M., 2000. SIMS determination of trace element partition coefficients between garnet, clinopyroxene and hydrous basaltic liquids at 2-7.5 GPa and 1080-1200 degrees C. Lithos, 53(3-4): 165-187.

Hartnady, C.J.H. and LeRoex, A.P., 1985. Southern-Ocean Hotspot Tracks and the Cenozoic Absolute Motion of the African, Antarctic, and South-American Plates. Earth and Planetary Science Letters, 75(2-3): 245-257.

Hoal, B.G., Hoal, K.E.O., Boyd, F.R. and Pearson, D.G., 1995. Age constraints on crustal and mantle lithosphere beneath the Gibeon kimberlite field, Namibia. South African Journal of Geology, 98(2): 112-118.

Hoal, K.E.O., Hoal, B.G., Erlank, A.J. and Shimizu, N., 1994. Metasomatism of the Mantle Lithosphere Recorded by Rare-Earth Elements in Garnets. Earth and Planetary Science Letters, 126(4): 303-313.

Ionov, D.A., Blichert-Toft, J. and Weis, D., 2005. Hf isotope compositions and HREE variations in off-craton garnet and spinel peridotite xenoliths from central Asia. Geochimica Et Cosmochimica Acta, 69(9): 2399-2418.

Jacobs, J., Pisarevsky, S., Thomas, R.J. and Beckere, T., 2008. The Kalahari Craton during the assembly and dispersal of Rodinia. Precambrian Research, 160(1-2): 142-158.

Janney, P.E. et al., 2010. Age, Composition and Thermal Characteristics of South African Off-Craton Mantle Lithosphere: Evidence for a Multi-Stage History. Journal of Petrology, 51(9): 1849-1890.

Kroner, A., Hegner, E., Wendt, J.I. and Byerly, G.R., 1996. The oldest part of the Barberton granitoid-greenstone terrain, South Africa: Evidence for crust formation between 3.5 and 3.7 Ga. Precambrian Research, 78(1-3): 105-124.

Kurszlaukis, S., Franz, L. and Lorenz, V., 1998. On the volcanology of the Gibeon Kimberlite Field, Namibia. Journal of Volcanology and Geothermal Research, 84(3-4): 257-272.

Lazarov, M., Unpublished results. Archean to present day evolution of the lithospheric mantle beneath the Kaapvaal craton – Processes recorded in subcalcic garnets, peridotites and polymict breccia. PhD thesis, Goethe-Univ. Frankfurt, Germany: 213 pp.

Lazarov, M., Brey, G.P. and Weyer, S., 2009. Time steps of depletion and enrichment in the Kaapvaal craton as recorded by subcalcic garnets from Finsch (SA). Earth and Planetary Science Letters, 279(1-2): 1-10.

Ludwig, K.R., 2008. Isoplot 3.7: A geochronological toolkit for Microsoft Excel. Berkley Geochronology Center, Spec. Pub. No. 4: 1-77.

Mather, K.A., Pearson, D.G., McKenzie, D., Kjarsgaard, B.A. and Priestley, K., 2011. Constraints on the depth and thermal history of cratonic lithosphere from peridotite xenoliths, xenocrysts and seismology. Lithos, 125(1-2): 729-742.

McDonough, W.F. and Sun, S.S., 1995. The Composition of the Earth. Chemical Geology, 120(3-4): 223-253.

Meisel, T., Walker, R.J., Irving, A.J. and Lorand, J.P., 2001. Osmium isotopic compositions of mantle xenoliths: A global perspective. Geochimica Et Cosmochimica Acta, 65(8): 1311-1323.

Mitchell, R.H., 1984. Garnet Lherzolites from the Hanaus-I and Louwrensia Kimberlites of Namibia. Contributions to Mineralogy and Petrology, 86(2): 178-188.

Muenker, C., Weyer, S., Scherer, E. and Mezger, K., 2001. Separation of High field strength elements (Nb, Ta, Zr, Hf) and Lu from rock samples for MC-ICPMS measurements. Geochemistry Geophysics Geosystems, 2(10.1029/2001GC000183).

Muller, M.R. et al., 2009. Lithospheric structure, evolution and diamond prospectivity of the Rehoboth Terrane and western Kaapvaal Craton, southern Africa: Constraints from broadband magnetotellurics. Lithos, 112: 93-105.

Nimis, P. and Grutter, H., 2010. Internally consistent geothermometers for garnet peridotites and pyroxenites. Contributions to Mineralogy and Petrology, 159(3): 411-427.

Nimis, P. and Taylor, W.R., 2000. Single clinopyroxene thermobarometry for garnet peridotites. Part I. Calibration and testing of a Cr-in-Cpx barometer and an enstatite-in-Cpx thermometer. Contributions to Mineralogy and Petrology, 139(5): 541-554.

Pearce, N.J.G. et al., 1997. A compilation of new and published major and trace element data for NIST SRM 610 and NIST SRM 612 glass reference materials. Geostandards Newsletter - the Journal of Geostandards and Geoanalysis, 21(1): 115-144.

Pearson, D.G., Irvine, G.J., Ionov, D.A., Boyd, F.R. and Dreibus, G.E., 2004. Re-Os isotope systematics and platinum group element fractionation during mantle melt extraction: a study of massif and xenolith peridotite suites. Chemical Geology, 208(1-4): 29-59.

Pearson, D.G. and Nowell, G.M., 2002. The continental lithospheric mantle: characteristics and significance as a mantle reservoir. Philosophical Transactions of the Royal Society a-Mathematical Physical and Engineering Sciences, 360(1800): 2383-2410.

Pin, C. and Zalduegui, J.F.S., 1997. Sequential separation of light rare-earth elements, thorium and uranium by miniaturized extraction chromatography: Application to isotopic analyses of silicate rocks. Analytica Chimica Acta, 339(1-2): 79-89.

Rudnick, R.L. and Walker, R.J., 2009. Interpreting ages from Re-Os isotopes in peridotites. Lithos, 112: 1083-1095.

Schmidt, A. et al., 2008. Rapid eclogitisation of the Dabie-Sulu UHP terrane: Constraints from Lu-Hf garnet geochronology. Earth and Planetary Science Letters, 273(1-2): 203-213.

Schmitz, M.D., Bowring, S.A., de Wit, M.J. and Gartz, V., 2004. Subduction and terrane collision stabilize the western Kaapvaal craton tectosphere 2.9 billion years ago. Earth and Planetary Science Letters, 222(2): 363-376.

Spriggs, A.J., 1988. An isotopic and geochemical study of kimberlites and associated alkaline rocks from Namibia. PhD thesis, University Leeds, England.

Tinker, J.H., de Wit, M.J. and Royden, L.H., 2004. Old, strong continental lithosphere with weak Archaean margin at similar to 1.8 Ga, Kaapvaal Craton, South Africa. South African Journal of Geology, 107(1-2): 255-260.

Van Schijndel, V., Cornell, D.H., Hoffmann, K.-H. and Frei, D., 2011. Three episodes of crustal developement in the Rehoboth Province, Namibia. In: Van Hinsbergen, D.J.J., Buiter, S.J.H., Torsvik, T.H., Gaina, C., Webb, S. (Eds.), The formation and evolution of Africa from the Archaean to Present. Geol. Soc. Spec. Pub.

Walker, R.J., Carlson, R.W., Shirey, S.B. and Boyd, F.R., 1989. Os, Sr, Nd, and Pb Isotope Systematics of Southern African Peridotite Xenoliths - Implications for the Chemical

Evolution of Subcontinental Mantle. Geochimica Et Cosmochimica Acta, 53(7): 1583-1595.

Wittig, N., Baker, J.A. and Downes, H., 2007. U-Th-Pb and Lu-Hf isotopic constraints on the evolution of sub-continental lithospheric mantle, French Massif Central. Geochimica Et Cosmochimica Acta, 71(5): 1290-1311.

Yang, Y.H., Wu, F.Y., Xie, L.W. and Zhang, Y.B., 2010. High-Precision Measurements of the 143Nd/144Nd Isotope Ratio in Certified Reference Materials without Nd and Sm Separation by Multiple Collector Inductively Coupled Plasma Mass Spectrometry. Analytical Letters, 43(1): 142-150.

Chapter 4:

U-Th-Pb and Hf isotope systematics of zircons from carbonatite and kimberlite derived crustal xenoliths: implications for the crustal evolution of the Rehoboth Terrane

4.1. Abstract

Knowledge about the crustal basement age of the Rehoboth Terrane in Namibia is only sketchy because of an extensive cover of Nama Group sediments. Known ages are Proterozoic. For this study we separated zircons from six crustal xenoliths from carbonatite dykes close to Gross Brukkaros, from one xenolith from the Louwrensia kimberlite diatreme and also from the matrix of the Louwrensia kimberlite. We determined the U-Pb ages of the zircons and their Hf isotopes by laser ablation ICPMS (Element 2 resp. Neptune from Finnigan). The xenoliths are high grade gneissic rocks of sedimentary origin.

Individual xenoliths give individual age spectra with main peaks at around 650 Ma, 1100-1200 and 1900 Ma. These ages also appear in the kimberlite matrix sample. The youngest ages are around 500 to 600 Ma. The kimberlite matrix contained a few zircons with ages of 2.4 to 2.9 Ga.

The combined Hf and U-Pb isotope data of zircon point to a prolonged history of juvenile crust formation, recycling and mixing.

The first crust may have been generated in the Archean from a primitive mantle source around 2.7 to 2.9 Ga ago or from a depleted source about 3.38 Ga ago with subsequent recycling around 1.9 to 2 Ga.

Palaeoproterozoic to Neoarchean crust was recycled during the attachment of the Rehoboth Terrane to the Kaapvaal craton at around 2.0 to 1.8 Ga. This coincides with the time of mantle enrichment as determined by the Lu-Hf isotope system on garnet peridotites from the Gibeon kimberlite field (Luchs et al., submitted, Precambrian Research).

Juvenile Mesoproterozoic crust was generated at around 1.5 to 1.6 Ga from a depleted mantle source, which was constantly recycled until 1.1 Ga and shows crustal mixing trend around 1.3

Ga. Nearly 60% of all datapoints are lying within this age range and are interpreted to mark a subduction process beneath the Kalahari plate (Becker et al., 2006).

More juvenile crust was formed at the boundary to the Neoproterozoic at 0.8 to 1.1 Ga that was subsequently recycling during the Namaquan and Pan African Orogeny.

4.2. Introduction

The Rehoboth Terrane in Namibia has often been described as an enigmatic province within the geotectonic framework of southern Africa (Hartnady et al., 1985) because of its patchy record of diverse crustal ages from scarce outcrops looking out from underneath a widely spread cover of Nama group sediments (Fig. 3.1 and 4.1). Crustal basement rocks can mainly be found in the Rehoboth Basement inlier which is situated in the north of the terrane, on the southern edge of the Ghanzi Chobe Belt. On its western border to the Proterozoic Namaqua Natal belt, the non diamondiferous Gibeon Kimberlite Province is situated. Kimberlitic volcanism as a consequence of the drifting of the African continent over the Vema Hot spot (Spriggs, 1988) lifted up numerous mantle and crustal xenoliths to the surface. These xenoliths were subject for several geochemical studies (e.g. Hoal et al., 1995; Franz et al., 1996b; Franz et al., 1996a; Pearson et al., 2004).

Analyses of these peridotites revealed a complex depletion and enrichment history of the upper mantle beneath Gibeon. Rhenium depletion ages for mantle xenoliths range from less than 0.5 up to 2.2 Ga (e.g. Hoal et al., 1995; Pearson et al., 2004) , whereas only the oldest ages have a geological significance as Rhenium depletion ages (T_{RD}). These ages can only be considered as minimum ages. Our major, trace and isotope (Sm-Nd, Lu-Hf) analyses of garnets and clinopyroxenes from garnet peridotites together with results from Re-Os (Pearson et al. (2004) indicate that the mantle underlying the Gibeon province is mainly made up of two different components (Luchs et al., submitted). A highly depleted and reenriched component with sigmoidal garnet REE patterns is possibly the residue of a first partial melting event at around 2.9 Ga (from Re-Os (Pearson et al., 2004); own interpretation). It may have been reenriched at around 1.9 Ga (Luchs et al., submitted) by a process connected with the collision of the Rehoboth Terrane with the Kaapvaal craton. The second, less depleted component (depletion age unknown) has flat middle to heavy garnet REE patterns with LREE enrichment. The Lu-Hf

isotope systematics give an age of around 850 Ma (Luchs et al., submitted) which corresponds to the very late stage of the Namaqua Natal orogeny. This mantle portion is thought to be a subducted addition to the Rehoboth mantle during the Namaqua Natal orogeny. Eventually, both mantle proportions were affected by a late enrichment around 460 Ma (Luchs et al., submitted).

In addition, a few zircon grains separated from a garnet peridotite of Hanaus I from Gibeon yielded three age clusters at 627, 751 and 1013 Ma, which can be related to magmatic events within the Damara belt (0.6 & 0.7 Ga) and the Namaqua Orogeny (1.0 Ga) (Liati et al., 2004).

The few crustal ages that have been determined in older studies from the Rehoboth Terrane revealed Proterozoic ages around 895 ± 7 Ma (K-Ar; (Rupprecht, unpublished results; PhD Thesis)) 1.7 ± 0.010 Ga (Nagel et al., 1996) and 1.7 – 2.3 Ga ($^{207}Pb/^{206}Pb$ and Nd model ages; (Ziegler and Stoessel, 1991)), whereas the Rehoboth basement inlier (RBI) is marked by an intrusive episode of 1210 ± 7 Ma and an episode of igneous activity from at least 1.23 to 1.09 Ga (Becker et al., 2006).

More recent studies by Cornell et al. (2011), Van Schijndel et al. (2011b) and Van Schijndel et al. (2011a) of zircon and baddeleyite grains extracted from mafic and granitic Dwyka tillite cobbles brought up new light into the development of the Rehoboth crust and extended the age range into the Archean with ages ranging up to 2.9 Ga for detrital zircons from the RBI (Van Schijndel et al., 2011a) and 2.9 Ga from granitic cobbles of Dwyka Tillites (Cornell et al., 2011). The age spectra of Van Schijndel et al. (2011a) additionally contains major peaks from 1.05 to 1.32 Ga and 1.9 to 2.2 Ga corresponding to the Namaquan orogeny and a major crust building phase for the Rehoboth Terrane respectively. Baddeleyite grains from mafic cobbles that were separated from Dwyka tillites of Van Schijndel et al. (2011b) were dated with U-Pb around 1.11 Ga.

In this study, we analyzed a new sample set of zircons that were derived as xenoliths in carbonatites and a kimberlite from the lower to the middle crust and one sample collected from the matrix of the Louwrensia kimberlite pipe in the Gibeon Kimberlite Field for U-Pb and Hf isotopic compositions. Our basic assumption was that the crustal xenoliths derived from the middle to lower crust could provide new information about the framework of the Gibeon crust. The zircon population in the gneisses would give the maximum possible age of the sedimentary precursor (= the youngest zircons) and the oldest ages of the hinterland from which the sediments were derived (= oldest zircons). Magmatic rocks give information of a magmatic event

in the crust and the detritus from a volcanic diatreme (zircons are from disintegrated crustal rocks) possibly a complete overview of the ages of the crust underneath the Gibeon province. We also tried to clarify the question of whether there is a connection between mantle and crustal processes and if there is an Archean component existent in the Rehoboth Terrane as proposed before in several former studies (e.g. Hoal et al., 1995; Cornell et al., 2011; Luchs et al., submitted).

4.3. Geological setting

On the western border to the Namaqua Natal belt, the Gibeon Kimberlite field forms part of the Rehoboth Terrane (see Fig.3.1), alternatively termed as the Namibia province or Maltahoehe province (Blignault et al., 1974; Tankard et al., 1982).

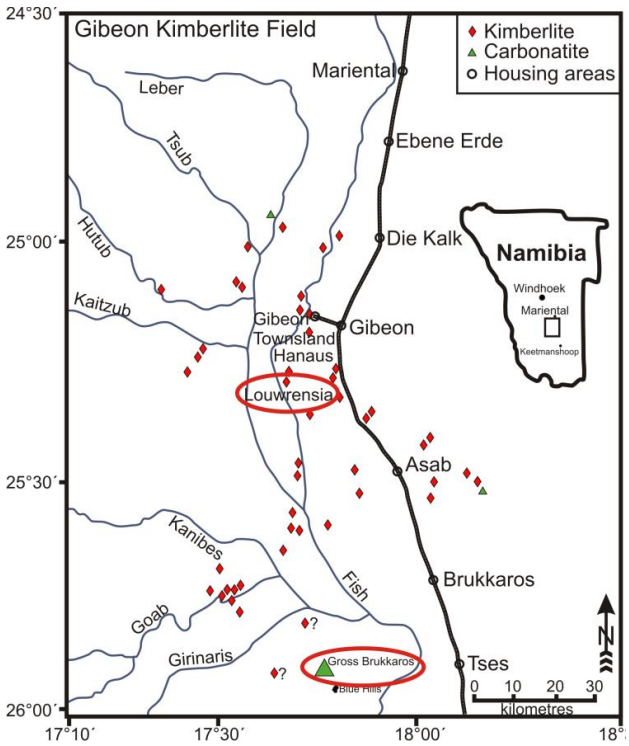

Fig.4.1: Location of the Gibeon Kimberlite field within the southern African framework (after Kurszlaukis et al. (1998)). Marked in red elipses are the sample locations for samples used in this study. A broader overview is given in Fig.3.1.

After the consolidation of the Kaapvaal craton at around 2.9 Ga, the Kheis-Magondi belt accreted along its western and south-western border, followed by the collision of the Rehoboth Terrane on its western margin at 1.9 Ga. At the time of collision of both Kaapvaal blocks, the

mantle of the Rehoboth Terrane probably already experienced its first depletion (Luchs et al., submitted) and crust had already existed (Cornell et al., 2011; Van Schijndel et al., 2011a).

Cornell et al. (2011) proposed an alternative scenario in which the Rehoboth Terrane and the Kaapvaal craton were attached from the Archaean, later separated, followed by a collision during which the Kheis-Magondi belt was formed.

During the Proterozoic, several terranes collided with the Kaapvaal craton and the Rehoboth Terrane in the west and in the south, forming the Namaqua-Natal belt with addition and enrichment of mantle components into the Rehoboth mantle around 0.8 to 0.9 Ga. At a later stage, during the Pan African orogeny, the Damara, Gariep and Saldania Belt were created. There is a general decrease of crustal basement ages away from the Archaean Kaapvaal craton towards the Atlantic Ocean, with some exceptions in between such as the Richtersveld subprovince with ages ranging from 2.0 to 1.7 Ga. It remains unclear if it represents a part that remained unaffected by the Namaqua orogeny or if had already formed in the protoatlantic and then collided with the Namaqua-Natal mobile belt (Hartnady et al., 1985).

The Rehoboth Terrane is largely hidden beneath a more than 1 km thick cover of Nama Group sediments, as evident from drilling operations (Aquitaine, 1971). Crustal basement is mainly exposed in the north, in the Rehoboth basement inlier (RBI) complex. The terrane is subdivided by a strong magnetic lineament which separates into the Aroab and the Tses subprovince (Hoal et al., 1995). Age dating of exposed gneissic rocks, very similar to crustal basement rocks in the Kheis Magondi belt, in the Aroab subprovince resulted in ages around 1.8 Ga, indicating the existence of lithospheric material of the adjacent domain (Blignault et al., 1974; Hoal et al., 1995).

The Gibeon Kimberlite field is located in the Tses subprovince and has an extension of 70 Km from East to west and 110 km from North to south (Kurszlaukis et al., 1998). It consists of more than 75 kimberlite diatremes and associated carbonatite vents. On its southern edge, the Gross Brukkaros and the Blue Hills as well as associated smaller carbonatite dykes are located. Carbonatite eruptions were also triggerd by the passing of the Discovery and eventually the Vema Hot spot (Davies et al., 2001).

Two samples used for this study were taken from the Kimberlite diatreme Louwrensia in the Gibeon kimberlite field and six stem from different carbonatite dykes, located close to the Gross Brukkaros (Fig.4.1).

4.4. Material and Methods

4.4.1. Sample description and Preparation

In total, this work investigates six crustal xenoliths from carbonatite diatremes around the Gross Brukkaros which accompanied kimberlite eruptions around 72.5 Ma ago (Davies et al., 2001) and one xenolith and one detritus sample (GLZ-1) from the Louwrensia kimberlite pipe in Gibeon. Samples from the Gross Brukkaros area were kindly provided by the University of Wuerzburg and collected and petrographically described by Rupprecht (unpublished results; PhD Thesis). Except for GLZ-1, all samples have an average diameter of 5 to 10 cm. The following petrographic descriptions of the carbonatite derived samples are based on the correspondent descriptions by Rupprecht (unpublished results; PhD Thesis).

KJA91-7 is a medium grained high grade-fenite from the carbonatite close to Jakkalsdraii. It does not show a sign of visible layering. The mineral assemblage is made up of aegirine-augite, alkali feldspar, plagioclase, calcite, apatite, ilmenite and magnetite.

KK3VB is a layered mafic granulite / garnet pyrobolite which is mainly made up of plagioclase, amphibole, clinopyroxene and garnets with diameters of up to 2 mm. Aluminosilicates and opaque minerals are visible as accessory phases.

K3e is a hornblende pyroxenefels from the carbonatite vent A2. The sample contains several xenoliths within the carbonatite matrix. Parts of the carbonatite matrix were crushed during the preparation process. K3eb is one of the xenoliths entrained in K3e and can be described as a clinopyroxene-amphibole felse with apatite and phlogopite as accessory mineral phases.

GLZ-2 is a high grade granulite, containing garnet and feldspar.

Except for the detritus samples, all samples were crushed in a SelFrag® Fragmentation system using voltages of 90 to 120 kV with a 1 mm built in sieve. Thereby a current runs between two electrodes in vessel filled with water in which the samples are placed. Using this technique allows the liberation of single grains, such as zircons, without cracking them as the minerals are separated along their grain boundaries. Contamination is kept to zero because the cleaning of the sample vessels is easy and very effective. Support for this efficiency may be the fact that not a single zircon grain was found in the amphibolites.

Crushing was followed by heavy liquid separation with Bromoform and sorting using a Frantz® magnetic separator. Amperage for the magnetic separation was adjusted up to 1.6 A with several steps in between. The least magnetic fraction, which contains the zircons, was treated with 6 M ultrapure HCl for 1 hour at 50°C to reduce the amount of apatite, which can easily be mistaken for zircon. Cleaned fractions were sieved with one time use fabric sieves, followed by hand picking with a stereo microscope.

Zircons were mounted on round holders with a diameter of one inch, embedded in epoxy and polished. As a preliminary work for laser ablation analyses, internal growth patterns of the zircons were revealed by cathodoluminescence imaging, using a Gatan MiniCL detector that is attached to a Jeol JSM-6490 electron microscope. Prior to this work, all mounts were coated with a thin layer of gold. We used a probe current of around 5 to 6 nA and a high voltage of 15 KV with a working distance of 15 mm.

4.4.2. LA-SF-ICPMS U-Th-Pb analysis

Prior to laser ablation analysis, gold coating was removed with ultrapure Ethanol. In order to remove any common lead from the surface that could stem from the preparation process, zircon mounts where cleaned with 2 % ultraclean nitric acid for 30s.

U-Pb dating was performed with a Thermo Finnigan Element 2 coupled to a Laser ablation system at the Goethe University in Frankfurt, Germany (GUF) in several sessions. For the majority of the samples, a New Wave UP213 Nd Yag laser with a teardrop shaped low volume sample cell was used, for the remaining samples (GLZ-1, GLZ-2, K3eb) a RESOlution M-50 193nm Excimer laser (Resonetics) was used. Samples ablated with the Resonetics M-50 laser were pre-ablated with 3 shots of the same energy as used for the following ablation in order to remove any surface contamination. Analysis was delayed to avoid the measurement of pre-ablated material. Spot sizes for all analyses varied from 20 µm to 33 µm and a fluence of 4-6 J cm^2. Laser holes were drilled with penetration depths of about 20 µm. A detailed description of the analytical procedures used here for U-Pb dating is described in Gerdes and Zeh (2006; 2009). For internal standardization the GJ-1 zircon (Jackson et al., 2004) was used as primary standard and the Plešovice zircon (Slama et al., 2008) was used as a secondary standard to check the accuracy and quality of the analyses.

Offset for $^{238}U/^{206}Pb$ ratios compared to the reference value of GJ-1 (Jackson et al., 2004) ranged in most sessions between 7 and 25%, whereas in two sessions, the offset was around 50 %.

Multiple analyses of the Plešovice standard resulted in an age of 346 ± 8 Ma and is in good agreement to reference values as published by Slama et al. (2008).

Data processing was performed, using an inhouse macro-based Excel® spreadsheet, created by A. Gerdes. The U-Pb data was usually corrected for common Pb using the measured Hg-interference corrected ^{204}Pb signal and a Stacey and Kramers (1975) compostion. However, for many analyses the ^{204}Pb was so low that it was below detection limit. Age probability-density plots were created using the Excel® spreadsheet of Sircombe (Sircombe, 2004). Concordia diagrams were created, using Isoplot 3.7 (Ludwig, 2008). Some of the data points as listed in Table A.4.1, were saturated in the signal for ^{238}U due to the usage of the counting mode, plotting above the Concordia line. These points were not considered for the Concordia diagrams.

4.4.3. LA-SF-ICPMS Hf analysis

Hafnium isotope measurements were performed with a Thermo-Finnigan Neptune multicollector (MC)-ICPMS at the Goethe University Frankfurt, coupled to New Wave UP213 Nd YAG laser (first part of the study) and a Resolution M-50 (Resonetics) 193 nm ArF excimer laser (CompexPro 102, Coherent) system, respectively, following the procedures described in Gerdes and Zeh (2006). Laser spots with diameter 40 µm were drilled with a frequency of 5.5 Hz and an energy density of 6 J/cm^2 during 55 s of data acquisition. The 40 µm Hf analysis spot was set on top or just next to the U-Th-Pb spot in the same growth domain as indicated by CL images. Penetration depths of the laser spots are in the range of about 40 to 50 µm.

Data were processed by the adjustment of all analyses to a $^{176}Hf/^{177}Hf$ isotope ratio of 0.282160 of reference standard JMC475. GJ-1 and Plešovice standards were measured in every measurement session to ensure high quality analyses. Average $^{176}Hf/^{177}Hf$ isotope ratios of GJ-1 in 84 analyses were at 0.282017 ± 0.00007 (2 sigma) and 0.282490 ± 0.000055 (2 sigma) for 38 analyses of the Plešovice standard, which is in accordance to published reference values (Gerdes and Zeh, 2006; Slama et al., 2008).

$\varepsilon Hf(t)_{initial}$ values were calculated by first substracting the amount of radiogenic ^{176}Hf from the $^{176}Hf/^{177}Hf$ ratios with the use of the corresponding age as obtained before by the U-Th-Pb analyses. Additionally, $^{176}Lu/^{177}Hf$ and $^{176}Hf/^{177}Hf$ ratios of 0.0336 and 0.282785 were used (Bouvier et al., 2008) along with a decay constant of $1.867*10^{-11}$ (average Scherer et al., 2001; Söderlund et al., 2004). Only datapoints with concordant ages (90 – 110% concordance) and small errors were considered for further interpretations. Data in table A.4.2 without U-Pb ages did not have a concordant age.

4.5. Results

4.5.1. Zircon morphology

Samples GLZ-1, GLZ-2, and KK3VB contained up to several thousand zircons, whereas KJA 91-7 contained up to one hundred and K3e contained only up to 40 zircons. Only two zircons were found in sample K3eb and none in KK3V.

Most grain sizes ranged from 50 to 150 µm, a smaller number of single crystals were larger than 200 µm. Most of the grains do not contain xenocrystic cores and are euhedral to subrounded. Inclusions in predominant oscillatory zoned zircons are rare but a substantial amount of grains are marked by a thin, bright illuminating rim which could be measured only in few cases. Recrystallized grains were observed only in very few crystals.

4.5.2. U-Pb age spectra

We obtained a wide range of U-Pb ages from around 500 Ma up to 2.9 Ga (Fig.4.2, 4.3; Table A.4.1). Taking all samples together we obtained prominent age clusters with peaks at around 650 Ma, between 1.0 to 1.15 Ga, 1.2 to 1.4 Ga, and 1.7 to 1.8 Ga and four ages between 2.7 – 2.9 Ga. Sixty percent of the ages are between 1.0 and 1.4 Ga. However the samples vary individually.

Carbonatite sample K3e has major age peaks from 600 to 700 Ma, 1.1 to 1.25 Ga and an old component at 2.1 Ga with 14 concordant analyses. Carbonatite sample K3eb, which is an individual mafic component within sample K3e only yielded one concordant age at 1.1 Ga.

Most ages of sample KJA91-7 fall within the range of 1.2 or 1.3 to 1.4 Ga, with 60 concordant analyses.

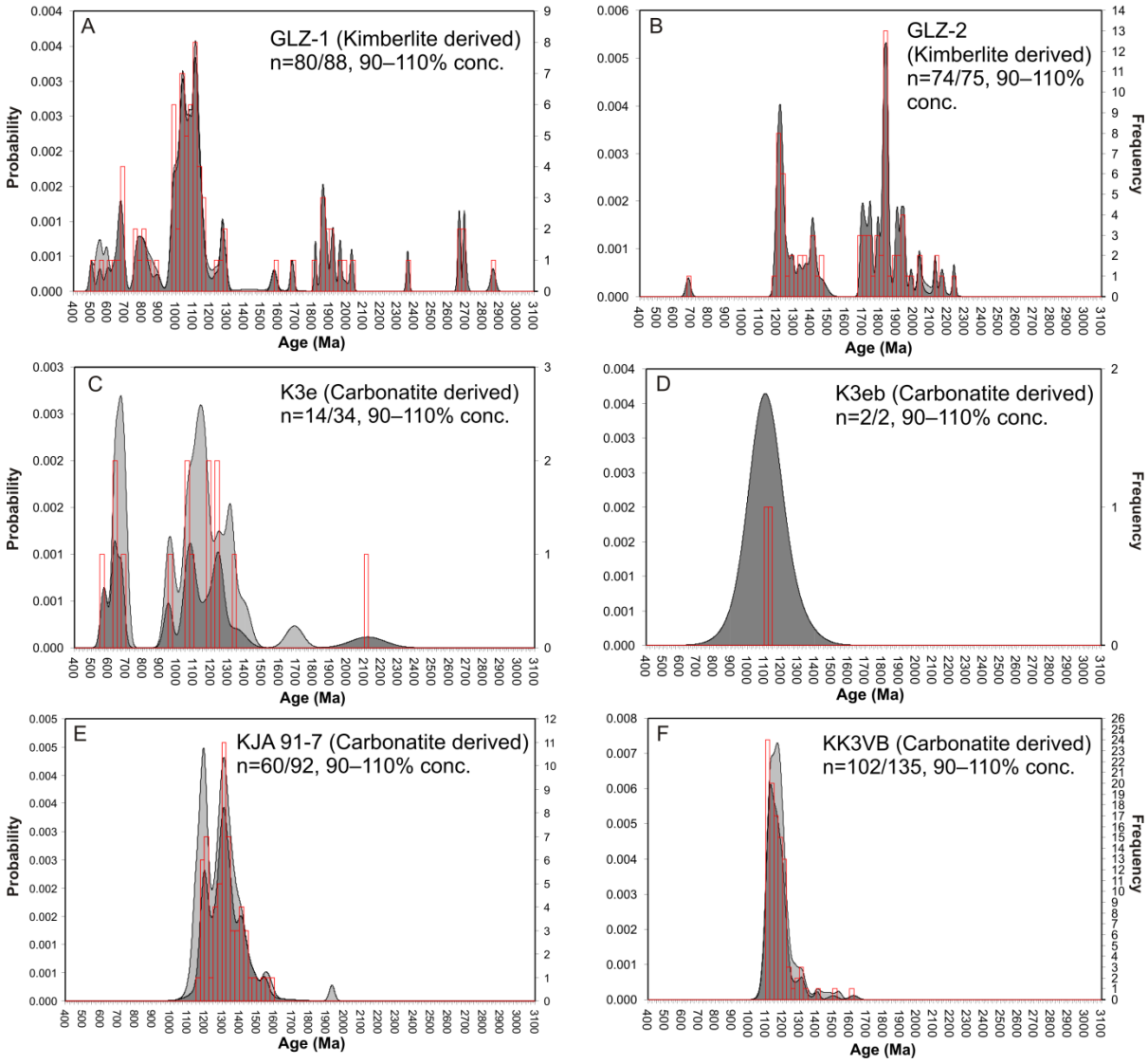

Fig.4.2: U-Pb age distribution patterns for each individual sample. Zircons from carbonatite derived xenoliths (C-F) show in general a smaller age range with mid-Proterozoic ages, while the kimberlite derived xenolith record events from 0.5 to 2.9 Ga (B). The sample from the matrix of the kimberlite shows a broader range in ages, as a result of the incorporation of Nama shale sediment zircons (A).

The last remaining sample, originating from a carbonatitic dyke, is KK3VB with 102 concordant analyses and a major peak around 1.1 to 1.2 Ga and some minor occurrences of ages between 1.4 and 1.6 Ga.

Sample GLZ-1 from the matrix of the Louwrensia Kimberlite pipe, has prominent peaks in all age clusters as mentioned above with 80 concordant analyses, while the most prominent peak is around 1.0 to 1.2 Ga. Four zircons give the oldes ages of around 2.7 to 2.9 Ga, overlapping with the Archean ages of the granite cobbles from Dwyka tillites reported by Cornell et al. (2011). The cathodoluminescence images of our old zircons testify a magmatic origin.

The kimberlite derived crustal xenolith GLZ-2 has two major age groups at around 1.2 Ga and 1.8 to 1.9 Ga, while there are some minor additional peaks around 0.6 to 0.7 Ga, 1.4 Ga, 1.7 Ga and 2.0 to 2.3 Ga.

Where possible, xenocrystic cores and surrounding rims were both analysed. In sample KK3VB, the ages of the core yielded ages of 1.2 Ga to 1.3 Ga with corresponding rims of around 1.15 Ga. For samples K3e, KJA91-7 and GLZ-2, cores yielded ages of 1.3 and 1.5 Ga with rims around 1.2 and 1.3, respectively. Sample GLZ-1 zircon show larger age variation and core-rim age determinations yielded core ages of around 0.8, 1.0, 1.1, 1.5 and 1.9 Ga and corresponding rim ages of 0.5, 0.6, 1.0, 1.1 and 1.8 Ga.

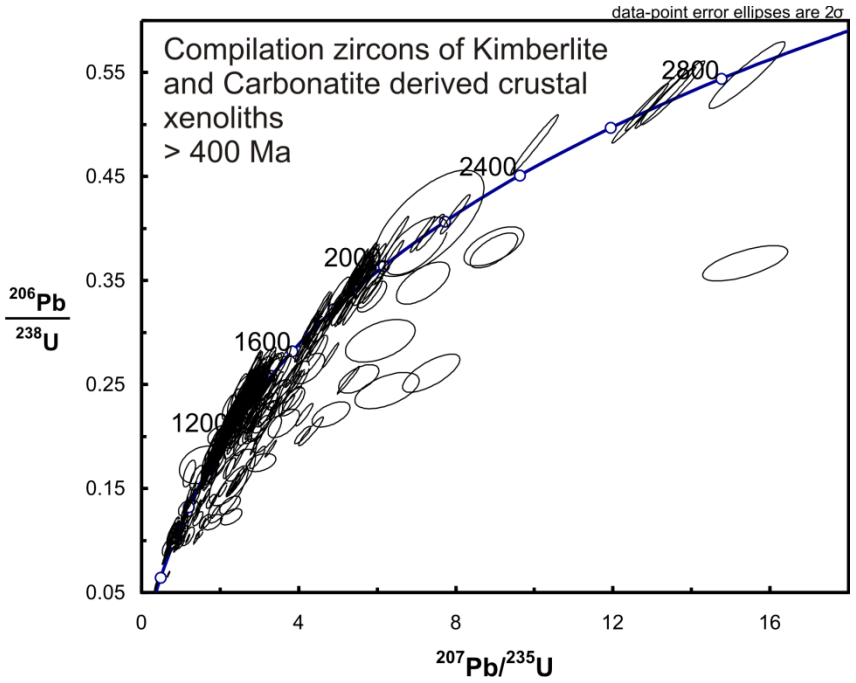

Fig.4.3 : Concordia diagram of all zircons from kimberlite and carbonatite derived xenoliths.

4.5.3. Hf isotopic composition

The data are given in Table A4.2 and shown in Fig.4.4 as εHf(*t*) values plotted against the U-Pb ages of the zircons.

Measured $^{176}Hf/^{177}Hf$ isotope ratios were calculated into εHf(*t*) values by using the corresponding U-Pb age. Except for one data point, all data plot below the evolution line for the depleted mantle (present day $^{176}Hf/^{177}Hf$ from (Chauvel and Blichert-Toft, 2001)), including the errors.

The majority of the analyses (~ 65%) are positive, with εHf(*t*) above the CHUR line. Generally the εHf(*t*) values increase from the Paleoproterozioc to the Mesoproterozoic, whereas the largest variation of the εHf(t) from +14.5 to -21 can be observed close to the boundary to the Neoproterozoic.

εHf(*t*) values for GLZ-1 range from around -20 to +14, for GLZ-2 from -12 to +12, for KJA91-7 from +2 to +11, for KK3VB from -12 to 15, for K3e from -2 to +14 and for K3eb around +1.

The four Archean-aged zircons of the sample GLZ-1 have εHf(*t*) values between +2 and -5. The age cluster between 1.7 and 2.2 Ga has εHf(*t*) values ranging from +5 to -9 belonging to samples GLZ-1 and GLZ-2. Ages between 1.6 and 1.2 Ga are characterized by εHf(*t*) values from +11 to -9, while there is a large vertical spread around 1.2 to 1.3 Ga with εHf(*t*) values from +5 to -10, including all samples of this study except for K3eb. Proterozoic ages from 1.1 to 0.9 Ga are between +11 to +2 εHf(*t*) units and belong to sample GLZ-1, KK3VB, K3e and K3eb. The most recent ages from 0.9 to 0.5 Ga (GLZ-1, K3e) range between +8 to -15 εHf(*t*) units.

A positive linear correlation between U-Pb and Hf model age shows no visible Pb loss in the sampleset used for this study (Fig.4.5).

4.6. Discussion

Provenance regions of the samples

It is important to note that crustal xenoliths investigated in this study that stem from carbonatite eruptions report mainly a time span between 1 to 1.5 Ga, whereas the kimberlite pipe derived xenolith and one sample from the matrix of the Louwrensia Kimberlite pipe, show a broader range of crustal events.

K3e shows a different age spectra, with additional age peaks around 500 to 700 Ma, and one single age at 2.1 Ga. These additional age peaks cannot be found in the other xenoliths originated from the carbonatites. They represent zircons derived from the carbonatite itself as during the preparation process parts of the carbonatite matrix was crushed and mixed with the enclosed crustal xenoliths.

For this reason, the maximum possible age for the precursor sediments of the carbonatites derived xenoliths is around 1 Ga, whereas that of the kimberlite derived xenoliths is only about 600 to 700 Ma. The carbonatite derived xenoliths may come from a stratigraphically different crustal part than the kimberlite derived xenoliths. Also, the sedimentary precursors may have sampled material from a different hinterland.

The kimberlite matrix sample potentially collected all these various layers and rare Archean magmatic rocks from the crust. There may, however, also be a component incorporated from the Nama sediments. It also yielded a substantial number of zircons with ages between 0.5 and 0.8 Ga, the age of the Pan African Orogeny, in which the Damara belt was created. A Pan African component has not been reported so far from the Rehoboth province and the origin of these zircons may be from the Nama group shales whose debris was incorporated into the kimberlite matrix during eruption.

It has been shown in former studies of detrital zircons, that zircons are able to survive long distance transports over time (e.g. Morag et al., 2011). On the other hand, a former study has shown that even though zircons are capable of surviving such long transports, it does not necessarily mean that they are being transported far away (Klama, Unpublished results; PhD Thesis). It is unlikely but it cannot completely be excluded that ages from sample GLZ-1 are not

made up of zircons from the Rehoboth Terrane itself but of neighbouring geotectonic domains such as the Kaapvaal craton.

Crust formation and recycling

This new U-Pb and Hf data bring up new aspects about the framework of the lower crust beneath the Rehoboth Terrane, in particular about the framework beneath the Gibeon kimberlite field. The question if there is any evidence for the Kheis Orogeny in the crustal record studied is also addressed.

Taking the the average crustal $^{176}Lu/^{177}Hf$ ratio of 0.0133 of Rudnick and Gao (2003) and projecting the Hf-isotope evolution back onto the depleted mantle, four periods of crustal growth (Fig.4.4) can be derived.

1. The oldest crustal components are represented by zircon with ages around 2.7 to 2.9 Ga and a Hf isotope composition similar to the primitive mantle at that time. Depleted mantle model ages range from 3.05 to 3.38 Ga. εHf(*t*) values of around -12 show subsequent recycling of this crust at a time around 1.9 to 2 Ga.
2. Palaeoproterozoic to Mesoproterozoic zircon suggest that juvenile crust was extracted from a depleted mantle source around 2.3 to 2.7 Ga. The most positive εHf(*t*) values of +5 yield Palaeoproterozoic grains. Recycling of this Palaeoproterozoic to Neoarchean crust during subsequent orogenic events is reflected by negative εHf(*t*) values around -14 to -22 in 1.0 to 1.2 Ga zircon.
3. Most Mesoproterozoic zircons in the interval 1.3 to 1.5 Ga are characterized by positive εHf(*t*) of +2 to +12 with a clear positive correlation between zircon age and εHf(*t*) pointing to an important juvenile crust forming event at around 1.5-1.6 Ga. The steepening slope between 1.3-1.1 Ga towards more negative εHf(*t*) is interpreted to reflect mixing of the juvenile and old crust during this time. It is worth noting that zircon affected by Pb-loss will also show a stronger decrease of the εHf(*t*) with age as the posulated crustal evolution trend with a $^{176}Lu/^{177}Hf$ ratio of 0.0113 (Rudnick and Gao, 2003). Juvenile growth of crustal material commenced around 1.8 to 1.9 Ga, whereas only few of

our data points are available from this event with εHf(*t*) values corresponding to a depleted mantle source.

The most prominent cluster of points have εHf(*t*) values are in the range of +5 to -3. The amount of ages in the range of 1.0 to 1.4 Ga make up about 60% of all measured data points overall and consist of data from all analyzed samples, whereas the major part stems from the sample KK3VB, a xenolith derived from a carbonatite vent near the Gross Brukkaros mountain, south of the Gibeon Kimberlite field.

4. Zircon formed in the late period of the Namaqua Orogeny at around 0.8 to 1.1 Ga, show εHf(*t*) values of around +14 to -22, with a maximum of around +4 to +10, +12 consistent with formation of juvenile crust from a depleted mantle source, recycling of old crust and the mixing of both components to variable degrees. This is evident from three samples, whereas the major part is derived from the sample GLZ-1. This newly formed crust has experienced recycling during the build-up of the Damara belt at the time of the Pan African Orogeny around 0.5 to 0.6 Ga. This late stage recycling is evident from the carbonatite derived xenoliths K3e and the kimberlite derived detritus sample GLZ-1.

One sample, the matrix of the Louwrensia Kimberlite (GLZ-1), shows a large range in ages, with oldest ages from 2.7 to 2.9 Ga. These ages are in accordance with ages determined by Cornell et al. (2011) in zircons from granite boulders in Dwyka tillites from Rietfontein and by Van Schijndel et al. (2011a) from detrital zircons of the Rehoboth Basement Inlier. The εHf(*t*) values are not very different to values for a primitive mantle at that time. Crustal growth may have commenced not too long before at around 3.1 Ga ago if these values are related to a depleted mantle. Cornell et al. (2011) determined the oxygen isotopes in their zircons, the $\delta^{18}O$ values are close to the mantle which indicates an immediate derivation from mantle derived rocks.

Evidence for a major event around 1.8 to 1.9 Ga in the Rehobotian crust is most obvious in both kimberlite derived samples (GLZ-1 and GLZ-2). This peak coincides with the age of the Kheis Orogeny (Tinker et al., 2004).

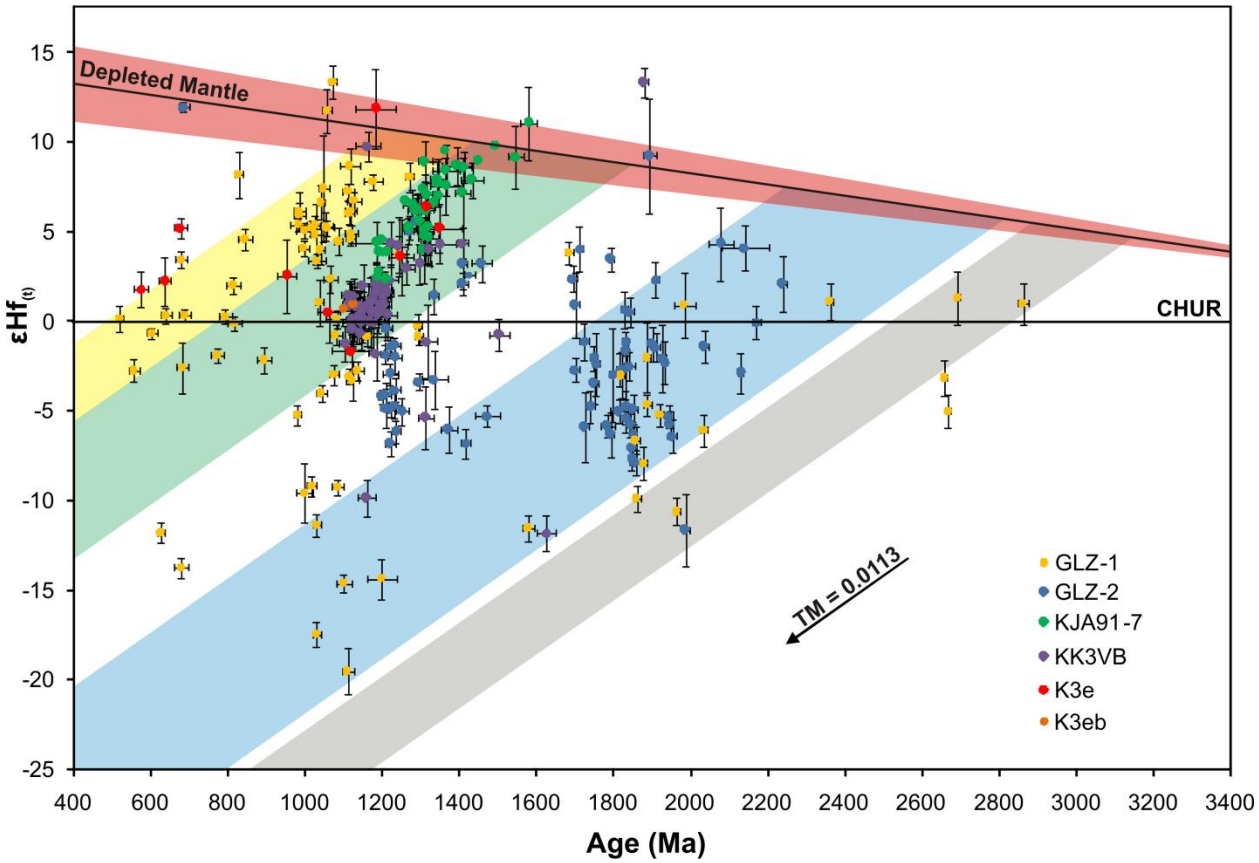

Fig.4.4: εHf(*t*) values and their corresponding U-Pb ages. Fields for crustal growth were calculated with a $^{176}Lu/^{177}Hf$ of 0.0113 (Rudnick and Gao, 2003) . The grey, blue, green and yellow field show juvenile crustal growth as well as crustal recycling and mixing of different crustal components.

Detrital zircons from a quartzite with a major peak around 1866 Ma are also well known from the Billstein Formation in the Rehoboth Basement Inlier to the north of Gibeon (Van Schijndel et al., 2011a). The εHf(*t*) values for this age group range are mostly negative (with extreme values down to -15 and a peak at around -5), but there is also a minority with εHf(*t*) up to +5 and an extreme value at +15). The debris from the Kheisian aged crust shows that it is a product of multiple stage crust recycling which was derived from a highly depleted mantle source. Calculated model ages point towards a primary source which may have originated in the late Archean.

Crust and Mantle

Two major theories about the generation of continental crust over time are competing. Pulsed growth of large volumes of continental crust stands in contrast to a model that describes steady accumulation of continental crust (as summarized by Pearson et al. (2007)). Newer evidence for pulsed crustal growth comes from Pearson et al. (2007) who compared U-Pb zircon data from crustal rocks with the distribution pattern of T_{RD} ages (Rhenium depletion ages) from platinum-group alloys (PGAs) and peridotites. They found a good correspondence of large crustal and mantle events which is in accordance to the theory of pulsed growth of the continental crust. Further evidence for pulsed growth was found in $^{4}He/^{3}He$ isotope ratios from ocean island basalts by Parman (2007).

With our new geochronological data from the Rehoboth crust and previously published age data for mantle events underneath the Rehoboth province (Hoal et al., 1995; Pearson et al., 2004; Janney et al., 2010; Luchs et al., submitted), we try to find further evidence for correspondence or disparity of major events (melting and / or reenrichment) in the mantle and the crust.

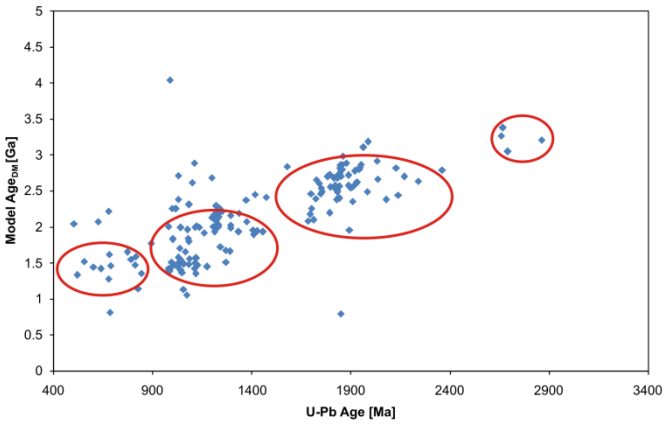

Fig.4.5 A linear correlation of U-Pb ages and model ages shows that there was hardly any lead loss. The four red elipses mark the four phases of crustal growth as recalculated in Fig.4.3

The oldest U-Pb zircon ages from this data set and that of Cornell et al. (2011) and Van Schijndel et al. (2011a) would correspond to a 2.9 Ga Re-Os isochron age inferred by us from the Re-Os data set of Pearson et al. (2004) on garnet peridotites from the neighbouring pipe Louwrensia (see Luchs et al., submitted and Chapter 1). The Rehoboth crust and mantle would

be closely genetically related if both of our assumptions i) that the old zircons are derived from the Rehoboth crust and ii) that the 2.9 Ga Re-Os isochron exists, are correct. The zircon εHf(*t*) values around zero and mantle values of $\delta^{18}O$ additionally point to a close link between mantle and overlying crust.

Subduction and enrichment of the Rehoboth mantle at the time of the collision of the Rehoboth Terrane and the Kaapvaal craton around 1.8 Ga has been proposed by Luchs et al. ((submitted) and Chapter 3) from Lu-Hf isotope systematics of garnet peridotites with sigmoidal garnet REE patterns from Gibeon Townsland and Hanaus. The time of this enrichment event by melts or fluids is also seen in the U-Pb zircon ages which peak around 1.8 to 1.9 Ga. The zircons have a large spread of εHf(*t*) with mostly negative values. This means major reworking of older crustal components (which may be as old as 2.5 Ga) at that period of time. Mixing of different crustal sources is the most probable reason for the vertical spread in εHf(*t*) values at this time. The age pattern of Cornell et al. (2011) from granitic cobbles, separated from Dwyka tillites in Rietfontein show a distinctive gap between 1.4 and 2 Ga, which lead them to a geotectonic model for the evolution of the assembly of the southern African terranes in which the Kheis thrust complex formed at around 1.2 Ga. As our sample area is far more north of Rietfontain, the existence of such ages that correspond to the Kheis belt in our sample set could mean that the evolution of the crustal domains of the different areas inside of the Rehoboth Terrane could have been different. Another explanation would be that the sampling sites of the tillites were not affected by the enrichment event that affected the underlying mantle.

Our data shows a distinctive gap of ages between 1.4 and 1.7 Ga which is in accordance with the results of Van Schijndel et al. (2011a). They interpreted this time interval as a quietsome period within the Rehoboth Terrane without significant magmatism, which seems to be valid for at least a large part of the Terrane.

Becker et al. (2006) proposed a northeast-directed subduction underneath the Kalahari Plate, starting with tonalitic intrusions around 1.37 Ga, followed by the Namaqua Orogeny around 1.1 Ga. We have a large cluster of ages from 1.5 to 1.1 Ga which could be related to this event. The data stems from all of the samples, whereas a major part comes from one sample that derived from a carbonatite vent associated to the Gross Brukkaros and from one crustal xenolith collected on the Louwrensia kimberlite pipe. Juvenile crustal growth started around 1.4 to 1.5 Ga. This crust has been recycled until 1.0 Ga, which can be observed from the εHf(*t*) values in

our data. At around 1.2 Ga, there is a large number of samples with a vertical spread in εHf(*t*) values. At this time, terranes of the later created Namaqua belt started to accret along the western border of the Rehoboth Terrane. Preexisting crust from these terranes has probably been mixed with crust from the Rehoboth Terrane and created the vertical crust evolution array (Becker et al., 2006).

The matrix sample from the Louwrensia Kimberlite pipe and one xenolith from the carbonatite pipe K3e, have a larger zircon population with ages between 1.1 and 0.9 Ga and with εHf values centering around +5 below the evolution curve for a depleted mantle. The ages correspond to the younger time of the Namaqua orogeny. Luchs et al. (submitted; see also Chapter 1) determined a mantle enrichment event underneath the Gibeon of 850 Ma which comes close to this event.

4.7. Conclusions

The Gibeon kimberlite field shows evidence for multiple large scale geotectonic events as recorded in the crustal xenoliths from carbonatite and kimberlite pipes and one sample collected from the detritus of the Louwrensia Kimberlite. It is also possible to make direct correlations of crustal events from this study to depletion and enrichment events in the mantle from a recent study (Luchs et al., submitted).

Our model for the evolution of the lower crust beneath Gibeon starts with the generation of Archean crust from a primitive mantle source which is in accordance to a new interpretation of Re-Os data (Pearson et al., 2004) by Luchs et al. (submitted) and recent studies from other regions of the Rehoboth Terrane (Cornell et al., 2011; Van Schijndel et al., 2011a), though it cannot be excluded that these zircons stem from the Kaapvaal craton as their model ages are in the range of the first crust generated in the Kaapvaal craton around 3.1 to 3.3 Ga. This episode is followed by juvenile crust generation around 2.3 to 2.7 Ga which was subsequently recycled during the attachment of the Rehoboth Terrane to the Kaapvaal craton around 1.8 to 1.9 Ga until it ended around 1 Ga. Recycling is supported by a Lu-Hf enrichment age of around 1.9 Ga of garnet peridotites from Gibeon (Luchs et al., submitted).

Crust generation around 1.2 to 1.5 Ga is probably related to a subduction process underneath the Kalahari Plate as proposed by Becker et al. (2006) and probably started around 1.8 Ga and marks the next greater crustal event within the southern African tectonic framework that did not affect the lithospheric mantle. Around 60 % of ages from this dataset lie in between this age range and support the significance of the event due to the high number of ages.

Juvenile crust was generated during the Namaquan Orogeny between 1.1 and 0.8 Ga which was subsequently recycled during the formation of the Damara belt at the time of the Pan African Orogeny.

Carbonatite and kimberlite derived xenoliths show slightly different age patterns, with a number of additional ages around 1.8 to 2.3 Ga for the latter. This age range is another confirmation for a palaeo-proterozoic Kheis Orogeny.

Our new crustal data, combined with geochronological data from garnet peridotites from Luchs et al. (submitted) further support the theory of pulsed crustal growth which is in contrast to a steady accumulation of newly grown crust through earth's history.

Our work on crustal xenoliths and a kimberlite matrix shows that the Gibeon volcanic field within the Rehoboth province is underlain by metamorphosed sediments which are not older than about 0.9 to 1 Ga without considering the age groups for the nama shale sediments. The metamorphosed sediments contain zircons from the two major tectonomagmatic events which were reported from outcrops to the north of the Gibeon field, namely of the Namaqua-Natal orogeny between 900 and 1200 Ma and from the Kheis-Maghondi event, mostly between 1700 – 1900 Ma (see compilation Janney et al., 2010). The sediments most have been deposited on older crust. The youngest possible age of this crust can be that of the Namaqua-Natal orogeny. It may be older and correspond to the Kheis-Maghondi event and it may even contain Archean components.

4.8. Acknowledgements

We owe thanks to H. Hoefer for assistance with the secondary electron microscope. A. Zeh is thanked for helpful discussions. For help during preparation, J. Heliosch and M. Krebs are thanked. This project was supported by the Deutsche Forschungsgemeinschaft, grant BR 1012/37-1.

4.9. References

Aquitaine, 1971. Aquitaine SWA and De Beers Oil Holdings well log. Open File Rep. Geological Survey of Namibia, MFN(0268/9).

Becker, T., Schreiber, U., Kampunzu, A.B. and Armstrong, R., 2006. Mesoproterozoic rocks of Namibia and their plate tectonic setting. Journal of African Earth Sciences, 46(1-2): 112-140.

Blignault, H.J., Jackson, M.P.A., Beukes, G.J. and D.J., T., 1974. The Namaqua tectonic province in South West Africa. Precambrian Res. Unit, Univ. Cape Town, Geol. Dep. Bull., 15: 29-47.

Bouvier, A., Vervoort, J.D. and Patchett, P.J., 2008. The Lu-Hf and Sm-Nd isotopic composition of CHUR: Constraints from unequilibrated chondrites and implications for the bulk composition of terrestrial planets. Earth and Planetary Science Letters, 273(1-2): 48-57.

Chauvel, C. and Blichert-Toft, J., 2001. A hafnium isotope and trace element perspective on melting of the depleted mantle. Earth and Planetary Science Letters, 190(3-4): 137-151.

Cornell, D.H. et al., 2011. Evidence from Dwyka tillite cobbles of Archaean basement beneath the Kalahari sands of southern Africa. Lithos, 125(1-2): 482-502.

Davies, G.R., Spriggs, A.J. and Nixon, P.H., 2001. A non-cognate origin for the Gibeon kimberlite megacryst suite, Namibia: Implications for the origin of Namibian kimberlites. Journal of Petrology, 42(1): 159-172.

Franz, L., Brey, G.P. and Okrusch, M., 1996a. Reequilibration of ultramafic xenoliths from Namibia by metasomatic processes at the mantle boundary. Journal of Geology, 104(5): 599-615.

Franz, L., Brey, G.P. and Okrusch, M., 1996b. Steady state geotherm, thermal disturbances, and tectonic development of the lower lithosphere underneath the Gibeon Kimberlite Province, Namibia. Contributions to Mineralogy and Petrology, 126(1-2): 181-198.

Gerdes, A. and Zeh, A., 2006. Combined U–Pb and Hf isotope LA-(MC-)ICP-MS analyses of detrital zircons: Comparison with SHRIMP and new constraints for the provenance and age of an Armorican metasediment in Central Germany. Earth and Planetary Science Letters, 249: 47-61.

Gerdes, A. and Zeh, A., 2009. Zircon formation versus zircon alteration - New insights from combined U-Pb and Lu-Hf in-situ LA-ICP-MS analyses, and consequences for the interpretation of Archean zircon from the Central Zone of the Limpopo Belt. Chemical Geology, 261(3-4): 230-243.

Hartnady, C., Joubert, P. and Stowe, C., 1985. Proterozoic Crustal Evolution in Southwestern Africa. Episodes, 8(4): 236-244.

Hoal, B.G., Hoal, K.E.O., Boyd, F.R. and Pearson, D.G., 1995. Age constraints on crustal and mantle lithosphere beneath the Gibeon kimberlite field, Namibia. South African Journal of Geology, 98(2): 112-118.

Jackson, S.E., Pearson, N.J., Griffin, W.L. and Belousova, E.A., 2004. The application of laser ablation-inductively coupled plasma-mass spectrometry to in situ U-Pb zircon geochronology. Chemical Geology, 211(1-2): 47-69.

Janney, P.E. et al., 2010. Age, Composition and Thermal Characteristics of South African Off-Craton Mantle Lithosphere: Evidence for a Multi-Stage History. Journal of Petrology, 51(9): 1849-1890.

Klama, K., Unpublished results. U-Pb Geochronologie, Hf Isotopie und Spurenelementgeochemie detritischer Zirkone aus rezenten Sedimenten des Orange- und Vaal River Flusssystems in Südafrika. PhD thesis, Goethe-Univ. Frankfurt, Germany: 179 pp.

Kurszlaukis, S., Franz, L. and Lorenz, V., 1998. On the volcanology of the Gibeon Kimberlite Field, Namibia. Journal of Volcanology and Geothermal Research, 84(3-4): 257-272.

Liati, A., Franz, L., Gebauer, D. and Fanning, C.M., 2004. The timing of mantle and crustal events in South Namibia, as defined by SHRIMP-dating of zircon domains from a garnet peridotite xenolith of the Gibeon Kimberlite Province. Journal of African Earth Sciences, 39(3-5): 147-157.

Luchs, T., Brey, G.P., A., G. and H.E., H., submitted. The lithospheric mantle underneath the Gibeon Kimberlite field (Namibia): a mix of old and young components - evidence from Lu-Hf and Sm-Nd systematics. Precambrian Research.

Ludwig, K.R., 2008. Isoplot 3.7: A geochronological toolkit for Microsoft Excel. Berkley Geochronology Center, Spec. Pub. No. 4: 1-77.

Morag, N., Avigad, D., Gerdes, A., Belousova, E. and Harlavan, Y., 2011. Detrital zircon Hf isotopic composition indicates long-distance transport of North Gondwana Cambrian-Ordovician sandstones. Geology, 39(10): 955-958.

Nagel, R., Warkus, F., Becker, T. and Hansen, B.T., 1996. U-Pb Zirkondatierungen der Gaub Valley Formation am Suedrand des Damara Orogens-Namibia und ihre Bedeutung fuer die Entwicklung des Rehoboth Basement Inlier. Zeitschrift fuer Geologische Wissenschaft, 24: 611.

Parman, S.W., 2007. Helium isotopic evidence for episodic mantle melting and crustal growth. Nature, 446(7138): 900-903.

Pearson, D.G., Irvine, G.J., Ionov, D.A., Boyd, F.R. and Dreibus, G.E., 2004. Re-Os isotope systematics and platinum group element fractionation during mantle melt extraction: a study of massif and xenolith peridotite suites. Chemical Geology, 208(1-4): 29-59.

Pearson, D.G., Parman, S.W. and Nowell, G.M., 2007. A link between large mantle melting events and continent growth seen in osmium isotopes. Nature, 449(7159): 202-205.

Rudnick, R.L. and Gao, S., 2003. Composition of the continental crust. In: Rudnick RL (ed) The crust. Treatise in Geochemistry 3: 1-64.

Rupprecht, P., unpublished results. Petrography, petrology and geochemistry of crustal xenoliths in kimberlites and carbonatites of the Gibeon Kimberlite Field, southern Namibia. PhD thesis: 326 pp.

Scherer, E., Munker, C. and Mezger, K., 2001. Calibration of the lutetium-hafnium clock. Science, 293(5530): 683-687.

Sircombe, K.N., 2004. AGEDISPLAY: an EXCEL workbook to evaluate and display univariate geochronological data using binned frequency histograms and probability density distributions. Computers & Geosciences, 30(1): 21-31.

Slama, J. et al., 2008. Plesovice zircon - A new natural reference material for U-Pb and Hf isotopic microanalysis. Chemical Geology, 249(1-2): 1-35.

Söderlund, U., Patchett, J.P., Vervoort, J.D. and Isachsen, C.E., 2004. The Lu-176 decay constant determined by Lu-Hf and U-Pb isotope systematics of Precambrian mafic intrusions. Earth and Planetary Science Letters, 219(3-4): 311-324.

Spriggs, A.J., 1988. An isotopic and geochemical study of kimberlites and associated alkaline rocks from Namibia. PhD thesis, University Leeds, England.

Stacey, J.S. and Kramers, J.D., 1975. Approximation of Terrestrial Lead Isotope Evolution by a 2-Stage Model. Earth and Planetary Science Letters, 26(2): 207-221.

Tankard, A.J. et al., 1982. Crustal evolution of southern Africa. 3.8 Billion Years of earths history. Springer Verlag, New York: 523 pp.

Tinker, J.H., de Wit, M.J. and Royden, L.H., 2004. Old, strong continental lithosphere with weak Archaean margin at similar to 1.8 Ga, Kaapvaal Craton, South Africa. South African Journal of Geology, 107(1-2): 255-260.

Van Schijndel, V., Cornell, D.H., Hoffmann, K.-H. and Frei, D., 2011a. Three episodes of crustal developement in the Rehoboth Province, Namibia. In: Van Hinsbergen, D.J.J., Buiter, S.J.H., Torsvik, T.H., Gaina, C., Webb, S. (Eds.), The formation and evolution of Africa from the Archaean to Present. Geol. Soc. Spec. Pub.

Van Schijndel, V., Cornell, D.H., Karlsson, L. and Olsson, J.R., 2011b. Baddeleyite geochronology and geochemistry of mafic cobbles from the Dwyka diamictite: New insights into the sub-Kalahari basement, South Africa. Lithos, 126(3-4): 307-320.

Ziegler, U.R.F. and Stoessel, G.F.U., 1991. Note: New constraints on the age of the Weener Intrusive Suite, the Gamsberg Granite and the crustal evolution of the Rehoboth Basement Inlier, Namibia. Communications Geological Survey of Namibia, 7: 75-78.

Chapter 5:

Lu-Hf, Sm-Nd and Sr isotope systematics of mantle xenoliths from Cabezo Negro de Tallante, Spain

5.1. Abstract

We have investigated clinopyroxenes, orthopyroxenes and plagioclases of spinel / plagioclase peridotites from the neogene volcano Cabezo Negro de Tallante in the South eastern volcanic province (Spain) for the major and trace element (clinopyroxene, orthopyroxene and plagioclase), as well as isotope characteristics (clinopyroxenes, plagioclases) with special regards to the Lu-Hf, Sm-Nd and Rb-Sr isotope system.

Three types of trace element patterns in the clinopyroxenes can be dinstiguished: the first are slightly depleted in light rare earth elements (LREE) and slightly enriched in middle rare earth elements, the second have flat REE patterns and the third are highly enriched in LREE.

Lu-Hf isotope systematics of the clinopyroxenes point towards a depletion event that might have occurred around 550 to 600 Ma ago. Older components could still be available as the model age of the most radiogenic sample is nearly Archean. Sm-Nd isotope systematics of the same minerals scatter but might still have retained the age of depletion, with data points scattering around the age obtained from Lu-Hf.

Sr isotope data of clinopyroxenes and plagioclases differ, with the clinopyroxenes having lower values that the plagioclases. The plagioclases have an isotopic signature corresponding to the alkaline melts that transported the mantle nodules to the surface, which means that the isotopic ratios of the plagioclases might have been changed by the rising alkaline melts.

5.2. Introduction

The neogene alkaline basaltic volcanism in the South eastern volcanic province (SEVP) of Spain is related to a young extensional phase in connection with the relative movements between the African and Iberian plate. Numerous mantle xenoliths have been transported to the surface by

the rising alkaline melts and have been the subject for several studies (e.g. Kogarko et al., 2001; Beccaluva et al., 2004; Bianchini et al., 2011).

Bellon et al. (1983) determined the K-Ar age of these to 2.6 to 2.8 Ma. The basalts and their explosive counterparts were erupted onto Permian mica shists.

The basalts and their tuffs carry abundant spinel and plagioclase peridotites, partly with amphibole and phlogopite, orthopyroxenites and amphibole, plagioclase and clinopyroxene megacrysts as well as some minor amount of crustal xenoliths.

However, not much is known about mantle depletion or enrichment processes and their timing in the mantle underneath the SEVP. A recent study of Bianchini et al. (2011) points towards a depletion process in the Proterozoic. These processes are key aspects for the understanding of the evolution of the whole lithosphere as the Iberian continent has experienced a complex tectonic history, including subduction and an extensional phase.

In this work, major and trace element as well as an isotope study of mantle peridotites and their corresponding minerals from Cabezo Negro de Tallante are presented. This volcano is situated within the SEVP in the Betic Cordillera. Our aim is to characterize the mantle underneath the SEVP for PT conditions, trace element content and to determine the time of depletion as well as the time of mantle metasomatism by Lu-Hf and Sm-Nd and Rb-Sr isotope systematics respectively. Sr isotope systematics of clinopyroxenes and plagioclases should enable us to clarify if the both mineral phases are cogenetic.

5.3. Geological background and previous work

Since the breakup of Gondwana, the African plate is showing a constant movement towards the north. It resulted in the convergence of the African and the Iberian plate, enclosing the Alboran microplate.

The subsequent evolution of the African-Alboran-Iberia region in the neogene is still highly disputed. Several models for the latest time span and the reason for the change from subduction like to intraplate like magmatism in the Alboran, the northern African and southern Spanish regions have been proposed from which we will only discuss the most important ones.

Eastward directed subduction of the Tethys slab is one possible scenario as proposed by e.g. Duggen et al. (2005). They suggested that slab derived fluids and melts caused subduction like magmatism. Roll back and delamination of subcontinental lithosphere is believed to be the process responsible for a westward migration of the subduction line, the extension of the basin and the upwelling of plume material, which is thought to have produced Si-poor and K-poor magmatism.

In contrast, Turner et al. (1999) suggest convective removal of lithospheric mantle beneath the Alboran basin to be the most likely process and to be responsible for extensional magmatism.

As an alternative scenario, the rising of a mantle diapir may have caused magmatism as proposed by Weijermars et al. (1985).

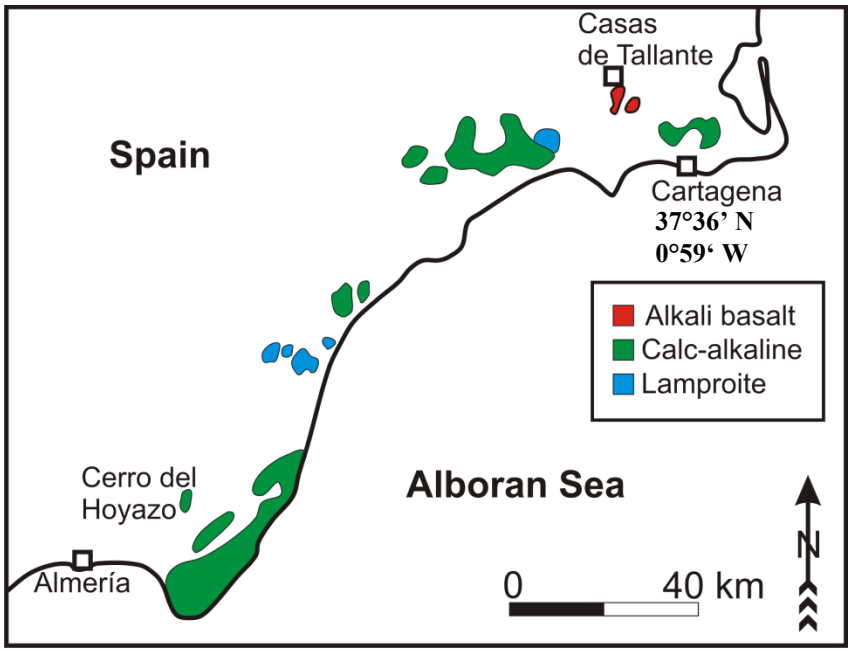

Fig.5.1: Map of the south-eastern coastline of Spain with the occurrences of neogene rocks that were emplaced into the Betic Cordillera. Marked in red are the alkali basalts together with Cabezo Negro de Tallante, from which the peridotites for this study were collected. Modified after Turner et al. (1999) and Venturelli et al. (1984).

Intraplate like magmatism also occurred in the south eastern coastline of Iberia, the south eastern volcanic province which forms part of the Betic cordillera.

The rocks related to the extensional phase of this African-Alboran-Iberian setting are made up of calc-alkaline, high-K calc alkaline and shoshonitish, ultrapotassic and alkaline basaltic volcanic rocks (see compilation Duggen et al., 2004).

Alkaline basalts are the most recent rocks in that area and were emplaced by phreatomagmatic eruptions, forming several small volcanic centers in the SEVP. Mantle xenoliths, megacrysts and crustal xenoliths, were entrained during the ascent of the magmas and can be collected on most of the outcrops.

Cabezo Negro de Tallante is one well-known volcano that was emplaced into the Permian mica shists 2.6 to 2.8 Ma ago (K-Ar; (Bellon et al., 1983)) and is situated close the small town of Tallante in the SEVP (Fig.5.1). A remarkable tuff layer can be found in between the basalts which has been deformed by volcanic bombs during the eruptions. The volcanic rocks contain numerous spinel and plagioclase lherzolithes with specimen sizes up to 20 cm, as well as megacrysts and few crustal xenoliths.

Mantle nodules from Cabezo Negro de Tallante have been the subject for several studies. The major part of the peridotites are spinel or plagioclase lherzolithes, with pressure and temperature ranges between 915 – 1030°C and 8 – 16 kbar respectively (Capedri et al., 1989; Beccaluva et al., 2004). Beccaluva et al. (2004) have subdivided the occurring peridotites into three groups: protogranular anhydrous spinel peridotites, amphibole/phlogopite-bearing harzburgites and orthopyroxenites with gabbronorite/anorthosite veinlets and amphibole/phlogopite bearing clinopyroxenites.

They often contain pyroxenite or gabbroic anorthosite veinlets which are due to their deformation and textural state not related to the alkaline basalts (Dupuy et al., 1986).

Diffusion profiles in minerals of spinel lherzolithes from Tallante by Kogarko et al. (2001) revealed that the peridotites ascended as a diapir with a velocity of 10 mm/a or less during a timeframe of about 3-4 Ma to a depths of 15 km in the crust before they were affected by the rising alkaline basalts that themselves have been molten in the garnet stability field (Dupuy et al., 1986). Mantle diapirism is also supported by investigations of spinel-pyroxene symplectites from Tallante (Shimizu et al., 2008).

They are thought to have been affected by two types of metasomatism, with one that has an anorogenic and another one with clear subduction related characters. This can be seen from the differently enriched Sr and Nd isotopic systematics of the xenoliths (Beccaluva et al., 2004).

Sr isotope ratios suggest that mantle xenoliths, megacrysts and the host alkaline basalts have different magmatic sources.

Based on major and trace element studies, a complex history of the upper mantle underlying Tallante has been suggested (Dupuy et al., 1986) with multiple melting events and metasomatism that may have produced heterogenous peridotite portions whitin very short scale distances.

Hafnium isotope studies of mantle peridotites by Bianchini et al. (2011) revealed a Hafnium model age of the most radiogenic sample of 1.6 Ga for CHUR and 1.28 Ga for the depleted mantle. No further age determinations considering the mantle underlying the SEVP are available.

The crustal framework of the deeper crust is still unknown. U-Pb investigations of zircons from a graphitic shist of the Alpine Alpujárride nappe complex (Zeck and Williams, 2001) and a dacite from Cerro del Hoyazo (Zeck and Williams, 2002) revealed a wide age spectra of the crust from 320 Ma to 2.8 Ga with distinct age groups in between and a gap from 1.2 to 1.8 Ga. As both areas are located within the Betic Cordillera, these results can be regarded as being a potential reference for the makeup of the lower crust beneath Cabezo Negro de Tallante.

5.4. Materials and Methods

Remaining fragments of the host alkaline basaltic rocks were removed with a stone saw from the plagioclase and spinel peridotites.

Thick sections of each sample were prepared for major and trace element analyses as well as for in-situ Strontium isotope ratio determinations.

5.4.1. Sample description

We have collected plagioclase and spinel peridotites from the hill slopes of Cabezo Negro de Tallante with sizes mostly between 5 and 10 cm. One sample (CNTP-11) was more than 20 cm

in its longest extension. Alteration status for all samples can be described as fresh. From the collected samples, we selected 11 samples with differing clinopyroxene modal abundances with the intention to analyse a sample set for the Sm-Nd, Rb-Sr and Lu-Hf isotope systems with the largest possible spread in these element ratios.

The samples are spinel / plagioclase peridotites with olivine, orthopyroxene, clinopyroxene, spinel and plagioclase. The amount of clinopyroxene varies, with CNTP-2 having the least amount. Plagioclase could only be found in the samples CNTP-3, 5, 7, 9, 11, with only 3 to 5 grains per thin section, whereas spinel was present in all samples.

According to the classification scheme of Beccaluva et al. (2004), which is based on petrographic descriptions and major and trace element contents of the peridotite xenoliths from Tallante, all our samples can be assigned to the protogranular anhydrous spinel-peridotites with clinopyroxene rich lherzolites that can contain plagioclase.

5.4.2. Major element analysis

First paragraph of the following descriptions for major element analysis are taken from chapter 3.4.1 as there is no difference in the set-up, configuration and method for the analysis of the major elements.

Major elements were determined in olivine, orthopyroxene, clinopyroxene and garnet with a Jeol JXA 8900RL Superprobe with five spectrometers in WDS mode with a beam size of 3 µm, an acceleration voltage of 15 kV and a probe current of 20 nA. For each sample and each mineral, three grains were analysed, with three analyses from core to rim to test for homogeneity. Peak measuring times varied between 20 to 30 s, background measuring times were 10 to 30 s. Standards were a mix of natural minerals and pure oxides and metals. CITZAF© algorithm by John T. Armstrong was used for matrix correction.

For the determination of Sr in Plagioclase, peak and background measurement times were increased to 40 s in order to lower the detection limit to about 400 ppm.

Calcium in olivine was determined as described by Koehler and Brey (1990) with peak and background measurement times increased to 120 s by using olivine SCKA as a secondary Ca standard. By applying this method, the detection limit for Ca was lowered to 30 ppmw (Koehler

and Brey, 1990). Average Ca concentrations in standard SCKA were around 524 ppm which is in perfect agreement to reference values as published by Koehler and Brey (1990).

5.4.3. Trace element analysis

Following descriptions for trace element analysis are taken from chapter 3.4.2 as set-up and configuration for the analysis are exactly the same.

Trace elements were analysed by Laser Ablation Inductively Coupled Plasma Mass Spectrometry (LA-ICPMS) using a Resonetics M-50 laser coupled with a Thermo-Finnigan® Element 2 at the Goethe University of Frankfurt.

Only unaltered and clear grains were considered for trace element analyses. For each sample, three grains of clinopyroxene and orthopyroxene were analysed with three laserspots from core to rim.

Analyses were performed with a spot size of 40 µm, an energy density of c. 4-6 Jcm^{-1} and a frequency of 10 Hz. We used as external standard a Nist 612 glass and CaO from microprobe analyses as an internal standard. Reference values for Nist 612 were taken from Pearce et al. (1997). The data were processed with the Gemoc GLITTER© software. USGS standard Bir-1G was always measured several times during an analytical session as secondary standard to monitor the machine performance and estimate the analytical precision and accuracy of the method. The obtained accuracy and precision for all analysed elements lie in the range of 2 to 15 %.

5.4.4. Sr isotope analyses of plagioclase

Strontium isotope analyses were performed using a Thermo Scientific Neptune multicollector ICPMS with Ni skimmer and sample cones coupled to a Resonetics M-50 laser. Spot sizes varied between 108 and 160 µm with a repetition rate of 12 Hz at 110 mJ. ^{87}Sr was corrected for interference with ^{87}Rb. The limited grain size of the plagioclase grains made it impossible to make core-rim measurements with the laser spots necessary for achieving a signal that is high enough for a good signal. Nevertheless, where possible, several measurements per grain were carried out. Several analyses of Mir A as a standard were carried out and average $^{87}Sr/^{88}Sr$ isotope ratios of 0.70308 were corrected to its reference value of 0.703096 as published by

Rankenburg et al. (2004). Additionaly, Nist 610 was measured at the beginning and the end of the session.

Errors (2 sigma) for $^{87}Sr/^{88}Sr$ range between 0.00003 to 0.00014.

5.4.5. Isotope dilution (ID) analyses – Lu-Hf and Sr and Sm-Nd

Based on their trace element patterns and the size of the hand specimens, samples were chosen for isotope dilution measurements considering Lu-Hf, Rb-Sr and Sm-Nd isotope systems.

Samples were crushed in a SelFrag® Lab system with a built-in sieve of 1 mm mesh size. Voltage was adjusted between 90 – 130 kV and electrode distance was reduced to a minimum level of 10 mm. Mineral separates were dried for several hours in a drying oven at 100°C followed by a separation with a Frantz magnetic separator and currents up to 1.6 A. Only clinopyroxenes with grain sizes smaller than 1 mm were considered during the handpicking process, using a stereomicroscope. Only clear fresh, unaltered and clean crystals were chosen for isotope dilution measurements.

Following descriptions for the preparation and the chromatographic separation are taken from chapter 3.4.3 with minor modifications as same procedures were used.

They were subsequently leached for 10 min in 2 M HCl which does not fractionate Hafnium or Neodymium isotopes as demonstrated by previous studies with 6 M HCl (DeWolf et al., 1996; Wittig et al., 2007). After rinsing with Milli-Q® H_2O, samples were re-examined and then cleaned with Milli-Q® H_2O in an ultrasonic bath for at least 1 hour. Each sample was weighed in and spiked with a ^{176}Lu-^{180}Hf and ^{149}Sm-^{150}Nd spike. Chemical separation of the desired elements was performed in one session ('batch') with 9 samples, including one column for a blank and one for standard BCR-1.

The samples were dissolved in 5 mL 3:1 HF (24 M): HNO_3 (15 M) solution in closed Savillex® teflon beakers at 120°C for 24 hours. Before fuming off, 150 µL of 11.6 M perchloric acid was added in order to prevent the formation of fluorides. After evaporation to dryness, the sample cake was re-dissolved in 6 M HCl and placed with the closed lid overnight on the hotplate at 120°C.

Samples were dried down and taken up in 3 M HCl in which 0.1 M ascorbic acid was added. Ascorbic acid is needed to reduce Fe^{3+} to Fe^{2+}, as Fe^{3+} may block the resin in the column

(Muenker et al., 2001). Before loading the columns, each sample was centrifuged in order to remove any possible left over inclusions.

For the separation of Lu and Hf we followed the procedures of Muenker et al. (2001), using Eichrom® Ln.spec resin. The procedures of Muenker et al. (2001), were slightly modified by omitting the zirconium washing step and by using 2 M HF instead of 6 M HCl with 0.2 M HF for collecting Hf. Washing out the zirconium would result in a partial loss of Hf, which is not desirable considering the low amounts of Hf down to 10 ng.

Following the procedures of Pin and Zalduegui (1997), light rare earth elements (LREE) and Sr were separated from the dissolved sample using Biorad 50Wx8 resin, while the separation of Sm and Nd were performed in Ln.Spec resin, using the same columns and digestion batch that were used for the Lu and Hf separation.

Because of the small amounts of samples, column sizes were reduced from conventional sizes to 1 mL resin volume for Ln.Spec columns and 1.5 mL in case of Biorad 50Wx8 columns.

Samples were measured using a Thermo-Finnigan® Neptune MC-ICPMS at the Goethe University Frankfurt with Ni x cones following the method described in Schmidt et al. (2008). In case of Lu and Hf isotope measurements a CETAC Aridus™ nebulization system (ca. 70 µL/min) was used to enhance sensitivity (e.g., Hf, 500-800 $Vppm^{-1}$). A conventional glass spray chamber was used as a sample introduction system for Sm and Nd. Procedural blanks were generally below 25 pg for Hf, below 10 pg for Lu, around 20 pg for Nd, and around 13 pg for Sm. Mass bias was corrected using of 0.7325 for the $^{179}Hf/^{177}Hf$ and 0.7219 for $^{143}Nd/^{144}Nd$ (Blichert-Toft et al., 1997). The mass bias for Yb was monitored with $^{173}Yb/^{171}Yb = 1.1248$ and used for interference correction of ^{176}Lu and ^{176}Yb on mass 176. JMC 475, Merck and Ames standards were measured during the analytical sessions to assure high quality isotope measurements of Hf and Nd isotopes. The comparison with published reference values (Blichert-Toft et al., 1997; Caro et al., 2006) shows that this was mostly achieved but a small offset correction had to be performed for Hf with isotope ratios of 0.282137 ± 0.000011 for $^{176}Hf/^{177}Hf$ before blank correction and 0.51174 ± 0.000025 for $^{143}Nd/^{144}Nd$ (Merck) and 0.51197 ± 0.000032 for $^{143}Nd/^{144}Nd$ (Ames).

Measurements of the standard BCR-1 yielded isotope ratios of 0.282875 ± 0.000011 for $^{176}Hf/^{177}Hf$ and 0.512667 ± 0.000025 for $^{143}Nd/^{144}Nd$. The measured ratios are in good agreement with published data for Hf (see compilation Chu et al. (2002)) and Nd (see

compilation Yang et al. (2010)). The data were processed using in-house Excel® spreadsheets. Age calculations, following isotope ratio calculations were performed using Isoplot 3.7 (Ludwig, 2008).

Due to non negligible amounts of Sr in the blanks, measured $^{86}Sr/^{87}Sr$ isotope ratios had to be corrected for their blanks. Routinely, after each sample measurement, blank concentrations were measured and substracted automatically by the Sequence editor software of the instrument. Strontium standard solution SRM987 and measured $^{86}Sr/^{87}Sr$ isotope ratios are in good agreement to literature data with ratios of 0.710145 ± 0.000011 (Balcaen et al., 2005) after blank correction.

Errors for Lu-Hf and Sm-Nd are error propagations of the spike calibration and standard analyses of the corresponding isotope ratios. For $^{176}Lu/^{177}Hf$ they are around 0.2 % (1 sigma), for $^{176}Hf/^{177}Hf$ they range around 0.0019 % (1 sigma). $^{147}Sm/^{144}Nd$ isotope ratios have an error around 0.2 % (1 sigma), whereas $^{143}Nd/^{144}Nd$ has an error of around 0.0023 % (1 sigma).

$^{87}Sr/^{88}Sr$ isotope ratios are afflicted by errors between 0.001 to 0.002 % (1 sigma).

5.5. Results

5.5.1. Pressure and Temperature estimates

We used the two pyroxene thermometer of Brey and Koehler (1990) in combination with the Ca in olivine barometer of Koehler and Brey (1990) to determine pressures and temperatures of crystallization. The results are given in Table 5.1 and shown in Fig. 5.2. Temperatures for all samples range between 900 and 1000°C and pressures from 7 to 20 kbar. Three samples plot within an area around 900 to 920°C and pressures between 7 to 10 kbar, five samples have temperatures from 940 to 960°C and pressures from 12 to 15 kbar, whereas the remaining three samples plot around 980°C with pressures around 16 to 20 kbar, following a smooth trend that does not correspond to a geothermal gradient.

A previous study of mantle xenoliths from Cabezo Negro de Tallante of Capedri et al. (1989) revealed pressures and temperatures around 8 to 15 kbar and 900 to 1050°C, giving a much

steeper trend. They used the pressure dependent thermometer of Nickel et al. (1985) and the barometer of Mercier (1980).

Table 5.1: Geothermobarometrical data, isotope characteristics and classification from the clinopyroxenes of the analysed samples.

Sample	T [°C]	P [Kbar]	$^{176}Lu/^{177}Hf$	$^{176}Hf/^{177}Hf$	$^{147}Sm/^{144}Nd$	$^{143}Nd/^{144}Nd$	$^{87}Rb/^{86}Sr$*	$^{87}Sr/^{86}Sr$	Type
CNTP-1	916	7.8	0.0322	0.283312	0.1868	0.512976	0.0053	0.703645	1
CNTP-2	983	16.1	0.0830	0.284920	0.1584	0.513103	0.0008	0.702774	2
CNTP-3	985	19.4	-	-	-	-	-	-	1
CNTP-4	957	14.0	0.0254	0.283597	0.2065	0.513222	0.0013	0.702622	1
CNTP-5	944	12.4	0.0364	0.283441	0.2107	0.513127	0.0198	0.702100	1
CNTP-6	955	12.9	-	-	-	-	-	-	2
CNTP-7	910	8.3	-	-	-	-	-	-	3
CNTP-8	975	16.3	0.0288	0.283558	0.2057	0.513116	0.0019	0.702778	2
CNTP-9	947	14.4	0.0314	0.283397	0.2270	0.513206	0.0119	-	1
CNTP-10	962	13.5	-	-	-	-	-	-	1
CNTP-11	916	9.5	0.0325	0.283411	0.2295	0.513248	0.0129	-	1
TL-1[1]	-	-	0.0272	0.283348	-	-	-	-	-

* calculated by the concentrations of Rb and Sr as determined by LA-ICPMS and their relative isotopic abundances

[1] from Beccaluva et al. (2004) and Bianchini et al. (2011); $^{176}Hf/^{177}Hf$ as given by Bianchini et al. (2011)$^{176}Lu/^{177}Hf$ calculated from the Lu and Hf concentrations as given by Beccaluva et al. (2004) and the natural abundance of the corresponding isotopes

Pressures as determined by Mercier (1980) are affected by a degree of uncertainty as the aluminum isopletes in the spinel stability field are not pressure dependent but only dependent on the temperature (Sachtleben and Seck, 1981).

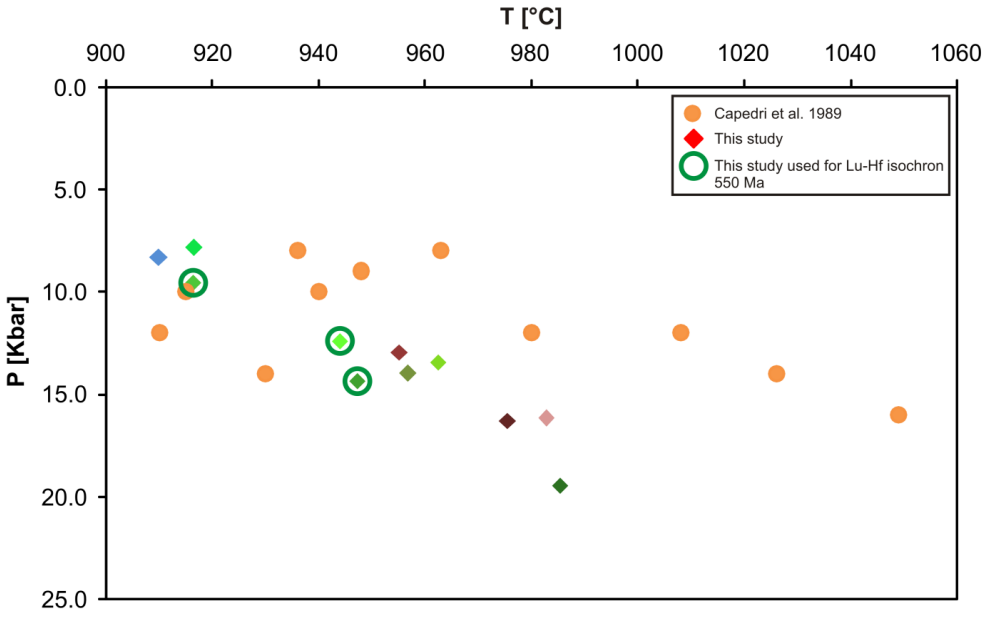

Fig.5.2: Pressures and temperatures as calculated by the two pyroxene thermometer of Brey and Koehler (1990) and Ca in olivine barometer of Koehler and Brey (1990) of this study (as marked by the diamond symbols) in comparison to P, T estimates as published by Capedri et al. (1989) (circles).

5.5.2. Plagioclase major element compositions

Plagioclases were measured from core to rim for samples CNTP-3, 5, 7, 9 and 11. The results are presented in Table A5.1 and Fig.5.2 .They are variable in their Albite and Anorthite contents, with $CaO/(CaO/Na_2O)$ compositions ranging from around 0.55 to 0.72. Core and rim compositions are very similar for all samples except for CNTP-7 with one grain having values from 0.55 to 0.61.

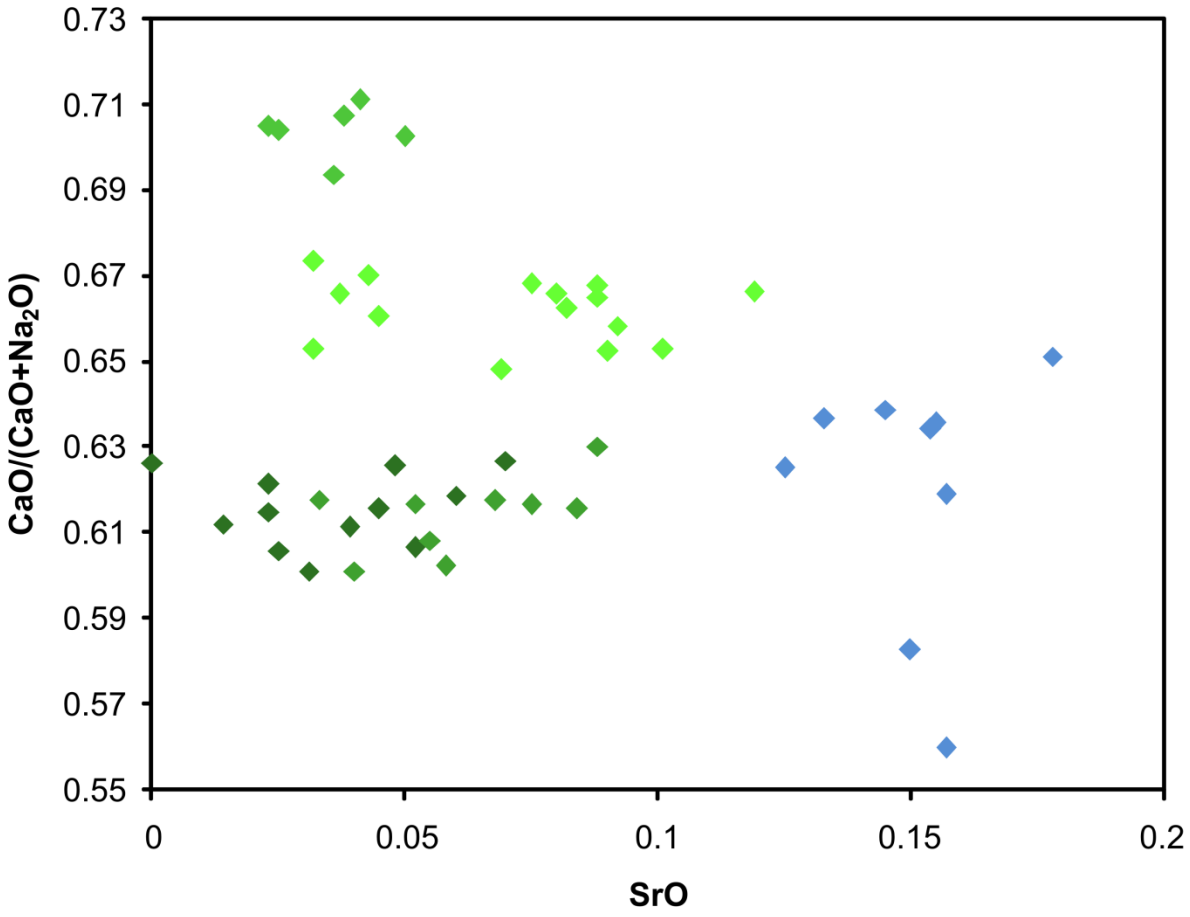

Fig.5.3: SrO concentrations as a function of the amount of Anorthite of the plagioclases analysed by Laser ablation ICPMS. Different colors of the diamond symbols are corresponding to the different types of samples, as defined earlier.

CNTP-5 and CNTP-11 have slightly higher Anorthite contents than CNTP 3, 7 and 9 with values from 0.65 to 0.72 in contrast to 0.55 to 0.63. SrO contents range from about 0.2 to about 0.18 wt%.

5.5.3. Trace elements

Trace elements were determined in clinopyroxene and orthopyroxene. They are given in Table A5.2 and shown as REE and extended trace element patterns in Fig 5.4 and Fig. 5.5.

We distinguish three types of rare earth element patterns which are not correlated with pressure and temperature.

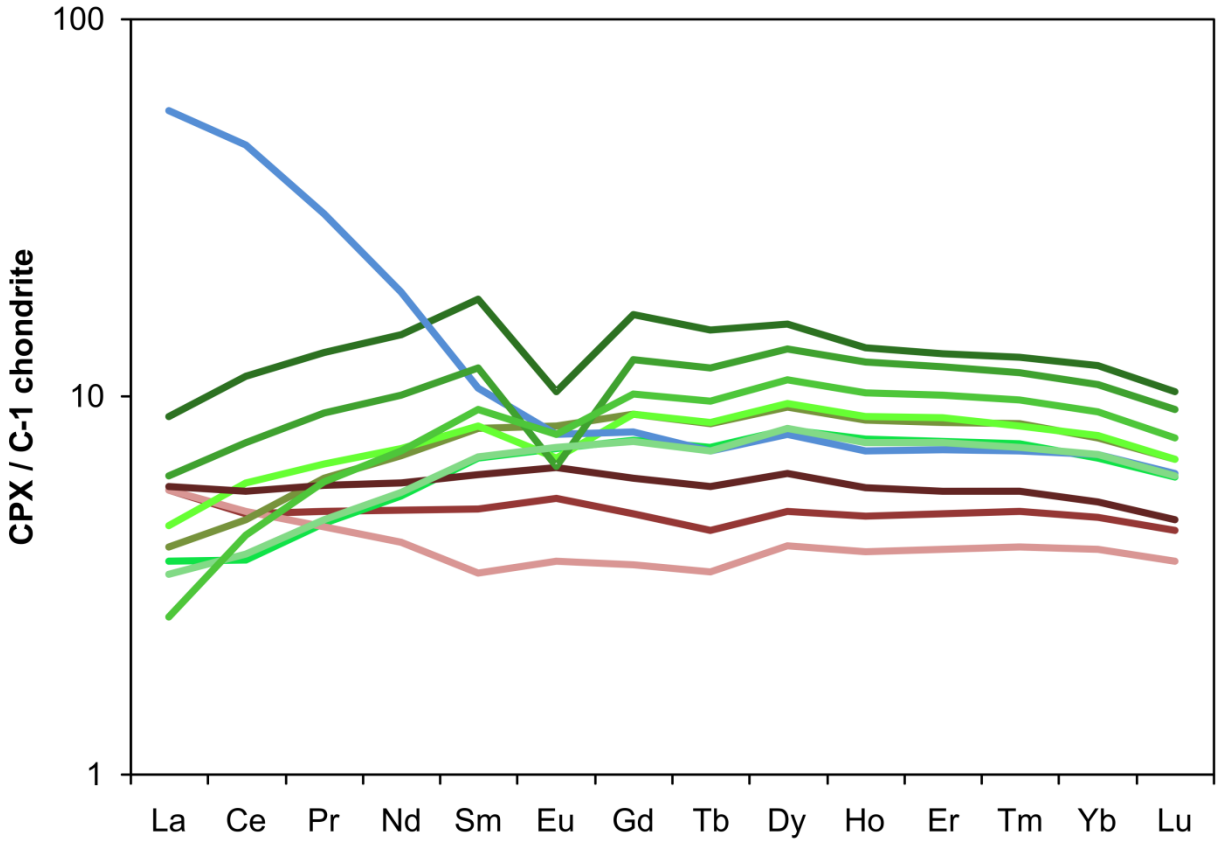

Fig.5.4: Rare earth element concentrations of the analyzed samples normalized to chondrite (McDonough and Sun, 1995). Three types of REE patterns are distinguished. Samples in green (type 1) have elevated MREE and slightly depleted LREE. Red lines correspond to samples with mostly flat REE patterns (type 2), while the blue sample shows highly elevated LREE contents (type 3).

Type one (shown in shades of green colors in Fig. 5.3) has elevated MREE and comparatively lower light and heavy REE, consisting of seven samples. Four out of these seven samples have strong Eu anomalies due to the presence of plagioclase. Sm_N/Yb_N ratios range from 0.98 to 1.49, indicating a minor enrichment for middle rare earth elements. Light rare earth elements show signs of minor depletion with La_N/Yb_N element ratios from 0.28 to 0.73.

Type two comprises three samples, shown in red colors here. The REE abundances are lower compared to type 1 and the patterns of two of the samples gently increase from Lu towards the LREE.

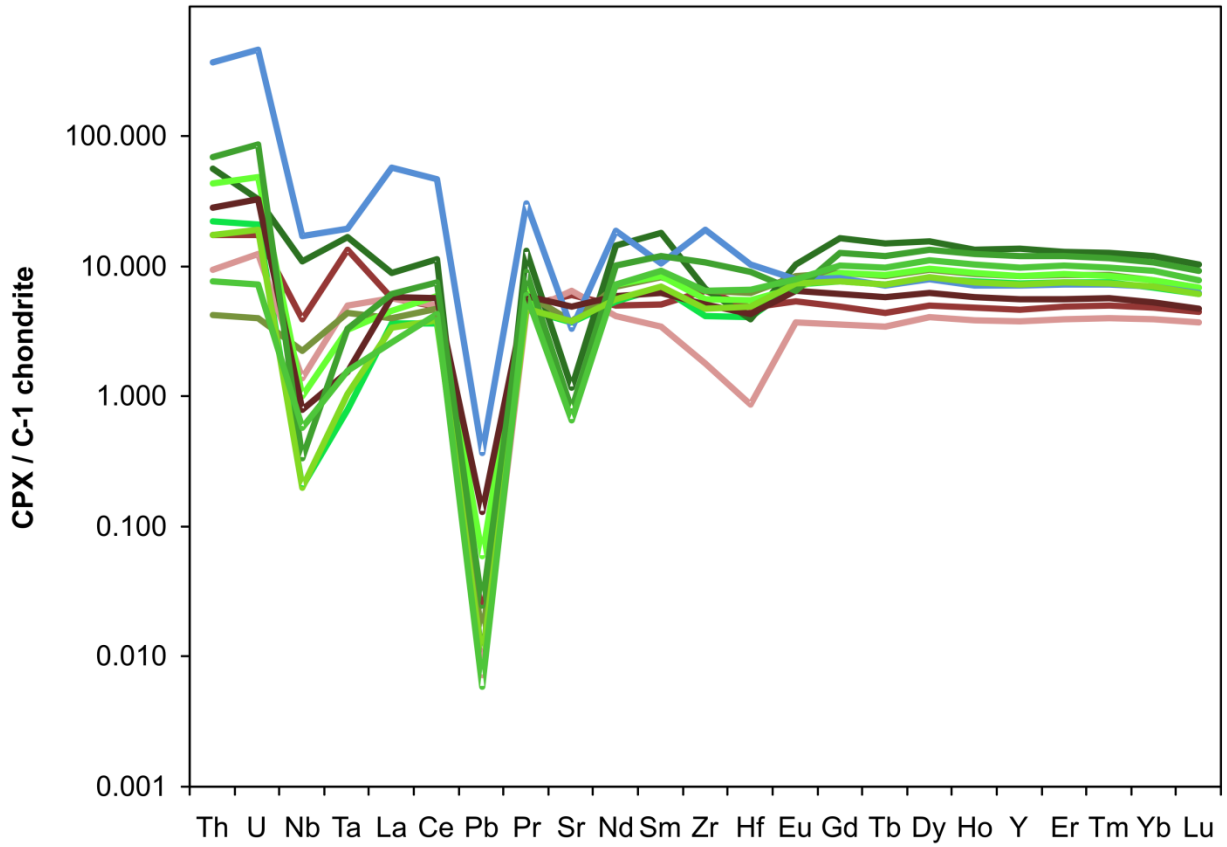

Fig.5.5: Extended trace element patterns of the three types of samples as distinguished by their REE patterns. Th and U contents vary by a factor of around 10 for all samples. Concentrations were normalized on C1 (McDonough and Sun, 1995).

An exceptional sample is sample CNTP-7 as shown in blue which defines type three. Most MREE and HREE overlap with Type 1 but the MREE increase steeply from Eu onwards to La which has a more than 60 times chondritic abundance.

Extended trace element patterns of the clinopyroxenes for all samples reveal elevated thorium and uranium contents with a scatter by a factor of 10, which is in accordance to published values of additional samples from Tallante by Rampone et al. (2010). Minor to strong negative Sr anomalies can be assigned to all samples of the first type. One sample of the second type shows a minor to negligible negative strontium anomaly, whereas the remaining two samples even have a slightly positive peak for strontium.

Hafnium contents range from +4 to +10 for all samples, except for sample CNTP-2 that has the lowest abundance of hafnium with a value below 1 to chondrite.

5.5.4. Isotope systematics

5.5.4.1. Lutetium-Hafnium

The analytical data are given in Table 5.1 and shown in Fig.5.6 in an isochron diagram.

$^{176}Lu/^{177}Hf$ ratios are generally very low, with ratios around 0.03 for six samples and 0.08 for one sample (CNTP-2), while $^{176}Hf/^{177}Hf$ ratios for six samples plot from 0.2832 to 0.2836 and for one sample (CNTP-2) at higher values around 0.2849. No obvious correlation regarding time constraints between all of the samples is possible due to scattering of the datapoints and the limited range in $^{176}Lu/^{177}Hf$.

All analysed clinoyproxene separates show radiogenic Hf isotopic compositions with εHf values around +25 which is higher than the present day value for the depleted mantle (Chauvel and Blichert-Toft, 2001). One sample (CNTP-2) is much more radiogenic, having an extremely high εHf value of around +75 (Fig.5.7).

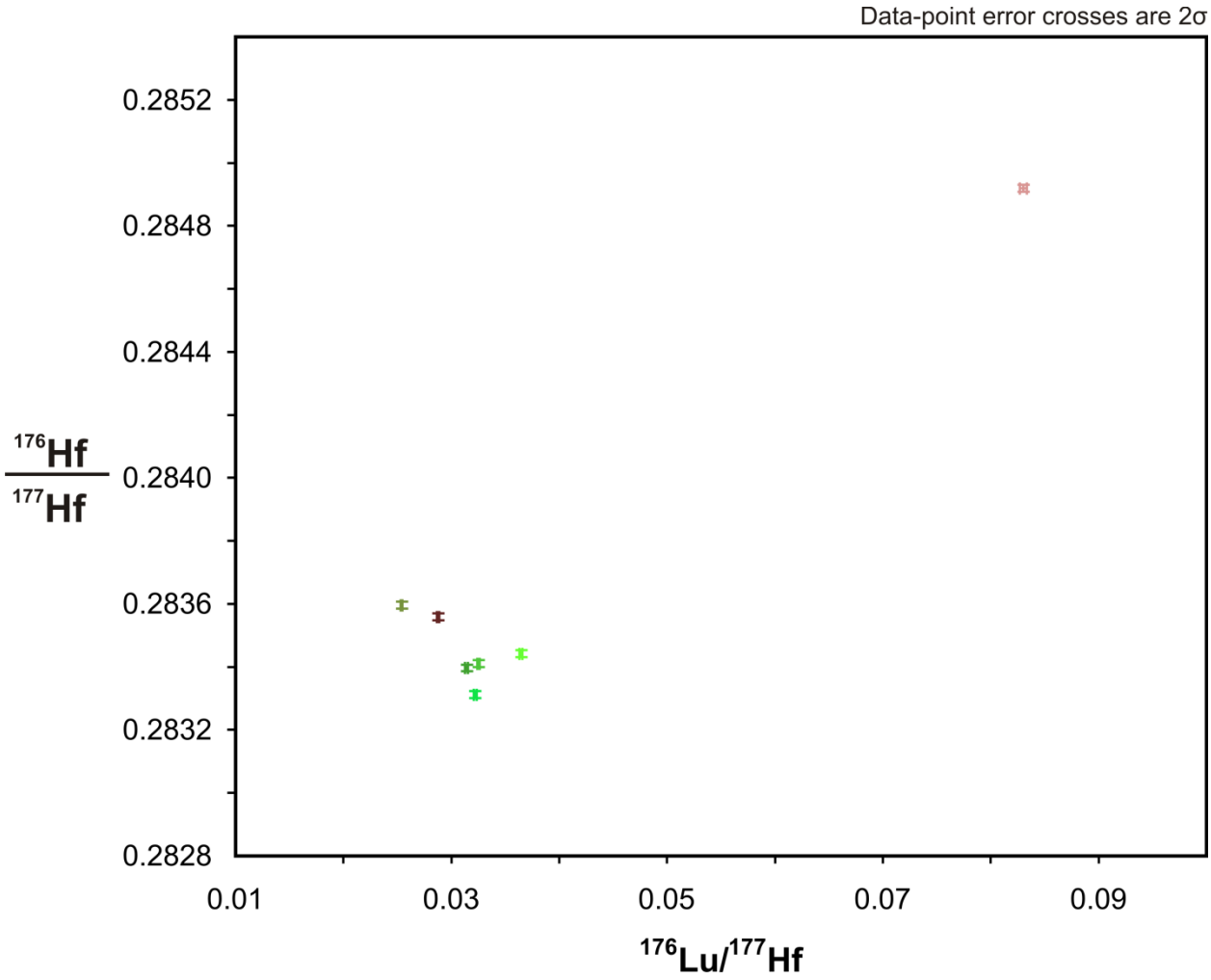

Fig.5.6: Lu-Hf isotope characteristics of the clinopyroxenes of seven samples analyzed from the samples of this study. Most samples are in the $^{176}Lu/^{177}Hf$ range around 0.02 to 0.04 and between 0.2832 and 0.2836 for $^{176}Hf/^{177}Hf$. Only one sample plots higher for both isotope ratios.

Model ages, considering CHUR and the depleted mantle as the source of melt extraction result in negative values due to the fact that most $^{176}Lu/^{177}Hf$ ratios of the samples are smaller than the $^{176}Lu/^{177}Hf$ ratio of the respective reservoir. Positive model ages could therefore be calculated for only two samples, with only one (CNTP-2) giving a possible meaningful model age of 2.0 and 2.2 Ga for the depleted mantle and CHUR respectively.

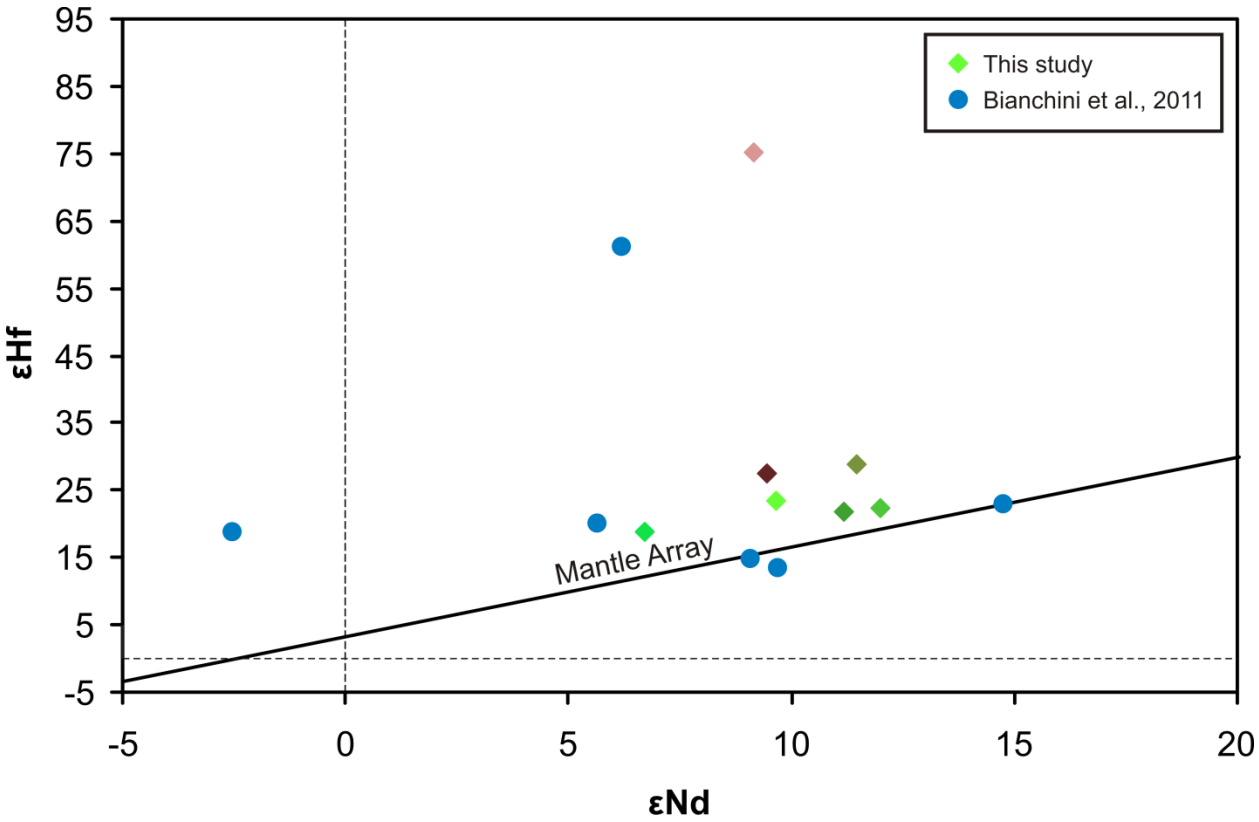

Fig.5.7: Hf versus Nd of own data (diamonds) and data from Bianchini et al. (2011) (circles). The mantle array was calculated, according to Vervoort et al. (1999).

5.5.4.2. Samarium-Neodymium

Isotope ratios of $^{147}Sm/^{144}Nd$ and $^{143}Nd/^{144}Nd$ are given in Table 5.1 and are visualized in Fig.5.8. There is no obvious linear correlation of the $^{147}Sm/^{144}Nd$ and $^{143}Nd/^{144}Nd$ isotope ratios when plotted into an isochron diagram. Only a rough trend can be obtained that does not allow precise isochron calculations. The projection of a 550 Ma reference isochron into the diagram shows that the data scatters around the projection. The scatter could be related to the narrow spread of $^{147}Sm/^{144}Nd$ isotope ratios or that the samples have experienced a minor enrichment that was not able to overprint the age of depletion.

Radiogenic neodymium isotope contents in the samples are moderate with εNd values ranging from +6 to +13. $^{147}Sm/^{144}Nd$ isotope ratios for all samples show a small spread, with ratios from 0.14 to 0.24. In contrast to the results for Lu-Hf, sample CNTP-2 does not show extraordinary

high radiogenic εNd values. In this case, the Sm-Nd and Lu-Hf isotope system seem to be decoupled (see Fig.5.7).

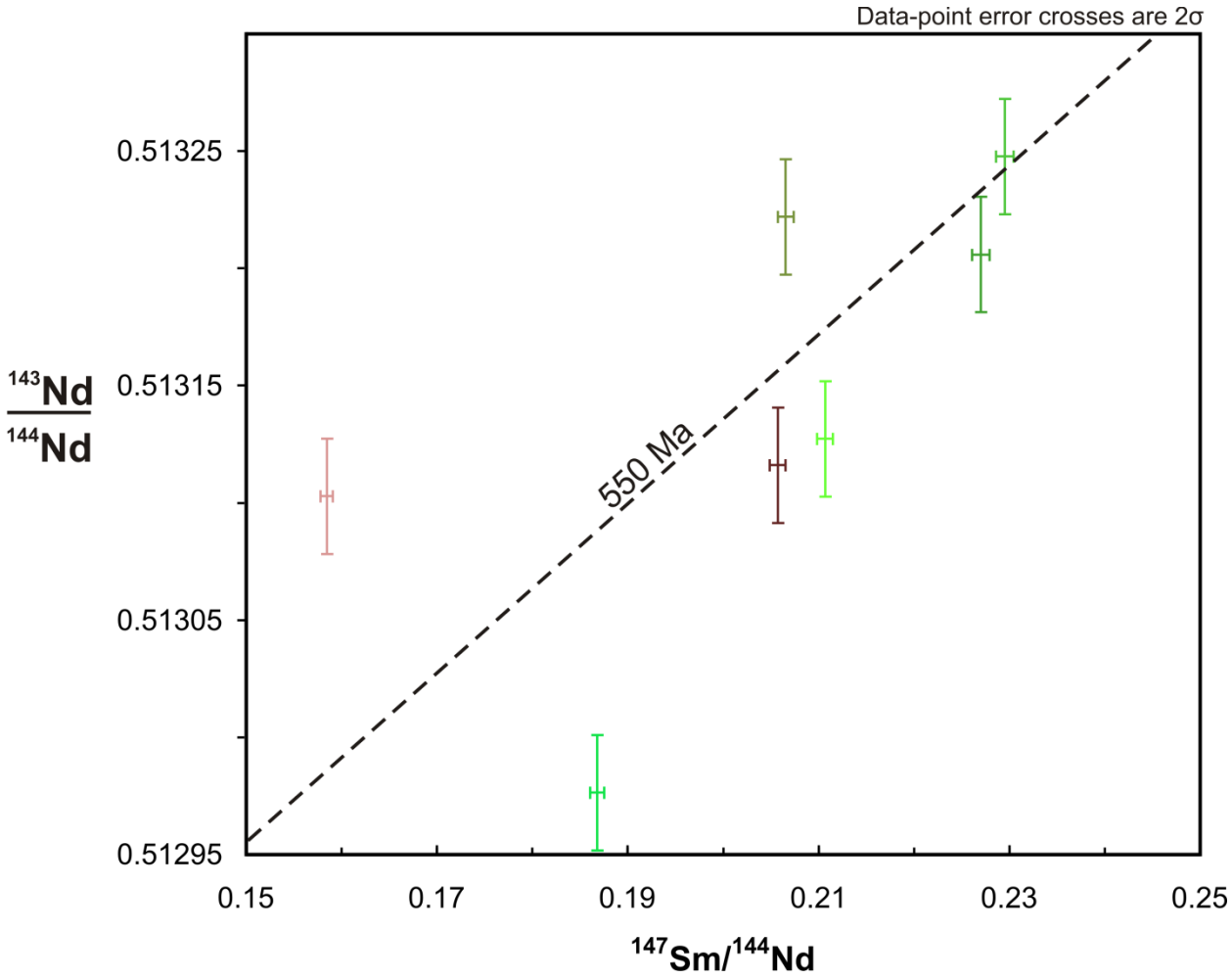

Fig.5.8: Sm-Nd isochron diagram with a reference isochron of 550 Ma

5.5.4.3. Strontium isotopes in clinopyroxene

The results are given in Table 5.2 and shown Fig.5.9. Only five samples could be analysed because of analytical problems (strong decrease of the signal during autosampler mode). $^{87}Rb/^{86}Sr$ ratios were calculated based on the corresponding concentrations as determined by LA-ICPMS. Four samples have calculated $^{87}Rb/^{86}Sr$ ratios between 0.0008 to 0.005, while an additional sample is around 0.019.

$^{87}Sr/^{86}Sr$ ratios vary, two samples have extreme $^{87}Sr/^{86}Sr$ ratios at 0.70210 and 0.70364, while three samples are in a very restricted range from 0.70262 to 0.70277. Any age correlations using

the isochron method are not applicable as the range is very narrow and no obvious trends or other correlations are visible.

5.5.4.4. Strontium plagioclase

The results are given in Table 5.2 and initial values are shown in Fig.5.9. Strontium isotope ratios could successfully be measured in-situ by laser ablation ICPMS in plagioclase of five samples.

Sample	$^{87}Rb/^{86}Sr$*	$^{87}Sr/^{86}Sr_{Rb}$	$^{87}Sr/^{86}Sr_{initial\ (600\ Ma)}$
CNTP3 plag1 p1	0.0389	0.70476	0.70443
CNTP3 plag1 p2	0.5817	0.70906	0.70408
CNTP3 plag2 p1	0.0324	0.70393	0.70365
CNTP3 plag2 p2	0.0398	0.70400	0.70366
CNTP3 plag4 p1	0.0665	0.70351	0.70294
CNTP3 plag5 p2	0.0732	0.70327	0.70265
CNTP3 plag5 p3	0.1070	0.70343	0.70251
CNTP5 plag1 p1	0.0044	0.70481	0.70477
CNTP5 plag1 p2	0.0045	0.70483	0.70479
CNTP5 plag2 p1	0.0058	0.70478	0.70473
CNTP5 plag2 p2	0.0068	0.70474	0.70468
CNTP5 plag3 p1	0.0059	0.70470	0.70465
CNTP5 plag3 p2	0.0068	0.70479	0.70473
CNTP5 plag4 p1	0.0117	0.70341	0.70331
CNTP5 plag4 p2	0.0091	0.70343	0.70335
CNTP5 plag5 p1	0.0109	0.70345	0.70336
CNTP5 plag5 p2	0.0181	0.70346	0.70331
CNTP7 plag4 p1	0.0106	0.70467	0.70458
CNTP7 plag4 p2	0.0109	0.70461	0.70452
CNTP7 plag5 p1	0.0073	0.70462	0.70456
CNTP7 plag5 p2	0.0322	0.70471	0.70444
CNTP7 plag5 p3	0.0114	0.70452	0.70443
CNTP7 plag5 p4	0.7389	0.71034	0.70401
CNTP7 plag5 p5	0.0160	0.70470	0.70456
CNTP7 plag6 p1	0.0081	0.70464	0.70457
CNTP7 plag6 p2	0.0085	0.70468	0.70460
CNTP9 plag2 p1	0.0061	0.70386	0.70380
CNTP9 plag2 p2	0.0066	0.70388	0.70382
CNTP9 plag5 p1	0.0350	0.70385	0.70355
CNTP9 plag5 p2	0.0199	0.70394	0.70377
CNTP9 plag6 p2	0.0076	0.70386	0.70380
CNTP11 plag1 p1	0.1186	0.70300	0.70199
CNTP11 plag1 p2	0.0081	0.70259	0.70252
CNTP11 plag1 p3	0.0090	0.70261	0.70254
CNTP11 plag4 p2	0.0081	0.70254	0.70247
CNTP11 plag4 p1	0.0054	0.70271	0.70267

* calculated

Table 5.2: Sr isotope systematics of the plagioclases. $^{87}Rb/^{86}Sr$ and $^{87}Sr/^{86}Sr_{Initial}$ ratios were calculated by the amount of Rb in the individual sample and based on an assumed equilibration age of around 600 Ma for the latter.

Strontium concentrations range from several hundred ppm up to 1300 ppm. Unfortunately, the Rb-Sr isotope systematics of clinopyroxenes could not be determined in the same samples by

solution MC-ICPMS because of analytical problems (strong decrease of the signal during autosampler mode) except for sample CNTP-5.

Where possible, several grains per sample have been measured. The $^{87}Sr/^{86}Sr$ istope ratios range between 0.70258 up to 0.70480. Calculated $^{86}Rb/^{87}Sr$ ratios are range in most cases from 0.0044 to 0.0732 with two exceptions showing values higher than 0.5

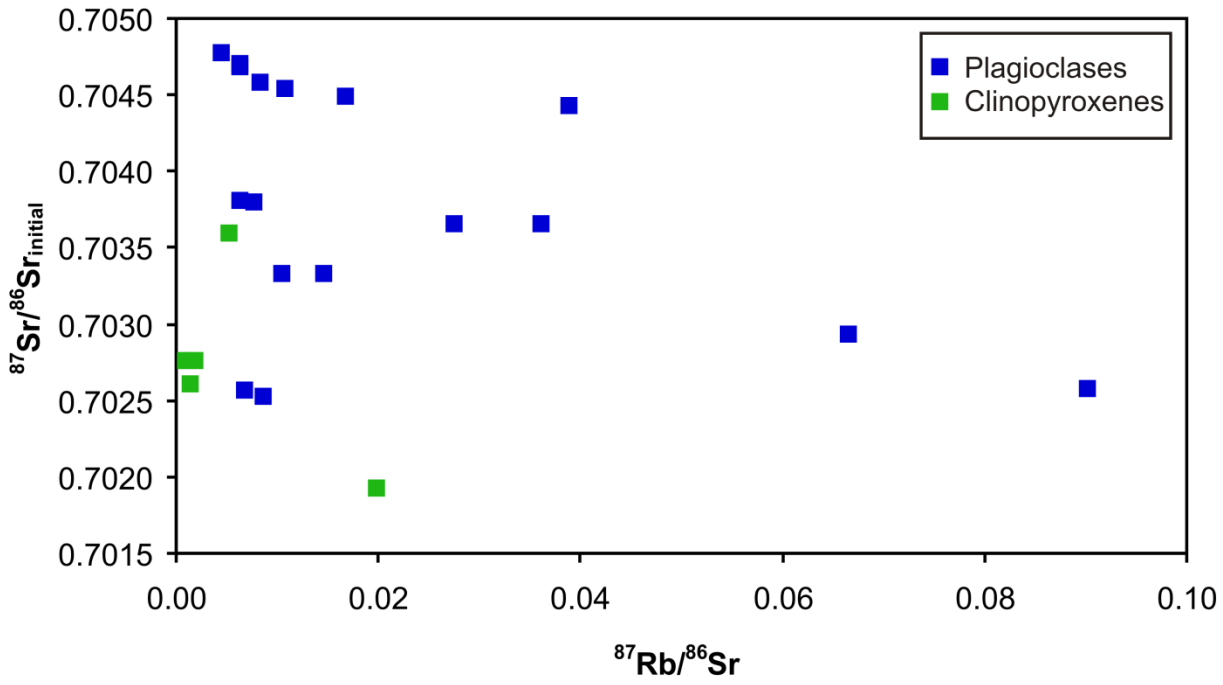

Fig.5.9: Initial $^{87}Sr/^{86}Sr$ isotope ratios of plagioclases and clinopyroxenes as calculated for t = 600 Ma, with the latter plotting in general in lower values than for the clinopyroxenes.

5.6. Discussion

Trace element characteristics

The plagioclase and spinel peridotites from Tallante analysed here contain a complex heterogenous record in their trace element patterns and isotopic compositions, even though they all stem from the same sample site at Cabezo Negro de Tallante.

The volcanic eruptions have transported mantle nodules with mostly similar chemical trace element compositions from different depths to the surface. Three types of rare earth patterns could be distinguished. Type 1 has slightly depleted LREE contents relative to its slightly elevated MREE. Type 2 shows flat REE patterns, while type 3 is highly enriched in LREE but the MREE and HREE follow the patterns of type 1.

Most samples show distinctive negative peaks for Ti and some show less pronounced negative anomalies for Zr.

These features in the trace element patterns of clinopyroxene in spinel peridotites have been interpreted in a former study as a worldwide distinct layer in the upper mantle which is depleted in high field strength elements (Rampone et al., 1991; Hellebrand et al., 2005). Rampone et al. (1991) showed that positive titanium and zirconium anomalies in corresponding trace element patterns of orthopyroxene compensate the depletion of the HFSE in clinopyroxene and thus no such depleted layer in the upper mantle exists. Furthermore, a depletion of HFSE in clinopyroxene would mean that a non negligible portion of hafnium is in the corresponding orthopyroxenes and that it would have to be considered for hafnium isotope analyses, depending on the modal amount of orthopyroxene in the peridotite. On the other hand Choi et al. (2010) have shown that the amount of Hf in orthopyroxene is insignificant for spinel peridoties. All of our clinopyroxenes show a depletion of titanium with a positive Ti peak in the patterns of the corresponding orthopyroxenes (Fig.5.10). A stronger negative zirconium anomaly in the clinopyroxene is only visible for CNTP-2 and 3 and minor to negligible negative zirconium anomalies are visible for the rest of the samples. Positive zirconium anomalies in orthopyroxene can be found in all samples. The same systematics can be found for Hf, with positive anomalies in orthopyroxene and negative anomalies in the corresponding clinopyroxene, meaning that an age calculated for these samples which is only based on the analysis of clinopyroxene is only a minimum age and must be slightly older, according to the modal abundance of orthopyroxene.

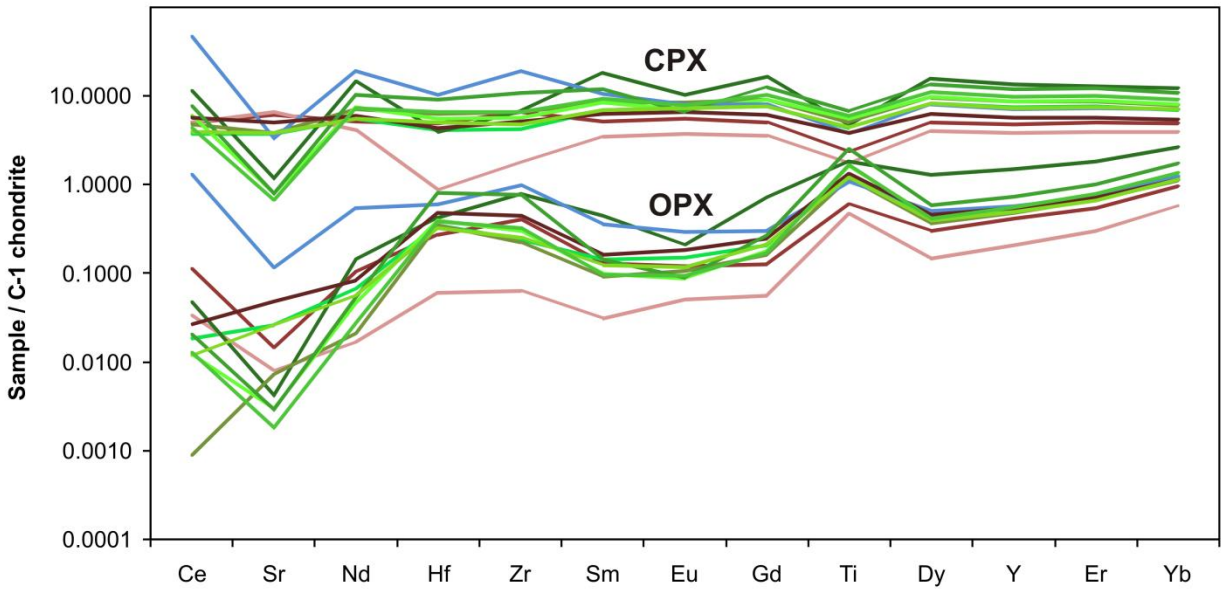

Fig.5.10: Trace element concentrations of clinopyroxene and orthopyroxene normalized to chondrite (McDonough and Sun, 1995) with visible negative Zr and Ti anomalies for the clinopyroxene and corresponding positive Zr and Ti anomalies for orthopyroxene.

In order to visualize depletion or enrichment trends of trace elements, we have normalized selected trace elements of our samples to the sample Vitim 314-56 (Ionov et al., 2005) which we consider as a primitive sample (Fig.5.11). Based on the HREE, we have retraced the former state of trace element partitioning, as indicated by the colored fields.

LREE are elevated for all three sample types, as indicated by the arrows in blue, green and red.

Group 1 and 3 samples are slightly elevated for the MREE, whereas group 2 samples plot around 1 or slightly below. Hf does not seem to be enriched except for minor additions to CNTP-7 and CNTP-9. Considering that some Hafnium is retained in orthopyroxene, whole rock contents of Hf could be higher or in extreme cases even enriched. For Sm and Nd, obvious enrichment can only be seen for sample CNTP-7. This means that age correlations for all other samples, except for CNTP-7, considering the Sm-Nd isotope system could be related to the age of depletion unless there was a fractionation or other disturbances of the system.

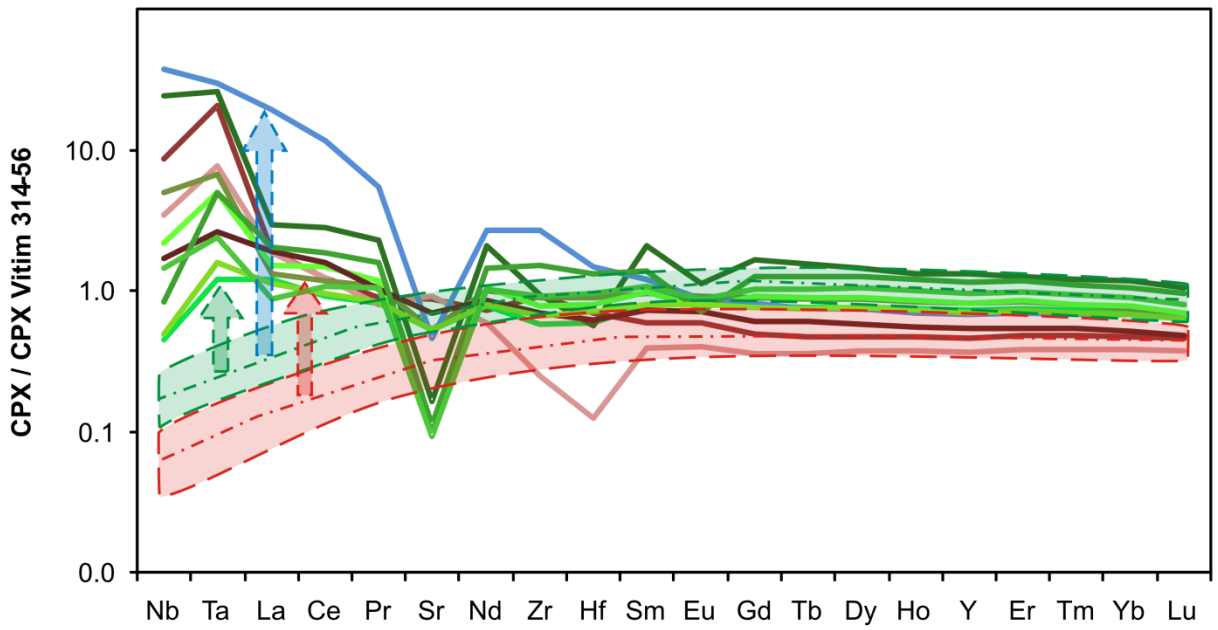

Fig.5.11: Trace elements normalized to corresponding clinopyroxene concentrations of the primitive sample Vitim 314-56 (Ionov et al., 2005). The green arrow displays enrichment relative to Vitim 314-56 for group 1 samples, the red arrow displays enrichment for group 2 samples and the blue arrow if for the group 3 sample.

Time constraints

We have analyzed Hafnium isotope systematics of clinopyroxenes in order to calculate the timing of mantle depletion. Our main assumption was that clinopyroxene is the main carrier of trace elements in the spinel / plagioclase lherzolithes. Our samples plot in a very narrow range for $^{176}Lu/^{177}Hf$ and $^{176}Hf/^{177}Hf$ ratios for most samples, and are thus very restricted in their spread.

Initial $^{176}Hf/^{177}Hf$ values of the clinopyroxenes were calculated in order to determine similar mantle sources to the melt extracted (Fig.5.12). Three samples out of this dataset (all type 1; CNTP-5,9,11) and one sample (TL1) that was published earlier in Bianchini et al. (2011), stem from the same mantle source when corrected for radiogenic ^{176}Hf contents with an estimated depletion age of around 600 Ma, which can be regarded as a reasonable age for the correction as this is the timing of the assembly of Gondwana.

Only $^{176}Hf/^{177}Hf$ ratios from the sample published by Bianchini et al. (2011) were available. The corresponding $^{176}Lu/^{177}Hf$ ratios were calculated from the content of Lu and Hf and the abundance of ^{176}Lu and ^{177}Hf, which creates a large error for the ratio but enabled us to use it for our age calculations.

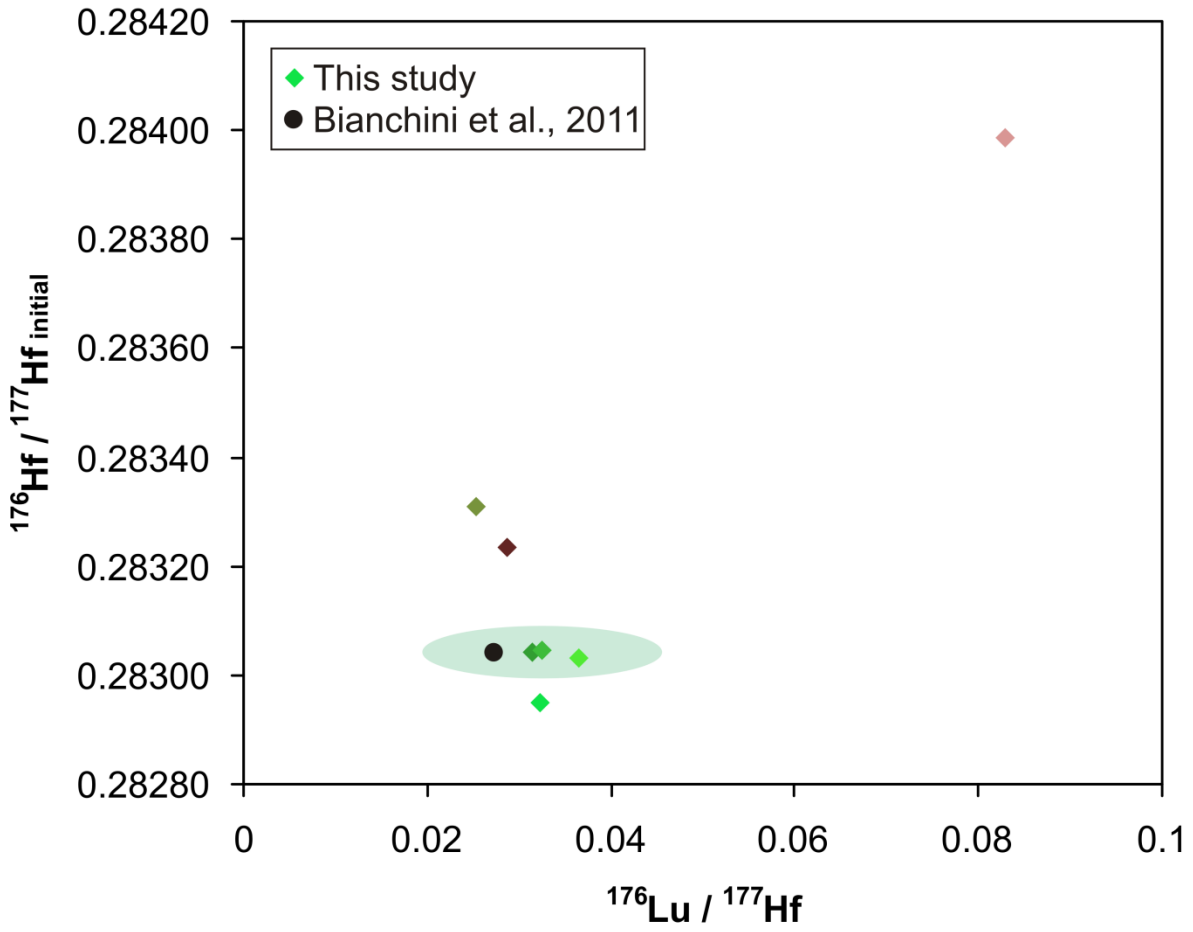

Fig.5.12: $^{176}Hf/^{177}Hf_{initial}$ ratios for all samples of this study and one sample (TL16) of Bianchini et al. (2011) as corrected for 600 Ma.

Present day $^{176}Hf/^{177}Hf_{initial}$ values of these samples are around 0.28303 to 0.28304 which correspond to around + 20 εHf units. A correlation of these samples in an isochron diagram resulted in an age of around 543 Ma, with a large error, due to the narrow $^{176}Lu/^{177}Hf$ range (Fig.5.13) and the high error of the $^{176}Lu/^{177}Hf$ ratio for sample 'TL1'. The elevated εHf initial value of around + 22 points towards a highly depleted mantle as the source of melt extraction. Because of the trace element characteristics of corresponding clinopyroxenes and

orthopyroxenes, as metioned before, the real age must be slightly older, depending on the modal amounts of orthopyroxene in the individual samples.

Another two samples from the dataset published in Beccaluva et al. (2004) and Bianchini et al. (2011) show a good agreement of initial $^{176}Hf/^{177}Hf$ isotopic compositions, which supports the idea of melt extraction around 550 to 600 Ma.

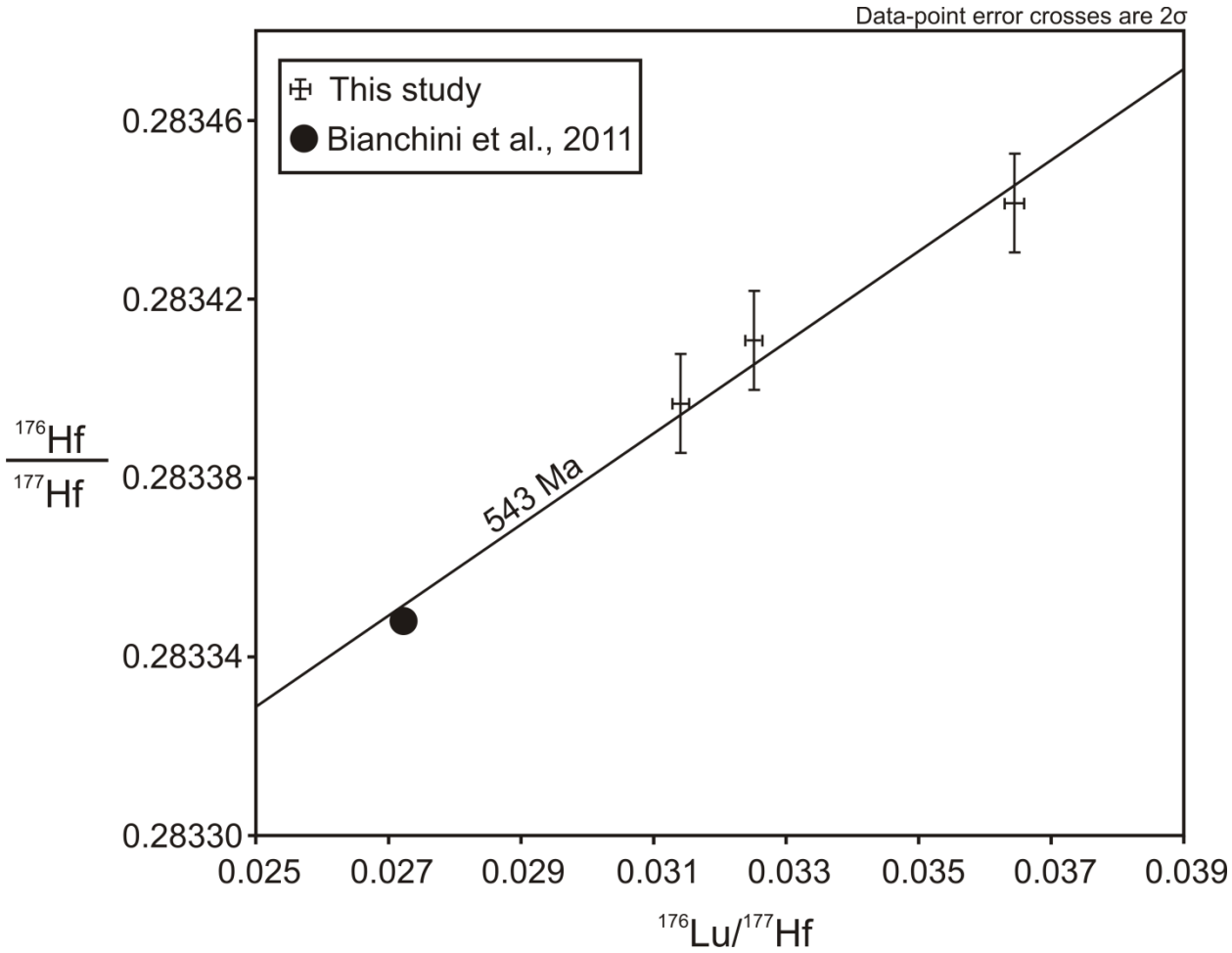

Fig.5.13 Lu-Hf reference Isochron of 543 Ma for three samples from this study and an additional one from Bianchini et al. (2011), with no errors displayed for the latter (see text).

Our remaining three samples do not show any correlation of initial values (0.2829 to 0.2833) or model ages and show that the mantle underneath Tallante seems to be very heterogenous with respect to its isotopic composition. The sample with the highest $^{176}Lu/^{177}Hf$ ratio shows initial $^{176}Hf/^{177}Hf$ ratios that cannot be correlated to any other sample and can therefore not be accounted for any isochron calculation in this dataset.

Except for CNTP-5 and CNTP-2, all other samples have $^{176}Lu/^{177}Hf$ values lower than the chondritic value or the depleted mantle and therefore result in negative model age. The most primitive sample of this dataset (CNTP-2) with very low Hafnium contents (0.16 ppm) is very radiogenic for Hafnium and has a Proterozoic model age for CHUR with 2.27 Ga and 1.97 Ga for the depleted mantle, suggesting an ancient mantle component. CNTP-5 has a negative model age for the depleted mantle but a model age of 1.11 Ga for CHUR.

As described before, Nd was slightly affected by enrichment due to mantle metasomatism. Isotope systematics of Sm and Nd therefore scatter and no reliable age for depletion or enrichment can be obtained. Nevertheless, a rough trend with an age of possibly 550 Ma between the data points can be correlated. Possibly this trend can be correlated to a depletion, given that the enrichment of Nd was not high enough to overprint the timing of depletion.

Similarities between the Ronda peridotite and different other European localities have been discussed in several other studies (e.g. Beccaluva et al., 2004; Bianchini et al., 2011). It has been shown by Beccaluva et al. (2004) that there is a great isotopic overlap of the Tallante anhydrous xenoliths, the Ronda peridotites (Reisberg et al., 1989), the Vulture peridotite xenoliths (Downes et al., 2002), Massif Central peridotite xenoliths (Downes and Dupuy, 1987; Zangana et al., 1997), Sardinia peridotite xenoliths (Beccaluva et al., 2001), Pyrenean peridotites (Downes et al., 1991) and the Lanzo Peridotites (Bodinier et al., 1991) concerning Neodymium and Strontium isotopic signatures. Multiple depletion events of the Rhonda peridotite have been dated to mid-Proterozoic ages (T_{RD}) by Re-Os in-situ laser ablation ICPMS analyses of sulfides (Marchesi et al., 2010). The existence of mantle components with similar ages underneath the SEVP are indicated by sample CNTP-2 with Hf model ages of 2.3 for CHUR and 2.0 for the depleted mantle and another sample from a study of Bianchini et al. (2011) with a Hf model age of 1.6 Ga for CHUR and around 1.2 Ga for the depleted mantle. Radiogenic Neodymium isotope systematics of different European localities that have been summarized by Downes (2001) may indicate a late Proterozoic to early Palaeozoic depletion event but are considered to be more a mixed signature of depleted and enriched xenoliths. Therefore the timing of depletion is estimated based on Os isotope systematics to range from 1.2 to 2 Ga.

Nature of metasomatism

Trace element enrichment due to mantle metasomatism can be seen from the trace element patterns of the clinopyroxenes by normalizing on a primitive spinel peridotite, which was for our samples a primitive sample from Siberia, reffered to as Vitim 314-56 by Ionov et al. (Ionov et al., 2005). A LREE enrichment has affected Nd compositions which are elevated in comparison to the corresponding HREE. Beccaluva et al. (2004) have differentiated between anorogenic and subduction related metasomatism of samples from Cabezo Negro de Tallante. Metasomatism was expressed in elevated $^{87}Sr/^{86}Sr$ and $^{143}Nd/^{144}Nd$ isotopic ratios. They found that a melt, undersaturated in silica produced typically $^{87}Sr/^{86}Sr$ ratios between 0.70213 and 0.70476 and $^{143}Nd/^{144}Nd$ ratios between 0.51339 and 0.5125. Metasomatism due to subduction with oversaturated silica characteristics is expressed in isotope ratios between 0.70672 and 0.70856 for $^{143}Nd/^{144}Nd$ and 0.51213 to 0.51211 for $^{87}Sr/^{86}Sr$. As already seen from the elevated light rare earth element contents, a minor enrichment has affected samples used for this study. Further confirmation comes from isotope analysis of clinopyroxene and plagioclase for Strontium, Samarium and Neodymium that are within the range as defined for anorogenic metasomatism by Beccaluva et al. (2004).

Correction of the clinopyroxenes for $^{87}Sr/^{86}Sr$ ratios for radiogenic ^{87}Sr due to the decay of ^{87}Rb for the calculation of $^{87}Sr/^{86}Sr_{initial}$ values for 600 Ma, has only a minor effect as the amount of Rb in most samples is nearly negligible. Four samples change in the fifth decimal place, whereas for one sample with the highest $^{87}Rb/^{86}Sr$ ratio, the change is on the third decimal place. $\varepsilon Sr_{initial}$ values are in the range between +45 and +69.

Plagioclase in anhydrous spinel peridotites are described as being the product of reequilibration of spinel under new P, T conditions (Bianchini et al., 2011). Therefore $^{87}Sr/^{86}Sr_{initial}$ ratios of clinopyroxenes and plagioclases can be compared if corrected for the same time since the last reequilibration.

Plagioclases corrected for radiogenic ^{87}Sr, due to the decay of ^{87}Rb for 600 Ma, changes the $^{87}Sr/^{86}Sr_{initial}$ values mostly in the fourth digital place, ranging from 0.70253 up to 0.70478. In two samples, there are two groups of plagioclase grains within one sample, having different $^{87}Sr/^{86}Sr_{initial}$ ratios. In CNTP-5 one group gives low values of 0.7034 and the other, 0.7047. For

CNTP-3, the lower values range from 0.7025 to 0.7036 and the higher have 0.7044. Plagioclases from sample CNTP-7 with highly enriched LREE in the clinopyroxenes also have high $^{87}Sr/^{86}Sr_{initial}$ values of 0.70478.

In general, Strontium isotope ratios of the plagioclases are elevated in comparison to the isotope dilution measurements of the clinopyroxenes. For sample CNTP-5, corresponding $^{87}Sr/^{86}Sr_{initial}$ ratios of clinopyroxene mineral concentrates are considerably lower with 0.70193.

$^{87}Sr/^{86}Sr$ isotope ratios of the alkali basalts from Cabezo Negro de Tallante have an average value of 0.70437, as determined by Capedri et al. (1989). It is therefore possible that the plagioclases of CNTP-7, CNTP-5 and CNTP-3 have been affected by the rising alkali basalts and changed their isotopic signature according to the infiltrating melts, whereas for CNTP-3 and CNTP-5, not all of the analyzed spots on the grains have such elevated values.

Kogarko et al. (2001) analyzed plagioclases of mantle xenoliths from Cabezo Negro de Tallante for Ca and Na compositions from core to rim. The cores of the plagioclases were more Na rich than the outer rim, being more calcic. Based on one concentration profile of their work, the rims have diameters around 10 – 20 µm. Due to the large diameter of the laser spots (> 100 µm) that we used in this study to determine Sr isotope systematics, rim composition could theoretically only be measured if the crystal was cut in the right orientation. Based on our results for major element compositions for the plagioclases, we do not see core-rim differences for the individual grains as described by Kogarko et al. (2001). Only for sample CNTP-7, the amount of SrO varies slightly with two points being slighty more rich in Anorthite, which is not expressed in $^{87}Sr/^{86}Sr$ isotopic ratios.

5.7. Conclusions

New Lu-Hf, Sm-Nd and Sr isotopic determinations have been carried out to shed new light into the development of the mantle underneath the SEVP and to reveal the timing of depletion and enrichment.

Three types of rare earth element patterns are characterisitic for the clinopyroxenes in this study, with an enrichment of light rare earth elements to different degrees for all three types. This

enrichment can also be detected from $^{87}Sr/^{86}Sr$ and $^{143}Nd/^{144}Nd$ isotope systematics and is related to anorogenic metasomatism as described by Beccaluva et al. (2004).

Our new studies of Lu-Hf isotope systematic suggest that the xenoliths sampled stem from several mantle domains with different geochemical characteristics and different timings of depletion.

Correlation of a group of samples indicates extraction during the Caledonian Orogeny, whereas two more samples suggest depletion in mid to late Proterozoic times. The latter are in agreement other localities all over the European continent (Beccaluva et al., 2001; Downes, 2001; Bianchini et al., 2007).

The timing of subsequent enrichment that has affected this sample set can neither be deciphered from Sm-Nd nor Sr isotopic systematics. The Sm-Nd istotopic system was probably reenriched during the ascent with the alkaline basalts in the Neogene but did not have enough time to reequilibrate, or the enrichment was not high enough. It seems that some of the samples even seem to have kept the isotopic record of depletion for Neodymium.

Strontium isotopic systematics of some rare plagioclase grains indicate that they have been more strongly affected by the alkaline basalts, as they kept the corresponding isotopic signature of the alkali basalts. Whereas Strontium isotopic systematics of the clinopyroxenes are in general lower and still have values corresponding to the mantle. Recalculated $\varepsilon Hf_{initial}$ values for clinopyroxenes and plagioclases differ, which is either related to the enrichment of the plagioclases by the infiltrating melts or the fact that their source of melt extraction is different.

5.8. Acknowledgements

We thank A. Neumann for help in the laboratory, J. Heliosch for the preparation of the sample mounts and M. Krebs for help with the mineral separation. This research was funded by DFG Grant BR 1012/37-1.

5.9. References

Balcaen, L., De Schrijver, I., Moens, L. and Vanhaecke, F., 2005. Determination of the Sr-87/Sr-86 isotope ratio in USGS silicate reference materials by multi-collector ICP-mass spectrometry. International Journal of Mass Spectrometry, 242(2-3): 251-255.

Beccaluva, L., Bianchini, G., Bonadiman, C., Siena, F. and Vaccaro, C., 2004. Coexisting anorogenic and subduction-related metasomatism in mantle xenoliths from the Betic Cordillera (southern Spain). Lithos, 75(1-2): 67-87.

Beccaluva, L. et al., 2001. Multistage evolution of the European lithospheric mantle: new evidence from Sardinian peridotite xenoliths. Contributions to Mineralogy and Petrology, 142(3): 284-297.

Bellon, H., Bordet, P. and Montenat, C., 1983. Chronology of the Neogene Magmatism from Betic Ranges (Southern Spain). Bulletin De La Societe Geologique De France, 25(2): 205-217.

Bianchini, G. et al., 2007. Evidence of diverse depletion and metasomatic events in harzburgite-lherzolite mantle xenoliths from the Iberian plate (Olot, NE Spain): Implications for lithosphere accretionary processes. Lithos, 94(1-4): 25-45.

Bianchini, G., Beccaluva, L., Nowell, G.M., Pearson, D.G. and Siena, F., 2011. Mantle xenoliths from Tallante (Betic Cordillera): Insights into the multi-stage evolution of the south Iberian lithosphere. Lithos, 124(3-4): 308-318.

Blichert-Toft, J., Chauvel, C. and Albarede, F., 1997. Separation of Hf and Lu for high-precision isotope analysis of rock samples by magnetic sector multiple collector ICP-MS. Contributions to Mineralogy and Petrology, 127(3): 248-260.

Bodinier, J.L., Menzies, M.A. and Thirlwall, M.F., 1991. Continental to Oceanic Mantle Transition-REE and Sr-Nd Isotopic Geochemistry of the Lanzo Lherzolite Massif. Journal of Petrology: 191-210.

Brey, G.P. and Koehler, T., 1990. Geothermobarometry in 4-Phase Lherzolites .2. New Thermobarometers, and Practical Assessment of Existing Thermobarometers. Journal of Petrology, 31(6): 1353-1378.

Capedri, S., Venturelli, G., Salviolimariani, E., Crawford, A.J. and Barbieri, M., 1989. Upper-Mantle Xenoliths and Megacrysts in an Alkali Basalt from Tallante, Southeastern Spain. European Journal of Mineralogy, 1(5): 685-699.

Caro, G., Bourdon, B., Birck, J.L. and Moorbath, S., 2006. High-precision Nd-142/Nd-144 measurements in terrestrial rocks: Constraints on the early differentiation of the Earth's mantle. Geochimica Et Cosmochimica Acta, 70(1): 164-191.

Chauvel, C. and Blichert-Toft, J., 2001. A hafnium isotope and trace element perspective on melting of the depleted mantle. Earth and Planetary Science Letters, 190(3-4): 137-151.

Choi, S.H., Suzuki, K., Mukasa, S.B., Lee, J.I. and Jung, H., 2010. Lu-Hf and Re-Os systematics of peridotite xenoliths from Spitsbergen, western Svalbard: Implications for mantle-crust coupling. Earth and Planetary Science Letters, 297(1-2): 121-132.

Chu, N.C. et al., 2002. Hf isotope ratio analysis using multi-collector inductively coupled plasma mass spectrometry: an evaluation of isobaric interference corrections. Journal of Analytical Atomic Spectrometry, 17(12): 1567-1574.

DeWolf, C.P., Zeissler, C.J., Halliday, A.N., Mezger, K. and Essene, E.J., 1996. The role of inclusions in U-Pb and Sm-Nd garnet geochronology: Stepwise dissolution experiments and trace uranium mapping by fission track analysis. Geochimica Et Cosmochimica Acta, 60(1): 121-134.

Downes, H., 2001. Formation and modification of the shallow sub-continental lithospheric mantle: a review of geochemical evidence from ultramafic xenolith suites and tectonically emplaced ultramafic massifs of western and central Europe. Journal of Petrology, 42(1): 233-250.

Downes, H., Bodinier, J.L., Thirlwall, M.F., Lorand, J.P. and Fabries, J., 1991. REE and Sr-Nd Isotopic Geochemistry of Eastern Pyrenean Peridotite Massifs: Sub-Continental Lithospheric Mantle Modified by Continental Magmatism. Journal of Petrology: 97-115.

Downes, H. and Dupuy, C., 1987. Textural, Isotopic and Ree Variations in Spinel Peridotite Xenoliths, Massif-Central, France. Earth and Planetary Science Letters, 82(1-2): 121-135.

Downes, H. et al., 2002. Geochemistry and Sr-Nd isotopic compositions of mantle xenoliths from the Monte Vulture carbonatite-melilitite volcano, central southern Italy. Contributions to Mineralogy and Petrology, 144(1): 78-92.

Duggen, S., Hoernle, K., Van den Bogaard, P. and Garbe-Schonberg, D., 2005. Post-collisional transition from subduction- to intraplate-type magmatism in the westernmost Mediterranean: Evidence for continental-edge delamination of subcontinental lithosphere. Journal of Petrology, 46(6): 1155-1201.

Duggen, S., Hoernle, K., van den Bogaard, P. and Harris, C., 2004. Magmatic evolution of the Alboran region: The role of subduction in forming the western Mediterranean and causing the Messinian Salinity Crisis. Earth and Planetary Science Letters, 218(1-2): 91-108.

Dupuy, C., Dostal, J. and Boivin, P.A., 1986. Geochemistry of ultramafic xenoliths and their host alkali basalts from Tallante, southern Spain. Mineralogical Magazine, 50(356): 231-239.

Hellebrand, E., Snow, J.E., Mostefaoui, S. and Hoppe, P., 2005. Trace element distribution between orthopyroxene and clinopyroxene in peridotites from the Gakkel Ridge: a SIMS and NanoSIMS study. Contributions to Mineralogy and Petrology, 150(5): 486-504.

Ionov, D.A., Blichert-Toft, J. and Weis, D., 2005. Hf isotope compositions and HREE variations in off-craton garnet and spinel peridotite xenoliths from central Asia. Geochimica Et Cosmochimica Acta, 69(9): 2399-2418.

Koehler, T.P. and Brey, G.P., 1990. Calcium Exchange between Olivine and Clinopyroxene Calibrated as a Geothermobarometer for Natural Peridotites from 2 to 60 Kb with Applications. Geochimica Et Cosmochimica Acta, 54(9): 2375-2388.

Kogarko, L.N., Ryabchikov, I.D., Brey, G.P., Santin, S.F. and Pacheco, H., 2001. Mantle rocks uplifted to crustal levels: Diffusion profiles in minerals of spinel-plagioclase lherzolites from Tallante, Spain. Geochemistry International, 39(4): 311-326.

Kohler, T.P. and Brey, G.P., 1990. Calcium Exchange between Olivine and Clinopyroxene Calibrated as a Geothermobarometer for Natural Peridotites from 2 to 60 Kb with Applications. Geochimica Et Cosmochimica Acta, 54(9): 2375-2388.

Ludwig, K.R., 2008. Isoplot 3.7: A geochronological toolkit for Microsoft Excel. Berkley Geochronology Center, Spec. Pub. No. 4: 1-77.

Marchesi, C., Griffin, W.L., Garrido, C.J., Bodinier, J.L. and Pearson, N.J., 2010. Persistence of mantle lithospheric Re-Os signature during asthenospherization of the subcontinental lithospheric mantle: insights from in situ isotopic analysis of sulfides from the Ronda peridotite (Southern Spain). Contributions to Mineralogy and Petrology, 159(3): 315-330.

McDonough, W.F. and Sun, S.S., 1995. The Composition of the Earth. Chemical Geology, 120(3-4): 223-253.

Mercier, J.C.C., 1980. Single-Pyroxene Thermobarometry. Tectonophysics, 70(1-2): 1-37.

Muenker, C., Weyer, S., Scherer, E. and Mezger, K., 2001. Separation of High field strength elements (Nb, Ta, Zr, Hf) and Lu from rock samples for MC-ICPMS measurements. Geochemistry Geophysics Geosystems, 2(10.1029/2001GC000183).

Nickel, K.G., Brey, G.P. and Kogarko, L., 1985. Orthopyroxene-Clinopyroxene Equilibria in the System Cao-Mgo-Al2o3-Sio2 (Cmas) - New Experimental Results and Implications for 2-Pyroxene Thermometry. Contributions to Mineralogy and Petrology, 91(1): 44-53.

Pearce, N.J.G. et al., 1997. A compilation of new and published major and trace element data for NIST SRM 610 and NIST SRM 612 glass reference materials. Geostandards Newsletter - the Journal of Geostandards and Geoanalysis, 21(1): 115-144.

Pin, C. and Zalduegui, J.F.S., 1997. Sequential separation of light rare-earth elements, thorium and uranium by miniaturized extraction chromatography: Application to isotopic analyses of silicate rocks. Analytica Chimica Acta, 339(1-2): 79-89.

Rampone, E., Bottazzi, P. and Ottolini, L., 1991. Complementary Ti and Zr Anomalies in Ortho-Pyroxene and Clinopyroxene from Mantle Peridotites. Nature, 354(6354): 518-520.

Rampone, E., Vissers, R.L.M., Poggio, M., Scambelluri, M. and Zanetti, A., 2010. Melt Migration and Intrusion during Exhumation of the Alboran Lithosphere: the Tallante Mantle Xenolith Record (Betic Cordillera, SE Spain). Journal of Petrology, 51(1-2): 295-325.

Rankenburg, K., Lassiter, J.C. and Brey, G., 2004. Origin of megacrysts in volcanic rocks of the Cameroon volcanic chain - constraints on magma genesis and crustal contamination. Contributions to Mineralogy and Petrology, 147(2): 129-144.

Reisberg, L., Zindler, A. and Jagoutz, E., 1989. Further Sr and Nd Isotopic Results from Peridotites of the Ronda Ultramafic Complex. Earth and Planetary Science Letters, 96(1-2): 161-180.

Sachtleben, T. and Seck, H.A., 1981. Chemical Control of Al-Solubility in Ortho-Pyroxene and Its Implications on Pyroxene Geothermometry. Contributions to Mineralogy and Petrology, 78(2): 157-165.

Schmidt, A. et al., 2008. Rapid eclogitisation of the Dabie-Sulu UHP terrane: Constraints from Lu-Hf garnet geochronology. Earth and Planetary Science Letters, 273(1-2): 203-213.

Shimizu, Y., Arai, S., Morishita, T. and Ishida, Y., 2008. Origin and significance of spinel-pyroxene symplectite in lherzolite xenoliths from Tallante, SE Spain. Mineralogy and Petrology, 94(1-2): 27-43.

Turner, S.P. et al., 1999. Magmatism associated with orogenic collapse of the Betic-Alboran Domain, SE Spain. Journal of Petrology, 40(6): 1011-1036.

Venturelli, G. et al., 1984. The ultrapotassic rocks from southeastern Spain. Lithos, 17: 37 - 54.

Vervoort, J.D., Patchett, P.J., Blichert-Toft, J. and Albarede, F., 1999. Relationships between Lu-Hf and Sm-Nd isotopic systems in the global sedimentary system. Earth and Planetary Science Letters, 168(1-2): 79-99.

Weijermars, R., Roep, T.B., Vandeneeckhout, B., Postma, G. and Kleverlaan, K., 1985. Uplift History of a Betic Fold Nappe Inferred from Neogene-Quaternary Sedimentation and Tectonics (in the Sierra Alhamilla and Almeria, Sorbas and Tabernas Basins of the Betic Cordilleras, Se Spain). Geologie En Mijnbouw, 64(4): 397-411.

Wittig, N., Baker, J.A. and Downes, H., 2007. U-Th-Pb and Lu-Hf isotopic constraints on the evolution of sub-continental lithospheric mantle, French Massif Central. Geochimica Et Cosmochimica Acta, 71(5): 1290-1311.

Yang, Y.H., Wu, F.Y., Xie, L.W. and Zhang, Y.B., 2010. High-Precision Measurements of the 143Nd/144Nd Isotope Ratio in Certified Reference Materials without Nd and Sm Separation by Multiple Collector Inductively Coupled Plasma Mass Spectrometry. Analytical Letters, 43(1): 142-150.

Zangana, N.A., Downes, H., Thirlwall, M.F. and Hegner, E., 1997. Relationship between deformation, equilibration temperatures, REE and radiogenic isotopes in mantle xenoliths (Ray Pic, Massif Central, France): An example of plume-lithosphere interaction? Contributions to Mineralogy and Petrology, 127(1-2): 187-203.

Zeck, H.P. and Williams, I.S., 2001. Hercynian metamorphism in nappe core complexes of the Alpine Betic-Rif belt, Western Mediterranean - a SHRIMP zircon study. Journal of Petrology, 42(7): 1373-1385.

Zeck, H.P. and Williams, I.S., 2002. Inherited and magmatic zircon from Neogene Hoyazo cordierite dacite, SE Spain - Anatectic source rock provenance and magmatic evolution. Journal of Petrology, 43(6): 1089-1104.

Chapter 6:

Combined U-Th-Pb and Hf isotope analyses of zircons from the South eastern volcanic Province (SEVP), Spain - evidence for intensive nappe stacking

6.1. Abstract

Zircons from three localities within the South Eastern volcanic Province (SEVP) were subject for this study. The aim was to obtain an age spectra of the underlying crust by U-Pb analyses and information about how the crust developed over time by Hf isotope analyses of the same spots on the corresponding zircon grains.

U-Pb analyses of all three localities are very similar and show a very large spread in ages from the Neogene to the Archean, with major age distributions around 0.3 to 0.4 Ga, 0.5 Ga and 0.6 to 0.7 Ga, while some minor age distributions are around 1 Ga to 1.1 Ga, 1.8 Ga to 2.2 Ga, 2.4 to 2.6 Ga and 2.9 to 3 Ga. Neogene ages are prominent in all localites with ages around 2.6 Ma and some minor age distributions from 4 to 8 Ma, reflecting eruption ages of the alkali basalts and Sr-K rich melts further to the Southwest of the SEVP.

Two major trends for crustal evolution from a depleted mantle source are visible from Hf isotope analyses, with the first starting from 1.0 to 1.5 Ga from the depleted mantle and being recycled during the Caledonian and Variscan events and the second starting in the Archean and being recycled at a time around 2.1 to 1.8 Ga. Mixing of different crustal sources occurred at a time around 0.5 to 0.6 Ga.

Most zircons are probably derived from a provenance region that is related to the time of the assembly of Gondwana, with some zircons being transported from the West African Craton and the Arabian Nubian shield.

Comparison to age results from other localities within the Betic Cordillera shows that the crust is a product of intensive nappe stacking.

6.2. Introduction

The Betic Cordillera and in particular the South Eastern Volcanic Province, has been the subject of many geological and geochemical studies. The interest stems from the changing geotectonic situations as a result of the relative movements of the African and the Ibearian plate with time and their ongoing convergence. The geotectonic situations resulted in a change of magmatism from subduction related calc-alkali magmatism to rift-related basaltic magmatism in the volcanic centers close to the village of Casas de Tallante.

The alkali basaltic eruptions at Cabezo Negro de Tallante have transported numerous (plagioclase-) spinel lherzolithe xenoliths together with amphibole, plagioclase and clinopyroxene megacrysts and crustal xenoliths to the surface, which were subject for several geochemical investigations (e.g. Dupuy et al., 1986; Schaefer et al., 2000; Kogarko et al., 2001; Rampone et al., 2010; Bianchini et al., 2011). The peridotites stem from a narrow temperature- and pressure range between 900 – 1000°C and 7 – 20 kbar respectively (see chapter 5.5.1). Kogarko et al. (2001) suggested that they were part of a rising mantle diapir which was metasomatized by melts similar to the host Si-poor, Na-rich alkali basalts / basanits up to tephrites and hawaiites (Duggen et al., 2003; Duggen et al., 2005). The timing of depletion of these mantle xenoliths has been, based on a Hf model age of one sample from Cabezo Negro de Tallante, estimated to be 1.6 Ga with respect to the CHUR (Chrondiritc Uniform Reservoir) (Bianchini et al., 2011). From own work (see chapter 5.6), we suggest an age of depletion to be around 450 Ma, based on a Lu-Hf isochron of three samples from own work and one sample of Bianchini et al. (2011) and Beccaluva et al. (2004).

Not much is known about the crust underneath the SEVP. Crustal rocks investigated are gneisses, graphitic schists, a dacit and its Al-rich restitic enclaves of more distant regions of the Betic Cordillera near Almería (Zeck and Whitehouse, 1999; Zeck and Williams, 2001; i.e. Zeck and Williams, 2002). The age distribution of the grains in these rocks is well documented by the work of these authors. It will serve as a comparison for our work on the zircon age distribution of the volcanics from the Tallante region. Thus we compare the crust from a subduction with a rift setting. The age of the crust underneath the SEVP is completely unknown. We therefore carried out U-Pb isotope measurements on zircons from tuff layers of three localities close to the village of Casas de Tallante combined with in situ Hf isotope analyses. Information should be obtained

on crustal evolution trends (juvenile crust accretion, crust recycling, crustal mixing), as well as provenance regions.

Additionally, the question whether components of detrital origin, e.g. Gondwana derived sediments are a part of the lower crust beneath the SEVP, should be considered. Previous studies have shown that the palaeoposition of Iberia during the assembly of Gondwana plays an important role in the structural makeup of the Iberian crust (Fernandez et al., 2010).

6.3. Geological Setting and previous work

The content of this chapter stems mostly from chapter 5.2 with minor modifications at the end.

Since the breakup of Gondwana, the African plate is showing a constant movement towards the north. It resulted in the convergence of the African and the Iberian plate, enclosing the Alboran microplate.

The subsequent evolution of the African-Alboran-Iberia region in the neogene is still highly disputed. Several models for the latest timespan and the reason for the change from subduction like to intraplate like magmatism in the Alboran, the northern African and southern Spanish regions have been proposed from which we will only discuss the most important ones.

Eastward directed subduction of the Tethys slab is one possible scenario as proposed by e.g. Duggen et al. (2005). They suggested that slab derived fluids and melts caused subduction like magmatism. Roll back and delamination of subcontinental lithosphere is believed to be the process responsible for a westward migration of the subduction line, the extension of the basin and upwelling of plume material, which is thought to have produced Si-poor and K-poor magmatism.

In contrast, Turner et al. (1999) suggest convective removal of lithospheric mantle beneath the Alboran basin to be the most likely process and to be responsible for extensional magmatism.

As an alternative scenario, the rising of a mantle diapir may have caused magmatism as proposed by Weijermars et al. (1985).

Intraplate like magmatism also occurred in the south eastern coastline of Iberia, the south eastern volcanic province which forms part of the Betic Cordillera.

The rocks related to the extensional phase of this African-Alboran-Iberian setting, are made up of calc-, high-K calc alkaline and shoshonitic, ultrapotassic and alkali basaltic volcanic rocks (see compilation Duggen et al., 2004).

Alkali basalts are the most recent rocks in that area and were emplaced by phreatomagmatic eruptions, forming several small volcanic centers in the SEVP. Mantle xenoliths, megacrysts and crustal xenoliths, were entrained during the ascent of the magmas and can be collected on most of the outcrops.

Cabezo Negro de Tallante is one well-known volcano that was emplaced into the Permian mica shists 2.6 to 2.8 Ma ago (K-Ar; (Bellon et al., 1983)) and is situated close the small town of Cases de Tallante in the SEVP (see Fig.5.1). A remarkable tuff layer can be found in between the basalts which has been deformed by volcanic bombs during the eruptions. The volcanic rocks contain numerous spinel and plagioclase lherzolithes with specimen sizes up to 20 cm, as well as megacrysts and few crustal xenoliths.

Mantle nodules from Cabezo Negro de Tallante were subject for several studies. The major part of the peridotites are spinel or plagioclase lherzolithes, with pressure and temperature ranges between 915 – 1030°C and 8 – 16 kbar respectively (Capedri et al., 1989; Beccaluva et al., 2004). Beccaluva et al. (2004) have subdivided the occurring peridotites into three groups: protogranular anhydrous spinel peridotites, amphibole/phlogopite-bearing harzburgites and orthopyroxenites with gabbronorite/anorthosite veinlets and amphibole/phlogopite bearing clinopyroxenites.

They often contain pyroxenite or gabbroic anorthosite veinlets which are due to their deformation and textural state not related to the alkali basalts (Dupuy et al., 1986).

Diffusion profiles in minerals of spinel lherzolithes from Tallante by Kogarko et al. (2001) revealed that the peridotites ascended as a diapir with a velocity of 10 mm/a or less during a timeframe of about 3-4 Ma to a depths of 15 km in the crust before they were affected by the rising alkali basalts that themselves have been molten in the garnet stability field (Dupuy et al., 1986). Mantle diapirism is also supported by investigations of spinel-pyroxene symplectites from Tallante (Shimizu et al., 2008).

They are thought to have been affected by two types of metasomatism, with one that has an anorogenic and another one with clear subduction related characters. This can be seen from the differently enriched Sr and Nd isotopic systematics of the xenoliths (Beccaluva et al., 2004).

Strontium isotope ratios suggest that mantle xenoliths, megacrysts and the host alkali basalts have different magmatic sources.

Based on major and trace element studies, a complex history of the upper mantle underlying Tallante has been suggested (Dupuy et al., 1986) with multiple melting events and metasomatism that may have produced heterogenous peridotite portions whitin very short scale distances.

Hafnium isotope studies of mantle peridotites by Bianchini et al. (2011) revealed a Hafnium model age of the most radiogenic sample of 1.6 Ga for CHUR and 1.28 Ga for the depleted mantle. No further age determinations considering the mantle underlying the SEVP are available.

The crustal framework of the deeper crust is still unknown. U-Pb investigations of zircons from a graphitic shist of the Alpine Alpujárride nappe complex (Zeck and Williams, 2001) and the xenoliths of a dacite from Cerro del Hoyazo (Zeck and Williams, 2002) revealed a wide age spectra of the crust from 320 Ma to 2.8 Ga with distinct age groups in between and a gap from 1.2 to 1.8 Ga. As both areas are located within the Betic Cordillera, these results can be regarded as being a potential reference for the makeup of the lower crust beneath Cabezo Negro de Tallante.

Samples for this study were collected from Cabezo Negro de Tallante (see Fig.5.1), a place next to the Highway close to San Isidro and Alto de las Cutandas, which are all alkali volcanic outcrops within a short scale distance of a few kilometers to each other, close to the town of Casas de Tallante.

6.4. Material and Methods

We have collected samples from three alkali basaltic outcrops within the SEVP Alto de Las Cutandas (ALCS), Cabezo Negro de Tallante (CNTS) and close to San Isidro (CG)). Samples were either taken from the tuff layers (ALCS, CNTS), which also contained mantle xenoliths or from the detritus of the disintegrated basalts (CG).

The samples were sieved in the field to grain sizes less than 1000 µm. These layers are very soft and could therefore be sieved very easy. The tuff layers contain numerous fragments of the

crust that they erupted through and zircons extracted from there were used to reconstruct a section through the lower crust.

In a further step, samples were deposited in which great care was taken in order not to lose a population with only few tens of µm in diameter, potentially containing zircons. Depositing was followed by heavy liquid segregation using bromoform with a density of 2.9 g/cm³ and subsequent treatment of the heavy mineral fraction with a Frantz® magnetic separator. Amperage of the instrument was increased up to 1.6 A in several lower steps before and only grains from more than 1.6 A were considered for further preparation steps. Mineral separates were treated with 6 M ultrapure HCl for one hour on a hotplate at 50°C in order to remove minerals such as apatite that can easily be mistaken for zircon and sieved with mesh sizes of 50 µm and 100 µm. For each sample, sieve fractions with grain sizes < 50 µm, 50 – 100 µm and > 100 µm were acquired. Samples from all localities contained up to several thousand grains, with most grain sizes smaller than 50 µm and only a small fraction greater than 100 µm. Zircons were carefully pipetted or handpicked with the use of a stereomicroscope, embedded in epoxy resin and polished.

Prior to analysis, the zircon mounts were cleaned in an ultrasonic bath with ultrapure benzine and coated with gold. Cathodoluminescence images, produced with a Joel JSM-6490 and a Gatan MiniCL detector revealed internal structures and growing patterns of the single crystals which enabled us to distinguish between different growth domains within the crystals for precise measurements by laser ablation ICPMS later.

6.4.1. LA-ICPMS U-Th-Pb analysis

The descriptions of the measurement conditions in this chapter for U-Th-Pb isotopes are taken from chapter 4.4.2 and were slightly modified.

From each sieve fraction of each sample locality, zircons were mounted, polished and analyzed for U-Th-Pb isotope ratios by laser ablation ICP-MS.

Where possible, core and rim domains were analysed, using a New Wave Research® UP-213 ultraviolet laser system with a teardrop shape low-volume laser cell, for a fast washout, connected to a Thermo-Finnigan® Scientific Element 2 ICPMS with Ni X skimmer and Al

sample cones. Several hundred grains per sample were analyses, with laserspot diameters varying from 20 to 40 µm, depending on the grainsize.

Measurements were performed, following the procedures of Gerdes and Zeh (2006; 2009). For data evaluation and as an external standard, we used standard GJ-1. Data was processed, using a self-created Excel® spreadsheet by A. Gerdes. Raw data was corrected for common lead, elemental fractionation and instrumental mass discrimination. Only concordant ages (90 – 110% concordance) were considered for further interpretation and discussion.

Prior to laser ablation analysis, gold coating was removed with ultrapure Ethanol. In order to remove any common lead from the surface that could stem from the preparation process, zircon mounts where cleaned with 2 % ultraclean nitric acid for 30s.

Spot sizes for all analyses varied from 20 µm to 33 µm and the fluence was around 4-6 J cm^2. Laser holes were drilled with penetration depths of about 20 µm. A detailed description of the analytical procedures used here for U-Pb dating is described in Gerdes and Zeh (2006; 2009). For internal standardization, we used as primary standard GJ-1 zircon (Jackson et al., 2004).

The Plešovice zircon standard (Slama et al., 2008) is routinely measured in the laboratory of the GUF and yields a concordant age of 338 ± 2 Ma, which is in perfect agreement to data published by Slama et al. (2008) from other laboratories.

Measurement were perfomed in several sessions, with offset values for $^{238}U/^{206}Pb$ for the major part of the sessions being in the range between 1 to 15 % and for one day with a value around 50% compared to the reference values for GJ-1.

Usually the U-Pb data was corrected for common Pb using the measured Hg-interference corrected ^{204}Pb signal and a Stacey and Kramers (1975) compostion. However, for many analyses the ^{204}Pb was below detection limit. Age propability-density plots were created using the Excel® spreadsheet of Sircombe (Sircombe, 2004). Concordia diagrams were created using Isoplot 3.7 (Ludwig, 2008). Some of the data points as listed in Table A.6.1, were saturated in the signal for ^{238}U due to the usage of the counting mode, plotting above the concordia line. These points were not considered for the concordia diagrams.

6.4.2. LA-MC-ICPMS Hafnium analysis

The following descriptions of the Hf isotope measurements are taken from chapter 4.4.3 with minor modifications.

Hafnium isotope measurements were performed with a Thermo-Finnigan Neptune multicollector (MC)-ICPMS at GUF coupled to New Wave UP213 NdYAG laser, following the procedures described in Gerdes and Zeh (2006; 2009). Laser spots with diameter 40 µm were drilled with repetition rate of 5.5 Hz and an energy density of 6 J/cm^2 during 55 s of data acquisition. The 40 µm Hf analysis spot was set on top or just next to the U-Th-Pb spot in the same growth domain as indicated by CL images. Penetration depths of the laser spots are in the range of about 40 to 50 µm.

Data were processed by the adjustment of all analyses to a $^{176}Hf/^{177}Hf$ isotope ratio of 0.282160 of reference standard JMC475. GJ-1 and Plešovice standards were measured during every measurement session to ensure high Accuracy and reproducibility. Average $^{176}Hf/^{177}Hf$ isotope ratios of GJ-1 in 7 analyses were at 0.282025 ± 0.00002 (2 sigma), which is in accordance to published reference values (Gerdes and Zeh, 2006).

$\varepsilon Hf(t)_{initial}$ values were calculated from the measurend $^{176}Hf/^{177}Hf$ and $^{176}Lu/^{177}Hf$ ratios, using the corresponding age as obtained before by the U-Th-Pb analyses and the CHUR values for $^{176}Lu/^{177}Hf$ and $^{176}Hf/^{177}Hf$ of 0.0336 and 0.282785 (Bouvier et al., 2008) and a decay constant of $1.867*10^{-11}$ (average Scherer et al., 2001; Söderlund et al., 2004). Only datapoints with concordant ages (90 – 110% concordance) and small errors were considered for further interpretations. Data in table A.4.2 without U-Pb ages did not have a concordant age.

6.5. Results

6.5.1. Zircon morphology

Grainsizes < 50 µm and between 50 to 100 µm are most abundant; only a minor fraction of the zircons in each sample is larger than 100 µm.

Most of the zircons from grain sizes < 50 µm and 50 – 100 µm have oscillary zoning, are monophase and colourless or reddish. They are subrounded to rounded, and seem to be detrital. Strong variations in the U contents of the grains can be seen in the cathodoluminescence images by different levels of brightness. This was confirmed by the obtained uranium contents ranging from < 100 ppm up to > 700 ppm.

A remarkable feature of some of the small sized zircons is a thin, illuminating rim with diameters of around 10 µm.

Zircons > 100 µm are mostly subeuhedral with partly rounded edges and show indications of a magmatic origin while a few of them show multi-phase growth (Fig.6.1).

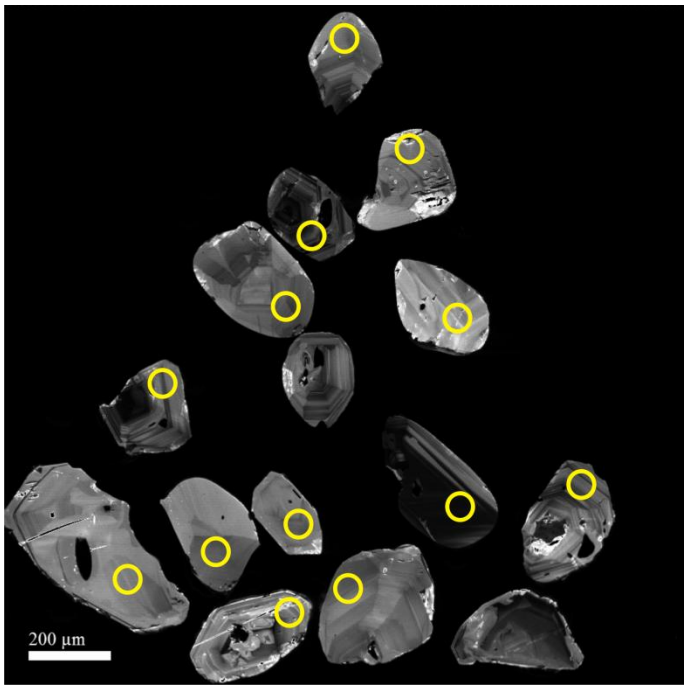

Fig.6.1: Cathodoluminescence images of subeuhedral zircons grains > 100 µm from Cabezo Negro de Tallante. Yellow circles indicate positions for the laser spots used for the determination of the U-Pb ages and Hf isotopic composition. U-Pb ages are around 2.6 Ma, corresponding to the age of eruption of the alkali basalts.

6.5.2. U-Pb age determinations

Results are listed in Table A.6.1. Only ages with concordance levels of 90 to 110 % for $^{206}U/^{238}Pb$ and $^{207}Pb/^{206}Pb$ were considered in the following interpretation (Fig.6.2, 6.3).

For the sample from Alto de las Cutandas (ALCS-1), only 24 out of 67 ages from the timespan > 100 Ma are clearly concordant. Thirty five zircons have ages younger than 5 Ma with a major age peak around 2.6 Ma. For such young zircons, ^{204}Pb and ^{207}Pb cannot by analyzed precise enough so that $^{207}Pb/^{206}Pb$ ages cannot be determined and there is no obvious concordance. However, in most cases, we see good correlations of $^{207}U/^{235}Th$ with $^{206}U/^{238}Pb$ and therefore consider these young ages to be real. Older ages peak around 0.3, 0.5 – 0.6, 0.8, 1.0, 1.4, 1.6, 1.8 – 2.2, 2.4 and 2.8 Ga.

86 out of 151 zircons from San Isidro (CG-Z1 – CG-Z3) with ages more than 100 Ma give concordant results, whereas a minor part of 32 zircons with ages is less than 10 Ma. Most ages range from around 0.3 to around 3 Ga with a major age peak at around 600 Ma. Minor age distributions are around 0.3, 0.7, 1.0, 1.2, 1.8 – 2.2, 2.4 – 2.6 and 2.9 – 3.0 Ga. Ages less than 10 Ma are mostly between 2 to 3 Ma and around 4.2, 5.5 and 6.5 Ma.

Nearly half of the zircons (62 out of 119) from Cabezo Negro de Tallante CNTS-1 are concordant with additionally 25 grains that are less than 10 Ma old. Zircons with ages older than 100 Ma have main age peaks around 0.3, 0.5 to 0.8, 1.0, 1.8 to 2.1 and 2.4 Ga. Young zircons peak around 2 to 3, 4, 6 to 7 and 7 to 8 Ma.

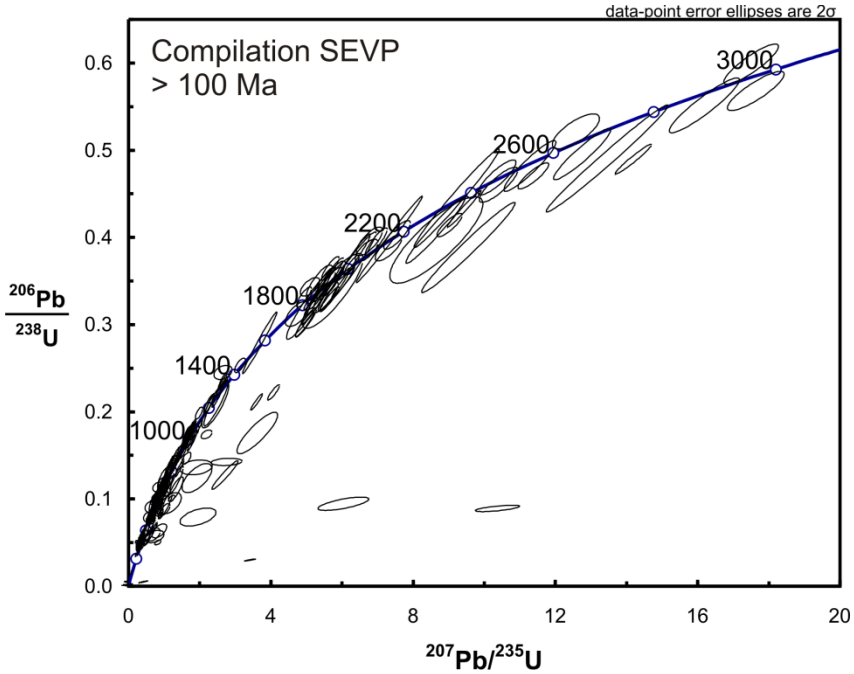

Fig.6.2 : Concordia diagram of all analyses > 100 Ma for all three localities.

All three sample localities give completely overlapping age spectra including the one from the weathered matrix of the basalts (CG-Z1 – CG-Z3). As a characteristic feature, all three sample localities show a wide range of ages from the Neogene up to the Archean. Major age clusters are around 300 to 400 Ma, 500 to 700 Ma, 1 Ga to 1.1 Ga, 1.8 Ga to 2.2 Ga, 2.4 to 2.6 Ga and 2.9 to 3 Ga. Oldest ages are achieved by samples from Alto de las Cutandas and San Isidro, whereas ages for Cabezo Negro de Tallante reach only up to 2.4 to 2.5 Ga.

The highest percentages of concordant ages for all localities are achieved for analyses from 300 to 400 Ma and 600 to 700 Ma.

For all sample localities, there is a remarkable gap of ages between 1.1 and 1.8 Ga, which can clearest be seen in the age spectra of CNTS-1.

Zircons younger than 10 Ma can be found in all samples. They generally occur in the fraction with grain sizes larger than 100 µm. A major age peaks is around 2.6 Ma, the age of the volcanic activity in Tallante. Minor age peaks are between 4 and 5 Ma and 7 and 8 Ma, the ages of the Ca-alkaline volcanism, a few tens of kilometers further west and around 150 kilometers further to the SW (Turner et al., 1999; Duggen et al., 2004).

No analysis of the thin illuminating rim around most zircons was possible, because its average diameter smaller than the laserspots used.

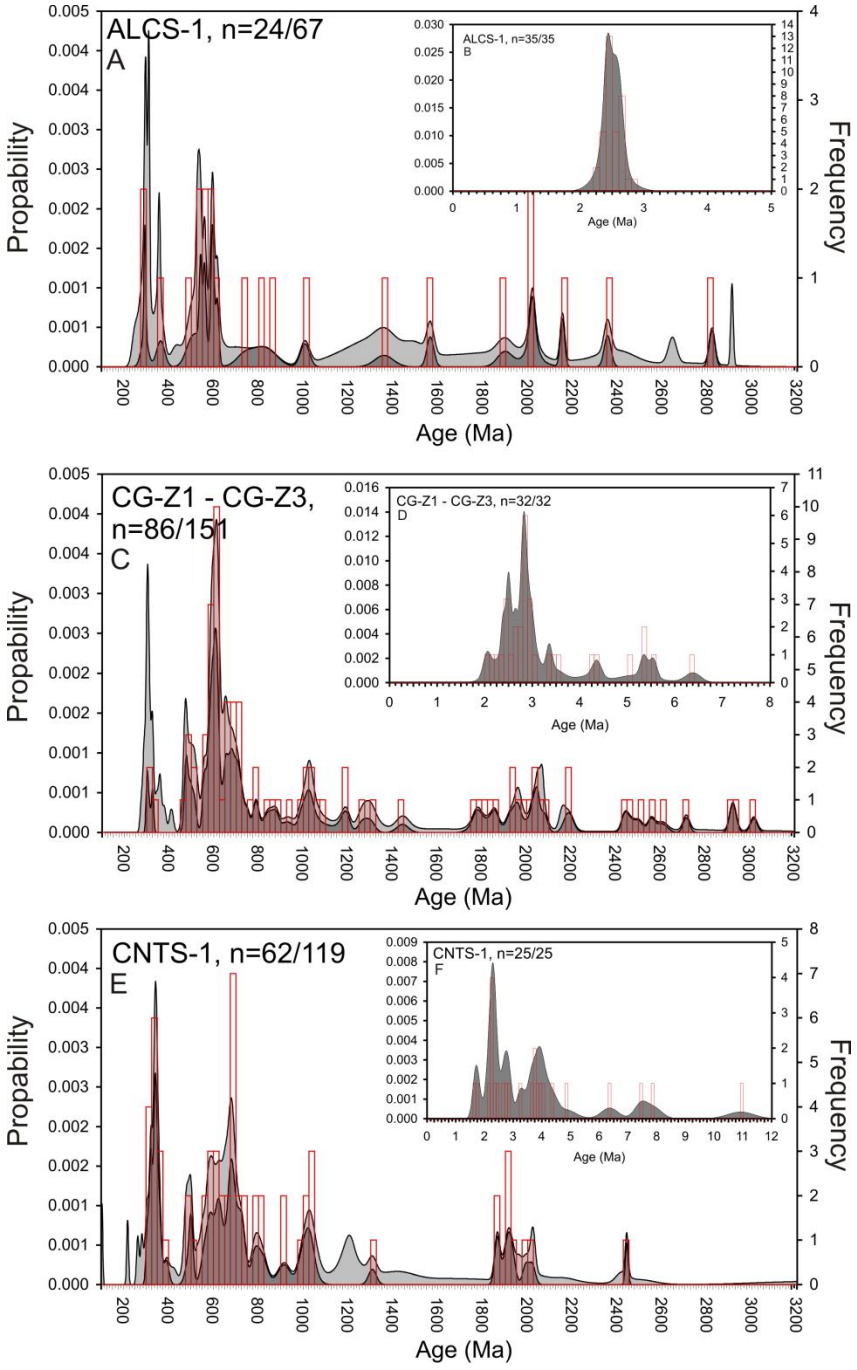

Fig.6.3: U-Pb based age distribution pattern of Alto de las Cutandas (ALCS; A-B), Cabezo Negro de Tallante (CNTS; C-D) and San Isidro (CG; E-F) with corresponding age pattern of zircons younger than 10 Ma inserted in each figure.

6.5.3. Initial Hafnium isotopic compositions

The Hf isotope compositions are reported in the εHf(*t*) notation. In general, $^{176}Lu/^{177}Hf$ isotope ratios are below 0.002, which is expected as Lu has only very low abundances in zircon crystals (Patchett et al., 1981). Therefore, the correction of $^{176}Hf/^{177}Hf$ isotope ratios for radiogenic ^{176}Hf does only have a minor effect on the isotope ratio. εHf(*t*) of all samples are below the evolution line for the depleted mantle for the corresponding age with values ranging from -25.3 to 8.8 εHf(*t*), while the major part is in the range between -9 and +8. The combination of the εHf(*t*) with their corresponding U-Pb ages shows one vertical trend from εHf(*t*) around 10 down to -15 εHf(*t*) units and two diagonal trends with εHf(*t*) values becoming less the younger the ages are.

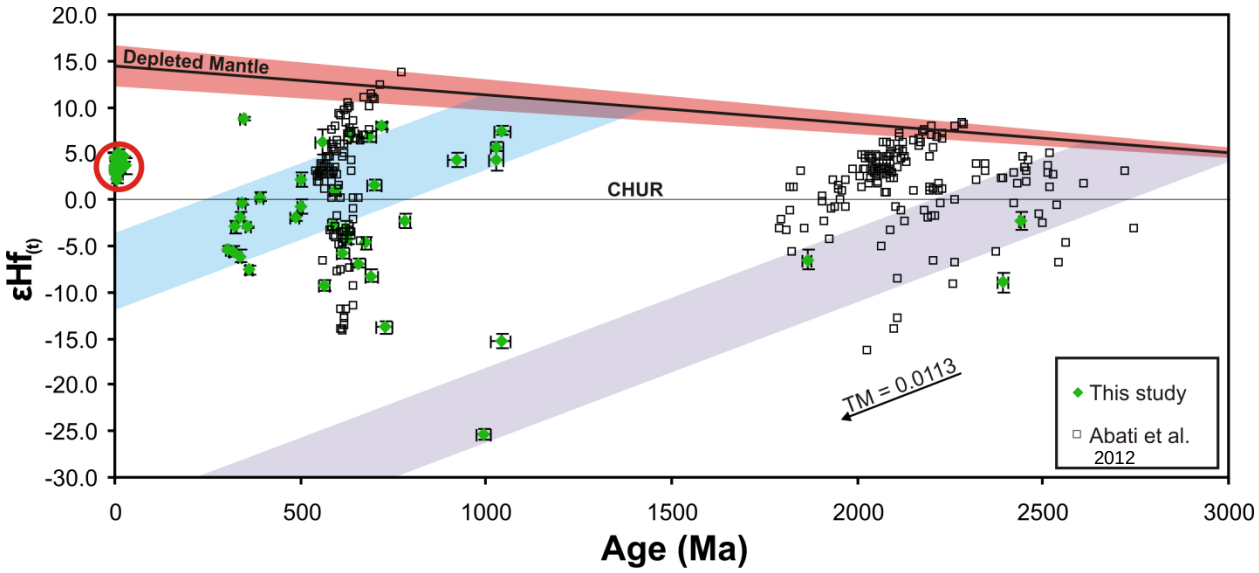

Fig.6.4: Hf evolution diagram for Cabezo Negro de Tallante (green) and additional data from the West African Craton (black squares; (Abati et al., 2012). εHf(*t*) values were plotted against their corresponding U-Pb ages. Crustal evolution trends are shown in blue and red, with an assumed $^{176}Lu/^{177}Hf$ isotope ratio of 0.0113 (Rudnick and Gao, 2003). The red circle surrounds ages younger than 10 Ma with εHf(*t*) values close to the chondritic value. For a more detailed illustration of these young ages, see Fig.6.7.

One group of samples with ages below 10 Ma, results in a very narrow εHf(*t*) range of around 2 to 5 (Fig 4.6). Three age groups can be distinguished with one at around 2 to 3 Ma, followed by a group from 4 to 5 Ma and another one at around 8 Ma. εHf(*t*) values of all groups are nearly

constant with some ages being slightly higher or lower than the average that is around 3 to 4 εHf(*t*) units.

By plotting these values into a Hf evolution diagram, crustal evolution trends, starting from the depleted mantle can be projected and compared to the sampleset (Fig.6.4). A $^{176}Lu/^{177}Hf$ of 0.0113 was chosen for the calculation of crustal evolution trends (Rudnick and Gao, 2003).

6.6. Discussion

6.6.1. Origin of the Zircons

Zircons were collected from the tuffs and the weathered matrix of the volcanic edifices (see above). They should be the debris of the metamorphic crustal xenoliths which are included in the volcanics but it cannot be excluded that there is also debris from the immediately underlying Permian mica schists included. As the results of zircon analyses from the restitic enclaves of a dacite in Cerro del Hoyazo by Zeck and Williams (2002) match in most points the age distribution pattern of this study, it can be said that we either did not have a recent addition of zircons close to the tuff layers or that if there was an addition of zircons, they have a similar age spectra like the crust beneath Cabezo Negro de Tallante.

The wide range of ages from Neogene to Archean implies that some of the zircons analyzed could have been transported from a more distant region to the SEVP as no Proterozoic or Archean rocks are reported from the Betic cordillera. Previous studies have shown that, zircons are able to survive long distance transports without being destroyed (Morag et al., 2011). During the assembly of Gondwana, zircons that are Archean in age could have been transported from the West African craton onto the Iberian plate before the breakup of Gondwana (Fernandez et al., 2010).

6.6.2. Age distribution and crustal evolution

So far, no data about the geochronological makeup of the crust beneath the Tallante region exists, so that we do not have any direct database to compare our geochronological records with. However, age information is available on the crustal make beneath Cerro del Hoyazo, which is

located around 150 km to the southwest of Cabezo Negro de Tallante (Zeck and Williams, 2002) and the crust from the Alpujárride graphitic schist, close to Cerro del Hoyazo (Zeck and Whitehouse, 1999), which is about the same age as the mica schists around Cabezo Negro de Tallante. These regions are all located within the Betic Cordillera, which assumes that both areas could have a similar history in age.

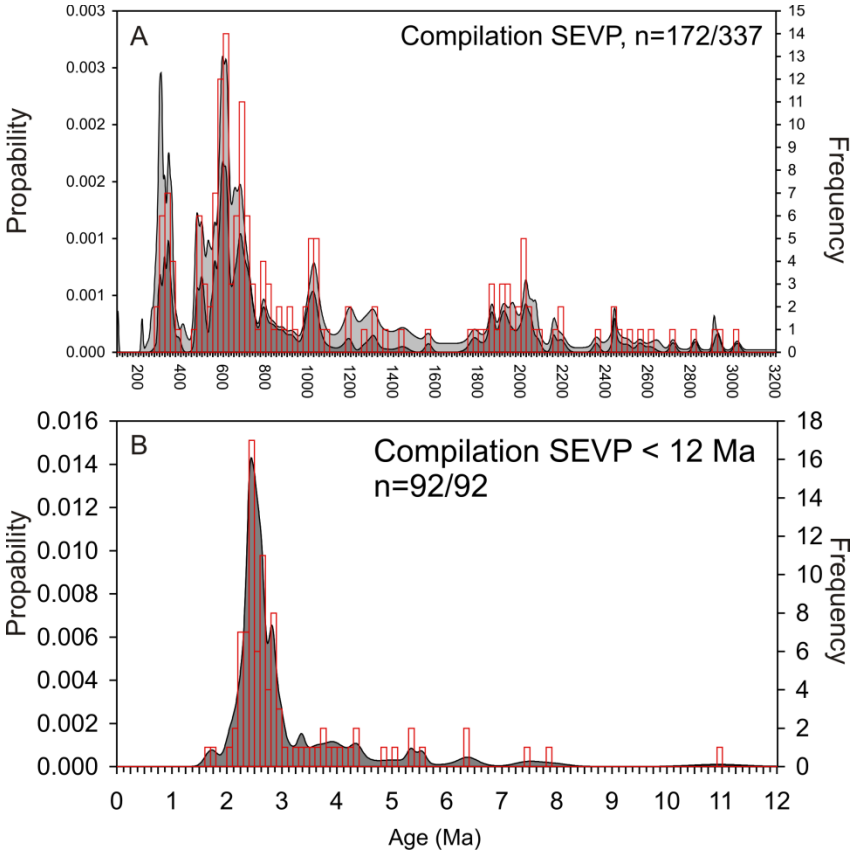

Fig.6.5: Compilation of U-Pb ages of all three localities from the SEVP, with ages from 0.1 to around 3 Ga (A) and Neogene ages of around 2 to 11 Ma (B).

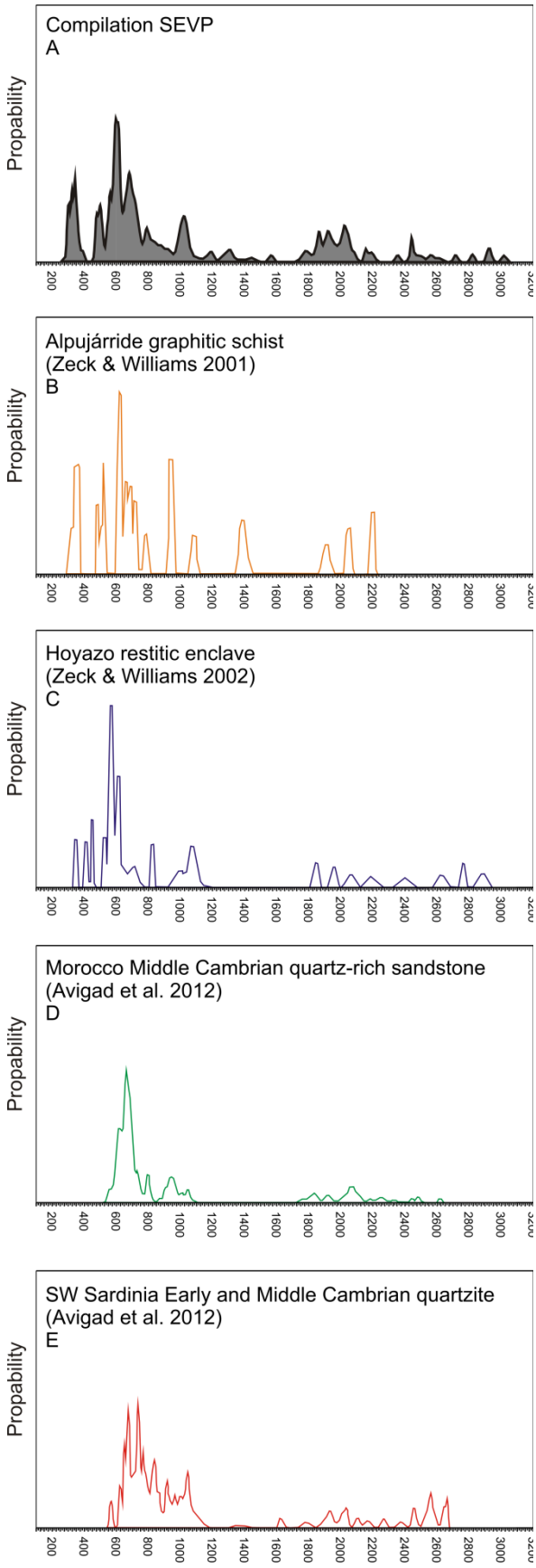

Fig.6.6: Comparison of the age distributions of the SEVP (A) to the results of the Alpujárride graphitic schist (Zeck and Williams, 2001) (B), the xenoliths of the dacite of Cerro del Hoyazo (Zeck and Williams, 2002) (C), a middle Cambrian quartz-rich sandstone in Morocco (Avigad et al., 2012) (D) and a middle Cambrian quartzite in SW Sardinia (Avigad et al., 2012) (E).

Additionally, detrital zircons from Morocco and Sardinia can be taken as a reference for this study (Avigad et al., 2012) as they were connected with each other during the assembly of Gondwana.

The age distribution patterns of of all three localities analyzed in this study are very similar (Fig.6.3). Differences are expressed in the maximum age of crystallization that is the highest for San Isidro or the occurrence of few ages in the timespan between 1.0 and 1.8 Ga. These differences are not significant though and can partly be explained by the number of concordant ages for each locality. San Isidro has the oldest U-Pb ages but is also the locality with the most data available.

The age distribution patterns between the three localities around Casas de Tallante and Cerro del Hoyazo have nearly the same range in ages, starting from around 300 Ma up to 2.8 Ga. Major age peaks of the dacite xenoliths comprise 320 to 350 Ma, 650 to 550 Ma, 0.9 to 1.1 Ga, 1.9 to 2.1 Ga and 2.5 to 2.8 Ga. These results are in good agreement to our results as described earlier. As a difference, no data older than 2.9 Ga is existent in their dataset (Zeck and Williams, 2002), which points to a slightly different stratigraphic unit. From the coincidence of the age distribution between the two localities we conclude that the zircons for Tallante are derived directly from the disintegrated crustal xenoliths there.

The age spectrum of the Alpujárride graphitic schist (Zeck and Williams, 2001) has the highest peak at around 0.6 to 0.7 Ga and some minor peaks around 0.3 to 0.4, 0.9, 1.1, 1.4 and 1.9 to 2.2 Ga. This is mostly in accordance to our own results of the SEVP with the difference that no ages older than 2.2 Ga are present in the age spectrum of the graphitic schist. Because of a similar age of this schist and the mica schists, surrounding the alkali basalts in the SEVP, we take its age spectra as a representative of the mica schists. By doing so, it can be seen that most ages from our samples match the ages of the surrounding country rocks. The absence of ages older than 2.2 Ga can probably be related to a smaller number of analyses (statistical effect).

Age spectra of Morocco and SW Sardinia (Avigad et al., 2012) are nearly the same with major age peaks around 0.6 to 0.8 Ga and minor age distributions around 0.9 to 1.0, 1.6, 1.8 to 2.2 and 2.4 to 2.7 Ga. Compared to the results of the SEVP, there is no evidence for the Variscan

orogeny in the Moroccan and Sardinian zircons, as ages around 0.3 Ga are completely missing, which was expected as the sediments are Cambrian.

Age spectras of the Alpujárride graphitic schist and the xenoliths within the dacite are very similar, which can be interpreted as as a stacking of nappes within the Betic cordillera. This stacking can also be observed for the SEVP, as the age spectra of these samples is very similar to those of Cerro del Hoyazo, with the mica schists being equivalent to the graphitic schist, while some older ages might point to a slightly different stratigraphic unit or may be a statistical effect.

In general, the comparison to these four other localities show very similar age spectra, pointing towards a Gondwanan source of detrital zircons.

More information on crustal evolution and crustal reworking can be obtained from the Hf isotopes of the zircons and the comparison with the mantle evolution line (Fig 6.4). We only analyzed the zircons from Cabezo Negro de Tallante as representative for the whole volcanic field. Two major crust building phases, probably starting from a depleted mantle source, show an obvious trend.

It appears from the projection of the Hf-isotopes onto the depleted mantle that the same primary crustal source rocks with ages between 1 to 1.5 Ga have been reworked during the assembly of Rodinia, the Caledonian orogeny and the Variscan orogeny. No crustal rocks from Iberia fall into that age range of 1 to 1.5 Ga, which means that the zircons, derived from a depleted mantle around that time must stem from somewhere else than Iberia.

In addition, the timespan between 500 and 600 Ma shows a distinct vertical array of $\varepsilon Hf(t)$. During this time span, further crustal components with widely different primary ages seem to have been reworked, mixed and homogenized, resulting in this remarkable trend that goes down to around -14 εHf units.

Ages between 1.0 and 1.8 Ga are very scarce in all localities, which is typical for a Gondwanan to Peri Gondwanan provenance (Zeh and Gerdes, 2010) like the SEVP.

Ages between 1.8 and 2.5 are more common again followed intermittently by few ages up to 3 Ga. The projection back to the depleted mantle evolution line of the late Proterozoic to Proterozoic zircons from Cabezo Negro de Tallante indicates the formation of juvenile crust sometime in the late Archean (Fig.6.4). The existence of such old zircon grains and their

morphological features, with special regard to their size and their roundness, implies that these zircons are detrital and do not have a direct magmatic origin from within the Betic Cordillera.

Looking back in the Earth's history, it can be seen that before the breakup of Gondwana, the Iberian Plate was attached to the West African Craton (Avigad et al., 2012). By comparison of the U-Pb age spectra of this study with age distributions of zircons from Cambrian sandstones of Morocco and Sardinia (Avigad et al., 2012), we can see a good agreement with the older ages (Fig.6.6). A geochronological study of zircons from the Anti-Atlas mountains, a part of to the West African Craton, is also in good agreement with the Palaeoproterozoic and Archean ages and the Caledonian crustal mixing trend (Abati et al., 2012). It also shows that most of the zircons of the SEVP could stem from the West African Craton and have been recycled and mixed in Caledonian and Variscan times. It implies that detrital zircons have been transported in Gondwanan times to the Iberian Plate, which were than in a later period (e.g. Variscian) metamorphosed and are now a part of the crust of the Betic Cordillera.

Rocks with U-Pb ages around 1 Ga, were found in the Arabian Nubian Shield and are probably another provenance region for the SEVP (Be'eri-Shlevin et al., 2012). These zircons were reworked and recycled during the Caledonian and variscian orogeny.

Our new U-Pb results and the Hf isotope data for Cabezo Negro de Tallante and the comparison to areas nearby (Zeck and Williams, 2001; Zeck and Williams, 2002) and the age signature of the West African Craton, implies that it is made up of zircons from the West African Craton that were transported during the time of the assemblage of the Gondwana terranes onto the Iberian plate and were reworked during the Caledonian and Variscan Orogeny. During the Alpine orogeny, the Betic cordillera was formed and caused a stacking of nappes. The samples collected in this study showed the characteristics of this part of the crust but did not allow a characterisation of the basement underneath it.

6.6.3. Magmatic zircons younger than 10 Ma

The sampleset of each locality around Casas de Tallante contains small amounts of zircons > 100 µm with subeuhedral shapes that are slightly only rounded on the edges (Fig.6.1). These

zircons have shown to be Neogene in age, with a large fraction that is 2 to 3 Ma and minor age distributions around 4, 5 – 6, 7 – 8 and 11 Ma.

Zircons that are of magmatic origin have been described to be euhedral in shape and to be larger in grain size (Hollis and Sutherland, 1985). The zircons described above match the morphological criterias for magmatic zircons and are in good agreement with their corresponding U-Pb ages (which are in good agreement to the U-Th ages) to the K-Ar ages of the Tallante basalts of Bellon et al. (1983). The roundness can be explained as being the result of interaction of the zircons grains with the basaltic melts. Therefore it cannot be excluded that these zircons are cogenetic with the basalts and record the time of eruption.

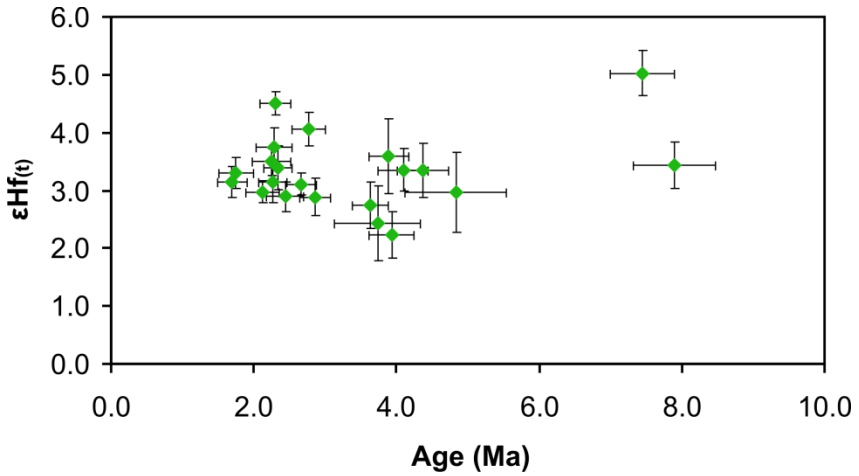

Fig.6.7: εHf(*t*) distribution of zircons from Cabezo Negro de Tallante with ages < 10 Ma. Values scatter from around 2 to 5 εHf units according to a slightly depleted mantle source.

In that case, the Hf isotopes provide information onthe mantle source of of the basanites. The εHf values range between +2 and +5 εHf(*t*) (Fig.6.7) for all three age groups as discussed earlier. These characteristics indicate that these zircons could be derived from a depleted mantle source that has been recycled later or that the source of melt extraction is a slightly depleted to a primitive mantle source. An origin from the depleted mantle is though unlikely as we do not find any evidence for zircons that are on the same line for a crustal evolution and the fact that these zircons all show, within a certain range, similar εHf(*t*) values. It is therefore very likely that the basaltic rocks were extracted from slightly depleted to primitive mantle source and that there is no cogenetic relationship towards the rest of the zircon population analyzed for this locality. These findings are in accordance to the results of a study of Cebria et al. (2009). They propose a

model in which the alkali basalts are derived from a primitive mantle source that has experienced minor interaction with metasomatized lithospheric mantle melts. Similar young ages (around 6 Ma), were obtained from euhedral zircons in a dacite (Zeck and Williams, 2002) and are thought to represent the age of eruption of the corresponding area.

Ages from around 6 to 8 Ma could be related to the extrusion of Ca-alkaline melts in the Miocene, further to the West and Southwest of Cabezo Negro de Tallante (Turner et al., 1999; Duggen et al., 2004).

6.7. Conclusions

This study was set out to clarify the question of how the lower crust beneath the SEVP is built up in terms of the geochronological record and the origin of melt extraction, to be clarified by U-Pb and Hf isotope analyses. The extensive study of crustal zircons, collected from the Tuff layers of Cabezo Negro de Tallante, Alto de Las Cutandas and San Isidro, all located in the SEVP, has shown a wide age range from the Neogene up to the Archean. All three localities show almost the same age patterns. The comparison of the ages from all three localities and Hf isotope systematics from Cabezo Negro de Tallante to crustal age distributions and Hf isotope systematics from selected other localities allowed us to get a better view in the understanding of the crust beneath the SEVP.

Before the breakup of Gondwana, the Iberian plate was in direct connection to the West African craton from which zircons have probably been transported onto the Iberian plate. These zircons have late Proterozoic ages which were mixed and reworked during the Caledonian orogeny. Hf isotope data from Cabezo Negro de Tallante suggests that juvenile crust formation occured around 1 to 1.5 Ga, whereas no rocks of this age are known in the Betics. These zircons are probably also Gondwana derived from a locality, situated in the Arabian Nubian Shield (Be'eri-Shlevin et al., 2012). They were recycled during the Caledonian and the Variscan orogeny, creating the younger array of crustal development. A vertical trend around 0.6 Ga, shows that zircons with different Hf isotopic compositions have interacted, forming a crustal mixing trend at the time of the Caledonian orogeny.

A minor part of the zircon population of all three localities is related to the magmatism that brought up the mantle xenoliths to the surface and formed the alkali basaltic hills in the SEVP. They are subeuhedral in shape and are in general bigger in their grain size than the rest of the zircon population with diameters greater than 100 µm. Their initial $^{176}Hf/^{177}Hf$ isotopic signatures are, if correlated to their U-Pb age, corresponding to a slightly depleted mantle source. The major part of these zircons have ages around 2.6 Ma, which is in good agreement to K-Ar geochronological data for the alkali basalts as published by Bellon et al. (1983). A minor part yields ages from 6 to 8 Ma, which corresponds to the age of the calc alkaline melts that can be found around further Southwest of Cabezo Negro de Tallante (Turner et al., 1999; Duggen et al., 2004).

Our new data, in comparison to data from the West African Craton and more localities within the Betic cordillera shows that the lower crust beneath the SEVP records extensive recycling and crustal mixing of detrital zircons that were transported from the West African craton during the assemblage of Gondwana onto the Iberian Plate. The lower and the upper crust are a product of intensive nappe stacking during major tectonic events.

6.8. Acknowledgements

We are grateful to J. Heliosch for the preparation of the zircon mounts and A. Zeh for helpful discussions.

This project has been supported by the DFG (Deutsche Forschungsgemeinschaft), project grant 1012/37-1.

6.9. References

Abati, J., Aghzer, A.M., Gerdes, A. and Ennih, N., 2012. Insights on the crustal evolution of the West African Craton from Hf isotopes in detrital zircons from the Anti-Atlas belt. Precambrian Research, 212 - 213: 263 - 274.

Avigad, D., Gerdes, A., Morag, N. and Bechstadt, T., 2012. Coupled U-Pb-Hf of detrital zircons of Cambrian sandstones from Morocco and Sardinia: Implications for provenance and Precambrian crustal evolution of North Africa. Gondwana Research, 21(2-3): 690-703.

Be'eri-Shlevin, Y., Eyal, M., Eyal, Y., Whitehouse, M.J. and Litvinovsky, B., 2012. The Sa'al volcano-sedimentary complex (Sinai, Egypt): A latest Mesoproterozoic volcanic arc in the northern Arabian Nubian Shield Geology, 40: 403-406.

Beccaluva, L., Bianchini, G., Bonadiman, C., Siena, F. and Vaccaro, C., 2004. Coexisting anorogenic and subduction-related metasomatism in mantle xenoliths from the Betic Cordillera (southern Spain). Lithos, 75(1-2): 67-87.

Bellon, H., Bordet, P. and Montenat, C., 1983. Chronology of the Neogene Magmatism from Betic Ranges (Southern Spain). Bulletin De La Societe Geologique De France, 25(2): 205-217.

Bianchini, G., Beccaluva, L., Nowell, G.M., Pearson, D.G. and Siena, F., 2011. Mantle xenoliths from Tallante (Betic Cordillera): Insights into the multi-stage evolution of the south Iberian lithosphere. Lithos, 124(3-4): 308-318.

Bouvier, A., Vervoort, J.D. and Patchett, P.J., 2008. The Lu-Hf and Sm-Nd isotopic composition of CHUR: Constraints from unequilibrated chondrites and implications for the bulk composition of terrestrial planets. Earth and Planetary Science Letters, 273(1-2): 48-57.

Capedri, S., Venturelli, G., Salviolimariani, E., Crawford, A.J. and Barbieri, M., 1989. Upper-Mantle Xenoliths and Megacrysts in an Alkali Basalt from Tallante, Southeastern Spain. European Journal of Mineralogy, 1(5): 685-699.

Cebria, J.M., Lopez-Ruiz, J., Carmona, J. and Doblas, M., 2009. Quantitative petrogenetic constraints on the Pliocene alkali basaltic volcanism of the SE Spain Volcanic Province. Journal of Volcanology and Geothermal Research, 185(3): 172-180.

Duggen, S., Hoernle, K., Van den Bogaard, P. and Garbe-Schonberg, D., 2005. Post-collisional transition from subduction- to intraplate-type magmatism in the westernmost

Mediterranean: Evidence for continental-edge delamination of subcontinental lithosphere. Journal of Petrology, 46(6): 1155-1201.

Duggen, S., Hoernle, K., van den Bogaard, P. and Harris, C., 2004. Magmatic evolution of the Alboran region: The role of subduction in forming the western Mediterranean and causing the Messinian Salinity Crisis. Earth and Planetary Science Letters, 218(1-2): 91-108.

Duggen, S., Hoernle, K., van den Bogaard, P., Rupke, L. and Morgan, J.P., 2003. Deep roots of the Messinian salinity crisis. Nature, 422(6932): 602-606.

Dupuy, C., Dostal, J. and Boivin, P.A., 1986. Geochemistry of ultramafic xenoliths and their host alkali basalts from Tallante, southern Spain. Mineralogical Magazine, 50(356): 231-239.

Fernandez, R.D. et al., 2010. U-Pb ages of detrital zircons from the Basal allochthonous units of NW Iberia: Provenance and paleoposition on the northern margin of Gondwana during the Neoproterozoic and Paleozoic. Gondwana Research, 18(2-3): 385-399.

Gerdes, A. and Zeh, A., 2006. Combined U–Pb and Hf isotope LA-(MC-)ICP-MS analyses of detrital zircons: Comparison with SHRIMP and new constraints for the provenance and age of an Armorican metasediment in Central Germany. Earth and Planetary Science Letters, 249: 47-61.

Gerdes, A. and Zeh, A., 2009. Zircon formation versus zircon alteration - New insights from combined U-Pb and Lu-Hf in-situ LA-ICP-MS analyses, and consequences for the interpretation of Archean zircon from the Central Zone of the Limpopo Belt. Chemical Geology, 261(3-4): 230-243.

Hollis, J.D. and Sutherland, F.L., 1985. Occurences and Origins of Gem Zircons in Eastern Australia. Records of the Australian Museum, 36: 299-311.

Jackson, S.E., Pearson, N.J., Griffin, W.L. and Belousova, E.A., 2004. The application of laser ablation-inductively coupled plasma-mass spectrometry to in situ U-Pb zircon geochronology. Chemical Geology, 211(1-2): 47-69.

Kogarko, L.N., Ryabchikov, I.D., Brey, G.P., Santin, S.F. and Pacheco, H., 2001. Mantle rocks uplifted to crustal levels: Diffusion profiles in minerals of spinel-plagioclase lherzolites from Tallante, Spain. Geochemistry International, 39(4): 311-326.

Ludwig, K.R., 2008. Isoplot 3.7: A geochronological toolkit for Microsoft Excel. Berkley Geochronology Center, Spec. Pub. No. 4: 1-77.

Morag, N., Avigad, D., Gerdes, A., Belousova, E. and Harlavan, Y., 2011. Detrital zircon Hf isotopic composition indicates long-distance transport of North Gondwana Cambrian-Ordovician sandstones. Geology, 39(10): 955-958.

Patchett, P.J., Kouvo, O., Hedge, C.E. and Tatsumoto, M., 1981. Evolution of Continental-Crust and Mantle Heterogeneity - Evidence from Hf Isotopes. Contributions to Mineralogy and Petrology, 78(3): 279-297.

Rampone, E., Vissers, R.L.M., Poggio, M., Scambelluri, M. and Zanetti, A., 2010. Melt Migration and Intrusion during Exhumation of the Alboran Lithosphere: the Tallante Mantle Xenolith Record (Betic Cordillera, SE Spain). Journal of Petrology, 51(1-2): 295-325.

Rudnick, R.L. and Gao, S., 2003. Composition of the continental crust. In: Rudnick RL (ed) The crust. Treatise in Geochemistry 3: 1-64.

Schaefer, B.F. et al., 2000. Re-Os isotope characteristics of postorogenic lavas: Implications for the nature of young lithospheric mantle and its contribution to basaltic magmas. Geology, 28(6): 563-566.

Scherer, E., Munker, C. and Mezger, K., 2001. Calibration of the lutetium-hafnium clock. Science, 293(5530): 683-687.

Shimizu, Y., Arai, S., Morishita, T. and Ishida, Y., 2008. Origin and significance of spinel-pyroxene symplectite in lherzolite xenoliths from Tallante, SE Spain. Mineralogy and Petrology, 94(1-2): 27-43.

Sircombe, K.N., 2004. AGEDISPLAY: an EXCEL workbook to evaluate and display univariate geochronological data using binned frequency histograms and probability density distributions. Computers & Geosciences, 30(1): 21-31.

Slama, J. et al., 2008. Plesovice zircon - A new natural reference material for U-Pb and Hf isotopic microanalysis. Chemical Geology, 249(1-2): 1-35.

Söderlund, U., Patchett, J.P., Vervoort, J.D. and Isachsen, C.E., 2004. The Lu-176 decay constant determined by Lu-Hf and U-Pb isotope systematics of Precambrian mafic intrusions. Earth and Planetary Science Letters, 219(3-4): 311-324.

Stacey, J.S. and Kramers, J.D., 1975. Approximation of Terrestrial Lead Isotope Evolution by a 2-Stage Model. Earth and Planetary Science Letters, 26(2): 207-221.

Turner, S.P. et al., 1999. Magmatism associated with orogenic collapse of the Betic-Alboran Domain, SE Spain. Journal of Petrology, 40(6): 1011-1036.

Weijermars, R., Roep, T.B., Vandeneeckhout, B., Postma, G. and Kleverlaan, K., 1985. Uplift History of a Betic Fold Nappe Inferred from Neogene-Quaternary Sedimentation and Tectonics (in the Sierra Alhamilla and Almeria, Sorbas and Tabernas Basins of the Betic Cordilleras, Se Spain). Geologie En Mijnbouw, 64(4): 397-411.

Zeck, H.P. and Whitehouse, M.J., 1999. Hercynian, Pan-African, Proterozoic and Archean ion-microprobe zircon ages for a Betic-Rif core complex, Alpine belt, W Mediterranean - consequences for its P-T-t path. Contributions to Mineralogy and Petrology, 134(2-3): 134-149.

Zeck, H.P. and Williams, I.S., 2001. Hercynian metamorphism in nappe core complexes of the Alpine Betic-Rif belt, Western Mediterranean - a SHRIMP zircon study. Journal of Petrology, 42(7): 1373-1385.

Zeck, H.P. and Williams, I.S., 2002. Inherited and magmatic zircon from Neogene Hoyazo cordierite dacite, SE Spain - Anatectic source rock provenance and magmatic evolution. Journal of Petrology, 43(6): 1089-1104.

Zeh, A. and Gerdes, A., 2010. Baltica- and Gondwana-derived sediments in the Mid-German Crystalline Rise (Central Europe): Implications for the closure of the Rheic ocean. Gondwana Research, 17(2-3): 254-263.

Supplement

Table A3.1 Major element compositions of the analyzed samples. Values are reported in weight percent.

Sample	SiO_2	TiO_2	Al_2O_3	Cr_2O_3	FeO	MnO	MgO	CaO	NiO	Na_2O	K_2O	P_2O_5	Total
Gibtown 93 1/1 Ol1 rim	40.11	0.01	0.02	0.03	8.89	0.10	51.31	0.03	0.35	0.00	0.00	0.02	100.88
Ol1 intermediate	39.98	0.00	0.01	0.01	9.02	0.12	51.26	0.01	0.41	0.02	0.00	0.01	100.84
Ol1 core	40.15	0.02	0.01	0.01	8.77	0.11	51.23	0.03	0.39	0.03	0.00	0.03	100.78
Ol2 rim	40.45	0.00	0.02	0.02	8.85	0.12	51.29	0.04	0.41	0.02	0.00	0.01	101.22
Ol2 intermediate	40.07	0.00	0.03	0.03	8.84	0.11	51.24	0.04	0.41	0.01	0.01	0.00	100.80
Ol2 core	39.93	0.00	0.02	0.03	8.90	0.11	51.07	0.04	0.38	0.03	0.02	0.01	100.53
Ol3 rim	40.25	0.02	0.03	0.00	8.91	0.12	51.07	0.03	0.38	0.00	0.00	0.02	100.83
Ol3 intermediate	40.03	0.02	0.02	0.00	8.83	0.11	51.15	0.03	0.40	0.03	0.00	0.00	100.61
Ol3 core	40.19	0.02	0.02	0.00	8.98	0.09	51.24	0.03	0.41	0.02	0.00	0.01	101.02
Gibtown 93 1/1 OPX1 rim	57.42	0.09	1.03	0.27	5.39	0.12	35.31	0.56	0.11	0.12	0.00	0.00	100.43
OPX1 intermediate	57.24	0.12	1.04	0.26	5.35	0.15	35.33	0.57	0.09	0.11	0.02	0.01	100.29
OPX1 core	57.18	0.10	1.03	0.26	5.45	0.14	35.31	0.54	0.12	0.10	0.01	0.00	100.22
OPX2 rim	57.43	0.02	0.93	0.26	5.26	0.12	35.46	0.45	0.12	0.12	0.01	0.00	100.17
OPX2 intermediate	57.46	0.04	0.90	0.27	5.29	0.12	35.62	0.44	0.10	0.11	0.00	0.00	100.36
OPX2 core	57.33	0.03	0.89	0.28	5.35	0.13	35.65	0.43	0.11	0.10	0.00	0.00	100.30
OPX3 rim	57.32	0.07	1.03	0.28	5.42	0.13	35.23	0.54	0.08	0.11	0.00	0.00	100.21
OPX3 intermediate	57.61	0.10	1.03	0.28	5.52	0.14	35.44	0.54	0.09	0.11	0.00	0.00	100.85
OPX3 core	57.41	0.05	0.99	0.26	5.46	0.14	35.57	0.49	0.10	0.10	0.01	0.00	100.58
Gibtown 93 1/1 CPX1 core	55.30	0.29	2.64	2.14	2.37	0.10	16.16	19.62	0.05	2.25	0.01	0.02	100.95
CPX1 rim	55.38	0.23	2.64	2.28	2.49	0.10	16.32	19.27	0.05	2.25	0.02	0.03	101.05
CPX1 intermediate	55.24	0.26	2.73	2.25	2.47	0.09	16.44	19.15	0.02	2.27	0.00	0.00	100.92
CPX2 core	55.15	0.24	2.66	2.13	2.44	0.08	16.54	19.31	0.08	2.31	0.02	0.00	100.95
CPX2 rim	55.12	0.25	2.71	2.16	2.47	0.07	16.41	19.39	0.09	2.17	0.01	0.03	100.88
CPX2 intermediate	55.19	0.24	2.71	2.24	2.47	0.09	16.38	19.30	0.04	2.21	0.02	0.02	100.90
CPX3 rim	54.82	0.24	2.70	2.28	2.45	0.09	16.40	19.23	0.06	2.29	0.01	0.03	100.60
CPX3 rim	55.11	0.25	2.66	2.25	2.44	0.08	16.35	19.18	0.08	2.21	0.02	0.00	100.62
CPX3 intermediate	54.76	0.24	2.71	2.26	2.47	0.08	16.35	19.31	0.05	2.27	0.02	0.02	100.54
Gibtown 93 1/1 Grt1 core	42.24	0.27	20.31	4.46	7.54	0.41	20.39	5.35	0.02	0.05	0.01	0.04	101.08
Grt1 intermediate	42.66	0.26	20.25	4.52	7.57	0.38	20.31	5.28	0.01	0.06	0.00	0.04	101.34
Grt1 rim	42.51	0.28	20.36	4.44	7.54	0.41	20.45	5.34	0.00	0.05	0.00	0.04	101.42
Grt2 core	42.70	0.23	20.51	4.41	7.44	0.39	20.73	5.20	0.00	0.03	0.00	0.04	101.67
Grt2 rim	42.77	0.23	20.44	4.45	7.72	0.43	20.64	5.27	0.03	0.05	0.02	0.03	102.07
Grt2 intermediate	42.49	0.24	20.54	4.39	7.45	0.39	20.58	5.28	0.01	0.05	0.01	0.02	101.45
Grt3 rim	42.43	0.25	20.56	4.37	7.54	0.39	20.57	5.22	0.03	0.05	0.00	0.04	101.44
Grt3 rim	42.39	0.27	20.43	4.44	7.47	0.40	20.61	5.25	0.00	0.04	0.00	0.01	101.33
Grt3 intermediate	42.44	0.26	20.35	4.46	7.41	0.41	20.64	5.17	0.00	0.04	0.00	0.03	101.21
Gibtown 93-11 Ol1 rim	40.47	0.02	0.03	0.00	8.42	0.09	51.68	0.03	0.39	0.02	0.00	0.02	101.17
Ol1 intermediate	40.26	0.01	0.01	0.02	8.41	0.13	51.58	0.03	0.38	0.04	0.00	0.02	100.88
Ol1 core	40.66	0.01	0.02	0.03	8.34	0.12	51.92	0.03	0.41	0.04	0.00	0.02	101.59
Ol2 rim	40.47	0.05	0.03	0.02	8.40	0.14	51.63	0.04	0.35	0.02	0.00	0.00	101.15
Ol2 intermediate	40.09	0.02	0.03	0.02	8.41	0.10	51.49	0.04	0.36	0.02	0.00	0.01	100.58
Ol2 core	40.58	0.02	0.01	0.01	8.37	0.10	51.92	0.03	0.39	0.03	0.00	0.02	101.49
Ol3 rim	40.24	0.03	0.02	0.02	8.47	0.14	51.61	0.02	0.37	0.02	0.00	0.00	100.94
Ol3 intermediate	40.44	0.00	0.04	0.03	8.42	0.10	51.57	0.01	0.39	0.01	0.00	0.01	101.01
Ol3 core	40.72	0.00	0.02	0.02	8.41	0.08	51.39	0.03	0.40	0.02	0.01	0.02	101.12
Gibtown 93-11 OPX1 rim	57.38	0.11	1.15	0.45	4.97	0.14	35.39	0.53	0.11	0.13	0.00	0.01	100.37
OPX1 intermediate	57.20	0.09	1.01	0.37	5.03	0.13	35.68	0.43	0.11	0.12	0.00	0.01	100.19
OPX1 core	57.78	0.11	1.00	0.38	5.02	0.14	35.65	0.44	0.12	0.11	0.01	0.02	100.76
OPX2 rim	58.01	0.12	0.89	0.35	5.07	0.13	35.69	0.41	0.10	0.09	0.00	0.00	100.87
OPX2 intermediate	57.87	0.13	0.91	0.36	5.08	0.12	35.71	0.40	0.13	0.12	0.00	0.00	100.85
OPX2 core	57.51	0.12	0.94	0.34	5.03	0.14	35.70	0.42	0.14	0.11	0.01	0.01	100.46
OPX3 rim	57.80	0.13	1.08	0.41	5.12	0.11	35.54	0.53	0.14	0.11	0.01	0.01	100.98
OPX3 intermediate	57.53	0.09	1.05	0.41	5.08	0.12	35.54	0.49	0.10	0.12	0.00	0.00	100.53
OPX3 core	57.54	0.10	0.99	0.39	4.97	0.10	35.51	0.49	0.09	0.13	0.00	0.02	100.32
Gibtown 93-11 CPX1 rim	54.81	0.30	2.54	2.05	2.36	0.07	15.95	19.36	0.08	2.21	0.00	0.00	99.72
CPX1 core	54.64	0.28	2.63	2.23	2.37	0.08	16.20	19.51	0.05	2.21	0.00	0.01	100.21
CPX1 intermediate	54.64	0.24	2.57	2.15	2.35	0.08	15.95	19.59	0.04	2.13	0.02	0.01	99.76
CPX2 rim	54.69	0.26	2.61	2.19	2.42	0.07	16.18	19.16	0.07	2.13	0.01	0.01	99.81
CPX2 core	54.69	0.27	2.64	2.12	2.42	0.11	16.37	19.23	0.06	2.16	0.01	0.02	100.10
CPX2 intermediate	54.72	0.22	2.68	2.23	2.46	0.10	16.27	19.08	0.03	2.19	0.01	0.02	100.00
CPX3 rim	54.62	0.26	2.61	2.30	2.43	0.09	16.34	19.09	0.05	2.14	0.00	0.02	99.94
CPX3 core	54.47	0.23	2.63	2.22	2.43	0.09	16.31	18.98	0.05	2.19	0.02	0.01	99.64
CPX3 intermediate	54.49	0.24	2.63	2.19	2.41	0.07	16.35	18.96	0.08	2.17	0.01	0.00	99.61
Gibtown 93-11 Grt1 rim	42.24	0.28	20.39	4.21	7.46	0.36	20.73	5.17	0.02	0.05	0.00	0.01	100.93
Grt1 intermediate	41.99	0.29	20.24	4.30	7.47	0.41	20.57	5.20	0.00	0.05	0.00	0.02	100.54
Grt1 core	42.17	0.31	20.30	4.46	7.61	0.38	20.55	5.18	0.00	0.05	0.00	0.03	101.04
Grt2 rim	42.32	0.33	20.07	4.50	7.60	0.36	20.38	5.36	0.00	0.05	0.00	0.03	101.00
Grt2 intermediate	42.30	0.29	20.21	4.50	7.68	0.41	20.35	5.35	0.01	0.06	0.01	0.02	101.20
Grt2 core	41.85	0.32	20.02	4.47	7.62	0.43	20.29	5.33	0.00	0.07	0.01	0.01	100.42
Grt3 rim	42.04	0.30	20.25	4.40	7.60	0.41	20.60	5.22	0.03	0.06	0.00	0.02	100.93
Grt3 intermediate	42.14	0.28	20.06	4.32	7.67	0.44	20.37	5.27	0.00	0.05	0.01	0.04	100.65
Grt3 core	41.93	0.30	20.27	4.37	7.67	0.38	20.41	5.35	0.03	0.06	0.00	0.01	100.78

Sample	SiO_2	TiO_2	Al_2O_3	Cr_2O_3	FeO	MnO	MgO	CaO	NiO	Na_2O	K_2O	P_2O_5	Total
SKGG IV OPX1 intermediate	57.32	0.09	0.84	0.29	5.30	0.13	35.93	0.45	0.10	0.12	0.00	0.00	100.57
OPX1 core	57.01	0.08	0.84	0.29	5.40	0.14	35.95	0.39	0.13	0.10	0.00	0.00	100.33
OPX1	57.37	0.09	0.93	0.30	5.38	0.11	35.92	0.43	0.09	0.11	0.00	0.00	100.73
OPX2 rim	58.27	0.09	0.83	0.25	5.32	0.11	36.07	0.40	0.10	0.11	0.00	0.00	101.56
OPX2 intermediate	58.06	0.08	0.86	0.29	5.36	0.10	35.95	0.40	0.09	0.08	0.01	0.02	101.30
OPX2 core	58.11	0.12	0.85	0.26	5.40	0.13	36.12	0.42	0.10	0.10	0.00	0.00	101.60
OPX3 rim	57.77	0.10	0.87	0.27	5.30	0.15	36.06	0.43	0.09	0.09	0.00	0.00	101.13
OPX3 intermediate	57.79	0.11	0.84	0.29	5.31	0.11	35.92	0.40	0.13	0.09	0.00	0.01	101.00
OPX3 core	57.79	0.09	0.84	0.24	5.30	0.13	36.07	0.43	0.13	0.09	0.01	0.02	101.14
OPX4 rim	57.79	0.12	0.82	0.26	5.41	0.12	35.93	0.43	0.07	0.12	0.01	0.00	101.06
OPX4 intermediate	57.62	0.14	0.82	0.28	5.24	0.13	36.01	0.43	0.09	0.12	0.00	0.01	100.88
OPX4 core	57.77	0.10	0.79	0.26	5.33	0.13	35.72	0.44	0.12	0.13	0.01	0.00	100.80
OPX5 rim	58.05	0.11	0.85	0.27	5.30	0.15	35.99	0.41	0.11	0.11	0.00	0.00	101.33
OPX5 intermediate	58.21	0.12	0.85	0.25	5.39	0.16	35.91	0.41	0.07	0.10	0.01	0.01	101.49
OPX5 core	58.06	0.10	0.86	0.27	5.37	0.12	35.91	0.39	0.10	0.12	0.01	0.01	101.33
OPX6 rim	57.85	0.11	0.82	0.33	5.29	0.13	35.96	0.43	0.10	0.11	0.00	0.00	101.12
OPX6 intermediate	57.81	0.11	0.83	0.29	5.27	0.15	35.87	0.42	0.10	0.11	0.00	0.01	100.96
OPX6 core	58.01	0.11	0.84	0.28	5.32	0.12	35.99	0.44	0.13	0.11	0.01	0.00	101.36
SKGG IV CPX1 rim	54.50	0.21	2.62	1.67	2.59	0.10	16.64	19.59	0.04	1.91	0.01	0.02	99.88
CPX1 intermediate	54.53	0.21	2.64	1.59	2.57	0.09	16.51	19.61	0.06	2.06	0.00	0.04	99.90
CPX1 core	54.65	0.22	2.59	1.70	2.60	0.06	16.69	19.54	0.00	2.01	0.01	0.01	100.08
CPX2 rim	54.52	0.23	2.67	1.67	2.58	0.06	16.66	19.53	0.03	1.96	0.01	0.03	99.95
CPX2 intermediate	54.50	0.20	2.63	1.56	2.56	0.07	16.73	19.55	0.03	1.97	0.02	0.02	99.83
CPX2 core	54.58	0.22	2.64	1.56	2.57	0.08	16.83	19.65	0.01	1.93	0.01	0.00	100.08
CPX3 rim	54.46	0.22	2.54	1.74	2.51	0.09	16.52	19.71	0.10	1.97	0.00	0.00	99.86
CPX3 intermediate	54.29	0.21	2.55	1.66	2.55	0.11	16.66	19.50	0.05	1.95	0.01	0.02	99.55
CPX3 core	54.60	0.19	2.54	1.71	2.54	0.07	16.89	19.58	0.03	2.00	0.00	0.03	100.19
SKGG IV Grt1 rim	41.99	0.26	21.01	3.18	8.08	0.39	20.39	4.96	0.00	0.05	0.00	0.03	100.34
Grt1 intermediate	42.31	0.26	20.97	3.28	8.03	0.42	20.40	5.00	0.03	0.06	0.00	0.03	100.79
Grt1 core	42.25	0.26	20.95	3.31	8.10	0.42	20.57	4.93	0.01	0.05	0.01	0.03	100.90
Grt2 rim	42.71	0.22	21.46	3.02	8.02	0.38	20.69	4.87	0.00	0.03	0.00	0.03	101.43
Grt2 intermediate	42.17	0.24	21.41	3.03	7.97	0.38	20.86	4.93	0.05	0.06	0.00	0.04	101.13
Grt2 core	42.27	0.24	21.32	3.01	7.98	0.37	20.62	4.91	0.03	0.03	0.01	0.02	100.82
Grt3 rim	42.39	0.25	21.18	3.16	8.00	0.38	20.52	4.94	0.00	0.06	0.01	0.03	100.91
Grt3 intermediate	42.31	0.23	21.25	3.17	7.94	0.39	20.58	4.95	0.04	0.04	0.00	0.03	100.93
Grt3 core	42.22	0.26	21.24	3.23	7.98	0.40	20.62	4.93	0.03	0.04	0.00	0.05	101.00
SKGG IVa OPX1 rim	57.80	0.17	1.44	0.61	4.77	0.09	35.00	0.83	0.15	0.17	0.01	0.00	101.03
OPX1 core	58.26	0.14	1.28	0.55	4.77	0.14	35.20	0.76	0.16	0.16	0.00	0.00	101.42
OPX1 intermediate	58.20	0.10	1.33	0.49	4.70	0.12	35.26	0.73	0.10	0.16	0.01	0.00	101.21
OPX2 intermediate	58.08	0.12	1.40	0.58	4.75	0.13	35.44	0.67	0.13	0.14	0.01	0.00	101.46
OPX2 intermediate	57.81	0.15	1.43	0.60	4.77	0.12	35.24	0.72	0.12	0.16	0.00	0.00	101.12
OPX2 intermediate	57.67	0.17	1.50	0.66	4.85	0.13	35.06	0.79	0.08	0.18	0.00	0.00	101.09
OPX3 intermediate	57.69	0.17	1.42	0.60	4.80	0.12	35.23	0.79	0.11	0.15	0.00	0.03	101.11
OPX3 intermediate	57.84	0.13	1.46	0.62	4.77	0.13	35.33	0.78	0.12	0.16	0.00	0.00	101.34
OPX3 intermediate	57.66	0.17	1.50	0.64	4.71	0.09	35.28	0.80	0.12	0.16	0.00	0.00	101.12
SKGG IVa CPX1 rim	55.07	0.15	2.74	1.48	2.58	0.09	17.08	19.63	0.04	1.86	0.02	0.00	100.73
CPX1 intermediate	55.29	0.17	2.67	1.47	2.62	0.08	17.01	19.52	0.08	1.85	0.01	0.02	100.79
CPX1 core	55.09	0.16	2.64	1.44	2.60	0.10	16.90	19.68	0.08	1.81	0.02	0.02	100.53
CPX2 rim	55.21	0.10	2.58	1.46	2.53	0.09	16.94	19.91	0.06	1.82	0.01	0.01	100.71
CPX2 intermediate	55.17	0.11	2.45	1.37	2.51	0.11	16.78	20.03	0.06	1.85	0.01	0.02	100.48
CPX2 core	55.24	0.10	2.47	1.43	2.50	0.12	16.85	20.03	0.03	1.79	0.01	0.01	100.60
CPX3 rim	55.30	0.13	2.32	1.47	2.54	0.07	16.86	20.26	0.06	1.81	0.01	0.00	100.84
CPX3 intermediate	55.25	0.09	2.27	1.52	2.56	0.10	16.83	20.21	0.06	1.73	0.02	0.01	100.65
CPX3 core	55.41	0.12	2.27	1.46	2.56	0.07	16.88	20.27	0.07	1.78	0.01	0.02	100.92
SKGG IVa Grt1 core	42.85	0.06	20.23	5.23	7.07	0.43	20.77	5.28	0.01	0.02	0.00	0.00	101.96
Grt1 rim	41.63	0.10	16.23	5.30	6.53	0.54	24.36	5.30	0.01	0.05	0.00	0.00	100.04
Grt1 intermediate	42.57	0.06	19.96	5.46	6.88	0.41	21.03	5.22	0.01	0.03	0.00	0.01	101.64
Grt2 rim	42.67	0.04	19.61	5.77	6.45	0.36	21.08	5.33	0.00	0.01	0.00	0.01	101.33
Grt2 core	42.66	0.14	19.82	5.67	6.32	0.37	21.31	5.30	0.00	0.02	0.00	0.02	101.63
Grt2 intermediate	42.51	0.08	19.99	5.49	6.62	0.38	21.03	5.16	0.00	0.01	0.00	0.02	101.29
SKGG IVb OPX1 rim	57.50	0.23	1.46	0.61	4.77	0.13	35.35	0.85	0.11	0.15	0.00	0.00	101.15
OPX1 intermediate	57.67	0.20	1.54	0.66	4.81	0.11	35.52	0.82	0.10	0.20	0.01	0.00	101.65
OPX1 core	57.40	0.18	1.45	0.64	4.75	0.14	35.09	0.85	0.11	0.16	0.00	0.00	100.76
OPX2 rim	57.09	0.18	1.46	0.63	4.70	0.14	35.07	0.83	0.12	0.17	0.00	0.01	100.40
OPX2 intermediate	56.88	0.17	1.47	0.61	4.76	0.11	35.08	0.85	0.11	0.18	0.00	0.00	100.23
OPX2 core	57.08	0.18	1.43	0.69	4.82	0.13	34.98	0.91	0.13	0.17	0.04	0.01	100.56
OPX3 rim	57.41	0.16	1.35	0.52	4.76	0.12	35.33	0.81	0.12	0.14	0.00	0.00	100.71
OPX3 intermediate	57.56	0.14	1.34	0.49	4.78	0.14	35.30	0.80	0.13	0.14	0.00	0.01	100.83
OPX3 core	57.11	0.18	1.37	0.54	4.74	0.11	35.27	0.84	0.16	0.15	0.00	0.00	100.46

Sample	SiO_2	TiO_2	Al_2O_3	Cr_2O_3	FeO	MnO	MgO	CaO	NiO	Na_2O	K_2O	P_2O_5	Total
SKGG IVb Grt1 rim	41.76	0.32	19.30	5.85	6.44	0.34	21.21	5.70	0.02	0.04	0.00	0.01	100.99
Grt1 core	41.96	0.05	20.00	5.54	6.86	0.35	21.30	5.26	0.03	0.00	0.01	0.02	101.37
Grt1 intermediate	41.72	0.13	19.92	5.65	6.54	0.34	21.45	5.33	0.00	0.04	0.01	0.01	101.14
Grt2 rim	41.11	0.05	20.03	5.46	7.15	0.43	20.93	5.25	0.03	0.02	0.00	0.03	100.47
Grt2 core	42.01	0.06	19.92	5.69	7.01	0.39	21.18	5.28	0.00	0.03	0.00	0.03	101.60
Grt2 intermediate	42.04	0.06	19.91	5.54	7.00	0.37	21.11	5.29	0.02	0.02	0.00	0.02	101.39
Grt3 rim	42.12	0.04	20.20	5.51	6.83	0.39	21.33	5.28	0.01	0.02	0.01	0.00	101.74
Grt3 core	42.14	0.05	20.24	5.46	7.17	0.38	21.07	5.40	0.03	0.02	0.00	0.02	101.98
Grt3 intermediate	42.16	0.09	20.11	5.47	6.92	0.39	21.24	5.30	0.00	0.03	0.00	0.01	101.72
SKGG IVc Ol1 rim	40.90	0.03	0.05	0.07	7.96	0.12	52.01	0.08	0.37	0.01	0.00	0.00	101.60
Ol1 intermediate	40.70	0.03	0.03	0.05	7.90	0.12	51.81	0.08	0.41	0.02	0.00	0.00	101.15
Ol1 core	40.66	0.05	0.03	0.05	7.72	0.12	51.76	0.06	0.36	0.02	0.01	0.01	100.86
Ol2 rim	40.85	0.03	0.02	0.05	8.01	0.11	51.73	0.07	0.39	0.02	0.00	0.01	101.29
Ol2 intermediate	40.69	0.03	0.03	0.06	8.05	0.09	51.89	0.07	0.40	0.03	0.00	0.01	101.36
Ol2 core	40.78	0.01	0.04	0.03	7.97	0.11	51.78	0.07	0.39	0.02	0.01	0.02	101.23
Ol3 rim	40.66	0.04	0.04	0.05	7.94	0.11	51.83	0.06	0.42	0.02	0.00	0.02	101.18
Ol3 intermediate	40.61	0.02	0.04	0.05	8.04	0.13	51.89	0.09	0.44	0.01	0.01	0.00	101.31
Ol3 core	40.57	0.00	0.02	0.05	7.99	0.13	51.58	0.07	0.38	0.03	0.01	0.00	100.84
SKGG IVc OPX1 rim	57.14	0.18	1.72	0.53	4.86	0.11	35.03	1.15	0.12	0.18	0.00	0.00	101.04
OPX1 intermediate	57.39	0.21	1.71	0.55	4.91	0.09	35.11	1.09	0.14	0.20	0.00	0.00	101.40
OPX1 core	57.07	0.20	1.69	0.53	4.89	0.12	34.89	1.11	0.13	0.17	0.00	0.00	100.79
OPX2 rim	56.93	0.19	1.72	0.53	4.90	0.12	35.01	1.13	0.14	0.17	0.01	0.00	100.84
OPX2 intermediate	57.22	0.22	1.71	0.54	4.90	0.13	35.04	1.07	0.11	0.17	0.01	0.00	101.12
OPX2 core	57.53	0.22	1.69	0.52	5.01	0.14	35.06	1.07	0.11	0.14	0.00	0.01	101.50
OPX3 intermediate	56.91	0.19	1.75	0.54	4.84	0.10	35.25	1.12	0.13	0.17	0.00	0.00	100.99
OPX3 core	57.30	0.19	1.70	0.52	4.79	0.14	35.08	1.10	0.12	0.18	0.01	0.00	101.12
SKGG IVc CPX1 rim	54.74	0.37	2.52	1.46	2.77	0.06	18.88	18.88	0.08	1.32	0.03	0.02	101.11
CPX1 core	55.17	0.34	2.57	1.50	2.79	0.08	18.74	18.63	0.07	1.32	0.02	0.00	101.24
CPX1 intermediate	54.99	0.36	2.57	1.50	2.76	0.08	18.89	18.85	0.05	1.31	0.02	0.01	101.38
SKGG IVc Grt1 rim	42.58	0.21	20.59	4.69	6.48	0.30	21.70	5.42	0.03	0.04	0.00	0.03	102.07
Grt1 core	42.49	0.14	20.51	4.77	6.65	0.34	21.31	5.39	0.01	0.05	0.00	0.04	101.70
Grt1 intermediate	42.23	0.16	20.59	4.68	6.44	0.31	21.76	5.39	0.02	0.02	0.00	0.00	101.60
SKGG IVd Ol1 rim	40.38	0.00	0.03	0.02	8.50	0.12	51.42	0.02	0.41	0.02	0.00	0.02	100.94
Ol1 intermediate	40.33	0.00	0.02	0.01	8.57	0.10	51.20	0.01	0.39	0.01	0.00	0.00	100.64
Ol1 core	40.90	0.01	0.02	0.02	8.55	0.10	51.22	0.01	0.41	0.01	0.00	0.01	101.26
Ol2 rim	40.25	0.02	0.01	0.01	8.66	0.11	51.27	0.02	0.39	0.03	0.01	0.00	100.80
Ol2 intermediate	40.69	0.02	0.00	0.02	8.58	0.14	51.37	0.02	0.44	0.01	0.00	0.01	101.30
Ol2 core	40.23	0.01	0.03	0.01	8.60	0.13	51.46	0.02	0.42	0.02	0.00	0.00	100.93
Ol3 rim	40.30	0.02	0.02	0.01	8.70	0.10	51.49	0.02	0.43	0.02	0.00	0.00	101.11
Ol3 intermediate	40.74	0.01	0.01	0.02	8.61	0.14	51.62	0.02	0.40	0.02	0.01	0.01	101.61
Ol3 core	40.18	0.01	0.02	0.00	8.51	0.11	51.53	0.03	0.41	0.02	0.00	0.00	100.82
SKGG IVd OPX1 rim	57.57	0.03	1.04	0.34	5.26	0.11	35.75	0.38	0.10	0.04	0.01	0.00	100.64
OPX1 intermediate	57.26	0.01	1.04	0.34	5.22	0.13	35.88	0.37	0.11	0.05	0.00	0.00	100.40
OPX1 core	57.65	0.03	1.05	0.34	5.24	0.12	35.72	0.36	0.09	0.05	0.00	0.00	100.64
OPX2 rim	57.69	0.02	0.49	0.29	5.13	0.12	35.86	0.38	0.10	0.10	0.00	0.01	100.18
OPX2 intermediate	57.73	0.04	0.78	0.35	5.22	0.13	35.87	0.36	0.10	0.10	0.00	0.01	100.68
OPX2 core	57.53	0.01	1.02	0.36	5.25	0.14	35.65	0.36	0.09	0.05	0.00	0.00	100.44
OPX3 rim	57.29	0.01	1.03	0.35	5.19	0.12	35.74	0.36	0.08	0.04	0.00	0.00	100.23
OPX3 intermediate	57.13	0.02	1.02	0.33	5.21	0.12	35.66	0.34	0.11	0.05	0.00	0.02	100.01
OPX3 core	57.14	0.01	1.01	0.34	5.28	0.12	35.70	0.37	0.11	0.04	0.01	0.00	100.13
SKGG IVd CPX1 rim	55.51	0.03	1.68	1.24	1.88	0.07	17.19	22.24	0.07	1.28	0.00	0.00	101.18
CPX1 core	55.76	0.05	1.82	1.23	1.99	0.08	17.07	22.05	0.05	1.45	0.00	0.00	101.55
CPX1 intermediate	54.72	0.06	1.96	1.18	2.09	0.09	16.80	22.05	0.06	1.41	0.17	0.10	100.67
CPX2 rim	55.29	0.05	1.74	1.27	1.97	0.06	17.10	22.19	0.05	1.35	0.00	0.01	101.09
CPX2 core	55.11	0.03	1.66	1.30	1.94	0.08	17.23	22.33	0.03	1.35	0.00	0.00	101.04
CPX2 intermediate	55.14	0.04	1.63	1.18	2.08	0.07	17.19	22.08	0.06	1.41	0.00	0.01	100.89
CPX3 rim	55.54	0.03	1.66	1.25	1.85	0.07	17.37	22.25	0.06	1.19	0.00	0.01	101.27
CPX3 core	54.61	0.04	1.68	1.21	1.82	0.08	17.29	22.40	0.04	1.27	0.00	0.01	100.45
CPX3 intermediate	55.36	0.04	1.63	1.24	1.91	0.08	17.30	22.52	0.05	1.21	0.00	0.00	101.33
SKGG IVe OPX1 rim	57.11	0.03	0.93	0.23	5.32	0.14	35.44	0.44	0.11	0.12	0.00	0.00	99.86
OPX1 intermediate	56.86	0.03	0.95	0.27	5.41	0.13	35.83	0.44	0.11	0.10	0.00	0.02	100.15
OPX1 core	57.55	0.06	0.94	0.24	5.56	0.11	35.78	0.46	0.10	0.10	0.00	0.01	100.91
OPX2 rim	56.94	0.04	1.01	0.26	5.39	0.13	35.38	0.49	0.09	0.12	0.00	0.01	99.87
OPX2 intermediate	57.18	0.06	1.02	0.24	5.48	0.10	35.37	0.48	0.12	0.11	0.01	0.00	100.17
OPX2 core	57.19	0.07	1.05	0.27	5.40	0.12	35.44	0.52	0.09	0.14	0.03	0.01	100.31
OPX3 rim	57.34	0.09	1.11	0.25	5.42	0.12	35.30	0.52	0.12	0.15	0.01	0.00	100.43
OPX3 intermediate	57.18	0.06	1.02	0.23	5.46	0.15	35.57	0.47	0.11	0.10	0.00	0.00	100.34
OPX3 core	57.67	0.06	0.98	0.26	5.50	0.12	35.62	0.48	0.11	0.11	0.00	0.00	100.91
SKGG IVe CPX1 rim	53.80	0.37	2.92	1.09	2.79	0.08	16.99	21.84	0.05	0.96	0.01	0.02	100.92
CPX1 core	55.26	0.11	2.34	1.30	2.63	0.09	17.14	20.59	0.04	1.70	0.01	0.00	101.21
CPX1 intermediate	55.11	0.12	2.36	1.35	2.62	0.08	17.16	20.28	0.05	1.74	0.01	0.00	100.87

Sample	SiO_2	TiO_2	Al_2O_3	Cr_2O_3	FeO	MnO	MgO	CaO	NiO	Na_2O	K_2O	P_2O_5	Total
CPX2 rim	54.09	0.15	2.50	1.26	2.62	0.08	17.24	20.13	0.05	1.77	0.02	0.01	99.91
CPX2 core	55.16	0.13	2.47	1.30	2.68	0.09	17.20	20.21	0.06	1.77	0.01	0.03	101.11
CPX2 intermediate	55.24	0.14	2.49	1.32	2.63	0.11	17.25	20.25	0.08	1.79	0.02	0.00	101.31
CPX3 rim	54.70	0.18	2.57	1.42	2.73	0.09	16.73	22.00	0.05	1.17	0.00	0.01	101.64
CPX3 core	55.76	0.07	2.40	1.33	2.56	0.08	17.04	20.38	0.08	1.70	0.00	0.00	101.40
CPX3 intermediate	55.17	0.12	2.43	1.30	2.57	0.08	16.84	20.24	0.05	1.90	0.07	0.00	100.78
SKGG IVe Grt1 rim	43.40	0.08	22.16	2.70	8.22	0.35	21.03	4.89	0.00	0.02	0.00	0.02	102.87
Grt1 core	42.61	0.07	22.00	2.63	8.17	0.42	21.03	4.92	0.00	0.02	0.00	0.00	101.87
Grt1 intermediate	42.84	0.07	22.23	2.67	8.27	0.42	21.20	4.94	0.01	0.03	0.00	0.01	102.69
Grt2 rim	42.70	0.08	22.02	2.76	7.85	0.38	21.08	4.87	0.00	0.02	0.00	0.03	101.79
Grt2 core	42.18	0.07	22.01	2.70	7.96	0.38	21.11	4.83	0.00	0.03	0.00	0.03	101.30
Grt2 intermediate	42.79	0.07	22.05	2.75	8.06	0.41	20.96	4.89	0.03	0.02	0.00	0.04	102.07
Grt3 rim	42.72	0.03	22.05	2.63	8.10	0.38	21.20	4.87	0.00	0.03	0.00	0.03	102.04
Grt3 core	42.85	0.06	22.09	2.66	7.99	0.39	21.08	4.86	0.00	0.00	0.00	0.03	102.01
Grt3 intermediate	42.71	0.06	21.95	2.71	7.93	0.37	21.10	4.81	0.01	0.03	0.00	0.04	101.72
KGG 91-20c Ol1 rim	39.93	0.02	0.00	0.05	9.40	0.12	51.03	0.06	0.42	0.01	0.00	0.00	101.03
Ol1 intermediate	39.78	0.03	0.04	0.06	9.48	0.13	50.99	0.06	0.38	0.03	0.00	0.00	100.98
Ol1 core	39.77	0.04	0.07	0.04	9.45	0.11	50.88	0.09	0.39	0.06	0.00	0.01	100.90
Ol2 rim	39.85	0.04	0.04	0.03	9.49	0.12	50.59	0.06	0.37	0.02	0.01	0.01	100.64
Ol2 intermediate	39.96	0.05	0.04	0.06	9.57	0.12	50.86	0.08	0.40	0.03	0.00	0.01	101.18
Ol2 core	40.14	0.05	0.02	0.07	9.50	0.14	50.70	0.08	0.43	0.02	0.00	0.00	101.15
Ol3 rim	39.40	0.04	0.04	0.06	9.55	0.14	50.89	0.06	0.38	0.02	0.00	0.01	100.60
Ol3 intermediate	39.18	0.04	0.05	0.05	9.46	0.12	50.73	0.09	0.38	0.02	0.01	0.00	100.13
Ol3 core	39.51	0.01	0.02	0.03	9.72	0.12	49.96	0.09	0.35	0.02	0.01	0.01	99.86
KGG 91-20c OPX1 rim	57.39	0.26	1.70	0.53	5.52	0.13	34.36	1.04	0.11	0.19	0.01	0.00	101.25
OPX1 intermediate	57.01	0.29	1.73	0.53	5.61	0.14	34.47	1.01	0.12	0.20	0.01	0.00	101.11
OPX1 core	57.03	0.28	1.71	0.54	5.46	0.13	34.39	1.00	0.14	0.20	0.00	0.00	100.88
OPX2 rim	56.86	0.29	1.75	0.53	5.60	0.13	34.35	1.06	0.14	0.23	0.00	0.00	100.93
OPX2 intermediate	56.70	0.31	1.76	0.52	5.62	0.10	34.35	1.14	0.10	0.18	0.00	0.00	100.77
OPX2 core	56.75	0.30	1.73	0.53	5.54	0.13	34.54	1.09	0.12	0.18	0.00	0.00	100.91
OPX3 rim	56.77	0.27	1.70	0.45	5.89	0.13	34.47	1.06	0.12	0.22	0.00	0.00	101.09
OPX3 intermediate	57.27	0.28	1.76	0.46	5.84	0.12	34.42	1.13	0.12	0.19	0.01	0.01	101.60
OPX3 core	57.25	0.28	1.75	0.49	5.73	0.13	34.36	1.12	0.11	0.25	0.03	0.00	101.49
KGG 91-20c CPX1 rim	53.98	0.49	2.74	1.63	3.22	0.08	18.19	17.92	0.06	1.58	0.02	0.02	99.93
CPX1 intermediate	54.30	0.53	2.73	1.60	3.23	0.12	18.16	17.83	0.10	1.59	0.03	0.00	100.21
CPX1 core	54.07	0.52	2.78	1.53	3.26	0.10	18.30	17.89	0.06	1.58	0.04	0.01	100.14
CPX2 rim	54.15	0.52	2.74	1.41	3.21	0.10	18.30	17.81	0.03	1.55	0.03	0.02	99.87
CPX2 intermediate	54.10	0.50	2.76	1.41	3.27	0.11	18.37	17.84	0.08	1.55	0.04	0.01	100.03
CPX2 core	54.29	0.49	2.74	1.39	3.20	0.11	18.22	17.92	0.08	1.57	0.03	0.00	100.04
CPX3 rim	54.07	0.53	2.75	1.65	3.23	0.10	18.23	17.97	0.06	1.60	0.03	0.00	100.21
CPX3 intermediate	54.20	0.51	2.71	1.55	3.18	0.11	18.23	17.94	0.06	1.54	0.04	0.01	100.08
CPX3 core	54.19	0.50	2.73	1.36	3.16	0.10	18.25	18.00	0.06	1.56	0.02	0.02	99.95
KGG 91-20c Grt1 rim	42.46	0.35	19.56	5.66	6.68	0.34	21.33	5.58	0.00	0.04	0.00	0.05	102.05
Grt1 core	41.43	0.38	19.74	5.38	6.70	0.34	21.42	5.53	0.03	0.04	0.00	0.00	100.99
Grt1 intermediate	41.80	0.38	19.81	5.54	6.71	0.35	21.45	5.49	0.04	0.06	0.00	0.04	101.67
Grt2 rim	42.08	0.38	19.73	5.72	6.64	0.32	21.30	5.65	0.03	0.04	0.00	0.06	101.95
Grt2 core	41.90	0.34	19.39	5.97	6.73	0.38	21.18	5.68	0.01	0.06	0.00	0.03	101.67
Grt2 intermediate	42.20	0.34	19.62	5.80	6.80	0.37	21.30	5.62	0.01	0.04	0.00	0.06	102.16
Grt3 rim	41.94	0.41	19.73	5.20	6.76	0.32	21.35	5.42	0.01	0.05	0.01	0.03	101.23
Grt3 core	41.48	0.39	19.80	5.26	6.72	0.34	21.48	5.41	0.00	0.05	0.01	0.02	100.96
Grt3 intermediate	41.85	0.37	19.73	5.23	6.76	0.36	21.30	5.37	0.01	0.02	0.00	0.04	101.05
KGG 91-37 Ol1 rim	40.82	0.03	0.03	0.04	7.78	0.10	51.97	0.04	0.39	0.03	0.00	0.01	101.23
Ol1 intermediate	40.99	0.00	0.01	0.03	7.68	0.09	51.84	0.04	0.37	0.02	0.00	0.00	101.07
Ol1 core	40.73	0.01	0.04	0.05	7.77	0.08	51.62	0.05	0.42	0.03	0.00	0.00	100.80
Ol2 rim	40.04	0.00	0.04	0.06	7.84	0.10	52.03	0.05	0.39	0.02	0.00	0.00	100.57
Ol2 intermediate	40.16	0.02	0.02	0.05	7.80	0.11	51.92	0.05	0.41	0.02	0.00	0.00	100.56
Ol2 core	40.19	0.01	0.04	0.05	7.73	0.14	52.07	0.05	0.48	0.02	0.00	0.00	100.78
Ol3 rim	39.42	0.02	0.03	0.05	7.85	0.09	52.06	0.04	0.42	0.02	0.00	0.01	100.01
Ol3 intermediate	40.57	0.02	0.03	0.04	7.72	0.10	51.90	0.04	0.38	0.02	0.00	0.00	100.81
Ol3 core	40.21	0.00	0.04	0.04	7.91	0.11	51.92	0.05	0.41	0.03	0.00	0.01	100.72
KGG 91-37 OPX1 rim	56.79	0.27	1.50	0.56	4.90	0.10	35.43	0.94	0.12	0.15	0.00	0.00	100.76
OPX1 intermediate	57.52	0.10	1.13	0.49	4.81	0.13	36.09	0.65	0.13	0.13	0.00	0.00	101.16
OPX1 core	57.45	0.09	1.20	0.51	4.76	0.08	35.87	0.79	0.11	0.15	0.00	0.00	101.00
OPX2 rim	56.85	0.09	1.32	0.55	4.77	0.11	35.79	0.79	0.12	0.15	0.00	0.00	100.54
OPX2 intermediate	56.81	0.08	1.34	0.56	4.80	0.12	35.75	0.75	0.10	0.15	0.00	0.00	100.44
OPX2 core	56.75	0.11	1.30	0.55	4.62	0.11	35.67	0.79	0.14	0.14	0.02	0.00	100.19
OPX3 rim	57.36	0.10	1.23	0.48	4.72	0.08	35.95	0.62	0.12	0.13	0.00	0.00	100.79
OPX3 intermediate	57.47	0.09	1.28	0.49	4.70	0.09	35.69	0.66	0.10	0.15	0.01	0.01	100.73
OPX3 core	57.19	0.10	1.36	0.53	4.65	0.10	35.57	0.69	0.10	0.15	0.00	0.00	100.45
KGG 91-37 CPX1 rim	55.72	0.18	2.12	2.44	2.29	0.10	17.71	19.27	0.06	1.67	0.03	0.00	101.60
CPX1 core	55.77	0.17	2.15	2.53	2.31	0.09	17.60	19.41	0.05	1.74	0.03	0.01	101.85
CPX1 intermediate	55.38	0.17	2.15	2.55	2.28	0.08	17.51	19.31	0.03	1.72	0.02	0.01	101.21
CPX2 rim	55.52	0.17	2.29	2.56	2.23	0.08	17.45	19.40	0.06	1.78	0.02	0.00	101.56
CPX2 core	55.65	0.18	2.22	2.59	2.34	0.08	17.62	19.17	0.08	1.85	0.01	0.01	101.81
CPX2 intermediate	55.78	0.17	2.03	2.34	2.30	0.09	17.92	19.44	0.05	1.70	0.02	0.00	101.84

Sample	SiO_2	TiO_2	Al_2O_3	Cr_2O_3	FeO	MnO	MgO	CaO	NiO	Na_2O	K_2O	P_2O_5	Total
CPX3 rim	55.89	0.18	2.08	1.90	2.30	0.08	17.84	19.66	0.04	1.61	0.02	0.02	101.61
CPX3 core	55.20	0.17	2.24	2.53	2.27	0.09	17.44	19.48	0.03	1.76	0.03	0.00	101.24
CPX3 intermediate	55.51	0.16	2.28	2.44	2.26	0.10	17.55	19.56	0.04	1.81	0.02	0.03	101.76
KGG 91-37 Grt rim	42.64	0.23	19.81	5.39	7.03	0.41	20.92	5.54	0.01	0.03	0.00	0.02	102.03
Grt core	42.40	0.22	19.73	5.61	6.92	0.35	20.97	5.60	0.00	0.05	0.00	0.01	101.86
Grt intermediate	42.38	0.24	19.80	5.67	6.97	0.38	21.03	5.64	0.04	0.04	0.01	0.02	102.21
Grt2 rim	42.90	0.24	19.56	5.72	7.08	0.38	20.66	5.68	0.03	0.05	0.01	0.00	102.31
Grt2 core	42.42	0.21	19.67	5.84	7.11	0.35	20.77	5.74	0.00	0.05	0.00	0.05	102.21
Grt2 intermediate	42.38	0.23	19.62	5.75	7.06	0.42	20.78	5.70	0.01	0.05	0.00	0.04	102.04
Grt3 rim	43.00	0.23	19.87	5.45	6.86	0.37	20.94	5.53	0.00	0.02	0.01	0.02	102.30
Grt3 core	42.70	0.23	19.97	5.32	6.97	0.37	20.90	5.51	0.00	0.02	0.00	0.01	101.99
Grt3 intermediate	42.69	0.21	20.07	5.29	7.04	0.38	20.94	5.51	0.04	0.05	0.00	0.01	102.22
KGG 91-46 Ol1 rim	40.22	0.00	0.04	0.04	7.67	0.11	52.12	0.08	0.44	0.03	0.00	0.01	100.75
Ol1 intermediate	40.41	0.00	0.05	0.05	7.74	0.12	52.02	0.07	0.43	0.03	0.00	0.00	100.92
Ol1 core	40.67	0.01	0.06	0.06	7.52	0.12	51.91	0.07	0.40	0.03	0.00	0.00	100.85
Ol2 rim	40.95	0.01	0.01	0.04	7.59	0.09	51.88	0.07	0.43	0.02	0.01	0.00	101.11
Ol2 intermediate	40.71	0.01	0.04	0.04	7.71	0.11	51.77	0.07	0.45	0.02	0.00	0.00	100.93
Ol2 core	40.59	0.03	0.04	0.04	7.56	0.12	51.85	0.05	0.43	0.02	0.01	0.01	100.74
Ol3 rim	40.76	0.01	0.04	0.03	7.77	0.11	51.89	0.08	0.41	0.01	0.00	0.00	101.11
Ol3 intermediate	40.64	0.00	0.05	0.05	7.72	0.11	51.86	0.07	0.39	0.02	0.00	0.02	100.93
Ol3 core	40.47	0.00	0.03	0.05	7.68	0.10	52.02	0.05	0.41	0.04	0.00	0.00	100.85
KGG 91-46 OPX1 rim	56.94	0.03	1.62	0.45	4.62	0.13	35.08	1.11	0.14	0.14	0.00	0.02	100.27
OPX1 intermediate	56.97	0.04	1.65	0.47	4.68	0.12	35.18	1.08	0.14	0.16	0.02	0.00	100.51
OPX1 core	57.43	0.05	1.65	0.45	4.75	0.10	35.26	1.05	0.13	0.13	0.00	0.00	100.99
OPX3 rim	57.19	0.03	1.62	0.47	4.60	0.12	35.15	1.10	0.12	0.13	0.01	0.01	100.55
OPX3 intermediate	57.07	0.05	1.61	0.43	4.59	0.14	35.04	1.09	0.12	0.14	0.01	0.01	100.31
OPX3 core	57.30	0.06	1.61	0.41	4.52	0.10	35.03	1.09	0.12	0.15	0.01	0.02	100.41
KGG 91-46 CPX1 rim	55.38	0.05	2.34	1.17	2.39	0.11	18.80	19.54	0.05	1.19	0.05	0.01	101.08
CPX1 intermediate	55.52	0.07	2.26	1.18	2.37	0.07	18.77	19.51	0.07	1.18	0.07	0.01	101.08
CPX1 core	55.15	0.06	2.32	1.17	2.34	0.08	18.82	19.44	0.08	1.18	0.08	0.02	100.73
CPX2 rim	55.53	0.04	2.24	1.18	2.31	0.09	18.79	19.70	0.07	1.17	0.08	0.02	101.21
CPX2 intermediate	55.67	0.07	2.26	1.20	2.37	0.07	18.85	19.58	0.06	1.16	0.07	0.01	101.38
CPX2 core	55.60	0.06	2.23	1.20	2.37	0.07	18.77	19.65	0.05	1.14	0.07	0.00	101.22
CPX3 rim	55.52	0.05	2.33	1.16	2.46	0.08	18.83	19.44	0.08	1.17	0.06	0.00	101.17
CPX3 intermediate	55.18	0.07	2.37	1.12	2.36	0.10	18.87	19.42	0.09	1.15	0.06	0.01	100.81
CPX3 core	55.39	0.09	2.28	1.24	2.42	0.08	18.81	19.36	0.06	1.19	0.08	0.01	101.01
KGG 91-46 Grt1 rim	43.66	0.18	21.05	4.02	5.82	0.25	22.22	5.51	0.00	0.02	0.00	0.02	102.74
Grt1 core	43.11	0.16	21.21	4.04	5.82	0.26	22.02	5.46	0.00	0.02	0.01	0.04	102.15
Grt1 intermediate	42.97	0.13	21.23	3.98	5.90	0.28	22.13	5.40	0.00	0.03	0.00	0.05	102.10
Grt2 rim	43.08	0.06	21.51	3.52	6.23	0.31	22.06	4.97	0.01	0.01	0.00	0.05	101.81
Grt2 core	42.88	0.06	21.57	3.53	6.27	0.32	22.22	4.99	0.01	0.02	0.00	0.05	101.92
Grt2 intermediate	42.96	0.05	21.49	3.46	6.12	0.33	22.11	5.02	0.03	0.00	0.00	0.03	101.61
Grt3 rim	42.84	0.09	21.13	4.06	5.85	0.28	22.48	5.14	0.01	0.01	0.00	0.04	101.93
Grt3 core	42.52	0.08	21.31	3.96	5.84	0.29	22.12	5.22	0.00	0.00	0.00	0.05	101.39
Grt3 intermediate	42.59	0.06	21.30	3.86	5.86	0.27	22.17	5.15	0.02	0.01	0.00	0.05	101.34
KGG 91-60 Ol1 rim	40.17	0.02	0.03	0.03	8.98	0.09	50.97	0.04	0.41	0.02	0.01	0.01	100.77
Ol1 intermediate	40.33	0.02	0.03	0.01	9.10	0.10	51.02	0.04	0.39	0.03	0.01	0.02	101.09
Ol1 core	40.50	0.01	0.02	0.05	9.01	0.13	50.77	0.03	0.40	0.02	0.00	0.02	100.96
Ol2 rim	40.22	0.02	0.03	0.02	9.08	0.11	51.15	0.03	0.42	0.03	0.00	0.01	101.13
Ol2 intermediate	40.04	0.02	0.01	0.01	8.93	0.10	51.02	0.02	0.38	0.01	0.00	0.00	100.54
Ol2 core	39.78	0.01	0.03	0.00	9.03	0.10	50.97	0.04	0.44	0.02	0.00	0.00	100.42
Ol3 rim	39.75	0.03	0.03	0.02	9.11	0.12	51.04	0.04	0.37	0.01	0.01	0.01	100.54
Ol3 intermediate	40.25	0.03	0.03	0.03	9.09	0.10	51.19	0.05	0.44	0.03	0.00	0.01	101.25
Ol3 core	40.48	0.02	0.02	0.02	9.02	0.10	50.92	0.02	0.39	0.02	0.00	0.01	101.01
KGG 91-60 OPX1 rim	57.21	0.09	1.00	0.40	4.98	0.16	35.98	0.43	0.12	0.12	0.00	0.00	100.49
OPX1 intermediate	57.34	0.11	0.99	0.40	5.04	0.11	35.80	0.40	0.12	0.12	0.00	0.00	100.42
OPX1 core	57.30	0.12	1.03	0.40	5.04	0.11	35.95	0.45	0.11	0.13	0.00	0.00	100.64
KGG 91-60 CPX1 rim	54.85	0.28	1.42	1.45	2.59	0.10	17.16	21.57	0.07	1.20	0.01	0.01	100.72
CPX1 core	55.04	0.28	2.89	1.38	2.63	0.06	16.48	19.93	0.05	2.17	0.01	0.00	100.92
CPX1 intermediate	55.12	0.29	2.87	1.40	2.67	0.08	16.32	19.65	0.05	2.14	0.00	0.00	100.59
CPX2 rim	53.84	0.37	2.47	1.32	2.68	0.09	17.11	21.27	0.05	1.15	0.02	0.01	100.37
CPX2 core	55.06	0.28	2.89	1.32	2.75	0.06	16.75	19.51	0.06	2.00	0.00	0.01	100.70
CPX2 intermediate	55.00	0.29	3.07	1.32	2.78	0.10	16.53	19.32	0.03	2.18	0.01	0.01	100.64
CPX3 rim	55.30	0.31	2.87	1.35	2.79	0.07	16.63	19.26	0.06	2.11	0.01	0.01	100.77
CPX3 core	54.98	0.31	2.96	1.35	2.79	0.09	16.61	19.10	0.05	2.19	0.00	0.00	100.43
CPX3 intermediate	55.00	0.28	3.02	1.36	2.76	0.04	16.59	19.25	0.03	2.09	0.01	0.02	100.45
KGG 91-60 Grt1 rim	42.76	0.27	21.94	2.46	8.46	0.42	20.92	4.79	0.00	0.05	0.00	0.02	102.09
Grt1 core	42.46	0.28	21.78	2.41	8.29	0.37	20.77	4.77	0.03	0.04	0.01	0.02	101.23
Grt1 intermediate	42.80	0.30	21.89	2.49	8.38	0.36	20.81	4.69	0.03	0.04	0.00	0.04	101.82
Grt2 rim	42.82	0.22	22.04	2.36	8.35	0.39	20.92	4.75	0.00	0.03	0.01	0.03	101.92

Sample	SiO_2	TiO_2	Al_2O_3	Cr_2O_3	FeO	MnO	MgO	CaO	NiO	Na_2O	K_2O	P_2O_5	Total
Grt2 core	42.75	0.26	22.10	2.36	8.43	0.39	20.99	4.73	0.00	0.06	0.00	0.01	102.09
Grt2 intermediate	42.76	0.27	22.23	2.45	8.37	0.39	21.01	4.79	0.00	0.06	0.01	0.03	102.37
Grt3 rim	42.37	0.27	21.71	2.51	8.16	0.37	20.56	4.85	0.03	0.04	0.00	0.03	100.90
Grt3 core	42.39	0.29	21.79	2.51	8.28	0.41	20.62	4.83	0.00	0.06	0.00	0.01	101.19
Grt3 intermediate	42.74	0.28	21.90	2.49	8.32	0.36	20.92	4.79	0.00	0.06	0.00	0.04	101.90
KGG 91-62 Ol1 rim	40.41	0.02	0.03	0.03	9.23	0.12	50.90	0.03	0.40	0.01	0.01	0.00	101.19
Ol1 intermediate	40.20	0.03	0.03	0.03	9.17	0.12	51.01	0.03	0.39	0.03	0.00	0.00	101.04
Ol1 core	40.25	0.01	0.02	0.03	9.07	0.14	50.85	0.01	0.41	0.02	0.00	0.00	100.82
Ol3 rim	40.10	0.02	0.03	0.03	9.01	0.13	50.86	0.03	0.44	0.03	0.00	0.01	100.69
Ol3 intermediate	39.77	0.03	0.02	0.02	9.09	0.11	51.14	0.02	0.38	0.01	0.00	0.01	100.60
Ol3 core	39.81	0.02	0.02	0.02	9.09	0.09	51.07	0.03	0.37	0.00	0.00	0.00	100.52
KGG 91-62 OPX1 rim	57.60	0.14	0.93	0.41	5.57	0.15	35.58	0.46	0.10	0.12	0.00	0.00	101.05
OPX1 intermediate	57.20	0.13	0.91	0.40	5.64	0.15	35.65	0.43	0.09	0.13	0.00	0.00	100.71
OPX1 core	57.52	0.14	0.92	0.43	5.60	0.14	35.76	0.46	0.09	0.15	0.00	0.00	101.21
OPX2 rim	57.17	0.12	0.94	0.39	5.48	0.14	35.62	0.43	0.12	0.12	0.00	0.00	100.53
OPX2 intermediate	57.24	0.15	0.87	0.37	5.54	0.13	35.59	0.43	0.14	0.15	0.00	0.00	100.60
OPX2 core	57.52	0.15	0.88	0.39	5.42	0.15	35.69	0.39	0.13	0.14	0.01	0.00	100.87
OPX3 rim	57.02	0.14	0.90	0.36	5.44	0.15	35.79	0.39	0.14	0.13	0.00	0.00	100.45
OPX3 intermediate	56.80	0.14	0.90	0.38	5.57	0.12	35.77	0.40	0.13	0.10	0.00	0.01	100.32
OPX3 core	57.26	0.14	0.90	0.36	5.47	0.12	35.70	0.43	0.14	0.11	0.00	0.01	100.64
KGG 91-62 CPX1 rim	54.97	0.34	2.65	2.44	2.63	0.08	16.22	19.02	0.05	2.38	0.03	0.00	100.81
CPX1 core	54.27	0.34	1.53	2.67	2.66	0.09	17.06	20.47	0.04	1.47	0.00	0.00	100.60
CPX1 intermediate	54.95	0.36	2.65	2.49	2.63	0.09	16.22	19.12	0.05	2.34	0.02	0.03	100.95
CPX2 rim	54.60	0.35	1.65	2.74	2.57	0.08	16.59	20.78	0.05	1.70	0.00	0.02	101.12
CPX2 core	54.96	0.31	2.60	2.43	2.65	0.08	16.22	19.05	0.05	2.37	0.01	0.00	100.73
CPX2 intermediate	54.64	0.31	2.56	2.43	2.62	0.06	16.10	19.04	0.05	2.31	0.01	0.01	100.15
CPX3 rim	54.05	0.37	2.27	2.51	2.58	0.08	16.52	21.38	0.05	1.38	0.01	0.01	101.22
CPX3 core	54.79	0.33	2.60	2.42	2.68	0.08	16.16	19.02	0.04	2.35	0.00	0.01	100.48
CPX3 intermediate	55.10	0.36	2.62	2.37	2.65	0.08	16.30	19.07	0.08	2.38	0.01	0.01	101.03
KGG 91-62 Grt1 rim	42.20	0.33	19.71	5.10	8.40	0.40	19.86	5.43	0.01	0.07	0.01	0.04	101.56
Grt1 core	42.28	0.29	19.61	5.10	8.41	0.42	19.90	5.52	0.00	0.05	0.01	0.00	101.59
Grt1 intermediate	42.37	0.31	19.74	5.02	8.34	0.43	20.04	5.57	0.01	0.06	0.00	0.02	101.91
Grt2 rim	42.10	0.35	19.50	5.38	8.46	0.38	19.77	5.67	0.03	0.07	0.00	0.03	101.73
Grt2 core	42.16	0.38	19.49	5.30	8.45	0.41	19.82	5.60	0.00	0.07	0.00	0.02	101.70
Grt2 intermediate	42.20	0.37	19.62	5.24	8.47	0.47	19.86	5.64	0.00	0.06	0.01	0.03	101.97
Grt3 rim	42.22	0.35	19.51	5.12	8.46	0.42	19.84	5.61	0.03	0.06	0.00	0.01	101.63
Grt3 core	42.14	0.33	19.62	5.19	8.44	0.44	19.84	5.50	0.01	0.07	0.00	0.03	101.60
Grt3 intermediate	42.30	0.31	19.75	5.14	8.33	0.43	20.04	5.52	0.00	0.06	0.00	0.03	101.91
KGG 91-65 Ol1 rim	40.74	0.01	0.02	0.02	8.24	0.10	51.57	0.02	0.39	0.00	0.00	0.02	101.13
Ol1 intermediate	40.43	0.03	0.04	0.03	8.13	0.13	51.59	0.03	0.42	0.02	0.00	0.02	100.87
Ol1 core	40.75	0.04	0.04	0.03	8.10	0.09	51.55	0.03	0.36	0.02	0.00	0.00	101.01
Ol2 rim	40.19	0.02	0.02	0.03	8.22	0.08	51.79	0.03	0.40	0.03	0.01	0.01	100.82
Ol2 intermediate	40.16	0.00	0.02	0.02	8.29	0.13	51.76	0.04	0.42	0.02	0.01	0.00	100.87
Ol2 core	40.15	0.02	0.02	0.02	8.10	0.13	51.70	0.04	0.37	0.02	0.00	0.00	100.56
Ol3 rim	40.36	0.03	0.03	0.03	8.20	0.11	51.74	0.03	0.39	0.03	0.00	0.00	100.95
Ol2 intermediate	40.34	0.02	0.04	0.04	8.24	0.10	51.83	0.02	0.38	0.01	0.00	0.00	101.03
Ol3 core	40.15	0.02	0.02	0.03	8.14	0.11	51.77	0.03	0.36	0.02	0.00	0.00	100.64
KGG 91-65 OPX1 rim	58.19	0.09	0.99	0.39	5.09	0.12	35.97	0.42	0.08	0.12	0.00	0.00	101.47
OPX1 intermediate	57.92	0.13	0.97	0.38	5.01	0.11	36.08	0.41	0.14	0.11	0.01	0.01	101.28
OPX1 core	57.52	0.10	1.02	0.41	5.08	0.09	35.97	0.44	0.09	0.12	0.00	0.00	100.83
KGG 91-65 CPX1 rim	55.04	0.26	2.69	2.36	2.38	0.09	16.42	19.28	0.04	2.27	0.00	0.02	100.85
CPX1 core	54.34	0.24	1.29	2.39	2.35	0.09	17.12	21.20	0.08	1.26	0.00	0.01	100.37
CPX1 intermediate	54.97	0.20	1.46	1.89	2.31	0.09	17.22	21.12	0.05	1.35	0.01	0.00	100.66
CPX2 rim	54.21	0.29	1.47	2.68	2.26	0.09	16.90	21.15	0.04	1.36	0.01	0.01	100.47
CPX2 core	54.85	0.26	2.68	2.36	2.41	0.08	16.31	19.26	0.03	2.26	0.00	0.00	100.50
CPX2 intermediate	54.53	0.24	1.85	2.49	2.22	0.10	16.47	21.01	0.06	1.59	0.01	0.00	100.57
CPX3 rim	54.01	0.28	1.73	2.07	2.27	0.07	16.90	21.40	0.03	1.13	0.00	0.02	99.91
CPX3 core	54.86	0.24	1.44	2.20	2.36	0.11	17.26	21.03	0.06	1.29	0.00	0.01	100.86
CPX3 intermediate	54.84	0.20	1.30	1.93	2.40	0.06	17.43	21.32	0.06	1.14	0.00	0.00	100.68
KGG 91-65 Grt1 rim	41.91	0.33	20.11	4.58	7.62	0.40	20.41	5.34	0.00	0.04	0.02	0.00	100.75
Grt1 core	42.27	0.30	20.40	4.61	7.63	0.42	20.67	5.31	0.02	0.06	0.00	0.00	101.70
Grt1 intermediate	42.37	0.29	20.37	4.52	7.63	0.35	20.72	5.34	0.02	0.05	0.00	0.02	101.68
Grt2 rim	42.10	0.30	20.21	4.57	7.57	0.41	20.61	5.31	0.00	0.03	0.01	0.03	101.15
Grt2 core	42.29	0.31	20.13	4.58	7.67	0.40	20.72	5.30	0.03	0.06	0.00	0.00	101.48
Grt2 intermediate	42.29	0.31	20.30	4.62	7.54	0.39	20.59	5.32	0.00	0.07	0.00	0.01	101.44
Grt3 rim	42.40	0.27	20.36	4.50	7.63	0.38	20.93	5.21	0.02	0.05	0.00	0.01	101.77
Grt3 core	42.41	0.25	20.39	4.45	7.43	0.37	20.87	5.20	0.03	0.05	0.00	0.00	101.44
KHA 91-29 Ol3 rim	40.24	0.02	0.02	0.00	8.22	0.14	51.90	0.00	0.40	0.00	0.00	0.00	100.94
Ol3 intermediate	40.96	0.00	0.02	0.00	8.29	0.11	51.96	0.01	0.48	0.02	0.01	0.00	101.86
Ol3 core	40.92	0.00	0.03	0.00	8.21	0.09	51.92	0.02	0.40	0.03	0.01	0.00	101.64

Sample	SiO_2	TiO_2	Al_2O_3	Cr_2O_3	FeO	MnO	MgO	CaO	NiO	Na_2O	K_2O	P_2O_5	Total
KHA 91-29 OPX1 rim	57.37	0.00	1.54	0.40	4.98	0.10	35.59	0.28	0.09	0.05	0.00	0.00	100.41
OPX1 intermediate	57.47	0.00	1.49	0.38	5.14	0.11	35.63	0.29	0.08	0.03	0.00	0.01	100.63
OPX1 core	57.43	0.01	1.55	0.42	5.15	0.13	35.68	0.29	0.11	0.03	0.00	0.00	100.80
OPX2 rim	57.79	0.00	1.18	0.32	5.08	0.13	35.86	0.33	0.11	0.02	0.00	0.00	100.82
OPX2 intermediate	57.63	0.00	1.17	0.32	5.16	0.14	35.96	0.32	0.09	0.04	0.00	0.01	100.84
OPX2 core	57.52	0.00	1.20	0.34	5.12	0.11	35.85	0.30	0.09	0.04	0.00	0.00	100.57
OPX3 rim	56.68	0.01	1.87	0.44	4.99	0.12	35.33	0.30	0.07	0.03	0.00	0.01	99.87
OPX3 intermediate	56.78	0.01	1.90	0.47	5.22	0.10	35.69	0.30	0.11	0.03	0.00	0.01	100.63
OPX3 core	56.72	0.00	1.92	0.49	5.13	0.10	35.30	0.31	0.07	0.04	0.00	0.00	100.07
KHA 91-29 CPX1 rim	55.38	0.00	1.59	0.88	1.57	0.05	17.48	22.94	0.04	0.84	0.00	0.03	100.79
CPX1 core	55.33	0.00	1.57	0.91	1.56	0.07	17.36	23.04	0.05	0.85	0.00	0.01	100.75
CPX1 intermediate	55.46	0.00	1.54	0.90	1.58	0.09	17.48	23.18	0.05	0.83	0.00	0.00	101.11
CPX2 rim	55.09	0.03	1.56	0.87	1.56	0.07	17.43	23.08	0.02	0.87	0.00	0.01	100.58
CPX2 core	55.13	0.00	1.60	0.87	1.53	0.07	17.40	23.07	0.04	0.89	0.00	0.01	100.62
CPX2 intermediate	55.15	0.00	1.52	0.94	1.54	0.06	17.45	23.29	0.04	0.88	0.00	0.03	100.90
CPX3 rim	55.27	0.00	1.55	0.84	1.59	0.09	17.35	23.30	0.07	0.87	0.00	0.04	100.96
CPX3 core	55.14	0.01	1.56	0.87	1.59	0.05	17.39	23.10	0.04	0.83	0.00	0.01	100.59
CPX3 core	55.02	0.02	1.52	0.86	1.59	0.07	17.41	23.14	0.07	0.83	0.01	0.02	100.56
KHA 91-29 Grt1 rim	42.52	0.00	22.47	2.15	8.10	0.50	20.31	5.38	0.00	0.02	0.01	0.01	101.47
Grt1 core	42.43	0.01	22.45	2.10	8.12	0.47	20.19	5.44	0.01	0.01	0.00	0.00	101.23
Grt1 intermediate	42.58	0.01	22.37	2.10	8.07	0.50	20.33	5.37	0.00	0.00	0.01	0.02	101.36
KHA 91-93 Ol1 rim	40.53	0.04	0.06	0.12	8.50	0.13	51.34	0.10	0.39	0.03	0.00	0.01	101.24
Ol1 intermediate	40.57	0.04	0.06	0.15	8.55	0.13	51.47	0.10	0.37	0.05	0.01	0.00	101.49
Ol1 core	40.82	0.03	0.07	0.13	8.37	0.10	51.08	0.09	0.42	0.04	0.00	0.00	101.15
Ol2 rim	40.60	0.02	0.05	0.10	8.55	0.13	51.27	0.11	0.38	0.02	0.00	0.00	101.21
Ol2 intermediate	40.64	0.00	0.05	0.10	8.59	0.12	51.18	0.10	0.41	0.02	0.01	0.01	101.23
Ol2 core	40.79	0.04	0.05	0.16	8.35	0.11	51.14	0.12	0.36	0.04	0.01	0.01	101.17
Ol3 rim	40.51	0.03	0.04	0.09	8.51	0.17	51.09	0.10	0.39	0.04	0.01	0.02	100.99
Ol3 intermediate	40.59	0.00	0.04	0.12	8.50	0.13	51.23	0.10	0.38	0.03	0.01	0.02	101.14
Ol3 core	40.56	0.04	0.09	0.16	8.33	0.13	50.90	0.11	0.38	0.05	0.01	0.00	100.76
KHA 91-93 OPX1 rim	55.92	0.19	2.00	1.09	5.04	0.12	33.67	1.41	0.10	0.19	0.01	0.00	99.74
OPX1 intermediate	56.39	0.21	2.01	1.07	5.23	0.16	33.78	1.42	0.14	0.23	0.00	0.00	100.64
OPX1 core	55.94	0.23	2.01	1.07	5.20	0.13	33.80	1.42	0.10	0.24	0.00	0.02	100.15
OPX2 rim	56.38	0.21	2.00	1.12	5.09	0.12	33.67	1.38	0.11	0.24	0.01	0.00	100.33
OPX2 intermediate	56.16	0.20	2.01	1.07	5.05	0.14	33.77	1.36	0.12	0.22	0.01	0.00	100.10
OPX2 core	56.18	0.23	2.02	1.06	5.11	0.13	33.84	1.39	0.10	0.24	0.00	0.00	100.30
OPX3 rim	56.37	0.20	2.02	1.06	5.23	0.13	33.84	1.36	0.13	0.25	0.01	0.00	100.61
OPX3 intermediate	56.31	0.24	2.00	1.08	5.12	0.13	33.86	1.37	0.13	0.23	0.01	0.01	100.49
OPX3 core	56.48	0.22	1.99	1.09	5.20	0.13	33.77	1.40	0.11	0.23	0.01	0.00	100.62
KHA 91-93 CPX2 rim	54.59	0.06	2.38	1.08	2.39	0.09	18.73	19.64	0.07	1.08	0.06	0.00	100.17
CPX2 intermediate	55.12	0.06	2.37	1.11	2.33	0.11	18.81	19.44	0.05	1.16	0.07	0.00	100.64
CPX2 core	55.03	0.07	2.35	1.11	2.35	0.10	18.82	19.37	0.09	1.16	0.07	0.03	100.54
CPX3 rim	55.20	0.05	2.30	1.15	2.39	0.10	18.83	19.40	0.08	1.19	0.07	0.01	100.77
CPX3 intermediate	54.67	0.08	2.34	1.15	2.39	0.07	18.92	19.45	0.09	1.08	0.08	0.01	100.32
CPX3 core	55.02	0.08	2.28	1.17	2.42	0.08	18.87	19.45	0.06	1.11	0.06	0.00	100.59
KHA 91-93 Grt1 rim	41.38	0.75	16.75	8.82	6.37	0.27	20.34	6.95	0.01	0.06	0.01	0.02	101.73
Grt1 core	41.35	0.72	16.71	8.86	6.29	0.30	20.38	6.86	0.04	0.08	0.00	0.05	101.63
Grt1 intermediate	41.44	0.70	16.69	8.82	6.26	0.28	20.31	6.93	0.03	0.06	0.02	0.01	101.55
Grt2 rim	41.03	0.64	16.81	8.85	6.22	0.29	20.47	6.82	0.00	0.04	0.00	0.02	101.19
Grt2 core	40.91	0.58	16.80	8.96	6.24	0.28	20.64	6.56	0.02	0.05	0.01	0.00	101.04
Grt2 intermediate	40.45	0.53	16.84	9.03	6.16	0.27	20.66	6.53	0.03	0.05	0.00	0.00	100.55
Grt3 rim	41.00	0.74	16.72	8.76	6.34	0.32	20.26	6.96	0.03	0.05	0.00	0.05	101.22
Grt3 core	40.71	0.65	16.95	8.73	6.21	0.30	20.52	6.82	0.00	0.05	0.01	0.01	100.96
Grt3 intermediate	40.67	0.68	16.94	8.70	6.26	0.27	20.54	6.76	0.02	0.05	0.00	0.01	100.90
KHA 91-94 OPX1 rim	57.53	0.11	0.93	0.28	5.56	0.11	35.48	0.37	0.12	0.06	0.00	0.03	100.58
OPX1 intermediate	57.41	0.12	0.93	0.29	5.59	0.13	35.45	0.40	0.11	0.10	0.00	0.00	100.52
OPX1 core	57.50	0.12	0.91	0.28	5.60	0.08	35.47	0.42	0.11	0.08	0.00	0.01	100.58
OPX2 rim	57.56	0.14	0.99	0.29	5.49	0.14	35.36	0.43	0.08	0.10	0.00	0.00	100.58
OPX2 intermediate	57.44	0.11	1.00	0.27	5.51	0.12	35.37	0.41	0.14	0.10	0.00	0.00	100.47
OPX2 core	57.65	0.13	0.98	0.32	5.49	0.14	35.44	0.40	0.12	0.09	0.01	0.00	100.76
OPX3 rim	57.57	0.10	1.09	0.31	5.50	0.11	35.26	0.48	0.13	0.10	0.00	0.01	100.66
OPX3 intermediate	57.51	0.12	1.07	0.31	5.59	0.08	35.29	0.47	0.10	0.07	0.01	0.00	100.62
OPX3 core	57.60	0.11	1.02	0.31	5.53	0.12	35.12	0.47	0.12	0.11	0.00	0.01	100.53
KHA 91-94 CPX1 core	55.01	0.24	2.54	1.52	2.64	0.09	16.82	20.21	0.05	1.80	0.01	0.01	100.94
CPX1 rim	56.05	0.27	2.56	1.54	2.73	0.09	16.48	19.77	0.06	1.72	0.01	0.00	101.28
CPX1 intermediate	55.24	0.22	2.57	1.57	2.61	0.08	16.77	20.02	0.07	1.82	0.01	0.00	100.98
CPX2 core	55.04	0.25	2.37	1.46	2.64	0.09	16.78	20.31	0.06	1.74	0.00	0.01	100.75
CPX2 intermediate	55.07	0.23	2.37	1.51	2.18	0.09	16.81	20.34	0.07	1.75	0.01	0.02	100.46
CPX2 core	55.48	0.24	2.37	1.47	2.63	0.07	17.02	20.20	0.04	1.79	0.02	0.01	101.34
CPX3 rim	54.73	0.23	2.45	1.50	2.67	0.09	16.27	19.56	0.05	1.78	0.01	0.02	99.36

Sample	SiO_2	TiO_2	Al_2O_3	Cr_2O_3	FeO	MnO	MgO	CaO	NiO	Na_2O	K_2O	P_2O_5	Total
KHA 91-94 Grt1 core	42.45	0.27	21.02	3.25	8.29	0.42	20.16	5.28	0.03	0.03	0.00	0.01	101.21
Grt1 intermediate	41.93	0.26	20.70	3.27	8.32	0.40	19.69	5.31	0.02	0.04	0.00	0.02	99.95
Grt1 rim	41.70	0.26	20.60	3.34	8.12	0.40	19.79	5.24	0.00	0.05	0.00	0.02	99.51
KHA 91-100 OPX2 rim	57.48	0.10	1.40	0.37	5.25	0.11	35.13	0.71	0.10	0.14	0.00	0.00	100.79
OPX2 intermediate	57.14	0.10	1.38	0.34	5.31	0.11	35.14	0.67	0.08	0.13	0.01	0.00	100.42
OPX2 core	57.17	0.08	1.47	0.38	5.32	0.11	35.05	0.79	0.13	0.15	0.00	0.00	100.64
OPX3 rim	56.93	0.09	1.37	0.35	5.20	0.10	35.14	0.58	0.12	0.12	0.01	0.01	100.02
OPX3 intermediate	56.88	0.08	1.26	0.33	5.21	0.14	35.38	0.51	0.11	0.12	0.00	0.00	100.02
OPX3 core	56.88	0.09	1.23	0.32	5.28	0.15	35.35	0.51	0.14	0.14	0.00	0.01	100.09
KHA 91-100 CPX1 rim	54.25	0.52	2.13	1.14	2.66	0.09	17.44	22.11	0.05	0.75	0.00	0.01	101.15
CPX1 core	55.03	0.23	2.81	1.53	2.70	0.09	17.61	19.41	0.02	1.76	0.02	0.02	101.23
CPX1 intermediate	55.13	0.24	2.80	1.52	2.72	0.11	17.47	19.41	0.04	1.71	0.00	0.02	101.16
CPX2 rim	55.20	0.24	2.91	1.47	2.81	0.09	17.54	19.33	0.06	1.77	0.02	0.01	101.44
CPX2 core	54.86	0.24	2.79	1.68	2.71	0.08	17.37	19.48	0.05	1.75	0.01	0.00	101.01
CPX2 intermediate	54.50	0.19	2.67	1.66	2.59	0.10	17.06	19.95	0.05	1.73	0.02	0.03	100.54
CPX3 rim	54.74	0.15	2.65	1.69	2.52	0.08	16.83	20.15	0.05	1.90	0.01	0.01	100.79
CPX3 core	55.08	0.16	2.67	1.73	2.50	0.06	16.74	20.22	0.05	2.00	0.00	0.00	101.21
CPX3 intermediate	54.74	0.16	2.67	1.68	2.58	0.11	16.99	20.08	0.06	1.83	0.00	0.00	100.90
KHA 91-100 Grt1 rim	43.00	0.14	21.81	3.04	7.40	0.37	21.54	4.91	0.02	0.03	0.00	0.03	102.30
Grt1 core	42.51	0.13	21.60	3.22	7.74	0.40	21.23	4.96	0.00	0.04	0.00	0.01	101.85
Grt1 intermediate	42.73	0.15	21.70	3.19	7.73	0.39	21.17	4.97	0.04	0.02	0.01	0.01	102.11
Grt2 rim	43.09	0.13	21.68	3.05	7.87	0.38	21.27	4.89	0.00	0.04	0.01	0.00	102.41
Grt2 core	42.83	0.14	21.43	3.36	7.95	0.40	20.89	5.07	0.00	0.05	0.01	0.01	102.15
Grt2 intermediate	42.53	0.17	21.47	3.23	7.95	0.39	21.06	5.05	0.01	0.02	0.00	0.01	101.89
Grt3 rim	43.00	0.13	21.95	2.84	7.65	0.41	21.37	4.88	0.00	0.03	0.01	0.02	102.29
Grt3 core	42.93	0.14	21.80	2.92	8.03	0.41	21.14	4.89	0.02	0.05	0.01	0.04	102.37
Grt3 intermediate	42.83	0.12	21.66	2.87	7.97	0.38	21.14	4.82	0.01	0.03	0.00	0.00	101.83
HAN 93-20 Ol1 rim	40.35	0.02	0.05	0.07	9.99	0.14	49.86	0.10	0.43	0.02	0.00	0.00	101.01
Ol1 intermediate	40.46	0.05	0.05	0.07	10.05	0.13	49.84	0.12	0.38	0.03	0.00	0.01	101.17
Ol1 core	40.35	0.02	0.06	0.07	9.91	0.14	49.98	0.08	0.37	0.03	0.00	0.01	101.02
Ol2 rim	40.11	0.03	0.04	0.07	10.03	0.13	50.23	0.08	0.39	0.05	0.00	0.00	101.15
Ol2 intermediate	39.87	0.01	0.05	0.08	10.00	0.14	50.37	0.09	0.38	0.04	0.00	0.01	101.03
Ol3 rim	40.15	0.02	0.05	0.04	10.10	0.15	50.36	0.10	0.40	0.04	0.01	0.02	101.44
Ol3 rim	39.67	0.02	0.05	0.05	9.99	0.14	50.16	0.09	0.37	0.03	0.01	0.00	100.59
Ol3 intermediate	39.48	0.03	0.05	0.05	10.10	0.12	50.29	0.08	0.42	0.05	0.00	0.01	100.68
Ol3 core	40.13	0.02	0.05	0.04	9.97	0.12	50.21	0.09	0.39	0.05	0.01	0.00	101.08
HAN 93-20 OPX1 rim	56.28	0.27	2.11	0.64	5.93	0.16	33.51	1.35	0.13	0.21	0.01	0.01	100.60
OPX1 intermediate	56.34	0.28	2.14	0.64	6.09	0.13	33.41	1.37	0.13	0.21	0.00	0.00	100.74
OPX1 core	56.35	0.30	2.11	0.62	6.06	0.14	33.46	1.33	0.12	0.21	0.00	0.00	100.69
OPX2 rim	56.37	0.28	2.12	0.65	6.02	0.15	33.34	1.35	0.11	0.20	0.01	0.00	100.60
OPX2 intermediate	56.63	0.29	2.17	0.64	6.00	0.16	33.41	1.33	0.13	0.20	0.00	0.00	100.95
OPX2 core	56.28	0.27	2.17	0.68	5.99	0.15	33.35	1.35	0.13	0.21	0.00	0.00	100.57
OPX3 rim	56.04	0.27	2.16	0.50	6.28	0.15	33.55	1.35	0.14	0.22	0.00	0.01	100.67
OPX3 intermediate	56.08	0.30	2.18	0.53	6.24	0.13	33.45	1.36	0.11	0.20	0.00	0.01	100.58
OPX3 core	55.95	0.26	2.19	0.54	6.26	0.13	33.33	1.38	0.11	0.21	0.00	0.00	100.35
HAN 93-20 CPX1 rim	53.99	0.49	3.03	1.34	3.79	0.12	18.84	17.07	0.07	1.52	0.01	0.01	100.28
CPX1 core	54.39	0.52	3.03	1.39	3.80	0.11	18.60	17.05	0.06	1.50	0.01	0.01	100.46
CPX1 intermediate	54.61	0.51	3.02	1.35	3.77	0.14	18.76	17.20	0.07	1.42	0.02	0.02	100.88
CPX2 rim	54.50	0.48	3.08	1.25	3.74	0.12	18.84	17.08	0.08	1.51	0.02	0.00	100.69
CPX2 core	54.53	0.45	3.01	1.35	3.76	0.12	18.80	17.00	0.04	1.57	0.01	0.00	100.64
CPX2 intermediate	54.52	0.50	3.04	1.38	3.72	0.13	18.76	17.02	0.05	1.46	0.01	0.01	100.60
CPX3 intermediate	54.03	0.54	3.25	1.28	3.81	0.12	18.49	17.08	0.09	1.45	0.03	0.00	100.17
CPX3 intermediate	54.27	0.48	3.01	1.29	3.74	0.12	18.54	16.89	0.07	1.49	0.03	0.02	99.94
CPX3 intermediate	54.35	0.52	3.08	1.27	3.73	0.09	18.59	17.05	0.07	1.50	0.01	0.00	100.26
HAN 93-20 Grt1 rim	42.10	0.82	19.28	5.17	7.35	0.29	20.42	5.99	0.00	0.06	0.01	0.03	101.51
Grt1 intermediate	42.09	0.77	18.87	5.56	7.33	0.30	20.20	6.08	0.02	0.07	0.00	0.04	101.32
Grt1 rim	42.21	0.71	20.00	4.22	7.35	0.29	20.74	5.72	0.04	0.07	0.00	0.05	101.40
Grt2 core	42.12	0.78	18.53	5.82	7.35	0.28	20.12	6.22	0.04	0.04	0.01	0.03	101.34
Grt2 intermediate	42.10	0.76	19.38	4.80	7.39	0.28	20.59	5.91	0.03	0.06	0.00	0.02	101.31
Grt2 rim	42.58	0.75	19.66	4.52	7.29	0.29	20.62	5.86	0.04	0.07	0.00	0.02	101.69
Grt3 core	41.90	0.80	19.11	5.03	7.37	0.27	20.29	5.95	0.02	0.07	0.00	0.03	100.84
Grt3 intermediate	42.11	0.77	19.34	4.92	7.33	0.26	20.22	5.98	0.02	0.04	0.00	0.01	101.01

Table A3.2 Trace element composition of the analyzed samples. Values are reported in ppm.

Gibtown 93 1/1 CPX	A01	A02	A03	A04	A05	A06	A07	A08	A09
Li	0.457	0.535	0.785	0.576	0.444	0.551	0.552	0.449	0.731
Sc	24.07	25.38	26.63	24.94	26.58	26.03	28.22	30.15	30.87
V	6.15	6.34	6.27	7.06	5.75	6.3	5.69	5.25	5.49
Cr	10438.67	11495.68	11383.29	11290.2	10804.8	11380.43	10533.31	10387.54	10179.68
Co	13.9	15.51	15.36	16.3	16.17	16.21	14.8	14.32	14.39
Ni	213.36	238.04	232.85	254.04	239.23	248.38	222.86	218.28	216.42
Cu	0.647	0.944	1.498	0.94	0.95	0.963	1.435	1.351	1.557
Zn	9.95	11.4	14.73	11.92	10.85	11.41	14.24	12.22	14.48
Rb	<0.0227	<0.0203	2.06	<0.0190	0.205	0.0443	0.0994	0.0234	0.0949
Sr	151.37	199.63	177.33	200.59	208.55	204.51	191.47	190.57	199.96
Y	0.821	1.461	1.096	1.561	1.607	1.634	1.762	1.904	1.931
Zr	14.64	23.49	19.13	24.15	24.46	25.93	27.56	29.06	29.05
Nb	0.6	0.79	2.334	0.681	1.201	0.818	1.037	0.869	1.315
Ba	0.49	1.806	21.87	0.186	8.23	1.362	3.87	2.03	9.53
La	2.85	3.91	4.6	3.47	4.3	3.65	3.81	3.79	4.18
Ce	11.64	16.96	16.64	16.92	17.56	17.21	15.49	14.68	15.94
Pr	2.15	2.81	2.69	2.79	2.87	2.91	2.78	2.77	2.92
Nd	8.27	11.04	10.11	11.13	11.55	11.78	11.72	11.94	12.4
Sm	1.151	1.706	1.453	1.835	1.783	1.98	1.91	2.12	2.08
Eu	0.35	0.531	0.434	0.553	0.537	0.559	0.588	0.589	0.603
Gd	0.753	1.223	0.97	1.157	1.252	1.292	1.299	1.337	1.85
Tb	0.0691	0.1056	0.0852	0.1162	0.1085	0.1133	0.126	0.1211	0.1346
Dy	0.3	0.454	0.362	0.474	0.502	0.539	0.554	0.612	0.593
Ho	0.0375	0.0593	0.0464	0.0584	0.0569	0.0666	0.0741	0.0774	0.0779
Er	0.0622	0.1018	0.0852	0.1144	0.1151	0.1322	0.1306	0.147	0.154
Tm	0.0076	0.0112	0.00854	0.0146	0.0119	0.0129	0.0144	0.0165	0.0158
Yb	0.0376	0.0552	0.0548	0.0714	0.0701	0.0829	0.0806	0.0897	0.0955
Lu	0.00467	0.00781	0.00637	0.00872	0.0072	0.00843	0.00924	0.0085	0.0108
Hf	0.792	0.945	0.895	0.94	0.928	1.076	1.196	1.238	1.316
Ta	0.0477	0.0784	0.1408	0.0646	0.0897	0.0814	0.0905	0.0807	0.1061
Pb	0.312	0.265	0.49	0.218	0.24	0.231	0.256	0.222	0.368
Th	0.0711	0.0514	0.2074	0.0365	0.0848	0.0523	0.0739	0.0625	0.093
U	0.01126	0.01048	0.0375	0.00971	0.0204	0.01088	0.01418	0.00971	0.01408

Gibtown 93 1/1 Grt	A01	A02	A03	A04	A05	A06	A07	A08	A09
Li	0.069	0.094	0.095	0.069	0.132	0.109	0.041	<0.030	0.065
Sc	129.72	124.28	118.97	111.19	107.57	102.75	113.65	114.92	110.72
V	175.39	174.31	185.71	196.98	202.12	200.81	140.95	137.15	139.28
Cr	29704.14	30884.42	32383.61	34241.98	35934.34	35810.59	27115.97	27585.08	27734.67
Co	39.69	41.32	42.06	41.91	43.34	42.66	31.69	31.91	30.71
Ni	38.85	40.61	38.11	35.57	36.65	36.77	29.94	31.66	28.7
Cu	0.33	0.273	0.162	0.172	0.185	<0.150	6.6	0.52	1.51
Zn	15.12	16.04	14.2	16.12	14.63	15.13	33.27	15.46	39.31
Ga	5.94	6.13	6.15	6.09	6.21	6.15	4.76	4.75	4.67
Rb	0.47	0.123	0.061	<0.058	<0.061	<0.058	<0.043	<0.042	<0.043
Sr	0.259	0.228	0.185	0.206	0.159	0.203	0.264	0.225	0.311
Y	8.8	8.76	8.63	8.45	8.21	8.1	10.64	11.26	10.96
Zr	24.05	24.03	23.71	24.58	24.27	23.36	27.5	29.51	27.95
Nb	0.404	0.374	0.207	0.212	0.197	0.224	0.41	0.376	0.292
Ba	<0.0204	<0.0204	<0.0227	0.0348	<0.0164	<0.0195	0.308	0.0237	0.118
La	0.0181	0.0184	0.0129	0.0139	0.0145	0.0077	0.156	0.0205	0.0153
Ce	0.268	0.258	0.1958	0.223	0.2073	0.215	0.398	0.242	0.195
Pr	0.1086	0.1036	0.0884	0.0911	0.0893	0.0914	0.1023	0.1098	0.102
Nd	0.895	0.94	0.818	0.897	0.857	0.859	0.928	1.068	0.984
Sm	0.632	0.615	0.563	0.579	0.596	0.556	0.659	0.699	0.648
Eu	0.338	0.351	0.331	0.344	0.352	0.324	0.336	0.368	0.358
Gd	1.059	1.073	1.058	0.991	1.02	1.01	1.23	1.33	1.22
Tb	0.218	0.231	0.213	0.205	0.206	0.199	0.262	0.267	0.26
Dy	1.63	1.62	1.61	1.5	1.49	1.47	1.91	2.07	1.9
Ho	0.321	0.329	0.329	0.326	0.321	0.314	0.395	0.419	0.413
Er	0.973	0.945	1.01	0.901	0.94	0.9	1.14	1.25	1.23
Tm	0.146	0.141	0.147	0.141	0.149	0.136	0.184	0.197	0.186
Yb	1.14	1.15	1.18	1.14	1.16	1.11	1.38	1.44	1.44
Lu	0.165	0.16	0.163	0.162	0.162	0.162	0.215	0.208	0.215
Hf	0.391	0.374	0.39	0.454	0.449	0.399	0.477	0.453	0.477
Ta	0.0127	0.0109	0.0087	0.0085	0.0046	0.007	0.018	0.0179	0.009
Pb	0.0608	0.0951	0.0716	0.1112	0.0684	0.0611	1.93	0.1765	0.971
Th	0.0056	0.0079	0.0086	0.0103	0.0082	0.0086	0.011	0.0104	0.0099
U	0.0155	0.01701	0.01506	0.01608	0.01657	0.01618	0.01094	0.01252	0.01272

Gibtown 93-11 CPX	A01	A02	A03	A04	A05	A06	A07	A08
Li	0.508	0.417	0.45	0.416	0.393	0.491	0.392	0.6
Sc	26.29	25.88	27.02	26.11	25.72	26.42	25.5	26.19
V	1428.47	1445.74	1401.59	1397.59	1403.05	1459.37	1382.95	1452.27
Cr	8153.28	8499.47	8765.76	8974.17	8940.51	8624.74	9083.79	9245.67
Co	10.67	10.67	11.58	11.64	11.63	10.95	11.87	11.71
Ni	171.88	174.93	187.62	187.92	185.96	180.38	187.35	187.97
Cu	12.41	23.19	50.31	41.4	19.28	3.29	23.96	59.08
Zn	14.94	16.67	25.21	22.87	18.22	15.23	20.23	33.83
Rb	0.106	0.0211	<0.0200	0.0256	0.0315	0.0213	0.0407	0.0277
Sr	145.81	147.36	189.24	186.67	183.43	151.7	180.26	167.53
Y	1.005	1.041	2.072	1.954	1.922	1.22	1.836	1.807
Zr	20.16	21.23	35.96	33.78	32.08	22.59	31.8	34.71
Nb	0.722	0.734	0.772	0.758	0.767	0.747	0.713	0.761
Ba	0.2359	0.2299	0.2169	0.1691	0.1641	0.345	0.1871	0.2804
La	3.5	3.42	3.92	3.8	3.78	3.72	3.71	4.15
Ce	10.66	10.59	12.99	13.15	12.95	11.31	13.14	13.28
Pr	2.332	2.34	2.793	2.818	2.775	2.476	2.735	2.762
Nd	9.46	9.71	12.89	12.91	12.5	10.55	12.11	12.34
Sm	1.386	1.375	2.279	2.137	2.138	1.538	2.152	2.065
Eu	0.388	0.4	0.618	0.61	0.614	0.431	0.611	0.579
Gd	0.873	0.877	1.401	1.423	1.38	0.996	1.358	1.265
Tb	0.0825	0.0867	0.1377	0.1464	0.1404	0.0998	0.1347	0.1291
Dy	0.34	0.342	0.643	0.616	0.595	0.391	0.538	0.55
Ho	0.04	0.0417	0.0813	0.0802	0.0745	0.0555	0.0747	0.0754
Er	0.0833	0.0796	0.1781	0.1596	0.1536	0.0882	0.1379	0.153
Tm	0.00932	0.00538	0.0191	0.0162	0.0152	0.0091	0.0163	0.0147
Yb	0.0366	0.041	0.0945	0.0888	0.0859	0.0548	0.0934	0.088
Lu	0.00465	0.00511	0.0116	0.00958	0.0098	0.00605	0.01005	0.0115
Hf	0.944	1.03	1.306	1.212	1.165	1.052	1.16	1.355
Ta	0.0591	0.0637	0.1086	0.0872	0.086	0.0758	0.087	0.0899
Pb	25.87	32.38	5.35	5.01	29.04	23	10.59	6.94
Th	0.0731	0.0698	0.0423	0.0462	0.0425	0.0539	0.0411	0.0536
U	0.00893	0.00924	0.0107	0.00902	0.00739	0.00761	0.00816	0.0104

Gibtown 93-11 Grt	A01	A02	A03	A04	A05	A06	A07	A08
Li	0.085	0.054	0.071	0.088	0.078	0.079	<0.069	<0.066
Sc	87.77	89.21	88.08	88.8	89.99	87.99	89.14	91.83
V	148.73	151.01	158.26	157.64	155.44	154.96	151.61	148.63
Cr	23506.51	23801.77	24991.88	23867.38	23850.78	24209.77	22127.25	22555.99
Co	32.12	32.19	32.43	30.32	29.94	30.11	28.47	27.99
Ni	27.1	27.67	27.37	24.47	24.21	24.81	23.18	22.53
Cu	<0.112	<0.109	0.412	1.92	1.58	1.51	<0.26	<0.270
Zn	15.79	14.88	14.91	15.53	13.89	18.28	12.74	13.17
Ga	4.7	4.68	4.77	4.31	4.33	4.22	3.99	3.8
Rb	<0.043	<0.040	<0.040	<0.041	<0.040	<0.040	<0.097	<0.091
Sr	0.215	0.192	0.178	0.194	0.188	0.205	0.214	0.185
Y	9.16	9.27	9.9	10.24	10.16	9.93	10.16	10.74
Zr	25.26	25.75	27.85	33.08	32.27	31.69	29.75	31.41
Nb	0.1781	0.2011	0.1228	0.1407	0.1328	0.1299	0.1257	0.1166
Ba	0.0048	<0.0077	0.0088	0.0611	<0.0096	0.0283	0.0173	<0.0247
La	0.0156	0.00988	0.0108	0.01436	0.01279	0.0152	0.0115	0.0164
Ce	0.1742	0.1786	0.1601	0.1661	0.1609	0.1678	0.1347	0.148
Pr	0.0886	0.0937	0.0915	0.0984	0.0962	0.0923	0.0885	0.0889
Nd	0.838	0.864	0.923	0.984	0.953	0.997	0.92	1.057
Sm	0.628	0.613	0.66	0.661	0.691	0.683	0.662	0.664
Eu	0.338	0.347	0.349	0.38	0.388	0.361	0.367	0.363
Gd	1.117	1.099	1.199	1.277	1.289	1.265	1.344	1.38
Tb	0.219	0.238	0.239	0.256	0.254	0.24	0.256	0.28
Dy	1.642	1.744	1.763	1.86	1.837	1.702	1.849	1.842
Ho	0.354	0.339	0.38	0.394	0.386	0.38	0.378	0.405
Er	1.039	1.028	1.16	1.154	1.165	1.04	1.125	1.242
Tm	0.1587	0.1642	0.176	0.1786	0.175	0.167	0.1591	0.1763
Yb	1.235	1.288	1.301	1.386	1.355	1.266	1.312	1.415
Lu	0.1823	0.1989	0.1931	0.2029	0.2057	0.2026	0.188	0.219
Hf	0.448	0.484	0.571	0.754	0.728	0.728	0.634	0.708
Ta	0.0057	0.0072	0.00436	0.0073	<0.0035	0.0053	<0.0054	0.0046
Pb	0.244	0.178	1.248	7.2	4.32	7.04	0.064	0.111
Th	0.00881	0.0092	0.0091	0.0091	0.00883	0.00973	0.0127	0.0103
U	0.01243	0.0139	0.01105	0.01264	0.0131	0.0131	0.0129	0.0141

SKGG IV CPX	A01	A02	A03	A04	A05	A06
Li	0.548	0.518	0.769	0.497	0.474	0.442
Sc	21.67	21.68	19.59	21.44	22.43	23.06
V	9.91	11.5	254.72	12.61	10.6	9.95
Cr	7734.73	7783.24	10288.99	7311.73	7247.45	6592.77
Co	15.5	15.49	20.04	14.73	14.76	13.2
Ni	244.59	243.22	303.55	232.23	230.48	206.2
Cu	2.04	1.64	1.19	1.21	1.05	1.11
Zn	7.76	7.21	8.61	6.96	7.38	6.22
Rb	<0.0158	<0.0157	<0.047	<0.0136	<0.0142	0.0142
Sr	148.19	154.42	143.93	151.04	148.53	144.42
Y	1.534	1.645	1.395	1.67	1.67	1.68
Zr	17.15	18.16	16.21	18.5	18.37	18.63
Nb	0.286	0.271	0.253	0.292	0.293	0.273
Ba	0.188	0.1882	0.238	0.1719	0.1705	0.1589
La	3.92	4.08	3.94	3.98	3.96	4.06
Ce	15.19	15.38	19.13	14.56	14.34	13.32
Pr	2.487	2.546	2.75	2.468	2.5	2.389
Nd	10.63	11.06	10.98	10.67	10.75	10.86
Sm	1.922	1.87	1.747	1.822	1.841	1.835
Eu	0.494	0.477	0.483	0.485	0.502	0.467
Gd	1.005	1.106	1.143	1.099	1.075	1.155
Tb	0.1064	0.1115	0.1156	0.113	0.1123	0.1178
Dy	0.499	0.515	0.458	0.532	0.501	0.494
Ho	0.0655	0.0701	0.0595	0.0675	0.0744	0.0703
Er	0.117	0.1312	0.095	0.1372	0.143	0.1412
Tm	0.013	0.014	0.0145	0.015	0.0165	0.0155
Yb	0.0763	0.072	0.069	0.0829	0.0904	0.0892
Lu	0.00884	0.0117	0.0085	0.00717	0.0118	0.0109
Hf	0.664	0.668	0.639	0.688	0.688	0.689
Ta	0.0242	0.0228	0.0197	0.027	0.0263	0.0277
Pb	0.777	0.643	0.65	0.51	0.452	0.792
Th	0.1015	0.1044	0.0997	0.1022	0.1033	0.1066
U	0.017	0.0159	0.0217	0.0174	0.0149	0.0143

SKGG IV Grt	A01	A02	A03	A04	A05	A06	A07	A08	A09
Li	0.065	0.083	0.084	0.084	0.086	0.086	0.081	0.125	0.086
Sc	91.4	90.6	91.32	91.92	89.38	89.8	80.98	80.16	80.73
V	128.82	125.55	126.67	124.64	129.37	136.22	140.09	139.86	146.21
Cr	15728.1	15464.92	15802.78	15973.63	16481.36	17468.47	18217.96	18390.78	19574.06
Co	27.47	26.86	27.36	25.1	25.64	26.93	29.37	29.6	31.59
Ni	22.74	21.8	22.16	20.68	21.08	22.29	24.32	24.53	26.5
Cu	0.296	0.27	0.274	0.437	0.134	0.442	0.522	2.2	6.83
Zn	8.18	7.18	7.76	7.3	7.42	7.81	8.46	8.33	9.06
Ga	4.42	4.32	4.39	4.38	4.56	4.73	4.82	4.93	5.24
Rb	<0.045	<0.040	<0.038	<0.038	<0.034	<0.037	<0.042	<0.043	<0.045
Sr	0.197	0.147	0.16	0.143	0.158	0.163	0.157	0.169	0.176
Y	12.2	12.33	12.41	13.28	13.5	13.67	10.97	11.04	11.05
Zr	20.38	19.97	19.99	20.57	21.6	21.63	17.77	18.3	17.51
Nb	0.0755	0.081	0.0701	0.073	0.0836	0.0763	0.0767	0.0967	0.0831
Ba	<0.0151	<0.0091	0.0136	<0.0107	<0.0076	0.0098	0.0065	<0.0131	<0.0146
La	0.00845	0.00852	0.00961	0.0106	0.01025	0.00927	0.00959	0.0085	0.00967
Ce	0.137	0.1337	0.1347	0.145	0.1457	0.1509	0.144	0.152	0.169
Pr	0.0717	0.0734	0.0718	0.0749	0.0725	0.075	0.0709	0.0716	0.0738
Nd	0.852	0.8	0.845	0.862	0.905	0.906	0.783	0.798	0.817
Sm	0.708	0.698	0.677	0.705	0.787	0.801	0.709	0.701	0.684
Eu	0.316	0.327	0.333	0.353	0.341	0.366	0.327	0.33	0.351
Gd	1.239	1.291	1.265	1.407	1.395	1.345	1.219	1.173	1.17
Tb	0.27	0.271	0.279	0.308	0.287	0.295	0.247	0.258	0.239
Dy	2.15	2.18	2.11	2.32	2.3	2.31	1.87	1.89	1.95
Ho	0.491	0.485	0.49	0.528	0.516	0.532	0.438	0.457	0.425
Er	1.499	1.539	1.488	1.694	1.64	1.63	1.382	1.34	1.32
Tm	0.232	0.23	0.232	0.267	0.266	0.253	0.208	0.225	0.194
Yb	1.777	1.808	1.79	1.981	1.98	1.964	1.711	1.754	1.653
Lu	0.277	0.293	0.273	0.317	0.32	0.318	0.2427	0.26	0.255
Hf	0.428	0.425	0.42	0.428	0.454	0.443	0.361	0.36	0.332
Ta	<0.0040	<0.0037	0.0057	<0.0045	0.0057	0.0074	0.0063	0.0039	0.0063
Pb	0.231	0.2047	0.288	0.208	0.252	0.221	0.491	0.822	2.03
Th	0.00508	0.00625	0.0064	0.00866	0.00758	0.00698	0.00623	0.0065	0.0076
U	0.00723	0.009	0.00766	0.00882	0.0091	0.0095	0.0085	0.01	0.0091

SKGG IVa CPX	A01	A02	A03	A04
Li	0.385	0.463	0.695	0.401
Sc	19.75	20.51	20.28	18.01
V	154.03	156.07	158.16	160.08
Cr	5438.88	5423.41	5434.68	5563.05
Co	12.69	12.91	12.64	12.9
Ni	191.51	196.67	192.89	192.42
Cu	91.01	203.96	71.93	399.35
Zn	140.2	147.83	25.04	62.98
Rb	<0.030	0.065	<0.0257	<0.031
Sr	89.78	91.02	87.53	92.76
Y	3.12	3.23	3.03	2.58
Zr	107.83	109.12	67.71	88.16
Nb	0.0793	0.1168	0.0641	0.0744
Ba	0.226	0.454	0.0996	1.018
La	0.635	0.744	0.633	2.066
Ce	3.06	3.31	3.1	6.33
Pr	0.9	0.951	0.909	1.314
Nd	5.8	6.13	6.06	6.72
Sm	1.68	1.792	1.734	1.481
Eu	0.534	0.541	0.547	0.464
Gd	1.349	1.49	1.4	1.043
Tb	0.189	0.183	0.17	0.139
Dy	0.945	0.928	0.93	0.718
Ho	0.137	0.137	0.139	0.119
Er	0.289	0.3	0.27	0.241
Tm	0.0403	0.0395	0.0314	0.0352
Yb	0.228	0.223	0.174	0.178
Lu	0.0304	0.0335	0.0256	0.0335
Hf	2.8	2.91	2.11	1.66
Ta	0.1228	0.1374	0.024	0.124
Pb	41.02	25.21	50.86	24.02
Th	0.0426	0.0517	0.0099	0.0397
U	0.033	0.0379	0.00299	0.0336

SKGG IVa Grt	A01	A02	A03	A04	A05	A06
Li	1.022	0.09	<0.0255	0.036	0.039	<0.032
Sc	150.21	143.19	142.6	133.81	131.49	126.03
V	168.75	166.71	153.18	176.95	172.46	178.99
Cr	36176.77	37318.17	34334.42	37225.28	37388.86	40956.79
Co	33.57	33.7	30	35.39	34.66	35.35
Ni	45.92	47.04	42.32	31.43	29.85	40.91
Cu	1.157	0.596	0.252	0.434	0.504	0.204
Zn	11.81	11	8.87	10.69	12.78	10.52
Ga	5	2.75	2.44	2.89	2.77	2.98
Rb	0.264	<0.043	<0.036	<0.041	<0.042	<0.046
Sr	6.89	1.009	0.407	0.442	0.551	0.537
Y	1.582	1.754	1.834	1.248	1.196	1.454
Zr	7.16	9.4	13.43	5.04	4.87	6.37
Nb	0.506	0.368	0.2268	0.765	0.749	0.545
Ba	33.65	1.045	0.233	0.0377	0.0648	0.237
La	0.1197	0.0639	0.0339	0.0659	0.0633	0.0586
Ce	0.93	0.789	0.549	0.95	0.966	0.913
Pr	0.291	0.2731	0.2421	0.3005	0.307	0.309
Nd	2.337	2.495	2.464	2.452	2.425	2.588
Sm	0.86	1.004	1.221	0.943	0.925	0.961
Eu	0.276	0.329	0.372	0.263	0.282	0.289
Gd	0.504	0.569	0.625	0.395	0.408	0.524
Tb	0.0497	0.0559	0.0601	0.0286	0.0287	0.0499
Dy	0.248	0.297	0.277	0.1246	0.1496	0.249
Ho	0.0542	0.0619	0.0661	0.0397	0.041	0.0526
Er	0.218	0.258	0.252	0.201	0.213	0.207
Tm	0.0594	0.055	0.0598	0.0525	0.0554	0.0485
Yb	0.642	0.643	0.69	0.632	0.631	0.606
Lu	0.1243	0.1206	0.1245	0.1186	0.1126	0.1088
Hf	0.151	0.1821	0.235	0.0781	0.0735	0.122
Ta	0.0448	0.0364	0.0254	0.0452	0.0442	0.0342
Pb	0.308	0.479	0.37	0.162	0.0946	0.0172
Th	0.0393	0.0326	0.0133	0.047	0.0527	0.0389
U	0.0394	0.037	0.0199	0.0649	0.0674	0.0516

SKGG IVb Grt	A01	A02	A03	A04	A05	A06	A07	A08	A09
Li	<0.070	<0.068	<0.069	<0.083	<0.080	<0.080	<0.078	<0.074	<0.076
Sc	168.02	163.24	156.23	152.31	151.85	144.06	138.08	136.28	136.28
V	180.04	185.42	193.6	198.88	195.71	222.96	233.81	233.68	242.97
Cr	35780.01	37872.25	40436.08	42622.79	42729.37	47150.2	49199.14	50059.64	51922.36
Co	30.44	31.8	33.05	33.53	33.84	37.99	39.29	39.2	41.15
Ni	28.07	34.2	40.87	39.88	39.37	39.55	47.95	50.64	49.16
Cu	<0.072	0.185	0.665	0.097	0.125	0.146	0.144	0.15	0.127
Zn	7.28	8	8.73	8.63	8.51	9.4	9.87	10.31	10.62
Ga	2.48	2.55	2.71	2.78	2.86	3.17	3.06	3.2	3.35
Rb	<0.040	<0.038	<0.039	<0.045	<0.043	<0.045	<0.043	<0.042	<0.044
Sr	0.396	0.395	0.409	0.383	0.386	0.372	0.339	0.352	0.336
Y	2.32	2.55	2.76	2.94	2.86	2.39	2.19	2.26	2.15
Zr	9.88	10.16	10.14	12.57	10.01	9.51	8.53	10.21	8.49
Nb	0.702	0.573	0.483	0.344	0.445	0.442	0.408	0.356	0.424
Ba	<0.0115	0.0101	0.0163	<0.0105	<0.0115	<0.0094	<0.0085	<0.0093	<0.0081
La	0.0844	0.0639	0.0603	0.043	0.0665	0.0448	0.039	0.0382	0.0389
Ce	0.821	0.789	0.755	0.655	0.829	0.789	0.702	0.653	0.732
Pr	0.321	0.315	0.313	0.337	0.346	0.33	0.281	0.275	0.293
Nd	3.03	3.03	2.96	3.54	3.22	3.11	2.578	2.718	2.738
Sm	1.289	1.302	1.271	1.491	1.304	1.277	1.051	1.126	1.072
Eu	0.344	0.342	0.332	0.415	0.354	0.358	0.314	0.339	0.316
Gd	0.653	0.702	0.752	0.894	0.794	0.753	0.625	0.667	0.639
Tb	0.051	0.0618	0.0689	0.089	0.0839	0.0735	0.0628	0.0628	0.0628
Dy	0.268	0.348	0.394	0.469	0.468	0.377	0.337	0.335	0.332
Ho	0.0783	0.0815	0.0892	0.097	0.1025	0.086	0.0751	0.0726	0.0747
Er	0.402	0.383	0.387	0.412	0.392	0.351	0.304	0.311	0.294
Tm	0.1021	0.1012	0.0923	0.098	0.0937	0.0815	0.0705	0.0722	0.069
Yb	1.092	1.013	0.965	0.952	0.937	0.875	0.806	0.742	0.773
Lu	0.238	0.226	0.206	0.199	0.205	0.18	0.1567	0.1531	0.165
Hf	0.213	0.219	0.218	0.264	0.233	0.204	0.192	0.212	0.178
Ta	0.0548	0.0466	0.041	0.0311	0.04	0.0336	0.029	0.0267	0.0279
Pb	0.00507	0.0986	0.1904	0.0186	0.00289	0.0184	0.037	0.0455	0.0563
Th	0.0708	0.0466	0.0359	0.0167	0.047	0.0258	0.0236	0.0172	0.0197
U	0.0648	0.0562	0.0503	0.034	0.0541	0.0498	0.0477	0.0384	0.048

SKGG IVc CPX	A02	A03
Li	0.637	0.966
Sc	17.78	18.59
V	152.61	152.98
Cr	7458.46	7756.51
Co	21.68	22.28
Ni	354.76	348.29
Cu	1.412	2.105
Zn	10.65	11.85
Rb	<0.0196	0.339
Sr	122	135.64
Y	1.795	1.893
Zr	10.17	11.31
Nb	0.193	0.994
Ba	0.326	8.06
La	1.922	2.852
Ce	7.07	8.76
Pr	1.297	1.516
Nd	6.65	7.47
Sm	1.416	1.494
Eu	0.386	0.397
Gd	1.053	1.156
Tb	0.1098	0.1196
Dy	0.516	0.518
Ho	0.0711	0.0782
Er	0.1613	0.1743
Tm	0.015	0.0201
Yb	0.1052	0.106
Lu	0.01242	0.0133
Hf	0.625	0.642
Ta	0.0225	0.0872
Pb	0.2582	0.527
Th	0.0263	0.1216
U	0.00577	0.0204

SKGG IVc Grt	A01	A02	A03
Li	0.069	0.032	0.07
Sc	108.09	110.91	112.54
V	226.77	211.21	192.81
Cr	37046.98	34868.98	34785.16
Co	39.9	36.68	37.18
Ni	71.01	57.62	66.76
Cu	<0.099	0.217	0.266
Zn	11.3	9.81	10.41
Ga	4.71	4.36	3.98
Rb	<0.029	<0.0233	<0.0229
Sr	0.387	0.387	0.424
Y	6.97	7.13	8.82
Zr	14.08	13.82	21.53
Nb	0.406	0.421	0.371
Ba	0.0235	0.0245	<0.0120
La	0.0531	0.0442	0.04
Ce	0.479	0.411	0.454
Pr	0.1362	0.1154	0.1528
Nd	1.184	1.128	1.471
Sm	0.794	0.799	0.932
Eu	0.313	0.304	0.357
Gd	0.957	0.981	1.19
Tb	0.1659	0.1671	0.2095
Dy	1.22	1.192	1.51
Ho	0.262	0.26	0.322
Er	0.809	0.82	0.985
Tm	0.1271	0.1283	0.155
Yb	1.014	1.046	1.178
Lu	0.1645	0.1716	0.1747
Hf	0.345	0.325	0.444
Ta	0.0269	0.0269	0.022
Pb	0.1519	0.2026	0.1405
Th	0.0186	0.0262	0.01301
U	0.0356	0.045	0.0178

SKGG IVd CPX	A01	A02	A03	A04	A05	A06	A07	A08	A09
Li	0.607	0.598	0.717	0.466	0.664	0.516	0.583	0.605	0.521
Sc	17.75	18.66	19.04	28.12	18.89	19.14	17.83	17.92	18.33
V	5.4	5.77	5.79	5.38	5.2	5.17	7.76	5.38	6.5
Cr	5744.99	5913.38	5913.85	5738.57	5308.14	5343.11	6665.65	6628.11	6484.02
Co	16.28	16.66	16.27	15.55	14.56	14.63	18.13	17.9	17.74
Ni	278.41	287.48	281.91	255	250.38	246.68	321.74	307.09	305.08
Cu	0.55	0.301	0.569	0.635	0.295	0.487	0.225	0.187	0.201
Zn	7.1	7.66	7.13	7.67	6.43	6.12	8.06	7.37	7.31
Rb	2.36	0.352	0.454	0.707	0.439	0.423	<0.0190	0.0815	0.0242
Sr	139.59	117.46	155.62	187.88	119.6	119.29	99.47	122.05	120.66
Y	0.53	0.394	0.413	2.68	0.477	0.417	0.0981	0.1953	0.2342
Zr	11.96	9.76	10.38	52.61	11.82	10.71	5.14	6.27	6.85
Nb	1.954	1.798	1.517	2.817	2.091	2.095	0.357	0.541	0.53
Ba	27.86	18.08	14.15	26.02	16.99	19.29	1.077	1.857	1.818
La	10.73	10.32	13.59	8.31	11.04	11.19	8.52	11.24	11.19
Ce	22.63	20.72	28.29	19.18	18.77	19.38	17.12	24.94	23.76
Pr	2.439	2.155	2.735	2.975	2.2	2.198	1.738	2.258	2.215
Nd	8.14	7.11	8.21	13.38	7.8	7.56	5.6	6.49	6.51
Sm	0.977	0.876	0.858	2.514	0.988	0.867	0.637	0.697	0.676
Eu	0.2128	0.1822	0.1848	0.669	0.2141	0.1927	0.1193	0.1369	0.1456
Gd	0.604	0.506	0.512	1.806	0.586	0.541	0.314	0.352	0.378
Tb	0.0417	0.0336	0.0332	0.1812	0.0407	0.0329	0.0168	0.0209	0.0232
Dy	0.1547	0.1352	0.1345	0.828	0.1658	0.1399	0.0409	0.0687	0.0915
Ho	0.0203	0.0153	0.0175	0.1116	0.0231	0.018	0.00387	0.0073	0.00926
Er	0.0381	0.0312	0.0292	0.2091	0.0423	0.0375	0.0109	0.0158	0.0201
Tm	0.00434	0.00458	0.00431	0.0231	0.00557	0.00466	<0.00131	0.00148	0.0027
Yb	0.0296	0.0215	0.0239	0.1176	0.0264	0.0205	0.0099	0.012	0.0112
Lu	0.00342	0.00182	0.00312	0.01343	0.00436	0.00326	<0.00092	0.00224	0.00203
Hf	0.365	0.334	0.318	1.831	0.386	0.328	0.231	0.2243	0.2455
Ta	0.134	0.1205	0.1081	0.1633	0.139	0.1285	0.0466	0.0634	0.0591
Pb	2.111	0.656	1.018	0.62	0.659	0.635	0.748	0.585	0.591
Th	0.799	0.982	0.631	0.685	1.278	1.063	1.233	0.674	0.727
U	0.0509	0.0709	0.0501	0.06	0.0748	0.0647	0.0775	0.0453	0.0458

SKGG IVe CPX	A01	A02	A03	A04	A05	A06	A07	A08
Li	2.3	1.069	0.758	0.931	1.462	1.155	1.546	1.453
Sc	19.66	19.79	20.56	21.39	21.6	21.8	21	21.1
V	6.65	5.54	5.53	5.94	6.2	5.91	6.47	5.84
Cr	6255.07	6274.63	6087.76	5933.14	5832.14	5883.17	6195.74	6128.44
Co	20.21	19.89	19.35	19.21	19.17	19.18	19.79	19.81
Ni	394.99	323.93	310.98	314.23	329.06	320.21	340.02	346.98
Cu	3.41	1.616	1.357	1.433	1.355	1.433	2.08	2.69
Zn	15.23	9.81	9.58	9.35	10.7	9.45	10.5	12.46
Rb	0.618	0.0566	<0.0173	0.1503	0.171	0.215	0.247	0.382
Sr	180.41	117.42	116.94	122.92	124.44	121.78	121.38	141.26
Y	1.687	1.019	1.218	1.371	1.366	1.373	1.335	1.364
Zr	13.01	6.67	9.06	9.96	10.05	9.62	9.68	10.46
Nb	6.48	1.806	1.221	1.528	1.952	1.623	1.349	2.964
Ba	30.72	8.69	0.673	5.34	9.67	4.46	1.254	11.1
La	11.12	7.25	5.15	4.76	5.02	4.41	4.47	6.7
Ce	27.05	16.39	13.92	13.34	13.41	12.47	13.43	17.23
Pr	3.143	1.92	1.896	1.864	1.864	1.798	1.861	2.164
Nd	10.68	6.4	6.89	6.98	7.04	6.71	6.81	7.67
Sm	1.244	0.728	0.888	0.934	0.939	0.901	0.873	0.981
Eu	0.334	0.1917	0.2286	0.247	0.2478	0.2374	0.2465	0.2515
Gd	0.917	0.693	0.604	0.636	0.667	0.639	0.625	0.66
Tb	0.087	0.0514	0.0637	0.0705	0.066	0.0694	0.067	0.0646
Dy	0.425	0.265	0.326	0.347	0.353	0.347	0.325	0.335
Ho	0.0638	0.0391	0.0489	0.0548	0.0565	0.0511	0.0499	0.0522
Er	0.1418	0.0851	0.1069	0.1203	0.1229	0.1319	0.113	0.1235
Tm	0.0171	0.01112	0.01281	0.01533	0.01505	0.01491	0.01454	0.0154
Yb	0.1186	0.0603	0.0808	0.0812	0.0799	0.0896	0.0907	0.0939
Lu	0.0155	0.00786	0.00924	0.0113	0.01064	0.01188	0.01172	0.01079
Hf	0.32	0.1643	0.263	0.383	0.368	0.376	0.37	0.348
Ta	0.576	0.2025	0.2191	0.2337	0.26	0.249	0.2257	0.309
Pb	1.963	0.542	0.633	0.359	0.375	0.338	0.776	1.096
Th	0.566	0.1449	0.0526	0.0764	0.1266	0.0892	0.0534	0.1485
U	0.1141	0.0186	0.01072	0.01515	0.029	0.0168	0.0143	0.024

SKGG IVe Grt	A01	A02	A03	A04	A05	A06	A07	A08	A09
Li	0.071	0.05	0.056	0.056	0.064	0.07	0.079	0.091	0.101
Sc	111.27	107.86	115.87	100.78	102.33	105.56	114.44	110.62	110.36
V	182.89	195.04	161.97	181.16	176.21	163.7	146.93	147.18	152.99
Cr	21542.67	22892.99	19395.76	23073	22696.85	21209.42	18439.79	18592.7	19053.62
Co	51.13	52.81	44.64	51.5	50.86	46.74	40.8	41.46	41.39
Ni	40.88	42.04	35.71	46.48	47.04	45.51	37.23	37.37	36.01
Cu	<0.121	<0.120	0.17	0.164	<0.110	0.15	0.14	<0.084	<0.080
Zn	12.34	13.06	10.31	12.83	12.84	11.59	9.44	9.99	9.85
Ga	6.35	6.57	5.5	6.27	6.25	5.65	4.94	5.13	5.27
Rb	0.245	<0.036	<0.0271	<0.030	<0.033	<0.0257	<0.0240	<0.0245	<0.0231
Sr	0.1014	0.0979	0.1046	0.1065	0.103	0.1058	0.1226	0.1048	0.0928
Y	10.27	9.39	10.82	8.52	9.04	9.48	10.83	10.31	10.15
Zr	4.34	3.99	4.19	4.4	5.63	5.39	5.04	4.91	4.71
Nb	0.69	0.728	0.67	0.727	0.763	0.781	0.665	0.662	0.648
Ba	<0.0120	<0.0132	0.0139	<0.0103	0.0206	<0.0111	0.0133	0.0114	<0.0091
La	0.0315	0.0291	0.0317	0.0276	0.0271	0.0305	0.0315	0.0315	0.0286
Ce	0.29	0.283	0.2503	0.276	0.285	0.271	0.249	0.2363	0.2345
Pr	0.0856	0.0747	0.0766	0.0705	0.0786	0.0785	0.0733	0.071	0.0708
Nd	0.574	0.583	0.604	0.564	0.606	0.614	0.603	0.582	0.563
Sm	0.325	0.302	0.304	0.285	0.322	0.302	0.312	0.299	0.291
Eu	0.1467	0.141	0.1388	0.1382	0.1479	0.1402	0.1367	0.1382	0.1411
Gd	0.555	0.471	0.557	0.477	0.542	0.587	0.61	0.583	0.595
Tb	0.1458	0.132	0.1396	0.1259	0.138	0.1364	0.152	0.139	0.144
Dy	1.29	1.182	1.367	1.128	1.256	1.262	1.413	1.339	1.348
Ho	0.365	0.33	0.388	0.304	0.327	0.337	0.387	0.375	0.365
Er	1.293	1.198	1.36	1.062	1.131	1.226	1.371	1.304	1.31
Tm	0.221	0.215	0.239	0.181	0.191	0.199	0.235	0.226	0.225
Yb	1.854	1.731	1.94	1.546	1.662	1.67	1.95	1.88	1.91
Lu	0.289	0.265	0.312	0.236	0.257	0.268	0.309	0.309	0.313
Hf	0.0575	0.0546	0.0631	0.0575	0.0657	0.0688	0.0707	0.0672	0.0729
Ta	0.0351	0.0354	0.0318	0.0363	0.041	0.0399	0.0318	0.0335	0.031
Pb	0.00346	0.0197	0.00711	0.008	0.123	0.0118	0.00911	0.00766	0.0099
Th	0.0308	0.0297	0.0298	0.0236	0.02	0.0205	0.036	0.026	0.028
U	0.0624	0.0735	0.0628	0.0641	0.0532	0.0489	0.0554	0.0553	0.0598

KGG 91-20c CPX	1	2	3	4	5	6	7	8	9
Li	1.047	11.59	6.29	2.042	3.19	0.998	3.24	15.15	0.29
Sc	22.45	23.02	22.8	21.83	24.1	22.85	22.21	22.69	22.83
V	237.53	241.26	240.6	241.4	246.2	241.85	238.88	244.11	240.4
Cr	11346.5	11435.12	11002.96	9776.72	10192.7	9776.85	11476.38	10717.75	9405.47
Co	769.54	804.21	776	774.95	777.79	781.87	802.82	798.48	804.16
Ni	27.71	28.72	28.21	28.3	27.94	28.3	29.03	28.97	28.87
Cu	464.67	486.06	473.75	481.91	489.52	490.57	489.49	490.73	492.29
Zn	4.57	4.61	4.53	5.03	4.32	4.54	5.28	4.48	4.52
Rb	0.0185	<0.0176	0.0887	0.0496	<0.0131	0.254	0.0563	<0.0143	<0.0127
Sr	109.14	116.07	110	110.46	114.95	114.5	120.22	119.57	120.47
Y	3.03	3.28	3.17	3.12	3.39	3.24	3.15	3.28	3.29
Zr	17.44	18.75	18.61	16.76	19.92	18.7	17.41	18.2	18.15
Nb	0.1709	0.1526	0.199	<0.0171	0.1936	0.189	0.1822	0.1754	0.1778
Ba	0.075	0.169	0.321	1.376	0.242	0.535	3.94	0.087	0.221
La	1.96	2.123	2.105	2.024	2.197	2.164	2.079	2.129	2.065
Ce	7.2	7.78	7.66	7.43	7.77	7.85	7.59	7.94	7.9
Pr	1.283	1.385	1.346	1.319	1.38	1.407	1.372	1.396	1.43
Nd	6.86	7.35	7.05	6.87	7.42	7.32	7.36	7.64	7.58
Sm	1.716	1.938	1.776	1.726	1.922	1.859	1.92	1.925	1.911
Eu	0.528	0.583	0.572	0.573	0.569	0.576	0.575	0.611	0.593
Gd	1.503	1.591	1.523	1.448	1.644	1.517	1.581	1.621	1.648
Tb	0.1871	0.194	0.1887	0.1852	0.204	0.1976	0.18	0.2007	0.201
Dy	0.942	0.983	0.976	0.971	0.987	0.976	0.969	0.992	0.981
Ho	0.1317	0.1444	0.1439	0.1348	0.1515	0.1393	0.1349	0.1419	0.1405
Er	0.28	0.314	0.299	0.268	0.333	0.312	0.283	0.293	0.292
Tm	0.0289	0.03	0.0319	0.0268	0.0348	0.0316	0.0296	0.0289	0.0234
Yb	0.161	0.167	0.157	0.14	0.187	0.151	0.149	0.157	0.177
Lu	0.017	0.0203	0.0184	0.0168	0.0178	0.019	0.014	0.0186	0.0147
Hf	1.066	1.085	1.12	1.093	1.265	1.148	1.052	1.098	1.062
Ta	0.0165	0.021	0.0276	0.0165	0.0219	0.0251	0.0342	0.1722	0.0472
Pb	0.1012	0.0929	0.1168	0.1168	0.1034	0.1076	0.0977	0.1085	0.1215
Th	0.0129	0.0225	0.0244	0.0088	0.025	0.024	0.0062	0.0195	0.0216
U	<0.0025	0.0056	0.00373	<0.0026	0.00424	0.00741	<0.0060	0.00227	0.00271

KGG 91-20c Grt	A01	A02	A03	A04	A05	A06	A07	A08	A09
Li	<0.083	<0.081	<0.080	0.079	<0.074	<0.079	<0.079	0.074	<0.077
Sc	130.94	131.59	130.68	126.19	125.04	123.77	125.16	128.05	126.89
V	199.34	194.91	195.95	199.41	199.84	208.03	213.45	207.86	213.47
Cr	42461.38	41543.68	41860.28	45666.32	45431.87	47226.62	45509.48	43887.56	44826.59
Co	37.81	37.06	36.61	35.94	35.55	37.63	38.47	37.72	38.18
Ni	71.49	70.42	69.24	64.23	62.64	69.55	71.56	70.16	71.77
Cu	0.228	0.285	0.276	0.308	0.338	0.31	0.291	0.353	0.284
Zn	11.79	11.9	11.89	11.17	10.97	12.03	12.38	12.09	12.01
Ga	4.28	4.14	4.12	4.11	4.13	4.44	4.45	4.39	4.41
Rb	<0.044	<0.045	<0.043	<0.040	<0.039	<0.041	<0.041	<0.040	<0.039
Sr	0.486	0.468	0.466	0.428	0.438	0.42	0.445	0.41	0.419
Y	23.13	22.62	22.07	20.63	20.22	20.3	20.49	21.24	20.98
Zr	66.63	64.81	63.1	59.72	59.4	59.5	57.66	58.56	58.72
Nb	0.252	0.2311	0.2284	0.25	0.24	0.241	0.246	0.24	0.234
Ba	<0.0091	<0.0104	<0.0100	<0.0112	<0.0102	0.0087	<0.0132	<0.0103	<0.0100
La	0.041	0.0377	0.0389	0.0351	0.0389	0.037	0.0359	0.032	0.0327
Ce	0.399	0.384	0.377	0.255	0.259	0.279	0.272	0.263	0.269
Pr	0.1043	0.0948	0.0902	0.0784	0.075	0.0783	0.0858	0.0823	0.0793
Nd	0.842	0.827	0.747	1.152	1.182	1.118	1.154	1.164	1.149
Sm	1.362	1.252	1.241	1.336	1.34	1.336	1.254	1.296	1.271
Eu	0.705	0.688	0.666	0.687	0.685	0.702	0.662	0.653	0.657
Gd	2.84	2.715	2.72	2.552	2.521	2.521	2.41	2.502	2.463
Tb	0.581	0.566	0.549	0.529	0.511	0.522	0.497	0.523	0.52
Dy	4.25	4.18	3.99	3.7	3.69	3.78	3.76	3.89	3.84
Ho	0.891	0.864	0.842	0.766	0.761	0.761	0.767	0.815	0.785
Er	2.488	2.413	2.373	2.133	2.036	2.173	2.182	2.33	2.28
Tm	0.366	0.361	0.343	0.299	0.29	0.302	0.318	0.342	0.331
Yb	2.644	2.526	2.524	2.107	1.981	2.126	2.287	2.517	2.42
Lu	0.405	0.379	0.37	0.305	0.292	0.314	0.337	0.358	0.355
Hf	1.166	1.141	1.092	1.028	0.999	1.021	0.968	0.993	0.983
Ta	0.0187	0.0158	0.0166	0.0219	0.0174	0.0201	0.0186	0.0218	0.0213
Pb	0.0103	0.00389	0.00607	0.0122	0.00652	0.0724	0.0155	0.00695	0.00763
Th	0.00512	0.00458	0.00646	0.00451	0.00511	0.00508	0.00573	0.00528	0.00493
U	0.0064	0.00652	0.00623	0.00537	0.00579	0.00594	0.00639	0.00635	0.00563

KGG 91-37 CPX	A01	A02	A03	A04	A05	A06	A07	A08	A09
Li	5.34	0.63	0.631	1.106	0.969	3.37	2.32	1.014	0.931
Sc	17.25	21.21	21.08	18.59	20.31	21.63	19.66	23.16	21.54
V	6.41	7.21	6.56	6.36	6.36	6.86	5.98	6.93	7.24
Cr	11461.85	13553.1	12566.95	10392.44	12473.57	12634.28	12043.04	12213.92	12914.62
Co	20.82	21.96	20.43	25.97	20.52	23.4	19.61	21.56	21.29
Ni	350.35	359.28	346.36	333.31	337.32	347	331.59	337.49	365.7
Cu	1.912	1.875	1.98	3.53	2.075	3.48	1.146	2.2	4.56
Zn	9.54	9.53	9.6	15.74	9.89	11.27	8.83	10.1	11.39
Rb	0.142	<0.0195	<0.0179	0.269	0.0457	0.1381	0.0679	0.1061	<0.0194
Sr	135.66	124.67	122.08	142.74	124.43	144.33	128.73	145.4	132.26
Y	1.578	1.385	1.43	1.981	1.708	1.632	1.748	1.507	1.547
Zr	12.64	12.9	12.67	16.99	14.52	14.72	14.74	16.09	14.37
Nb	0.345	0.375	0.289	2.65	0.506	0.602	0.464	0.771	0.351
Ba	1.407	0.74	0.435	15.85	1.819	3.72	1.902	3.81	0.1932
La	1.823	1.749	1.704	4.07	1.994	2.228	2.044	2.505	1.87
Ce	7.82	7.74	7.35	11.58	7.76	8.27	7.87	9.48	8.23
Pr	1.315	1.307	1.251	1.767	1.345	1.39	1.382	1.625	1.399
Nd	6.36	6.35	6.07	8.12	6.66	6.85	6.89	7.89	6.88
Sm	1.229	1.213	1.24	1.592	1.349	1.399	1.397	1.484	1.367
Eu	0.361	0.347	0.338	0.415	0.379	0.373	0.384	0.398	0.378
Gd	0.87	0.834	0.867	1.119	0.923	0.973	0.95	0.99	0.908
Tb	0.0999	0.0882	0.0833	0.1125	0.1046	0.1033	0.1057	0.1028	0.095
Dy	0.465	0.423	0.426	0.557	0.485	0.491	0.523	0.44	0.467
Ho	0.0624	0.0533	0.0533	0.0801	0.0653	0.0675	0.0706	0.0656	0.0657
Er	0.1526	0.1102	0.1237	0.1595	0.1401	0.129	0.1472	0.1087	0.1299
Tm	0.0105	0.01243	0.012	0.018	0.01595	0.01463	0.01563	0.01059	0.01327
Yb	0.0807	0.0688	0.0558	0.0868	0.0761	0.0739	0.089	0.0665	0.0733
Lu	0.01067	0.00782	0.00786	0.0121	0.00867	0.00891	0.00958	0.00734	0.00885
Hf	0.806	0.826	0.792	0.925	0.895	0.934	0.91	0.976	0.883
Ta	0.0419	0.0384	0.0366	0.1586	0.0498	0.0551	0.0493	0.0685	0.0475
Pb	0.283	0.483	0.613	2.074	1.465	0.856	0.256	1.024	1.964
Th	0.0264	0.0187	0.0177	0.2196	0.0399	0.0776	0.0327	0.0654	0.0237
U	0.00929	0.01441	0.01621	0.085	0.0257	0.0508	0.0086	0.031	0.00634

KGG 91-37 Grt	A01	A02	A04	A05	A06	A07	A08
Li	<0.041	0.162	0.071	0.108	0.108	0.05	<0.033
Sc	112.45	112.91	114.66	113.68	111.31	114.23	113.14
V	207.94	205.27	183.61	186.97	188.83	190.02	194.28
Cr	40138.48	41552.28	37755.74	38854.11	40010.83	37388.43	40158.67
Co	39.29	38.9	33.42	33.79	34.45	34.23	36.27
Ni	40.95	42.43	32.06	33.55	35	40.21	40.67
Cu	<0.100	0.13	0.182	0.164	0.183	0.144	0.135
Zn	10.02	10.04	8.29	8.28	8.53	9.47	9.56
Ga	5.25	5.21	3.93	3.96	4.13	4.75	4.94
Rb	0.562	<0.039	<0.0275	<0.0260	<0.0274	<0.040	<0.031
Sr	0.286	0.296	0.2346	0.2279	0.2339	0.358	0.2701
Y	12.85	12.84	14.4	14.39	14.38	14.48	14.08
Zr	28.91	28.93	33.63	33.19	32.98	31.9	31.29
Nb	0.427	0.426	0.496	0.495	0.505	0.439	0.444
Ba	<0.0108	<0.0097	0.0995	0.0159	<0.0076	0.1155	0.0141
La	0.0306	0.0306	0.0539	0.0534	0.0521	0.0375	0.0351
Ce	0.388	0.39	0.36	0.367	0.374	0.351	0.362
Pr	0.1165	0.124	0.1163	0.1126	0.1131	0.1198	0.1197
Nd	1.156	1.16	1.17	1.169	1.116	1.195	1.171
Sm	0.804	0.775	0.885	0.871	0.87	0.824	0.842
Eu	0.379	0.383	0.405	0.411	0.398	0.391	0.386
Gd	1.382	1.414	1.584	1.548	1.547	1.539	1.498
Tb	0.291	0.281	0.337	0.33	0.321	0.322	0.316
Dy	2.243	2.161	2.501	2.448	2.458	2.432	2.414
Ho	0.482	0.468	0.53	0.525	0.521	0.519	0.525
Er	1.417	1.401	1.441	1.472	1.46	1.584	1.516
Tm	0.2018	0.1982	0.2031	0.2074	0.2029	0.2248	0.2307
Yb	1.472	1.482	1.427	1.473	1.44	1.607	1.606
Lu	0.207	0.2148	0.2167	0.2158	0.2162	0.2401	0.2458
Hf	0.613	0.591	0.752	0.73	0.736	0.664	0.644
Ta	0.0248	0.0244	0.0184	0.0181	0.0193	0.0275	0.0209
Pb	0.0264	0.0185	0.01793	0.00851	0.01749	0.0483	0.00955
Th	0.0271	0.0194	0.0638	0.0685	0.066	0.035	0.037
U	0.0543	0.0442	0.0639	0.0653	0.071	0.0439	0.0495

KGG 91-46 CPX	A01	A02	A03	A04	A05	A06	A07	A08	A09
Li	0.362	0.537	0.315	0.372	0.36	0.353	0.515	0.37	0.434
Sc	13.79	13.04	13.49	14.36	14.04	14.03	13.66	14.36	14.37
V	134.07	129.31	133.69	122.94	127.58	122.54	123.64	118.42	116.44
Cr	5443.11	5358.12	5398.23	5195.05	5390.79	5351.88	5279.75	5218.98	5124.95
Co	20.23	20	19.47	18.65	19.13	19.32	20.48	18.94	19.16
Ni	357.52	352.11	346.88	327	341.11	342.65	358.25	339.67	337.01
Cu	0.47	1.14	0.613	0.678	0.566	0.522	4.62	0.562	0.436
Zn	8.45	9.02	8.25	4.99	8.34	7.84	8.72	8.18	7.93
Rb	<0.0240	0.579	<0.0220	<0.0195	<0.0201	<0.0211	0.1103	0.0406	<0.0208
Sr	75.72	86.8	77.73	77.6	81.54	88.79	102.38	90.61	83.84
Y	0.506	0.571	0.51	0.573	0.565	0.631	0.636	0.64	0.632
Zr	6.17	6.17	6.08	6.59	6.39	6.42	6.29	6.45	6.41
Nb	0.308	0.393	0.327	0.298	0.286	0.295	0.336	0.309	0.302
Ba	0.648	2.316	0.788	0.1909	0.098	0.1064	13.84	3.031	0.1241
La	0.471	0.485	0.47	0.468	0.47	0.472	0.507	0.504	0.495
Ce	2.093	2.182	2.066	1.977	2.101	2.113	2.295	2.259	2.179
Pr	0.579	0.619	0.583	0.588	0.609	0.627	0.663	0.67	0.649
Nd	3.91	4.18	4	4.17	4.22	4.33	4.58	4.65	4.56
Sm	1.09	1.124	1.094	1.135	1.169	1.205	1.222	1.309	1.222
Eu	0.298	0.316	0.299	0.307	0.313	0.318	0.347	0.36	0.332
Gd	0.544	0.532	0.558	0.603	0.586	0.618	0.616	0.659	0.662
Tb	0.0431	0.0509	0.0454	0.0471	0.0487	0.0512	0.0561	0.0552	0.0549
Dy	0.188	0.188	0.1498	0.195	0.196	0.231	0.219	0.24	0.227
Ho	0.0186	0.0214	0.0203	0.019	0.0215	0.0252	0.0252	0.026	0.0272
Er	0.0447	0.0465	0.0411	0.0486	0.0464	0.0524	0.0571	0.0542	0.0573
Tm	0.00581	0.00592	0.00534	0.00565	0.00536	0.00705	0.00648	0.00718	0.00689
Yb	0.0314	0.0391	0.038	0.0393	0.034	0.0394	0.0446	0.041	0.044
Lu	0.00557	0.00558	0.00698	0.00568	0.00617	0.00594	0.00611	0.00653	0.00737
Hf	0.336	0.379	0.34	0.37	0.357	0.388	0.388	0.397	0.386
Ta	0.0392	0.0432	0.0381	0.0395	0.0407	0.0382	0.0417	0.0452	0.0419
Pb	0.00764	0.0094	0.0434	0.0346	0.00659	0.348	0.0378	0.00784	0.00867
Th	0.00555	0.00816	0.00555	0.00599	0.00533	0.00638	0.00623	0.00759	0.0065
U	0.00184	0.00234	0.00223	0.00177	0.00211	0.00192	0.00476	0.002	0.00178

KGG 91-46 Grt	A01	A02	A03	A04	A05	A06	A07	A08	A09
Li	0.041	0.049	0.052	0.042	0.045	0.041	0.053	0.063	<0.037
Sc	109.61	111.52	110.52	111.28	111.51	108.6	107.11	105.45	104.8
V	198.83	196.51	192.89	204.06	205.85	206.02	189.51	189.44	194.26
Cr	30490.06	30519.1	30489.94	29005.51	29017.93	29211.71	31174.36	30494.96	32240.33
Co	39.29	39.44	38.26	41.58	41.79	41.74	39.45	39.46	40.87
Ni	76.12	77.87	75.7	68.84	68.44	69.91	78.46	78.47	81.68
Cu	<0.097	<0.089	<0.085	<0.089	0.09	<0.082	0.102	<0.077	0.163
Zn	10.61	10.69	10.45	10.95	10.73	10.75	10.59	10.48	10.87
Ga	2.406	2.431	2.282	2.701	2.726	2.73	2.531	2.507	2.656
Rb	0.201	<0.032	<0.029	<0.031	<0.031	<0.029	<0.0276	<0.0278	<0.0285
Sr	0.2572	0.2617	0.2555	0.282	0.2372	0.2333	0.2317	0.2185	0.2111
Y	3.63	4.04	4.07	2.725	2.556	2.598	2.775	2.738	2.765
Zr	41.76	45.04	45.59	26.61	26.06	25.97	31.49	30.65	30.72
Nb	0.596	0.593	0.564	0.271	0.271	0.29	0.546	0.51	0.527
Ba	<0.0135	<0.0070	<0.0099	<0.0113	<0.0079	<0.0119	<0.0086	<0.0101	0.0083
La	0.00851	0.00757	0.00881	0.0136	0.00852	0.01015	0.00865	0.00775	0.00813
Ce	0.1377	0.1384	0.1322	0.314	0.298	0.302	0.1132	0.1051	0.1077
Pr	0.0742	0.0743	0.0728	0.1701	0.1758	0.1721	0.0763	0.0705	0.0744
Nd	1.032	1.045	1.045	1.919	1.959	1.972	1.258	1.243	1.351
Sm	0.973	1.014	1.02	1.263	1.2	1.193	1.224	1.204	1.238
Eu	0.418	0.428	0.434	0.431	0.427	0.425	0.451	0.45	0.483
Gd	1.194	1.261	1.271	1.054	1.036	1.031	1.129	1.098	1.125
Tb	0.1617	0.175	0.1727	0.102	0.1074	0.1116	0.1243	0.1213	0.1287
Dy	0.804	0.871	0.916	0.545	0.52	0.505	0.547	0.566	0.562
Ho	0.137	0.15	0.1554	0.0997	0.0856	0.0908	0.0978	0.0945	0.0976
Er	0.389	0.417	0.399	0.305	0.294	0.289	0.305	0.311	0.327
Tm	0.0666	0.0704	0.0704	0.0681	0.0576	0.0589	0.0584	0.0591	0.0616
Yb	0.609	0.676	0.643	0.664	0.604	0.605	0.628	0.59	0.606
Lu	0.1199	0.1176	0.1225	0.1209	0.1129	0.1177	0.1153	0.1169	0.1163
Hf	0.875	0.959	1.009	0.452	0.433	0.452	0.55	0.55	0.551
Ta	0.0659	0.0695	0.0677	0.0412	0.0338	0.0355	0.0494	0.0556	0.0439
Pb	0.0077	0.00439	0.00606	0.024	0.0301	0.0136	0.01423	0.00787	0.021
Th	0.00221	0.00321	0.00293	0.008	0.00551	0.00612	0.00201	0.00238	0.00359
U	0.00653	0.00734	0.00654	0.026	0.0252	0.0235	0.00654	0.00561	0.00683

KGG 91-60 CPX	A01	A02	A03	A04	A05	A06	A07	A08	A09
Li	4.85	0.562	4.17	5.57	0.618	0.737	0.715	0.665	0.667
Sc	27.7	27.83	30.92	27.04	28	26.44	27.81	26.87	26.99
V	6.03	6.03	3.79	4.47	6.19	6.12	6	5.91	6.08
Cr	7469.59	7323.61	7888.33	7461.93	7172.6	7494.35	7108.74	7076.81	6994.51
Co	19.53	15.37	18.89	19.1	17.24	17.19	16.86	17.27	17.06
Ni	287.48	254.5	271.01	317.98	282.52	283.86	278.08	282.84	282.08
Cu	14.15	1.12	5.41	5.05	1.341	1.452	1.316	1.427	1.546
Zn	8.26	6.88	8.24	10.98	7.58	7.74	7.63	7.65	7.94
Rb	5.03	<0.0112	1.436	7.83	<0.0120	0.0234	0.0492	<0.0109	<0.0112
Sr	226.41	106.65	278.52	177.85	149	143.85	148.25	148.52	150.02
Y	2.19	1.87	2.01	2.97	2.73	2.68	2.8	2.72	2.74
Zr	13.24	12.93	14.68	14.11	16.66	16.46	17.24	16.83	16.89
Nb	0.886	0.535	0.466	1.067	0.496	0.527	0.575	0.536	0.545
Ba	4.96	0.1259	8.75	17.38	0.1147	1.329	0.623	0.1468	0.253
La	2.476	1.936	2.94	5.17	2.392	2.338	2.65	2.41	2.44
Ce	7.44	5.62	7.71	14.04	10.14	10.12	10.41	10.15	10.13
Pr	1.293	0.976	1.249	2.274	1.972	1.939	2.034	1.987	1.987
Nd	6.4	5.06	6.12	10.57	9.99	9.6	10.34	9.97	10.11
Sm	1.553	1.336	1.515	2.208	2.163	2.078	2.167	2.18	2.191
Eu	0.489	0.434	0.47	0.641	0.621	0.616	0.653	0.646	0.639
Gd	1.262	1.069	1.209	1.545	1.532	1.504	1.603	1.552	1.568
Tb	0.1335	0.1198	0.1326	0.1683	0.1662	0.1626	0.1705	0.1665	0.1682
Dy	0.64	0.533	0.595	0.793	0.776	0.751	0.793	0.79	0.772
Ho	0.0826	0.0726	0.0826	0.112	0.1027	0.1025	0.112	0.1084	0.1083
Er	0.1572	0.1354	0.1498	0.217	0.2	0.199	0.214	0.215	0.219
Tm	0.0166	0.01519	0.0136	0.0227	0.0221	0.0221	0.0236	0.0227	0.0218
Yb	0.0793	0.0678	0.0732	0.1286	0.1143	0.1131	0.1162	0.12	0.1083
Lu	0.01076	0.00739	0.00885	0.01341	0.01271	0.0138	0.0142	0.0143	0.013
Hf	0.604	0.593	0.665	0.57	0.648	0.641	0.668	0.659	0.655
Ta	0.056	0.0657	0.0413	0.0958	0.0807	0.0868	0.0923	0.0875	0.0941
Pb	1.112	0.2214	0.317	0.441	0.216	28.4	2.36	2.59	102.28
Th	0.0438	0.0785	0.1097	0.296	0.0218	0.0229	0.0261	0.0226	0.0254
U	0.0188	0.0065	0.0346	0.065	0.00424	0.00453	0.00515	0.0041	0.00482

KGG 91-60 Grt	A01	A02	A03	A04	A05	A06	A07	A08	A09
Li	0.114	0.141	0.131	0.119	0.103	0.127	0.116	0.15	0.133
Sc	88.14	87.17	87.84	91.81	91.63	90.21	90.31	89.48	89.75
V	148.12	155.24	154.18	140.24	143.94	151.08	146.46	150.4	152.72
Cr	17161.94	17260.83	17602.9	16721.8	16951.63	17709.71	17231.17	17260.81	17862.1
Co	38.22	37.81	38.81	38.68	39.48	40.06	38.5	37.75	38.66
Ni	30.85	30.79	31.65	30.93	31.83	32.41	31.76	31	32.26
Cu	<0.115	0.109	<0.112	<0.112	0.128	0.154	<0.121	<0.120	<0.104
Zn	9.18	9.16	9.58	9.2	9.52	9.4	9.5	9.01	9.29
Ga	6.78	6.69	7.07	6.85	7.14	7.15	7.21	6.94	7.08
Rb	0.0838	<0.0227	<0.0231	<0.0232	<0.0229	<0.0231	<0.0249	<0.0247	<0.0217
Sr	0.0972	0.0935	0.0927	0.1036	0.117	0.0965	0.1035	0.1062	0.1303
Y	17.47	16.68	16.98	18.29	18.13	18.06	19.34	18.63	18.87
Zr	18.9	18.63	18.65	16.72	16.6	16.57	20.28	20.22	19.98
Nb	0.1008	0.087	0.0976	0.1348	0.1238	0.1208	0.0934	0.0947	0.0856
Ba	<0.0117	<0.0081	<0.0114	<0.0135	<0.0162	<0.0113	0.0152	<0.0125	<0.0115
La	0.00545	0.00455	0.00359	0.00714	0.00524	0.00583	0.00532	0.00723	0.00594
Ce	0.0438	0.045	0.0426	0.0672	0.0541	0.0538	0.0471	0.05	0.0453
Pr	0.0233	0.0222	0.0241	0.0312	0.0245	0.0255	0.0242	0.0248	0.0227
Nd	0.327	0.328	0.345	0.356	0.339	0.351	0.363	0.35	0.325
Sm	0.546	0.502	0.522	0.502	0.513	0.5	0.539	0.586	0.573
Eu	0.338	0.324	0.343	0.316	0.325	0.32	0.346	0.338	0.339
Gd	1.425	1.369	1.437	1.374	1.479	1.39	1.566	1.577	1.532
Tb	0.332	0.318	0.329	0.335	0.343	0.339	0.371	0.357	0.351
Dy	2.88	2.68	2.81	2.84	2.83	2.84	3.06	3.03	2.96
Ho	0.658	0.625	0.638	0.672	0.667	0.679	0.684	0.692	0.685
Er	2.084	1.967	2.054	2.091	2.149	2.099	2.288	2.205	2.164
Tm	0.318	0.306	0.32	0.326	0.331	0.328	0.337	0.349	0.34
Yb	2.48	2.31	2.343	2.477	2.508	2.466	2.543	2.521	2.505
Lu	0.363	0.335	0.354	0.374	0.373	0.368	0.382	0.381	0.381
Hf	0.409	0.43	0.437	0.307	0.29	0.313	0.444	0.465	0.449
Ta	0.00701	0.00663	0.00657	0.0113	0.00802	0.0064	0.0073	0.00656	0.0058
Pb	0.153	0.0846	0.0882	0.0892	0.1149	0.0626	0.0476	0.0462	0.129
Th	0.0065	0.00759	0.00559	0.00801	0.00617	0.00792	0.00689	0.00594	0.00508
U	0.01053	0.01084	0.00992	0.01282	0.01368	0.014	0.00915	0.01034	0.01092

KGG 91-62 CPX	A01	A02	A03	A04	A05	A06	A07	A08	A09
Li	15.71	12.6	17.38	18.73	0.998	13.33	10.44	0.726	13.42
Sc	31.35	32.66	32.58	33.24	32.24	31.57	25.53	31.24	30.29
V	6.67	5.47	5.91	5.4	6.86	6.85	6.25	6.49	6.23
Cr	11963.09	11513.83	11913.17	11529.98	12890.46	12577.93	11090.05	12688.43	11962.09
Co	16.24	15.51	17.12	15.84	16.96	17.4	14.72	16.53	16.08
Ni	260.4	251.63	265.11	256.34	283.52	279.72	233.55	273.05	262.05
Cu	1.484	0.688	1.929	1.087	1.536	2.04	0.433	1.378	1.112
Zn	7.52	6.8	7.68	7.44	8.01	8.5	7.44	7.38	8.01
Rb	0.0958	0.409	0.0864	0.357	0.0453	2.96	1.206	<0.0127	0.341
Sr	151.63	195.53	175.94	164.16	154.36	188.9	225.11	152.28	184.19
Y	1.558	1.948	1.793	1.844	1.586	1.583	1.988	1.47	1.587
Zr	20.96	22.02	21.62	23.13	21.38	20.9	19.14	19.9	20.66
Nb	0.1985	0.834	0.706	0.477	0.1217	0.486	1.837	0.1155	1.154
Ba	1.335	4.41	2.206	6.93	5.13	29.57	13.69	0.403	15.39
La	7.07	10.39	8.55	8.16	7.31	8.1	8.72	6.75	8.3
Ce	17.09	23.91	20.58	18.33	18.97	18.97	24.8	17.73	19.68
Pr	2.309	3.23	2.807	2.505	2.454	2.44	3.33	2.365	2.529
Nd	9.44	12.62	11.26	10.45	9.83	9.67	13.06	9.3	10.02
Sm	1.732	2.069	1.926	1.936	1.814	1.734	2.089	1.667	1.72
Eu	0.457	0.569	0.532	0.528	0.508	0.487	0.563	0.469	0.492
Gd	1.147	1.328	1.237	1.292	1.226	1.15	1.404	1.056	1.15
Tb	0.1143	0.1304	0.1268	0.1336	0.1148	0.112	0.1277	0.1072	0.1122
Dy	0.49	0.583	0.533	0.592	0.542	0.475	0.561	0.458	0.512
Ho	0.0665	0.076	0.0734	0.0716	0.0669	0.062	0.0792	0.0596	0.0646
Er	0.1169	0.1342	0.1322	0.1317	0.1132	0.1098	0.1381	0.1042	0.1204
Tm	0.01073	0.01469	0.01304	0.01238	0.01166	0.01214	0.0145	0.01051	0.01265
Yb	0.1015	0.0794	0.0668	0.069	0.0582	0.0564	0.0891	0.049	0.0677
Lu	0.00682	0.01005	0.00632	0.0076	0.0082	0.00651	0.00945	0.0072	0.00756
Hf	1.088	1.008	0.999	1.204	1.086	1.059	0.821	0.989	1.024
Ta	0.01219	0.0592	0.0304	0.0272	0.0144	0.0169	0.1017	0.00981	0.0467
Pb	0.334	0.2461	0.38	0.39	0.5	0.483	0.277	0.334	0.89
Th	0.1613	0.1735	0.1572	0.1986	0.1476	0.1593	0.259	0.1361	0.286
U	0.0296	0.01701	0.0275	0.0309	0.0301	0.056	0.0859	0.0244	0.0442

KGG 91-62 Grt	A01	A02	A03	A04	A05	A06	A07	A08	A09
Li	0.097	1.037	2.43	0.105	0.102	0.117	0.143	0.159	0.101
Sc	126.34	126.54	130.87	128.21	122.17	118.68	112.27	111.65	109.78
V	176.56	176.62	183.71	168.6	171.03	173.6	184.34	174.75	186.38
Cr	33696.8	32508.43	32377.63	33865.43	34552.21	35775.29	38979.93	37358.75	39799.09
Co	34.54	32.69	32.34	31.16	31.97	32.6	36.57	34.66	37.58
Ni	31.45	34.02	39.43	27.46	27.68	28.67	32.87	32.14	34.38
Cu	<0.145	9.76	13.54	<0.122	<0.122	<0.110	<0.112	1.455	0.112
Zn	8.79	10.56	11.79	7.7	7.68	7.98	8.94	8.47	9.3
Ga	6.55	8.38	12.23	5.72	5.76	5.95	6.8	6.36	7.03
Rb	0.164	3.47	11.11	<0.0281	<0.0277	<0.0261	<0.0269	0.0633	<0.0279
Sr	0.1627	3.92	9.3	0.1483	0.1679	0.1877	0.1464	0.583	0.1621
Y	17.2	17.16	18.65	19.57	18.32	17.49	16.79	16.12	16.91
Zr	33.75	33.36	36.2	37.67	34.97	33.61	33.18	31.53	33.31
Nb	0.0811	0.2049	0.47	0.0764	0.0775	0.0773	0.0911	0.0845	0.0902
Ba	<0.0119	23.96	65.7	<0.0160	0.0543	0.0149	<0.0091	0.25	<0.0082
La	0.0277	0.0602	0.378	0.0207	0.0266	0.0243	0.0195	0.0422	0.0281
Ce	0.1946	0.2271	0.475	0.1514	0.1803	0.1785	0.27	0.2189	0.2059
Pr	0.0738	0.0762	0.1115	0.0673	0.0684	0.0687	0.072	0.0745	0.078
Nd	0.8	0.853	0.985	0.863	0.813	0.806	0.841	0.83	0.879
Sm	0.885	0.859	0.902	0.97	0.873	0.875	0.884	0.794	0.918
Eu	0.474	0.453	0.465	0.481	0.452	0.452	0.466	0.446	0.493
Gd	1.947	1.927	2.152	2.226	2.017	1.884	1.878	1.795	1.955
Tb	0.401	0.401	0.426	0.458	0.413	0.401	0.389	0.366	0.406
Dy	3.05	3.07	3.19	3.5	3.19	3.09	3.01	2.82	3.05
Ho	0.656	0.637	0.675	0.724	0.677	0.636	0.624	0.589	0.644
Er	1.829	1.833	1.95	2.067	1.911	1.848	1.8	1.667	1.833
Tm	0.2699	0.2672	0.288	0.299	0.282	0.2635	0.2594	0.2477	0.27
Yb	1.893	1.881	2.001	2.056	1.927	1.901	1.919	1.782	1.966
Lu	0.29	0.286	0.308	0.319	0.299	0.287	0.28	0.259	0.295
Hf	0.579	0.56	0.622	0.672	0.618	0.586	0.57	0.511	0.572
Ta	0.00706	0.00433	0.00469	<0.00259	0.004	0.00342	0.0042	0.0047	0.00485
Pb	0.0702	0.218	0.378	0.0799	0.0331	0.0422	0.0449	0.0326	0.027
Th	0.0181	0.0207	0.0224	0.0306	0.0201	0.0175	0.0162	0.0187	0.0187
U	0.0238	0.0348	0.0721	0.0204	0.0215	0.0213	0.024	0.0335	0.0246

KGG 91-65 CPX	A01	A02	A03	A04	A05	A06	A07	A08	A09
Li	0.777	1.084	2.42	1.386	0.697	0.792	2.13	1.43	1.63
Sc	29.11	30.46	26.89	28.37	28.25	29.56	30.95	32.15	31.79
V	7.55	7.29	7.04	7.12	7.19	6.74	6.89	6.97	7.13
Cr	13267.01	12839.49	12242.51	12999.98	13279.97	12255.31	10503.4	11228.06	9935.22
Co	17.87	18.05	19.26	18.75	17.22	16.2	19.12	21.47	19.91
Ni	282.02	280.65	281.3	263.88	284.12	263.06	248.22	278	268.79
Cu	0.963	5.06	6.87	0.596	1.147	1.018	3.66	69.24	17.05
Zn	7.46	7.98	9.28	9.29	8.15	7.08	8.94	10.97	9.2
Rb	0.0372	0.0414	2.08	1.588	0.0253	<0.0110	2.86	1.244	2.42
Sr	159.45	166.5	206.46	174.21	159.14	161.09	240.8	193.57	240
Y	2.49	2.63	2.75	2.6	2.45	2.85	3.14	3.1	3.1
Zr	46.24	48.76	33.52	34.53	45.26	51.86	41.48	40.35	39.61
Nb	0.531	0.627	0.961	0.997	0.545	0.572	1.37	1.049	1.6
Ba	0.1516	0.857	8.3	3.11	0.1647	0.2064	14.18	3.08	11.05
La	3.56	4.03	8.28	5.86	3.48	3.72	9.54	8.18	9.83
Ce	13.58	13.85	23.45	16.33	13.42	12.65	24.14	20.15	24.59
Pr	2.291	2.395	3.2	2.488	2.276	2.298	3.62	3.03	3.54
Nd	10.88	11.29	13.47	11.11	10.61	11.29	15.94	13.81	15.37
Sm	2.338	2.459	2.581	2.354	2.218	2.393	3	2.78	2.95
Eu	0.68	0.706	0.749	0.662	0.677	0.697	0.807	0.773	0.808
Gd	1.602	1.66	1.698	1.567	1.543	1.719	2.036	1.889	2.048
Tb	0.1693	0.1729	0.1841	0.1712	0.1666	0.1813	0.2089	0.2058	0.2049
Dy	0.77	0.768	0.883	0.805	0.773	0.853	0.947	0.893	0.941
Ho	0.1055	0.1093	0.1152	0.1091	0.1037	0.1151	0.1219	0.1265	0.1287
Er	0.2065	0.216	0.225	0.2138	0.214	0.218	0.241	0.254	0.246
Tm	0.0217	0.0218	0.0226	0.0216	0.0211	0.024	0.0258	0.0252	0.025
Yb	0.1036	0.1152	0.1238	0.1219	0.1162	0.1174	0.1287	0.1332	0.1329
Lu	0.01279	0.01294	0.01515	0.01189	0.01221	0.0126	0.01688	0.01448	0.0156
Hf	1.769	1.835	1.404	1.526	1.801	1.987	1.616	1.622	1.6
Ta	0.067	0.0731	0.0371	0.0338	0.0705	0.077	0.0699	0.0477	0.0528
Pb	0.672	0.485	0.533	14.27	21.24	5.21	0.619	0.937	0.702
Th	0.0517	0.0592	0.1999	0.1601	0.0522	0.0518	0.2531	0.336	0.384
U	0.01055	0.01472	0.0409	0.0251	0.01085	0.01016	0.0475	0.0379	0.0525

KGG 91-65 Grt	A01	A02	A03	A04	A05	A06	A07
Li	0.09	0.07	0.088	0.118	0.113	0.089	0.121
Sc	101.01	100.08	97.55	98.17	97.77	99.14	100.48
V	191.01	197.47	201.45	198.54	191.82	186.07	192.8
Cr	32513.52	34854.58	35659.48	35538.49	34212.25	33337.53	35793.93
Co	34.32	37.16	37.34	36.85	35.53	34.38	37.04
Ni	30.03	32.14	33.09	32.7	30.48	29.67	34.96
Cu	<0.114	0.159	0.156	0.15	<0.110	<0.108	0.34
Zn	8.16	8.91	9.36	8.72	8.09	7.87	8.61
Ga	5.36	5.85	5.83	5.72	5.4	5.28	5.67
Rb	0.0494	<0.0238	<0.0263	<0.0246	<0.0226	<0.0219	<0.0236
Sr	0.172	0.1504	0.133	0.1804	0.1897	0.1816	0.2306
Y	15.19	15.53	13.03	13.77	14.82	15.09	13.92
Zr	41.69	41.7	32.56	35.71	40.38	40.51	32.19
Nb	0.1339	0.1559	0.1825	0.1495	0.1358	0.1478	0.2079
Ba	<0.0120	<0.0098	0.0124	<0.0103	<0.0133	<0.0091	0.201
La	0.01382	0.01341	0.01357	0.0115	0.01782	0.01657	0.01596
Ce	0.1255	0.1381	0.1633	0.1383	0.1298	0.1291	0.1512
Pr	0.0535	0.0582	0.0572	0.0572	0.0563	0.0551	0.0573
Nd	0.74	0.754	0.625	0.678	0.738	0.737	0.676
Sm	0.858	0.864	0.69	0.752	0.843	0.849	0.735
Eu	0.455	0.465	0.386	0.401	0.445	0.434	0.388
Gd	1.713	1.799	1.369	1.483	1.721	1.667	1.437
Tb	0.349	0.36	0.282	0.302	0.338	0.35	0.301
Dy	2.68	2.73	2.161	2.26	2.55	2.66	2.37
Ho	0.572	0.593	0.482	0.493	0.554	0.58	0.506
Er	1.784	1.785	1.461	1.485	1.676	1.748	1.491
Tm	0.26	0.278	0.22	0.2222	0.254	0.265	0.237
Yb	1.995	2.096	1.7	1.685	1.952	1.948	1.776
Lu	0.286	0.302	0.249	0.246	0.286	0.296	0.267
Hf	0.901	0.873	0.58	0.664	0.866	0.891	0.508
Ta	0.00698	0.0102	0.01096	0.0074	0.0285	0.00671	0.0084
Pb	0.1072	0.1039	0.1185	0.0398	0.0319	0.0258	0.0695
Th	0.0181	0.0172	0.0202	0.0213	0.0169	0.0166	0.0137
U	0.0183	0.0207	0.0175	0.0141	0.0198	0.0168	0.0193

KHA 91-29 CPX	A01	A02	A03	A04	A05	A06	A07	A08	A09
Li	0.442	0.461	0.493	0.432	0.411	0.401	0.366	0.38	0.37
Sc	26.82	26.7	26.75	27.74	32.62	30.27	30.58	30.88	30.51
V	59.3	48.96	80.18	9.24	9.84	10.73	93.28	16.32	60.38
Cr	4589.04	4707.93	4816.48	4495.89	4132.4	4262.35	4118.74	4135.42	4140.92
Co	14.02	14.41	14.61	13.29	12.36	12.48	12.01	11.96	11.9
Ni	249.7	259.84	264.94	236.31	222.01	226.28	221.4	219.46	218.09
Cu	0.35	0.5	0.459	0.369	0.429	0.379	0.399	0.397	0.386
Zn	4.74	5.11	5.13	4.17	4.11	4.24	4.27	4.2	4.33
Rb	<0.0144	<0.0143	<0.0140	<0.0118	<0.0108	0.0378	<0.0119	<0.0107	<0.0107
Sr	82.15	83.03	82.18	80.95	81.05	80.41	80	79.14	78.59
Y	0.0482	0.0512	0.0523	0.0517	0.0549	0.0499	0.0471	0.0497	0.0528
Zr	1.812	1.697	1.663	2.137	2.202	1.931	2.056	2.055	2.173
Nb	0.361	0.346	0.352	0.507	0.475	0.495	0.371	0.393	0.412
Ba	0.0889	0.0987	0.0961	1.773	3.048	1.227	0.1112	0.1331	0.1608
La	9.01	8.9	8.84	8.91	9.55	9.39	9.51	9.39	9.46
Ce	15.64	16.37	16.55	15.06	14.16	14.54	13.84	13.71	13.65
Pr	1.738	1.776	1.764	1.683	1.687	1.688	1.662	1.643	1.639
Nd	5.83	5.83	5.74	5.73	6.13	6.05	6.02	6	6
Sm	0.548	0.545	0.536	0.55	0.624	0.608	0.586	0.611	0.584
Eu	0.1046	0.1034	0.1055	0.0986	0.1013	0.1028	0.1014	0.1019	0.0982
Gd	0.18	0.16	0.178	0.194	0.192	0.182	0.182	0.179	0.176
Tb	0.00876	0.00725	0.00841	0.00863	0.0101	0.00779	0.01018	0.0093	0.00863
Dy	0.0278	0.0289	0.0214	0.0191	0.0372	0.0228	0.0274	0.0275	0.028
Ho	0.00232	0.00303	0.00337	0.00189	0.00152	0.00272	0.00274	0.00301	0.00297
Er	0.0057	0.0049	0.0078	0.0052	0.00671	0.00463	0.00562	0.00625	0.00623
Tm	<0.00102	0.00076	0.00119	0.00061	0.00118	0.00116	0.00083	0.0012	0.00099
Yb	0.0039	0.0055	0.0074	<0.0027	0.0062	0.00517	<0.0033	0.0034	0.0038
Lu	0.00087	0.00084	0.00065	0.00136	0.00101	0.00077	0.00098	<0.00067	0.00115
Hf	0.0422	0.0403	0.0383	0.0466	0.0485	0.0436	0.0501	0.0441	0.0442
Ta	0.039	0.0383	0.0368	0.0543	0.0492	0.047	0.0453	0.0459	0.0584
Pb	0.684	0.695	0.671	0.607	0.566	0.572	30.38	25.58	42.07
Th	0.581	0.59	0.562	0.611	0.692	0.67	0.689	0.688	0.713
U	0.0711	0.0733	0.0735	0.0703	0.0654	0.0672	0.0617	0.0651	0.0656

KHA 91-29 Grt	A01	A02	A03
Li	<0.043	<0.045	<0.042
Sc	188.97	175.44	178.98
V	100.28	109.46	110.68
Cr	13019.53	14636.92	15060.95
Co	33.01	37.13	37.27
Ni	16.22	18.42	18.62
Cu	<0.118	<0.114	<0.109
Zn	5.61	6.55	6.25
Ga	1.388	1.593	1.605
Rb	<0.0264	<0.0250	<0.0241
Sr	0.0392	0.0373	0.0428
Y	0.753	0.74	0.754
Zr	4.34	4.36	4.2
Nb	0.1454	0.1635	0.1487
Ba	<0.0153	<0.0126	<0.0107
La	0.0206	0.0194	0.0184
Ce	0.159	0.1778	0.1672
Pr	0.0607	0.06	0.0579
Nd	0.638	0.593	0.587
Sm	0.35	0.355	0.361
Eu	0.1257	0.1305	0.1382
Gd	0.332	0.305	0.316
Tb	0.0337	0.0306	0.0351
Dy	0.16	0.168	0.158
Ho	0.0266	0.0244	0.0276
Er	0.0837	0.074	0.093
Tm	0.0159	0.0153	0.0155
Yb	0.137	0.117	0.117
Lu	0.0235	0.0213	0.0222
Hf	0.027	0.0258	0.0233
Ta	0.00419	0.0047	0.00453
Pb	0.1151	0.155	0.0686
Th	0.018	0.0219	0.0239
U	0.0384	0.046	0.0426

KHA 91-93 CPX	A01	A02	A06	A07
Li	0.398	0.462	2.9	2.76
Sc	15.77	15.07	7.48	7.53
V	112.31	110.05	132.51	131.21
Cr	5114.91	4940.24	5288.74	5599.02
Co	18.13	19.33	27.04	22.98
Ni	308.79	317.21	363.41	358.66
Cu	1.23	4.79	13.22	5.04
Zn	4.35	3.33	3.15	2.97
Rb	0.0414	0.063	0.792	0.37
Sr	90.89	89.99	123.39	107.69
Y	0.715	0.901	1.147	1.038
Zr	6.85	8.71	12.4	10.27
Nb	0.327	0.33	0.7	0.54
Ba	0.316	5.52	5.83	3.65
La	0.492	0.517	1.862	1.249
Ce	2.031	1.907	5.07	3.6
Pr	0.621	0.608	1.117	0.884
Nd	4.52	4.66	6.84	6.15
Sm	1.239	1.351	1.93	1.658
Eu	0.332	0.328	0.451	0.43
Gd	0.652	0.749	0.864	0.945
Tb	0.0526	0.0694	0.12	0.0977
Dy	0.256	0.273	0.503	0.352
Ho	0.0282	0.0396	0.0655	0.0436
Er	0.0666	0.0726	0.136	0.06
Tm	0.00779	0.007	0.0149	0.0127
Yb	0.0556	0.0523	0.077	0.069
Lu	0.00583	0.0108	0.012	0.0069
Hf	0.402	0.499	0.676	0.559
Ta	0.0499	0.0508	0.11	0.0933
Pb	0.917	2.106	0.279	0.235
Th	0.00572	0.0087	0.0552	0.0338
U	0.00218	0.0244	0.0213	0.0071

KHA 91-93 Grt	A01	A02	A03	A04	A05	A06	A07	A08	A09
Li	<0.090	<0.077	<0.074	<0.078	<0.072	0.075	<0.066	<0.062	<0.062
Sc	183.57	180.35	173.94	198.43	199.39	197.18	171.08	168.24	166.39
V	205.91	195.38	198.42	200.5	198.08	196.51	196.31	195.16	196.96
Cr	65713.57	62819.44	63063.04	71051.68	71256.49	71614.92	67871.48	69264.19	71027.65
Co	36.29	33.15	32.61	36.19	35.63	34.61	32.78	31.95	32.49
Ni	91.38	83.7	81.94	89.91	88.44	85.79	83.77	80.74	82.28
Cu	0.152	0.198	0.325	0.339	0.38	0.301	0.37	0.322	0.346
Zn	11.37	10.24	9.89	11.19	10.94	10.54	10.76	9.78	10.19
Ga	3.94	3.78	3.87	3.31	3.31	3.27	4.23	4.07	4.16
Rb	0.173	<0.040	<0.039	<0.042	<0.040	<0.038	<0.038	<0.035	<0.036
Sr	1.045	1.005	0.981	1.08	1.066	1.056	1.043	1.044	1.031
Y	11.46	11.73	13.64	7.92	8.22	8.22	15.53	15.96	15.43
Zr	102.83	100.04	97.19	81.88	85.14	87.49	100.95	100.58	98.33
Nb	0.343	0.331	0.327	0.371	0.397	0.382	0.334	0.328	0.327
Ba	<0.0101	<0.0096	<0.0090	<0.0110	<0.0118	<0.0127	0.011	<0.0104	0.0141
La	0.0978	0.087	0.088	0.1008	0.0988	0.1	0.0914	0.0931	0.0886
Ce	0.91	0.827	0.808	0.946	0.954	0.918	0.828	0.845	0.83
Pr	0.345	0.3174	0.3051	0.354	0.352	0.347	0.3186	0.326	0.3202
Nd	3.43	3.3	3.23	3.59	3.58	3.58	3.35	3.37	3.34
Sm	2.637	2.512	2.349	2.529	2.585	2.592	2.576	2.439	2.555
Eu	1.093	1.073	1.067	0.904	0.946	0.957	1.117	1.093	1.114
Gd	3.54	3.56	3.69	2.469	2.56	2.631	3.96	3.96	3.85
Tb	0.484	0.511	0.556	0.284	0.32	0.321	0.638	0.622	0.632
Dy	2.609	2.647	3.1	1.508	1.546	1.551	3.57	3.64	3.61
Ho	0.401	0.399	0.484	0.2633	0.2683	0.2627	0.586	0.591	0.578
Er	1.04	1.042	1.196	0.799	0.837	0.841	1.424	1.45	1.401
Tm	0.1723	0.1722	0.182	0.1436	0.1536	0.1567	0.2123	0.2124	0.206
Yb	1.492	1.405	1.489	1.339	1.385	1.397	1.637	1.624	1.618
Lu	0.2639	0.264	0.2613	0.2482	0.261	0.2658	0.2756	0.2809	0.2833
Hf	2.126	2.101	2.11	1.298	1.447	1.483	2.255	2.224	2.208
Ta	0.0245	0.0183	0.0203	0.0258	0.0225	0.0247	0.0202	0.021	0.0191
Pb	0.00582	0.00356	0.00453	0.00801	0.00513	0.0043	0.00659	0.0062	0.043
Th	0.01262	0.012	0.01292	0.0138	0.01314	0.01505	0.01339	0.01201	0.01112
U	0.01233	0.01051	0.01021	0.01114	0.01361	0.01236	0.0107	0.01131	0.01107

KHA 91-94 CPX	A01	A02	A03	A04	A05	A06	A08	A09
Li	0.453	0.396	0.428	0.367	0.351	0.43	0.456	0.768
Sc	23.12	21.74	22.57	21.61	21.43	22.13	24.6	27.05
V	5.31	4.91	5.39	5.46	5.67	5.59	6.14	6.42
Cr	8007.35	7324.21	7486.41	7418.45	7038.79	7343.91	7708.82	8216.46
Co	15.11	15.36	15.32	15.28	15.26	16.18	16.97	18.11
Ni	241.79	235.44	237.65	235.18	233.24	250.26	255.77	274.05
Cu	3.45	2.85	1.798	1.146	1.593	1.509	2.65	3.22
Zn	12.73	16.37	17.22	9.62	10.22	11.8	13.73	15.26
Rb	0.0738	0.0137	0.0272	<0.0138	<0.0165	<0.0145	<0.0143	0.303
Sr	130.77	137.16	132.57	131.18	109.76	142.31	137.86	179.89
Y	1.602	1.452	1.483	1.451	1.148	1.489	1.7	2.2
Zr	33.86	31.07	31.75	29.63	20.23	31.06	35.2	43.23
Nb	0.312	0.286	0.265	0.283	0.317	0.363	0.305	2.11
Ba	0.824	0.464	0.168	0.18	0.27	1.8	0.197	5.45
La	3.22	2.49	2.68	3.27	3.58	2.65	2.98	5.29
Ce	13.12	11.57	11.94	13.29	12.58	12.82	13.5	18.72
Pr	2.09	1.93	1.98	2.03	1.82	2.06	2.19	2.84
Nd	9.21	8.62	8.82	8.8	7.61	8.98	9.86	12.27
Sm	1.752	1.658	1.703	1.653	1.286	1.749	1.83	2.29
Eu	0.506	0.474	0.501	0.475	0.359	0.518	0.531	0.68
Gd	1.049	1.007	0.994	0.987	0.741	1.017	1.135	1.48
Tb	0.1102	0.1084	0.1109	0.1037	0.0777	0.103	0.123	0.158
Dy	0.522	0.461	0.499	0.48	0.364	0.476	0.555	0.76
Ho	0.0697	0.0547	0.0673	0.0618	0.0462	0.0613	0.0734	0.0973
Er	0.1373	0.1191	0.1212	0.1192	0.094	0.1205	0.1307	0.19
Tm	0.0125	0.012	0.0132	0.0129	0.0119	0.0123	0.0158	0.0175
Yb	0.0775	0.078	0.0636	0.0646	0.0571	0.0578	0.077	0.1085
Lu	0.00948	0.00727	0.00703	0.00798	0.00633	0.00768	0.0099	0.0139
Hf	1.151	1.171	1.108	0.989	0.681	1.155	1.14	1.93
Ta	0.0501	0.0379	0.034	0.0357	0.0396	0.0408	0.0417	0.187
Pb	0.184	0.215	0.216	0.2	0.266	0.176	0.256	0.171
Th	0.0647	0.0286	0.0255	0.0309	0.0507	0.0367	0.0297	0.186
U	0.0369	0.0061	0.00558	0.00591	0.00776	0.0124	0.01	0.11

KHA 91-94 Grt	A01	A02	A03	A07
Li	0.076	0.084	0.099	0.109
Sc	88.08	87.88	86.33	84.35
V	144.5	147.37	147.53	148.93
Cr	18388.9	18611.21	18372.19	19842.69
Co	34.08	34.1	34.87	35.11
Ni	25.85	27.33	28.09	26.44
Cu	2.04	2.04	2.37	1.9
Zn	14.16	15.13	15.78	13.94
Ga	4.99	4.97	4.94	5.27
Rb	0.07	<0.038	<0.035	0.063
Sr	0.233	0.1625	0.303	0.203
Y	9.09	9.17	9.01	8.84
Zr	18.51	18.58	20.23	18.17
Nb	0.0915	0.0953	0.136	0.0995
Ba	0.0474	0.0312	0.139	0.0432
La	0.01363	0.01306	0.0226	0.01105
Ce	0.1384	0.1331	0.1831	0.1375
Pr	0.0559	0.0553	0.0641	0.0549
Nd	0.619	0.597	0.641	0.6
Sm	0.508	0.517	0.495	0.504
Eu	0.2354	0.241	0.26	0.2386
Gd	0.788	0.767	0.814	0.771
Tb	0.1618	0.1711	0.168	0.1653
Dy	1.435	1.447	1.373	1.47
Ho	0.343	0.34	0.321	0.34
Er	1.132	1.104	1.162	1.063
Tm	0.1789	0.175	0.173	0.172
Yb	1.524	1.542	1.465	1.522
Lu	0.227	0.225	0.21	0.206
Hf	0.396	0.402	0.406	0.398
Ta	0.0048	0.0037	0.0072	0.005
Pb	0.106	0.149	0.1198	0.1035
Th	0.0057	0.0046	0.0046	0.00535
U	0.00737	0.00668	0.00617	0.0064

KHA 91-100 CPX	A01	A02	A03	A04	A05	A06	A07	A08	A09	A10
Li	<1.82	0.705	0.829	0.723	0.542	0.776	0.759	0.489	0.476	0.578
Sc	27.23	23.94	24.58	23.98	27.06	26.69	27.17	27.8	27.25	26.87
V	259.78	7.78	7.17	7.18	6.93	6.71	6.56	7.03	6.84	6.98
Cr	7333.09	9388.04	8891.26	8389.36	8204.73	8723.5	8735.39	8380.44	8590.03	8953.49
Co	20.84	22.68	22.26	22.14	16.9	19.55	19.02	16.63	15.86	17.2
Ni	293.27	375.01	364.29	364.77	266.54	317.77	308.54	270.81	263.3	284.31
Cu	<2.36	2.37	1.92	1.892	1.298	1.635	1.559	1.365	1.232	1.46
Zn	3.52	11.93	12.06	11.69	7.85	9.85	10.07	8.28	8.29	8.59
Rb	<0.96	<0.033	<0.032	0.043	<0.0255	0.058	0.145	<0.029	<0.0272	<0.027
Sr	85.17	114.16	122.77	119.98	132.81	118.59	116.88	134.74	144.47	139.48
Y	1.8	2.3	2.22	2.35	1.31	2.29	2.08	1.388	1.11	1.177
Zr	24.88	37.73	38.09	38.47	23.15	40.87	37.34	24.8	13.18	17.12
Nb	0.77	0.414	0.466	0.635	0.318	0.757	0.484	0.284	0.2773	0.315
Ba	15.57	0.911	8.43	13.67	0.621	5.04	1.774	0.1357	0.2454	0.287
La	1.57	1.997	1.983	2.231	2.863	2.293	2.164	3.28	5.31	4.44
Ce	4.84	8.38	8.49	8.9	9.12	8.01	7.57	9.47	12.36	11.31
Pr	0.711	1.513	1.518	1.58	1.55	1.511	1.443	1.567	1.714	1.627
Nd	3.87	7.71	7.65	8.09	7.16	7.94	7.64	7.39	7.17	6.96
Sm	0.36	1.791	1.776	1.875	1.358	1.853	1.707	1.427	1.27	1.208
Eu	0.184	0.544	0.541	0.56	0.38	0.538	0.494	0.395	0.351	0.352
Gd	0.97	1.384	1.364	1.425	0.919	1.383	1.289	0.978	0.816	0.818
Tb	<0.044	0.1515	0.1529	0.155	0.0968	0.156	0.1393	0.1016	0.08	0.0809
Dy	0.61	0.702	0.696	0.726	0.425	0.687	0.638	0.423	0.369	0.366
Ho	<0.038	0.1041	0.0972	0.0963	0.0552	0.092	0.0872	0.0587	0.0458	0.05
Er	<0.16	0.192	0.186	0.204	0.0965	0.184	0.17	0.1018	0.083	0.0901
Tm	<0.0180	0.018	0.0184	0.0196	0.01123	0.0187	0.018	0.0128	0.00869	0.0085
Yb	<0.068	0.1136	0.1177	0.1092	0.0618	0.1093	0.0999	0.0508	0.044	0.0469
Lu	<0.0152	0.0109	0.011	0.0118	0.00673	0.0113	0.0125	0.00671	0.00434	0.00672
Hf	<0.23	1.65	1.63	1.65	0.601	1.61	1.37	0.681	0.508	0.552
Ta	<0.045	0.0431	0.0506	0.0579	0.0413	0.0687	0.052	0.041	0.0368	0.0372
Pb	<0.075	0.377	0.1954	0.1888	0.2045	0.2247	0.1926	0.241	0.59	0.475
Th	<0.031	0.036	0.0325	0.0536	0.0285	0.0665	0.0532	0.0262	0.0404	0.0321
U	<0.019	0.0503	0.009	0.0236	0.00929	0.0625	0.0557	0.00347	0.00598	0.01066

KHA 91-100 Grt	A01	A02	A03	A04	A05	A06	A07	A08	A09
Li	<0.127	<0.111	<0.122	<0.107	<0.106	<0.131	<0.111	<0.106	<0.103
Sc	103.87	104.71	100.05	117.08	111.35	103.55	103.38	103.49	104.2
V	162.06	161.01	169.72	137.94	148.54	160.62	153.38	160.57	155.05
Cr	21977.12	22556.39	23824.12	19067.13	20948.09	23278.35	20503.01	21315.17	20663
Co	36.97	35.08	39.21	31.53	33.37	37.07	37.39	37.77	37.61
Ni	44.26	34.47	42.49	30.9	31.72	36.01	39.95	36.07	36.28
Cu	<0.130	0.12	0.137	0.113	0.178	<0.113	0.108	0.221	0.22
Zn	10.66	9.7	11.56	8.67	9.31	10.04	10.33	9.95	9.93
Ga	5.94	5.84	6.42	5.09	5.54	6.02	5.87	6.06	6
Rb	<0.065	<0.058	<0.061	<0.054	<0.052	<0.060	<0.054	<0.050	<0.046
Sr	0.1546	0.1537	0.1542	0.1364	0.1529	0.1379	0.1331	0.1328	0.131
Y	11.14	11.38	10.82	14.1	13.15	12.11	11.21	11.06	11.25
Zr	14.25	14.65	14.01	17.97	16.86	15.71	14.2	13.86	14.03
Nb	0.2344	0.2105	0.2444	0.1945	0.1976	0.2231	0.2186	0.2297	0.2271
Ba	<0.0158	<0.0153	<0.0164	<0.0125	0.0216	<0.0159	0.0128	<0.0129	<0.0110
La	0.0222	0.0222	0.0236	0.0217	0.0227	0.024	0.0211	0.0221	0.02008
Ce	0.1898	0.1942	0.2014	0.1648	0.188	0.1987	0.178	0.185	0.169
Pr	0.0636	0.0656	0.0666	0.0651	0.063	0.0685	0.0612	0.0632	0.0628
Nd	0.636	0.659	0.671	0.654	0.683	0.674	0.633	0.633	0.623
Sm	0.499	0.53	0.506	0.589	0.561	0.578	0.543	0.55	0.545
Eu	0.284	0.2762	0.289	0.297	0.285	0.299	0.29	0.299	0.2776
Gd	1.115	1.099	1.095	1.315	1.301	1.284	1.102	1.096	1.108
Tb	0.2306	0.2347	0.2283	0.2726	0.269	0.2693	0.2398	0.231	0.2322
Dy	1.811	1.855	1.797	2.261	2.198	2.069	1.907	1.824	1.864
Ho	0.415	0.417	0.412	0.535	0.495	0.461	0.418	0.408	0.41
Er	1.294	1.288	1.218	1.601	1.5	1.418	1.315	1.277	1.266
Tm	0.203	0.2047	0.1942	0.252	0.2312	0.2286	0.2093	0.2016	0.2008
Yb	1.53	1.571	1.476	1.878	1.763	1.698	1.575	1.611	1.576
Lu	0.2482	0.2447	0.2331	0.315	0.3	0.2707	0.2495	0.253	0.2499
Hf	0.1982	0.2199	0.2015	0.265	0.253	0.2314	0.1987	0.2051	0.2085
Ta	0.0129	0.0144	0.0136	0.0135	0.0124	0.0158	0.014	0.0125	0.01425
Pb	0.0547	0.061	0.0728	0.2989	0.1806	0.1791	0.1429	0.0945	0.1758
Th	0.0343	0.0254	0.0296	0.0335	0.0306	0.0309	0.0298	0.0294	0.0289
U	0.0445	0.034	0.0466	0.0365	0.0322	0.0424	0.0403	0.043	0.0382

HAN 93-20 CPX	A04	A05	A06	A07	A08	A09
Li	0.682	0.68	0.864	0.727	0.766	0.834
Sc	16.79	17.83	19.49	18.27	18.56	17.57
V	95.1	114.46	114.37	81.09	77.57	81.82
Cr	7569.88	6826.42	7821.98	6916.65	6948.64	7075.8
Co	28.69	25.86	29.1	25.72	26.54	25.95
Ni	389.01	354.82	403.56	348.02	360.56	356.15
Cu	2.65	1.86	2.51	1.96	2.21	2.26
Zn	28.89	24.36	26.67	24.46	24.21	23.84
Rb	0.0208	0.0155	<0.0163	<0.0152	<0.0148	<0.0151
Sr	109.6	108.14	108.74	103.56	101.62	103.42
Y	2.49	2.55	2.61	2.76	2.8	2.74
Zr	8.14	8.54	9.01	9.29	9.27	9.09
Nb	0.1096	0.1125	0.1229	0.1234	0.1153	0.1192
Ba	0.276	0.445	2.582	0.2371	0.2451	0.24
La	1.605	1.619	1.628	1.669	1.597	1.627
Ce	7.8	7.17	7.69	7.13	7.01	7.21
Pr	1.234	1.242	1.258	1.206	1.212	1.239
Nd	5.76	5.98	6	5.91	5.81	5.96
Sm	1.438	1.402	1.484	1.517	1.437	1.477
Eu	0.49	0.512	0.525	0.503	0.511	0.49
Gd	1.123	1.119	1.175	1.217	1.253	1.149
Tb	0.1235	0.1455	0.1418	0.1526	0.1531	0.1541
Dy	0.666	0.734	0.689	0.766	0.739	0.799
Ho	0.1017	0.1078	0.1117	0.1126	0.1063	0.1092
Er	0.22	0.226	0.254	0.26	0.238	0.232
Tm	0.0181	0.0265	0.0266	0.0275	0.0264	0.0263
Yb	0.1512	0.1377	0.1416	0.1386	0.154	0.1474
Lu	0.0122	0.0099	0.016	0.0158	0.0148	0.0152
Hf	0.45	0.473	0.473	0.478	0.499	0.52
Ta	0.0082	0.013	0.0121	0.011	0.0124	0.0128
Pb	0.255	0.128	0.1368	0.1215	0.145	0.1109
Th	0.0147	0.0168	0.0146	0.01385	0.0166	0.0175
U	0.00314	0.00816	0.0094	0.00281	0.00306	0.00252

HAN 93-20 Grt	A01	A02	A03	A04	A05	A06	A07	A08	A09
Li	0.28	0.36	0.334	0.177	0.148	0.131	0.111	0.139	0.12
Sc	108.2	112.36	111.04	101.3	93.59	94.26	104.11	100.65	100.24
V	329.6	349.9	341.64	199.34	197.13	194.25	144.02	147.05	156.62
Cr	65666.89	67263.56	68569.45	34264.36	42776.14	41312.81	29231.05	31655.35	30609.84
Co	86.91	79.18	86.44	47.61	44.77	45.03	33.12	32.07	35.19
Ni	196.07	173.69	194.15	101.25	97.22	97.48	70.6	70.25	75.32
Cu	1.14	1.255	1.09	0.642	0.802	0.697	1.957	1.299	0.498
Zn	53.93	48.51	50.37	23.87	25.44	24.32	32.72	21.38	20.32
Ga	19.34	18.48	19.76	8.98	8.95	8.75	6.42	6.23	6.69
Rb	0.165	<0.102	<0.113	<0.053	<0.047	<0.046	<0.033	0.121	<0.038
Sr	0.73	0.892	0.835	0.632	0.645	0.595	0.75	1.118	0.633
Y	24.79	24.13	24.86	19.79	19.77	19.42	24.52	24.23	22.37
Zr	49.54	48.12	50.06	41.52	40.51	39.79	48.15	47.44	44.69
Nb	0.247	0.307	0.273	0.1978	0.219	0.204	0.1878	0.216	0.1948
Ba	<0.04	0.25	0.207	0.0874	0.0377	<0.0155	0.25	0.449	0.0787
La	0.0487	0.0588	0.0535	0.0358	0.0461	0.0396	0.042	0.0746	0.042
Ce	0.803	0.873	0.874	0.569	0.627	0.589	0.485	0.578	0.483
Pr	0.2032	0.1984	0.2083	0.1719	0.1874	0.1829	0.1691	0.186	0.1632
Nd	1.864	1.854	1.778	1.528	1.701	1.541	1.664	1.788	1.551
Sm	1.469	1.391	1.431	1.252	1.369	1.243	1.286	1.341	1.243
Eu	0.771	0.76	0.807	0.713	0.721	0.716	0.739	0.767	0.731
Gd	2.66	2.59	2.56	2.172	2.312	2.157	2.541	2.513	2.312
Tb	0.624	0.579	0.583	0.461	0.474	0.466	0.555	0.544	0.497
Dy	4.53	4.49	4.65	3.66	3.78	3.67	4.36	4.33	4.04
Ho	1.007	0.985	0.989	0.786	0.797	0.754	0.961	0.96	0.894
Er	2.99	2.74	2.96	2.267	2.212	2.174	2.89	2.84	2.611
Tm	0.413	0.398	0.422	0.343	0.319	0.303	0.416	0.41	0.384
Yb	3.2	3.02	3.33	2.543	2.337	2.377	3.02	2.97	2.823
Lu	0.409	0.414	0.409	0.329	0.288	0.295	0.408	0.386	0.376
Hf	1.111	0.998	1.041	0.87	0.86	0.846	1.062	1.099	0.962
Ta	0.0109	<0.0082	<0.0101	0.0122	0.0137	0.0083	0.0107	0.0113	0.0127
Pb	0.204	0.223	0.231	0.1191	0.1367	0.1158	0.295	0.1195	0.0668
Th	0.0104	0.0059	0.0103	0.00457	0.0054	0.00505	0.00716	0.01051	0.00568
U	0.0165	0.015	0.0128	0.00743	0.00748	0.00813	0.00526	0.009	0.00622

Table A4.1 Results of U-Pb isotope analyzes from the zircons collected on the Rehoboth Terrane.

sample	207	U (ppm)	Pb (ppm)	Th/U	206*/238	1s%	7/35r	2s%	208/232	1s%	207*/206*	1s%	206/238	2s	207/206	2s	conc%
GLZ-1																	
A04	22255	112	19.3	0.32	0.1986	0.95	1.6642	5.1	0.064	1	0.073	0.42	984	45	1020	28	96
A05	20899	159	18.6	0.26	0.1339	0.65	1.1058	5.5	0.070	6	0.055	5.81	679	30	991	59	69
A06	42823	188	38.6	0.43	0.2303	0.80	2.0223	5.0	0.070	1	0.071	1.32	1126	50	1117	31	101
A07	21699	108	22.2	0.74	0.2141	0.83	1.8153	5.1	0.073	1	0.070	2.49	1053	47	1048	32	100
A08	22248	111	20.7	0.36	0.2150	0.73	1.7846	5.0	0.073	2	0.070	1.68	1056	46	1005	33	105
A09	156465	102	70.2	0.96	0.6612	0.78	15.4119	5.1	0.154	1	0.204	0.82	2813	110	2861	28	98
A10	22257	108	22.7	0.64	0.2284	1.34	1.9991	5.9	0.091	7	0.071	1.85	1115	54	1115	53	100
A11	8764	89	8.4	0.55	0.1086	1.42	0.7394	5.7	0.014	3	0.060	0.65	554	28	594	44	93
A12	599185	1207	295.1	0.62	0.2485	1.69	4.3680	5.9	0.077	1	0.148	1.50	1203	62	2395	32	50
A13	41181	332	43.3	0.69	0.1427	0.87	1.1674	5.2	0.053	2	0.064	2.52	718	33	982	39	73
A14	55893	213	47.3	0.67	0.2382	1.30	2.2476	5.3	0.064	2	0.083	0.40	1156	55	1269	22	91
A15	10886	64	15.5	0.24	0.3013	13.82	2.3884	28.1	0.066	2	0.070	0.86	1430	370	920	44	155
A16	18762	91	19.0	0.69	0.2209	0.52	1.8492	4.9	0.068	1	0.072	1.72	1078	46	1033	34	104
A17	22495	105	23.0	0.86	0.2221	0.90	1.9089	5.1	0.068	1	0.072	1.05	1083	49	1087	29	100
A18	16140	79	14.8	0.77	0.2002	1.17	1.7025	5.3	0.021	5	0.075	0.44	983	46	1067	30	92
A19	16734	143	17.6	0.57	0.1347	1.83	0.9444	6.0	0.042	7	0.062	1.73	677	37	668	36	101
A20	480	4	0.7	0.00	0.2104	3.39	1.6127	29.8	-456.702	-52	10.000	3.17	1028	82	857	594	120
A21	30469	201	33.4	0.65	0.1806	0.57	1.3797	4.8	0.057	1	0.066	1.10	892	39	851	28	105
A22	4777	26	5.0	0.48	0.2225	1.14	1.8690	5.8	0.089	5	0.073	4.41	1081	50	1048	56	103
A23	57412	364	63.7	0.94	0.1959	6.51	2.3695	20.0	0.061	32	0.094	6.13	961	125	1748	265	55
A24	21527	80	17.1	0.47	0.2307	0.55	2.3378	6.5	0.105	4	0.070	6.32	1117	48	1418	86	79
A25	117527	559	91.4	0.28	0.1926	0.97	1.6422	5.2	0.058	2	0.075	0.61	945	43	1081	34	87
A26	31423	288	32.8	0.30	0.1359	0.96	0.9438	5.3	0.042	2	0.061	0.89	680	32	656	43	104
A27	40888	407	25.1	0.22	0.0685	2.60	0.4332	7.6	0.011	16	0.056	0.40	352	24	453	71	78
A28	20680	71	16.0	0.37	0.2486	0.61	2.7329	6.0	0.142	4	0.079	6.23	1193	51	1576	71	76
A32	23141	76	17.8	0.39	0.2547	0.71	3.0751	6.2	0.164	3	0.080	7.33	1217	53	1754	72	69
A33	15623	75	16.8	0.75	0.2330	0.89	1.9848	5.1	0.078	2	0.078	1.30	1121	50	1089	31	103
A34	23239	110	21.5	0.38	0.2305	0.68	1.9140	4.9	0.080	2	0.072	1.30	1110	48	1039	27	107
A35	60476	70	30.9	0.66	0.4819	0.78	4.3283	6.2	0.011	13	0.080	0.54	2134	88	1197	78	178
A36	45771	218	45.8	0.56	0.2183	4.08	2.5884	12.5	0.182	17	0.077	10.35	1054	92	1726	153	61
A37	42995	346	37.5	0.48	0.1159	0.59	0.9482	5.3	0.044	3	0.073	0.99	581	26	1012	51	57
A38	192845	189	109.9	0.86	0.5914	0.91	10.0271	4.9	0.151	1	0.150	0.66	2531	102	2360	16	107
A39	10962	65	9.2	0.50	0.1454	0.94	1.6807	7.8	0.099	2	0.065	12.64	720	33	1682	111	43
A40	38248	248	39.8	1.11	0.1489	0.68	1.4919	6.7	0.071	3	0.059	9.28	736	33	1415	90	52
A41	60804	314	58.4	1.85	0.1516	1.06	2.3445	9.2	0.059	2	0.080	13.08	748	36	2205	134	34
A42	68472	104	45.3	0.79	0.4491	0.63	5.9168	4.8	0.130	1	0.118	0.47	2002	81	1924	19	104
A43	68868	617	64.8	0.22	0.1312	0.60	1.0310	4.9	0.044	3	0.062	1.91	652	29	937	32	70
A44	70863	663	139.4	0.35	0.2708	1.43	2.3321	5.7	0.074	6	0.076	1.67	1278	62	1124	40	114
A45	71120	449	49.3	0.19	0.1284	2.72	1.2462	10.7	0.209	9	0.067	12.51	637	43	1360	155	47
A46	154477	233	102.9	1.06	0.4543	0.49	6.3441	4.7	0.103	1	0.120	0.86	2018	80	2032	16	99
A47	15131	75	14.3	0.35	0.2256	0.63	1.8693	5.0	0.074	2	0.071	1.67	1080	47	1050	34	103
A48	372884	246	149.4	0.43	0.6503	0.54	13.3417	4.7	0.187	1	0.182	0.32	2722	104	2691	11	101
A49	40611	46	18.6	0.59	0.3226	1.73	7.4030	8.0	0.196	13	0.123	12.42	1492	78	2875	90	52
A50	33235	163	28.2	0.77	0.1659	1.45	2.3085	9.4	0.115	5	0.072	23.46	810	42	2030	136	40
A51	41032	210	41.6	0.71	0.2117	0.70	1.7120	4.9	0.064	1	0.072	0.82	1016	44	1006	24	101
A52	49467	238	44.9	0.43	0.2167	0.68	1.7551	4.8	0.069	1	0.073	0.71	1038	45	1011	22	103
A53	58440	262	50.5	0.37	0.2275	0.62	1.8824	4.8	0.105	14	0.075	0.63	1085	47	1055	22	103
A54	16195	176	18.4	0.30	0.1289	0.57	0.8551	4.9	0.043	2	0.061	1.26	637	28	595	33	107
A55	130153	698	112.9	0.11	0.2023	0.76	1.7913	5.3	0.147	4	0.068	2.90	972	43	1193	46	82
A59	73613	266	62.9	0.51	0.2684	0.78	2.4733	4.9	0.079	1	0.083	0.53	1258	55	1276	18	99
A60	46977	74	32.1	0.76	0.4323	1.04	5.8230	5.9	0.162	3	0.108	3.93	1920	83	1982	56	97
A61	31338	267	32.4	0.72	0.1286	0.90	1.0955	7.3	0.050	6	0.056	7.93	633	29	1123	109	56
A62	28792	332	34.1	0.67	0.1154	0.82	0.7768	5.0	0.033	1	0.060	0.93	570	26	637	32	89
A63	68903	196	53.3	0.20	0.3370	0.97	3.6273	5.2	0.101	3	0.095	1.24	1540	68	1577	31	98
A64	33632	181	32.1	0.22	0.2208	0.49	1.8649	4.8	0.075	3	0.074	1.45	1049	45	1109	29	95
A65	15157	86	15.5	0.61	0.1965	0.45	1.7359	5.4	0.071	4	0.070	4.58	941	40	1200	56	78
A66	142085	744	143.3	0.32	0.2357	0.47	2.1689	4.8	0.082	1	0.077	1.05	1113	47	1281	29	87
A67	6575	52	8.3	0.67	0.1782	0.99	1.2640	5.5	0.061	3	0.063	4.39	858	40	755	52	114
A68	21798	183	28.1	0.98	0.1593	0.58	1.1664	4.9	0.049	1	0.068	1.02	772	34	822	30	94
A69	49544	327	40.5	0.26	0.1484	0.47	1.3092	5.1	0.068	3	0.073	2.76	722	31	1201	43	60
A70	56365	92	42.7	1.21	0.4437	0.56	5.5467	4.7	0.123	1	0.112	0.65	1953	79	1859	17	105
A71	4567	50	5.8	0.39	0.1408	0.79	0.9700	5.6	0.070	5	0.060	8.11	686	31	698	63	98
A72	12858	62	14.7	0.81	0.2582	0.81	2.3204	5.2	0.088	1	0.076	2.83	1206	53	1241	38	97
A73	11897	167	19.1	1.36	0.1083	0.74	0.6692	5.1	0.033	1	0.054	2.49	533	24	464	40	115
A74	29559	150	28.2	0.38	0.2257	0.67	1.8636	5.0	0.076	2	0.073	1.85	1064	46	1076	36	99
A75	46125	81	35.6	0.92	0.4549	0.66	5.6597	4.8	0.129	1	0.112	0.64	1990	81	1856	20	107
A76	83411	149	61.0	0.61	0.4578	0.61	5.7579	4.8	0.124	1	0.112	0.91	2000	81	1877	18	107
A77	14925	69	13.9	0.49	0.2345	0.58	2.0305	5.3	0.090	3	0.068	3.82	1101	47	1174	51	94
A78	17480	115	17.7	0.51	0.1758	0.85	1.3351	5.0	0.065	1	0.070	1.41	842	38	910	31	93
A79	35557	185	32.8	0.42	0.2103	0.52	1.7128	4.8	0.073	2	0.072	1.45	995	43	1054	27	94
A80	40832	211	40.0	0.36	0.2263	0.61	1.9412	6.7	0.105	2	0.085	3.65	1064	46	1159	95	92
A81	27195	126	23.8	0.35	0.2287	0.99	1.8695	5.1	0.077	2	0.076	0.83	1073	49	1064	27	101
A82	30479	128	25.6	0.14	0.2594	0.64	2.1682	4.8	0.080	3	0.076	0.62	1204	52	1110	25	109
A83	20115	207	25.3	0.62	0.1399	0.44	0.9311	4.9	0.047	1	0.061	1.91	677	30	639	36	106
A84	42134	197	39.2	0.42	0.2383	0.88	1.9268	5.0	0.075	1	0.075	0.81	1113	50	1045	22	106
A88	67813	112	47.4	0.84	0.4357	0.62	5.5662	4.8	0.133	1	0.112	0.85	1905	77	1918	20	99
A89	233004	430	180.1	0.77	0.4563	0.45	5.5159	4.6	0.120	0	0.111	0.22	1981	79	1819	13	109
A90	6113	61	6.9	0.48	0.1314	0.56	0.9751	5.4	0.055	4	0.061	5.85	635	28	877	57	72
A91	20654	93	21.2	0.84	0.2443	0.67	2.0200	4.9	0.073	1	0.076	1.29	1134	49	1099	30	103
A92	7647	18	5.9	1.24	0.2967	0.81	3.8741	7.1	0.123	3	0.060	17.74	1353	59	1961	92	69
A93	17498	127	17.4	0.41	0.1659	0.58	1.2090	4.9	0.058	2	0.066	1.37	791	35	844	32	94
A94	9344	59	6.2	0.05	0.1345	0.93	1.1200	5.8	0.350	6	0.072	4.23	648	30	1117	63	58
A95	40203	180	27.1	0.31	0.1840	0.98	1.4967	5.3	0.074	2	0.071	2.27	870	40	1071	41	81
A96	59450	241	39.8	0.18	0.2130	0.51	1.6568	4.8	0.072	1	0.071	0.68	997	43	982	24	102
A97	73940	78	34.6	0.57	0.4950	0.83	6.4541	4.9	0.138	1	0.120	0.48	2116	87	1963	15	108
A98	12420	65	7.5	0.27	0.1384	0.71	1.1726	6.7	0.091	5	0.064	7.21	664	30	1156	94	57
A99	35909	241	25.0	0.12	0.1385	0.57	0.9160	4.8	0.051	2	0.061	0.65	664	29	646	24	103
A100	59123	155	29.0	0.06	0.2474	0.88	2.0831	5.1	0.097	5	0.078	0.68	1142	51	1146	31	100

sample	207	U (ppm)	Pb (ppm)	Th/U	206*/238	1s%	7/35r	2s%	208/232	1s%	207*/206*	1s%	206/238	2s	207/206	2s	conc%
A101	28959	74	17.7	0.99	0.2484	0.64	2.0979	4.9	0.072	1	0.074	1.22	1146	49	1152	28	99
A102	52797	158	27.5	0.22	0.2236	0.64	1.7556	4.8	0.073	1	0.073	0.59	1040	45	1007	20	103
A103	49689	132	27.6	0.59	0.2419	0.77	1.9483	4.9	0.071	1	0.072	1.32	1117	49	1060	26	105
A104	4180	20	2.3	0.77	0.1253	0.79	1.0649	6.8	0.065	2	0.071	6.67	602	28	1169	97	52
A105	3967	20	2.2	0.52	0.1308	0.97	0.8910	5.6	0.040	9	0.070	5.53	627	29	716	60	88
A106	2988	8	1.2	0.48	0.1508	1.37	1.8828	10.2	0.149	5	0.112	11.21	717	36	1896	157	38
A107	14884	100	8.4	0.42	0.1043	0.48	0.6424	4.9	0.032	2	0.058	1.72	504	22	501	37	101
A108	17544	43	7.8	0.54	0.2144	0.54	1.6660	4.9	0.070	1	0.074	1.20	997	43	993	35	100
A109	8844	35	4.1	0.80	0.1235	0.54	0.9902	6.4	0.054	2	0.067	6.95	592	26	1059	90	56
A110	13064	42	5.9	0.41	0.1722	0.61	1.1844	4.9	0.057	1	0.067	1.13	811	36	743	32	109
A111	33092	71	12.5	0.31	0.2195	0.69	1.7028	4.9	0.075	2	0.072	0.70	1017	44	994	24	102
A112	40795	33	11.5	0.69	0.3900	0.69	4.3185	4.8	0.112	1	0.104	0.75	1708	71	1683	21	102
A116	15736	47	5.4	0.46	0.1326	0.45	1.0031	7.2	0.044	1	0.071	2.72	632	28	948	114	67
A117	12256	55	5.2	0.25	0.1233	0.58	0.7581	5.0	0.050	3	0.063	1.61	589	26	510	38	116
A118	45935	66	13.4	0.32	0.2505	0.68	2.3670	5.0	0.125	2	0.083	1.24	1144	50	1391	32	82
A119	7165	13	3.0	1.06	0.2400	0.70	1.8834	5.1	0.066	2	0.075	3.74	1099	48	1027	40	107
A120	21440	37	6.8	0.40	0.2228	0.72	1.7297	4.9	0.074	2	0.074	1.03	1026	45	1006	29	102
A121	22758	35	6.4	0.29	0.2279	0.55	1.7746	4.8	0.074	1	0.072	1.02	1047	45	1013	28	103
A122	218295	45	27.9	0.57	0.6771	0.78	13.1006	4.8	0.183	1	0.182	0.20	2715	106	2666	11	102
A123	124581	24	14.5	0.31	0.6858	0.69	13.5297	4.9	0.217	2	0.185	0.49	2742	106	2699	19	102
A124	7031	23	2.4	0.50	0.1264	0.81	0.8079	5.3	0.042	3	0.066	2.37	601	27	604	50	99
A125	14113	30	4.5	0.77	0.1644	0.68	1.1232	5.1	0.050	1	0.065	2.34	771	34	747	39	103
A126	28538	57	8.3	0.51	0.1743	0.56	1.1972	4.8	0.056	1	0.064	0.80	814	36	760	28	107
A127	24940	26	5.0	0.38	0.2200	0.62	2.2949	5.7	0.087	5	0.089	2.78	1010	44	1588	61	64
A128	33441	42	8.0	0.26	0.2415	0.52	1.9730	4.9	0.097	2	0.074	1.88	1101	47	1118	33	98
A129	24243	26	6.8	1.53	0.2374	0.71	1.9490	5.2	0.067	1	0.080	1.65	1083	47	1129	43	96
A130	34907	49	7.6	0.23	0.1998	0.55	1.5772	4.9	0.049	3	0.072	1.61	922	40	1051	30	88
A131	22921	29	5.4	0.49	0.2250	0.83	1.7006	5.0	0.066	2	0.076	0.93	1029	46	964	27	107
A132	70484	27	11.2	0.95	0.4386	0.81	5.3058	4.9	0.126	1	0.113	0.44	1874	78	1866	18	100
A133	18220	22	3.9	0.42	0.2243	0.48	1.7371	4.8	0.077	1	0.073	1.38	1025	44	1016	29	101
A134	34128	34	7.1	0.61	0.2403	0.54	1.9637	5.0	0.079	1	0.076	1.67	1092	47	1125	35	97
A135	5561	4	0.9	0.38	0.2766	1.37	3.6754	8.8	0.194	9	0.087	14.74	1241	60	2036	124	61
A136	11885	13	2.2	0.50	0.2143	0.77	1.7016	5.2	0.067	3	0.083	1.34	981	43	1070	43	92
A137	29216	31	5.6	0.33	0.2319	0.74	1.8028	4.9	0.073	2	0.075	0.85	1055	46	1029	26	103
A138	133915	19	11.7	0.62	0.6661	0.52	12.7008	4.7	0.177	1	0.180	0.24	2659	101	2657	13	100
A139	9593	5	1.6	0.97	0.3137	0.92	3.5394	7.2	0.128	4	0.077	9.90	1388	61	1746	98	79
A140	15111	34	4.5	1.88	0.1150	0.54	0.7301	5.0	0.036	1	0.061	2.34	544	24	609	44	89
A141	3849	9	1.0	0.94	0.1184	0.91	0.7091	5.9	0.037	4	0.063	4.88	559	26	483	73	116
A142	51642	16	6.9	1.00	0.4611	0.94	5.6087	5.0	0.137	1	0.112	1.00	1947	82	1886	23	103
A143	21711	20	3.8	0.52	0.2292	0.75	1.7628	4.9	0.077	1	0.074	1.38	1041	46	1014	28	103
A144	28088	26	4.6	0.47	0.2091	1.03	1.7021	5.4	0.069	2	0.081	1.45	955	44	1129	42	85
A145	43975	24	5.8	0.41	0.2978	0.66	2.6339	4.8	0.097	1	0.086	0.69	1321	56	1293	22	102
GLZ-2																	
A04	162825	701	165.1	1.29	0.2619	0.80	2.8211	4.0	0.050	1	0.090	1.63	1212	41	1605	26	76
A05	196740	650	182.7	1.59	0.3208	0.67	4.0342	3.8	0.040	1	0.106	1.06	1454	47	1889	20	77
A06	78961	412	86.5	1.29	0.2031	0.58	1.8974	3.7	0.049	1	0.084	1.23	958	32	1337	22	72
A07	166775	597	119.6	1.68	0.1937	0.64	2.4531	3.8	0.023	2	0.108	1.10	916	31	1905	20	48
A08	83570	169	67.5	0.52	0.4573	0.57	5.7993	3.7	0.148	1	0.112	0.71	1983	61	1907	16	104
A09	68105	140	56.6	0.74	0.4407	0.61	5.3416	3.7	0.131	1	0.109	0.71	1920	60	1827	21	105
A10	76621	675	86.5	1.55	0.1297	0.52	1.2449	3.7	0.027	1	0.083	0.83	626	21	1393	21	45
A11	71718	179	64.3	0.76	0.3903	0.71	4.4083	3.8	0.119	1	0.103	0.60	1725	55	1700	19	102
A12	189572	719	133.3	1.40	0.1957	2.50	2.3839	6.1	0.034	3	0.109	0.68	922	52	1839	15	50
A13	87646	197	80.0	1.01	0.4581	1.01	5.5494	4.0	0.135	1	0.111	0.68	1981	67	1830	16	108
A14	60988	122	48.8	0.73	0.4357	0.64	5.3339	3.7	0.132	1	0.112	0.51	1896	59	1850	18	103
A15	60655	141	53.9	0.91	0.4006	0.70	4.6478	3.8	0.127	1	0.104	1.04	1762	56	1753	20	100
A16	59390	118	52.2	1.15	0.4375	0.70	5.5291	3.8	0.124	1	0.115	0.77	1901	60	1909	18	100
A17	212789	634	156.0	1.95	0.2569	0.48	4.1470	4.0	0.037	1	0.127	1.82	1183	38	2339	32	51
A18	143645	219	64.0	1.18	0.3247	1.30	5.3197	4.3	0.028	7	0.149	0.36	1461	56	2365	13	62
A19	28496	111	30.7	0.63	0.3173	0.53	2.9367	3.8	0.105	1	0.083	1.35	1431	45	1332	25	107
A20	99668	234	93.8	1.41	0.3815	0.66	4.4002	3.7	0.096	0	0.106	0.47	1684	54	1747	17	96
A21	21322	102	23.4	0.61	0.2609	0.68	2.2625	3.9	0.088	1	0.082	1.05	1197	40	1207	30	99
A22	18170	84	20.8	0.63	0.2835	0.51	2.4568	3.8	0.092	1	0.076	1.46	1290	41	1207	29	107
A23	92058	228	78.4	0.56	0.4128	1.15	4.6575	4.2	0.113	2	0.104	0.35	1802	64	1710	16	105
A24	84827	625	91.0	0.91	0.1713	0.62	1.5166	3.8	0.029	1	0.079	0.87	809	27	1251	22	65
A25	58946	171	62.7	0.94	0.4164	0.58	4.6530	3.7	0.129	1	0.103	0.68	1814	56	1694	19	107
A26	197027	719	138.5	1.23	0.2052	1.91	2.5907	5.2	0.035	4	0.108	1.18	957	45	1917	21	50
A27	71189	88	46.4	0.92	0.4905	1.06	8.9923	6.8	0.228	8	0.117	9.69	2088	73	2563	92	81
A28	3277	12	5.1	2.61	0.3418	1.34	3.3839	5.4	0.112	2	0.113	5.58	1522	58	1471	64	104
A32	78640	489	80.5	1.33	0.1773	1.02	1.8304	5.6	0.005	272	0.065	36.33	832	31	1554	75	54
A33	78793	210	53.8	0.50	0.3058	1.17	3.4606	4.5	0.081	7	0.101	2.19	1374	51	1725	36	80
A34	90827	174	64.8	0.71	0.4108	0.46	5.1917	3.6	0.123	0	0.118	0.38	1785	54	1926	15	93
A35	139329	620	141.8	2.24	0.2480	1.29	2.9796	4.3	0.031	1	0.106	0.83	1135	44	1836	16	62
A36	49963	108	36.0	0.50	0.3289	1.32	5.5650	7.6	0.259	9	0.115	12.12	1465	58	2436	105	60
A37	40467	187	48.9	0.55	0.3150	0.43	3.0306	3.8	0.120	1	0.083	1.83	1409	44	1425	28	99
A38	73906	291	71.9	0.37	0.3104	0.34	2.9584	3.6	0.096	1	0.090	0.37	1390	43	1408	19	99
A39	42975	189	48.7	2.07	0.2638	0.86	2.2806	4.0	0.100	2	0.081	0.56	1199	41	1220	28	98
A40	94912	239	83.8	0.99	0.3668	0.71	4.1283	3.8	0.094	1	0.105	0.77	1611	52	1722	22	94
A41	149781	1020	143.0	1.64	0.1506	0.58	1.6442	3.6	0.023	1	0.099	0.54	711	24	1667	15	43
A42	60082	475	55.1	1.20	0.1324	1.23	1.4671	4.5	0.024	1	0.092	2.05	628	25	1696	30	37
A43	152586	582	213.8	1.56	0.4192	1.38	5.1730	4.8	0.092	1	0.112	1.10	1809	69	1892	34	96
A44	28530	128	30.0	0.40	0.2891	0.49	2.5532	3.8	0.094	2	0.084	1.03	1300	41	1267	27	103
A45	34652	116	31.6	0.57	0.3059	1.14	3.8963	5.3	0.056	6	0.094	3.88	1367	51	1951	60	70

sample	207	U (ppm)	Pb (ppm)	Th/U	206*/238	1s%	7/35r	2s%	208/232	1s%	207*/206*	1s%	206/238	2s	207/206	2s	conc%
A46	170445	1164	179.8	1.35	0.1794	1.22	1.9068	4.3	0.036	1	0.093	0.81	836	33	1622	21	52
A47	55863	260	68.7	1.46	0.2697	0.84	2.4614	5.2	0.064	43	0.083	18.58	1218	42	1334	68	91
A48	240207	1049	189.7	0.34	0.2309	1.43	2.5189	4.5	0.056	2	0.099	0.92	1056	43	1673	18	63
A49	54530	209	51.5	0.44	0.2894	0.62	2.9758	4.0	0.107	1	0.090	0.94	1298	42	1563	32	83
A50	53953	215	40.6	1.08	0.2025	3.28	2.4395	7.7	0.047	6	0.105	1.93	934	64	1856	39	50
A51	22867	76	21.8	0.72	0.3246	0.64	3.0705	3.9	0.100	1	0.089	1.21	1438	46	1407	30	102
A52	20995	78	21.7	1.04	0.2806	0.49	2.9572	4.4	0.107	2	0.089	3.36	1260	40	1612	51	78
A53	59617	107	42.2	0.61	0.4349	0.66	5.9191	5.2	0.196	6	0.114	6.28	1859	59	2076	65	90
A54	74564	179	60.3	0.86	0.3699	0.83	4.4860	3.9	0.104	2	0.110	0.66	1613	54	1871	19	86
A55	29562	134	32.3	0.72	0.2707	0.69	2.3338	3.9	0.086	1	0.081	1.20	1217	40	1232	27	99
A59	47097	231	62.6	0.76	0.3270	0.62	3.1607	4.5	0.074	3	0.085	2.41	1442	46	1456	51	99
A60	56334	444	79.4	3.14	0.1708	0.50	1.5266	3.7	0.026	1	0.080	1.11	793	26	1307	25	61
A61	98139	493	99.3	2.18	0.1943	0.61	2.1334	4.2	0.041	2	0.085	3.03	894	30	1697	39	53
A62	24119	82	27.8	1.56	0.3158	0.60	2.9827	3.8	0.092	1	0.091	0.95	1395	45	1415	25	99
A63	94648	238	67.6	1.65	0.3018	0.73	3.7744	3.9	0.029	6	0.112	1.08	1339	44	1935	23	69
A64	181851	469	144.8	1.88	0.3639	0.54	4.8561	3.6	0.033	2	0.125	0.43	1582	50	2051	14	77
A65	46917	89	39.0	0.98	0.4571	0.69	5.7602	3.8	0.132	1	0.119	0.75	1931	61	1951	20	99
A66	60261	127	50.6	0.74	0.4534	0.65	5.3396	3.7	0.136	1	0.112	0.65	1917	60	1830	18	105
A67	60462	119	45.0	0.40	0.4598	0.75	5.4659	3.8	0.125	1	0.114	0.63	1939	62	1847	19	105
A68	125198	438	94.4	1.38	0.2468	0.68	3.3425	3.7	0.020	6	0.126	0.62	1112	37	2081	14	53
A69	222876	1030	162.6	0.67	0.1966	0.52	2.3747	3.7	0.025	2	0.115	0.46	900	30	1879	20	48
A70	163594	768	149.1	2.41	0.2093	0.57	2.5800	3.7	0.026	1	0.108	1.20	954	32	1916	21	50
A71	19221	94	21.4	0.58	0.2708	0.64	2.3141	3.9	0.091	2	0.081	1.61	1209	40	1231	30	98
A72	18439	86	19.6	0.60	0.2719	0.58	2.3078	4.1	0.086	3	0.065	4.61	1213	39	1218	41	100
A73	26355	21	13.1	0.27	0.4817	0.90	15.3678	5.8	1.157	3	0.304	2.09	2013	66	3491	67	58
A74	49269	239	52.0	1.37	0.2397	1.62	2.0729	4.8	0.046	5	0.079	1.06	1079	47	1257	21	86
A75	34168	143	62.8	4.05	0.2765	0.80	2.3800	4.1	0.079	1	0.084	1.15	1230	42	1249	34	98
A76	143273	302	109.8	0.72	0.4144	0.60	4.8550	3.7	0.107	1	0.112	0.31	1764	55	1830	14	96
A77	10214	23	9.5	1.03	0.4445	0.83	5.0735	4.3	0.123	3	0.106	2.65	1875	61	1783	38	105
A78	7562	28	8.0	0.71	0.3248	0.87	2.9737	4.4	0.106	4	0.083	4.14	1420	48	1371	42	104
A79	114008	187	83.5	1.10	0.4606	0.89	5.7427	3.9	0.124	1	0.119	0.38	1931	64	1945	15	99
A80	116527	237	94.5	0.84	0.4415	0.61	5.2052	3.7	0.118	1	0.112	0.34	1861	58	1845	14	101
A81	59910	602	96.6	2.98	0.1646	1.03	1.4688	4.3	0.026	1	0.085	0.68	758	28	1325	32	57
A82	101990	707	115.6	1.68	0.1817	0.56	1.6310	3.7	0.030	1	0.081	0.80	831	28	1338	20	62
A83	66711	220	62.5	0.86	0.3434	1.06	3.9142	4.2	0.045	2	0.103	1.10	1490	53	1786	22	83
A84	1578	18	2.1	0.39	0.1479	1.26	0.9609	6.4	0.107	12	0.028	52.46	684	27	684	103	100
A88	53044	86	41.2	0.86	0.5076	2.42	7.0325	9.2	1.123	7	0.167	25.32	2091	107	2139	124	98
A89	62143	130	47.8	0.69	0.4190	0.67	4.9063	3.8	0.114	1	0.111	0.56	1771	56	1841	19	96
A90	146058	208	87.5	0.31	0.5228	0.60	7.1875	3.7	0.166	1	0.131	0.43	2143	65	2128	15	101
A91	37359	91	24.4	1.09	0.2319	0.76	3.0936	10.1	-0.003	-103	0.065	24.45	1039	38	2076	164	50
A92	43230	187	49.0	1.07	0.2799	0.70	2.3699	3.8	0.083	1	0.082	0.62	1233	41	1234	22	100
A93	47142	100	36.5	0.98	0.4005	0.68	4.3297	3.8	0.110	1	0.103	0.73	1699	54	1699	21	100
A94	107121	171	72.0	1.30	0.4221	0.65	4.9495	3.7	0.117	0	0.113	0.39	1778	56	1848	16	96
A95	51592	65	26.0	3.17	0.3436	0.66	3.8614	3.8	0.115	1	0.108	0.78	1482	48	1772	21	84
A96	71784	152	41.6	0.79	0.3000	0.71	3.3996	3.8	0.095	1	0.109	0.59	1311	43	1788	17	73
A97	114160	449	83.4	1.13	0.2227	1.09	1.9260	4.1	0.037	2	0.082	0.50	998	37	1280	16	78
A98	34705	113	23.5	0.62	0.2595	0.58	2.1750	3.7	0.074	1	0.081	0.96	1148	37	1220	21	94
A99	23133	30	12.3	1.04	0.4380	0.60	5.0998	3.9	0.125	1	0.115	1.09	1832	57	1840	27	100
A100	75937	103	38.0	0.76	0.4317	0.69	4.9536	3.8	0.120	1	0.110	0.66	1809	58	1815	19	100
A101	71518	54	21.4	1.16	0.4630	1.48	6.0034	4.6	0.143	2	0.128	0.58	1921	75	2035	18	94
A102	123296	128	45.4	0.15	0.4716	0.35	5.7655	3.5	0.148	2	0.117	0.45	1951	58	1931	14	101
A103	21095	53	11.4	0.49	0.2658	0.78	2.2331	4.1	0.094	2	0.080	1.67	1170	40	1230	35	95
A104	44981	102	22.5	0.66	0.2631	0.74	2.1730	3.8	0.081	1	0.081	0.60	1159	39	1198	22	97
A105	93429	103	44.5	1.07	0.4944	0.76	5.7879	3.8	0.144	1	0.113	0.46	2029	64	1856	17	109
A106	31721	50	11.2	0.50	0.2848	1.11	2.9104	4.2	0.069	3	0.098	1.11	1245	46	1607	25	77
A107	54619	97	20.5	0.15	0.2889	0.73	2.5020	3.8	0.106	2	0.085	0.50	1260	42	1293	21	97
A108	28414	58	13.1	0.60	0.2731	0.65	2.2745	3.8	0.085	1	0.080	0.87	1197	39	1218	23	98
A109	23034	44	10.1	0.62	0.2797	0.57	2.3191	3.8	0.089	1	0.080	1.17	1223	40	1210	26	101
A110	20534	37	8.7	0.73	0.2766	0.64	2.2879	3.9	0.089	1	0.080	1.38	1210	40	1206	29	100
A111	100448	82	32.0	0.88	0.4352	0.62	5.0436	3.7	0.119	1	0.113	0.37	1812	57	1843	16	98
A112	7289	11	2.7	0.65	0.2931	0.81	2.5243	4.5	0.096	3	0.076	3.40	1274	43	1288	47	99
A116	64599	102	23.6	1.30	0.2652	0.69	2.4413	4.4	0.063	1	0.090	1.18	1161	39	1419	49	82
A117	99658	234	29.3	0.97	0.1425	0.51	1.5310	4.6	0.036	2	0.086	3.30	649	22	1711	56	38
A118	87132	61	22.4	0.72	0.4300	0.77	4.9263	3.8	0.115	1	0.107	0.83	1788	58	1829	19	98
A119	101054	170	34.9	1.36	0.2420	1.67	3.0067	5.6	0.069	2	0.104	4.58	1066	47	1975	51	54
A120	38980	27	10.5	1.13	0.4094	0.69	4.6440	4.4	0.125	2	0.096	3.17	1711	55	1813	46	94
A121	46092	32	11.5	1.10	0.3849	1.06	4.2144	4.1	0.120	1	0.103	0.66	1620	57	1749	21	93
A122	35744	23	9.0	1.13	0.4070	0.78	4.4276	3.9	0.129	1	0.100	1.56	1701	56	1738	21	98
A123	53044	35	12.9	1.15	0.3854	0.88	4.3246	4.0	0.117	1	0.106	0.84	1620	54	1796	23	90
A124	88896	29	14.5	0.57	0.5113	0.60	9.0129	5.5	0.586	19	0.089	20.75	2071	65	2582	68	80
A125	105305	52	19.6	0.69	0.4344	0.62	5.2820	3.7	0.130	1	0.118	0.53	1798	56	1942	19	93
A126	210059	175	50.9	0.21	0.4022	0.98	4.4967	4.0	0.050	3	0.107	0.49	1680	58	1792	14	94
A127	167317	217	35.4	0.89	0.1721	0.97	1.9439	4.3	0.064	1	0.090	2.91	772	28	1812	35	43
A128	78686	42	14.5	0.77	0.3952	0.75	4.5111	3.8	0.105	1	0.110	0.80	1653	54	1831	18	90
A129	33819	12	5.4	0.71	0.5358	0.65	7.3909	3.8	0.167	1	0.135	0.76	2151	66	2168	22	99
A130	26673	50	12.1	0.96	0.2995	1.47	3.2196	5.0	0.114	2	0.097	3.15	1289	52	1723	40	75
A131	113736	59	17.6	0.34	0.3924	0.76	4.2160	3.8	0.070	2	0.104	0.53	1640	54	1724	18	95
A132	44433	39	10.8	1.25	0.2982	0.78	2.6560	4.1	0.097	1	0.076	2.79	1282	43	1372	32	93
A133	17522	15	4.1	1.03	0.2942	0.61	2.4362	3.9	0.091	1	0.081	1.31	1266	41	1231	31	103
A134	102514	57	17.1	1.44	0.3412	0.92	3.9401	3.9	0.059	1	0.110	0.74	1447	50	1858	17	78
A135	63850	16	8.3	0.92	0.5609	0.79	8.0295	3.8	0.180	1	0.141	0.92	2230	70	2238	17	100
A136	65527	18	10.2	1.94	0.4715	1.70	7.2131	7.6	0.171	4	0.133	6.13	1922	80	2353	101	82
A137	45531	16	7.1	1.20	0.4595	0.55	5.8634	4.2	0.158	1	0.114	2.53	1878	58	2039	40	92
A138	223728	98	28.9	1.74	0.3003	0.98	4.1981	4.2	0.069	1	0.125	1.19	1287	46	2200	29	59
A139	289561	111	37.8	0.70	0.4421	1.50	5.4704	4.6	0.043	2	0.119	0.81	1815	72	1986	19	91
A140	104454	49	19.6	0.97	0.4805	1.51	5.6604	4.6	0.147	1	0.114	0.44	1950	76	1899	17	103
A141	85642	162	15.5	1.41	0.0920	0.87	0.7540	4.0	0.026	1	0.077	1.23	421	15	1220	23	35
A142	93108	41	10.3	0.44	0.3109	0.70	3.4793	3.7	0.108	1	0.109	0.54	1326	44	1808	16	73
A143	119764	112	19.6	1.41	0.1948	0.96	1.7068	4.1	0.046	1	0.080	1.15	861	31	1352	27	64
A144	65379	37	9.7	0.96	0.2950	0.49	2.7926	3.8	0.099	1	0.086	1.38	1263	40	1500	29	84
A145	101435	188	13.3	1.46	0.0643	2.89	0.5658	6.8	0.021	2	0.078	2.08	297	19	1361	28	22

sample	207	U (ppm)	Pb (ppm)	Th/U	206*/238	1s%	7/35r	2s%	208/232	1s%	207*/206*	1s%	206/238	2s	207/206	2s	conc%
K3e																	
A02	11509	452	122.4	0.19	0.2148	0.72	3.1370	6.1	0.084	6	0.079	1.95	1519	73	1329	58	114
A03	10617	744	127.0	0.01	0.1464	1.65	1.8421	6.8	0.048	109	0.069	2.29	1073	61	1034	62	104
A04	20203	866	182.0	0.01	0.1793	0.68	2.5107	6.0	0.200	13	0.080	2.03	1292	62	1247	55	104
A05	375	10	4.6	0.38	0.3270	4.48	7.3529	15.6	0.407	19	0.130	33.67	2191	195	2122	204	103
A06	14369	598	140.9	0.15	0.1901	0.98	2.6647	6.4	0.065	5	0.076	2.54	1362	68	1248	64	109
A07	15163	689	159.2	0.04	0.1965	1.32	2.5484	6.8	0.110	12	0.075	2.55	1403	73	1095	70	128
A08	5227	465	57.6	0.12	0.1023	2.69	1.2488	9.9	0.061	22	0.053	8.43	769	54	971	132	79
A09	560	63	9.5	0.01	0.1328	1.94	1.2782	10.6	1.380	16	0.096	11.86	981	59	467	187	210
A10	2361	87	23.1	0.47	0.1860	1.08	2.7448	8.2	0.063	8	0.053	12.55	1336	68	1348	116	99
A11	16398	746	156.9	0.04	0.1787	0.62	2.3861	5.8	0.025	29	0.078	1.46	1289	62	1152	49	112
A12	6630	177	69.9	0.42	0.3009	1.24	5.3304	7.9	0.100	8	0.096	4.57	2042	101	1692	100	121
A13	2746	142	29.6	0.23	0.1623	0.86	2.1063	7.5	0.048	13	0.078	5.38	1181	59	1095	103	108
A14	3165	194	37.4	0.32	0.1450	0.79	1.7518	6.5	0.054	6	0.070	4.27	1065	53	950	76	112
A15	4261	235	44.6	0.10	0.1568	0.77	1.9620	7.2	0.026	42	0.065	4.54	1145	56	1020	96	112
A16	2543	163	27.0	0.21	0.1282	1.06	1.5734	7.5	0.055	12	0.078	5.83	951	49	980	103	97
A17	8935	535	114.6	0.61	0.1441	1.29	1.8345	6.4	0.041	5	0.069	2.84	1060	56	1054	58	100
A18	12602	719	142.7	0.52	0.1355	1.19	1.8496	6.5	0.049	2	0.074	1.93	1001	53	1194	65	84
A19	367	46	5.1	0.35	0.0847	4.28	0.9017	17.8	0.024	83	10.000	4.19	644	62	684	314	94
A20	349	41	4.9	0.46	0.0859	2.93	0.9863	12.9	0.058	14	0.102	17.52	653	49	842	215	78
A21	14897	652	167.4	0.15	0.2074	1.21	2.9799	6.4	0.056	5	0.078	1.90	1476	75	1293	56	114
A22	7958	394	81.3	0.04	0.1736	0.71	2.3507	7.1	-0.157	-23	0.077	3.73	1257	61	1177	92	107
A23	530	68	7.4	0.52	0.0749	2.29	0.7467	15.6	-0.011	-60	10.000	3.43	573	38	541	306	106
A24	2892	387	37.4	0.02	0.0842	1.14	0.8155	7.2	0.079	44	0.060	3.04	641	34	475	99	135
A25	3518	435	42.4	0.03	0.0833	0.74	0.8932	6.4	0.056	26	0.055	4.80	634	32	697	74	91
A26	20191	1087	346.7	0.30	0.2578	2.97	3.4542	11.1	0.064	8	0.065	5.49	1789	124	1155	156	155
A27	4669	190	42.7	0.28	0.1565	0.73	2.6334	7.6	0.089	15	0.074	6.96	1144	56	1593	101	72
A28	6081	291	67.7	0.38	0.1634	1.11	2.4493	8.0	0.074	9	0.069	5.97	1191	61	1373	110	87
A29	3566	221	47.0	0.45	0.1527	0.74	1.9100	7.3	0.032	7	0.054	5.32	1119	55	1016	101	110
A30	2497	153	29.8	0.29	0.1489	0.97	1.8449	7.5	0.037	21	0.065	8.94	1094	55	996	102	110
A32	3962	283	40.8	0.24	0.1054	0.86	1.2638	16.0	0.032	12	0.070	7.37	793	41	928	309	85
A33	1691	243	41.0	0.46	0.1289	1.63	1.4895	10.3	0.040	5	0.051	13.77	958	54	852	173	112
A34	176	157	2.2	0.28	0.0099	8.22	0.1305	25.8	0.011	85	10.000	7.96	79	14	1112	384	7
A36	2247	273	33.6	0.36	0.0925	1.13	0.9365	7.4	0.041	6	0.064	5.28	702	37	570	106	123
A37	27943	1173	300.9	0.21	0.2029	0.86	2.9571	5.8	0.064	3	0.084	1.32	1450	71	1316	39	110
A38	27482	1601	1057.9	0.23	0.5537	4.70	7.3045	10.9	0.052	2	0.074	1.16	3376	288	1120	40	301
A39	34690	1800	694.2	0.07	0.3264	2.39	4.3578	7.4	0.046	6	0.078	1.02	2196	132	1144	45	192
A40	22133	1946	669.3	0.11	0.2899	3.98	3.9255	9.7	0.029	5	0.071	1.39	1984	164	1172	42	169
A41	3736	472	58.8	0.40	0.0918	0.95	0.9121	6.6	0.038	3	0.056	4.44	697	36	529	80	132
A42	2933	351	39.0	0.19	0.0889	0.82	0.9414	6.8	0.031	15	0.054	6.71	676	35	665	90	102
A43	6550	534	61.4	0.14	0.0947	1.39	1.1696	6.7	0.015	27	0.069	2.74	718	40	985	68	73
A44	1001	58	10.3	0.26	0.1333	2.79	1.8142	10.1	-0.020	-111	0.065	16.42	989	70	1180	132	84
A45	860	118	13.4	0.29	0.0872	1.74	0.8598	9.1	0.051	14	0.086	8.32	664	39	511	147	130
A46	1015	135	14.4	0.14	0.0880	1.41	0.9027	8.3	0.061	23	0.087	5.36	670	37	595	127	113
k3eb																	
A04	7169	49	#BEZUG!	2.60	0.1717	0.84	1.9679	9.5	0.058	3	10.000	0.98	1105	38	1103	175	100
A05	4073	28	#BEZUG!	2.14	0.1849	1.01	2.1355	15.1	0.064	4	10.000	1.04	1178	44	1127	290	105
KJA 91-7 gross																	
A01	29647	229	61.9	1.01	0.4483	0.85	2.4631	4.7	0.190	2	0.093	2.97	1292	50	1209	38	107
A02	36100	252	71.6	1.06	0.4628	0.82	2.6739	5.4	0.216	2	0.090	1.61	1331	51	1305	66	102
A03	34338	263	72.6	0.92	0.4719	0.98	2.6082	4.8	0.230	6	0.085	2.34	1356	54	1217	39	111
A04	72585	578	173.4	1.11	0.4902	0.99	2.6823	4.7	0.231	2	0.086	1.12	1404	56	1195	34	118
A05	66394	226	76.5	0.87	0.4451	0.82	4.8641	8.0	0.226	5	0.080	3.51	1288	52	2450	112	53
A06	31829	239	65.3	0.81	0.4747	0.87	2.5836	4.6	0.257	3	0.089	2.95	1367	53	1181	32	116
A07	40416	317	89.5	1.06	0.4614	0.85	2.4779	4.6	0.246	3	0.083	1.82	1333	52	1152	36	116
A08	51390	216	62.6	0.63	0.4381	0.83	2.8749	5.7	0.313	2	0.102	1.01	1273	50	1538	69	83
A09	69599	415	118.9	0.89	0.4684	0.88	2.4244	5.7	0.209	3	0.080	1.56	1354	53	1075	74	126
A10	53278	398	103.7	0.68	0.4640	1.09	2.5594	4.9	0.222	2	0.082	1.37	1344	55	1199	38	112
A11	108435	944	321.0	0.25	0.6995	1.80	3.6415	5.5	0.201	5	0.081	0.81	1933	90	1082	31	179
A12	68874	527	145.5	1.03	0.4516	0.71	2.4718	4.4	0.210	2	0.085	2.76	1316	50	1176	29	112
A13	63921	484	131.0	0.96	0.4460	0.86	2.4532	4.7	0.216	2	0.088	1.09	1302	51	1184	36	110
A14	85179	433	136.6	0.84	0.4912	0.93	3.2768	5.3	0.336	2	0.103	1.20	1422	56	1554	56	91
A15	89383	602	198.8	1.30	0.4962	1.08	2.9920	5.0	0.272	3	0.083	1.23	1436	58	1360	45	106
A16	48769	268	71.2	0.69	0.4253	1.31	2.3679	7.8	0.156	7	0.085	2.98	1251	54	1202	123	104
A17	66319	356	120.3	1.17	0.4959	0.98	3.2122	4.9	0.298	1	0.099	0.86	1438	57	1493	42	96
A18	117708	355	131.5	0.53	0.5261	1.05	4.3078	7.7	0.244	20	0.125	2.82	1517	61	1922	113	79
A19	15658	117	34.2	1.33	0.4291	1.02	2.3919	5.1	0.219	5	0.087	2.59	1264	51	1199	49	105
A20	41357	258	73.1	0.84	0.4609	1.13	2.6510	6.0	0.206	2	0.088	1.87	1350	55	1259	77	107
A21	53566	349	91.1	0.71	0.4250	1.21	2.8776	5.2	0.265	5	0.089	1.23	1255	53	1569	44	80
A22	38020	295	80.2	0.90	0.4476	0.85	2.5176	4.9	0.209	5	0.091	1.34	1317	51	1211	48	109
A23	10762	79	19.8	0.51	0.4568	1.43	2.5935	5.6	0.240	23	0.088	5.06	1345	59	1223	54	110
A24	28228	116	38.3	0.97	0.4868	1.65	2.9443	13.6	0.211	8	0.092	5.79	1425	67	1345	242	106
A25	54788	319	98.8	1.27	0.4525	0.76	3.1812	5.5	0.201	2	0.081	1.42	1336	51	1628	65	82
A26	67710	381	117.5	1.30	0.4477	0.73	2.2791	5.9	0.190	2	0.077	1.54	1324	51	1000	84	132
A27	64210	477	145.3	1.42	0.4580	1.14	2.5290	4.8	0.196	1	0.086	2.74	1353	56	1161	32	117
A28	150451	1165	1400.6	0.12	2.4933	2.37	14.6505	6.9	0.203	3	0.091	1.64	5292	226	1281	61	413
A29	40618	287	82.3	1.04	0.4529	0.84	2.7379	5.2	0.208	2	0.088	2.67	1342	52	1334	56	101
A30	11070	75	20.4	0.58	0.4719	1.29	2.9123	5.9	0.188	12	0.095	4.99	1394	59	1372	68	102
A31	48385	344	94.8	0.96	0.4437	0.79	2.6583	4.9	0.219	3	0.081	1.29	1319	51	1313	46	101
A32	38149	288	77.4	0.81	0.4517	0.94	2.5459	4.9	0.170	3	0.082	1.57	1342	53	1191	45	113
A33	20741	159	39.2	0.88	0.4109	0.69	2.3320	5.2	0.162	3	0.070	2.88	1233	47	1203	62	102
A34	35418	278	73.6	1.23	0.4091	0.71	2.3151	4.5	0.155	1	0.081	1.46	1231	47	1192	35	103
A35	66072	498	140.3	1.29	0.4315	0.92	2.4544	4.6	0.178	1	0.085	1.02	1293	51	1200	29	108
A36	5480	35	9.5	0.66	0.4379	2.20	3.2457	6.9	0.148	30	0.150	7.26	1312	70	1702	65	77
A37	40246	206	59.4	1.09	0.4194	0.64	2.6446	5.3	0.194	2	0.094	1.06	1263	48	1396	62	90
A38	94657	677	195.5	1.44	0.4220	0.93	2.4816	4.7	0.179	1	0.081	0.88	1271	50	1259	35	101
A39	31382	244	62.0	1.06	0.4056	0.96	2.3014	4.8	0.159	3	0.078	1.51	1227	49	1187	39	103

sample	207	U (ppm)	Pb (ppm)	Th/U	206*/238	1s%	7/35r	2s%	208/232	1s%	207*/206*	1s%	206/238	2s	207/206	2s	conc%
A40	18867	154	37.6	0.42	0.4637	1.09	2.5765	5.0	0.203	8	0.087	3.76	1387	56	1143	43	121
A41	38417	304	66.3	0.16	0.4344	0.87	2.4194	4.6	0.185	8	0.089	1.42	1309	51	1146	33	114
A42	24872	197	48.8	0.59	0.4433	0.94	2.4797	4.7	0.199	3	0.084	2.09	1334	53	1152	36	116
A43	11340	75	20.7	0.90	0.4416	0.99	2.8436	5.3	0.217	5	0.090	3.89	1331	53	1425	56	93
A44	27588	202	61.3	1.42	0.4541	1.12	2.6027	4.9	0.200	3	0.084	2.13	1368	56	1193	36	115
A45	20588	131	38.2	1.09	0.4472	0.91	2.9235	5.0	0.209	3	0.089	2.77	1351	53	1446	48	93
A46	12481	93	23.9	0.75	0.4325	1.46	2.4937	5.7	0.186	5	0.074	3.61	1312	58	1200	56	109
A47	10199	77	20.7	1.04	0.4315	1.47	2.3921	5.5	0.208	4	0.095	3.08	1310	58	1121	52	117
A48	16188	116	30.7	0.98	0.4162	1.34	2.4378	5.3	0.131	5	0.084	3.40	1269	55	1227	45	103
A49	22289	73	23.3	1.15	0.3830	1.67	2.1781	9.9	0.156	11	0.084	3.59	1178	57	1167	166	101
A50	8092	62	15.4	0.63	0.4324	1.04	2.4481	5.3	0.223	5	0.102	2.54	1316	53	1156	56	114
A51	11842	68	18.3	1.09	0.3883	1.06	2.8698	6.9	0.125	7	0.076	5.26	1195	49	1664	98	72
A52	18134	143	37.8	0.98	0.4270	1.19	2.4191	5.2	0.179	3	0.077	2.76	1304	54	1153	49	113
A53	13255	99	22.6	0.29	0.4262	1.29	2.4858	5.5	0.011	213	0.079	4.58	1303	56	1209	55	108
A54	66834	487	141.2	0.42	0.5417	1.78	3.2494	5.8	0.187	2	0.083	1.40	1616	76	1262	45	128
A55	56558	323	102.8	1.14	0.4729	0.94	3.4536	4.8	0.248	1	0.107	0.92	1434	56	1635	38	88
KJA 91-7 klein																	
A01	22220	181	54.0	1.07	0.4558	0.89	2.8552	6.1	0.197	3	0.082	3.11	1412	73	1306	38	108
A02	35979	278	88.1	1.09	0.4692	1.05	2.9278	6.5	0.225	3	0.084	1.33	1449	76	1299	56	112
A03	71750	253	104.0	0.88	0.5436	0.86	6.1180	11.8	0.582	3	0.152	5.08	1651	84	2369	176	70
A04	42438	358	114.6	1.37	0.4660	1.20	2.9357	6.2	0.200	2	0.082	1.30	1439	77	1318	32	109
A05	29291	229	70.0	1.13	0.4558	1.00	3.0073	6.1	0.191	3	0.090	3.09	1411	74	1407	38	100
A06	33318	260	85.4	1.31	0.4710	1.37	3.0088	6.6	0.191	2	0.093	1.80	1453	80	1345	47	108
A07	18391	106	34.6	0.86	0.4808	1.43	3.2362	8.0	0.268	5	0.091	2.39	1480	82	1446	98	102
A08	20766	177	51.0	1.13	0.4288	1.08	2.6874	6.3	0.175	5	0.091	2.07	1335	71	1309	44	102
A09	27815	234	72.6	1.23	0.4600	1.14	2.9395	6.3	0.194	2	0.090	2.99	1422	76	1347	40	106
A10	1072995	242	379.7	1.24	0.0393	64.84	1.9407	130.5	-3.051	-9	2.016	35.92	134	175	4663	164	3
A11	27821	197	59.5	0.94	0.4589	1.07	3.3108	6.3	0.228	3	0.092	1.21	1419	75	1578	43	90
A12	20669	210	51.9	0.59	0.4230	0.97	2.5019	6.0	0.197	4	0.082	1.93	1318	69	1197	32	110
A13	22745	196	57.6	1.15	0.4387	0.95	2.7577	6.4	0.197	2	0.092	1.84	1362	71	1317	55	103
A14	25062	218	64.5	1.21	0.4399	1.16	2.7568	6.3	0.215	2	0.095	1.29	1365	73	1311	43	104
A15	33525	468	102.7	0.28	0.4219	2.18	2.4468	7.4	0.184	4	0.087	2.27	1314	84	1159	47	113
A16	25940	247	72.4	1.18	0.4407	1.15	2.7588	6.3	0.173	2	0.091	1.98	1367	73	1309	39	104
A17	11735	106	40.6	1.76	0.5429	2.73	3.3775	8.7	0.239	6	0.100	3.53	1646	113	1297	77	127
A18	10230	76	24.0	0.87	0.4741	2.63	3.4430	14.0	0.042	74	0.095	12.98	1459	100	1592	221	92
A19	7992	83	24.1	0.89	0.4638	1.22	2.9173	6.9	0.238	13	0.115	3.62	1430	77	1319	65	108
A20	28976	238	77.5	1.45	0.4510	0.84	3.1921	6.1	0.203	2	0.092	1.65	1395	72	1545	40	90
A21	19693	182	51.4	0.95	0.4427	1.27	2.8186	6.5	0.204	7	0.093	2.88	1372	75	1343	50	102
A22	56433	362	126.1	0.93	0.5184	1.00	4.4156	6.7	0.367	2	0.115	1.64	1579	82	1886	61	84
A23	7325	65	17.2	0.19	0.4823	1.40	3.0627	7.2	-0.112	-248	0.084	9.74	1480	82	1340	74	110
A24	7122	68	22.0	0.98	0.5119	1.78	3.1907	7.0	0.205	13	0.118	5.48	1561	91	1304	52	120
A25	21678	210	62.1	1.13	0.4463	1.05	2.7720	6.2	0.179	3	0.084	1.64	1380	73	1297	41	106
A26	30999	263	83.6	1.13	0.4805	1.33	2.8477	6.9	0.219	3	0.080	1.57	1475	81	1206	66	122
A27	24123	222	65.3	1.32	0.4146	1.11	2.7608	6.6	0.195	3	0.087	1.77	1291	69	1432	58	90
A28	33900	308	94.1	1.13	0.4550	1.08	2.9978	6.2	0.211	2	0.088	1.64	1404	74	1411	41	99
A29	52701	574	156.0	0.93	0.4499	1.62	2.7824	6.6	0.192	4	0.085	1.63	1390	80	1290	32	108
A30	41965	493	109.9	0.78	0.3834	2.11	2.3233	7.3	0.128	6	0.082	1.11	1202	76	1250	47	96
A31	38673	215	74.3	1.24	0.4561	1.13	2.9564	7.6	0.207	4	0.088	1.86	1406	75	1381	92	102
A32	32855	222	55.7	0.59	0.3838	1.36	2.2496	8.4	0.141	9	0.079	2.53	1203	67	1185	114	101
A33	18488	195	54.4	0.99	0.4392	1.03	2.7057	6.1	0.168	3	0.095	2.96	1359	72	1284	38	106
A34	66612	831	193.5	0.34	0.4406	1.12	2.6041	6.1	0.133	3	0.083	0.86	1363	73	1203	29	113
A35	49646	543	142.0	0.61	0.4511	1.02	2.7576	6.1	0.213	3	0.086	1.18	1392	73	1269	35	110
A36	28479	306	90.9	1.37	0.4280	1.04	2.6705	6.2	0.173	2	0.083	1.77	1327	70	1309	38	101
A37	47299	476	141.7	0.98	0.4701	1.18	2.9396	6.2	0.193	2	0.085	1.09	1444	77	1314	31	110
A38	20704	215	69.9	1.68	0.4432	1.25	2.7362	6.4	0.186	2	0.084	2.03	1369	74	1289	41	106
A39	54124	553	195.9	1.81	0.4972	1.56	3.2074	6.7	0.222	2	0.087	1.35	1518	86	1375	43	110
A40	20262	196	56.1	1.43	0.4100	0.99	3.1908	7.9	0.188	3	0.076	2.90	1276	68	1727	98	74
A41	29488	231	87.7	1.56	0.4615	1.75	3.0028	7.6	0.199	6	0.077	2.67	1419	83	1392	76	102
A42	19619	146	51.7	1.54	0.4721	1.88	3.9151	8.4	0.202	6	0.088	5.87	1448	87	1844	94	79
A43	5174	58	13.9	0.95	0.3776	1.47	2.3851	7.3	0.098	15	0.070	6.94	1183	67	1335	76	89
A44	6358	73	20.3	1.54	0.4046	1.33	2.4792	6.7	0.157	7	0.096	5.87	1260	70	1277	53	99
A45	20507	178	51.4	1.29	0.3972	1.67	3.0552	8.7	0.152	6	0.078	3.79	1238	73	1708	107	73
A46	12834	130	36.0	1.02	0.4265	1.36	2.8771	6.9	0.131	6	0.080	3.90	1321	73	1462	60	90
A47	15575	152	42.7	1.18	0.4148	0.75	2.9270	7.1	0.154	2	0.076	2.38	1288	66	1548	80	83
A48	13571	158	41.1	1.25	0.3860	1.16	2.4502	6.9	0.138	5	0.075	3.65	1206	66	1346	69	90
A49	11098	125	33.4	1.28	0.3961	1.37	2.5357	7.5	0.166	3	0.071	4.46	1235	69	1363	83	91
A50	21018	168	44.9	0.91	0.3788	2.27	3.2611	9.2	-0.012	-133	0.077	8.47	1185	78	1914	105	62
A51	91485	991	358.2	1.28	0.5695	1.18	3.6723	6.2	0.198	2	0.081	1.13	1708	90	1377	36	124
A52	68011	495	106.8	0.87	0.2708	7.22	2.2531	18.6	-1.401	-16	0.072	5.91	869	127	1852	187	47
A53	31861	359	112.2	1.24	0.4694	1.22	3.0739	6.6	0.193	2	0.084	1.61	1439	78	1408	55	102
A54	45273	612	187.1	1.94	0.4225	0.91	2.6732	6.1	0.171	1	0.079	1.84	1308	69	1342	38	98
A55	19379	246	65.9	1.11	0.4086	0.85	2.5860	6.1	0.159	3	0.080	2.18	1269	66	1343	40	95
KK3VB gross																	
A01	31842	467	93.8	0.02	0.3826	1.05	2.3032	4.3	0.087	146	0.082	1.09	1249	44	1150	35	109
A02	35526	549	103.6	0.02	0.3623	1.15	2.1828	4.3	-0.011	-639	0.077	1.24	1178	43	1170	33	101
A03	21675	355	62.0	0.02	0.3397	1.02	1.9543	4.1	-0.197	-35	0.076	1.52	1101	39	1098	31	100
A04	15797	256	46.5	0.06	0.3521	1.03	2.0436	4.3	-0.034	-132	0.084	3.51	1128	40	1134	40	100
A05	16149	256	47.3	0.05	0.3623	1.20	2.0486	4.5	0.188	29	0.076	3.16	1148	43	1100	41	104
A06	28406	441	94.3	0.41	0.3803	1.07	2.1822	4.2	0.190	3	0.081	0.95	1191	42	1148	31	104
A07	16888	264	56.2	0.32	0.3912	1.07	2.2847	4.4	0.170	5	0.079	3.11	1212	43	1200	41	101
A08	19949	306	76.4	1.05	0.3951	0.92	2.3358	4.3	0.137	3	0.086	1.85	1213	41	1242	43	98
A09	20390	332	67.3	0.03	0.4113	0.88	2.3901	4.3	0.003	2199	0.083	2.88	1248	42	1226	44	102
A10	10123	174	31.9	0.08	0.3712	0.93	2.1020	4.5	0.141	53	0.084	3.29	1127	39	1192	51	95
A11	10705	197	36.3	0.03	0.3842	1.06	2.0924	4.4	-0.184	-67	0.082	3.80	1154	41	1132	41	102
A12	58501	995	395.0	0.02	0.8533	1.40	4.5570	4.5	-0.039	-97	0.077	0.85	2279	83	1145	29	199
A13	9061	155	25.7	0.02	0.3574	1.74	1.8940	5.5	0.412	79	0.084	3.36	1046	46	1146	55	91
A14	20938	395	81.9	0.05	0.4461	1.36	2.3729	4.6	0.158	20	0.082	2.71	1272	49	1170	34	109
A15	7761	172	33.0	0.12	0.4135	1.18	2.0606	4.7	0.083	39	0.081	3.48	1178	43	1057	50	111
A16	8028	149	33.2	0.06	0.4877	1.90	2.5433	5.8	0.066	116	0.080	4.18	1358	62	1164	56	117
A17	23385	306	100.2	0.34	0.6773	2.16	4.2549	5.7	0.227	10	0.101	1.79	1804	86	1539	33	117
A18	6302	151	27.6	0.01	0.4123	1.58	2.0972	5.6	0.962	35	0.080	2.63	1149	48	1147	65	100

sample	207	U (ppm)	Pb (ppm)	Th/U	206*/238	1s%	7/35r	2s%	208/232	1s%	207*/206*	1s%	206/238	2s	207/206	2s	conc%
A19	20137	555	121.0	0.30	0.4532	1.44	2.3556	4.7	0.223	5	0.082	2.96	1243	49	1205	35	103
A20	4864	115	22.4	0.02	0.4455	1.74	2.1988	5.8	0.355	110	0.085	5.37	1215	53	1119	66	109
A21	9788	84	28.6	0.32	0.5285	2.26	6.2927	10.6	0.084	114	0.068	12.50	1408	73	2716	146	52
A22	50253	1137	292.8	0.37	0.5498	1.37	2.7613	4.4	0.206	3	0.080	2.68	1448	55	1185	25	122
A23	6863	245	49.7	0.24	0.4582	1.25	2.1347	4.7	0.290	8	0.080	3.80	1203	45	1081	44	111
A24	20650	658	148.5	0.27	0.5085	1.17	2.4529	4.4	0.197	4	0.079	2.69	1313	48	1166	35	113
A25	21122	603	153.2	0.50	0.5465	1.14	2.8174	4.4	0.198	3	0.082	1.31	1392	50	1311	38	106
A26	14518	501	96.8	0.03	0.4699	1.06	2.2016	4.4	-0.141	-85	0.080	3.00	1206	43	1138	39	106
A27	14728	656	146.2	0.10	0.5342	1.20	2.7187	4.8	0.195	13	0.078	3.11	1345	49	1315	49	102
A28	3944	155	28.2	0.03	0.4473	1.40	2.0677	5.5	-0.355	-112	0.079	5.44	1137	45	1141	68	100
A29	2525	121	24.4	0.05	0.4990	2.10	2.2527	6.7	2.886	17	0.097	7.77	1248	61	1108	82	113
A30	10134	581	105.0	0.03	0.4532	0.79	2.0039	4.1	0.016	1161	0.081	3.49	1135	38	1081	38	105
A31	13144	596	127.9	0.08	0.5305	1.48	2.5792	4.8	0.378	14	0.086	2.96	1302	52	1283	37	101
A32	14791	1157	215.6	0.02	0.4748	1.68	2.1076	5.2	-0.030	-410	0.074	3.13	1169	50	1118	45	105
A33	5766	517	115.0	0.81	0.4736	1.53	2.1485	5.2	0.173	8	0.079	5.39	1159	48	1175	52	99
KK3VB klein																	
A01	27710	612	119.9	0.01	0.2315	1.04	2.2543	4.7	0.364	23	0.084	1.45	1223	49	1154	33	106
A02	30148	591	152.2	0.47	0.2452	0.70	2.4844	4.5	0.086	1	0.080	1.31	1288	48	1233	32	104
A03	26312	537	108.7	0.02	0.2379	0.87	2.3238	4.5	0.179	12	0.080	0.90	1252	49	1162	26	108
A04	45195	932	203.5	0.09	0.2472	0.79	2.4662	4.4	0.093	7	0.082	0.76	1296	50	1205	24	108
A05	31953	641	183.6	0.60	0.2522	1.04	2.5370	4.6	0.095	2	0.081	0.82	1319	53	1222	27	108
A06	44301	855	175.7	0.01	0.2354	1.20	2.3262	5.3	0.086	34	0.080	1.15	1239	52	1188	52	104
A07	41893	910	179.4	0.01	0.2339	0.96	2.2330	4.6	-0.010	-408	0.076	1.20	1231	49	1121	30	110
A08	6776	164	29.5	0.03	0.2115	1.37	1.9688	5.5	-0.090	-52	0.085	4.41	1122	49	1071	54	105
A09	16946	375	71.8	0.07	0.2202	1.01	2.1066	4.8	0.102	10	0.080	1.61	1164	47	1126	39	103
A10	27528	604	112.5	0.03	0.2176	0.94	2.1240	4.5	0.097	10	0.082	1.14	1151	46	1168	28	99
A11	30135	679	123.5	0.01	0.2159	0.91	2.0736	4.6	0.356	17	0.078	1.31	1142	45	1136	34	101
A12	111947	1201	395.5	0.31	0.3457	1.44	3.3811	5.1	0.113	1	0.080	0.75	1742	74	1173	28	148
A13	5548	94	23.9	0.18	0.2685	1.35	2.8694	6.5	0.130	13	0.095	4.20	1391	60	1347	85	103
A14	178155	1979	1557.9	0.01	0.9341	1.94	9.5340	6.1	0.062	26	0.083	1.24	3922	164	1259	51	311
A15	147726	1642	1008.5	0.05	0.7200	2.51	7.4683	6.9	0.092	7	0.084	1.29	3209	163	1291	55	249
A18	92938	1810	1600.0	0.01	1.0515	3.45	10.6068	8.0	0.096	16	0.081	0.60	4275	252	1240	23	345
A19	9277	197	35.4	0.02	0.2128	2.54	2.1087	7.4	0.122	94	0.084	3.54	1123	66	1205	73	93
A20	62411	1367	436.4	0.15	0.3602	2.13	3.5331	6.0	0.096	1	0.080	0.80	1799	91	1187	30	152
A21	39705	803	172.4	0.05	0.2504	1.19	2.4302	4.9	0.114	5	0.083	1.24	1303	54	1165	32	112
A22	28790	581	133.7	0.18	0.2512	0.98	2.4903	4.8	0.128	2	0.084	1.29	1306	52	1208	37	108
A23	29901	699	144.4	0.04	0.2425	1.60	2.2689	5.4	0.138	6	0.083	1.31	1264	58	1094	38	116
A24	34824	659	136.0	0.01	0.2451	1.51	2.3875	5.3	0.254	16	0.080	0.85	1276	57	1175	38	109
A25	12133	282	47.7	0.02	0.2008	1.46	1.8979	5.5	-0.087	-48	0.083	2.72	1063	48	1116	51	95
A26	20335	426	78.8	0.04	0.2155	1.32	2.1084	5.0	0.117	8	0.083	1.23	1134	49	1185	33	96
A27	31786	611	152.8	0.01	0.2986	1.39	2.9476	5.1	0.124	50	0.081	1.44	1522	65	1204	35	126
A28	7168	157	29.9	0.06	0.2218	1.24	2.1006	5.4	0.188	12	0.097	2.83	1163	49	1123	55	104
A29	9528	145	36.3	0.29	0.2427	1.25	2.6899	5.2	0.141	6	0.105	3.51	1262	53	1430	47	88
A30	10174	229	44.9	0.04	0.2294	1.04	2.2105	5.2	0.249	14	0.087	2.68	1198	49	1159	55	103
A31	34220	685	134.6	0.02	0.2330	1.14	2.2769	4.8	0.199	9	0.084	1.21	1215	50	1188	31	102
A32	8304	192	38.4	0.04	0.2344	1.04	2.2403	5.0	0.166	17	0.087	3.41	1221	49	1145	48	107
A33	47063	955	285.2	0.02	0.3565	1.06	3.4345	4.7	0.529	6	0.083	1.47	1775	69	1162	29	153
A34	8222	162	28.8	0.03	0.2113	1.63	1.9701	5.8	0.179	26	0.082	2.49	1109	52	1097	57	101
A35	43030	808	169.5	0.01	0.2519	0.97	2.4015	4.6	0.054	54	0.078	1.13	1302	52	1143	32	114
A36	19896	379	77.8	0.05	0.2416	0.81	2.2546	4.7	0.128	11	0.076	1.91	1253	48	1101	40	114
A37	33058	603	124.0	0.10	0.2289	1.03	2.2289	4.8	0.126	7	0.080	1.30	1192	48	1186	38	101
A38	15313	153	47.2	0.39	0.2979	1.17	3.6442	5.2	0.125	3	0.101	2.02	1512	61	1624	49	93
A39	86922	1058	562.5	0.01	0.6391	2.97	6.2150	7.4	0.062	24	0.080	0.97	2894	168	1186	40	244
A40	20942	357	101.1	0.02	0.3334	1.71	3.5174	6.1	0.028	94	0.087	2.57	1669	77	1346	60	124
A41	11654	173	35.3	0.01	0.2457	1.72	2.2788	5.7	0.349	24	0.081	2.53	1269	60	1094	47	116
A42	35060	462	183.5	0.02	0.4740	1.96	4.8737	6.5	-0.175	-24	0.077	2.34	2259	106	1298	68	174
A43	10551	145	30.0	0.01	0.2468	2.10	2.3752	7.9	-0.162	-85	0.084	3.48	1273	67	1169	107	109
A44	12287	162	27.5	0.01	0.2051	0.96	1.9201	4.8	-0.085	-93	0.075	2.34	1075	43	1115	41	96
A45	11877	147	28.9	0.08	0.2272	0.92	2.1342	4.8	0.124	8	0.080	2.67	1180	47	1123	43	105
A46	51587	524	118.4	0.08	0.2613	1.26	2.5275	4.9	0.124	4	0.083	0.87	1339	56	1182	30	113
A47	20100	221	43.8	0.03	0.2364	1.32	2.2287	5.0	0.055	29	0.082	1.58	1223	53	1132	33	108
A48	6340	54	13.7	0.25	0.2704	1.62	2.7687	6.0	0.131	6	0.087	3.95	1380	63	1295	62	107
A49	26893	180	53.0	0.30	0.3034	0.98	3.2912	4.6	0.108	2	0.097	1.34	1529	60	1407	29	109
A50	50855	424	106.4	0.01	0.3037	1.18	2.9323	4.7	-0.177	-21	0.081	0.94	1530	62	1182	26	129
A51	17498	141	32.2	0.16	0.2474	1.47	2.4865	5.3	0.133	6	0.091	1.61	1272	57	1262	42	101
A52	9573	85	15.4	0.02	0.2181	0.99	2.0225	5.2	0.056	86	0.073	2.37	1133	46	1104	55	103
A53	20018	157	30.9	0.02	0.2339	0.86	2.2989	4.7	0.152	13	0.083	1.18	1207	47	1220	37	99
A54	29747	234	44.1	0.01	0.2270	1.08	2.1844	4.8	0.151	23	0.082	1.33	1174	48	1179	34	100
A55	79594	530	217.8	0.06	0.4896	1.20	4.7357	4.8	0.098	3	0.080	0.63	2309	89	1190	25	194
KK3VB klein																	
A01	33399	697	135.1	0.01	0.2436	0.98	2.2490	5.8	0.199	11	0.078	0.97	1199	60	1191	37	101
A02	32198	631	132.1	0.16	0.2418	0.96	2.2331	5.7	0.097	3	0.082	1.06	1192	60	1191	30	100
A03	12081	246	51.4	0.18	0.2381	1.08	2.2194	5.9	0.076	8	0.080	2.13	1175	60	1209	41	97
A04	21880	491	89.8	0.04	0.2269	0.85	2.0533	5.6	0.115	9	0.081	1.26	1125	56	1150	34	98
A05	19446	332	84.6	0.38	0.2625	1.19	2.5930	5.8	0.092	2	0.084	1.54	1285	66	1321	29	97
A06	9985	214	40.3	0.01	0.2379	1.09	2.1567	6.1	0.348	18	0.087	1.55	1175	60	1152	49	102
A07	30959	629	135.5	0.16	0.2488	1.09	2.2404	5.9	0.082	3	0.078	0.92	1225	62	1138	41	108
A08	33006	637	136.0	0.01	0.2702	1.04	2.5158	5.7	0.297	10	0.083	0.87	1320	66	1204	28	110
A09	11272	203	35.7	0.02	0.2093	1.51	1.9344	9.1	0.383	14	0.080	3.38	1046	58	1188	137	88
A10	25185	567	100.7	0.02	0.2238	1.09	2.0045	5.8	0.181	15	0.078	1.18	1113	57	1126	32	99
A11	13641	299	56.8	0.01	0.2401	1.29	2.1831	6.0	0.160	39	0.081	1.89	1187	62	1155	38	103
A12	70951	865	293.5	0.01	0.4303	1.12	3.9227	5.8	0.147	18	0.080	0.82	1993	96	1160	33	172
A13	47328	1019	191.0	0.08	0.2273	1.25	2.0564	5.9	0.056	5	0.078	0.99	1130	59	1143	34	99
A14	31061	636	123.6	0.02	0.2433	1.08	2.2458	5.9	0.139	15	0.080	0.97	1203	61	1183	40	102
A15	36172	728	133.8	0.01	0.2311	0.99	2.1262	5.7	0.165	14	0.081	0.97	1148	58	1176	35	98
A16	29922	642	120.0	0.02	0.2344	1.25	2.1248	6.0	0.068	24	0.077	1.24	1163	61	1146	38	102
A17	9615	212	34.9	0.02	0.2070	1.06	1.8811	6.0	0.078	62	0.084	2.07	1038	53	1150	44	90
A18	48334	1079	193.5	0.02	0.2244	1.05	2.0086	5.7	0.110	7	0.079	0.49	1118	57	1120	26	100
A19	31779	640	155.4	0.44	0.2523	1.34	2.3598	6.1	0.054	8	0.082	1.09	1245	66	1206	37	103
A20	29010	661	116.9	0.01	0.2232	1.01	1.9871	5.7	0.160	16	0.078	1.19	1113	56	1107	32	101

sample	207	U (ppm)	Pb (ppm)	Th/U	206*/238	1s%	7/35r	2s%	208/232	1s%	207*/206*	1s%	206/238	2s	207/206	2s	conc%
A21	36432	792	156.1	0.04	0.2441	0.94	2.1949	5.7	0.170	16	0.078	1.14	1209	60	1126	34	107
A22	5467	127	25.7	0.23	0.2346	2.07	2.1476	7.3	0.071	11	0.077	3.84	1166	70	1162	64	100
A23	63002	881	213.4	0.01	0.3053	1.12	2.8837	5.7	0.068	91	0.080	0.81	1480	74	1223	27	121
A24	38709	729	252.2	0.01	0.4259	1.64	4.4942	6.5	0.164	32	0.081	1.35	1983	104	1436	46	138
A25	8030	114	32.3	0.26	0.3100	1.36	3.3876	6.4	0.121	10	0.105	1.43	1501	78	1502	52	100
A26	31209	650	132.1	0.02	0.2545	1.23	2.3101	6.0	0.014	59	0.078	0.92	1257	65	1142	41	110
A27	13432	310	56.9	0.01	0.2308	1.10	2.0739	6.0	-0.129	-28	0.082	1.66	1150	59	1121	43	103
A28	16763	390	70.8	0.03	0.2253	1.26	1.9970	6.0	0.032	42	0.075	1.38	1126	59	1093	41	103
A29	21317	501	90.6	0.01	0.2272	1.14	2.0306	5.9	0.156	16	0.079	1.31	1134	58	1109	39	102
A30	19545	377	74.9	0.01	0.2491	1.76	2.3432	6.5	0.293	20	0.083	1.43	1234	70	1210	36	102
A31	12297	257	54.6	0.04	0.2603	1.33	2.4258	6.3	-0.225	-32	0.082	2.59	1285	67	1191	53	108
A32	16902	407	73.1	0.03	0.2230	0.99	2.0012	5.8	0.058	19	0.075	1.21	1116	56	1116	41	100
A33	19187	463	84.5	0.06	0.2233	0.88	1.9748	5.7	0.135	4	0.076	1.25	1118	56	1086	35	103
A34	34619	749	132.6	0.01	0.2225	0.99	2.0147	5.6	0.049	29	0.076	0.81	1114	56	1133	25	98
A35	33722	642	120.3	0.01	0.2347	0.92	2.1846	5.7	0.108	17	0.078	0.93	1171	58	1185	34	99
A36	31804	605	107.3	0.01	0.2213	0.88	2.0583	5.6	0.161	13	0.080	0.84	1110	55	1183	32	94
A37	47630	887	163.8	0.03	0.2284	0.80	2.0911	5.5	0.109	10	0.079	0.72	1143	56	1152	29	99
A38	62133	1023	187.9	0.01	0.2298	0.93	2.1220	5.6	0.075	16	0.080	0.65	1149	57	1169	24	98
A39	15199	256	46.0	0.01	0.2259	1.07	2.0321	5.9	0.202	27	0.082	1.80	1132	58	1116	43	101
A40	11618	185	32.8	0.04	0.2173	0.98	1.9639	6.0	0.115	19	0.078	1.55	1092	55	1125	51	97
A41	18129	291	51.7	0.03	0.2198	0.96	1.9820	5.7	0.137	11	0.081	1.02	1104	56	1120	30	99
A42	14920	193	35.8	0.05	0.2254	1.30	2.1114	6.1	0.082	16	0.079	1.86	1130	60	1195	39	95
A43	9931	142	24.9	0.02	0.2186	0.95	1.9960	5.9	0.127	32	0.082	2.30	1099	55	1144	47	96
A44	16919	234	40.4	0.04	0.2128	0.74	1.9137	5.7	0.069	13	0.079	1.60	1073	53	1112	42	96
A45	53526	679	119.6	0.01	0.2204	0.92	1.9956	5.5	0.094	19	0.077	0.65	1109	55	1124	22	99
A46	41313	472	79.4	0.03	0.2055	1.12	1.9064	5.8	0.043	26	0.079	0.81	1040	54	1172	32	89
A47	48580	523	104.2	0.03	0.2449	0.97	2.3059	5.7	0.059	17	0.080	0.95	1222	61	1201	30	102
A48	12678	126	25.4	0.06	0.2445	1.08	2.2533	6.0	0.118	10	0.079	1.70	1220	62	1158	44	105
A49	48897	513	103.8	0.03	0.2500	1.07	2.3116	5.9	0.086	6	0.079	0.87	1245	63	1164	38	107
A50	54507	480	112.7	0.01	0.2925	1.61	2.7734	6.2	0.107	12	0.081	0.75	1435	78	1213	28	118
A51	17366	108	35.1	0.31	0.3443	1.36	3.7315	6.5	0.138	3	0.096	2.28	1660	85	1471	58	113
A52	9633	78	16.7	0.13	0.2479	1.38	2.3535	6.2	0.067	17	0.082	2.89	1237	66	1214	44	102
A53	59091	413	104.5	0.01	0.3157	1.02	2.9688	5.8	0.105	27	0.080	0.85	1538	76	1195	37	129
A54	32903	270	81.6	0.86	0.2486	0.75	2.3114	5.7	0.097	1	0.083	1.06	1241	60	1172	39	106
A55	8813	77	14.5	0.04	0.2322	1.10	2.1024	6.5	0.089	24	0.071	2.74	1166	60	1119	68	104

Table A4.2 Results of Hf isotope analyzes from the zircons collected in the Rehoboth Terrane.

sample	$^{176}Yb/^{177}Hf$	1se %	$^{176}Lu/^{177}Hf$	1se	$^{178}Hf/^{177}Hf$ (1)	1se %	Hf_{total}(V)	$(176/177)Hf_{Lu}$	$\varepsilon Hf_{Lu\text{-}T}$	+/– 2σ	Age (Ma)	2s abs
K3eb 40 3	0.0193	2.432	0.00065	1.974	1.4673	0.0014	15.30	0.282096	0.9	1.4	1127	10
K3eb 33 2	0.0096	0.299	0.00034	0.457	1.4673	0.0025	10.24	0.282104	0.7	1.3	1103	10
GLZ2b 40 130	0.0951	2.087	0.00272	1.581	1.4674	0.0012	15.89	0.281929	-30.3	1.0		
GLZ2b 40 129	0.0445	3.635	0.00134	3.784	1.4673	0.0011	15.41	0.282006	-27.5	0.4		
GLZ2b 40 128	0.0931	1.157	0.00292	2.024	1.4674	0.0013	19.04	0.281954	-29.4	1.4		
GLZ2b 40 127	0.0617	2.712	0.00200	1.835	1.4673	0.0011	18.09	0.281560	-43.3	0.8		
GLZ2b 40 126	0.0716	3.062	0.00222	2.731	1.4673	0.0009	20.76	0.281906	-31.1	0.8		
GLZ2b 40 125	0.0538	6.046	0.00167	5.809	1.4673	0.0012	14.59	0.281536	-1.3	1.0	1899	9
GLZ2b 40 124	0.0469	2.183	0.00147	2.507	1.4673	0.0013	10.38	0.281187	-11.7	2.0	1986	10
GLZ2b 40 123	0.0860	1.952	0.00298	2.372	1.4673	0.0017	10.54	0.281308	-52.2	1.0		
GLZ2b 40 122	0.0206	6.303	0.00075	5.557	1.4673	0.0025	10.45	0.281554	-43.5	2.6		
GLZ2b 40 121	0.0510	3.280	0.00180	2.866	1.4673	0.0027	6.10	0.281595	-42.1	3.9		
GLZ2b 40 120	0.0394	3.107	0.00133	2.624	1.4673	0.0011	13.87	0.281410	2.1	1.5	2238	8
GLZ2b 40 119	0.0751	1.334	0.00229	1.285	1.4673	0.0014	14.42	0.281579	-42.7	0.4		
GLZ2b 40 117	0.0613	6.607	0.00214	5.818	1.4673	0.0027	7.02	0.281896	-0.6	7.2	1372	16
GLZ2b 40 116	0.0732	2.043	0.00254	1.712	1.4673	0.0012	19.56	0.281520	-5.9	1.9	1724	9
GLZ2b 40 115	0.0481	5.939	0.00132	5.400	1.4673	0.0011	13.06	0.281520	-44.7	1.4		
GLZ2b 40 114	0.0175	1.631	0.00053	1.627	1.4673	0.0010	21.46	0.281395	-0.1	0.9	2168	11
GLZ2b 40 113	0.0239	1.755	0.00071	1.408	1.4673	0.0007	21.60	0.281568	-1.7	0.7	1831	9
GLZ2b 40 112	0.0709	3.108	0.00215	2.339	1.4673	0.0006	21.69	0.281739	3.4	0.7	1792	7
GLZ2b 40 110	0.0452	2.069	0.00154	2.055	1.4673	0.0009	20.58	0.281395	-5.3	0.6	1942	10
GLZ2b 40 109	0.0675	3.114	0.00228	2.989	1.4673	0.0009	21.92	0.281556	-43.5	0.5		
GLZ2b 40 108	0.0496	3.038	0.00158	3.035	1.4673	0.0013	15.03	0.281555	-3.0	2.6	1796	11
GLZ2b 40 107	0.0384	1.857	0.00128	2.116	1.4673	0.0009	20.69	0.281542	-4.8	0.9	1738	11
GLZ2b 40 106	0.0326	1.427	0.00118	1.361	1.4673	0.0009	14.63	0.281572	-3.5	1.2	1749	10
GLZ2b 40 105	0.0511	1.500	0.00177	1.131	1.4673	0.0010	16.52	0.281486	-5.0	0.7	1813	23
GLZ2b 40 104	0.0694	1.508	0.00225	1.212	1.4673	0.0012	13.91	0.281752	-36.5	0.7		
GLZ2b 40 103	0.0413	3.670	0.00143	3.079	1.4673	0.0011	19.18	0.281543	-2.6	1.7	1829	9
GLZ2b 40 102	0.0572	3.781	0.00189	3.814	1.4673	0.0009	21.19	0.281961	-29.2	0.5		
GLZ2b 33 118	0.0226	2.582	0.00079	1.773	1.4673	0.0017	10.13	0.281871	-4.7	0.7	1231	16
GLZ2b 33 111	0.0581	3.129	0.00197	2.666	1.4673	0.0013	13.27	0.281464	-6.3	1.3	1792	7
GLZ2a 40 101	0.0490	4.003	0.00158	2.735	1.4673	0.0010	20.37	0.281897	-31.4	0.3		
GLZ2a 40 100	0.0247	0.266	0.00089	0.504	1.4673	0.0010	16.77	0.282126	5.6	0.6	1288	24
GLZ2a 40 99	0.0411	1.440	0.00148	1.980	1.4673	0.0010	18.47	0.281445	-5.8	0.7	1843	8
GLZ2a 40 98	0.0275	1.677	0.00092	2.021	1.4673	0.0007	19.90	0.281968	-1.8	0.5	1206	14
GLZ2a 40 97	0.0282	3.124	0.00094	3.009	1.4673	0.0012	15.34	0.282005	-0.4	0.6	1210	13
GLZ2a 40 96	0.0224	1.613	0.00070	0.483	1.4673	0.0010	18.80	0.281973	-1.4	0.5	1218	12
GLZ2a 40 95	0.0646	1.618	0.00222	1.913	1.4673	0.0008	22.47	0.281869	-3.4	0.4	1293	10
GLZ2a 40 94	0.0334	0.632	0.00121	0.667	1.4673	0.0012	15.83	0.281828	-33.9	0.3		
GLZ2a 40 93	0.0564	2.276	0.00176	2.305	1.4673	0.0011	19.56	0.281379	-7.9	0.7	1856	9
GLZ2a 40 92	0.0340	1.952	0.00121	2.472	1.4673	0.0011	18.56	0.281907	-4.2	0.4	1198	11
GLZ2a 40 91	0.0308	2.204	0.00110	2.699	1.4673	0.0010	18.92	0.281947	-2.0	0.9	1230	18
GLZ2a 40 90	0.0240	2.294	0.00071	2.706	1.4673	0.0011	19.38	0.281486	-2.3	1.2	1931	7
GLZ2a 40 89	0.0224	1.174	0.00072	1.274	1.4673	0.0011	18.84	0.281443	-1.4	0.9	2035	9
GLZ2a 40 88	0.0259	2.764	0.00090	1.809	1.4673	0.0010	20.16	0.281551	-2.7	0.9	1815	10
GLZ2a 40 87	0.0312	0.692	0.00104	1.500	1.4672	0.0011	15.88	0.281540	-2.5	0.8	1840	13
GLZ2a 40 86	0.0553	5.106	0.00176	5.360	1.4673	0.0007	21.98	0.281872	-4.9	0.4	1220	11
GLZ2a 40 85	0.0524	1.714	0.00151	2.023	1.4673	0.0008	21.74	0.281780	-35.5	0.1		
GLZ2a 40 84	0.0655	2.510	0.00185	1.389	1.4673	0.0014	20.32	0.281573	-42.9	1.2		
GLZ2a 40 83	0.0369	5.433	0.00114	4.429	1.4673	0.0011	18.39	0.281563	-43.2	0.1		
GLZ2a 40 82	0.0477	1.246	0.00170	1.031	1.4673	0.0009	19.23	0.281428	-6.3	0.7	1848	8
GLZ2a 40 81	0.0439	3.806	0.00136	3.778	1.4673	0.0009	20.13	0.281626	-2.7	0.7	1699	10
GLZ2a 40 80	0.0353	1.273	0.00128	1.025	1.4673	0.0008	16.52	0.281828	-6.2	0.6	1234	11
GLZ2a 40 79	0.0317	2.757	0.00118	3.128	1.4673	0.0008	17.07	0.281946	-29.7	0.6		
GLZ2a 40 78	0.0653	7.437	0.00197	7.333	1.4673	0.0009	22.59	0.281342	-2.9	1.1	2128	7
GLZ2a 40 77	0.0228	2.528	0.00078	1.868	1.4673	0.0009	17.41	0.281624	0.5	0.8	1841	9
GLZ2a 40 76	0.0213	1.333	0.00076	1.056	1.4673	0.0010	17.18	0.281531	4.1	1.2	2139	62
GLZ2a 40 75	0.0136	0.501	0.00053	0.386	1.4673	0.0010	18.45	0.282691	12.0	0.2	684	14
GLZ2a 40 74	0.0525	3.575	0.00157	3.521	1.4673	0.0009	19.55	0.281651	-40.1	0.3		
GLZ2a 40 73	0.0748	3.045	0.00200	1.857	1.4673	0.0008	22.41	0.281823	-34.0	0.2		
GLZ2a 40 72	0.1062	4.321	0.00291	3.345	1.4673	0.0009	16.53	0.281797	-35.0	0.2		
GLZ2a 40 71	0.0384	3.519	0.00128	3.204	1.4673	0.0007	19.73	0.281390	-7.7	0.6	1845	7
GLZ2a 40 70	0.0285	0.840	0.00099	0.647	1.4673	0.0009	18.20	0.281379	-5.8	0.8	1945	7
GLZ2a 40 69	0.0265	4.447	0.00075	4.029	1.4673	0.0011	14.11	0.281743	-6.0	1.3	1371	21
GLZ2a 40 68	0.0173	2.083	0.00056	1.218	1.4673	0.0009	20.05	0.281483	-5.9	0.6	1783	19
GLZ2a 40 67	0.0311	1.883	0.00094	1.435	1.4673	0.0008	20.52	0.281582	-1.2	0.7	1830	7
GLZ2a 40 66	0.0412	2.095	0.00121	1.609	1.4672	0.0013	12.24	0.281850	-5.0	0.7	1249	17
GLZ2a 40 65	0.0332	2.978	0.00113	2.558	1.4673	0.0007	21.01	0.281934	-30.1	0.2		
GLZ2a 40 64	0.0267	8.063	0.00094	7.865	1.4673	0.0007	21.35	0.282263	-18.5	0.1		
GLZ2a 40 63	0.0175	1.324	0.00063	1.364	1.4673	0.0009	17.75	0.281929	-2.9	0.6	1218	20
GLZ2a 40 62	0.0230	1.395	0.00069	1.184	1.4673	0.0010	20.10	0.281965	-1.4	0.5	1231	15
GLZ2a 40 61	0.1058	4.804	0.00281	5.561	1.4673	0.0009	22.59	0.281469	-46.5	0.7		
GLZ2a 40 60	0.0525	2.303	0.00152	2.805	1.4673	0.0010	24.22	0.281487	-45.9	0.5		
GLZ2a 40 59	0.0566	6.825	0.00163	6.035	1.4673	0.0008	23.62	0.281450	-47.2	0.1		
GLZ2a 40 58	0.0589	2.975	0.00199	3.068	1.4673	0.0010	20.71	0.281405	-7.1	0.8	1847	9
GLZ2a 40 57	0.0213	2.029	0.00075	1.980	1.4673	0.0008	18.23	0.281464	-5.5	0.7	1830	9
GLZ2a 40 56	0.0494	1.563	0.00168	1.835	1.4673	0.0008	17.77	0.281358	-6.4	0.9	1951	10
GLZ2a 40 55	0.0616	2.837	0.00199	3.375	1.4673	0.0008	17.33	0.281522	-44.7	0.3		
GLZ2a 40 54	0.0402	2.673	0.00136	1.816	1.4673	0.0008	19.03	0.281540	-44.0	0.3		
GLZ2a 40 53	0.0252	1.322	0.00089	1.731	1.4673	0.0011	17.63	0.281693	-6.8	0.8	1415	13
GLZ2a 40 52	0.0403	1.788	0.00134	1.824	1.4673	0.0012	20.04	0.282100	-24.2	0.7		
GLZ2a 40 51	0.0579	3.171	0.00192	2.306	1.4673	0.0008	18.15	0.281757	-36.4	0.1		
GLZ2a 40 50	0.0234	0.751	0.00084	0.797	1.4673	0.0010	11.02	0.281950	3.2	1.0	1456	26
GLZ2a 40 49	0.0366	1.702	0.00134	1.238	1.4673	0.0010	10.26	0.281895	-3.8	0.7	1232	13
GLZ2a 40 48	0.0187	4.620	0.00067	4.594	1.4673	0.0014	10.88	0.281543	-43.9	0.8		
GLZ2a 40 47	0.0287	4.378	0.00083	4.454	1.4673	0.0016	9.73	0.281578	4.3	2.1	2076	32
GLZ2a 40 46	0.0625	3.070	0.00224	3.277	1.4673	0.0014	15.56	0.281966	-29.0	1.7		

sample	$^{176}Yb/^{177}Hf$	1se %	$^{176}Lu/^{177}Hf$	1se	$^{178}Hf/^{177}Hf$ (1)	1se %	Hf_{total}(V)	(176/177)Hf_{Lu}	$\varepsilon Hf_{Lu\text{-}T}$	+/– 2σ	Age (Ma)	2s abs
GLZ2a 40 45	0.0315	1.913	0.00104	0.846	1.4673	0.0011	13.53	0.281949	2.1	0.6	1407	15
GLZ2a 40 44	0.0376	3.997	0.00113	3.872	1.4673	0.0007	22.41	0.281675	-39.2	1.3		
GLZ2a 40 43	0.0646	0.892	0.00196	1.454	1.4673	0.0009	19.59	0.281893	-31.6	0.4		
GLZ2a 40 42	0.0963	5.045	0.00253	5.422	1.4673	0.0012	27.74	0.281393	-49.2	0.4		
GLZ2a 40 41	0.0523	1.793	0.00173	2.398	1.4673	0.0010	14.66	0.281846	-3.2	1.6	1334	34
GLZ2a 40 40	0.0894	6.416	0.00243	6.337	1.4673	0.0010	16.51	0.281710	-38.0	0.9		
GLZ2a 40 39	0.0652	2.236	0.00256	2.453	1.4673	0.0018	9.05	0.282208	-20.4	0.9		
GLZ2a 40 38	0.0522	2.804	0.00201	2.621	1.4673	0.0015	9.42	0.282122	5.0	0.7	1267	13
GLZ2a 40 37	0.0772	5.023	0.00221	5.073	1.4674	0.0022	8.41	0.281837	9.2	3.2	1892	17
GLZ2a 40 36	0.0587	3.259	0.00149	3.906	1.4673	0.0016	12.54	0.281920	-30.6	1.0		
GLZ2a 40 35	0.1079	4.085	0.00316	3.496	1.4673	0.0008	22.36	0.281555	-43.5	0.2		
GLZ2a 40 34	0.0568	1.639	0.00204	1.731	1.4673	0.0009	18.35	0.281655	-1.1	1.0	1722	11
GLZ2a 40 33	0.0402	2.766	0.00133	2.366	1.4673	0.0010	17.73	0.281818	-6.9	0.7	1220	14
GLZ2a 40 32	0.0470	1.626	0.00152	2.168	1.4673	0.0016	13.40	0.281980	3.2	1.4	1408	9
GLZ2a 40 31	0.0467	0.694	0.00171	0.548	1.4673	0.0017	5.52	0.281951	2.6	2.8	1425	14
GLZ2a 40 30	0.0489	0.973	0.00152	1.205	1.4673	0.0012	15.77	0.281971	-28.8	0.8		
GLZ2a 40 29	0.0794	3.794	0.00217	3.947	1.4673	0.0014	20.39	0.281499	-45.5	1.3		
GLZ2a 40 28	0.0421	6.406	0.00128	5.500	1.4673	0.0011	18.42	0.281497	-2.1	1.9	1926	8
GLZ2a 40 27	0.0796	2.344	0.00233	2.335	1.4673	0.0010	21.92	0.281596	-42.1	1.0		
GLZ2a 40 26	0.0570	2.784	0.00185	2.211	1.4673	0.0017	15.03	0.281891	-31.6	1.8		
GLZ2a 40 25	0.0290	1.494	0.00084	1.063	1.4673	0.0012	15.98	0.281700	-5.3	0.6	1471	32
GLZ2a 40 24	0.0375	5.068	0.00114	4.562	1.4673	0.0006	20.76	0.281532	-44.3	0.2		
GLZ2a 40 23	0.0984	4.692	0.00272	4.357	1.4673	0.0012	26.07	0.281554	-43.5	0.5		
GLZ2a 40 22	0.0444	2.878	0.00135	2.319	1.4673	0.0011	18.45	0.281772	2.4	0.7	1694	9
GLZ2a 40 21	0.0642	4.018	0.00162	4.703	1.4673	0.0012	22.47	0.281851	-33.0	0.3		
GLZ2a 40 20	0.0655	5.189	0.00185	6.105	1.4673	0.0009	25.06	0.281808	4.0	1.2	1710	8
GLZ2a 40 17	0.0722	1.777	0.00250	1.473	1.4673	0.0010	19.66	0.281613	-2.1	0.7	1747	9
GLZ2a 40 16	0.0210	1.163	0.00067	1.068	1.4673	0.0010	20.23	0.281979	1.4	1.0	1332	13
GLZ2a 40 15	0.0309	5.641	0.00091	5.868	1.4673	0.0011	17.65	0.281395	-49.1	1.5		
GLZ2a 40 14	0.0555	3.183	0.00170	2.904	1.4673	0.0012	17.58	0.281642	-40.4	1.8		
GLZ2a 40 13	0.0476	1.969	0.00163	2.024	1.4673	0.0013	18.77	0.281525	-1.5	0.8	1909	9
GLZ2a 40 12	0.0290	5.553	0.00101	5.462	1.4673	0.0012	16.79	0.281600	-2.4	1.8	1753	10
GLZ2a 40 11	0.0213	1.456	0.00070	1.828	1.4673	0.0012	20.29	0.281466	-4.9	0.8	1850	9
GLZ2a 40 10	0.0697	2.185	0.00207	2.787	1.4673	0.0010	19.05	0.281482	-4.8	0.9	1830	8
GLZ2a 40 9	0.0740	3.351	0.00212	3.373	1.4673	0.0009	21.40	0.281515	-44.9	0.8		
GLZ2a 40 8	0.0314	1.395	0.00100	2.288	1.4673	0.0010	19.67	0.281727	0.9	1.8	1700	10
GLZ2a 40 7	0.0584	2.851	0.00164	1.838	1.4673	0.0012	19.92	0.281824	-34.0	0.5		
GLZ2a 40 6	0.0441	4.329	0.00141	3.767	1.4673	0.0009	21.09	0.281638	0.7	1.0	1827	10
GLZ2a 40 5	0.0359	2.399	0.00098	1.613	1.4673	0.0010	15.54	0.281632	2.3	1.0	1907	8
GLZ2a 40 4	0.0842	4.713	0.00264	4.128	1.4673	0.0010	23.47	0.281551	-43.6	0.2		
GLZ2a 40 3	0.0557	4.426	0.00178	3.507	1.4673	0.0011	17.10	0.281911	-30.9	0.6		
GLZ2a 40 2	0.1181	2.007	0.00386	2.194	1.4673	0.0013	18.51	0.281634	-40.7	0.6		
GLZ2a 40 1	0.1153	1.319	0.00357	1.535	1.4673	0.0010	18.30	0.281589	-42.3	0.3		
GLZ2a 33 19	0.0283	1.031	0.00096	0.721	1.4672	0.0013	10.46	0.281902	-4.1	0.7	1207	15
GLZ2a 33 18	0.0274	1.100	0.00095	0.885	1.4673	0.0015	10.39	0.281883	-4.8	1.1	1207	15
GLZ1a 40 130	0.0026	2.063	0.00007	0.696	1.4673	0.0009	16.23	0.281940	-0.8	0.5	1293	11
GLZ1a 40 129	0.0062	10.625	0.00019	10.493	1.4673	0.0009	22.48	0.282017	-27.2	0.2		
GLZ1a 40 128	0.0224	2.785	0.00073	2.031	1.4673	0.0011	19.58	0.282013	-4.0	0.5	1041	14
GLZ1a 40 127	0.0218	0.321	0.00078	0.689	1.4673	0.0012	19.38	0.281449	-4.7	0.6	1886	12
GLZ1a 40 126	0.0086	1.963	0.00030	1.717	1.4673	0.0010	19.06	0.282354	-15.2	0.1		
GLZ1a 40 125	0.0324	5.542	0.00103	5.133	1.4673	0.0013	14.81	0.282307	-16.9	0.3		
GLZ1a 40 124	0.0523	2.459	0.00175	2.357	1.4673	0.0010	13.69	0.281961	-29.1	0.2		
GLZ1a 40 123	0.0308	1.107	0.00103	0.775	1.4673	0.0009	17.42	0.280988	-3.2	1.0	2657	6
GLZ1a 40 122	0.0152	1.020	0.00063	1.685	1.4674	0.0018	14.86	0.282448	11.7	1.2	1055	13
GLZ1a 40 121	0.0198	1.745	0.00073	1.401	1.4673	0.0010	18.22	0.282316	5.4	0.3	981	21
GLZ1a 40 120	0.0137	0.778	0.00050	0.975	1.4673	0.0014	17.07	0.282313	-16.7	0.4		
GLZ1a 40 119	0.0279	3.213	0.00094	2.389	1.4673	0.0008	20.77	0.282261	6.7	0.5	1125	18
GLZ1a 40 118	0.0140	2.269	0.00048	2.605	1.4673	0.0010	21.84	0.282287	5.4	0.5	1025	14
GLZ1a 40 117	0.0155	2.401	0.00050	1.891	1.4673	0.0016	12.83	0.281524	-2.0	1.9	1886	9
GLZ1a 40 116	0.0221	2.177	0.00077	2.116	1.4673	0.0009	19.90	0.282228	3.4	0.4	1029	23
GLZ1a 40 113	0.0100	0.518	0.00036	0.914	1.4673	0.0008	22.08	0.282213	4.9	0.5	1118	16
GLZ1a 40 112	0.0144	0.641	0.00049	0.825	1.4673	0.0009	17.21	0.282183	-21.3	0.2		
GLZ1a 40 111	0.0267	1.412	0.00086	0.925	1.4673	0.0011	20.49	0.282266	-0.1	0.4	814	18
GLZ1a 40 110	0.0288	2.060	0.00095	1.884	1.4673	0.0008	20.52	0.282244	-1.9	0.4	771	17
GLZ1a 40 109	0.0152	0.981	0.00051	0.231	1.4673	0.0009	18.63	0.282387	-0.7	0.3	601	14
GLZ1a 40 107	0.0321	1.647	0.00105	1.113	1.4673	0.0010	15.69	0.280929	-5.0	0.9	2666	6
GLZ1a 40 106	0.0288	2.324	0.00093	3.019	1.4674	0.0013	17.38	0.282331	7.4	3.0	1047	14
GLZ1a 40 105	0.0524	5.809	0.00164	4.745	1.4674	0.0013	15.10	0.282272	4.8	1.7	1026	14
GLZ1a 40 104	0.0301	1.973	0.00105	1.745	1.4673	0.0008	16.88	0.281676	-14.6	0.5	1099	20
GLZ1a 40 103	0.0213	2.796	0.00071	2.956	1.4673	0.0016	9.27	0.282230	-19.6	0.8		
GLZ1a 40 100	0.0231	0.248	0.00076	0.538	1.4673	0.0009	17.18	0.281820	3.8	0.6	1683	10
GLZ1a 40 99	0.0376	1.815	0.00133	1.150	1.4673	0.0009	16.27	0.282287	5.2	0.4	1017	22
GLZ1a 40 98	0.0258	1.983	0.00084	2.225	1.4673	0.0009	18.44	0.282329	2.0	0.5	811	18
GLZ1a 40 97	0.0346	2.529	0.00119	2.366	1.4673	0.0010	16.21	0.282319	-16.5	0.2		
GLZ1a 40 96	0.0162	1.331	0.00056	0.785	1.4673	0.0009	19.88	0.282296	5.1	0.4	997	21
GLZ1a 40 95	0.0068	1.709	0.00027	1.409	1.4673	0.0014	17.63	0.282095	-13.2	2.4	502	11
GLZ1a 40 93	0.0251	3.419	0.00092	2.952	1.4673	0.0013	13.08	0.282407	-13.4	0.1		
GLZ1a 40 92	0.0216	2.204	0.00074	2.320	1.4673	0.0009	14.50	0.282456	-11.6	0.2		
GLZ1a 40 91	0.1079	1.902	0.00320	1.286	1.4673	0.0010	14.70	0.282207	4.6	0.4	1117	13
GLZ1a 40 90	0.0274	0.685	0.00086	0.309	1.4673	0.0012	11.20	0.282313	6.6	1.0	1040	10
GLZ1a 40 86	0.0119	4.621	0.00039	3.703	1.4673	0.0010	18.31	0.282453	-11.7	0.1		
GLZ1a 40 85	0.0159	1.711	0.00056	1.072	1.4673	0.0008	19.65	0.281232	-10.6	0.8	1963	8
GLZ1a 40 84	0.0496	1.401	0.00156	0.932	1.4673	0.0017	21.00	0.281883	-9.6	1.6	997	21
GLZ1a 40 83	0.0330	2.227	0.00111	2.778	1.4673	0.0009	22.96	0.281890	-31.6	0.2		
GLZ1a 40 81	0.0461	1.214	0.00160	1.087	1.4673	0.0009	16.28	0.282292	0.2	0.4	791	17
GLZ1a 40 80	0.0330	2.081	0.00111	2.839	1.4673	0.0012	15.14	0.282006	-27.6	0.4		
GLZ1a 40 79	0.0247	1.382	0.00083	0.823	1.4673	0.0008	19.62	0.281988	-2.8	0.5	1134	15
GLZ1a 40 78	0.0019	1.456	0.00005	1.401	1.4673	0.0008	20.32	0.282346	-15.5	0.1		

sample	$^{176}Yb/^{177}Hf$	1se %	$^{176}Lu/^{177}Hf$	1se	$^{178}Hf/^{177}Hf$ (1)	1se %	Hf_{total}(V)	(176/177)Hf_{Lu}	$\varepsilon Hf_{Lu\text{-}T}$	+/– 2σ	Age (Ma)	2s abs
GLZ1a 40 77	0.0139	3.363	0.00057	2.277	1.4674	0.0010	16.36	0.281539	-3.0	1.3	1819	6
GLZ1a 40 76	0.0255	1.710	0.00087	2.036	1.4673	0.0009	16.82	0.281412	-5.2	0.6	1918	10
GLZ1a 40 75	0.0308	2.846	0.00107	1.812	1.4673	0.0013	14.68	0.282250	6.0	0.6	1113	11
GLZ1a 40 74	0.0175	0.720	0.00060	0.731	1.4673	0.0008	16.06	0.282455	3.4	0.5	677	15
GLZ1a 40 73	0.0099	1.046	0.00033	1.585	1.4673	0.0011	18.83	0.282229	-19.7	0.2		
GLZ1a 40 72	0.0119	0.807	0.00042	1.590	1.4673	0.0009	18.80	0.282021	-3.0	0.6	1073	13
GLZ1a 40 71	0.0291	2.228	0.00096	2.392	1.4674	0.0008	17.38	0.282025	-0.9	0.5	1159	47
GLZ1a 40 70	0.0195	3.247	0.00062	1.975	1.4673	0.0008	21.30	0.282270	4.1	0.4	995	14
GLZ1a 40 69	0.0230	5.296	0.00078	5.400	1.4673	0.0010	15.78	0.282381	4.6	0.6	842	19
GLZ1a 40 68	0.0139	0.720	0.00049	0.387	1.4673	0.0009	17.13	0.282260	7.8	0.4	1174	25
GLZ1a 40 67	0.0346	2.200	0.00138	2.399	1.4674	0.0010	14.73	0.281363	-7.9	0.9	1877	9
GLZ1a 40 66	0.0238	1.052	0.00087	0.369	1.4673	0.0010	16.81	0.281413	-6.6	0.8	1856	10
GLZ1a 40 65	0.0232	2.933	0.00076	3.079	1.4673	0.0011	18.54	0.282177	2.3	0.7	1064	18
GLZ1a 40 64	0.0224	7.555	0.00074	6.818	1.4673	0.0009	16.22	0.282343	-15.6	0.2		
GLZ1a 40 63	0.0200	0.581	0.00077	0.710	1.4674	0.0018	9.93	0.282103	3.8	1.0	1241	19
GLZ1a 40 62	0.0180	5.743	0.00061	5.562	1.4673	0.0012	14.47	0.282361	0.3	0.4	686	16
GLZ1a 40 61	0.0112	0.524	0.00039	0.097	1.4673	0.0010	15.42	0.281320	-9.9	0.7	1859	9
GLZ1a 40 58	0.0251	1.090	0.00086	1.813	1.4673	0.0011	20.83	0.282290	-17.5	0.3		
GLZ1a 40 57	0.0213	3.645	0.00066	2.910	1.4673	0.0008	29.03	0.282178	-21.5	0.9		
GLZ1a 40 56	0.0275	0.884	0.00086	1.200	1.4674	0.0012	20.34	0.282074	-25.2	0.7		
GLZ1a 40 55	0.0153	1.980	0.00052	2.173	1.4676	0.0007	22.33	0.281531	-19.5	1.3	1109	15
GLZ1a 40 54	0.0190	0.928	0.00066	0.592	1.4675	0.0009	21.27	0.281456	-11.6	0.7	1577	16
GLZ1a 40 53	0.0372	4.002	0.00130	3.036	1.4675	0.0010	20.35	0.282351	-15.4	0.2		
GLZ1a 40 52	0.0494	3.125	0.00168	1.641	1.4676	0.0022	17.41	0.282421	-12.9	4.9		
GLZ1a 40 51	0.0244	9.584	0.00073	11.080	1.4675	0.0017	12.17	0.281543	0.9	1.8	1982	28
GLZ1a 40 50	0.0388	8.543	0.00112	9.038	1.4675	0.0010	19.87	0.281958	-0.3	0.6	1291	10
GLZ1a 40 48	0.0188	4.437	0.00058	4.922	1.4675	0.0009	19.62	0.282392	0.3	0.5	637	14
GLZ1a 40 47	0.0378	2.434	0.00123	2.343	1.4674	0.0011	19.25	0.282223	4.5	0.8	1085	11
GLZ1a 40 46	0.0536	2.830	0.00176	2.686	1.4674	0.0014	13.97	0.282240	4.0	0.8	1038	11
GLZ1a 40 45	0.0254	0.506	0.00091	1.174	1.4674	0.0010	23.96	0.281882	-9.2	0.6	1016	12
GLZ1a 40 44	0.0236	5.346	0.00082	4.729	1.4674	0.0010	15.53	0.282421	-12.9	0.2		
GLZ1a 40 42	0.0272	2.122	0.00106	1.318	1.4674	0.0012	16.80	0.281090	1.3	1.5	2691	6
GLZ1a 40 41	0.0182	5.641	0.00047	2.361	1.4675	0.0023	12.56	0.282263	5.7	5.1	1080	17
GLZ1a 40 40	0.0307	3.268	0.00103	3.563	1.4674	0.0011	16.88	0.281315	-6.1	0.9	2032	8
GLZ1a 40 39	0.0186	3.745	0.00054	3.072	1.4674	0.0009	20.35	0.282300	-17.2	0.9		
GLZ1a 40 38	0.0221	2.822	0.00062	3.341	1.4674	0.0010	19.51	0.282299	-17.2	0.7		
GLZ1a 40 37	0.0404	2.536	0.00138	2.510	1.4674	0.0008	18.46	0.282534	-8.9	0.5		
GLZ1a 40 35	0.0281	1.733	0.00093	1.946	1.4673	0.0018	20.14	0.282191	-21.0	1.2		
GLZ1a 40 34	0.0448	4.268	0.00139	4.486	1.4674	0.0016	17.36	0.282212	-20.3	2.4		
GLZ1a 40 33	0.0192	3.995	0.00062	3.320	1.4673	0.0012	16.31	0.282372	-14.6	0.2		
GLZ1a 40 32	0.0146	10.998	0.00050	11.336	1.4673	0.0007	21.86	0.281302	1.1	1.1	2360	8
GLZ1a 40 31	0.0392	2.499	0.00134	2.809	1.4673	0.0009	18.95	0.282385	-14.2	0.8		
GLZ1a 40 30	0.0382	1.483	0.00120	2.187	1.4673	0.0013	19.64	0.281889	-31.7	0.5		
GLZ1a 40 29	0.0207	1.483	0.00075	1.389	1.4673	0.0010	17.48	0.281620	-14.4	1.1	1197	39
GLZ1a 40 28	0.0317	3.458	0.00100	2.730	1.4673	0.0008	17.97	0.282285	7.2	0.5	1110	14
GLZ1a 40 27	0.0347	3.664	0.00112	2.746	1.4673	0.0010	17.96	0.281981	-3.3	1.1	1121	16
GLZ1a 40 26	0.0221	4.223	0.00084	4.060	1.4673	0.0016	11.46	0.282380	-14.3	1.0		
GLZ1a 40 25	0.0208	3.472	0.00070	3.596	1.4673	0.0016	14.65	0.282502	-10.0	0.5		
GLZ1a 40 24	0.0289	3.851	0.00092	2.467	1.4673	0.0009	24.85	0.282337	-15.9	0.2		
GLZ1a 40 23	0.0242	4.313	0.00084	4.459	1.4673	0.0012	18.40	0.282282	-2.6	1.4	680	16
GLZ1a 40 22	0.0248	2.578	0.00077	3.051	1.4673	0.0011	20.89	0.282388	-14.0	0.7		
GLZ1a 40 21	0.0389	2.391	0.00106	1.222	1.4679	0.0020	10.95	0.281975	-28.6	1.5		
GLZ1a 40 20	0.1214	2.555	0.00331	2.692	1.4672	0.0007	26.42	0.282484	-10.6	0.2		
GLZ1a 40 19	0.0185	8.682	0.00057	9.031	1.4672	0.0008	22.81	0.282103	0.1	0.5	1081	28
GLZ1a 40 18	0.0219	1.982	0.00073	1.741	1.4673	0.0010	18.23	0.282159	-2.2	0.7	892	19
GLZ1a 40 17	0.0027	4.612	0.00008	5.328	1.4673	0.0006	31.82	0.282437	-12.3	0.1		
GLZ1a 40 16	0.0207	7.388	0.00060	7.337	1.4673	0.0008	24.40	0.281969	-13.8	0.6	677	19
GLZ1a 40 15	0.0297	2.794	0.00095	2.647	1.4673	0.0009	23.85	0.282336	6.1	1.0	983	15
GLZ1a 40 14	0.0137	0.674	0.00048	0.785	1.4673	0.0007	22.03	0.281838	-9.3	0.4	1083	15
GLZ1a 40 13	0.0189	0.809	0.00068	0.645	1.4673	0.0012	16.81	0.282080	-0.8	0.6	1078	17
GLZ1a 40 12	0.0151	1.892	0.00056	1.740	1.4673	0.0011	16.06	0.282369	-14.7	0.5		
GLZ1a 40 11	0.0240	3.602	0.00074	2.886	1.4673	0.0011	22.59	0.282207	8.1	0.8	1269	11
GLZ1a 40 10	0.0423	1.603	0.00117	1.511	1.4673	0.0008	22.46	0.282354	-15.2	0.1		
GLZ1a 40 9	0.1049	3.025	0.00283	2.559	1.4673	0.0009	23.63	0.280960	-64.5	1.1		
GLZ1a 40 8	0.0464	0.599	0.00145	0.632	1.4673	0.0011	23.85	0.282358	-2.8	0.6	554	14
GLZ1a 40 7	0.0239	2.177	0.00076	2.090	1.4673	0.0012	16.74	0.282323	8.7	1.0	1115	27
GLZ1a 40 6	0.0532	0.525	0.00166	0.370	1.4673	0.0011	16.25	0.280969	1.0	1.2	2861	14
GLZ1a 40 5	0.0121	0.574	0.00042	0.385	1.4673	0.0010	20.64	0.282263	5.2	0.4	1056	17
GLZ1a 40 4	0.0697	3.360	0.00249	2.589	1.4673	0.0010	15.15	0.282267	5.3	0.8	1053	16
GLZ1a 40 3	0.0249	2.493	0.00086	2.317	1.4674	0.0010	19.53	0.282249	6.1	0.8	1117	15
GLZ1a 40 2	0.0273	3.002	0.00093	3.198	1.4674	0.0013	13.54	0.282559	-8.0	0.2		
GLZ1a 40 1	0.0275	2.262	0.00099	1.653	1.4674	0.0011	13.94	0.282329	5.9	0.7	984	14
GLZ1a 33 115	0.0211	1.346	0.00077	1.692	1.4673	0.0011	11.13	0.281813	-11.4	0.6	1028	10
GLZ1a 33 114	0.0479	5.810	0.00183	4.919	1.4673	0.0011	9.92	0.281641	-17.5	0.7	1028	10
GLZ1a 33 108	0.0155	2.004	0.00054	2.401	1.4673	0.0012	9.65	0.280947	-43.0	0.6	986	10
GLZ1a 33 102	0.0077	0.289	0.00027	0.481	1.4673	0.0014	10.54	0.282451	-11.8	0.2		
GLZ1a 33 101	0.0102	0.977	0.00036	0.667	1.4673	0.0012	9.98	0.282430	29.3	0.8	1848	10
GLZ1a 33 94	0.0080	0.738	0.00030	1.118	1.4673	0.0017	6.41	0.282484	13.3	0.9	1070	10
GLZ1a 33 89	0.0202	6.112	0.00076	4.627	1.4673	0.0010	10.58	0.281993	-3.1	0.4	1113	10
GLZ1a 33 88	0.0042	5.791	0.00019	4.057	1.4673	0.0016	9.46	0.282019	-5.2	0.6	978	10
GLZ1a 33 87	0.0093	1.153	0.00035	1.469	1.4673	0.0012	11.08	0.282494	8.2	1.3	826	10
GLZ1a 33 82	0.0083	3.800	0.00034	4.384	1.4673	0.0015	8.15	0.282463	0.1	0.7	517	10
GLZ1a 33 60	0.0083	3.854	0.00026	4.207	1.4673	0.0016	11.97	0.282058	-11.8	0.6	624	10
GLZ1a 33 59	0.0262	5.852	0.00083	6.092	1.4674	0.0017	8.13	0.282158	1.0	1.3	1035	10
KJA91-7 klein 40 seq1 A55	0.0628	1.783	0.00222	1.974	1.4669	0.0054	12.11	0.282150	7.7	1.3	1343	20
KJA91-7 klein 40 seq1 A55	0.0628	1.783	0.00222	1.974	1.4669	0.0054	12.11	0.282150	7.7	1.3	1343	20
KJA91-7 klein 40 seq1 A54	0.0640	1.985	0.00235	1.255	1.4670	0.0039	9.03	0.282155	7.9	1.0	1342	19
KJA91-7 klein 40 seq1 A52	0.0773	5.292	0.00286	4.996	1.4669	0.0047	9.51	0.282209	-20.4	1.1		

sample	$^{176}Yb/^{177}Hf$	1se %	$^{176}Lu/^{177}Hf$	1se	$^{178}Hf/^{177}Hf$ (1)	1se %	Hf_{total}(V)	(176/177)Hf_{Lu}	$\varepsilon Hf_{Lu\text{-}T}$	+/– 2σ	Age (Ma)	2s abs
KJA91-7 klein 40 seq1 A49	0.0687	1.297	0.00251	1.548	1.4668	0.0056	7.22	0.282132	7.5	1.6	1363	42
KJA91-7 klein 40 seq1 A48	0.0658	2.025	0.00232	1.118	1.4669	0.0046	7.68	0.282156	8.4	1.4	1364	35
KJA91-7 klein 40 seq1 A47	0.0642	1.479	0.00228	1.183	1.4670	0.0047	7.34	0.282208	-20.4	1.0		
KJA91-7 klein 40 seq1 A45	0.0525	4.073	0.00196	3.246	1.4673	0.0060	6.66	0.282192	-21.0	1.2		
KJA91-7 klein 40 seq1 A44	0.0569	0.943	0.00193	0.592	1.4670	0.0030	7.90	0.282157	6.5	0.8	1277	27
KJA91-7 klein 40 seq1 A42	0.0588	4.069	0.00203	3.172	1.4671	0.0038	9.05	0.282185	-21.2	0.5		
KJA91-7 klein 40 seq1 A41	0.0970	2.177	0.00319	1.348	1.4671	0.0031	7.29	0.282145	8.7	1.1	1392	38
KJA91-7 klein 40 seq1 A38	0.0704	1.360	0.00219	0.335	1.4671	0.0033	7.52	0.282145	6.3	0.8	1289	21
KJA91-7 klein 40 seq1 A37	0.0744	0.860	0.00256	1.133	1.4670	0.0029	7.52	0.282149	7.0	0.7	1314	15
KJA91-7 klein 40 seq1 A36	0.0588	4.028	0.00213	3.069	1.4670	0.0045	9.16	0.282205	8.9	1.1	1309	19
KJA91-7 klein 40 seq1 A35	0.0632	1.555	0.00234	0.498	1.4671	0.0027	12.91	0.282126	5.2	0.7	1269	17
KJA91-7 klein 40 seq1 A33	0.0694	0.800	0.00218	1.437	1.4671	0.0044	9.03	0.282144	6.2	0.7	1284	19
KJA91-7 klein 40 seq1 A32	0.0515	4.268	0.00192	1.582	1.4669	0.0070	8.73	0.282157	4.4	1.2	1185	57
KJA91-7 klein 40 seq1 A29	0.0733	2.616	0.00230	1.391	1.4672	0.0027	9.19	0.282139	6.2	1.0	1290	16
KJA91-7 klein 40 seq1 A28	0.0666	2.311	0.00209	1.195	1.4671	0.0031	8.62	0.282130	8.6	0.9	1411	20
KJA91-7 klein 40 seq1 A27	0.0648	2.037	0.00216	1.735	1.4670	0.0035	7.31	0.282096	7.9	1.0	1432	29
KJA91-7 klein 40 seq1 A26	0.0715	2.517	0.00239	1.367	1.4668	0.0053	6.54	0.282214	-20.2	0.9		
KJA91-7 klein 40 seq1 A25	0.0674	0.539	0.00240	1.102	1.4670	0.0067	5.69	0.282119	5.6	1.4	1297	20
KJA91-7 klein 40 seq1 A23	0.0600	1.904	0.00224	0.762	1.4670	0.0097	5.70	0.282192	-21.0	1.7		
KJA91-7 klein 40 seq1 A22	0.0742	2.821	0.00282	1.640	1.4668	0.0084	7.53	0.282212	-20.3	1.5		
KJA91-7 klein 40 seq1 A20	0.0563	1.181	0.00197	0.743	1.4670	0.0051	5.48	0.282060	9.2	1.7	1545	20
KJA91-7 klein 40 seq1 A17	0.0821	2.738	0.00283	1.953	1.4673	0.0063	5.97	0.282138	-22.9	1.0		
KJA91-7 klein 40 seq1 A16	0.0545	0.680	0.00195	1.120	1.4671	0.0082	5.34	0.282090	4.8	1.6	1309	19
KJA91-7 klein 40 seq1 A14	0.0564	1.462	0.00202	0.822	1.4671	0.0097	6.02	0.282127	6.2	2.0	1311	21
KJA91-7 klein 40 seq1 A13	0.0496	2.842	0.00183	1.790	1.4670	0.0079	5.87	0.282079	4.6	1.4	1317	27
KJA91-7 klein 40 seq1 A11	0.0373	2.184	0.00147	1.564	1.4669	0.0097	4.97	0.282092	11.1	2.0	1578	22
KJA91-7 klein 40 seq1 A10	0.0739	2.449	0.00261	2.042	1.4671	0.0092	7.91	0.282145	-22.6	1.5		
KJA91-7 klein 40 seq1 A08	0.0508	1.911	0.00179	1.163	1.4671	0.0066	5.97	0.282096	5.0	1.4	1309	22
KJA91-7 klein 40 seq1 A05	0.0623	3.617	0.00217	2.052	1.4670	0.0082	6.26	0.282092	7.2	2.0	1407	19
KJA91-7 klein 40 seq1 A04	0.0495	2.340	0.00185	1.086	1.4669	0.0069	5.85	0.282096	5.3	1.6	1318	16
KJA91-7 klein 40 seq1 A03	0.0805	3.257	0.00287	2.366	1.4671	0.0084	5.68	0.282169	-21.8	1.7		
KJA91-7 klein 40 seq1 A01	0.0644	1.193	0.00222	0.757	1.4669	0.0086	5.68	0.282068	4.0	1.8	1306	19
KK3Vbklein 40 seq3 A54	0.0424	5.441	0.00120	4.808	1.4673	0.0020	8.56	0.282053	0.4	0.8	1172	20
KK3Vbklein 40 seq3 A53	0.0275	11.826	0.00082	10.590	1.4675	0.0037	12.78	0.282123	-23.4	1.5		
KK3Vbklein 40 seq3 A52	0.0530	2.707	0.00159	2.182	1.4673	0.0020	7.98	0.282025	0.4	0.8	1214	22
KK3Vbklein 40 seq3 A51	0.0650	2.987	0.00222	3.432	1.4674	0.0034	11.76	0.282173	-21.6	3.2		
KK3Vbklein 40 seq3 A50	0.0313	2.443	0.00091	2.539	1.4673	0.0017	10.52	0.282056	-25.8	0.9		
KK3Vbklein 40 seq3 A48	0.0438	1.775	0.00130	1.243	1.4673	0.0016	9.82	0.281772	-9.9	1.0	1158	22
KK3Vbklein 40 seq3 A47	0.0459	1.810	0.00136	2.004	1.4674	0.0017	9.43	0.282046	0.8	0.8	1201	15
KK3Vbklein 40 seq3 A46	0.0475	3.103	0.00141	2.929	1.4672	0.0019	9.42	0.282082	-24.9	0.9		
KK3Vbklein 40 seq3 A45	0.0348	5.001	0.00104	4.703	1.4673	0.0015	10.40	0.282061	-0.4	0.7	1124	11
KK3Vbklein 40 seq3 A44	0.0043	1.686	0.00012	1.837	1.4673	0.0017	10.21	0.282120	1.4	0.8	1112	21
KK3Vbklein 40 seq3 A42	0.0074	6.851	0.00020	7.100	1.4673	0.0016	11.13	0.282088	2.2	0.9	1195	19
KK3Vbklein 40 seq3 A41	0.0073	3.414	0.00020	3.460	1.4673	0.0018	9.91	0.282078	0.1	0.8	1120	15
KK3Vbklein 40 seq3 A40	0.0051	7.845	0.00015	8.639	1.4673	0.0018	11.02	0.282109	1.3	1.1	1125	26
KK3Vbklein 40 seq3 A38	0.0189	2.226	0.00049	2.179	1.4673	0.0012	9.66	0.282059	0.5	0.9	1169	12
KK3Vbklein 40 seq3 A37	0.0247	9.055	0.00069	8.865	1.4672	0.0024	10.73	0.282055	0.0	1.0	1152	14
KK3Vbklein 40 seq3 A36	0.0140	9.217	0.00039	9.476	1.4673	0.0018	10.53	0.282094	2.1	1.0	1183	16
KK3Vbklein 40 seq3 A35	0.0131	3.132	0.00033	3.187	1.4672	0.0018	10.35	0.282083	1.8	0.9	1185	17
KK3Vbklein 40 seq3 A34	0.0316	2.617	0.00088	2.992	1.4673	0.0017	9.76	0.282085	0.8	0.8	1139	7
KK3Vbklein 40 seq3 A33	0.0121	5.749	0.00038	5.655	1.4673	0.0022	11.06	0.282107	1.1	1.1	1118	17
KK3Vbklein 40 seq3 A32	0.0254	9.109	0.00082	9.860	1.4674	0.0024	8.94	0.282101	0.8	1.4	1116	21
KK3Vbklein 40 seq3 A30	0.0512	2.476	0.00169	1.731	1.4674	0.0022	8.48	0.282061	1.6	0.9	1210	18
KK3Vbklein 40 seq3 A28	0.0039	3.243	0.00011	3.637	1.4673	0.0018	9.39	0.282094	0.8	1.1	1126	20
KK3Vbklein 40 seq3 A26	0.0179	7.276	0.00052	7.277	1.4673	0.0014	10.74	0.282084	0.8	0.9	1142	21
KK3Vbklein 40 seq3 A25	0.0259	2.085	0.00079	1.690	1.4673	0.0016	8.19	0.281808	-0.8	0.9	1502	26
KK3Vbklein 40 seq3 A22	0.0373	2.199	0.00118	2.954	1.4673	0.0023	6.88	0.282323	9.8	0.8	1162	32
KK3Vbklein 40 seq3 A21	0.0356	2.250	0.00102	2.416	1.4673	0.0023	7.30	0.282076	0.2	0.8	1126	17
KK3Vbklein 40 seq3 A19	0.0375	2.218	0.00108	1.928	1.4673	0.0023	6.86	0.282069	1.7	1.1	1206	19
KK3Vbklein 40 seq3 A18	0.0124	10.570	0.00037	10.612	1.4672	0.0021	8.08	0.282078	0.1	1.2	1120	13
KK3Vbklein 40 seq3 A16	0.0486	3.636	0.00144	3.490	1.4673	0.0020	7.63	0.282055	-0.1	1.1	1146	19
KK3Vbklein 40 seq3 A15	0.0175	11.632	0.00048	11.439	1.4673	0.0031	8.09	0.282076	1.3	1.2	1176	18
KK3Vbklein 40 seq3 A14	0.0142	5.653	0.00043	5.027	1.4673	0.0024	6.86	0.281984	-1.8	1.5	1183	20
KK3Vbklein 40 seq3 A13	0.0435	1.053	0.00125	0.816	1.4673	0.0028	7.08	0.282041	-0.7	0.9	1143	17
KK3Vbklein 40 seq3 A08	0.0326	6.005	0.00095	5.732	1.4673	0.0022	8.76	0.282061	1.4	1.0	1204	14
KK3Vbklein 40 seq3 A07	0.0227	4.920	0.00068	4.631	1.4673	0.0031	6.86	0.282070	0.2	1.5	1138	21
KK3Vbklein 40 seq3 A05	0.0373	2.103	0.00110	2.471	1.4672	0.0026	7.23	0.282058	4.0	0.9	1321	14
KK3Vbklein 40 seq3 A04	0.0384	2.001	0.00111	2.250	1.4673	0.0020	6.25	0.282111	2.0	1.2	1150	17
KK3Vbklein 40 seq3 A02	0.0383	14.701	0.00107	14.211	1.4673	0.0020	8.74	0.282049	0.7	0.8	1191	15
KK3Vbklein 40 seq3 A01	0.0378	1.474	0.00111	1.815	1.4673	0.0021	11.53	0.282055	0.9	0.8	1191	19
KK3Vbklein 40 seq2 A55	0.0206	3.292	0.00059	2.780	1.4673	0.0021	9.37	0.282102	-24.2	0.9		
KK3Vbklein 40 seq2 A54	0.0374	3.595	0.00110	3.758	1.4673	0.0014	9.59	0.282079	1.5	0.8	1179	17
KK3Vbklein 40 seq2 A53	0.0504	5.520	0.00150	5.435	1.4673	0.0014	9.59	0.282076	2.3	0.9	1220	19
KK3Vbklein 40 seq2 A51	0.0488	4.973	0.00144	4.944	1.4673	0.0019	9.80	0.282066	2.9	0.9	1262	21
KK3Vbklein 40 seq2 A49	0.0576	2.502	0.00171	2.066	1.4673	0.0020	9.78	0.282013	4.4	0.9	1407	15
KK3Vbklein 40 seq2 A48	0.0248	0.321	0.00072	0.462	1.4673	0.0020	6.94	0.282052	3.2	1.1	1295	31
KK3Vbklein 40 seq2 A46	0.0131	7.833	0.00035	7.644	1.4673	0.0020	9.36	0.282084	-24.8	0.8		
KK3Vbklein 40 seq2 A44	0.0475	10.531	0.00134	10.671	1.4674	0.0030	6.35	0.282105	0.9	1.2	1115	20
KK3Vbklein 40 seq2 A41	0.1041	2.916	0.00282	3.107	1.4673	0.0023	11.39	0.282107	-24.0	1.0		
KK3Vbklein 40 seq2 A38	0.0367	0.488	0.00112	0.702	1.4673	0.0019	7.44	0.281417	-11.8	1.0	1624	24
KK3Vbklein 40 seq2 A37	0.0429	5.688	0.00122	4.991	1.4673	0.0028	7.70	0.282079	1.6	1.0	1186	19
KK3Vbklein 40 seq2 A35	0.0180	4.960	0.00053	5.189	1.4673	0.0025	8.23	0.282111	-23.8	1.3		
KK3Vbklein 40 seq2 A31	0.0453	2.628	0.00136	2.794	1.4673	0.0030	6.61	0.282042	0.4	1.0	1188	16
KK3Vbklein 40 seq2 A29	0.0375	1.199	0.00116	1.107	1.4673	0.0031	5.44	0.281696	-38.5	1.2		
KK3Vbklein 40 seq2 A26	0.0445	0.823	0.00133	0.524	1.4673	0.0028	6.19	0.282099	2.3	1.0	1185	16
KK3Vbklein 40 seq2 A23	0.0264	1.473	0.00077	1.376	1.4673	0.0025	7.06	0.281468	-46.6	1.9		
KK3Vbklein 40 seq2 A20	0.0492	1.540	0.00145	1.065	1.4674	0.0023	7.57	0.282082	-24.8	0.9		
KK3Vbklein 40 seq2 A13	0.0232	1.786	0.00071	1.734	1.4673	0.0026	5.07	0.282050	4.3	1.1	1347	42

sample	$^{176}Yb/^{177}Hf$	1se %	$^{176}Lu/^{177}Hf$	1se	$^{178}Hf/^{177}Hf$ (1)	1se %	$Hf_{total}(V)$	$(176/177)Hf_{Lu}$	$\varepsilon Hf_{Lu\text{-}T}$	+/– 2σ	Age (Ma)	2s abs
KK3Vbklein 40 seq2 A11	0.0574	4.821	0.00169	4.814	1.4673	0.0024	8.00	0.282070	0.2	1.0	1136	17
KK3Vbklein 40 seq2 A08	0.0168	16.000	0.00051	16.422	1.4673	0.0028	7.98	0.282072	-0.1	1.4	1122	27
KK3Vbklein 40 seq2 A07	0.0450	0.437	0.00131	0.518	1.4673	0.0032	7.89	0.282063	-0.4	1.0	1121	15
KK3Vbklein 40 seq2 A05	0.0323	1.106	0.00096	0.909	1.4673	0.0032	5.68	0.282131	4.3	1.2	1222	14
KK3Vbklein 40 seq2 A03	0.0356	1.721	0.00104	1.770	1.4672	0.0032	6.71	0.282071	0.8	1.3	1162	13
KK3Vbklein 40 seq2 A1	0.0348	4.072	0.00101	4.224	1.4672	0.0031	6.32	0.282043	0.0	1.4	1167	9
KK3Vbgross 40 seq1 A33	0.0410	2.263	0.00115	1.893	1.4672	0.0036	4.26	0.282038	-0.1	1.7	1175	16
KK3Vbgross 40 seq1 A31	0.0201	3.070	0.00065	3.323	1.4672	0.0036	5.08	0.281813	-5.6	2.4	1283	19
KK3Vbgross 40 seq1 A27	0.1381	1.814	0.00386	1.474	1.4673	0.0039	4.81	0.281918	-1.1	2.0	1315	25
KK3Vbgross 40 seq1 A25	0.0243	0.694	0.00076	0.377	1.4673	0.0030	4.14	0.281801	-5.4	1.8	1311	19
KK3Vbgross 40 seq1 A24	0.0403	0.975	0.00113	0.585	1.4674	0.0044	4.31	0.282081	-24.9	1.4		
KK3Vbgross 40 seq1 A19	0.0270	1.025	0.00075	1.610	1.4672	0.0046	4.17	0.282046	0.9	1.7	1205	17
KK3Vbgross 40 seq1 A17	0.0312	4.308	0.00095	3.999	1.4672	0.0033	5.53	0.281698	-38.4	1.7		
KK3Vbgross 40 seq1 A16	0.0590	3.004	0.00169	2.976	1.4674	0.0031	5.78	0.282084	-24.8	0.9		
KK3Vbgross 40 seq1 A12	0.0664	1.803	0.00186	1.310	1.4673	0.0024	7.46	0.281961	13.3	0.8	1877	9
KK3Vbgross 40 seq1 A11	0.0253	9.505	0.00075	9.999	1.4674	0.0028	5.09	0.282075	0.3	1.5	1132	20
KK3Vbgross 40 seq1 A08	0.0154	3.237	0.00047	2.517	1.4673	0.0024	5.42	0.282114	4.2	1.7	1242	21
KK3Vbgross 40 seq1 A07	0.0504	4.625	0.00139	4.467	1.4672	0.0034	6.12	0.282062	1.3	1.1	1200	20
KK3Vbgross 40 seq1 A06	0.0322	2.065	0.00089	1.844	1.4673	0.0032	7.72	0.282064	0.2	1.2	1148	16
KK3Vbgross 40 seq1 A03	0.0301	5.635	0.00092	5.870	1.4673	0.0029	9.91	0.282051	-1.3	1.0	1101	16
KK3Vbgross 40 seq1 A02	0.0355	9.228	0.00102	9.637	1.4673	0.0035	8.02	0.282072	1.0	1.4	1170	16
KK3Vbgross 40 seq1 A01	0.0264	7.070	0.00077	7.313	1.4672	0.0026	7.20	0.282071	0.6	1.1	1150	17
KJA91 7 gross 40 seq1 A54	0.0403	0.840	0.00115	1.146	1.4671	0.0034	7.66	0.282116	-23.7	0.4		
KJA91 7 gross 40 seq1 A54	0.0403	0.840	0.00115	1.146	1.4671	0.0034	7.66	0.282116	-23.7	0.4		
KJA91 7 gross 40 seq1 A53	0.0849	0.777	0.00231	0.435	1.4672	0.0040	7.08	0.282127	3.9	0.9	1209	20
KJA91 7 gross 40 seq1 A51	0.0909	1.110	0.00251	1.595	1.4672	0.0052	7.16	0.282166	-21.9	0.9		
KJA91 7 gross 40 seq1 A49	0.0838	1.224	0.00234	1.495	1.4672	0.0041	6.82	0.282177	-21.5	0.5		
KJA91 7 gross 40 seq1 A47	0.0728	0.511	0.00212	0.625	1.4671	0.0042	6.96	0.282128	5.2	1.0	1268	14
KJA91 7 gross 40 seq1 A45	0.0779	0.897	0.00235	2.329	1.4669	0.0101	4.74	0.282118	9.0	2.2	1446	24
KJA91 7 gross 40 seq1 A44	0.1006	0.653	0.00280	0.706	1.4673	0.0117	5.12	0.282135	-23.0	1.8		
KJA91 7 gross 40 seq1 A41	0.0717	2.103	0.00211	2.009	1.4673	0.0081	3.80	0.282077	-25.1	1.5		
KJA91 7 gross 40 seq1 A39	0.0421	0.497	0.00122	0.773	1.4673	0.0110	4.33	0.282110	2.8	2.5	1187	19
KJA91 7 gross 40 seq1 A38	0.1474	0.762	0.00410	0.757	1.4672	0.0083	5.21	0.282175	6.7	2.2	1259	18
KJA91 7 gross 40 seq1 A35	0.0847	0.661	0.00242	0.879	1.4669	0.0117	5.26	0.282134	3.9	2.0	1200	15
KJA91 7 gross 40 seq1 A34	0.0865	1.135	0.00252	0.984	1.4672	0.0105	4.84	0.282138	3.9	2.0	1192	17
KJA91 7 gross 40 seq1 A32	0.0455	0.440	0.00126	0.508	1.4671	0.0043	6.37	0.282131	-23.1	0.8		
KJA91 7 gross 40 seq1 A29	0.0461	1.588	0.00132	1.201	1.4671	0.0056	5.91	0.282122	6.6	1.4	1334	28
KJA91 7 gross 40 seq1 A27	0.0737	0.736	0.00204	0.615	1.4671	0.0045	6.52	0.282166	-21.9	0.7		
KJA91 7 gross 40 seq1 A26	0.0809	0.824	0.00226	0.759	1.4670	0.0060	5.70	0.282186	-21.2	1.2		
KJA91 7 gross 40 seq1 A24	0.0724	0.640	0.00197	0.406	1.4669	0.0057	5.63	0.282130	7.1	1.2	1345	121
KJA91 7 gross 40 seq1 A22	0.0475	0.454	0.00131	0.716	1.4671	0.0064	5.75	0.282082	2.3	1.3	1211	24
KJA91 7 gross 40 seq1 A21	0.0630	2.744	0.00173	1.981	1.4672	0.0076	5.69	0.282155	-22.3	1.3		
KJA91 7 gross 40 seq1 A19	0.0922	1.151	0.00244	1.339	1.4670	0.0054	5.29	0.282152	4.5	1.1	1199	24
KJA91 7 gross 40 seq1 A17	0.0515	1.006	0.00140	0.674	1.4671	0.0044	5.62	0.282113	9.8	1.1	1493	21
KJA91 7 gross 40 seq1 A15	0.1301	0.674	0.00337	0.663	1.4671	0.0042	5.32	0.282191	9.6	1.4	1360	22
KJA91 7 gross 40 seq1 A13	0.0546	1.508	0.00150	1.798	1.4671	0.0050	6.28	0.282105	2.5	1.1	1184	18
KJA91 7 gross 40 seq1 A12	0.1010	1.647	0.00274	1.659	1.4671	0.0053	5.93	0.282205	-20.5	1.0		
KJA91 7 gross 40 seq1 A11	0.0700	1.367	0.00213	0.684	1.4669	0.0061	5.66	0.282146	-22.6	0.8		
KJA91 7 gross 40 seq1 A09	0.0604	0.567	0.00181	1.578	1.4670	0.0062	6.36	0.282149	-22.5	0.8		
KJA91 7 gross 40 seq1 A08	0.0422	0.980	0.00124	0.398	1.4672	0.0047	5.93	0.282137	-22.9	0.7		
KJA91 7 gross 40 seq1 A07	0.1139	1.022	0.00296	1.304	1.4672	0.0065	5.37	0.282204	-20.6	1.3		
KJA91 7 gross 40 seq1 A05	0.0409	0.929	0.00112	0.538	1.4671	0.0059	5.38	0.282126	-23.3	1.0		
KJA91 7 gross 40 seq1 A04	0.0971	1.166	0.00259	1.065	1.4671	0.0085	5.05	0.282204	-20.6	1.6		
KJA91 7 gross 40 seq1 A02	0.0638	1.728	0.00178	1.172	1.4671	0.0047	5.08	0.282164	7.4	1.8	1305	33
K3e 40 seq1 A46	0.0103	1.511	0.00031	1.861	1.4670	0.0042	7.24	0.282473	-11.0	0.4		
K3e 40 seq1 A45	0.0202	1.755	0.00057	1.993	1.4670	0.0041	6.78	0.282499	-10.1	0.8		
K3e 40 seq1 A44	0.0244	1.090	0.00094	1.039	1.4670	0.0049	5.97	0.282440	-12.2	0.9		
K3e 40 seq1 A43	0.0182	1.189	0.00056	1.565	1.4670	0.0030	9.87	0.282460	-11.5	0.3		
K3e 40 seq1 A42	0.0207	0.775	0.00060	0.722	1.4670	0.0035	8.65	0.282505	5.2	0.6	676	17
K3e 40 seq1 A39	0.0503	0.448	0.00146	0.631	1.4670	0.0032	8.68	0.281938	-29.9	0.6		
K3e 40 seq1 A38	0.0511	1.437	0.00132	1.515	1.4671	0.0038	11.05	0.282172	-21.7	0.7		
K3e 40 seq1 A37	0.0809	1.916	0.00222	1.451	1.4670	0.0031	10.28	0.282129	6.4	0.8	1316	20
K3e 40 seq1 A35	0.2522	3.266	0.00698	3.270	1.4666	0.0102	5.98	0.282646	-4.9	2.0		
K3e 40 seq1 A34	0.0035	3.571	0.00009	3.026	1.4672	0.0097	5.73	0.282758	-1.0	1.1		
K3e 40 seq1 A31	0.0482	2.190	0.00140	0.683	1.4670	0.0078	5.73	0.282529	-9.0	1.3		
K3e 40 seq1 A29	0.0509	1.367	0.00158	1.404	1.4668	0.0073	5.34	0.282029	-1.7	1.5	1119	51
K3e 40 seq1 A28	0.0443	1.019	0.00136	0.538	1.4667	0.0129	5.12	0.282436	-12.4	2.3		
K3e 40 seq1 A26	0.0300	11.372	0.00107	10.438	1.4666	0.0179	7.39	0.282204	-20.5	2.6		
K3e 40 seq1 A25	0.0229	3.389	0.00065	3.421	1.4671	0.0086	9.08	0.282448	2.2	1.4	634	16
K3e 40 seq1 A23	0.0239	2.009	0.00071	1.296	1.4671	0.0070	6.62	0.282474	1.8	1.0	573	19
K3e 40 seq1 A21	0.0093	1.960	0.00045	2.473	1.4671	0.0087	9.04	0.282093	-24.5	1.3		
K3e 40 seq1 A20	0.0317	2.548	0.00104	1.203	1.4669	0.0096	5.46	0.282339	-15.8	1.4		
K3e 40 seq1 A17	0.0875	5.096	0.00237	5.335	1.4669	0.0067	5.25	0.282128	0.5	1.7	1060	29
K3e 40 seq1 A16	0.0532	1.012	0.00157	1.238	1.4671	0.0099	6.42	0.282254	2.5	2.0	951	25
K3e 40 seq1 A14	0.0190	1.626	0.00060	2.156	1.4668	0.0119	5.70	0.282406	-13.4	1.7		
K3e 40 seq1 A13	0.0564	1.143	0.00181	0.824	1.4672	0.0093	4.90	0.282370	11.8	2.2	1181	51
K3e 40 seq1 A12	0.0545	1.167	0.00195	1.743	1.4669	0.0142	6.21	0.281803	-34.7	1.8		
K3e 40 seq1 A10	0.0432	0.776	0.00130	0.802	1.4671	0.0083	4.15	0.282075	5.2	1.4	1348	58
K3e 40 seq1 A08	0.0487	17.244	0.00132	14.665	1.4668	0.0105	5.42	0.282411	-13.2	1.4		
K3e 40 seq1 A07	0.0092	7.053	0.00041	5.748	1.4667	0.0161	6.47	0.282124	-23.4	2.4		
K3e 40 seq1 A06	0.0091	4.105	0.00038	3.818	1.4671	0.0130	7.92	0.282094	3.6	2.1	1248	32
K3e 40 seq1 A05	0.0636	2.987	0.00240	2.665	1.4671	0.0142	3.24	0.282067	22.7	3.2	2122	102
K3e 40 seq1 A02	0.0389	1.538	0.00137	2.315	1.4670	0.0067	6.12	0.282035	-26.5	1.5		

Table A5.1 Major element compositions of the analyzed samples. Values are reported in weight percent.

Sample	SiO_2	TiO_2	Al_2O_3	Cr_2O_3	FeO	MnO	MgO	CaO	NiO	Na_2O	K_2O	P_2O_5	SrO	Total
CNTP1 CPX1 rim	52.30	0.43	5.56	1.02	2.22	0.06	15.83	22.34	0.03	0.73	0.00	0.02	n.d.	100.54
CPX1 intermediate	51.90	0.45	6.00	1.12	2.16	0.09	15.71	22.47	0.04	0.73	0.01	0.01	n.d.	100.69
CPX1 core	52.83	0.36	4.72	0.76	2.24	0.08	16.25	22.19	0.04	0.70	0.01	0.02	n.d.	100.20
CPX2 rim	52.68	0.32	5.22	1.01	2.17	0.10	16.04	22.38	0.07	0.70	0.01	0.00	n.d.	100.69
CPX2 intermediate	51.53	0.47	6.03	1.15	2.27	0.10	15.72	22.15	0.07	0.76	0.01	0.00	n.d.	100.26
CPX2 core	51.22	0.45	5.76	1.17	2.27	0.06	15.42	21.97	0.04	0.77	0.01	0.01	n.d.	99.15
CPX3 rim	51.70	0.44	5.32	1.03	2.30	0.06	15.82	22.11	0.06	0.67	0.00	0.02	n.d.	99.53
CPX3 intermediate	51.32	0.33	4.94	0.96	2.29	0.09	16.04	22.29	0.00	0.66	0.01	0.02	n.d.	98.95
CPX3 core	50.88	0.46	5.97	1.13	2.28	0.08	15.60	22.10	0.05	0.74	0.02	0.00	n.d.	99.29
CNTP 1 OPX1 core	55.44	0.12	4.42	0.55	6.04	0.13	33.33	1.03	0.09	0.06	0.01	0.00	n.d.	101.22
OPX1 intermediate	55.33	0.13	4.46	0.53	6.05	0.14	33.31	0.73	0.08	0.03	0.00	0.00	n.d.	100.78
OPX1 rim	55.95	0.10	3.81	0.41	6.18	0.13	33.86	0.70	0.07	0.04	0.00	0.02	n.d.	101.26
OPX2 core	55.63	0.14	4.36	0.53	6.01	0.13	33.38	0.73	0.11	0.05	0.00	0.02	n.d.	101.09
OPX2 intermediate	55.11	0.12	4.27	0.50	6.05	0.14	32.88	1.21	0.08	0.05	0.00	0.00	n.d.	100.40
OPX2 rim	55.55	0.08	3.51	0.41	6.12	0.14	33.83	0.67	0.11	0.03	0.02	0.00	n.d.	100.47
OPX3 core	55.50	0.12	4.61	0.57	6.10	0.15	33.44	0.70	0.07	0.04	0.00	0.00	n.d.	101.28
OPX3 intermediate	55.48	0.10	4.53	0.57	6.11	0.17	33.33	0.68	0.08	0.03	0.00	0.00	n.d.	101.08
OPX3 rim	55.68	0.13	4.41	0.51	6.21	0.12	33.59	0.70	0.11	0.03	0.00	0.01	n.d.	101.50
CNTP1 Ol1 core	40.15	n.d.	n.d.	n.d.	9.10	0.14	49.30	0.06	0.39	n.d.	n.d.	n.d.	n.d.	99.13
Ol1 intermediate	40.53	n.d.	n.d.	n.d.	9.08	0.15	49.88	0.06	0.38	n.d.	n.d.	n.d.	n.d.	100.08
Ol1 rim	40.62	n.d.	n.d.	n.d.	9.09	0.15	49.74	0.05	0.36	n.d.	n.d.	n.d.	n.d.	100.02
Ol2 core	40.59	n.d.	n.d.	n.d.	9.06	0.13	49.87	0.05	0.37	n.d.	n.d.	n.d.	n.d.	100.07
Ol2 intermediate	40.23	n.d.	n.d.	n.d.	9.09	0.14	49.33	0.06	0.39	n.d.	n.d.	n.d.	n.d.	99.24
Ol2 rim	40.52	n.d.	n.d.	n.d.	9.08	0.13	49.77	0.05	0.37	n.d.	n.d.	n.d.	n.d.	99.92
Ol3 core	40.42	n.d.	n.d.	n.d.	9.16	0.13	49.66	0.05	0.36	n.d.	n.d.	n.d.	n.d.	99.77
Ol3 intermediate	40.58	n.d.	n.d.	n.d.	9.09	0.13	49.86	0.06	0.36	n.d.	n.d.	n.d.	n.d.	100.07
Ol3 rim	40.58	n.d.	n.d.	n.d.	9.10	0.14	49.85	0.05	0.36	n.d.	n.d.	n.d.	n.d.	100.08
CNTP2 CPX1 rim	52.52	0.13	5.03	1.40	2.25	0.09	15.88	21.07	0.05	1.22	0.00	0.00	n.d.	99.63
CPX1 core	58.32	0.14	5.20	1.60	2.29	0.10	12.93	17.69	0.05	1.07	0.09	0.00	n.d.	99.48
CPX1 btw	53.64	0.15	5.09	1.58	2.26	0.09	14.81	20.69	0.07	1.10	0.03	0.00	n.d.	99.52
CPX2 rim	53.22	0.09	4.86	1.54	2.15	0.08	15.88	21.62	0.04	1.05	0.01	0.01	n.d.	100.55
CPX2 btw	53.99	0.18	5.30	1.60	2.27	0.09	15.30	20.56	0.07	1.27	0.03	0.00	n.d.	100.66
CPX2 core	52.73	0.12	4.35	1.35	2.16	0.10	16.12	21.47	0.02	1.11	0.00	0.02	n.d.	99.54
CPX3 rim	51.85	0.14	4.81	1.48	2.17	0.09	15.92	21.75	0.05	0.98	0.00	0.00	n.d.	99.24
CPX3 btw	52.75	0.15	4.66	1.30	2.22	0.11	16.05	21.78	0.00	0.93	0.00	0.02	n.d.	99.97
CPX3 core	53.52	0.20	4.87	1.46	2.12	0.07	15.94	21.37	0.07	1.12	0.02	0.00	n.d.	100.75
CNTP 2 OPX1 core	56.23	0.03	3.50	0.63	5.75	0.14	34.07	0.63	0.10	0.04	0.00	0.00	n.d.	101.13
OPX1 intermediate	56.39	0.02	3.10	0.55	5.76	0.16	34.19	0.61	0.08	0.03	0.00	0.00	n.d.	100.88
OPX1 rim	56.58	0.04	2.98	0.49	5.84	0.13	34.36	0.62	0.10	0.03	0.01	0.02	n.d.	101.20
OPX2 core	56.42	0.04	2.96	0.53	5.80	0.16	34.24	0.65	0.12	0.04	0.00	0.00	n.d.	100.97
OPX2 intermediate	56.41	0.06	3.01	0.56	5.66	0.15	33.74	1.24	0.13	0.07	0.01	0.00	n.d.	101.03
OPX2 rim	56.42	0.04	3.10	0.54	5.80	0.12	34.24	0.71	0.08	0.04	0.01	0.00	n.d.	101.10
OPX3 core	56.30	0.07	3.46	0.64	5.77	0.15	34.00	0.72	0.10	0.06	0.01	0.00	n.d.	101.28
OPX3 intermediate	56.25	0.05	3.59	0.65	5.85	0.13	34.09	0.72	0.08	0.04	0.01	0.00	n.d.	101.45
OPX3 rim	56.03	0.05	3.17	0.53	5.75	0.16	34.23	0.62	0.11	0.05	0.00	0.00	n.d.	100.69
CNTP2 Ol1 core	40.73	n.d.	n.d.	n.d.	8.59	0.12	50.16	0.05	0.39	n.d.	n.d.	n.d.	n.d.	100.03
Ol1 intermediate	40.84	n.d.	n.d.	n.d.	8.53	0.14	50.50	0.05	0.38	n.d.	n.d.	n.d.	n.d.	100.44
Ol1 rim	40.55	n.d.	n.d.	n.d.	8.50	0.12	50.24	0.05	0.39	n.d.	n.d.	n.d.	n.d.	99.84
Ol2 core	40.54	n.d.	n.d.	n.d.	8.65	0.12	49.93	0.06	0.39	n.d.	n.d.	n.d.	n.d.	99.68
Ol2 intermediate	41.14	n.d.	n.d.	n.d.	8.63	0.14	50.32	0.06	0.38	n.d.	n.d.	n.d.	n.d.	100.67
Ol2 rim	40.73	n.d.	n.d.	n.d.	8.59	0.14	50.22	0.05	0.40	n.d.	n.d.	n.d.	n.d.	100.13
Ol3 core	40.85	n.d.	n.d.	n.d.	8.51	0.12	50.35	0.06	0.38	n.d.	n.d.	n.d.	n.d.	100.27
Ol3 intermediate	40.94	n.d.	n.d.	n.d.	8.54	0.14	50.60	0.05	0.38	n.d.	n.d.	n.d.	n.d.	100.65
Ol3 rim	40.70	n.d.	n.d.	n.d.	8.59	0.13	50.56	0.05	0.38	n.d.	n.d.	n.d.	n.d.	100.41
CNTP3 CPX1 rim	52.74	0.47	5.46	1.45	2.08	0.08	15.51	21.82	0.05	0.98	0.00	0.00	n.d.	100.64
CPX1 intermediate	52.65	0.48	5.44	1.48	2.13	0.08	15.59	21.84	0.07	0.95	0.02	0.00	n.d.	100.72
CPX1 core	53.87	0.33	4.27	1.33	2.20	0.08	15.85	21.59	0.06	0.84	0.01	0.00	n.d.	100.44
CPX2 rim	53.06	0.47	4.64	1.34	2.19	0.08	16.18	22.27	0.04	0.84	0.00	0.00	n.d.	101.12
CPX2 intermediate	53.20	0.51	5.20	1.44	2.23	0.09	15.54	21.57	0.02	0.93	0.00	0.03	n.d.	100.75
CPX2 core	51.96	0.43	5.84	1.41	2.14	0.08	15.51	21.75	0.05	1.01	0.00	0.03	n.d.	100.21
CPX3 rim	52.92	0.71	4.13	1.21	2.19	0.07	16.33	22.06	0.05	0.89	0.01	0.01	n.d.	100.56
CPX3 intermediate	51.89	0.49	5.25	1.32	2.37	0.09	16.66	20.96	0.07	0.88	0.00	0.01	n.d.	99.99
CPX3 core	53.81	0.45	5.06	1.36	2.67	0.10	17.60	17.96	0.06	0.83	0.03	0.00	n.d.	99.91
CNTP 3 OPX1 core	55.36	0.20	3.56	0.82	5.82	0.16	32.97	1.79	0.07	0.10	0.01	0.00	n.d.	100.85
OPX1 intermediate	55.58	0.21	3.55	0.81	5.65	0.14	32.45	2.35	0.10	0.12	0.00	0.00	n.d.	100.96
OPX1 rim	56.02	0.15	2.86	0.53	6.00	0.18	34.19	0.70	0.11	0.03	0.01	0.00	n.d.	100.78
OPX2 core	55.95	0.21	3.19	0.66	5.87	0.16	33.46	1.48	0.09	0.07	0.01	0.00	n.d.	101.14
OPX2 intermediate	56.06	0.18	2.77	0.51	5.95	0.14	34.25	0.68	0.09	0.04	0.00	0.00	n.d.	100.67
OPX2 rim	56.41	0.15	2.57	0.47	5.96	0.16	34.38	0.66	0.06	0.05	0.00	0.00	n.d.	100.87
OPX3 core	55.66	0.16	2.96	0.54	5.99	0.17	34.09	0.87	0.08	0.04	0.00	0.00	n.d.	100.57
OPX3 intermediate	56.05	0.14	2.79	0.47	5.94	0.15	34.18	0.71	0.07	0.02	0.01	0.00	n.d.	100.53
OPX3 rim	56.17	0.08	2.76	0.40	5.99	0.12	34.35	0.66	0.09	0.03	0.00	0.01	n.d.	100.66
CNTP3 Ol1 core	40.65	n.d.	n.d.	n.d.	8.77	0.13	50.27	0.05	0.38	n.d.	n.d.	n.d.	n.d.	100.25
Ol1 intermediate	40.77	n.d.	n.d.	n.d.	8.79	0.15	50.27	0.05	0.38	n.d.	n.d.	n.d.	n.d.	100.40
Ol1 rim	40.69	n.d.	n.d.	n.d.	8.80	0.14	50.25	0.05	0.39	n.d.	n.d.	n.d.	n.d.	100.31
Ol2 core	40.53	n.d.	n.d.	n.d.	8.86	0.14	49.56	0.05	0.37	n.d.	n.d.	n.d.	n.d.	99.50
Ol2 intermediate	40.31	n.d.	n.d.	n.d.	8.84	0.13	49.72	0.05	0.37	n.d.	n.d.	n.d.	n.d.	99.42
Ol2 rim	40.87	n.d.	n.d.	n.d.	8.89	0.15	50.10	0.05	0.38	n.d.	n.d.	n.d.	n.d.	100.43
Ol3 core	40.63	n.d.	n.d.	n.d.	8.87	0.15	50.12	0.05	0.38	n.d.	n.d.	n.d.	n.d.	100.20
Ol3 intermediate	41.08	n.d.	n.d.	n.d.	8.84	0.14	50.47	0.05	0.39	n.d.	n.d.	n.d.	n.d.	100.97
Ol3 rim	39.53	n.d.	n.d.	n.d.	8.91	0.13	48.45	0.05	0.39	n.d.	n.d.	n.d.	n.d.	97.46

Sample	SiO_2	TiO_2	Al_2O_3	Cr_2O_3	FeO	MnO	MgO	CaO	NiO	Na_2O	K_2O	P_2O_5	SrO	Total
CNTP3 Plag1 core	56.25	0.00	26.47	0.02	0.11	0.00	0.04	9.33	0.00	6.05	0.34	0.00	0.052	98.66
Plag1 intermediate	56.75	0.01	26.78	0.00	0.11	0.02	0.04	9.38	0.00	6.10	0.31	0.00	0.025	99.53
Plag1 rim	57.14	0.01	27.08	0.00	0.10	0.05	0.07	9.36	0.00	6.21	0.35	0.00	0.031	100.40
Plag2 core	56.89	0.04	27.33	0.00	0.11	0.00	0.04	9.55	0.00	6.07	0.34	0.00	0.039	100.41
Plag2 intermediate	56.32	0.00	26.91	0.00	0.10	0.02	0.05	9.60	0.00	6.01	0.34	0.00	0.023	99.37
Plag2 rim	56.53	0.04	27.11	0.00	0.07	0.00	0.06	9.68	0.04	6.04	0.31	0.00	0.045	99.93
Plag4 core	56.32	0.02	27.16	0.00	0.16	0.01	0.05	9.66	0.02	6.12	0.29	0.00	0.014	99.81
Plag4 intermediate	56.18	0.01	27.30	0.02	0.15	0.00	0.04	9.93	0.00	5.92	0.29	0.00	0	99.84
Plag4 rim	56.16	0.00	27.24	0.01	0.18	0.00	0.06	9.73	0.00	5.93	0.28	0.00	0.023	99.61
Plag5 core	56.12	0.01	27.50	0.03	0.14	0.02	0.08	9.79	0.02	6.03	0.22	0.00	0.06	100.01
Plag5 intermediate	56.14	0.03	27.66	0.00	0.17	0.01	0.05	10.08	0.00	6.00	0.23	0.00	0.07	100.44
Plag5 rim	56.27	0.00	27.50	0.00	0.12	0.02	0.07	10.01	0.00	5.99	0.22	0.00	0.048	100.24
CNTP4 CPX1 rim	52.42	0.41	5.70	1.20	2.25	0.09	15.76	21.86	0.06	1.01	0.00	0.00	n.d.	100.76
CPX1 btw	52.92	0.45	5.42	1.15	2.20	0.09	15.94	22.11	0.06	0.88	0.00	0.01	n.d.	101.23
CPX1 core	52.12	0.44	5.46	1.13	2.26	0.09	15.62	21.76	0.06	0.87	0.00	0.00	n.d.	99.80
CPX2 rim	53.02	0.44	4.83	1.01	2.19	0.07	16.21	22.48	0.08	0.76	0.00	0.00	n.d.	101.08
CPX2 btw	52.48	0.43	5.89	1.31	2.23	0.08	15.61	21.74	0.04	0.90	0.02	0.03	n.d.	100.74
CPX2 core	52.56	0.43	5.81	1.25	2.30	0.09	15.71	21.71	0.02	1.05	0.00	0.00	n.d.	100.92
CPX3 rim	52.85	0.37	5.71	1.21	2.24	0.07	15.67	21.73	0.07	1.07	0.00	0.01	n.d.	101.00
CPX3 btw	52.04	0.37	5.94	1.34	2.22	0.07	15.54	21.71	0.04	1.06	0.01	0.01	n.d.	100.35
CPX3 core	52.18	0.39	6.03	1.32	2.24	0.08	15.68	21.35	0.07	1.00	0.02	0.01	n.d.	100.38
CNTP 4 OPX1 core	55.42	0.15	4.01	0.53	5.75	0.14	33.03	1.85	0.10	0.08	0.00	0.00	n.d.	101.07
OPX1 intermediate	55.80	0.13	3.96	0.50	6.02	0.17	33.82	0.76	0.11	0.04	0.00	0.00	n.d.	101.30
OPX1 rim	56.37	0.09	3.41	0.42	5.99	0.16	34.23	0.66	0.07	0.05	0.00	0.00	n.d.	101.46
OPX2 core	56.10	0.11	3.80	0.50	5.91	0.16	33.77	0.64	0.09	0.04	0.00	0.00	n.d.	101.11
OPX2 intermediate	56.32	0.11	3.58	0.45	5.98	0.13	33.86	0.68	0.11	0.03	0.00	0.00	n.d.	101.25
OPX2 rim	56.11	0.09	3.09	0.36	6.01	0.14	34.38	0.63	0.08	0.02	0.00	0.00	n.d.	100.90
OPX3 core	55.95	0.12	3.83	0.49	5.92	0.14	33.74	0.75	0.09	0.04	0.01	0.00	n.d.	101.08
OPX3 intermediate	56.14	0.13	3.68	0.47	5.84	0.16	33.83	0.62	0.09	0.05	0.01	0.02	n.d.	101.04
OPX3 rim	56.03	0.10	3.58	0.46	5.96	0.13	33.99	0.64	0.11	0.03	0.01	0.00	n.d.	101.05
CNTP4 Ol1 core	40.69	n.d.	n.d.	n.d.	8.78	0.14	50.21	0.05	0.39	n.d.	n.d.	n.d.	n.d.	100.26
Ol1 intermediate	40.60	n.d.	n.d.	n.d.	8.75	0.13	50.11	0.05	0.38	n.d.	n.d.	n.d.	n.d.	100.02
Ol1 rim	40.49	n.d.	n.d.	n.d.	8.75	0.12	49.78	0.05	0.38	n.d.	n.d.	n.d.	n.d.	99.57
Ol2 core	40.67	n.d.	n.d.	n.d.	8.75	0.14	50.27	0.05	0.38	n.d.	n.d.	n.d.	n.d.	100.26
Ol2 intermediate	40.37	n.d.	n.d.	n.d.	8.69	0.14	49.92	0.05	0.39	n.d.	n.d.	n.d.	n.d.	99.57
Ol2 rim	40.60	n.d.	n.d.	n.d.	8.76	0.15	50.11	0.05	0.38	n.d.	n.d.	n.d.	n.d.	100.04
Ol3 core	38.24	n.d.	n.d.	n.d.	8.72	0.15	46.74	0.06	0.35	n.d.	n.d.	n.d.	n.d.	94.26
Ol3 intermediate	40.61	n.d.	n.d.	n.d.	8.60	0.13	48.67	0.07	0.39	n.d.	n.d.	n.d.	n.d.	98.47
Ol3 rim	40.49	n.d.	n.d.	n.d.	8.76	0.13	49.94	0.05	0.37	n.d.	n.d.	n.d.	n.d.	99.74
CNTP5 CPX1 rim	54.24	0.26	3.43	0.75	2.40	0.09	16.70	22.33	0.08	0.83	0.01	0.01	n.d.	101.12
CPX1 btw	53.16	0.50	4.31	1.10	2.27	0.07	16.09	22.17	0.07	0.88	0.00	0.03	n.d.	100.65
CPX1 core	53.20	0.58	4.76	1.29	2.19	0.10	15.39	21.50	0.01	0.86	0.02	0.00	n.d.	99.90
CPX2 rim	52.34	0.47	4.51	1.17	2.31	0.09	16.17	22.03	0.04	0.95	0.00	0.01	n.d.	100.09
CPX2 btw	52.51	0.54	4.92	1.34	2.26	0.11	16.01	21.84	0.00	0.91	0.01	0.03	n.d.	100.48
CPX2 core	52.52	0.49	4.89	1.26	2.32	0.11	15.94	21.63	0.05	0.97	0.01	0.00	n.d.	100.20
CPX3 rim	52.92	0.54	4.44	1.14	2.27	0.09	15.80	21.93	0.07	0.88	0.01	0.00	n.d.	100.09
CPX3 btw	52.88	0.62	5.70	1.21	2.30	0.09	15.63	21.80	0.02	0.97	0.00	0.00	n.d.	101.22
CPX3 core	52.98	0.65	4.81	1.25	2.10	0.12	15.90	22.16	0.04	0.91	0.00	0.01	n.d.	100.92
CNTP 5 OPX1 core	55.50	0.17	3.68	0.70	5.98	0.16	33.19	1.13	0.10	0.05	0.01	0.00	n.d.	100.66
OPX1 intermediate	55.84	0.17	3.49	0.62	6.13	0.17	33.70	0.87	0.09	0.05	0.00	0.00	n.d.	101.12
OPX1 rim	56.70	0.12	2.86	0.43	6.21	0.17	33.97	0.63	0.08	0.02	0.00	0.00	n.d.	101.18
OPX2 core	55.64	0.19	3.59	0.68	6.02	0.15	33.30	1.23	0.06	0.05	0.01	0.00	n.d.	100.91
OPX2 intermediate	55.83	0.19	3.46	0.61	6.10	0.16	33.97	0.76	0.09	0.06	0.00	0.00	n.d.	101.23
OPX2 rim	55.93	0.18	3.16	0.52	6.21	0.16	34.01	0.75	0.08	0.05	0.00	0.00	n.d.	101.04
OPX3 core	56.10	0.16	3.16	0.56	6.13	0.15	33.71	0.79	0.06	0.05	0.01	0.00	n.d.	100.88
OPX3 intermediate	55.81	0.18	3.48	0.62	6.19	0.14	33.57	0.79	0.07	0.04	0.00	0.02	n.d.	100.92
OPX3 rim	55.98	0.14	3.27	0.56	6.14	0.17	33.65	0.77	0.09	0.05	0.00	0.00	n.d.	100.81
CNTP5 Ol1 core	40.61	n.d.	n.d.	n.d.	9.18	0.14	49.88	0.05	0.37	n.d.	n.d.	n.d.	n.d.	100.23
Ol1 intermediate	40.62	n.d.	n.d.	n.d.	9.09	0.14	50.01	0.05	0.37	n.d.	n.d.	n.d.	n.d.	100.27
Ol1 rim	40.70	n.d.	n.d.	n.d.	9.20	0.14	50.06	0.05	0.39	n.d.	n.d.	n.d.	n.d.	100.54
Ol2 core	40.89	n.d.	n.d.	n.d.	9.11	0.13	50.19	0.05	0.37	n.d.	n.d.	n.d.	n.d.	100.75
Ol2 intermediate	40.79	n.d.	n.d.	n.d.	9.12	0.14	50.04	0.05	0.36	n.d.	n.d.	n.d.	n.d.	100.50
Ol2 rim	40.79	n.d.	n.d.	n.d.	9.13	0.14	49.97	0.05	0.37	n.d.	n.d.	n.d.	n.d.	100.45
Ol3 core	40.57	n.d.	n.d.	n.d.	9.08	0.15	49.91	0.05	0.36	n.d.	n.d.	n.d.	n.d.	100.12
Ol3 intermediate	40.65	n.d.	n.d.	n.d.	9.06	0.13	49.90	0.05	0.35	n.d.	n.d.	n.d.	n.d.	100.14
Ol3 rim	39.46	n.d.	n.d.	n.d.	9.07	0.14	47.57	0.06	0.36	n.d.	n.d.	n.d.	n.d.	96.66
CNTP5 Plag1 core	55.42	0.01	28.20	0.01	0.05	0.00	0.04	10.71	0.00	5.39	0.30	0.00	0.088	100.21
Plag1 intermediate	55.10	0.04	28.19	0.02	0.08	0.01	0.06	10.64	0.01	5.42	0.33	0.00	0.082	99.99
Plag1 rim	55.55	0.00	27.92	0.00	0.18	0.03	0.06	10.41	0.01	5.53	0.36	0.00	0.101	100.14
Plag2 core	55.06	0.00	28.23	0.00	0.12	0.02	0.04	10.72	0.00	5.38	0.32	0.00	0.08	99.96
Plag2 intermediate	55.27	0.02	28.25	0.00	0.09	0.02	0.05	10.75	0.00	5.35	0.32	0.00	0.088	100.20
Plag2 rim	55.75	0.01	27.86	0.00	0.11	0.01	0.05	10.40	0.02	5.54	0.36	0.00	0.09	100.20
Plag3 core	55.11	0.00	28.23	0.00	0.09	0.05	0.04	10.81	0.04	5.41	0.34	0.00	0.119	100.24
Plag3 intermediate	55.38	0.04	28.16	0.00	0.11	0.00	0.04	10.93	0.00	5.43	0.31	0.00	0.075	100.47
Plag3 rim	55.31	0.00	28.05	0.00	0.18	0.00	0.07	10.62	0.00	5.51	0.34	0.00	0.092	100.17

Sample	SiO_2	TiO_2	Al_2O_3	Cr_2O_3	FeO	MnO	MgO	CaO	NiO	Na_2O	K_2O	P_2O_5	SrO	Total
Plag4 core	54.97	0.04	28.00	0.00	0.05	0.00	0.05	11.04	0.00	5.35	0.28	0.00	0.032	99.82
Plag4 intermediate	55.01	0.02	28.26	0.00	0.09	0.02	0.07	10.81	0.00	5.32	0.29	0.00	0.043	99.93
Plag4 rim	55.25	0.02	27.89	0.00	0.17	0.02	0.06	10.65	0.05	5.66	0.31	0.00	0.032	100.10
Plag5 core	55.07	0.02	27.91	0.01	0.08	0.02	0.04	10.74	0.00	5.39	0.34	0.00	0.037	99.65
Plag5 intermediate	55.28	0.03	27.98	0.02	0.10	0.01	0.05	10.77	0.04	5.53	0.36	0.00	0.045	100.20
Plag5 rim	55.45	0.02	27.67	0.00	0.14	0.00	0.04	10.33	0.00	5.61	0.38	0.00	0.069	99.70
CNTP6 CPX1 core	52.39	0.23	5.44	1.33	2.30	0.08	16.06	21.48	0.02	1.07	0.00	0.00	n.d.	100.39
CPX1 intermediate	52.38	0.22	5.48	1.28	2.31	0.09	16.02	21.18	0.04	1.12	0.01	0.00	n.d.	100.13
CPX1 rim	52.60	0.23	4.85	1.12	2.17	0.08	16.39	21.61	0.03	0.94	0.00	0.00	n.d.	100.02
CPX2 core	52.48	0.24	5.10	1.17	2.30	0.08	16.24	21.31	0.05	1.09	0.00	0.00	n.d.	100.06
CPX2 intermediate	52.94	0.23	4.65	0.98	2.28	0.09	16.47	21.79	0.00	0.97	0.01	0.02	n.d.	100.44
CPX2 rim	53.06	0.21	4.28	0.94	2.18	0.09	16.64	22.12	0.06	0.86	0.01	0.01	n.d.	100.45
CPX3 core	52.26	0.19	5.61	1.36	2.29	0.09	15.99	21.31	0.05	1.15	0.00	0.00	n.d.	100.30
CPX3 intermediate	52.28	0.22	5.55	1.34	2.25	0.07	16.02	21.30	0.07	1.12	0.01	0.00	n.d.	100.22
CPX3 rim	52.33	0.20	5.14	1.23	2.23	0.09	16.24	21.76	0.02	1.07	0.00	0.00	n.d.	100.31
CNTP6 OPX1 core	55.31	0.07	3.95	0.62	6.47	0.17	33.27	0.68	0.09	0.05	0.00	0.00	n.d.	100.67
OPX1 intermediate	55.46	0.05	3.57	0.58	6.53	0.18	33.72	0.66	0.08	0.08	0.00	0.01	n.d.	100.91
OPX1 rim	55.32	0.07	3.52	0.51	6.58	0.20	33.57	0.70	0.10	0.06	0.00	0.01	n.d.	100.63
OPX2 core	55.44	0.06	3.72	0.58	5.93	0.15	33.97	0.70	0.05	0.07	0.00	0.00	n.d.	100.66
OPX2 intermediate	55.24	0.06	3.70	0.57	5.97	0.17	33.82	0.70	0.10	0.05	0.01	0.00	n.d.	100.38
OPX2 rim	55.66	0.05	3.42	0.50	5.96	0.16	34.17	0.66	0.09	0.04	0.00	0.02	n.d.	100.72
OPX3 core	55.47	0.06	3.97	0.61	6.46	0.16	33.42	0.83	0.09	0.05	0.00	0.00	n.d.	101.11
OPX3 intermediate	55.39	0.03	3.80	0.55	6.46	0.14	33.38	0.75	0.07	0.07	0.00	0.01	n.d.	100.65
OPX3 rim	55.74	0.07	3.27	0.47	6.38	0.19	33.70	0.69	0.10	0.07	0.00	0.00	n.d.	100.66
CNTP6 Ol1 core	40.90	n.d.	n.d.	n.d.	8.89	0.13	50.53	0.05	0.38	n.d.	n.d.	n.d.	n.d.	100.89
Ol1 intermediate	40.97	n.d.	n.d.	n.d.	8.94	0.12	50.49	0.05	0.39	n.d.	n.d.	n.d.	n.d.	100.97
Ol1 rim	40.76	n.d.	n.d.	n.d.	8.99	0.13	50.25	0.05	0.38	n.d.	n.d.	n.d.	n.d.	100.56
Ol2 core	40.66	n.d.	n.d.	n.d.	9.03	0.12	50.18	0.05	0.37	n.d.	n.d.	n.d.	n.d.	100.41
Ol2 intermediate	40.48	n.d.	n.d.	n.d.	8.99	0.13	50.18	0.05	0.38	n.d.	n.d.	n.d.	n.d.	100.22
Ol2 rim	40.99	n.d.	n.d.	n.d.	8.99	0.15	50.77	0.05	0.37	n.d.	n.d.	n.d.	n.d.	101.32
Ol3 core	40.56	n.d.	n.d.	n.d.	9.65	0.15	49.55	0.05	0.38	n.d.	n.d.	n.d.	n.d.	100.34
Ol3 intermediate	40.63	n.d.	n.d.	n.d.	9.74	0.16	49.60	0.05	0.37	n.d.	n.d.	n.d.	n.d.	100.55
Ol3 rim	40.39	n.d.	n.d.	n.d.	9.64	0.16	49.38	0.05	0.38	n.d.	n.d.	n.d.	n.d.	100.00
CNTP7 CPX1 rim	51.46	0.38	6.18	1.08	2.39	0.08	15.36	22.04	0.02	1.11	0.00	0.02	n.d.	100.12
CPX1 btw	52.76	0.20	4.90	0.98	2.51	0.12	15.52	21.33	0.06	0.93	0.01	0.00	n.d.	99.32
CPX1 core	51.95	0.44	6.23	1.09	2.32	0.07	15.19	21.82	0.06	1.07	0.00	0.00	n.d.	100.23
CPX2 rim	52.38	0.24	4.97	1.04	2.36	0.05	15.78	21.84	0.07	0.89	0.00	0.00	n.d.	99.62
CPX2 btw	52.90	0.20	4.57	0.92	2.33	0.08	16.31	22.15	0.03	0.84	0.01	0.03	n.d.	100.37
CPX2 core	52.99	0.18	4.69	1.02	2.38	0.07	16.09	21.76	0.03	0.98	0.00	0.00	n.d.	100.18
CPX3 rim	52.86	0.29	4.45	0.85	2.47	0.07	16.30	22.09	0.05	0.81	0.00	0.02	n.d.	100.25
CPX3 btw	53.57	0.22	3.93	0.74	2.49	0.07	16.58	22.29	0.05	0.81	0.00	0.00	n.d.	100.75
CPX3 core	54.11	0.11	3.38	0.68	2.52	0.12	16.53	22.22	0.06	0.77	0.02	0.03	n.d.	100.55
CNTP 7 OPX1 core	54.84	0.12	4.17	0.44	7.48	0.16	32.55	0.78	0.06	0.06	0.00	0.00	n.d.	100.66
OPX1 intermediate	55.02	0.09	4.11	0.50	7.27	0.14	32.95	0.63	0.11	0.04	0.00	0.03	n.d.	100.88
OPX1 rim	55.46	0.07	3.82	0.40	7.58	0.16	33.04	0.65	0.12	0.05	0.00	0.01	n.d.	101.36
OPX2 core	54.92	0.11	4.90	0.60	6.38	0.14	33.06	0.68	0.10	0.05	0.01	0.02	n.d.	100.95
OPX2 intermediate	55.30	0.11	4.78	0.57	6.39	0.14	33.35	0.66	0.10	0.05	0.00	0.01	n.d.	101.45
OPX2 rim	55.99	0.09	3.10	0.39	6.50	0.17	33.73	0.64	0.09	0.03	0.00	0.00	n.d.	100.72
OPX3 core	54.74	0.13	4.48	0.51	7.64	0.16	32.24	0.92	0.10	0.09	0.01	0.02	n.d.	101.03
OPX3 intermediate	54.98	0.11	4.48	0.48	7.57	0.18	32.29	0.71	0.10	0.05	0.00	0.00	n.d.	100.96
OPX3 rim	54.50	0.11	4.43	0.50	7.72	0.17	32.24	0.70	0.12	0.05	0.01	0.00	n.d.	100.56
CNTP7 Ol1 core	40.08	n.d.	n.d.	n.d.	11.91	0.17	47.71	0.05	0.36	n.d.	n.d.	n.d.	n.d.	100.28
Ol1 intermediate	40.24	n.d.	n.d.	n.d.	11.81	0.17	47.73	0.05	0.37	n.d.	n.d.	n.d.	n.d.	100.37
Ol1 rim	40.18	n.d.	n.d.	n.d.	11.81	0.19	47.55	0.05	0.37	n.d.	n.d.	n.d.	n.d.	100.15
Ol2 core	40.56	n.d.	n.d.	n.d.	9.67	0.15	49.42	0.05	0.37	n.d.	n.d.	n.d.	n.d.	100.22
Ol2 intermediate	40.56	n.d.	n.d.	n.d.	9.56	0.16	49.50	0.05	0.38	n.d.	n.d.	n.d.	n.d.	100.21
Ol2 rim	40.60	n.d.	n.d.	n.d.	9.56	0.15	49.54	0.05	0.40	n.d.	n.d.	n.d.	n.d.	100.30
Ol3 core	40.47	n.d.	n.d.	n.d.	9.80	0.15	49.44	0.05	0.37	n.d.	n.d.	n.d.	n.d.	100.28
Ol3 intermediate	41.02	n.d.	n.d.	n.d.	9.76	0.14	49.97	0.05	0.41	n.d.	n.d.	n.d.	n.d.	101.35
Ol3 rim	40.41	n.d.	n.d.	n.d.	9.77	0.15	49.15	0.05	0.39	n.d.	n.d.	n.d.	n.d.	99.91
CNTP7 Plag4 core	55.75	0.00	27.21	0.00	0.15	0.02	0.06	9.73	0.03	5.99	0.38	0.03	0.157	99.49
Plag4 intermediate	57.56	0.00	26.08	0.00	0.23	0.00	0.05	8.42	0.00	6.62	0.46	0.03	0.157	99.59
Plag4 rim	57.49	0.02	26.33	0.02	0.20	0.01	0.05	8.90	0.00	6.37	0.46	0.05	0.15	100.04
Plag5 core	55.54	0.01	27.33	0.00	0.09	0.00	0.05	10.19	0.01	5.76	0.35	0.04	0.145	99.51
Plag5 intermediate	55.71	0.00	27.44	0.00	0.14	0.00	0.05	10.04	0.00	5.73	0.35	0.02	0.133	99.61
Plag5 rim	56.11	0.00	27.18	0.00	0.13	0.00	0.07	9.85	0.01	5.90	0.37	0.07	0.125	99.81
Plag6 core	55.26	0.02	27.83	0.00	0.14	0.00	0.05	10.44	0.01	5.59	0.30	0.03	0.178	99.85
Plag6 intermediate	55.74	0.02	27.41	0.00	0.15	0.03	0.07	10.15	0.00	5.85	0.34	0.02	0.154	99.93
Plag6 rim	55.66	0.00	27.42	0.02	0.19	0.04	0.06	10.21	0.01	5.85	0.38	0.01	0.155	100.00
CNTP8 CPX1 rim	52.86	0.45	5.29	0.91	2.75	0.08	15.84	21.95	0.03	0.86	0.00	0.00	n.d.	101.02
CPX1 core	52.01	0.49	6.65	1.12	2.48	0.07	15.31	21.55	0.05	0.99	0.01	0.01	n.d.	100.75
CPX1 btw	51.82	0.50	6.51	1.22	2.43	0.11	15.34	21.55	0.02	1.03	0.00	0.00	n.d.	100.53
CPX2 rim	52.50	0.47	5.92	0.78	2.67	0.09	15.89	21.57	0.08	0.92	0.11	0.01	n.d.	101.01
CPX2 core	52.71	0.55	5.61	0.98	2.62	0.09	15.51	22.05	0.04	0.85	0.00	0.00	n.d.	101.02
CPX2 btw	52.60	0.49	5.58	0.97	2.47	0.11	15.57	22.17	0.03	0.87	0.00	0.02	n.d.	100.88
CPX3 rim	52.84	0.43	5.29	0.91	2.65	0.11	15.92	21.81	0.06	0.89	0.02	0.02	n.d.	100.95
CPX3 core	52.32	0.47	6.24	1.04	2.33	0.09	15.52	21.54	0.07	0.98	0.00	0.00	n.d.	100.59
CPX3 btw	52.06	0.48	6.06	1.01	2.60	0.07	15.49	21.59	0.01	0.89	0.00	0.01	n.d.	100.27

Sample	SiO_2	TiO_2	Al_2O_3	Cr_2O_3	FeO	MnO	MgO	CaO	NiO	Na_2O	K_2O	P_2O_5	SrO	Total
CNTP 8 OPX1 core	55.61	0.12	4.41	0.57	6.21	0.13	33.00	1.23	0.10	0.08	0.00	0.00	n.d.	101.47
OPX1 intermediate	55.58	0.13	4.67	0.60	6.19	0.16	33.06	0.94	0.08	0.05	0.00	0.02	n.d.	101.47
OPX1 rim	55.48	0.13	4.59	0.57	6.28	0.16	33.43	0.69	0.12	0.05	0.00	0.00	n.d.	101.50
OPX2 core	55.57	0.15	4.65	0.56	6.21	0.13	33.15	0.69	0.08	0.04	0.00	0.01	n.d.	101.24
OPX2 intermediate	55.49	0.13	4.59	0.57	6.30	0.13	32.75	1.16	0.07	0.05	0.00	0.00	n.d.	101.23
OPX2 rim	55.95	0.13	4.28	0.50	6.32	0.16	33.42	0.69	0.07	0.04	0.01	0.02	n.d.	101.60
OPX3 core	55.47	0.13	4.48	0.55	6.18	0.16	33.13	0.90	0.13	0.07	0.01	0.00	n.d.	101.21
OPX3 intermediate	55.56	0.15	4.59	0.55	6.04	0.13	32.37	2.02	0.10	0.09	0.00	0.01	n.d.	101.61
OPX3 rim	56.07	0.14	3.78	0.44	6.39	0.15	33.54	0.66	0.13	0.05	0.01	0.00	n.d.	101.35
CNTP8 Ol1 core	40.59	n.d.	n.d.	n.d.	9.49	0.14	49.68	0.05	0.38	n.d.	n.d.	n.d.	n.d.	100.33
Ol1 intermediate	40.42	n.d.	n.d.	n.d.	9.47	0.15	49.53	0.05	0.36	n.d.	n.d.	n.d.	n.d.	99.99
Ol1 rim	40.43	n.d.	n.d.	n.d.	9.49	0.14	49.65	0.05	0.37	n.d.	n.d.	n.d.	n.d.	100.14
Ol2 core	40.51	n.d.	n.d.	n.d.	9.26	0.16	49.64	0.05	0.39	n.d.	n.d.	n.d.	n.d.	100.01
Ol2 intermediate	40.51	n.d.	n.d.	n.d.	9.27	0.15	49.46	0.05	0.37	n.d.	n.d.	n.d.	n.d.	99.81
Ol2 rim	40.51	n.d.	n.d.	n.d.	9.30	0.14	49.52	0.05	0.38	n.d.	n.d.	n.d.	n.d.	99.90
Ol3 core	40.42	n.d.	n.d.	n.d.	9.26	0.15	49.60	0.05	0.35	n.d.	n.d.	n.d.	n.d.	99.83
Ol3 intermediate	40.25	n.d.	n.d.	n.d.	9.37	0.15	49.69	0.05	0.37	n.d.	n.d.	n.d.	n.d.	99.88
Ol3 rim	40.24	n.d.	n.d.	n.d.	9.29	0.11	49.63	0.05	0.37	n.d.	n.d.	n.d.	n.d.	99.69
CNTP9 CPX1 rim	53.33	0.45	4.50	1.16	2.22	0.08	16.17	22.09	0.06	0.82	0.00	0.01	n.d.	100.89
CPX1 core	53.03	0.59	4.81	1.29	2.19	0.09	16.03	22.08	0.02	0.86	0.00	0.01	n.d.	101.01
CPX1 btw	52.64	0.77	4.87	1.27	2.20	0.07	15.82	21.84	0.00	0.91	0.00	0.00	n.d.	100.39
CPX2 rim	52.91	0.58	4.57	1.27	2.32	0.08	16.32	21.99	0.07	0.89	0.00	0.02	n.d.	101.01
CPX2 core	52.46	0.86	4.91	1.34	2.16	0.11	15.92	21.98	0.09	0.92	0.01	0.00	n.d.	100.74
CPX2 btw	52.93	0.57	4.56	1.27	2.26	0.08	16.07	21.88	0.01	0.87	0.00	0.01	n.d.	100.53
CPX3 rim	53.08	0.44	4.52	1.05	2.22	0.08	16.21	22.30	0.00	0.79	0.00	0.02	n.d.	100.72
CPX3 core	52.23	0.73	5.29	1.31	2.21	0.10	15.68	22.07	0.05	0.92	0.00	0.02	n.d.	100.59
CPX3 btw	52.66	0.61	5.16	1.20	2.27	0.07	15.97	22.04	0.06	0.87	0.00	0.00	n.d.	100.90
CNTP 9 OPX1 core	57.08	0.15	2.66	0.46	6.05	0.15	34.33	0.65	0.12	0.05	0.00	0.01	n.d.	101.70
OPX1 intermediate	56.45	0.25	3.25	0.56	6.07	0.13	34.00	0.71	0.11	0.04	0.00	0.00	n.d.	101.57
OPX1 rim	56.76	0.16	3.00	0.45	6.16	0.16	34.00	0.67	0.10	0.05	0.00	0.00	n.d.	101.51
OPX2 core	56.01	0.24	3.12	0.58	6.18	0.13	33.90	0.76	0.11	0.04	0.01	0.00	n.d.	101.08
OPX2 intermediate	55.69	0.26	3.21	0.65	6.11	0.15	33.63	0.82	0.09	0.04	0.01	0.00	n.d.	100.65
OPX2 rim	56.06	0.24	3.06	0.55	5.99	0.16	33.64	0.79	0.10	0.03	0.00	0.00	n.d.	100.62
OPX3 core	56.00	0.23	3.33	0.59	6.08	0.16	33.63	0.73	0.09	0.05	0.01	0.00	n.d.	100.90
OPX3 intermediate	56.50	0.21	3.12	0.53	5.98	0.13	34.07	0.71	0.09	0.07	0.01	0.00	n.d.	101.43
OPX3 rim	56.92	0.11	2.76	0.45	6.00	0.15	34.19	0.67	0.09	0.06	0.01	0.02	n.d.	101.43
CNTP9 Ol1 core	40.66	n.d.	n.d.	n.d.	8.89	0.12	49.67	0.04	0.41	n.d.	n.d.	n.d.	n.d.	99.80
Ol1 intermediate	40.62	n.d.	n.d.	n.d.	8.93	0.14	49.80	0.04	0.42	n.d.	n.d.	n.d.	n.d.	99.96
Ol1 rim	40.22	n.d.	n.d.	n.d.	8.83	0.14	49.42	0.05	0.39	n.d.	n.d.	n.d.	n.d.	99.04
Ol2 core	40.53	n.d.	n.d.	n.d.	8.93	0.14	49.99	0.05	0.39	n.d.	n.d.	n.d.	n.d.	100.03
Ol2 intermediate	40.70	n.d.	n.d.	n.d.	8.86	0.14	50.03	0.05	0.38	n.d.	n.d.	n.d.	n.d.	100.15
Ol2 rim	40.50	n.d.	n.d.	n.d.	8.87	0.15	49.83	0.05	0.41	n.d.	n.d.	n.d.	n.d.	99.81
Ol3 core	40.46	n.d.	n.d.	n.d.	8.88	0.14	49.70	0.06	0.41	n.d.	n.d.	n.d.	n.d.	99.65
Ol3 intermediate	40.71	n.d.	n.d.	n.d.	8.83	0.12	50.05	0.05	0.41	n.d.	n.d.	n.d.	n.d.	100.17
Ol3 rim	40.45	n.d.	n.d.	n.d.	8.72	0.12	49.84	0.12	0.41	n.d.	n.d.	n.d.	n.d.	99.66
CNTP9 Plag2 core	55.96	0.02	27.40	0.00	0.05	0.01	0.04	9.72	0.00	6.26	0.33	0.02	0.055	99.86
Plag2 intermediate	55.77	0.07	27.03	0.00	0.30	0.01	0.14	9.67	0.05	6.01	0.32	0.04	0.075	99.48
Plag2 rim	55.67	0.04	27.68	0.01	0.08	0.02	0.06	10.16	0.05	5.96	0.30	0.06	0.088	100.18
Plag5 core	55.98	0.02	27.22	0.01	0.12	0.02	0.05	9.65	0.01	6.37	0.28	0.04	0.058	99.83
Plag5 intermediate	56.22	0.03	27.22	0.00	0.11	0.02	0.05	9.48	0.02	6.29	0.33	0.01	0.04	99.83
Plag5 rim	55.90	0.00	27.47	0.00	0.21	0.02	0.04	9.88	0.00	6.11	0.34	0.05	0.033	100.05
Plag6 core	56.19	0.00	27.17	0.00	0.05	0.00	0.06	9.85	0.01	6.10	0.34	0.02	0.068	99.85
Plag6 intermediate	56.07	0.03	27.07	0.00	0.09	0.03	0.06	9.81	0.03	6.09	0.34	0.04	0.052	99.70
Plag6 rim	56.14	0.02	27.25	0.00	0.14	0.00	0.06	9.86	0.01	6.15	0.35	0.03	0.084	100.09
CNTP10 CPX rim	52.13	0.38	5.98	1.14	2.21	0.08	15.86	22.20	0.04	0.68	0.00	0.02	n.d.	100.73
CPX core	51.97	0.44	6.29	1.18	2.24	0.05	15.80	21.78	0.07	0.83	0.00	0.01	n.d.	100.66
CPX btw	52.43	0.44	5.84	1.10	2.23	0.10	15.75	22.26	0.04	0.73	0.01	0.02	n.d.	100.95
CPX2 rim	52.65	0.36	5.27	0.99	2.22	0.07	16.05	22.34	0.03	0.69	0.00	0.02	n.d.	100.68
CPX2 core	52.51	0.46	5.65	1.00	2.24	0.10	15.73	22.29	0.06	0.72	0.00	0.00	n.d.	100.77
CPX2 btw	52.41	0.40	6.27	1.15	2.30	0.07	15.74	22.03	0.01	0.82	0.00	0.01	n.d.	101.21
CPX3 rim	52.44	0.39	5.70	1.03	2.21	0.08	15.75	22.32	0.08	0.69	0.00	0.02	n.d.	100.70
CPX3 core	52.05	0.41	6.53	1.23	2.26	0.10	15.78	21.94	0.09	0.85	0.00	0.01	n.d.	101.25
CPX3 btw	52.65	0.44	5.46	1.01	2.16	0.09	15.98	22.23	0.07	0.67	0.00	0.01	n.d.	100.78
CNTP 10 OPX1 core	55.05	0.12	3.98	0.46	5.97	0.15	33.21	1.19	0.08	0.06	0.00	0.00	n.d.	100.26
OPX1 intermediate	55.34	0.11	4.16	0.47	5.95	0.13	33.42	0.75	0.10	0.05	0.01	0.00	n.d.	100.50
OPX1 rim	55.16	0.12	4.06	0.48	6.15	0.15	33.50	0.78	0.06	0.06	0.00	0.00	n.d.	100.52
OPX2 core	55.02	0.16	4.47	0.50	6.04	0.17	33.21	1.25	0.10	0.05	0.00	0.00	n.d.	100.97
OPX2 intermediate	54.92	0.13	4.54	0.54	6.07	0.15	32.98	1.17	0.10	0.06	0.00	0.00	n.d.	100.66
OPX2 rim	55.57	0.09	3.92	0.42	6.09	0.14	33.69	0.73	0.08	0.05	0.00	0.00	n.d.	100.78
OPX3 core	54.91	0.12	4.82	0.61	5.88	0.13	32.53	1.38	0.10	0.07	0.01	0.00	n.d.	100.56
OPX3 intermediate	54.58	0.15	5.02	0.60	6.02	0.15	33.06	0.80	0.09	0.04	0.00	0.01	n.d.	100.53
OPX3 rim	55.07	0.10	4.15	0.49	6.03	0.18	33.48	0.70	0.12	0.03	0.00	0.00	n.d.	100.35
CNTP10 Ol1 core	40.82	n.d.	n.d.	n.d.	9.11	0.13	49.83	0.06	0.39	n.d.	n.d.	n.d.	n.d.	100.34
Ol1 intermediate	40.73	n.d.	n.d.	n.d.	9.06	0.15	49.78	0.05	0.38	n.d.	n.d.	n.d.	n.d.	100.15
Ol1 rim	40.84	n.d.	n.d.	n.d.	9.07	0.14	49.88	0.05	0.40	n.d.	n.d.	n.d.	n.d.	100.38
Ol2 core	40.57	n.d.	n.d.	n.d.	9.14	0.12	49.74	0.05	0.40	n.d.	n.d.	n.d.	n.d.	100.02
Ol2 intermediate	40.64	n.d.	n.d.	n.d.	9.05	0.14	49.84	0.06	0.36	n.d.	n.d.	n.d.	n.d.	100.09
Ol2 rim	40.77	n.d.	n.d.	n.d.	9.10	0.14	49.91	0.06	0.39	n.d.	n.d.	n.d.	n.d.	100.36
Ol3 core	40.85	n.d.	n.d.	n.d.	9.09	0.13	50.06	0.05	0.37	n.d.	n.d.	n.d.	n.d.	100.55
Ol3 intermediate	40.72	n.d.	n.d.	n.d.	9.14	0.13	50.12	0.05	0.37	n.d.	n.d.	n.d.	n.d.	100.53
Ol3 rim	40.72	n.d.	n.d.	n.d.	9.03	0.15	49.97	0.06	0.39	n.d.	n.d.	n.d.	n.d.	100.32

Sample	SiO_2	TiO_2	Al_2O_3	Cr_2O_3	FeO	MnO	MgO	CaO	NiO	Na_2O	K_2O	P_2O_5	SrO	Total
CNTP11 CPX1 rim	52.53	0.57	4.46	0.83	2.24	0.08	16.21	22.28	0.06	0.77	0.00	0.00	n.d.	100.03
CPX1 core	52.28	0.59	4.95	1.10	2.20	0.10	15.75	22.35	0.06	0.78	0.00	0.00	n.d.	100.16
CPX1 btw	52.30	0.70	5.25	1.15	2.21	0.07	15.85	22.27	0.07	0.88	0.00	0.00	n.d.	100.74
CPX2 rim	53.41	0.48	4.42	0.89	2.28	0.10	16.45	22.29	0.04	0.72	0.00	0.02	n.d.	101.09
CPX2 core	51.88	0.70	5.37	1.06	2.29	0.09	15.84	22.02	0.09	0.84	0.00	0.00	n.d.	100.19
CPX2 btw	52.23	0.66	5.18	1.05	2.27	0.09	15.72	22.20	0.05	0.82	0.00	0.04	n.d.	100.31
CPX3 rim	51.56	0.55	5.12	1.09	2.29	0.08	15.71	22.08	0.04	0.83	0.00	0.00	n.d.	99.35
CPX3 core	52.23	0.68	5.48	1.09	2.17	0.11	15.61	22.22	0.06	0.83	0.00	0.03	n.d.	100.52
CPX3 btw	52.33	0.63	5.70	1.09	2.28	0.08	15.68	21.90	0.07	0.87	0.00	0.01	n.d.	100.64
CNTP 11 OPX1 core	56.13	0.17	3.70	0.56	6.31	0.13	33.43	0.78	0.05	0.34	0.02	0.00	n.d.	101.62
OPX1 intermediate	55.97	0.17	3.78	0.54	6.32	0.18	33.35	0.80	0.10	0.09	0.00	0.00	n.d.	101.30
OPX1 rim	56.23	0.13	3.43	0.49	6.28	0.15	33.45	0.71	0.06	0.07	0.01	0.00	n.d.	101.01
OPX2 core	56.01	0.19	3.78	0.58	6.07	0.14	32.61	1.87	0.08	0.07	0.01	0.00	n.d.	101.42
OPX2 intermediate	56.22	0.18	3.85	0.55	6.26	0.17	33.41	0.83	0.11	0.05	0.00	0.00	n.d.	101.62
OPX2 rim	56.62	0.12	3.31	0.39	6.32	0.17	33.86	0.67	0.13	0.03	0.00	0.00	n.d.	101.62
OPX3 core	56.11	0.18	3.64	0.52	6.28	0.17	33.45	0.73	0.09	0.05	0.00	0.00	n.d.	101.21
OPX3 intermediate	56.06	0.15	3.68	0.51	6.35	0.17	33.52	0.65	0.07	0.06	0.00	0.00	n.d.	101.21
OPX3 rim	56.45	0.09	3.15	0.34	6.24	0.18	33.64	0.65	0.11	0.04	0.01	0.01	n.d.	100.91
CNTP11 Ol1 core	40.66	n.d.	n.d.	n.d.	9.27	0.15	49.82	0.05	0.36	n.d.	n.d.	n.d.	n.d.	100.31
Ol1 intermediate	40.76	n.d.	n.d.	n.d.	9.25	0.13	49.91	0.05	0.37	n.d.	n.d.	n.d.	n.d.	100.48
Ol1 rim	40.59	n.d.	n.d.	n.d.	9.30	0.14	50.00	0.05	0.36	n.d.	n.d.	n.d.	n.d.	100.44
Ol2 core	40.76	n.d.	n.d.	n.d.	9.16	0.13	49.80	0.05	0.37	n.d.	n.d.	n.d.	n.d.	100.27
Ol2 intermediate	40.74	n.d.	n.d.	n.d.	9.22	0.14	49.92	0.05	0.36	n.d.	n.d.	n.d.	n.d.	100.44
Ol2 rim	40.51	n.d.	n.d.	n.d.	9.22	0.15	49.88	0.05	0.36	n.d.	n.d.	n.d.	n.d.	100.17
Ol3 core	40.65	n.d.	n.d.	n.d.	9.28	0.14	49.76	0.05	0.37	n.d.	n.d.	n.d.	n.d.	100.25
Ol3 intermediate	40.76	n.d.	n.d.	n.d.	9.25	0.13	49.94	0.05	0.38	n.d.	n.d.	n.d.	n.d.	100.52
Ol3 rim	40.45	n.d.	n.d.	n.d.	9.27	0.14	49.54	0.05	0.37	n.d.	n.d.	n.d.	n.d.	99.83
CNTP11 Plag1 core	53.68	0.00	28.80	0.02	0.07	0.00	0.05	12.06	0.01	5.07	0.03	0.01	0.025	99.82
Plag1 intermediate	53.71	0.02	28.78	0.02	0.07	0.00	0.05	11.86	0.01	5.02	0.04	0.00	0.05	99.63
Plag1 rim	53.80	0.02	28.55	0.00	0.10	0.03	0.05	11.83	0.03	5.22	0.05	0.01	0.036	99.73
Plag4 core	53.69	0.03	28.44	0.01	0.08	0.00	0.07	11.85	0.01	4.90	0.04	0.02	0.038	99.18
Plag4 intermediate	53.46	0.00	28.69	0.00	0.07	0.01	0.06	11.92	0.04	4.99	0.04	0.00	0.023	99.30
Plag4 rim	53.32	0.04	28.43	0.00	0.09	0.02	0.07	11.99	0.01	4.87	0.02	0.01	0.041	98.91

Table A5.2 Trace element compositions of the analysed samples. Values are reported in ppm.

CNTP1	CPX1	CPX1	CPX1	CPX2	CPX2	CPX2	CPX3	CPX3	CPX3
Li	4.89	5.65	5.8	6.05	5.8	6.05	6.85	5.95	5.38
Na	5525.74	4840.95	5267.54	5160.07	5363.12	5346.21	4247.97	5055.53	5389.49
Ca	n.d.	n.d.	n.d.	n.d.	n.d.	n.d.	n.d.	n.d.	n.d.
Sc	68.53	62.01	68.63	66.4	70.63	72.61	52.1	63.96	72.18
V	252.06	249.24	260.54	253.09	258.87	259.12	204.66	254.22	261.32
Cr	7356.17	7938.83	7418.49	8106.44	7251.2	7578.32	5697.36	7760.06	7412.37
Co	24.94	30.54	26.15	26.69	24.12	23.29	58.48	27.26	24.06
Ni	473.4	438.94	483.01	386.2	376.4	354.68	1534.15	394.93	388.44
Ga	3.15	3.86	3.34	3.32	3.21	3.26	2.63	3.41	3.32
Rb	0.0776	<0.0132	<0.0126	<0.0131	0.0167	<0.0130	0.19	<0.0130	0.0483
Sr	43.81	38.43	44.54	44.97	50.03	48.6	33.04	46.73	49.86
Y	17.12	15.33	17.45	17.27	18.01	18.91	11.38	16.57	18.38
Zr	27.41	21.3	23.02	23.09	24.17	27.43	16.11	21.39	23.84
Nb	0.0954	0.06	0.0734	0.036	0.0958	0.0745	0.0734	0.0991	0.0775
Ba	0.576	<0.0138	<0.0139	<0.0263	0.0072	<0.0138	1.014	<0.0114	0.054
La	2.23	1.561	1.662	1.092	1.156	1.247	0.929	1.075	1.175
Ce	4.73	3.7	3.94	3.2	3.48	3.62	2.53	3.25	3.43
Pr	0.741	0.603	0.678	0.646	0.658	0.686	0.461	0.619	0.627
Nd	4.13	3.66	4.01	3.97	4.22	4.22	2.77	3.89	4.04
Sm	1.59	1.491	1.68	1.72	1.7	1.82	1.047	1.572	1.74
Eu	0.663	0.583	0.685	0.664	0.688	0.694	0.468	0.639	0.666
Gd	2.45	2.3	2.47	2.47	2.51	2.54	1.59	2.3	2.55
Tb	0.439	0.402	0.441	0.437	0.469	0.477	0.291	0.432	0.452
Dy	3.08	2.92	3.22	3.28	3.45	3.65	2.06	3.14	3.4
Ho	0.669	0.609	0.679	0.69	0.72	0.74	0.43	0.667	0.721
Er	1.97	1.74	1.99	2.02	2.03	2.12	1.319	1.87	2.04
Tm	0.27	0.239	0.278	0.283	0.287	0.306	0.183	0.279	0.288
Yb	1.82	1.53	1.75	1.77	1.73	1.92	1.21	1.79	1.9
Lu	0.224	0.212	0.234	0.25	0.254	0.279	0.155	0.238	0.258
Hf	0.874	0.729	0.785	0.717	0.767	0.822	0.501	0.713	0.755
Ta	0.0322	0.0194	0.0275	0.0146	0.0226	0.0204	0.0072	0.019	0.0229
Pb	0.195	0.0354	0.0373	0.0143	0.0375	0.0191	0.084	0.0216	0.0238
Th	1.64	1.42	1.55	0.629	0.619	0.697	0.594	0.642	0.753
U	0.423	0.326	0.375	0.1665	0.1757	0.197	0.256	0.191	0.211

CNTP1	OPX1	OPX1	OPX1	OPX2	OPX2	OPX2	OPX3	OPX3	OPX3
Li	5.55	5.29	5.25	5.26	5.43	5.45	5.04	5.05	5.18
Na	313.23	322.84	291.34	314.83	311.77	326.86	290.46	325.38	314.41
Ca	n.d.	n.d.	n.d.	n.d.	n.d.	n.d.	n.d.	n.d.	n.d.
Sc	23.16	23.42	23.44	22.14	22.02	22.07	23.82	24.33	24.41
V	111.76	110.39	111.37	112.85	117.44	118.78	108.37	117.38	117.02
Cr	3691.91	3591.79	3407.39	3479.36	3804.14	3662.91	3386.25	3824.24	3928.83
Co	58.32	58.47	59.1	59.69	58.3	60.74	58.23	59.28	59.4
Ni	693.77	702.13	695.2	688.86	680.38	698.83	689.79	701.1	701.26
Ga	2.88	2.86	2.83	2.88	2.87	2.88	2.77	3.04	3.04
Rb	<0.0138	<0.0131	<0.0134	<0.0119	<0.0117	<0.0112	<0.0140	<0.0123	<0.0123
Sr	0.296	0.313	0.222	0.264	0.317	0.347	0.233	0.402	0.347
Y	1.153	1.179	1.182	1.103	1.086	1.109	1.211	1.278	1.267
Zr	0.361	1.61	1.63	0.433	1.59	1.58	1.316	1.74	1.46
Nb	<0.0038	<0.0055	0.0086	<0.0074	0.0108	0.0091	<0.0147	<0.0059	<0.0041
Ba	<0.0174	<0.0152	<0.0085	<0.0207	<0.0200	<0.0104	<0.113	<0.0200	<0.0111
La	0.0082	0.0068	0.0069	<0.0137	0.0128	0.0161	0.0075	0.0122	0.0133
Ce	0.0142	0.0063	0.027	<0.0072	0.0248	0.0429	<0.0159	<0.0084	0.0418
Pr	0.00782	0.007	0.00596	0.00451	0.0062	0.00887	0.00377	0.0077	0.00603
Nd	0.041	0.0424	0.0439	0.0289	0.0405	0.0548	0.0445	0.0601	0.0605
Sm	0.046	0.0287	0.0239	0.0292	0.0324	0.028	0.016	0.0409	0.0529
Eu	0.0124	0.0127	0.0098	0.0087	0.0117	0.0136	0.0148	0.0187	0.0134
Gd	0.0652	0.0543	0.0576	0.0532	0.0622	0.0553	0.0516	0.1	0.0595
Tb	0.0134	0.0167	0.0166	0.0083	0.0158	0.0138	0.0153	0.0164	0.0198
Dy	0.15	0.152	0.159	0.154	0.12	0.161	0.172	0.164	0.165
Ho	0.0427	0.0455	0.0393	0.0414	0.0429	0.0426	0.0378	0.0427	0.0507
Er	0.161	0.154	0.158	0.189	0.162	0.168	0.178	0.19	0.176
Tm	0.0364	0.0354	0.0385	0.0318	0.0316	0.0318	0.0293	0.0378	0.0349
Yb	0.308	0.275	0.274	0.287	0.283	0.259	0.297	0.341	0.317
Lu	0.0497	0.052	0.0572	0.0563	0.0517	0.0486	0.0553	0.0521	0.05
Hf	0.0721	0.0692	0.0711	0.0546	0.0701	0.0652	0.0397	0.0654	0.0408
Ta	0.0671	0.0601	0.0374	<0.0051	0.0157	0.0178	0.0124	0.0091	0.00219
Pb	0.1513	0.0052	0.0057	0.0621	0.0078	0.013	<0.0057	<0.00184	<0.0027
Th	0.0574	0.0943	0.0572	0.0526	0.0651	0.0723	0.0483	0.0809	0.0615
U	0.0088	0.0128	0.0086	0.0067	0.01038	0.0158	0.007	0.0121	0.0107

CNTP2	CPX1	CPX1	CPX1	CPX2	CPX2	CPX2	CPX3	CPX3	CPX3
Li	6.18	5.84	5.07	5.61	5.58	4.97	4.4	4.77	4.26
Na	10207.74	9722.05	8195.65	10398.67	9987.67	9348.78	7952.56	8092.56	7448.97
Ca43	n.d.	n.d.	n.d.	n.d.	n.d.	n.d.	n.d.	n.d.	n.d.
Sc	61.86	62.34	71.25	65.88	68.75	75.27	69.94	74.18	81.29
V	242.66	245.12	259.4	248.64	255.8	255.31	249.09	254.16	259.34
Cr	11915.04	11749.78	10215.81	11617.43	11434.94	10913.81	11007.32	11178.07	9219.65
Co	21.28	21.32	21.6	21.5	21.13	21.26	21.76	21.31	21.32
Ni	340.83	338.31	345.94	356.19	336.86	344.17	354.77	343.15	343.36
Ga	2.693	2.663	2.382	2.646	2.655	2.479	2.232	2.403	2.217
Rb	<0.0196	<0.0151	<0.0151	0.022	<0.0155	<0.0136	<0.0129	<0.0124	0.0247
Sr	82.27	80.21	77.21	82.21	85.28	83.18	67.53	70.12	70.79
Y	8.63	8.45	8.43	8.66	8.81	8.82	7.98	8.74	8.51
Zr	8.17	8.7	9.35	8.83	10.13	10.55	10.14	11.39	11.52
Nb	0.808	0.606	0.381	0.763	1.121	0.774	<0.022	0.1526	0.1052
Ba	<0.054	<0.034	0.0156	<0.070	<0.0137	<0.0103	<0.031	<0.036	0.135
La	2.11	2.21	2.33	2.09	2.15	2.08	1.793	1.921	1.98
Ce	4.92	4.6	5.1	4.67	5.17	4.99	4.37	4.58	4.37
Pr	0.693	0.656	0.67	0.675	0.685	0.67	0.574	0.32	0.613
Nd	3.1	2.93	2.98	3.02	3.12	3.01	2.59	2.78	2.79
Sm	0.798	0.814	0.753	0.803	0.79	0.838	0.763	0.768	0.777
Eu	0.33	0.355	0.31	0.35	0.331	0.332	0.279	0.306	0.291
Gd	1.135	1.097	1.06	1.185	1.15	1.12	1.026	1.072	1.018
Tb	0.195	0.193	0.196	0.215	0.206	0.205	0.183	0.204	0.196
Dy	1.506	1.545	1.435	1.549	1.576	1.579	1.421	1.615	1.608
Ho	0.323	0.323	0.335	0.334	0.339	0.335	0.32	0.33	0.335
Er	0.989	0.96	0.961	0.936	1.005	1.023	0.915	1.016	1.045
Tm	0.1443	0.1465	0.1428	0.1419	0.1472	0.1492	0.1229	0.1463	0.1437
Yb	1.018	0.966	1	0.98	0.976	0.99	0.904	0.977	0.984
Lu	0.141	0.1343	0.14	0.1476	0.1483	0.1415	0.1259	0.1411	0.1408
Hf	0.139	0.1308	0.166	0.123	0.16	0.166	0.128	0.184	0.214
Ta	0.179	0.1587	0.1265	0.1598	0.189	0.1608	0.0442	0.0908	0.0675
Pb	0.0348	0.0383	0.0311	0.0152	0.0204	0.0267	0.0259	0.0198	0.0273
Th	0.5	0.589	0.692	0.296	0.289	0.32	0.284	0.294	0.311
U	0.1743	0.2276	0.296	0.0916	0.1008	0.1286	0.0927	0.1281	0.1256

CNTP2	OPX1	OPX1	OPX1	OPX2	OPX2	OPX2	OPX3	OPX3	OPX3
Li	3.36	3.47	3.62	3.76	3.53	3.39	3.69	3.49	3.56
Na	282.83	287.16	291.05	372.11	309.63	280.57	330.81	326.81	303.4
Ca	n.d.	n.d.	n.d.	n.d.	n.d.	n.d.	n.d.	n.d.	n.d.
Sc	17.88	18.35	18.25	21.11	20.31	19.31	20.23	19.91	20.32
V	76.09	78.25	81.08	94.98	88.92	81.54	90.6	91.68	89.1
Cr	3510.95	3660.45	3784.89	4651.56	4246.27	3742.32	4407.36	4227.13	4000.07
Co	57.06	57.8	58.27	57.56	58.17	58.94	58.61	57.01	58.46
Ni	689.6	704.15	703.61	695.03	702.89	723.94	699.56	692.58	703.27
Ga	1.592	1.823	1.821	2.157	2.12	1.982	1.695	2.064	2.062
Rb	<0.0112	<0.0114	<0.0127	<0.0116	<0.0107	<0.0113	<0.0123	<0.0099	<0.0106
Sr	0.0308	0.0413	0.0505	0.358	0.112	0.0425	<0.0143	0.0992	0.1175
Y	0.409	0.421	0.421	0.566	0.488	0.454	0.45	0.495	0.508
Zr	<0.052	0.42	0.175	0.462	<0.045	0.565	<0.073	0.723	0.791
Nb	<0.0109	0.0257	<0.0058	0.0131	0.0126	0.0094	<0.0138	0.0199	0.029
Ba	<0.046	<0.0162	<0.044	<0.0167	0.0072	<0.0082	<0.062	0.0108	0.0198
La	<0.0046	<0.00234	<0.0034	0.0091	0.00339	0.00274	<0.019	0.00313	0.00765
Ce	<0.022	0.0043	<0.0066	0.0099	0.242	0.0054	<0.029	0.0272	<0.0079
Pr	<0.00188	<0.00119	<0.00197	0.00506	0.00209	0.00273	<0.0046	0.00258	0.00226
Nd	<0.0100	0.0095	<0.0112	0.0313	0.0112	0.015	<0.0134	0.018	0.0206
Sm	<0.0088	0.0123	<0.0054	0.0164	0.0068	0.0104	0.0113	<0.0062	0.0077
Eu	0.0034	0.00232	0.005	0.0063	0.0036	0.0047	0.0035	0.0045	0.0066
Gd	0.0151	<0.0132	0.0242	0.0328	0.0114	<0.0127	0.0266	0.0166	0.027
Tb	0.0047	0.00453	0.0026	0.0109	0.0076	0.00511	<0.0027	0.00536	0.00727
Dy	0.045	0.0474	0.0576	0.0742	0.0524	0.0593	0.0453	0.0498	0.0706
Ho	0.0128	0.0179	0.0152	0.0201	0.0157	0.0162	0.0172	0.0189	0.0211
Er	0.0611	0.0747	0.0698	0.0882	0.0727	0.0762	0.0666	0.0835	0.081
Tm	0.0139	0.0153	0.0147	0.0174	0.0155	0.0158	0.0143	0.0133	0.0166
Yb	0.105	0.139	0.129	0.182	0.135	0.138	0.14	0.146	0.152
Lu	0.0262	0.0219	0.0205	0.0319	0.0301	0.0275	0.0275	0.0311	0.0276
Hf	<0.0172	0.0111	<0.0056	0.0093	0.0176	0.012	<0.0198	0.0305	0.0174
Ta	<0.0038	<0.00100	0.0043	0.002	<0.00159	0.00072	<0.0053	0.0046	0.00424
Pb	<0.0097	<0.00175	<0.00158	0.0114	0.0032	0.00233	<0.0045	<0.00156	0.00291
Th	<0.0128	<0.0022	0.0049	0.0219	0.0086	0.00169	<0.0106	0.00295	0.0027
U	<0.0041	<0.0052	<0.00262	<0.0031	0.00469	0.00475	<0.0052	0.00158	<0.00178

CNTP3	CPX1	CPX1	CPX1	CPX2	CPX2	CPX2	CPX3	CPX3	CPX3
Li	5.98	6.1	5.02	5.83	5.75	5.86	5.94	5.58	5
Na	6752.19	7365.26	6491.36	7043.4	7002.4	7564.99	7602.73	7162.38	7039.2
Ca	n.d.	n.d.	n.d.	n.d.	n.d.	n.d.	n.d.	n.d.	n.d.
Sc	68.84	70.68	74.31	80.09	82.26	74.78	81.63	87.88	88.67
V	209.42	218.31	244.47	229.24	227.15	233.11	223.36	239.46	245.87
Cr	10502.95	10331.34	10100.27	10267.78	10000.15	10369.92	10652.82	10052.51	10446.84
Co	31.17	27.6	25.1	26.78	27.12	24.26	24.2	22.6	21.92
Ni	427.62	395.42	371.41	487.77	400.69	434.88	381.57	464.08	352.53
Ga	4.11	4.04	3.59	4.39	4.35	4.23	4.47	4.05	3.9
Rb	<0.0127	<0.0130	0.0311	0.0797	0.0186	0.0415	0.0369	<0.0174	0.0252
Sr	19.66	19.76	16.7	14.57	14.42	15.41	8.57	8.4	8.51
Y	16.79	19.08	20.32	28.91	28.55	29.14	43.01	45.69	43.69
Zr	19.49	23.28	24.91	33.48	33.68	33.38	52.44	59.57	55.52
Nb	4.57	5.4	3.05	4.27	4.05	4.82	3.7	3.8	3.56
Ba	<0.036	<0.0168	<0.0142	0.195	<0.0127	0.132	0.076	0.0514	0.0258
La	2.68	2.91	2.4	3.32	3.19	3.36	3.85	3.8	3.71
Ce	7.51	9.15	8	11.02	10.73	11.76	13.82	13	12.81
Pr	1.217	1.408	1.23	1.827	1.747	1.876	2.355	2.234	2.218
Nd	6.43	7.58	7.12	10.34	10.05	10.38	14.14	13.58	13.41
Sm	2.32	2.6	2.68	4.01	4.08	3.94	6.03	6.05	5.98
Eu	0.808	0.853	0.736	0.952	0.93	0.932	0.988	0.93	0.949
Gd	2.66	3.06	3.27	4.71	4.76	4.64	7.01	7.92	7.44
Tb	0.433	0.536	0.565	0.792	0.824	0.808	1.213	1.349	1.299
Dy	3.09	3.61	3.91	5.48	5.6	5.61	8.37	9.32	8.45
Ho	0.633	0.719	0.744	1.105	1.064	1.088	1.622	1.69	1.65
Er	1.82	2.07	2.31	3.12	3.06	3.08	4.44	4.71	4.5
Tm	0.269	0.302	0.311	0.458	0.426	0.435	0.629	0.622	0.609
Yb	1.89	2.11	2.24	2.95	2.88	3.05	3.98	4.02	3.92
Lu	0.267	0.281	0.291	0.406	0.382	0.395	0.499	0.518	0.497
Hf	0.562	0.537	0.554	0.631	0.653	0.651	0.795	0.957	0.977
Ta	0.2	0.268	0.207	0.442	0.437	0.43	0.704	0.672	0.606
Pb	0.0296	0.0248	0.0288	0.0391	0.0335	0.0322	0.0344	0.027	0.0432
Th	2.51	2.82	2.04	2.52	2.41	2.55	2.43	2.18	2.08
U	0.367	0.471	0.403	0.411	0.387	0.44	0.408	0.365	0.353

CNTP3	OPX1	OPX1	OPX1	OPX2	OPX2	OPX2	OPX3	OPX3	OPX3
Li	4.58	4.19	4.15	4.74	4.73	4.46	4.22	4.15	4.02
Na	387.31	280.44	266.29	430.78	377.07	387.51	340.32	315.62	280.79
Ca	n.d.	n.d.	n.d.	n.d.	n.d.	n.d.	n.d.	n.d.	n.d.
Sc	26.89	22.83	23.49	26.2	26.11	25.23	21.45	21.06	20.2
V	121.69	103.65	103.82	120.82	117.53	116.04	97.36	90.26	84.24
Cr	5036.82	4156.22	3774.42	5452.21	5302.55	5242.59	3898.87	3609.3	3174.08
Co	58.24	57.42	58.28	57.19	57.58	57.27	57	58.02	59.75
Ni	704.52	694.02	692.35	680.91	693.18	686.95	686.87	686.64	702.56
Ga	3.32	2.88	2.86	3.55	3.36	3.34	2.76	2.74	2.77
Rb	<0.0154	<0.0127	<0.0116	<0.0138	<0.0125	<0.0109	<0.0113	<0.0111	<0.0130
Sr	0.0923	0.0238	0.0226	0.1164	0.072	0.0748	0.0291	<0.0117	0.024
Y	4.6	3.4	3.33	4.42	4.06	4.01	2.59	2.36	1.99
Zr	5.56	4.34	4.6	5.93	5.38	5.16	3.36	2.95	2.25
Nb	<0.0121	0.0233	0.0737	0.0427	0.0305	0.0478	0.0758	0.1287	0.0714
Ba	<0.031	<0.056	<0.0082	<0.0270	<0.0194	<0.0265	<0.0101	<0.0096	<0.0084
La	0.0276	0.0081	0.0082	0.0403	0.0257	0.0221	0.0068	0.0075	0.00318
Ce	0.0194	0.0243	0.026	0.1466	0.0473	0.0852	0.0157	0.0281	0.022
Pr	0.0218	0.00646	<0.0038	0.0328	0.0188	0.0198	0.0097	0.0081	0.00521
Nd	0.167	0.0523	0.054	0.178	0.137	0.146	0.0677	0.0653	0.0527
Sm	0.155	0.0645	0.0726	0.166	0.126	0.128	0.0893	0.0687	0.0595
Eu	0.0206	0.0098	0.0147	0.0301	0.0206	0.0188	0.017	0.0212	0.0121
Gd	0.294	0.196	0.175	0.302	0.271	0.283	0.172	0.171	0.105
Tb	0.0806	0.0459	0.0444	0.0734	0.0708	0.0663	0.0437	0.0373	0.0269
Dy	0.637	0.481	0.471	0.634	0.638	0.61	0.364	0.346	0.244
Ho	0.153	0.1147	0.1205	0.153	0.152	0.1417	0.1023	0.0838	0.0748
Er	0.597	0.487	0.451	0.577	0.515	0.513	0.348	0.326	0.273
Tm	0.108	0.0826	0.0831	0.0948	0.0918	0.0918	0.0642	0.0587	0.0575
Yb	0.814	0.657	0.722	0.739	0.749	0.712	0.574	0.48	0.472
Lu	0.1186	0.1099	0.1181	0.1218	0.1214	0.1248	0.0951	0.086	0.0745
Hf	0.0734	0.0746	0.0944	0.0989	0.1109	0.1059	<0.0200	0.0718	0.0563
Ta	0.0077	0.0041	0.0072	0.0124	0.0063	0.0104	0.0093	0.0121	0.00461
Pb	<0.0043	0.00232	0.016	<0.0024	<0.00188	<0.00154	<0.0029	0.00194	0.0142
Th	0.184	0.0245	0.0089	0.214	0.1335	0.1089	0.0085	0.0179	0.006
U	0.0077	0.00424	0.0061	0.0159	0.0052	0.0065	0.0064	0.0083	0.00641

CNTP4	CPX1	CPX1	CPX1	CPX2	CPX2	CPX2	CPX3	CPX3	CPX3
Li	2.5	2.23	2.43	2.76	2.69	2.61	2.77	2.64	2.42
Na	6969.79	6681.35	7047.91	7768.4	7385.88	7244.58	7882.97	7520.16	7083.63
Ca	n.d.	n.d.	n.d.	n.d.	n.d.	n.d.	n.d.	n.d.	n.d.
Sc	75.64	91.38	80.02	71.41	78.02	76.56	70.06	71.7	71.93
V	233.95	248.44	242.08	230.26	238.82	244.67	232.18	234.53	241.02
Cr	8253.54	7379.53	7817.59	9481.82	9347.79	8923.88	9662.49	8915.07	8381.63
Co	25.6	23.56	24.01	23.07	23.41	22.11	24.34	24	21.45
Ni	372.07	371.16	359.58	352.01	376.54	349.72	352.73	372.86	346.37
Ga	3.05	3.04	3.13	3.22	3.23	3.21	3.4	3.46	3.09
Rb	0.0307	0.0159	<0.0133	<0.0145	0.0199	<0.0122	<0.0151	<0.0141	0.0174
Sr	48.62	47.7	50.07	43.76	40.65	42.59	48.16	45.13	37.87
Y	17.7	19.57	18.55	19.56	20.89	19.36	18.97	18.64	17.84
Zr	32.98	40.02	37.59	32.27	40.54	39.15	28.82	34.84	35.07
Nb	0.805	0.791	0.948	0.792	0.761	1.021	0.894	0.789	0.818
Ba	<0.054	0.065	<0.0134	<0.134	<0.095	0.0469	<0.064	<0.0186	<0.041
La	1.432	1.5	1.52	1.45	1.49	1.45	1.5	1.54	1.35
Ce	4.17	4.51	4.57	4.31	4.44	4.76	4.61	5.04	4.43
Pr	0.797	0.828	0.837	0.853	0.912	0.817	0.835	0.871	0.785
Nd	4.7	4.93	4.86	5.07	5.26	4.93	5.23	5	4.69
Sm	1.81	1.88	1.93	2.03	1.96	1.93	2	1.81	1.75
Eu	0.681	0.691	0.726	0.763	0.75	0.753	0.781	0.756	0.652
Gd	2.49	2.88	2.72	2.76	2.93	2.82	2.69	2.74	2.64
Tb	0.432	0.509	0.482	0.514	0.539	0.506	0.473	0.503	0.456
Dy	3.34	3.56	3.49	3.65	3.99	3.73	3.57	3.47	3.39
Ho	0.702	0.754	0.735	0.716	0.837	0.749	0.755	0.703	0.683
Er	2.05	2.2	2.14	2.09	2.34	2.14	2.13	2.09	2.02
Tm	0.28	0.312	0.303	0.3	0.332	0.309	0.302	0.294	0.286
Yb	1.76	1.99	1.85	2.01	2.16	1.93	1.94	1.89	1.83
Lu	0.229	0.269	0.282	0.252	0.278	0.264	0.255	0.261	0.256
Hf	1.13	1.248	1.264	1.085	1.23	1.151	0.913	1.033	0.98
Ta	0.1012	0.1215	0.1169	0.1136	0.1066	0.135	0.106	0.1158	0.1094
Pb	0.0769	0.0797	0.193	<0.0128	0.0513	0.0118	<0.0079	0.0225	0.0201
Th	0.207	0.197	0.199	0.154	0.1	0.176	0.186	0.216	0.19
U	0.0333	0.0545	0.057	0.0181	0.0517	0.0519	0.0272	0.0752	0.0667

CNTP4	OPX1	OPX1	OPX1	OPX2	OPX2	OPX2	OPX3	OPX3	OPX3
Li	2.12	2.01	1.88	1.85	1.78	1.717	1.77	1.716	1.675
Na	341.9	347.86	273.62	317.7	282.77	254.73	270.33	257.46	1162.24
Ca	n.d.	n.d.	n.d.	n.d.	n.d.	n.d.	n.d.	n.d.	n.d.
Sc	24.83	24.46	23.91	24.04	25.39	23.47	22.02	23.37	21.45
V	101.77	99.76	98.14	100.95	102.47	95.38	99.36	100.23	97.59
Cr	4104.61	4082.26	3720.84	3871.05	3752.94	3167.96	3689.39	3481.14	3181.2
Co	56.12	56.44	56.74	55.66	56.29	58.13	56.29	58.49	56.67
Ni	678.31	677.08	684.18	669.91	666.8	675.59	667.14	689.86	685.11
Ga	2.51	2.59	2.51	2.56	2.55	2.41	2.55	2.49	2.46
Rb	<0.0122	<0.0137	<0.0134	<0.0121	<0.0120	<0.0102	<0.0119	<0.0107	<0.0114
Sr	0.221	0.217	0.0621	0.1361	0.0572	0.0154	<0.0101	0.0277	0.0241
Y	1.212	1.21	1.038	1.156	1.173	0.98	0.969	0.999	0.888
Zr	<0.121	1.74	1.5	1.061	1.27	1.51	0.756	1.79	1.57
Nb	<0.024	<0.0078	<0.0085	<0.0130	<0.0167	<0.0085	<0.0113	0.0053	0.0084
Ba	<0.15	<0.037	<0.032	<0.101	<0.032	<0.0249	<0.030	<0.0116	<0.0113
La	<0.015	<0.0060	<0.0122	<0.0064	<0.0082	<0.0033	<0.0051	0.00406	<0.00183
Ce	<0.025	<0.0145	<0.0156	<0.038	<0.0080	<0.025	<0.016	0.0076	<0.017
Pr	<0.0030	<0.0044	<0.0041	<0.0035	<0.0032	<0.00180	<0.0030	0.00252	0.00241
Nd	<0.0212	0.0322	<0.0210	0.0279	0.0177	0.0115	0.0175	0.0116	0.0133
Sm	0.0221	0.04	0.025	0.0342	0.0202	0.0164	<0.0151	0.0197	0.0141
Eu	0.006	0.0115	0.0118	0.0124	0.0115	0.0089	0.0067	0.0079	0.0054
Gd	0.07	0.0429	0.0426	0.0632	0.0484	0.054	0.0267	0.0553	0.0372
Tb	0.0111	0.012	0.0115	0.016	0.0073	0.0101	0.0103	0.0106	0.009
Dy	0.17	0.169	0.125	0.161	0.165	0.133	0.117	0.109	0.113
Ho	0.0334	0.0423	0.0362	0.04	0.0393	0.0354	0.0359	0.0316	0.034
Er	0.182	0.196	0.177	0.179	0.19	0.133	0.155	0.167	0.134
Tm	0.0326	0.0317	0.0273	0.0303	0.0347	0.0318	0.0289	0.0338	0.024
Yb	0.3	0.234	0.288	0.296	0.289	0.271	0.273	0.274	0.255
Lu	0.0556	0.0531	0.045	0.0554	0.0546	0.0526	0.0505	0.0513	0.0494
Hf	0.074	0.0747	0.0835	0.0678	0.0872	0.0563	<0.0209	0.0656	0.0553
Ta	0.0091	0.0075	<0.00277	<0.018	<0.00217	<0.0040	<0.0054	<0.00136	0.00338
Pb	<0.0110	0.0113	0.0075	<0.0063	0.0056	0.0028	<0.0035	0.0039	0.0064
Th	<0.0088	0.0138	<0.0099	<0.0088	0.0027	<0.0041	<0.0027	0.00147	0.00057
U	<0.0077	<0.0043	<0.0042	<0.0055	<0.00247	<0.0028	<0.0037	0.00372	0.00286

CNTP5	CPX1	CPX1	CPX1	CPX2	CPX2	CPX2	CPX3	CPX3	CPX3
Li	5.14	4.74	5.22	4.35	4.22	3.55	4.96	4.29	3.71
Na	7694.27	7266.06	7481.85	6903.17	6865.43	6735.87	7820.9	7699.45	8308.11
Ca	154447.92	155132.19	150473.14	154165.73	157614.47	153247.47	148321.14	150763.97	155357.77
Sc	73.85	76.39	73.9	79.71	79.66	79.67	68.8	73.22	85.25
V	356.57	349.63	370.07	350.04	349.89	345.25	343.77	337.41	366.76
Cr	9793.08	9627.64	10120.8	8605.7	8910.32	7937.17	9316.94	8673.4	8378.96
Co	23.09	22.72	23.37	22.87	22.11	22.6	22.77	35.26	23.73
Ni	353.07	344.46	345.31	357.62	375.19	460.66	352.88	1248.37	375.57
Ga	4.07	4.05	3.93	3.55	3.7	3.35	3.96	3.91	4.02
Rb	0.0155	0.04	<0.0080	<0.0083	0.0778	0.0233	0.034	0.0939	0.1719
Sr	10.29	10.57	9.9	9.56	8.62	9.44	7.99	8.42	9
Y	21.15	19.95	20.02	18.1	18.66	16.8	19.3	18.36	18.09
Zr	38.04	36.25	34.76	32.02	32.63	29.51	29.44	29.27	18
Nb	0.571	0.342	0.742	0.1196	0.285	0.324	0.33	0.44	0.219
Ba	0.117	1.292	0.0069	<0.0190	0.501	0.17	<0.052	0.51	0.601
La	1.269	1.314	1.202	1.491	1.274	1.36	1.87	1.842	3.46
Ce	5.09	5.01	5.05	5.06	4.75	4.9	6.08	5.9	9.04
Pr	0.928	0.873	0.919	0.828	0.834	0.819	0.965	0.908	1.094
Nd	5.55	5.24	5.52	4.87	4.98	4.66	5.37	5.19	5.19
Sm	2.194	2.02	2.056	1.807	1.88	1.758	1.971	1.932	1.777
Eu	0.639	0.586	0.647	0.575	0.555	0.545	0.589	0.589	0.653
Gd	3.08	2.95	2.95	2.62	2.63	2.45	2.84	2.66	2.54
Tb	0.559	0.52	0.531	0.483	0.496	0.438	0.502	0.491	0.459
Dy	4.1	3.89	3.93	3.48	3.67	3.29	3.6	3.53	3.45
Ho	0.844	0.81	0.799	0.707	0.746	0.676	0.753	0.731	0.718
Er	2.47	2.3	2.3	2.084	2.19	1.97	2.186	2.08	2.119
Tm	0.324	0.316	0.312	0.288	0.299	0.264	0.303	0.292	0.288
Yb	2.13	2.062	2.035	1.966	1.878	1.724	1.97	1.903	1.952
Lu	0.279	0.27	0.265	0.259	0.252	0.243	0.27	0.247	0.259
Hf	1.077	1.159	1.082	1.068	1.008	0.968	0.914	0.959	0.622
Ta	0.1154	0.0972	0.1113	0.0631	0.076	0.0837	0.1058	0.0963	0.0201
Pb	0.1249	0.1642	0.0444	0.235	0.143	0.1576	0.227	0.326	0.51
Th	0.6	0.814	0.212	1.698	1.024	1.158	3.12	3.08	4.87
U	0.2019	0.289	0.0758	0.559	0.371	0.398	1.105	1.037	1.319

CNTP5	OPX1	OPX1	OPX1	OPX2	OPX2	OPX2	OPX3	OPX3	OPX3
Li	4.9	4.83	4.52	4.9	4.7	4.39	4.73	4.56	4.2
Na	404.29	407.9	326.67	382.16	325.65	305.17	318.86	303.56	319.37
Ca	6079.32	6733.28	4757.76	5621.06	5781.98	4791.82	5029.88	4637.73	3657.38
Sc	25.63	24.31	21.11	23.7	23.32	22.3	21.59	22.14	18.78
V	151.98	142.27	135.42	143.06	141.98	129.92	138.25	136.76	117.04
Cr	4895.8	4466.84	4129.33	4590.8	4344.23	3833.01	4230.09	4049.44	3492.44
Co	63.1	61.93	64.31	62.42	61.84	63.26	62.84	62.37	61.79
Ni	723.94	696.72	763.19	716.08	711.74	742.86	719.09	715.33	736.29
Ga	3.53	3.31	3.18	3.41	3.34	3.27	3.29	3.42	3.14
Rb	<0.0087	0.0086	<0.0079	<0.0087	<0.0076	<0.0079	<0.0084	<0.0079	<0.0074
Sr	0.0593	0.0636	<0.0111	0.0742	0.0218	0.0125	0.0146	0.0246	0.0505
Y	1.467	1.443	1.121	1.344	1.283	1.168	1.107	1.097	0.888
Zr	1.08	2.162	1.314	2.197	1.376	1.334	2.289	1.886	1.419
Nb	<0.0145	0.0272	<0.0098	<0.0051	0.0236	<0.0094	<0.0087	0.0244	0.0099
Ba	<0.030	<0.027	<0.030	0.0352	<0.0199	<0.0200	<0.043	<0.031	<0.0072
La	<0.0081	0.0119	<0.0036	0.0073	<0.0039	<0.00160	<0.0047	<0.0091	0.0138
Ce	<0.0127	0.0448	<0.0098	0.0087	<0.0073	<0.019	<0.023	0.0199	0.0309
Pr	0.00297	0.0094	0.00506	0.00722	0.00355	0.00259	<0.00149	0.00267	0.00446
Nd	0.0479	0.0555	0.0211	0.0198	0.0448	0.026	0.0123	0.0331	0.0343
Sm	0.0298	0.0295	0.0261	0.0179	0.0278	0.0225	0.0187	0.0202	0.0148
Eu	0.0132	0.0144	0.0078	0.0103	0.0104	<0.0035	<0.0096	0.00625	0.0072
Gd	0.0647	0.0763	0.0582	0.0688	0.0753	0.0479	0.0226	0.051	0.0302
Tb	0.017	0.0185	0.0163	0.0211	0.0169	0.0148	0.0143	0.0125	0.0105
Dy	0.197	0.198	0.15	0.183	0.186	0.161	0.124	0.142	0.1139
Ho	0.0509	0.0586	0.0415	0.0523	0.0484	0.0419	0.0383	0.0413	0.0327
Er	0.221	0.211	0.1621	0.206	0.193	0.1755	0.1572	0.1725	0.1416
Tm	0.0419	0.0385	0.0351	0.0404	0.0395	0.0387	0.037	0.0331	0.0305
Yb	0.379	0.344	0.275	0.358	0.349	0.292	0.309	0.316	0.236
Lu	0.0683	0.0661	0.0498	0.0582	0.0602	0.0599	0.0578	0.0546	0.047
Hf	0.0794	0.0807	0.1049	0.0778	0.071	0.05	0.0562	0.0711	0.0414
Ta	<0.00213	0.00361	<0.00217	0.00235	<0.00205	0.00126	<0.0024	0.0798	0.0162
Pb	0.0305	0.0056	<0.0039	<0.0031	<0.00212	0.0027	4.04	1.301	11.73
Th	0.0083	0.0112	0.006	0.0348	0.00483	0.0135	<0.0030	0.0126	0.0147
U	<0.0056	0.0067	<0.0048	0.0112	0.00317	0.0117	<0.0025	0.00979	0.0125

CNTP6	CPX1	CPX1	CPX1	CPX2	CPX2	CPX2	CPX3	CPX3	CPX3
Li	3.35	3.15	2.81	3.13	3.43	2.24	2.89	2.72	2.33
Na	7839.52	8071.76	7463.13	8107.66	8385.51	6935.39	8788.17	8484.06	8270.37
Ca	n.d.	n.d.	n.d.	n.d.	n.d.	n.d.	n.d.	n.d.	n.d.
Sc	69.88	69.96	71.87	71.21	65.65	81.28	68.49	69.11	73.45
V	237.02	231.31	242.83	239.14	240.79	236.16	236.85	242.64	236.07
Cr	9096.94	9037.44	8485.86	8416.62	9144.63	6516.04	9530.69	9697.29	9232.02
Co	20.79	21	20.82	22.06	21.15	20.92	21.39	21.08	21.05
Ni	337.13	328.31	335.84	345.4	338.62	341.92	332.73	334.36	333.29
Ga	2.546	2.678	2.465	2.562	2.699	2.226	2.77	2.76	2.589
Rb	0.0337	<0.0117	<0.0106	<0.0117	<0.0157	<0.0146	<0.0146	<0.0150	<0.0127
Sr	66.52	75.58	67.36	72.84	73.79	68.57	78.02	74.95	73.64
Y	10.2	10.78	10.31	10.65	10.61	10.27	10.56	10.82	11.05
Zr	35.09	36.08	34.71	35.57	35.35	34.55	36.54	37.34	38.62
Nb	1.068	1.743	1.143	1.57	1.687	1.183	1.755	1.605	1.477
Ba	<0.0225	<0.0086	<0.0123	<0.0182	<0.0093	<0.0105	<0.040	<0.0120	0.0199
La	2.33	1.747	1.816	1.691	1.761	1.557	2.11	2.61	3.15
Ce	4.97	4.25	4.26	4.15	4.33	3.77	4.69	5.43	6.43
Pr	0.699	0.675	0.61	0.648	0.678	0.564	0.721	0.732	0.816
Nd	3.43	3.6	3.32	3.49	3.68	3.12	3.73	3.8	3.98
Sm	1.193	1.216	1.083	1.162	1.2	1.037	1.199	1.237	1.218
Eu	0.464	0.5	0.442	0.459	0.481	0.424	0.47	0.509	0.486
Gd	1.375	1.541	1.437	1.54	1.564	1.346	1.584	1.562	1.546
Tb	0.24	0.26	0.244	0.26	0.263	0.247	0.259	0.275	0.266
Dy	1.85	1.965	1.855	1.864	1.95	1.842	1.885	1.93	1.97
Ho	0.409	0.43	0.403	0.404	0.401	0.398	0.414	0.426	0.416
Er	1.213	1.235	1.235	1.18	1.22	1.226	1.179	1.221	1.297
Tm	0.174	0.177	0.173	0.176	0.171	0.171	0.179	0.194	0.184
Yb	1.155	1.201	1.173	1.129	1.222	1.156	1.197	1.246	1.219
Lu	0.1734	0.1729	0.1606	0.173	0.17	0.1599	0.166	0.175	0.175
Hf	0.877	0.879	0.891	0.841	0.853	0.825	0.86	0.85	0.86
Ta	0.317	0.361	0.288	0.299	0.348	0.22	0.462	0.447	0.427
Pb	0.144	0.0248	0.0198	0.0162	0.0143	0.0171	0.0924	0.135	0.178
Th	0.988	0.258	0.624	0.255	0.263	0.316	0.752	1.401	1.77
U	0.311	0.077	0.2075	0.0727	0.0789	0.0961	0.2124	0.368	0.496

CNTP6	OPX1	OPX1	OPX1	OPX2	OPX2	OPX2	OPX3	OPX3	OPX3
Li	4.43	4.81	4.2	3.11	2.86	3.15	4.2	3.96	3.8
Na	515.51	453.06	499.9	403.23	337.65	333.39	441.61	410.17	399.21
Ca	n.d.	n.d.	n.d.	n.d.	n.d.	n.d.	n.d.	n.d.	n.d.
Sc	21.2	20.81	21.26	23.05	21.12	19.81	21.66	21.03	20.69
V	103.61	95.3	97.63	100.18	96.19	94.03	103.6	97.88	91.32
Cr	4699.95	4132.18	4221.08	4344.51	3781.5	3441.47	4376.84	4053.94	3749.64
Co	60.48	61.39	59.75	58.33	57.08	57.46	59.93	56.23	58.53
Ni	740.29	727.91	712.37	706.53	692.29	693.47	716.02	692.52	705.52
Ga	2.95	3.14	3.08	2.504	2.271	2.342	2.488	2.513	2.675
Rb	<0.0147	<0.0131	<0.0130	0.0365	<0.0131	0.1346	<0.0134	<0.0126	<0.0119
Sr	0.294	0.0565	0.239	0.252	0.0637	0.1773	0.214	0.1424	0.1032
Y	1.117	1.277	1.365	0.741	0.624	0.613	0.773	0.803	1.035
Zr	2.5	2.73	2.49	2.27	1.87	2.05	2.13	2.09	2.02
Nb	0.0195	0.024	0.0212	0.0244	0.0205	0.1072	0.0483	0.0347	0.0316
Ba	<0.080	<0.0123	<0.0237	0.0329	0.0236	0.099	<0.0129	<0.0134	0.0149
La	0.1048	0.0301	0.1245	0.0197	0.00628	0.0172	0.0128	0.0153	0.0139
Ce	0.281	0.1418	0.337	0.0404	0.0126	0.0485	0.0268	0.0428	0.0378
Pr	0.0323	0.0245	0.0486	0.0061	0.0023	0.00743	0.00301	0.00585	0.00855
Nd	0.118	0.125	0.204	0.0416	0.0237	0.0539	0.028	0.025	0.0452
Sm	0.0428	0.0466	0.063	0.017	0.0157	0.0204	0.0189	0.019	0.0258
Eu	0.0156	0.0118	0.0166	0.0112	0.0075	0.0095	0.0051	0.0086	0.0074
Gd	0.055	0.0695	0.0625	0.0292	0.0346	0.0188	0.0266	0.0132	0.0353
Tb	0.0157	0.0158	0.0191	0.0075	0.00683	0.0088	0.0089	0.0092	0.0064
Dy	0.137	0.179	0.167	0.0875	0.0786	0.0787	0.0861	0.102	0.1169
Ho	0.0382	0.0435	0.0485	0.0267	0.0218	0.0233	0.03	0.0256	0.0315
Er	0.151	0.19	0.183	0.132	0.0903	0.0938	0.1132	0.1209	0.156
Tm	0.0319	0.0359	0.0362	0.0235	0.0198	0.0233	0.0216	0.0242	0.0289
Yb	0.267	0.281	0.321	0.212	0.187	0.175	0.203	0.234	0.261
Lu	0.0497	0.0566	0.0564	0.0352	0.0389	0.0386	0.0409	0.0421	0.0441
Hf	<0.0214	0.0548	0.0538	0.0663	0.0586	0.051	0.0566	0.0548	0.0461
Ta	0.0111	0.00502	0.006	0.0155	0.00392	0.00238	0.0096	0.0081	0.00619
Pb	0.1679	0.1119	0.0382	0.203	0.0323	0.439	0.0488	0.0421	0.0909
Th	0.217	0.0551	0.186	0.044	0.0086	0.0187	0.018	0.0256	0.0163
U	<0.0079	0.0317	0.0594	0.0151	0.00725	0.0115	0.0152	0.02	0.0221

CNTP7	CPX1	CPX1	CPX1	CPX2	CPX2	CPX2	CPX3	CPX3	CPX3
Li	4.65	3.22	3.2	2.58	3.24	4.4	2.88	4.13	3.61
Na	8422.58	8792.8	8625.6	10546.11	9556.22	7423.41	9522.29	8398.8	7540.43
Ca	134958.38	142270.69	151515.33	141783.06	145086.38	153553.66	138437.44	157321.89	161636.39
Sc	52.59	54.68	57.37	62.31	60.48	59.13	61.31	58.03	63.72
V	250.05	257.68	256.97	297.17	277.39	262.38	276.2	258.27	258.74
Cr	8219.52	8026.58	8009.91	7643.72	6911.56	7368.2	6822.25	8061.95	7306.15
Co	30.49	26.8	25.98	27.96	26.16	22.78	27.7	23.97	23.25
Ni	459.72	436.05	419.87	515.23	452.07	367.13	588.85	395.04	412.79
Ga	5.56	5.55	5.31	12.02	7.84	3.63	10.48	5.03	4.67
Rb	0.711	0.811	0.775	2.33	1.26	0.0165	1.53	0.562	0.253
Sr	34.06	34.45	37.31	50.31	46.89	35.76	42.32	35.92	35.94
Y	13.05	14.29	15.74	19.54	18.22	13.96	15.8	16.4	16.28
Zr	30.84	76.63	63.24	220.18	179.08	39.86	213.7	46.97	86.23
Nb	1.731	1.99	1.653	19.75	10.34	0.592	17.56	2.102	1.401
Ba	6.58	6.55	6.63	36.14	18.33	0.0787	29.41	6.03	3.99
La	17.36	19.49	19.82	24.32	21.11	15.44	25.43	22.17	23.83
Ce	32.98	40.67	39.35	56.45	50.47	29.89	59.92	42.14	48.72
Pr	2.67	3.47	3.45	6.26	5.69	2.48	5.85	3.46	4.31
Nd	7.77	10.57	10.55	22.46	20.59	7.76	18.46	10.12	12.67
Sm	1.574	1.91	2.04	3.99	3.6	1.651	3.04	1.97	2.18
Eu	0.583	0.628	0.659	0.996	0.921	0.534	0.676	0.608	0.645
Gd	1.78	2.06	2.29	3.55	3.11	2.03	2.75	2.32	2.4
Tb	0.314	0.359	0.398	0.563	0.501	0.354	0.436	0.406	0.416
Dy	2.45	2.66	2.98	3.89	3.54	2.61	2.96	3.11	3.1
Ho	0.516	0.525	0.605	0.748	0.702	0.554	0.586	0.625	0.635
Er	1.538	1.614	1.765	2.12	2.06	1.584	1.79	1.9	1.82
Tm	0.225	0.243	0.25	0.295	0.279	0.226	0.254	0.269	0.264
Yb	1.496	1.66	1.78	1.99	1.9	1.573	1.69	1.78	1.83
Lu	0.207	0.23	0.251	0.279	0.249	0.208	0.227	0.245	0.254
Hf	0.451	0.837	0.742	4.98	4.31	0.598	3.29	0.64	0.837
Ta	0.0642	0.1105	0.0945	1.65	0.873	0.0641	1.46	0.129	0.131
Pb	1.177	1.306	1.44	1.51	1.044	0.737	2.65	1.173	1.075
Th	14.73	15.29	17.09	15.63	12.77	15.26	13.58	18.05	18.93
U	5.35	5.32	5.93	5.29	5.09	6.55	4.43	6.26	6.35

CNTP7	OPX1	OPX1	OPX1	OPX2	OPX2	OPX2	OPX3	OPX3	OPX3
Li	4.56	4.5	3.94	4.44	4.36	4.03	4.7	4.58	3.05
Na	357.71	344.84	308.71	818.82	369.27	351.24	545.38	410.85	1342.91
Ca	4787.84	4664.54	4239.38	5746	4899.4	5249.8	7895.59	5601.23	29841.74
Sc	20.29	20.29	19.51	19.95	20.69	20.79	22.44	21.47	26.71
V	119.9	119.08	108.17	117.98	120.32	114.41	123.15	121.01	121.79
Cr	3662.77	3582.81	3254.85	3514.62	3592.87	3459.12	4227.21	4042.91	4043.67
Co	63.14	63.75	64.63	62.73	62.93	62.38	61.89	62.81	55.68
Ni	712.11	729.01	755.29	742.91	733.69	730.68	708.27	732.08	710.79
Ga	2.97	3.16	3.99	3.31	3.35	3.21	3.13	2.71	3.89
Rb	0.1307	0.0117	0.1433	0.403	0.0122	<0.0075	<0.0085	<0.0086	1.025
Sr	0.1066	0.0698	0.263	1.76	0.1837	0.1419	0.752	0.237	8.78
Y	0.914	0.943	1.038	1.096	0.946	0.955	1.309	1.06	3.29
Zr	0.428	1.214	3.8	1.421	1.623	1.831	1.557	1.339	35.88
Nb	0.0111	0.0162	0.0932	0.1513	0.0265	0.0313	0.0305	0.0223	0.899
Ba	<0.0155	0.113	1.425	0.687	0.0937	0.0363	0.0825	<0.0144	1.515
La	0.0531	0.0449	0.0523	0.621	0.099	0.0873	0.555	0.1531	3.53
Ce	0.0447	0.1536	0.1839	1.216	0.326	0.2493	1.018	0.276	7.61
Pr	0.0161	0.0158	0.0232	0.109	0.0244	0.0243	0.0714	0.0237	0.763
Nd	0.0504	0.0497	0.0957	0.293	0.0936	0.077	0.2	0.0705	2.53
Sm	0.0148	0.0188	0.041	0.0488	0.0293	0.0191	0.0456	0.0274	0.494
Eu	0.0045	0.0053	0.0125	0.0214	0.0095	0.0105	0.0161	0.0101	0.1382
Gd	0.0409	0.0388	0.0362	0.057	0.0423	0.041	0.098	0.0485	0.434
Tb	0.0125	0.0113	0.0131	0.0163	0.0125	0.0131	0.0194	0.0123	0.0829
Dy	0.12	0.116	0.118	0.156	0.112	0.125	0.177	0.163	0.621
Ho	0.0346	0.0373	0.0377	0.034	0.0306	0.0338	0.0479	0.0388	0.1275
Er	0.1422	0.153	0.173	0.1421	0.147	0.1525	0.2	0.172	0.372
Tm	0.0278	0.0286	0.0323	0.0339	0.0309	0.0298	0.033	0.032	0.0681
Yb	0.265	0.26	0.314	0.292	0.288	0.284	0.289	0.278	0.478
Lu	0.0487	0.0493	0.057	0.0536	0.0448	0.0525	0.0517	0.0494	0.0774
Hf	0.0452	0.0458	0.0701	0.0403	0.0512	0.0462	0.0725	0.0497	0.546
Ta	<0.00155	0.00148	0.0082	0.0167	0.00254	0.00226	0.00395	0.00358	0.1081
Pb	0.0132	0.0095	0.0691	0.0987	0.0328	0.0187	0.075	0.1156	0.339
Th	0.147	0.1075	0.0578	0.596	0.301	0.192	1.329	0.526	2.79
U	0.0959	0.0916	0.0645	0.1849	0.1028	0.0982	0.376	0.2063	0.978

CNTP8	CPX1	CPX1	CPX1	CPX2	CPX2	CPX2	CPX3	CPX3	CPX3
Li	4.09	2.97	3.61	4.16	4.07	3.92	5.05	5.01	3.65
Na	7399.42	294.75	6763.95	7466.38	7693.66	7417.65	3149.05	2823.81	5495.38
Ca	160811.72	4877.72	157898.38	158845.91	161087.2	165658.08	69689.05	68385.95	132429.98
Sc	61.34	20.34	67.13	62.44	60.15	64.99	32.11	34.25	65.18
V	253.39	102.31	251.67	253.57	245.29	243.23	113.43	110.48	218.21
Cr	7948.85	3128.7	7141.25	7676.93	7747.64	7512.22	3131.89	2711.7	4966.49
Co	23.43	57.88	23.57	22.27	22.19	21.67	117.73	121.65	54.14
Ni	375.82	696.78	352.35	345.63	339.62	383.19	2289.32	2392.73	979.83
Ga	3.27	2.462	2.91	3.4	3.39	3.22	1.62	1.733	3.58
Rb	0.0356	0.0149	<0.0081	0.1293	0.0157	0.0267	0.1146	0.729	0.355
Sr	76.33	0.2218	72.1	79.65	82.07	82.59	31.32	32.89	69.24
Y	16.98	0.98	16.75	17.06	16.96	17.88	6.87	6.44	12.39
Zr	36.95	2.17	38.29	38.06	36.44	38.62	14.62	16.65	29.92
Nb	0.267	0.016	0.1809	0.288	0.303	0.32	0.278	0.492	0.494
Ba	0.113	0.0419	0.0255	0.461	0.0744	0.255	0.866	1.606	4.16
La	1.612	0.0041	1.941	2.73	2.48	2.48	1.684	1.693	4.52
Ce	4.99	<0.0049	5.36	6.72	6.74	6.45	3.83	3.75	10.66
Pr	0.874	0.00481	0.878	1	1.049	1.01	0.509	0.527	1.353
Nd	5.15	0.033	4.84	5.41	5.64	5.62	2.51	2.58	6.16
Sm	1.906	0.0278	1.78	1.975	1.948	2.033	0.8	0.791	1.72
Eu	0.783	0.0145	0.738	0.766	0.777	0.777	0.301	0.303	0.636
Gd	2.52	0.0584	2.43	2.55	2.56	2.66	0.996	1.002	1.999
Tb	0.438	0.0135	0.431	0.466	0.458	0.476	0.181	0.187	0.362
Dy	3.34	0.146	3.18	3.23	3.23	3.38	1.333	1.227	2.38
Ho	0.644	0.0398	0.652	0.682	0.681	0.681	0.264	0.253	0.506
Er	1.915	0.1332	1.84	1.905	1.883	1.98	0.745	0.729	1.433
Tm	0.27	0.0294	0.259	0.274	0.272	0.282	0.1057	0.1088	0.206
Yb	1.736	0.282	1.651	1.76	1.748	1.812	0.705	0.712	1.362
Lu	0.23	0.0522	0.229	0.231	0.241	0.237	0.1015	0.0995	0.197
Hf	1.013	0.0754	1.086	0.997	0.94	1.062	0.436	0.451	0.856
Ta	0.0537	<0.00145	0.0478	0.0605	0.057	0.0656	0.0197	0.0235	0.031
Pb	0.296	0.0143	0.401	0.556	0.341	0.351	0.556	0.695	1.022
Th	0.723	0.0086	1.225	1.82	1.565	1.535	0.928	0.867	2.06
U	0.296	0.00951	0.461	0.601	0.564	0.532	0.282	0.244	0.601

CNTP8	OPX1	OPX1	OPX1	OPX2	OPX2	OPX2	OPX3	OPX3	OPX3
Li	3.42	3.43	3.17	3.41	3.46	3.31	3.49	3.43	3.58
Na	424.31	447.58	313	374.61	388.99	306.94	398.31	425.87	307.55
Ca	6850.32	7551.26	4563.94	6190.76	6491.05	5079.25	6341.28	7074.83	4635.71
Sc	22.64	22.79	21.56	21.22	22.08	20.85	20.88	21.82	21.29
V	115.97	116.73	105.39	113.59	117.05	107.9	107.85	114.58	113.62
Cr	3860.49	4008.69	3180.01	3897.2	3874.74	3176.02	3865.67	4117.05	4051.34
Co	60.18	60.5	63	60.84	60.73	61.53	59.56	60.22	61.11
Ni	683.88	678.51	731.02	678.38	689.59	719.75	667.69	675.15	724.26
Ga	2.754	2.438	2.572	2.735	2.84	2.646	2.74	2.88	2.81
Rb	<0.0082	<0.0086	<0.0077	<0.0089	<0.0084	<0.0074	<0.0076	0.0087	0.0121
Sr	0.816	1.017	0.1537	0.504	0.663	0.314	0.648	0.813	0.272
Y	1.343	1.428	0.973	1.22	1.264	1.05	1.249	1.379	1.121
Zr	2.86	2.89	2.11	1.341	2.88	2.055	2.36	3.11	2.4
Nb	0.0085	0.0068	0.0094	<0.0162	0.0099	0.0061	<0.0149	<0.0073	0.0111
Ba	<0.037	<0.079	0.0067	<0.123	0.0289	<0.0127	<0.031	<0.0253	<0.16
La	0.0322	<0.0089	0.00674	<0.0084	0.0248	0.0091	<0.0062	0.0236	<0.0033
Ce	0.0306	<0.07	0.0219	<0.020	0.0685	0.0422	<0.020	0.0658	<0.0074
Pr	0.0133	0.0165	0.00421	0.0065	0.0122	0.00689	0.0079	0.0122	0.00567
Nd	0.0887	0.0912	0.0309	0.0297	0.0832	0.0385	0.0518	0.0903	0.0211
Sm	0.048	0.0617	0.021	0.0389	0.0476	0.024	0.0355	0.042	0.0205
Eu	0.0194	0.02	0.0112	0.0191	0.017	0.0117	0.0114	0.0244	0.0104
Gd	0.092	0.1109	0.0445	0.0801	0.0748	0.0448	0.0873	0.094	0.0562
Tb	0.0212	0.0235	0.0133	0.0162	0.0171	0.0148	0.0133	0.022	0.0125
Dy	0.189	0.168	0.141	0.184	0.195	0.152	0.183	0.214	0.142
Ho	0.0512	0.0543	0.036	0.0429	0.0446	0.0386	0.0438	0.0501	0.0377
Er	0.186	0.205	0.165	0.173	0.175	0.148	0.183	0.208	0.168
Tm	0.0363	0.0367	0.03	0.0304	0.0352	0.0298	0.0302	0.0379	0.0325
Yb	0.298	0.317	0.269	0.279	0.284	0.234	0.255	0.309	0.265
Lu	0.0487	0.0565	0.0522	0.0506	0.0544	0.0464	0.0456	0.0559	0.0559
Hf	0.0998	0.1016	0.0807	0.0664	0.0775	0.0677	0.084	0.1141	0.0891
Ta	<0.00160	0.00306	0.00094	<0.0033	0.00211	<0.00270	<0.0052	<0.0027	0.00186
Pb	<0.0103	0.0089	0.00309	0.0085	0.0115	<0.0038	0.0126	0.0312	0.0637
Th	0.0423	0.0466	0.0125	0.0096	0.023	0.0118	0.0146	0.0166	0.009
U	0.0215	0.0138	0.00962	<0.0031	0.0119	0.0054	<0.0043	0.0126	0.00739

CNTP9	CPX1	CPX1	CPX1	CPX2	CPX2	CPX2	CPX3	CPX3	CPX3
Li	5.16	3.64	4.36	5.38	5.45	5.34	5.74	5.78	5.35
Na	7703.95	7110.84	7378.13	7258.85	7284.14	1623.77	7201.08	6841.22	6858.82
Ca	160402.28	167721.64	160212.58	158975.31	161021.11	30397.83	153123.61	151691.92	156765.83
Sc	78.72	89.86	80.92	83.27	82.96	27.01	74.04	72.28	78.77
V	370.66	358.73	356.19	383.39	366.4	140.42	365.11	368.91	392.33
Cr	10395.14	9785.26	9416.94	9827.47	10127.28	3706.37	9798.68	9670.37	10102.37
Co	23.59	21.5	21.95	22.18	21.79	52.71	22.14	22.27	22.75
Ni	375.99	430.01	424.46	351.91	347.2	982.41	348.97	352.21	361.69
Ga	4.65	4.13	4.31	4.05	4.49	3.28	4.59	4.49	4.32
Rb	0.152	0.0196	0.0614	0.0328	0.0087	0.0355	0.0191	0.0097	0.0167
Sr	13.6	12.73	12.67	10.05	10.44	2.071	7.54	7.62	7.35
Y	28.28	33.9	26.75	31.66	31.72	4.61	29.73	28.2	28.02
Zr	73.04	86.45	73.29	73.28	74.07	11.04	50.99	47.62	49.71
Nb	<0.0173	0.214	0.0915	0.0606	0.0636	0.0765	0.1474	0.22	0.262
Ba	0.651	0.0972	0.394	<0.079	<0.0231	0.255	<0.046	0.0107	0.0278
La	3.53	3.16	3.34	2.01	2.05	0.377	2.07	1.98	1.95
Ce	8.65	8.54	8.73	7.09	7.64	1.276	7.97	7.64	7.83
Pr	1.32	1.451	1.286	1.423	1.429	0.208	1.402	1.353	1.355
Nd	7.45	8.79	7.12	8.61	8.63	1.154	8.07	7.65	7.58
Sm	2.83	3.48	2.71	3.36	3.44	0.419	2.96	2.84	2.87
Eu	0.576	0.645	0.552	0.663	0.665	0.0929	0.672	0.649	0.616
Gd	4.09	4.94	3.84	4.71	4.66	0.599	4.08	3.88	3.91
Tb	0.749	0.875	0.7	0.838	0.833	0.1133	0.737	0.701	0.717
Dy	5.33	6.52	5.18	6.06	6.08	0.846	5.46	5.24	5.37
Ho	1.109	1.32	1.077	1.217	1.231	0.178	1.153	1.105	1.113
Er	3.22	3.76	2.98	3.45	3.46	0.538	3.32	3.2	3.17
Tm	0.448	0.514	0.413	0.473	0.469	0.0811	0.469	0.438	0.422
Yb	2.83	3.32	2.63	2.91	3.02	0.619	3	2.92	2.82
Lu	0.368	0.424	0.349	0.403	0.398	0.0974	0.394	0.386	0.371
Hf	2.25	2.63	2.25	1.89	1.83	0.366	1.151	1.093	1.26
Ta	0.0842	0.1122	0.084	0.0901	0.1001	0.0092	0.1145	0.0875	0.0917
Pb	<0.038	0.1285	0.156	0.0733	0.0437	0.0314	0.227	0.0704	0.0783
Th	5.01	4.59	4.93	2.38	2.45	0.504	2.51	2.31	1.99
U	1.745	1.539	1.766	0.793	0.816	0.296	0.93	0.894	0.745

CNTP9	OPX1	OPX1	OPX1	OPX2	OPX2	OPX2	OPX3	OPX3	OPX3
Li	5.65	5.3	5.45	5.36	5.07	5.03	5.14	5.17	4.68
Na	345.09	306.21	300.44	318.54	281.71	280.22	308.82	338.24	297.38
Ca	5309.67	4637.48	4838.69	5619.23	5081.7	4562.46	5296.44	5756.6	4665.76
Sc	24.04	22.46	22.78	22.58	21.85	21.27	21.24	22.19	21.84
V	142.53	124.55	135.46	134.06	124.68	122.74	123.53	129.41	125.38
Cr	4679.83	4005.71	4526.83	4255.64	3919.1	3848.75	3976.2	4190.72	4252.87
Co	62.45	61.85	62.61	60.8	62.36	62.02	61.75	60.5	62.6
Ni	751.02	839.07	755.24	728.95	748.49	742.84	745.4	726.38	751.06
Ga	3.84	3.69	3.79	3.6	3.63	3.48	3.42	3.53	3.5
Rb	0.0104	0.0186	<0.0070	<0.0075	<0.0069	<0.0066	<0.0069	<0.0065	<0.0063
Sr	0.0626	0.162	0.0191	<0.0109	0.028	0.0218	<0.0088	<0.0106	0.0197
Y	1.713	1.471	1.428	1.71	1.571	1.479	1.74	1.96	1.75
Zr	5.1	4.22	4.33	3	4.93	4.16	3.26	5.24	4.3
Nb	0.0085	0.0243	0.0182	<0.021	0.0258	0.0288	<0.0147	0.0119	0.0916
Ba	<0.025	0.145	0.005	<0.088	0.0206	0.0437	<0.080	0.0232	0.033
La	0.0056	0.0124	0.00288	<0.0071	<0.00174	0.00449	<0.0098	0.0118	0.0043
Ce	<0.0134	0.0293	0.0104	<0.026	0.0229	0.0305	<0.030	0.0461	0.0359
Pr	0.0046	0.00482	0.00406	<0.0031	0.0047	0.00665	<0.00234	0.00889	0.00376
Nd	0.0345	0.038	0.0235	0.0231	0.0627	0.0348	0.0291	0.0637	0.0305
Sm	0.0308	0.0334	0.0264	0.0351	0.0337	0.0292	0.0327	0.0492	0.0283
Eu	0.0088	0.006	0.00558	0.0041	0.0111	0.0071	0.0072	0.0116	0.0089
Gd	0.0816	0.0753	0.0757	0.109	0.0722	0.0606	0.0961	0.0933	0.0729
Tb	0.019	0.0172	0.0154	0.0164	0.0206	0.0197	0.0142	0.0299	0.0212
Dy	0.212	0.196	0.167	0.222	0.216	0.205	0.242	0.28	0.243
Ho	0.0588	0.051	0.0554	0.0595	0.0521	0.0587	0.0626	0.0716	0.0658
Er	0.266	0.228	0.227	0.232	0.244	0.231	0.269	0.287	0.248
Tm	0.0543	0.0477	0.0496	0.0414	0.0492	0.0441	0.0453	0.0532	0.0511
Yb	0.456	0.426	0.401	0.417	0.431	0.392	0.454	0.48	0.443
Lu	0.0869	0.0769	0.0775	0.0804	0.0755	0.0754	0.0754	0.0844	0.0801
Hf	0.195	0.158	0.186	0.08	0.153	0.145	0.1	0.155	0.132
Ta	<0.0034	0.0016	0.00485	<0.0055	0.0054	0.00207	<0.0058	<0.00121	0.00393
Pb	<0.0025	0.0079	0.00323	<0.0049	0.0096	0.009	<0.0081	0.00362	0.0017
Th	0.0217	0.022	0.0092	<0.0072	0.0108	<0.0026	0.0053	0.0457	0.00556
U	0.0127	0.0234	0.0126	<0.0075	0.0105	0.00932	<0.0056	0.0064	0.00801

CNTP 10	CPX1	CPX1	CPX1	CPX2	CPX2	CPX2	CPX3	CPX3	CPX3
Li	6.96	6.85	5.81	6.15	5.78	6.7	6.14	6.8	5.33
Na	5947.52	5605.19	5404.92	5428.68	5080.79	5712.68	5766.7	6215.24	5198.01
Ca	165298.97	164226.17	173120.22	159755.2	152509.97	166344.38	158192.27	160242.3	157961.86
Sc	64.5	68.3	78.06	63.03	59.39	68.96	67.75	64.6	63.61
V	258.47	264.45	273.44	242.55	241.23	251.13	262.59	262.78	254.29
Cr	9220.52	9453.03	7514.38	8759.51	8734.67	8314.92	8426.01	8644.25	8317.08
Co	27.47	31.35	24.97	29.05	31.52	26.51	24.9	25.08	25.9
Ni	422.27	439.79	395.07	437.14	500.09	402.15	387.35	390.43	436.69
Ga	3.76	3.91	3.1	3.83	3.85	3.77	3.5	3.68	3.45
Rb	0.0194	0.0116	0.0664	0.0133	<0.0080	<0.0080	0.0292	0.0124	0.138
Sr	45.98	46.43	46.44	42.09	38.53	48.32	46.53	48.04	42.01
Y	17.37	17.17	16.39	16.03	14.76	17.09	16.26	16.55	14.78
Zr	27.32	27.86	29.03	24.88	23.33	26.39	27.1	26.35	25.45
Nb	0.0983	0.0783	0.064	0.0663	0.0527	0.0835	<0.043	0.1366	0.0995
Ba	0.14	0.012	0.268	<0.0225	0.0143	<0.0075	0.256	0.0312	0.921
La	1.199	1.19	1.165	1.172	1.026	1.244	1.418	1.425	1.352
Ce	3.58	3.64	3.54	3.32	3.14	3.82	4.08	4.15	3.79
Pr	0.667	0.694	0.626	0.616	0.562	0.673	0.674	0.679	0.634
Nd	4.38	4.22	3.86	3.88	3.53	4.13	3.98	3.99	3.71
Sm	1.75	1.69	1.62	1.57	1.434	1.65	1.66	1.58	1.448
Eu	0.678	0.677	0.641	0.622	0.589	0.674	0.638	0.658	0.584
Gd	2.48	2.51	2.28	2.31	2.14	2.45	2.35	2.41	2.1
Tb	0.442	0.456	0.418	0.4	0.382	0.433	0.431	0.432	0.372
Dy	3.24	3.31	3.09	3.16	2.91	3.33	3.06	3.36	2.88
Ho	0.673	0.707	0.658	0.639	0.595	0.664	0.628	0.645	0.58
Er	1.96	2.03	1.91	1.89	1.69	1.97	1.86	1.93	1.7
Tm	0.289	0.283	0.272	0.258	0.23	0.261	0.26	0.265	0.241
Yb	1.95	1.97	1.78	1.67	1.58	1.75	1.7	1.74	1.58
Lu	0.255	0.258	0.239	0.225	0.208	0.257	0.229	0.232	0.217
Hf	0.925	0.922	1.071	0.815	0.784	0.848	0.868	0.875	0.84
Ta	0.0266	0.0229	0.0246	0.0207	0.0176	0.0387	0.0378	0.0311	0.0255
Pb	0.0251	0.0192	0.076	0.018	0.0189	0.0204	0.0591	0.0249	0.0477
Th	0.79	0.831	0.723	0.67	0.602	0.687	0.816	0.777	0.815
U	0.221	0.234	0.228	0.203	0.177	0.225	0.285	0.259	0.263

CNTP 10	OPX1	OPX1	OPX1	OPX2	OPX2	OPX2	OPX3	OPX3	OPX3
Li	5.68	5.26	4.76	5.13	5.3	5.47	5.74	5.85	5.81
Na	327.17	238.49	242.54	326	276.64	247.19	404.71	418.66	356.9
Ca	6676.46	5460.95	4187.74	5776.13	5381.82	4628.75	7511.1	8613.7	6237.09
Sc	23.85	23.89	20.27	22.43	21.54	20.82	23.59	24.73	23.58
V	120.63	112.49	96.42	113.08	112.91	104.3	120.9	123.11	128
Cr	4035.21	3353.16	2777.05	3725.22	3600.68	3189.24	4602.55	4384.84	4541.31
Co	62.73	61.96	60.91	61.56	62.14	62.5	60.16	60.71	62.38
Ni	725.72	711.41	693.32	719.89	714.46	738.72	688.47	691.65	831.64
Ga	3.13	2.71	2.39	2.94	2.75	2.73	3.17	3.25	3.26
Rb	<0.0074	0.0087	<0.0070	<0.0077	<0.0076	0.0085	<0.0078	<0.0069	0.0106
Sr	0.354	0.0959	0.0413	0.278	0.168	0.0737	0.55	0.827	0.403
Y	1.11	1.099	0.907	1.052	1.013	0.937	1.234	1.37	1.156
Zr	1.99	1.85	1.3	1.8	1.68	1.44	0.097	2.05	0.208
Nb	0.0088	0.0088	0.0077	0.0082	0.0086	0.0118	<0.0163	<0.0154	<0.0116
Ba	0.006	<0.0059	<0.0065	<0.0131	<0.0054	0.0171	<0.054	<0.049	<0.086
La	0.0161	0.00506	0.00243	0.0103	0.0086	0.00309	<0.0115	0.0358	<0.0074
Ce	0.041	0.0161	0.00799	<0.0065	0.0228	0.014	<0.028	<0.0167	<0.0133
Pr	0.00776	0.00402	0.00177	0.00462	0.00475	0.0034	<0.10	<0.0043	<0.0025
Nd	0.0449	0.0271	0.0177	0.0316	0.0338	0.0198	0.0608	0.0749	0.0446
Sm	0.0319	0.0198	0.022	0.0319	0.0239	0.0179	0.039	0.0449	0.0273
Eu	0.0105	0.0088	0.0079	0.0093	0.0069	0.0096	0.0073	0.0196	0.0109
Gd	0.0636	0.052	0.0523	0.0688	0.0588	0.0522	0.0727	0.0987	0.0662
Tb	0.0167	0.013	0.011	0.0135	0.0133	0.0105	0.0125	0.0197	0.009
Dy	0.158	0.137	0.11	0.137	0.135	0.133	0.178	0.202	0.145
Ho	0.0427	0.0402	0.0324	0.0374	0.0343	0.0355	0.0392	0.0464	0.0374
Er	0.173	0.157	0.146	0.166	0.155	0.15	0.18	0.192	0.169
Tm	0.0362	0.0331	0.0331	0.0327	0.0332	0.0285	0.036	0.0371	0.0345
Yb	0.315	0.287	0.245	0.274	0.273	0.276	0.281	0.312	0.268
Lu	0.0542	0.0552	0.045	0.0506	0.0529	0.0443	0.0478	0.0529	0.0522
Hf	0.077	0.0786	0.0444	0.0775	0.0673	0.0573	<0.0225	0.0663	0.0523
Ta	0.00208	<0.00129	<0.00061	0.00129	<0.00063	<0.00077	<0.0069	<0.0035	<0.0033
Pb	0.00205	0.00213	0.00092	0.00174	0.00086	0.0043	<0.0074	0.006	0.06
Th	0.0667	0.0175	0.00571	0.0684	0.0579	0.0146	0.038	0.0797	0.024
U	0.0145	0.00641	0.00714	0.0103	0.0089	0.00765	<0.0043	0.0098	<0.013

CNTP 11	CPX1	CPX1	CPX1	CPX2	CPX2	CPX2	CPX3	CPX3	CPX3
Li	6.93	7.22	5.64	5.76	5.89	5.74	5.89	5.83	5.66
Na	7161.18	6691.52	6157.89	6616.41	6681.7	6732.94	6291.48	6143.07	6187.04
Ca	155854.52	158352.17	154820.91	157423.33	160727.09	152197.06	159206.27	162494.95	163786.84
Sc	68.4	75.35	75.37	76.2	79.36	72.07	78.36	86.48	87.25
V	313.42	313.98	298.29	336.03	332.35	340.37	331.56	325.99	329.4
Cr	8806.38	8947.88	7543.36	8663.79	8515.97	8609.98	8467.64	7941.91	7347.54
Co	25.07	26.7	27.58	23.67	24.61	23.92	24.63	24.95	25.17
Ni	350.83	372.07	473.1	350.28	366.19	376.47	363.52	379.08	388.31
Ga	4.2	4.4	3.66	3.73	4.03	3.96	3.75	3.63	3.76
Rb	0.009	0.0112	0.0994	0.0099	0.0143	0.115	<0.0079	0.007	0.0196
Sr	7.68	8.12	8.18	7.11	7.53	7.19	7.75	8.37	8.34
Y	21.98	23.83	19.24	21.67	23.36	21.15	22.47	21.68	22.55
Zr	32.76	37.2	33.04	35.39	38.37	34.88	37.25	38.19	37.96
Nb	0.357	0.471	0.56	<0.0118	0.0703	0.245	0.0354	0.0543	0.159
Ba	<0.060	0.0087	0.0806	<0.072	<0.0143	0.0331	<0.036	<0.0133	<0.0095
La	0.962	1.067	0.924	0.883	0.976	0.916	0.895	1.009	1.002
Ce	4.29	4.68	3.94	3.9	4.39	4.05	3.76	3.97	4.24
Pr	0.841	0.927	0.761	0.785	0.835	0.805	0.781	0.777	0.843
Nd	5.34	5.82	4.65	5.06	5.31	4.82	5.06	4.9	5.15
Sm	2.23	2.37	1.94	2.03	2.19	2.08	2.1	2.03	2.22
Eu	0.684	0.794	0.616	0.672	0.729	0.687	0.698	0.649	0.684
Gd	3.12	3.48	2.68	3.04	3.29	2.98	3.31	3.02	3.13
Tb	0.572	0.611	0.492	0.553	0.591	0.55	0.56	0.559	0.585
Dy	4.2	4.74	3.64	4.04	4.61	4.03	4.3	4.11	4.36
Ho	0.855	0.941	0.759	0.855	0.921	0.829	0.912	0.847	0.906
Er	2.49	2.73	2.23	2.48	2.61	2.37	2.55	2.51	2.66
Tm	0.35	0.377	0.311	0.351	0.366	0.325	0.357	0.357	0.354
Yb	2.24	2.48	1.96	2.18	2.39	2.2	2.34	2.27	2.38
Lu	0.297	0.32	0.259	0.295	0.303	0.287	0.301	0.304	0.308
Hf	1.16	1.3	1.14	1.15	1.22	1.12	1.17	1.22	1.18
Ta	0.0312	0.0509	0.0403	0.0399	0.0473	0.048	0.0284	0.0328	0.0483
Pb	<0.0108	0.0141	0.0519	<0.0092	0.013	0.0473	0.0212	0.0185	0.029
Th	0.0812	0.117	0.302	0.423	0.422	0.372	0.393	0.504	0.292
U	0.0215	0.0376	0.106	0.0281	0.125	0.119	0.111	0.143	0.1

CNTP 11	OPX1	OPX1	OPX1	OPX2	OPX2	OPX2	OPX3	OPX3	OPX3
Li	5.42	5.46	4.87	5.14	5.04	5.46	5.09	5.2	4.86
Na	352.88	343.1	261.9	291.54	289.56	303	291.66	288.19	295.93
Ca	6252.3	6158.84	4231.65	4966.98	5121.17	5195.57	4422.53	4340.8	4324.38
Sc	23.18	23.28	21.53	22.53	22.72	22.15	21.16	22.26	21.09
V	138.52	141.29	129.97	134.48	135.83	140	127.34	130.6	124.44
Cr	4174.06	4225.89	3435.07	3830.32	3832.79	4186.21	3879.66	3985.47	3303.33
Co	62.97	63.56	64.37	63.04	63.17	65.56	62.21	63.5	64.72
Ni	706	713.06	745.71	706.36	707.34	760.33	709.29	706.35	741.61
Ga	3.14	3.29	3.13	3.12	3.14	2.89	3.02	3.06	2.98
Rb	<0.0074	<0.0077	0.0187	<0.0075	<0.0075	<0.0075	<0.0073	<0.0077	<0.0067
Sr	0.0238	0.0291	0.0611	0.0087	0.0211	0.0176	0.0128	0.0121	0.0099
Y	1.44	1.46	1.2	1.35	1.4	1.34	0.99	1.08	1.02
Zr	1.44	2.41	1.87	2.03	1.99	1.68	1.46	1.72	1.54
Nb	<0.020	0.0225	0.0434	<0.016	<0.0045	<0.0053	<0.027	<0.0064	0.0127
Ba	<0.066	<0.084	0.0136	<0.0233	<0.075	<0.0248	<0.059	<0.0204	0.0142
La	<0.014	0.0178	<0.00156	<0.0031	<0.0065	<0.0068	<0.0039	0.00197	0.0075
Ce	<0.0136	0.0218	0.0053	0.0609	0.0096	<0.0092	<0.0066	<0.0048	0.0122
Pr	<0.0048	0.00581	0.00307	<0.00145	0.00495	0.00158	<0.00137	0.00193	0.00247
Nd	<0.0242	0.0432	0.0192	0.0203	0.0255	0.0288	0.011	0.0106	0.0185
Sm	0.0304	0.026	0.0229	0.023	0.0252	0.0307	0.0185	0.0125	0.0138
Eu	0.0087	0.0125	0.0115	<0.0046	0.011	0.0106	0.0064	0.0064	0.0061
Gd	0.0704	0.0655	0.0497	0.0591	0.0629	0.0509	0.0336	0.0432	0.0285
Tb	0.0147	0.0241	0.0162	0.0169	0.0153	0.0155	0.0111	0.0112	0.0132
Dy	0.191	0.207	0.137	0.196	0.165	0.16	0.12	0.117	0.109
Ho	0.0493	0.0569	0.0456	0.0497	0.0466	0.0482	0.0386	0.0401	0.0369
Er	0.24	0.224	0.172	0.219	0.209	0.21	0.162	0.165	0.163
Tm	0.0369	0.0458	0.0362	0.0439	0.0436	0.0421	0.03	0.0359	0.0297
Yb	0.364	0.34	0.348	0.363	0.373	0.337	0.296	0.308	0.309
Lu	0.0638	0.0697	0.0629	0.0661	0.0628	0.0612	0.0584	0.0586	0.0592
Hf	0.0703	0.092	0.068	0.108	0.082	0.0653	<0.0214	0.0815	0.0551
Ta	<0.0058	0.00379	0.00117	<0.00142	<0.00214	<0.0033	<0.00167	<0.00142	0.0067
Pb	<0.0048	<0.0115	0.0514	<0.00219	<0.00255	0.0023	<0.0025	0.00208	0.0048
Th	<0.0087	<0.0024	0.00287	0.0042	0.0109	0.00292	0.00262	<0.0058	0.00436
U	<0.0026	0.00336	0.00387	<0.00207	<0.00244	<0.0030	<0.0027	0.00168	0.00306

Tab A6.1 Results of U-Pb isotope analyzes from the zircons collected in the SEVP, Spain.

sample	207	U (ppm)	Pb (ppm)	Th/U	206*/238	1s%	7/35r	2s%	208/232	1s%	207*/206*	1s%	206/238	2s	207/206	2s	conc%
ALCS-1 Seq1																	
a1	415	432	0.5	6.79	0.0012	3.50	0.0023	10.3	0.003	12.1	0.1200	58.3	2.35	0.17	9	175	26
a2	243	858	0.5	1.84	0.0014	6.64	0.0029	15.1	0.003	17.1	0.4738	211.7	2.80	0.38	86	162	3
a3	421	624	0.5	3.15	0.0012	1.67	0.0025	7.6	0.002	3.6	0.0715	52.3	2.48	0.10	95	154	3
a4	63	371	0.2	0.82	0.0012	1.78	0.0021	21.3	0.000	#DIV/0!	0.7848	22.1	2.38	0.10	-234	529	-1
a5	234	1318	0.6	1.19	0.0012	1.05	0.0025	7.7	0.000	#DIV/0!	0.5944	83.8	2.41	0.07	88	168	3
a6	118	665	0.3	1.05	0.0012	2.58	0.0026	15.3	0.001	3.9	0.0931	99.5	2.56	0.14	55	339	5
a7	1263	638	0.6	1.01	0.0012	2.11	0.0028	14.3	0.001	4.5	0.0502	6.7	2.60	0.12	203	313	1
a8	537	1208	0.7	1.52	0.0012	1.08	0.0024	12.6	0.001	3	0.0444	6.0	2.54	0.07	-88	300	-3
a9	124	393	0.2	0.91	0.0011	2.41	0.0022	13.0	-0.002	-35	0.0414	5.6	2.44	0.13	-262	303	-1
a10	117	793	0.4	0.99	0.0010	1.97	0.0021	13.9	0.002	11	0.0231	18.1	2.37	0.10	-241	333	-1
a11	120	799	0.3	0.98	0.0010	2.94	0.0023	13.1	0.001	3	0.0235	17.7	2.34	0.15	-59	280	-4
a12	47423	659	13.2	3.03	0.0010	10.64	0.0022	38.9	0.000	-420	0.0415	16.2	2.48	0.53	-255	823	-1
a13	240	1175	0.6	1.37	0.0009	5.83	0.0025	15.6	0.001	8	0.0753	50.98	2.32	0.27	168	236	1
a14	40	277	0.1	0.64	0.0011	3.11	0.0024	27.8	0.001	5	0.5985	20.1	2.61	0.17	-141	669	-2
a15	113	1097	0.4	0.35	0.0010	1.70	0.0028	14.6	0.008	21	0.0200	1665.2	2.58	0.10	207	325	1
a16	137	1520	0.6	0.52	0.0010	1.61	0.0026	16.0	0.001	5	0.1282	108.5	2.47	0.09	163	364	2
a17	570	1257	0.6	0.47	0.0010	1.72	0.0026	20.4	-0.001	-28	0.0509	9.9	2.42	0.10	235	462	1
a18	1733	3964	2.0	0.58	0.0009	1.22	0.0027	17.2	0.001	21	0.0514	8.4	2.43	0.08	259	387	1
a19	489	382	0.6	4.39	0.0010	2.01	0.0027	7.4	0.007	6	0.1618	10.5	2.61	0.12	102	141	3
a20	246	585	0.4	3.88	0.0009	6.03	0.0021	13.8	0.001	4	0.0960	56.5	2.30	0.28	-185	159	-1
a21	40	251	0.1	0.89	0.0010	3.11	0.0027	22.8	0.001	12	0.7899	8.1	2.64	0.17	57	521	5
a22	293	756	0.4	2.16	0.0008	6.85	0.0023	15.1	0.001	3	0.1275	2.8	2.22	0.31	89	142	3
a23	796484	673	117.9	1.27	-0.0198	-4.99	-1.0039	10.3	-17.513	-8	0.9312	-82.9	-54.82	-5.59	5024	26	
a24	147	1011	0.4	0.63	0.0009	1.92	0.0027	12.9	0.012	17	0.3996	85.7	2.62	0.11	149	285	2
a25	104	683	0.3	0.77	0.0009	2.04	0.0028	22.8	0.026	17	0.6219	41.0	2.59	0.12	249	514	1
a26	499468	1263	312.4	1.03	0.1999	1.28	10.3814	4.8	1.163	3	1.8387	43.4	545.55	16.91	5012	51	
a27	135	990	0.4	0.71	0.0009	2.91	0.0026	18.5	0.001	6	0.1430	40.9	2.68	0.16	-80	426	-3
a28	221	1004	0.6	2.15	0.0009	3.13	0.0027	12.6	0.001	10	0.0451	628.3	2.60	0.17	80	255	3
a29	60	449	0.2	0.69	0.0009	2.04	0.0025	20.2	0.003	14	1.0000	1.0	2.59	0.12	-87	482	-3
a30	93346	1057	30.8	1.29	0.0015	14.53	0.0781	29.1	0.003	39.4	0.9214	-103.6	4.38	1.28	4979	17	0
a31	598282	656	199.2	0.83	0.0090	11.88	0.4670	24.5	-47.494	-10.8	0.0529	515.9	27.06	6.44	4931	80	1
a32	306	361	0.4	5.62	0.0008	4.44	0.0023	14.1	0.004	14.5	0.0506	100.0	2.42	0.22	-76	263	-3
a33	182	1143	0.5	0.80	0.0008	1.84	0.0025	6.6	0.003	13.5	0.0907	244.6	2.49	0.10	46	122	5
a34	2882528	1067	2945.6	0.88	3.1384	4.80	139.9010	16.2	4.962	10.2	0.7783	11.4	6019.59	395.37	4640	186	130
a35	42395	500	14.4	0.47	0.0007	34.47	0.0336	69.1	-0.234	-23.7	0.2112	173.1	2.10	1.45	4823	61	0
a36	293	414	0.5	4.68	0.0009	4.73	0.0027	19.0	0.004	8.6	0.0010	21868.9	2.73	0.26	-25	396	-11
a37	22204	4	2.8	0.41	-1.6049	-2.30	-82.3380	24.0	19.713	1.8	0.5439	69.6	-10394.99	-1182.93	4822	335	-216
a38	315299	863	104.3	1.04	0.0006	100.74	0.0351	201.5	-0.018	-25.1	0.9915	18.6	1.93	3.89	5010	20	0
a39	425	891	0.5	1.96	0.0006	12.25	0.0047	27.7	-0.001	-52.7	0.1908	21.0	1.88	0.46	1894	230	0
a40	2296	405	1.0	0.47	0.0010	22.66	0.0400	46.1	-0.001	-245.9	0.7382	30.3	3.18	1.44	4479	118	0
a41	11296	264	23.8	0.03	0.1912	0.46	0.8101	2.7	0.247	10.6	0.0620	1.9	597.83	12.46	620	34	96
a42	11757	288	25.6	0.03	0.1881	0.56	0.8012	2.5	0.175	7.9	0.0591	1.8	591.38	12.85	621	23	95
a44	162	1136	0.5	1.01	0.0007	1.56	0.0025	11.0	0.000	4.1	0.6118	50.5	2.49	0.09	75	247	3
a45	62	530	0.3	0.76	0.0008	2.01	0.0025	45.0	0.054	17.1	0.3392	38.9	2.65	0.12	-86	1098	-3
a46	117090	747	75.8	0.90	0.0559	1.48	3.4598	3.8	0.455	7.5	0.5551	22.6	186.80	6.56	5014	17	4
a47	77	509	0.2	0.54	0.0007	2.62	0.0028	23.2	0.013	16.0	0.7233	11.0	2.47	0.14	284	514	1
a48	107	848	0.4	0.84	0.0007	2.45	0.0026	23.0	0.001	4.9	0.0090	3582.3	2.42	0.13	191	521	1
a49	113	951	0.4	0.72	0.0007	1.90	0.0024	11.1	-0.003	-20.1	0.6894	-99.2	2.46	0.11	24	246	10
a50	10696	295	23.9	0.03	0.1635	0.52	0.7213	2.6	0.090	4.6	0.0578	2.8	542	12	592	29	91
a51	10927	288	24.1	0.03	0.1682	0.54	0.7528	2.7	0.190	9.6	0.0595	1.8	559	12	613	33	91
ALCS-1 Seq2																	
a1	5978	96	9.9	0.73	0.2004	1.21	0.8270	11.0	0.129	1.8	0.0531	5.7	564	56	794	80	71
a2	4906	102	7.4	0.26	0.1515	2.08	0.6768	12.3	0.088	18.0	0.0621	10.4	432	46	950	114	46
a3	3342	61	5.5	0.63	0.1784	1.08	0.6682	10.9	0.107	1.8	0.0575	11.5	506	50	578	78	88
a4	10336	17	7.4	0.51	0.8576	0.99	8.6683	12.4	0.578	1.5	0.1592	3.4	2151	191	2442	116	88
a5	1613	26	2.5	0.41	0.1978	1.53	0.7634	11.7	0.120	3.3	0.0533	17.1	566	57	615	110	92
a6	1921	28	2.6	0.19	0.2021	1.33	0.8064	11.5	0.106	5.5	0.0372	27.1	580	58	678	101	86
a7	5043	141	7.9	0.70	0.1035	1.44	0.3560	21.6	0.080	2.6	0.0535	9.4	305	31	341	426	89
a8	888	20	1.3	1.02	0.1121	1.44	-0.1888	220.3	0.095	2	-0.0261	-110.0	331	34	#ZAHL!	#####	#ZAHL!
a9	1039	26	1.7	0.54	0.1321	1.84	0.9049	18.8	0.047	24	0.0430	93.5	390	41	1720	284	23
a10	1590	10	2.3	0.58	0.4380	1.22	2.4838	12.3	0.338	2	0.0541	35.2	1216	116	1356	129	90
a11	2031	26	3.2	0.57	0.2326	1.26	1.3731	12.8	0.159	2	0.0572	33.4	677	67	1424	141	48
a12	5162	13	5.3	1.19	0.6705	1.27	5.1727	11.0	0.392	2	0.1109	10.9	1806	166	1896	65	95
a13	1692	63	2.9	0.45	0.0899	0.98	0.3440	11.5	0.057	3	0.0182	54.62	275	28	503	114	55
a14	7483	284	11.1	0.21	0.0810	2.10	0.3148	11.9	0.064	2	0.0542	3.9	249	27	527	103	47
a15	1656	35	2.7	0.20	0.1635	1.30	0.6335	11.5	0.121	3	0.0436	29.5	496	50	510	106	97
a16	3338	33	4.8	0.83	0.2480	0.98	1.3865	11.7	0.183	2	0.0554	14.8	741	72	1259	110	59
a17	2575	34	3.4	0.84	0.1692	2.04	0.7795	11.6	0.102	2	0.0609	13.3	517	54	861	84	60
a19	6982	147	13.8	3.18	0.0932	2.16	0.3368	18.3	0.065	1	0.0529	7.3	292	31	315	334	93
a20	10927	9	5.9	1.02	0.9797	0.88	13.4554	10.4	0.529	2	0.1880	2.4	2569	221	2820	26	91
a21	12282	24	9.3	0.68	0.6730	1.24	5.7713	12.1	0.303	3	0.1243	3.0	1877	171	2012	110	93
a22	24805	33	16.1	0.72	0.7686	2.10	9.5691	11.1	0.365	6	0.1693	2.4	2112	200	2644	37	80
a23	17313	59	13.1	0.85	0.3417	2.17	3.6422	12.8	0.188	6	0.1177	5.1	1038	106	2359	112	44
a24	1173	21	1.7	1.11	0.1142	1.80	0.7276	24.5	0.066	2	0.0697	29.3	368	38	1424	421	26
a25	1242	21	1.6	1.09	0.1087	1.50	0.7633	28.5	0.068	3	0.0646	44.4	352	36	1599	494	22
a26	1548	41	2.6	0.89	0.1008	1.37	0.5580	14.2	0.101	2	0.0271	66.0	329	34	1131	191	29
a27	12895	229	18.0	0.02	0.1638	1.09	0.6918	10.5	0.115	4	0.0537	30.1	528	53	558	45	95
a28	1006	19	0.8	1.21	0.1027	3.22	-3.7803	61.5	0.091	4	-0.5114	-30.1	338	39	#ZAHL!	#####	#ZAHL!
a29	9140	18	7.6	0.70	0.6839	1.10	6.1716	10.6	0.387	2	0.1268	3.2	1982	178	2020	46	98
a30	7450	36	8.3	0.46	0.3956	1.05	2.5073	11.2	0.332	2.0	0.0807	3.5	1225	116	1359	83	90
a31	1174	12	1.4	0.57	0.1474	1.79	1.9908	20.9	0.153	4.6	0.0636	69.9	486	50	2693	296	18
a32	40773	58	27.1	0.17	0.8319	1.19	9.2340	10.5	0.663	1.6	0.1472	1.4	2369	209	2355	30	101
a34	5951	72	6.9	0.58	0.1686	4.37	1.0863	14.9	0.048	10.6	0.0687	9.1	566	73	1334	128	42
a35	2125	60	3.8	0.57	0.1060	1.01	0.4309	11.6	0.063	2.4	0.0425	20.1	363	36	366	121	99
a36	14136	56	17.4	0.64	0.5057	1.28	3.7157	10.5	0.310	1.2	0.0952	2.3	1582	148	1565	31	101
a37	935	28	1.4	0.59	0.0844	1.87	0.4176	14.1	0.067	2.8	0.0316	57.8	294	31	773	191	38
a38	6024	43	6.0	0.25	0.2220	2.35	1.9591	17.5	0.169	30.7	0.0546	10.5	750	79	1883	243	40
a39	1052	18	1.3	0.55	0.1329	2.29	-1.1344	75.6	0.146	9.3	-0.1113	-37.4	461	49	#ZAHL!	#####	#ZAHL!
a40	3096	40	4.0	0.13	0.1681	1.17	1.2275	19.9	-1.438	-3.7	0.0471	23.6	581	58	1515	320	38
a41	6619	100	10.4	0.50	0.1722	1.07	0.8310	10.8	0.110	1.9	0.0607	4.1	598	59	675	65	89
a42	761	23	1.6	1.17	0.0996	1.20	0.4704	15.5	0.064	2.1	0.0587	38.0	354	36	618	249	57
a44	12800	121	18.3	0.68	0.2295	1.29	1.1884	12.3	0.140	2.4	0.0651	3.3	804	79	770	139	104
a47	669	22	1.3	0.66	0.0943	1.56	0.4236	12.8	0.055	2.8	0.0535	43.9	348	36	428	160	81
a48	22499	183	30.5	0.35	0.2743	1.16	1.6267	10.5	0.167	1.7	0.0683	2.3	969	94	1006	41	96
a49	1230	20	2.1	0.46	0.1684	1.14	0.8617	12.0	0.090	4.9	0.0564	19.2	615	61	688	128	89
a51	12165	368	25.2	1.76	0.0811	1.38	0.3476	17.8	0.056	1.1	0.0519	7.2	307	31	273	330	112
a52	1858	25	3.5	1.28	0.1841	1.53	1.0402	14.3	0.104	1.9	0.0418	22.6	680	68	862	201	79

sample	207	U (ppm)	Pb (ppm)	Th/U	206*/238	1s%	7/35r	2s%	208/232	1s%	207*/206*	1s%	206/238	2s	207/206	2s	conc%
a53	5277	69	9.3	0.88	0.1997	1.82	1.0851	17.9	0.104	2.2	0.0650	7.1	739	75	769	303	96
a54	42354	75	36.3	1.02	0.6496	0.85	7.3480	10.3	0.308	1.2	0.1331	0.7	2156	190	2154	20	100
a55	1464	20	2.9	0.29	0.2308	1.29	1.3255	11.6	0.156	2.5	0.0495	26.9	855	84	862	104	99
ALCS-1 Seq3																	
a1	13278	77	14.4	0.56	0.2368	0.57	2.7882	12.7	0.564	1.2	0.0562	9.8	853	19	2263	215	38
a2	7149	304	14.7	0.21	0.0827	0.67	0.3666	5.2	0.064	1.3	0.0500	3.8	311	8	362	102	86
a3	3315	119	6.6	0.60	0.0825	0.77	0.4344	6.4	0.073	1.3	0.0447	12.2	310	8	738	123	42
a4	64	82	0.1	0.48	0.0007	7.02	0.0081	53.6	0.001	19.5	1.0717	5.5	3	0	2115	906	0
a5	6621	44	9.6	0.85	0.2884	0.67	2.2341	5.3	0.251	1.7	0.0683	6.6	1029	24	1500	89	69
a6	2961	58	5.5	0.56	0.1432	1.03	0.7416	4.9	0.099	1.7	0.0542	10.0	532	15	691	82	77
a7	656	29	1.4	0.52	0.0774	0.99	0.3379	8.6	0.056	2.9	0.0297	83.1	294	8	311	183	94
a8	6583	211	10.6	0.22	0.0829	0.80	0.2917	13.9	0.082	2	0.0427	6.8	314	8	-205	343	-153
a9	2938	588	2.4	0.55	0.0036	3.28	0.1278	15.7	0.025	5	0.8849	56.8	14	1	4008	210	0
a10	90	190	0.1	1.10	0.0007	6.05	0.0069	52.8	0.001	12	0.8200	40.5	3	0	1974	915	0
a11	19	76	0.0	0.51	0.0007	8.16	0.0064	164.0	0.003	15	0.9249	17.0	3	0	1712	3001	0
a12	67	132	0.1	0.73	0.0012	7.05	0.0144	50.0	0.004	13	0.6202	18.0	5	1	2288	824	0
a13	10526	178	19.9	0.69	0.1650	0.68	0.8347	3.6	0.111	1	0.0584	2.57	616	15	617	55	100
a14	216	522	0.2	0.77	0.0007	3.02	-0.0086	414.1	0.001	3	-0.1540	-207.0	3	0	#ZAHL!	#####	#ZAHL!
a15	176676	169	103.8	0.79	0.8030	0.95	14.1999	2.9	0.459	1	0.2123	0.3	2568	60	2909	11	88
a16	1889	66	3.5	0.70	0.0777	0.83	0.4051	6.8	0.055	2	0.0539	19.0	299	8	672	133	44
a17	3676	76	6.6	0.43	0.1398	0.82	0.7581	6.0	0.083	1	0.0454	9.1	528	14	753	114	70
a18	23859	109	30.4	0.75	0.3994	0.85	2.6877	7.5	0.296	3	0.0805	3.5	1409	34	1192	139	118
a19	30096	36	20.1	0.74	0.7665	0.81	11.4002	3.1	0.422	1	0.1753	0.9	2481	55	2617	25	95
a20	31246	70	34.3	1.27	0.5992	0.71	6.3011	2.9	0.402	1	0.1236	0.9	2017	44	2020	23	100
a21	14434	428	25.0	0.34	0.0927	0.83	0.3912	6.7	0.077	2	0.0503	3.0	357	9	187	144	191
a22	93	214	0.1	0.95	0.0009	4.04	0.0074	39.6	0.001	11	1.9304	32.1	3	0	1640	719	0
CNTS-1 seq1																	
a1	775	323	5.2	2.59	0.0170	1.58	0.1206	8.6	0.001	3.0	0.0113	221.2	104	7	365	131	28
a2	22204	539	55.6	0.13	0.1075	1.19	0.9048	6.8	0.013	42.3	0.0637	1.6	633	36	730	70	87
a3	6365	250	26.4	0.77	0.0977	0.81	0.7618	6.2	0.040	1.0	0.0581	4.8	577	32	566	53	102
a4	1987	49	7.5	0.88	0.1411	1.14	1.2624	7.8	0.053	1.4	0.0532	20.5	820	46	852	106	96
a5	21826	717	103.8	0.95	0.1360	1.13	1.1168	6.2	0.040	0.7	0.0585	1.5	794	44	668	39	119
a6	6462	184	23.0	0.44	0.1232	0.81	1.0709	6.3	0.058	1.1	0.0639	4.5	724	39	786	53	92
a7	10397	307	36.4	0.84	0.1062	0.69	0.9989	6.1	0.045	0.8	0.0580	3.7	630	34	946	45	67
a8	42243	302	106.2	0.65	0.3511	1.08	5.8267	6.1	0.035	1	0.1165	0.9	1885	97	2021	27	93
a9	12143	438	44.2	0.87	0.0908	1.17	0.9514	6.9	0.027	1	0.0591	3.5	543	31	1159	70	47
a10	553138	434	318.6	0.33	0.0966	1.97	6.0667	9.6	3.079	7	0.0692	4.5	578	37	4148	102	14
a11	5521	182	19.3	0.71	0.0963	1.75	0.8317	7.8	0.037	1	0.0605	5.2	576	36	758	92	76
a12	3388	54	12.5	2.38	0.1381	1.23	1.1909	7.4	0.047	1	0.0516	25.2	815	46	745	92	109
a14	7641	555	34.9	0.86	0.0572	0.83	0.4149	6.8	0.022	1	0.0549	3.4	351	20	361	82	97
a16	17016	517	60.8	0.52	0.1145	0.86	0.9770	6.0	0.037	1	0.0621	1.7	686	38	711	35	97
a17	3781	129	16.5	1.83	0.0923	1.89	0.7275	26.0	0.033	2	0.0583	12.5	560	36	537	550	104
a18	4460	78	13.5	0.23	0.1785	1.02	1.7905	6.4	0.062	2	0.0699	7.5	1043	57	1040	51	100
a19	26084	166	79.3	2.20	0.3268	0.87	5.2610	5.9	0.116	1	0.1097	1.5	1799	91	1934	27	93
a20	14696	197	44.2	0.40	0.2230	1.15	2.5695	6.2	0.074	2	0.0827	2.0	1282	69	1308	35	98
a23	2603	67	9.0	0.39	0.1324	1.23	1.1957	7.1	0.049	1	0.0611	12.1	797	45	804	80	99
a24	33801	165	67.7	0.55	0.3784	0.91	6.3556	6.0	0.122	1	0.1228	1.1	2060	103	1992	27	103
a25	3857	155	13.9	0.64	0.0799	1.30	0.7066	7.4	0.036	1	0.0567	6.0	494	29	754	91	66
a26	3561	140	12.5	0.74	0.0789	1.01	0.5918	19.6	0.021	4	0.0546	9.3	489	28	392	421	125
a27	9185	288	40.9	1.55	0.1083	0.75	1.0009	6.1	0.039	1	0.0641	2.3	663	36	839	45	79
a28	46274	337	52.0	0.44	0.1266	4.53	2.7378	11.0	0.046	4	0.1569	1.5	769	77	2420	53	32
a29	15571	261	43.4	0.20	0.1653	1.16	1.8395	6.2	0.071	2	0.0714	1.9	988	55	1210	34	82
a30	24231	605	66.1	1.18	0.0910	1.09	0.7326	6.9	0.033	0.9	0.0582	1.8	564	32	536	79	105
a31	19504	637	73.1	0.35	0.1115	0.64	1.0727	6.0	0.045	1.5	0.0670	1.7	685	37	912	43	75
a32	9733	245	36.5	0.18	0.1527	0.70	1.5242	6.2	0.062	1.4	0.0713	3.3	922	49	984	52	94
a33	1978	101	7.9	0.34	0.0775	0.87	0.6205	7.7	0.026	2.1	0.0534	10.3	485	27	514	112	94
a34	13724	481	48.1	0.18	0.1025	0.67	0.8731	5.9	0.036	1.3	0.0605	1.7	637	34	639	34	100
a36	3425	96	11.0	1.17	0.0860	1.56	1.0647	9.7	0.027	2.8	0.0738	8.8	540	33	1391	142	39
a37	5831	506	26.5	0.48	0.0500	1.13	0.3748	7.0	0.017	1.3	0.0480	5.9	319	19	350	83	91
a38	16058	93	36.1	0.63	0.3445	1.07	5.6268	6.2	0.109	1.0	0.1137	1.8	1939	99	1900	35	102
a39	17126	294	58.3	0.74	0.1749	1.04	1.8083	6.2	0.059	1.2	0.0733	1.9	1058	57	1028	39	103
a40	16985	587	69.4	0.27	0.1167	0.82	1.0675	6.0	0.045	1.2	0.0638	1.9	726	39	772	35	94
a41	17191	523	62.0	0.47	0.1118	1.20	1.0152	6.2	0.040	1.1	0.0622	1.5	698	40	754	31	93
a42	16992	427	13.9	1.90	0.0135	1.28	0.1239	6.3	0.050	4.8	0.0503	3.4	88	5	777	37	11
a43	25075	716	112.2	1.11	0.1316	1.41	1.4805	6.5	0.043	1.1	0.0720	1.6	817	47	1185	41	69
a44	1926	151	9.3	0.62	0.0562	1.03	0.4272	7.8	0.020	1.6	0.0491	17.7	363	21	351	116	103
a45	1479	109	6.9	0.91	0.0535	0.92	0.4308	7.2	0.025	4.5	0.0506	12.5	346	20	476	96	73
a46	10258	391	41.2	0.55	0.0966	0.95	0.8522	6.2	0.035	0.8	0.0609	2.3	614	34	671	45	91
a47	19211	485	26.4	0.54	0.0506	0.95	0.3944	6.0	0.017	1.7	0.0540	1.4	329	19	395	36	83
a48	15080	711	45.2	0.42	0.0603	1.12	0.4669	6.2	0.022	1.2	0.0534	1.8	391	23	377	42	104
a49	4569	166	21.7	1.42	0.0975	1.28	0.8606	6.6	0.036	0.9	0.0565	7.7	621	36	663	55	94
a50	11657	402	44.6	0.44	0.1030	1.26	0.9006	6.3	0.037	1.0	0.0633	2.1	656	38	638	41	103
a51	3730	165	16.4	1.15	0.0731	1.24	0.6519	6.8	0.035	1.0	0.0639	5.9	473	27	679	69	70
a53	25440	150	59.8	0.89	0.3254	0.76	5.3437	5.8	0.103	0.6	0.1127	0.9	1886	94	1865	23	101
a54	4893	413	19.7	0.10	0.0486	0.80	0.3716	6.5	0.019	2.1	0.0543	5.2	320	18	329	70	97
CNTS-1 seq2																	
a1	8956	339	36.8	1.65	0.0769	0.88	0.7375	6.5	0.023	4.7	0.0585	3.9	479	17	910	111	53
a2	4229	331	17.0	0.32	0.0509	0.76	0.3708	14.6	0.018	3.3	0.0529	7.0	321	11	313	322	103
a3	7342	698	32.4	0.19	0.0482	1.23	0.3529	4.6	0.021	1.4	0.0510	3.1	305	12	323	54	94
a4	3918	165	15.9	0.60	0.0883	0.82	0.7750	5.4	0.029	2.4	0.0529	9.6	548	19	721	87	76
a5	36135	360	24.0	1.99	0.0443	1.39	0.4015	4.8	0.019	3.0	0.0596	1.2	281	12	787	47	36
a6	10338	428	46.2	0.90	0.0947	1.41	0.7864	4.7	0.030	1.5	0.0602	2.4	586	24	600	45	98
a7	13219	538	23.5	0.54	0.0414	1.44	0.3043	6.3	0.016	1.4	0.0532	2.3	263	11	328	106	80
a8	23654	386	87.7	0.59	0.2079	1.50	2.3233	4.7	0.079	1	0.0793	1.4	1225	49	1210	34	101
a9	2473	128	10.2	0.26	0.0801	0.71	0.6470	4.3	0.031	3	0.0588	10.7	500	17	537	57	93
a10	1652	80	8.6	1.46	0.0804	1.05	0.6444	5.6	0.031	1	0.0509	22.6	502	18	520	91	97
a11	8532	302	32.8	1.04	0.0913	1.26	0.9406	4.9	0.030	1	0.0622	2.3	567	22	1045	55	54
a12	46433	154	64.0	0.05	0.4033	3.47	8.6536	7.9	0.320	18	0.1934	1.0	2202	144	2392	32	92
a13	12250	474	59.6	1.32	0.0993	1.55	0.8199	6.9	0.035	1	0.0595	2.60	616	26	577	115	107
a14	16914	396	78.3	0.79	0.1757	1.59	1.7808	4.9	0.059	1	0.0731	2.1	1054	44	1007	38	105
a15	15878	514	70.4	0.57	0.1276	1.21	1.1530	4.6	0.050	1	0.0632	1.9	783	29	767	48	102
a16	10812	344	41.6	0.59	0.1099	1.16	1.0820	5.1	0.043	1	0.0589	2.5	680	25	945	68	72
a17	32145	500	37.8	0.86	0.0523	1.13	0.5910	4.8	0.045	3	0.0519	1.7	333	13	1219	54	27
a18	23589	708	77.8	0.45	0.1051	1.27	0.9412	4.5	0.027	2	0.0589	1.0	652	25	745	40	88
a19	16879	589	49.2	0.79	0.0732	1.94	0.6061	8.1	0.031	1	0.0595	3.1	461	22	576	137	80
a20	7768	274	29.7	0.24	0.1092	1.52	0.9632	5.1	0.043	2	0.0618	3.0	677	28	711	55	95
a21	3476	76	16.1	1.28	0.1757	1.28	1.7953	5.4	0.059	2	0.0775	5.4	1057	40	1016	71	104

sample	207	U (ppm)	Pb (ppm)	Th/U	206*/238	1s%	7/35r	2s%	208/232	1s%	207*/206*	1s%	206/238	2s	207/206	2s	conc%
a22	4607	157	17.6	0.32	0.1093	1.29	0.9625	5.7	0.044	3	0.0656	5.0	678	26	705	84	96
a23	15060	651	42.4	1.18	0.0531	1.05	0.3935	4.2	0.020	1	0.0529	1.2	339	13	323	42	105
a24	31136	426	68.0	1.49	0.0338	1.08	0.2419	4.8	0.156	1	0.0513	1.4	218	8	244	66	89
a25	3728	144	15.5	0.71	0.0949	1.79	0.8034	5.8	0.034	2	0.0588	5.0	594	27	616	70	96
a26	6290	543	36.1	1.20	0.0535	1.76	0.3984	5.4	0.018	1	0.0526	3.2	342	16	331	58	103
a27	5260	444	27.4	0.86	0.0537	1.33	0.4041	4.9	0.019	1	0.0577	4.0	343	14	353	60	97
a28	8630	180	36.5	1.20	0.1632	1.44	1.6501	4.8	0.057	1	0.0704	2.7	992	39	985	46	101
a29	14285	535	62.6	1.85	0.0663	3.63	0.6610	9.3	0.030	2	0.0568	3.7	422	32	955	98	44
a30	11371	368	47.6	0.75	0.1159	1.11	1.2119	4.8	0.044	2.0	0.0623	3.2	721	26	1050	56	69
a31	2268	35	6.0	1.34	0.1328	1.90	1.9408	19.6	0.049	2.2	0.0577	39.8	820	38	1693	350	48
a32	5362	190	24.2	0.80	0.1108	1.77	0.9750	5.8	0.040	1.2	0.0642	4.6	691	31	691	71	100
a34	7487	280	30.2	0.14	0.1108	1.77	1.0418	8.4	0.033	2.6	0.0606	4.4	693	31	825	145	84
a35	1317	53	5.5	1.09	0.0818	1.38	0.8971	9.4	0.041	1.7	0.0719	17.1	518	21	1139	167	46
a36	951	35	3.8	0.24	0.1102	1.86	0.9935	8.4	0.039	3.3	0.0626	25.1	690	32	736	144	94
a37	5799	177	22.4	0.47	0.1173	1.10	1.0964	5.0	0.041	2.3	0.0664	4.4	732	27	810	66	90
a38	10121	388	46.9	0.71	0.1080	0.91	0.9285	4.2	0.036	0.9	0.0602	2.2	677	23	632	47	107
a39	6215	266	26.0	0.39	0.0938	1.24	0.7703	4.7	0.033	1.3	0.0582	3.5	593	23	531	54	112
a40	41085	508	78.6	2.09	0.0908	1.07	0.8875	4.0	0.069	2.0	0.0639	0.8	575	21	899	28	64
a41	54604	550	134.6	0.85	0.2050	0.97	3.6201	3.9	0.067	0.8	0.1235	0.5	1232	42	2024	19	61
a42	106323	780	256.0	0.09	0.3230	0.88	5.3693	3.9	0.118	0.9	0.1178	0.7	1848	58	1915	25	97
a43	3282	134	16.6	1.06	0.1037	0.90	0.9855	5.1	0.040	0.9	0.0574	5.9	654	23	837	74	78
a45	5025	228	24.6	1.15	0.0828	0.83	0.7250	4.5	0.034	0.7	0.0617	4.5	528	18	661	58	80
a46	2998	257	14.9	0.58	0.0523	0.82	0.3997	4.7	0.020	1.4	0.0469	8.2	339	12	360	71	94
a47	230	448	0.2	1.25	0.0025	3.31	-0.3899	245.0	0.001	4.6	-1.1110	-122.4	16	1	#ZAHL!	#####	#ZAHL!
a48	2013	147	9.3	0.83	0.0533	1.19	0.4844	6.6	0.023	1.3	0.0513	7.8	345	13	738	113	47
a49	32	88	0.1	0.65	0.0006	7.91	0.0182	52.3	0.001	10.7	0.8181	5.4	4	1	3039	797	0
a50	163	659	0.5	0.78	0.0006	3.21	0.0106	33.0	0.001	7.3	1.1357	39.3	4	0	2056	569	0
a51	327	13	1.1	0.97	0.0963	1.61	-3.8328	159.7	0.039	2.9	-0.2803	-79.8	612	26	#ZAHL!	#####	#ZAHL!
a52	168	197	0.4	0.66	0.0007	7.20	0.0284	28.3	0.001	14.9	0.7422	18.9	5	1	3333	378	0
a53	82	408	0.3	0.59	0.0005	3.75	0.0068	54.9	0.000	8.2	0.7703	16.1	3	0	1584	1016	0
a54	48	686	0.3	0.56	0.0004	5.04	0.0033	64.1	0.000	7.5	0.6376	20.0	2	0	715	1342	0
a55	176	967	0.6	0.94	0.0006	9.02	-0.0084	153.2	0.000	-56.1	-0.1058	-76.0	4	1	#ZAHL!	#####	#ZAHL!
CNTS-1 seq3																	
a1	24464	345	136.1	2.85	0.3571	1.60	2.6828	5.1	-0.002	-85.2	0.0526	0.9	2035	87	304	30	669
a2	120	900	0.4	0.66	0.0003	3.88	0.0048	28.7	0.000	12.5	0.7750	32.4	2	0	1597	510	0
a3	16606	407	70.0	0.98	0.1400	0.58	1.6740	6.5	0.061	2.1	0.0690	2.6	877	33	1278	101	69
a4	210937	856	392.3	0.26	0.4142	0.56	9.4544	4.0	0.139	0.9	0.1586	0.3	2315	78	2442	13	95
a5	29727	650	119.1	0.40	0.1686	0.69	1.7866	4.4	0.078	1.9	0.0736	0.8	1046	39	1030	34	102
a6	17712	347	91.4	2.43	0.2396	4.35	2.0053	10.7	0.021	0.6	0.0495	2.6	1441	124	531	109	271
a7	54	640	0.3	0.53	0.0004	3.55	0.0036	32.5	0.000	9.9	0.4029	57.7	3	0	732	666	0
a8	17313	439	86.8	1.23	0.1557	0.58	1.6675	4.6	0.053	1	0.0675	2.0	975	36	1043	45	94
a9	42124	373	384.9	2.84	0.9241	1.99	8.4618	5.6	0.173	3	0.0604	0.9	4372	177	716	27	610
a10	26139	1014	126.3	0.55	0.1121	0.52	1.0545	4.3	0.040	1	0.0650	1.1	718	27	770	36	93
a11	58790	546	182.3	0.64	0.2850	0.64	4.9806	4.3	0.097	1	0.1176	0.7	1692	60	1962	26	86
a12	26429	1217	117.0	0.52	0.0871	2.61	0.6932	8.8	0.025	3	0.0546	3.0	568	35	396	135	143
a13	2591	139	14.0	0.41	0.0927	0.63	0.8521	6.4	0.041	2	0.0479	10.32	604	23	707	106	85
a14	884	990	6.6	1.13	0.0054	1.57	0.0413	9.0	0.002	2	0.0364	31.7	37	2	290	172	13
a15	145	1102	-0.2	0.51	0.0005	2.92	-0.1243	287.1	0.001	7	-1.5979	-143.4	4	0	#ZAHL!	#####	#ZAHL!
a16	2678	149	18.3	1.08	0.0961	0.76	0.8778	8.8	0.039	2	0.0557	7.7	626	24	687	167	91
a17	8135	1013	65.9	1.01	0.0536	1.23	0.4210	5.2	0.018	1	0.0506	3.4	358	16	351	60	102
a18	26811	1117	241.5	0.94	0.1974	2.95	1.7724	7.2	0.034	1	0.0593	1.0	1230	79	644	33	191
a19	22278	759	254.4	0.30	0.3371	3.25	2.8811	7.7	0.029	1	0.0575	1.0	1980	130	534	31	371
a20	25528	422	208.2	3.83	0.4436	2.23	3.4210	6.2	0.035	2	0.0524	0.9	2500	123	302	45	829
a21	32619	524	358.1	2.09	0.6513	4.21	5.4952	9.5	0.073	4	0.0572	1.1	3407	249	500	51	681
a22	18290	416	157.9	1.56	0.3710	2.40	2.8263	6.9	0.022	2	0.0516	1.5	2157	113	267	71	807
a23	6310	1031	59.8	0.78	0.0514	1.25	0.4117	5.1	0.013	1	0.0486	3.2	346	15	374	50	93
a24	75	1072	0.4	0.67	0.0003	3.78	0.0039	36.5	0.000	8	0.7469	49.2	2	0	1134	706	0
a25	790	511	2.1	1.42	0.0034	2.30	-0.1653	79.2	0.003	2	-0.3246	-39.4	24	1	#ZAHL!	#####	#ZAHL!
a26	17	597	0.1	0.72	0.0003	5.13	-0.0393	269.7	0.000	18	-0.8044	-134.4	2	0	#ZAHL!	#####	#ZAHL!
a27	111	734	1.0	1.57	0.0011	2.36	0.0129	19.1	0.000	3	0.4321	57.3	7	0	1225	356	1
a28	335	806	4.6	1.79	0.0040	2.65	-0.0352	110.2	0.002	2	-0.0586	-54.9	28	2	#ZAHL!	#####	#ZAHL!
a29	69	947	0.7	0.96	0.0006	3.82	0.0057	40.5	0.000	8	0.3546	38.0	4	0	794	830	1
a30	50	1084	0.4	1.00	0.0004	3.28	-0.0175	481.0	0.000	8.0	-0.2862	-240.4	3	0	#ZAHL!	#####	#ZAHL!
a31	97	625	1.3	1.47	0.0016	3.80	0.0119	21.4	0.001	3.4	0.2849	64.0	11	1	227	454	5
CNTS-1 seq4																	
a1	356	824	1.1	0.77	0.0006	3.52	-0.0099	598.9	0.001	3.9	-0.1167	-299.4	4	0	#ZAHL!	#####	#ZAHL!
a2	77	863	0.8	2.33	0.0012	3.04	-0.0672	238.6	0.000	6.4	-0.3954	-119.1	8	1	#ZAHL!	#####	#ZAHL!
a3	264	844	3.8	1.26	0.0034	3.74	-0.0704	199.4	0.001	3.1	-0.1470	-99.6	22	2	#ZAHL!	#####	#ZAHL!
a4	106	1328	1.2	0.90	0.0007	3.66	0.0086	43.1	0.000	9.6	0.1196	102.0	4	0	1472	802	0
a5	158	1042	1.3	1.64	0.0010	4.17	-0.0236	359.5	0.001	8.8	-0.1722	-179.6	6	1	#ZAHL!	#####	#ZAHL!
a6	150	1003	0.8	0.75	0.0005	3.67	0.0142	21.8	0.001	4.0	0.1273	292.2	3	0	3112	321	0
a7	34	1104	0.2	0.68	0.0003	6.73	-0.0215	297.8	0.000	13.1	-0.5708	-148.6	2	0	#ZAHL!	#####	#ZAHL!
a8	12	535	0.2	0.56	0.0004	5.64	0.0026	78.0	0.000	11	0.8807	19.4	2	0	335	1748	1
a9	36	986	0.4	0.55	0.0004	4.28	0.0044	36.5	0.000	11	0.8083	22.1	2	0	1397	675	0
a10	42	1169	0.4	0.72	0.0003	5.93	0.0037	58.8	0.000	11	0.5902	20.2	2	0	1668	1063	0
a11	39	1070	0.5	1.11	0.0004	5.09	0.0047	41.9	0.000	8	0.7971	26.5	2	0	1674	747	0
CG-Z1_klein_seq1																	
a1	3665	11	4.9	1.48	0.3373	0.87	5.3919	5.7	0.122	1.4	0.1002	7.9	1924	77	1840	60	105
a2	1435	60	3.1	0.46	0.0469	0.76	0.3720	6.8	0.023	1.5	0.0711	12.7	304	14	447	112	68
a3	10569	10	7.0	0.84	0.5348	0.88	16.1861	5.0	0.205	1.4	0.2159	1.1	2829	107	2929	30	97
a4	45167	110	39.2	0.20	0.3384	0.50	6.0693	4.5	0.128	0.9	0.1254	0.6	1926	74	2049	19	94
a5	88170	156	83.3	0.16	0.5066	0.87	9.1945	4.7	0.253	2.5	0.1265	0.3	2703	103	2071	14	130
a6	5058	93	11.1	1.04	0.0962	0.87	0.8407	5.3	0.038	1.1	0.0607	4.7	608	27	663	56	92
a7	1873	48	3.8	0.46	0.0748	0.82	0.6244	6.9	0.029	2.1	0.0559	7.2	477	21	565	112	84
a8	4243	30	7.6	1.25	0.2028	0.81	2.2711	5.2	0.078	1	0.0718	6.2	1218	51	1176	47	104
a9	2473	61	5.0	0.30	0.0801	0.71	0.6697	5.2	0.031	3	0.0588	10.7	509	22	574	57	89
a10	1652	38	4.2	1.66	0.0804	1.05	0.6663	6.3	0.031	1	0.0509	22.6	510	23	556	91	92

sample	207	U (ppm)	Pb (ppm)	Th/U	206*/238	1s%	7/35r	2s%	208/232	1s%	207*/206*	1s%	206/238	2s	207/206	2s	conc%
a11	952	18	2.2	0.74	0.1033	1.05	0.8590	6.1	0.040	2	0.0908	11.2	648	29	563	83	115
a12	3871	76	7.2	0.22	0.0945	0.57	0.8094	9.8	0.039	2	0.0601	4.3	594	25	633	188	94
a13	13021	39	15.6	0.68	0.3392	0.70	5.6704	5.0	0.146	1	0.1159	2.07	1917	75	1938	40	99
a14	985	16	2.6	2.39	0.1102	1.13	0.9442	7.0	0.038	1	0.0602	2.0	687	32	636	109	108
a15	3253	167	8.5	0.52	0.0482	0.72	0.3529	5.6	0.020	1	0.0412	10.8	309	14	289	77	107
a16	6547	79	12.0	0.61	0.1361	0.79	1.3306	5.3	0.053	1	0.0619	3.8	837	36	916	55	91
a17	1701	38	4.0	0.84	0.0912	0.93	0.7620	6.2	0.037	1	0.0580	14.7	572	26	587	88	97
a18	21508	27	16.2	0.75	0.4866	1.13	12.7644	5.1	0.184	1	0.1869	1.5	2592	104	2716	29	95
a19	7507	107	15.3	0.67	0.1283	0.63	1.1714	5.1	0.050	1	0.0581	4.5	790	33	779	51	101
a20	5127	199	11.6	0.58	0.0535	0.50	0.3774	14.1	0.021	1	0.0498	6.7	341	15	212	310	161
a21	628	26	1.5	0.50	0.0555	1.54	0.4392	9.9	0.024	3	0.0082	553.2	354	18	472	187	75
a22	805	9	1.7	1.32	0.1523	1.56	1.5325	7.6	0.061	2	0.0987	25.7	926	46	985	112	94
a23	1366	24	2.9	0.40	0.1173	0.91	1.0310	7.3	0.048	2	0.0502	19.1	723	32	708	119	102
a24	43426	94	52.2	0.20	0.5299	0.58	9.3990	4.6	0.260	3	0.1281	0.5	2767	101	2059	20	134
a25	1338	27	3.5	1.07	0.1081	0.85	0.9310	7.8	0.041	2	0.0438	29.7	669	29	666	134	100
a26	2837	84	6.2	0.17	0.0763	0.97	0.5910	5.5	0.031	2	0.0538	7.3	479	22	436	66	110
a27	4203	217	10.6	0.16	0.0507	0.88	0.3821	6.7	0.025	3	0.0592	5.1	322	15	377	108	85
a28	4406	102	10.9	0.80	0.0952	0.78	0.7780	5.1	0.039	1	0.0574	5.0	591	26	557	51	106
a29	3320	114	7.8	0.48	0.0652	0.82	0.5141	5.5	0.026	1	0.0576	8.5	410	18	482	68	85
a30	5473	265	12.5	0.16	0.0488	0.74	0.3624	5.5	0.021	1.6	0.0555	3.6	310	14	347	71	89
a31	2244	49	5.9	1.11	0.1006	1.01	0.8664	6.3	0.041	1.4	0.0477	14.4	622	28	675	89	92
a32	7017	155	15.9	0.54	0.0962	0.50	0.8591	5.3	0.038	1.1	0.0572	4.0	595	25	755	63	79
a33	1131	16	2.5	0.70	0.1411	0.85	1.3458	6.9	0.049	2.0	0.0732	15.8	855	37	893	105	96
a34	11320	435	44.3	0.76	0.0656	1.45	0.7666	6.6	0.126	2.0	0.0471	4.2	411	21	1302	80	32
a35	1897	41	4.4	0.37	0.1058	1.03	0.9013	6.4	0.037	2.7	0.0511	10.8	650	29	662	92	98
a36	16428	230	22.9	0.72	0.0827	1.09	0.9499	5.9	0.050	1.8	0.0580	3.4	513	24	1274	66	40
a37	2650	59	7.7	1.53	0.0994	0.97	0.8496	6.1	0.040	1.5	0.0611	9.6	612	27	672	84	91
a38	26186	100	30.7	0.17	0.3017	0.80	5.0222	4.9	0.115	1.3	0.1170	1.1	1700	69	1966	32	86
a39	6887	158	16.0	0.46	0.0972	0.72	0.8578	5.6	0.044	1.1	0.0558	3.9	598	26	743	70	80
a40	7461	55	13.8	0.69	0.2298	0.89	2.6725	5.1	0.085	1.1	0.0802	2.5	1332	56	1303	39	102
a41	2721	60	9.4	1.89	0.1176	0.69	1.0243	6.3	0.052	1.8	0.0735	7.5	716	31	717	93	100
a42	1998	22	4.3	1.01	0.1683	1.11	1.7589	6.3	0.074	1.1	0.0762	10.4	1001	45	1094	83	91
a43	6430	81	13.2	0.19	0.1661	0.94	1.6909	5.2	0.070	2.4	0.0684	4.2	988	43	1043	46	95
a44	19087	34	21.7	1.45	0.4836	1.25	11.2891	5.3	0.162	1.0	0.1649	1.8	2532	105	2559	32	99
a45	1738	41	4.6	0.93	0.0961	0.75	0.8540	7.1	0.039	1.9	0.0586	14.9	589	26	768	116	77
a46	3815	108	11.0	0.73	0.0946	0.82	0.7702	5.4	0.035	1.1	0.0592	6.6	579	25	584	63	99
a47	3346	91	7.6	0.06	0.0894	0.83	0.7408	5.4	0.037	3.8	0.0558	7.3	549	24	621	61	88
a48	2024	66	5.9	0.83	0.0802	0.73	0.6601	6.7	0.037	1.5	0.0669	9.6	494	22	609	106	81
a49	1814	112	4.9	0.32	0.0443	0.81	0.3309	6.0	0.018	2.6	0.0469	13.2	277	12	398	86	70
a50	5926	23	8.4	0.52	0.3339	0.62	5.5577	5.3	0.128	1.6	0.1177	3.2	1842	72	1983	52	93
a51	12398	279	29.6	0.48	0.1028	0.71	0.8706	4.9	0.040	1.4	0.0575	2.0	625	27	676	41	92
a52	852	19	2.0	0.33	0.1090	1.21	0.9986	7.9	0.052	2.1	0.0509	31.6	660	31	842	128	78
a53	3468	106	8.6	0.21	0.0842	0.92	0.6901	6.3	0.036	2.3	0.0552	7.5	515	23	609	92	85
a54	355	22	1.4	1.72	0.0465	1.51	0.3409	10.3	0.019	2.6	0.0077	479.1	290	15	361	201	80
a55	2090	126	6.0	0.36	0.0482	1.07	0.3554	6.3	0.020	1.7	0.0384	30.3	300	14	378	92	79
CG-Z1_klein_seq2																	
a1	3665	13	5.6	1.42	0.3368	0.66	5.1218	4.2	0.123	0.9	0.1002	7.9	1898	43	1774	60	107
a2	2499	51	5.4	0.54	0.0966	1.17	0.7923	5.4	0.035	2.3	0.0399	17.9	604	19	549	94	110
a3	1587	32	4.9	2.39	0.1021	1.71	1.0121	11.7	0.040	1.5	0.0172	106.2	637	25	949	224	67
a4	1158	53	2.8	0.59	0.0507	1.35	-0.0421	709.7	0.025	1.9	-0.0061	-354.9	324	11	#ZAHL!	#####	#ZAHL!
a5	7402	10	7.0	1.44	0.5122	1.11	12.5806	4.3	0.177	1.5	0.1730	2.9	2704	70	2607	48	104
a6	6518	17	7.7	0.88	0.3879	1.23	6.7858	4.4	0.154	2.2	0.1201	4.9	2144	61	2025	51	106
a7	30083	90	37.6	1.09	0.3386	0.88	5.7185	3.2	0.119	2.2	0.1223	1.3	1909	47	1962	27	97
a8	6558	17	7.5	0.81	0.3778	0.86	6.7215	3.9	0.145	1	0.1221	3.5	2097	51	2054	48	102
a9	2812	124	6.7	0.49	0.0510	1.08	0.3796	4.8	0.019	3	0.0514	13.4	326	10	331	84	98
a10	1896	89	4.8	0.76	0.0479	1.16	0.3416	5.4	0.020	2	0.0350	22.8	307	10	233	101	132
a11	2947	51	7.8	1.65	0.1137	1.05	1.0006	4.6	0.043	1	0.0603	10.0	706	21	698	74	101
a12	3073	155	7.9	0.57	0.0467	1.06	0.3343	5.3	0.018	2	0.0439	9.6	300	9	239	99	125
a13	28154	93	34.5	0.72	0.3228	1.34	5.6741	3.8	0.114	2	0.1268	0.91	1832	56	2032	24	90
a14	3068	56	7.4	1.44	0.0974	1.27	0.8679	5.0	0.041	2	0.0574	10.8	610	20	723	77	84
a15	5008	44	10.5	1.19	0.1942	0.95	2.0161	4.1	0.070	1	0.0802	3.3	1163	32	1040	57	112
a16	6532	35	9.5	0.53	0.2478	0.82	3.1654	3.9	0.093	2	0.0957	3.9	1451	36	1446	52	100
a17	2059	104	5.2	0.66	0.0449	1.09	0.3340	5.3	0.019	2	0.0389	17.5	288	9	328	97	88
a18	3147	88	7.0	0.52	0.0742	1.00	0.6348	5.0	0.026	2	0.0522	10.5	470	14	637	85	74
a19	18255	169	32.1	0.63	0.1705	0.73	1.7582	3.2	0.064	1	0.0750	1.3	1033	26	1025	35	101
a20	14466	306	31.8	0.80	0.0968	0.82	0.8059	3.3	0.028	4	0.0598	1.8	606	16	578	38	105
a21	2226	113	5.7	0.49	0.0474	1.16	0.3731	7.1	0.026	3	0.0409	15.7	304	10	452	141	67
a23	1887	30	4.2	0.80	0.1211	1.17	1.0745	5.9	0.048	2	0.0532	18.2	750	23	712	104	105
a24	264	5	0.6	1.76	0.1031	1.71	-2.8367	119.6	0.045	3	-0.2004	-59.7	645	25	#ZAHL!	#####	#ZAHL!
a25	4060	83	11.2	1.45	0.1042	0.81	0.8829	4.3	0.041	1	0.0530	8.2	651	17	614	72	106
a26	255	10	0.6	0.66	0.0619	1.88	-0.7369	121.5	0.026	6	-0.0867	-60.6	395	17	#ZAHL!	#####	#ZAHL!
a27	10828	39	15.5	1.06	0.3245	0.88	4.9666	3.5	0.110	1	0.1115	2.2	1843	46	1780	36	104
a28	1868	54	4.2	0.42	0.0749	1.17	0.5852	6.1	0.030	2	0.0464	11.9	474	15	436	115	109
a29	1857	45	4.7	0.63	0.0948	1.25	0.7762	5.9	0.038	2	0.0639	11.9	595	19	538	105	111
a30	4988	114	12.1	0.82	0.0927	1.01	0.7647	4.0	0.037	1.3	0.0585	5.0	582	17	555	57	105
a31	1731	90	5.1	1.00	0.0468	1.08	0.3457	5.8	0.018	1.5	0.0331	34.8	301	9	305	112	99
a32	67663	253	64.8	0.57	0.2172	1.08	4.1134	3.5	0.095	1.1	0.1379	0.7	1290	37	2159	26	60
a34	3981	61	7.7	0.23	0.1274	1.05	1.1693	4.4	0.052	2.8	0.0572	7.7	788	23	780	67	101
a35	4724	52	9.3	0.44	0.1687	1.16	1.6967	4.9	0.070	1.8	0.0660	5.3	1025	31	970	76	106
a36	5964	68	12.7	0.65	0.1694	0.89	1.6693	3.9	0.064	1.5	0.0701	4.3	1029	27	928	55	111
a37	8882	190	17.1	0.37	0.0836	1.33	0.7201	4.2	0.038	2.6	0.0590	2.9	528	18	647	52	82
a38	23127	85	32.0	0.31	0.3559	1.03	5.7010	3.5	0.117	2.4	0.1134	1.5	1999	53	1860	32	107
a39	618	13	1.5	0.92	0.1048	1.35	0.9648	9.1	0.045	3.0	0.0353	56.4	655	22	786	176	83
a40	5378	159	17.9	0.60	0.1072	1.28	0.9138	4.9	0.040	2.3	0.0570	5.5	670	22	623	76	108
a41	7507	300	18.4	0.41	0.0591	1.96	0.4368	5.4	0.029	2.4	0.0543	6.3	378	17	307	67	123
a42	659	7	1.2	0.76	0.1520	2.10	-0.2594	557.3	0.079	3.8	-0.0124	-278.6	930	41	#ZAHL!	#####	#ZAHL!
a43	6803	135	13.8	0.33	0.0983	1.13	0.8736	4.3	0.044	2.1	0.0638	3.3	617	19	711	60	87
a45	12830	40	17.1	0.91	0.3490	1.38	5.8099	4.3	0.121	1.5	0.1165	1.9	1967	61	1928	42	102
a46	4692	118	10.6	0.32	0.0879	0.97	0.7283	4.0	0.034	2.1	0.0523	5.8	554	16	560	58	99
a47	5585	85	10.5	0.50	0.1108	1.65	0.8792	14.7	0.016	19.7	0.0577	7.0	692	26	464	313	149
a48	4600	208	12.3	0.96	0.0485	1.90	0.3929	5.9	0.020	3.9	0.0566	5.8	312	13	509	85	61
a49	805	18	2.5	1.81	0.0997	1.31	0.9010	6.9	0.041	2.2	0.0334	67.2	626	21	744	127	84
a51	1003	9	1.8	0.84	0.1765	1.49	-2.2713	129.2	0.209	6.3	-0.0935	-64.5	1070	37	#ZAHL!	#####	#ZAHL!
a52	26413	51	24.4	0.62	0.4044	0.74	9.0350	3.2	0.156	1.3	0.1619	0.9	2232	51	2439	29	92
a53	2801	90	10.0	1.93	0.0777	1.12	0.6370	6.2	0.029	1.2	0.0532	9.3	493	15	533	115	92
a54	4102	46	9.1	0.95	0.1668	1.28	1.7134	5.6	0.063	1.4	0.0693	5.4	1016	32	1009	89	101
a55	1715	40	4.5	0.85	0.0962	1.26	0.8340	6.0	0.037	2.0	0.0480	22.4	605	20	655	107	92

sample	207	U (ppm)	Pb (ppm)	Th/U	206*/238	1s%	7/35r	2s%	208/232	1s%	207*/206*	1s%	206/238	2s	207/206	2s	conc%
CG-Z1_klein_seq3																	
a1	2067	3	#DIV/0!	#DIV/0!	0.0000	#DIV/0!	#DIV/0!	#DIV/0!	0.000	#DIV/0!	-1.5827	#DIV/0!	0	#WERT!	#ZAHL!	#####	#ZAHL!
a2	17336	54	27.4	1.06	0.3851	0.88	6.9918	3.7	0.140	1.1	0.1280	1.3	2142	60	2080	30	103
a3	3913	111	11.0	0.32	0.0947	0.75	0.8083	4.6	0.040	1.7	0.0616	4.2	596	18	621	72	96
a4	20287	214	40.7	0.30	0.1798	0.94	2.0256	3.7	0.058	2.2	0.0791	1.5	1089	34	1193	31	91
a5	3008	78	9.1	0.88	0.0941	0.89	0.7875	13.7	0.039	1.5	0.0597	6.6	592	19	580	288	102
a6	3156	53	9.7	1.09	0.1428	1.00	1.3366	4.6	0.051	1.6	0.0656	6.8	879	28	817	63	108
a7	110952	140	96.4	0.36	0.5847	0.75	17.4907	3.6	0.203	1.1	0.2136	0.7	3023	77	2921	27	103
a8	7247	21	9.0	0.30	0.3785	0.71	7.3263	4.1	0.140	3	0.1281	3.1	2110	57	2192	45	96
a9	5896	143	15.6	0.21	0.1094	0.71	0.9486	4.1	0.042	2	0.0662	2.3	684	20	655	55	104
a10	5270	#DIV/0!	#DIV/0!	######	#DIV/0!	#DIV/0!	#DIV/0!	#DIV/0!	0.203	1	1.7547	#DIV/0!	#WERT!	#WERT!	5859	#####	#WERT!
a11	8742	125	21.8	0.39	0.1632	0.81	1.6141	3.9	0.066	1	0.0706	2.5	995	30	933	44	107
a12	11849	300	21.9	0.39	0.0615	6.21	0.7367	13.3	-0.001	-519	0.0634	4.4	393	49	1315	74	30
a13	1542	50	5.9	1.11	0.0890	0.87	0.7266	5.3	0.034	1	0.0509	12.10	561	18	528	92	106
a14	3235	91	9.0	0.18	0.0980	1.01	0.8418	5.0	0.075	3	0.0576	7.5	616	20	636	79	97
a15	7318	208	13.0	0.55	0.0484	2.09	0.8644	8.8	0.061	3	0.0720	7.8	311	15	2053	127	15
a16	1159	59	3.5	0.61	0.0483	1.08	0.4942	9.7	0.015	3	0.0349	50.8	311	11	1002	185	31
a17	5728	222	17.3	0.27	0.0752	0.79	0.6032	3.9	0.031	2	0.0529	3.6	477	15	488	51	98
a18	22584	30	21.5	0.73	0.5551	0.79	17.6143	3.7	0.187	1	0.2277	1.2	2896	75	3018	30	96
a19	5757	118	18.5	1.86	0.0981	0.64	1.2582	5.2	0.048	1	0.0549	8.8	616	18	1448	79	43
a20	9582	22	11.9	0.44	0.4582	1.09	10.3689	4.1	0.160	2	0.1530	1.8	2475	73	2463	36	101
a21	26	104	0.1	-3.24	0.0005	5.23	0.0076	64.6	0.000	17	0.9539	5.0	3	0	1687	1174	0
a22	11956	38	16.2	0.26	0.3936	0.89	7.5781	4.0	0.152	2	0.1370	1.9	2178	62	2186	39	100
a23	12	217	0.1	-49.40	0.0004	3.49	0.0015	89.4	0.000	12	0.8321	21.3	3	0	#ZAHL!	#####	#ZAHL!
a24	1515	107	5.3	0.12	0.0506	0.92	0.3479	5.5	0.021	3	0.0399	16.4	325	11	140	103	232
a25	4567	126	13.8	0.09	0.1120	0.78	0.9602	4.4	0.042	3	0.0559	4.3	698	21	636	64	110
a26	2378	68	7.3	0.15	0.1089	0.98	0.9433	5.1	0.040	2	0.0576	7.5	680	22	657	83	103
a27	1592	46	5.4	0.54	0.1050	0.89	0.8913	5.8	0.047	1	0.0605	13.4	656	21	614	103	107
a28	10	130	0.1	55.70	0.0004	6.14	0.0020	78.7	0.000	15	0.9287	10.5	3	0	-704	2160	0
a29	383	11	1.5	1.29	0.1159	1.15	1.0238	10.8	0.041	4	0.1022	24.0	721	25	700	217	103
a30	858	13	2.6	0.59	0.1728	1.69	1.8151	8.6	0.059	3.0	0.0154	195.0	1047	42	1059	150	99
a31	280	10	0.8	0.46	0.0731	1.67	0.7063	10.5	0.049	5.6	0.0239	212.1	464	20	888	196	52
a32	3	112	0.0	#DIV/0!	0.0006	5.66	0.0009	373.4	0.000	21.1	1.0039	6.0	0	0	#ZAHL!	#####	#ZAHL!
a33	1630	43	5.7	1.06	0.1054	1.17	1.0986	8.8	0.052	1.6	0.0622	9.8	659	23	1043	161	63
a34	26259	70	37.9	0.61	0.4506	1.11	10.4240	4.2	0.154	1.1	0.1662	1.1	2438	73	2503	37	97
a35	2643	181	11.2	0.51	0.0563	0.94	0.3993	5.4	0.022	1.1	0.0497	5.9	360	12	216	97	167
a36	545	17	2.2	1.08	0.1016	1.51	0.8470	8.2	0.037	2.0	0.0535	24.8	636	25	578	154	110
a37	761	32	2.8	0.24	0.0806	1.66	0.6580	8.4	0.030	3.2	0.0307	36.2	509	21	531	158	96
a38	644	23	2.5	0.33	0.0940	1.16	0.8124	7.4	0.034	2.6	0.0201	54.9	590	21	658	138	90
a39	1766	11	4.7	1.60	0.3056	1.24	4.7821	5.8	0.120	1.6	0.1062	10.1	1748	57	1821	80	96
a40	7461	80	20.5	0.51	0.2298	0.89	2.6762	3.9	0.085	1.1	0.0802	2.5	1356	41	1266	39	107
a41	4647	170	15.0	0.02	0.0936	0.93	0.7921	5.5	0.096	8.7	0.0587	3.4	587	19	613	94	96
CG-Z2_seq2																	
a1	85	140	0.1	0.59	0.0006	3.29	0.0064	42.7	0.001	9.3	1.0196	18.8	3.1	0	1560	790	0
a2	583	481	-0.4	0.60	0.0004	3.53	-0.2144	218.4	0.000	-27.4	-4.9246	-109.1	2.0	0	#ZAHL!	#####	#ZAHL!
a3	265	585	0.3	0.55	0.0005	1.23	0.0044	19.6	0.000	3.7	0.0588	258.6	2.8	0	1020	391	0
a4	1169	1808	1.5	0.16	0.0010	0.71	0.0062	8.3	0.001	4.7	0.0273	52.1	5.5	0	304	178	2
a5	941	1587	1.2	0.04	0.0010	0.61	0.0053	6.8	0.001	9.0	0.0247	66.9	5.3	0	19	151	28
a6	333	159	0.1	0.41	0.0005	2.29	0.0147	92.9	0.001	5.3	0.8588	20.8	2.6	0	3295	1457	0
a7	1622	1145	1.1	0.30	0.0009	6.19	0.0157	73.9	0.002	8.1	0.1919	97.4	5.1	1	2274	1255	0
a8	364	529	-0.4	0.55	0.0010	9.70	-0.2509	208.4	0.003	18	-2.1952	-103.7	5.4	1	#ZAHL!	#####	#ZAHL!
a9	4052	419	0.6	0.56	0.0005	1.74	0.0258	104.2	0.002	6	1.1263	47.1	2.97	0	3932	1563	0
a10	3426	536	0.9	0.49	0.0008	1.77	0.0586	59.8	0.002	2	0.6318	29.8	4.36	0	4576	864	0
a11	885	459	0.4	0.83	0.0005	1.54	-0.0297	122.5	0.000	5	-0.4967	-61.2	2.81	0	#ZAHL!	#####	#ZAHL!
a12	539	768	0.4	0.34	0.0005	1.57	0.0053	15.1	0.002	3	0.0418	207.2	2.5	0	1613	272	0
a13	920	431	0.6	0.47	0.0006	1.30	0.0137	13.4	0.008	14	0.3470	84.74	3.4	0	2754	212	0
a14	105	682	0.3	0.72	0.0004	1.25	0.0013	28.8	0.000	6	0.5846	74.0	2.4	0	#ZAHL!	#####	#ZAHL!
a15	185	668	0.3	0.45	0.0005	1.22	0.0026	19.6	0.001	5	0.1715	213.0	2.65	0	33	463	8
a16	370	511	0.3	0.72	0.0005	1.99	0.0071	50.6	0.000	5	0.1061	274.3	2.8	0	1927	903	0
a17	170	301	0.2	0.48	0.0005	2.16	0.0052	41.6	0.000	9	0.1937	59.3	2.8	0	1362	797	0
a18	907	423	0.3	0.55	0.0004	5.09	0.0121	19.9	0.000	30	0.2533	74.6	2.4	0	3085	271	0
a19	21975	221	20.7	0.03	0.1171	0.45	0.8270	4.0	0.054	3	0.0604	1.5	613	15	608	67	101
a20	22837	216	20.2	0.03	0.1175	0.43	0.8155	3.8	0.050	4	0.0593	1.4	615	15	569	62	108
CG-Z3_seq1																	
a1	870	1049	#BEZUG!	0.44	0.0004	1.15	-0.0085	80.4	0.000	4.4	-0.1689	-40.1	2.50	0.08	#ZAHL!	#####	#ZAHL!
a2	251	415	#BEZUG!	0.47	0.0005	2.06	0.0046	39.2	0.001	6.8	0.2236	258.6	2.86	0.14	1062	783	0
a3	762	791	#BEZUG!	0.60	0.0005	1.74	-0.0010	544.0	0.000	5.9	-0.0183	-272.0	2.82	0.12	#ZAHL!	#####	#ZAHL!
a4	478	322	#BEZUG!	0.42	0.0005	2.22	-0.0165	339.9	0.000	6.5	-0.2760	-169.9	2.98	0.15	#ZAHL!	#####	#ZAHL!
a5	23976	241	#BEZUG!	0.03	0.1188	0.47	0.7466	4.8	0.052	2.3	0.0571	2.0	620.99	15.52	352	91	176
a6	22971	222	#BEZUG!	0.03	0.1186	0.40	0.7592	3.8	0.046	1.8	0.0585	1.4	617.23	15.18	404	63	153
CG-Z2_seq1																	
a1	17	71	#BEZUG!	0.62	0.0004	10.34	0.0049	79.7	0.000	13.4	0.8879	8.5	2.87	0.59	1197	1517	0
a2	17	63	#BEZUG!	0.49	0.0006	5.55	0.0046	165.6	0.001	10.8	0.9243	10.4	4.22	0.47	249	3802	2
a3	25	61	#BEZUG!	0.55	0.0003	11.77	0.0135	48.0	0.001	14.8	0.9175	6.5	2.23	0.53	3378	652	0
a4	49	168	#BEZUG!	0.34	0.0010	2.49	0.0066	31.2	0.001	12.2	0.2828	160.8	6.38	0.32	122	726	5
a5	20	99	#BEZUG!	0.75	0.0004	6.49	0.0035	66.9	0.000	13.0	0.8201	4.1	2.72	0.35	627	1414	0
a6	148	193	#BEZUG!	0.49	0.0003	6.57	0.0083	34.3	0.000	-61.6	0.8384	10.3	2.20	0.29	2614	527	0
a7	-1	36	#BEZUG!	0.51	0.0005	8.77	-0.0240	#ZAHL!	0.001	7.7	0.8273	2.1	3.52	0.62	#ZAHL!	#####	#ZAHL!

Tab A6.2 Results of Hf isotope analyzes of zircons from the SEVP, Spain.

sample	$^{176}Yb/^{177}Hf$	1se %	$^{176}Lu/^{177}Hf$	1se	$^{178}Hf/^{177}Hf$ (1)	1se %	Hf_{total}(V)	(176/177)Hf_{Lu}	εHf_{Lu-T}	+/– 2σ	Age (Ma)	2s abs
CNTS-1_seq4_A11	0.0184	1.721	0.00053	1.037	1.4672	0.0029	14.6	0.282868	3.0	0.2	2.1	0
CNTS-1_seq4_A10	0.0122	0.411	0.00039	0.197	1.4672	0.0021	14.0	0.282873	3.2	0.3	1.7	0
CNTS-1_seq4_A9	0.0085	2.210	0.00029	2.345	1.4672	0.0022	13.5	0.282911	4.5	0.2	2.3	0
CNTS-1_seq4_A8	0.0155	1.121	0.00056	0.861	1.4672	0.0024	12.0	0.282882	3.5	0.2	2.3	0
CNTS-1_seq4_A7	0.0099	0.700	0.00028	0.519	1.4672	0.0033	14.5	0.282877	3.3	0.3	1.8	0
CNTS-1_seq4_A6	0.0269	0.849	0.00091	0.575	1.4671	0.0021	11.1	0.282898	4.1	0.3	2.8	0
CNTS-1_seq4_A4	0.0422	1.273	0.00121	0.997	1.4672	0.0038	6.5	0.282877	3.3	0.5	4.4	0
CNTS-1_seq4_A3	0.0740	1.093	0.00195	0.291	1.4672	0.0041	6.3	0.282869	3.5	0.7	22.2	2
CNTS-1_seq4_A2	0.0598	2.097	0.00164	2.346	1.4672	0.0048	8.6	0.282877	3.4	0.4	7.9	1
CNTS-1_seq4_A1	0.0208	0.893	0.00062	0.440	1.4672	0.0035	10.7	0.282846	2.2	0.4	3.9	0
CNTS-1_seq3_A31	0.0598	2.356	0.00160	1.720	1.4673	0.0054	11.5	0.282863	3.0	0.2	10.9	1
CNTS-1_seq3_A30	0.0482	0.387	0.00135	0.245	1.4672	0.0046	9.5	0.282865	2.9	0.3	2.9	0
CNTS-1_seq3_A29	0.0296	0.729	0.00085	1.069	1.4672	0.0041	10.6	0.282877	3.4	0.4	4.1	0
CNTS-1_seq3_A28	0.1204	1.640	0.00311	1.179	1.4672	0.0045	9.2	0.282870	3.6	0.9	28.1	2
CNTS-1_seq3_A27	0.0340	1.177	0.00092	0.691	1.4671	0.0052	7.7	0.282923	5.0	0.4	7.4	0
CNTS-1_seq3_A26	0.0115	0.319	0.00034	0.887	1.4672	0.0030	10.4	0.282890	3.7	0.3	2.3	0
CNTS-1_seq3_A25	0.0485	0.725	0.00137	0.588	1.4672	0.0036	12.2	0.282900	4.6	0.2	23.8	1
CNTS-1_seq3_A24	0.0428	0.209	0.00121	0.683	1.4672	0.0057	9.4	0.282880	3.4	0.4	2.3	0
CNTS-1_seq3_A23	0.0631	1.045	0.00159	0.686	1.4673	0.0054	12.1	0.282815	8.8	0.3	346	8
CNTS-1_seq3_A22	0.0266	1.693	0.00095	1.563	1.4672	0.0037	10.4	0.282383	34.8	0.9		
CNTS-1_seq3_A21	0.1129	3.980	0.00314	3.353	1.4671	0.0033	7.2	0.282240	59.2	1.8		
CNTS-1_seq3_A20	0.0410	0.752	0.00154	0.682	1.4672	0.0027	14.9	0.282425	44.3	0.9		
CNTS-1_seq3_A19	0.0633	2.351	0.00177	1.607	1.4671	0.0025	16.0	0.282337	29.0	0.7		
CNTS-1_seq3_A17	0.0287	0.918	0.00081	0.855	1.4672	0.0030	18.7	0.282476	-3.0	0.2	358	8
CNTS-1_seq3_A16	0.0329	1.320	0.00086	0.895	1.4670	0.0072	11.4	0.282272	-4.2	0.6	626	12
CNTS-1_seq3_A15	0.0265	0.828	0.00070	0.442	1.4672	0.0084	10.3	0.282861	2.8	0.4	3.6	0
CNTS-1_seq3_A13	0.0114	0.635	0.00036	0.887	1.4672	0.0026	12.5	0.282328	-2.7	0.5		
CNTS-1_seq3_A12	0.0409	2.730	0.00123	1.953	1.4672	0.0021	16.8	0.282430	0.1	0.4		
CNTS-1_seq3_A11	0.0246	1.516	0.00087	1.609	1.4671	0.0034	10.8	0.281203	-11.7	0.7		
CNTS-1_seq3_A10	0.0814	1.208	0.00237	1.270	1.4671	0.0017	14.4	0.282558	8.0	0.4	718	13
CNTS-1_seq3_A09	0.0422	1.029	0.00141	1.604	1.4672	0.0032	15.4	0.282233	82.4	1.4		
CNTS-1_seq3_A08	0.0347	1.183	0.00133	1.318	1.4672	0.0036	14.8	0.282335	7.5	0.4	1043	23
CNTS-1_seq3_A07	0.0103	0.868	0.00031	0.653	1.4671	0.0028	13.1	0.282871	3.1	0.2	2.7	0
CNTS-1_seq3_A06	0.0536	0.645	0.00178	0.979	1.4673	0.0036	13.1	0.282485	21.9	0.7		
CNTS-1_seq3_A05	0.0276	0.355	0.00063	0.169	1.4672	0.0047	12.9	0.282294	5.7	0.4	1030	17
CNTS-1_seq3_A04	0.0040	0.967	0.00009	0.940	1.4673	0.0037	16.0	0.281153	-2.3	1.0	2442	6
CNTS-1_seq3_A03	0.0283	2.292	0.00082	1.610	1.4672	0.0026	15.4	0.281775	-7.0	0.5		
CNTS-1_seq3_A02	0.0152	1.039	0.00043	0.777	1.4672	0.0026	11.5	0.282872	3.1	0.3	2.3	0
CNTS-1_seq3_A01	0.0301	3.933	0.00089	3.536	1.4671	0.0019	19.9	0.282400	32.5	0.6		
CNTS-1_seq2_A55	0.0261	0.972	0.00081	0.677	1.4672	0.0023	12.7	0.282881	3.4	0.1		
CNTS-1_seq4_A5	0.0321	0.454	0.00104	0.161	1.4671	0.0066	4.2	0.282843	2.1	0.9		
CNTS-1_seq3_A14	0.0382	0.414	0.00113	0.458	1.4672	0.0035	5.5	0.283019	9.1	0.7		
CNTS-1_seq2_A54	0.0128	0.787	0.00035	0.506	1.4672	0.0025	6.7	0.282865	2.9	0.3	2.4	0
CNTS-1_seq2_A52	0.0235	2.922	0.00069	3.110	1.4672	0.0053	4.3	0.282866	3.0	0.7	4.8	1
CNTS-1_seq2_A51	0.0433	1.169	0.00131	0.815	1.4672	0.0044	3.7	0.282604	-6.4	0.8		10
CNTS-1_seq2_A50	0.0181	0.451	0.00048	0.267	1.4672	0.0044	4.6	0.282884	3.6	0.7	3.9	0
CNTS-1_seq2_A49	0.0148	2.515	0.00038	2.299	1.4672	0.0049	5.6	0.282851	2.4	0.6	3.7	1
CNTS-1_seq2_A48	0.0427	2.468	0.00121	1.313	1.4672	0.0042	6.7	0.282480	-3.1	0.6		
CNTS-1_seq2_A47	0.0676	1.321	0.00161	1.404	1.4671	0.0054	4.2	0.282872	3.1	0.8		
CNTS-1_seq2_A46	0.0416	1.334	0.00106	1.375	1.4671	0.0065	7.2	0.282400	-6.1	0.6	339	6
CNTS-1_seq2_A45	0.0437	0.858	0.00114	1.030	1.4672	0.0062	6.2	0.282083	-13.1	0.8		
CNTS-1_seq2_A41	0.0218	1.236	0.00091	0.622	1.4671	0.0039	7.0	0.281339	-5.4	1.1		
CNTS-1_seq2_A40	0.0921	2.692	0.00258	2.178	1.4672	0.0053	7.6	0.282092	-11.7	0.7		
CNTS-1_seq2_A39	0.0667	2.494	0.00235	2.918	1.4670	0.0045	7.1	0.282269	-5.0	0.8		
CNTS-1_seq2_A38	0.0623	2.803	0.00195	1.983	1.4671	0.0072	7.1	0.282226	-4.7	0.7	677	12
CNTS-1_seq2_A36	0.0200	6.849	0.00070	7.578	1.4673	0.0112	7.1	0.282638	10.2	1.5		
CNTS-1_seq2_A35	0.0741	1.160	0.00227	1.081	1.4671	0.0047	7.6	0.282455	13.9	0.9		
CNTS-1_seq2_A32	0.0304	1.582	0.00086	0.923	1.4671	0.0042	7.1	0.282117	-8.2	0.6	691	16
CNTS-1_seq2_A31	0.0149	3.310	0.00056	3.315	1.4671	0.0052	4.9	0.281809	3.7	1.1		
CNTS-1_seq2_A28	0.0325	1.277	0.00104	1.236	1.4672	0.0048	7.8	0.281442	-25.3	0.6	992	20
CNTS-1_seq2_A26	0.0318	1.375	0.00095	1.433	1.4672	0.0042	8.5	0.282562	-0.3	0.3	342	8
CNTS-1_seq2_A25	0.0481	2.048	0.00139	1.815	1.4672	0.0053	7.5	0.282440	1.0	0.5	594	14
CNTS-1_seq2_A24	0.1501	2.585	0.00401	2.044	1.4672	0.0033	7.6	0.282546	-3.6	1.1		
CNTS-1_seq2_A23	0.0548	2.140	0.00170	1.245	1.4671	0.0046	7.0	0.282520	-1.8	0.5	339	6
CNTS-1_seq2_A19	0.0646	3.470	0.00163	1.839	1.4673	0.0054	7.2	0.282183	-11.0	0.6		
CNTS-1_seq2_A17	0.0863	1.413	0.00300	0.763	1.4672	0.0043	10.1	0.282215	7.2	0.6		
CNTS-1_seq2_A15	0.0140	3.181	0.00050	3.121	1.4673	0.0052	6.8	0.282226	-2.3	0.8	783	15
CNTS-1_seq2_A12	0.0427	2.000	0.00128	0.876	1.4671	0.0061	7.6	0.280998	-9.0	1.1	2392	16
CNTS-1_seq2_A11	0.0516	2.164	0.00144	1.787	1.4672	0.0036	6.9	0.282613	17.4	0.7		
CNTS-1_seq2_A10	0.0254	2.013	0.00080	1.055	1.4672	0.0046	8.0	0.282529	2.2	0.7	502	9
CNTS-1_seq2_A9	0.0434	1.524	0.00128	2.336	1.4672	0.0050	5.9	0.282449	-0.7	0.7	500	8
CNTS-1_seq2_A7	0.0495	1.861	0.00157	2.597	1.4671	0.0060	9.5	0.282332	-10.2	0.4		
CNTS-1_seq2_A6	0.0088	1.591	0.00034	2.217	1.4672	0.0032	8.9	0.282339	-2.7	0.6	586	12
CNTS-1_seq2_A5	0.1051	1.038	0.00295	0.793	1.4672	0.0064	9.6	0.282483	-4.5	1.0		
CNTS-1_seq2_A4	0.0326	1.886	0.00105	2.805	1.4673	0.0051	5.7	0.282464	0.9	0.6		
CNTS-1_seq2_A3	0.0548	1.312	0.00181	1.115	1.4671	0.0060	7.7	0.282443	-5.3	0.3	305	6
CNTS-1_seq2_A2	0.0344	2.000	0.00124	2.183	1.4672	0.0038	5.6	0.282500	-2.9	0.6	321	5
CNTS-1_seq2_A1	0.0419	0.751	0.00145	0.541	1.4672	0.0050	5.8	0.282005	-16.9	0.7		
CNTS-1_seq1_A54	0.0327	4.648	0.00091	4.258	1.4670	0.0060	9.3	0.282425	-5.6	0.5	320	9
CNTS-1_seq1_A53	0.0230	0.608	0.00069	0.451	1.4671	0.0057	6.8	0.281412	-6.5	1.1	1865	12

sample	$^{176}Yb/^{177}Hf$	1se %	$^{176}Lu/^{177}Hf$	1se	$^{178}Hf/^{177}Hf$ (1)	1se %	Hf_{total}(V)	(176/177)Hf_{Lu}	$\varepsilon Hf_{Lu\text{-}T}$	+/– 2σ	Age (Ma)	2s abs
CNTS-1_seq1_A51	0.0443	2.783	0.00149	3.364	1.4670	0.0057	9.2	0.282347	-4.9	0.6		
CNTS-1_seq1_A50	0.0286	2.452	0.00090	1.776	1.4671	0.0050	7.1	0.282176	-6.9	0.5	656	19
CNTS-1_seq1_A49	0.0428	2.056	0.00157	2.131	1.4671	0.0044	5.5	0.282307	-3.0	0.7	621	18
CNTS-1_seq1_A48	0.0734	2.527	0.00230	2.160	1.4672	0.0051	8.9	0.282548	0.3	0.4	391	11
CNTS-1_seq1_A46	0.0418	2.548	0.00120	1.772	1.4671	0.0048	6.2	0.282235	-5.8	0.6	614	17
CNTS-1_seq1_A44	0.0556	1.961	0.00177	1.247	1.4670	0.0066	7.3	0.282343	-7.6	0.5	363	10
CNTS-1_seq1_A42	0.0717	0.889	0.00205	0.877	1.4673	0.0072	8.2	0.282508	-7.8	0.3		
CNTS-1_seq1_A41	0.0295	0.906	0.00099	0.964	1.4672	0.0038	9.3	0.282388	1.5	0.6	698	20
CNTS-1_seq1_A40	0.0534	1.124	0.00192	1.868	1.4670	0.0046	8.3	0.281937	-13.8	0.6	726	20
CNTS-1_seq1_A39	0.0952	3.423	0.00271	2.553	1.4672	0.0056	9.4	0.282254	4.2	1.0	1028	20
CNTS-1_seq1_A34	0.0283	0.635	0.00087	1.280	1.4671	0.0062	6.7	0.282581	7.0	0.9	637	17
CNTS-1_seq1_A33	0.0666	1.388	0.00200	1.512	1.4673	0.0057	8.6	0.282423	-2.0	0.4	485	13
CNTS-1_seq1_A32	0.0648	1.108	0.00207	1.745	1.4671	0.0043	8.0	0.282323	4.3	0.7	922	24
CNTS-1_seq1_A31	0.0311	2.599	0.00101	2.594	1.4672	0.0045	8.0	0.282428	2.7	0.7		
CNTS-1_seq1_A30	0.0561	1.134	0.00195	1.825	1.4670	0.0078	6.2	0.282169	-9.2	0.6	564	16
CNTS-1_seq1_A26	0.0481	1.932	0.00168	1.841	1.4671	0.0054	4.3	0.282345	-4.7	1.3		
CNTS-1_seq1_A18	0.0112	2.177	0.00037	1.317	1.4671	0.0047	6.5	0.281696	-15.2	0.8	1040	25
CNTS-1_seq1_A17	0.0593	1.693	0.00213	1.637	1.4671	0.0043	3.8	0.282608	6.2	1.4	560	18
CNTS-1_seq1_A16	0.0412	4.340	0.00136	4.768	1.4671	0.0058	8.2	0.282546	6.9	0.6	686	19
CNTS-1_seq1_A10	0.0627	1.661	0.00194	1.306	1.4672	0.0039	6.4	0.282198	75.6	1.7		
CNTS-1_seq1_A2	0.0617	1.888	0.00169	1.786	1.4671	0.0047	7.5	0.282222	-5.8	0.7		

Acknowledgements

First of all I would like to express my gratitude to my supervisor Gerhard Brey for choosing me to work on this interesting and challenging project. Thank you for allowing me to go to so many international conferences to present my data and to meet highly recognized scientists from all over the world. Thank you for providing a sampleset that looked so inconspicuous first but turned out to contain so many interesting results! You always managed to encourage me when I was unsatisfied!

Axel Gerdes for being a great advisor in the laboratory! You introduced me into the fascinating world of mass spectrometry and isotope geochemistry and awoke my own passion for trace element and isotope analytics. Thank you for taking so much time to help me when I experienced problems in the lab and for the numerous hours we spent talking about the evaluation and interpretation of my results.

Heidi Höfer for teaching me how to use the electron microprobe, the SEM and various preparation instruments. Your teachings allowed me to be able to work with the instruments beyond the knowledge of a regular user.

Marina Lazarov for teaching me how to do isotope dilution measurements and for the nice time we had while sharing an office.

Armin Zeh for help with the evaluation of zircon data and a lot of fruitful discussions.

Alexander Schmidt for teaching me how to use the SelFrag instrument.

Sonja Aulbach for helpful discussions about Re-Os isotope geochemistry.

Michael Seitz for help in the mass spectrometer lab.

Jan Heliosch for the preparation of my sample mounts.

Martin Okrusch for providing crustal xenoliths samples from Namibia.

Anna Neumann and Janina Schastock for their support in the clean lab.

Mandy Krebs for help during the preparation process.

Margaret Hanrahan-Denk for careful proofreading.

All other collegues at the institute of Mineralogy for having a good time, lots of good food and a nice working environment.

I am grateful for constant support by my family, Hans-Werner, Ursula and Kathrin Luchs.

I would like to express my heartfelt gratitude to Nadin Graf. Thank you for your throughout support and your understanding during my work. You helped me to keep up my motivation!

TIMO LUCHS

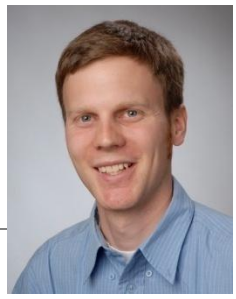

PERSONAL DATA

- Date and place of birth: 30.04.1984, Paderborn, Germany
- Nationality: German

EDUCATION

Since 01.11.2008	Ph.D. studies at Goethe University, Frankfurt am Main, Petrology and Geochemistry **Thesis:** Coupling of geological processes in the Earth's crust and mantle **Supervisor:** Prof. Dr. Brey	Frankfurt a.M.
Summer Term 2008	Graduation of Geology Studies: Diplom Geologe (Dipl.Geol.) (equal to MSc.) **Thesis:** Optimierung des Langzeitverhaltens von Hohlfasermembranmodulen zur Sanierung von kontaminierten Grundwässern **Supervisors:** Prof. Dr. Schüth (thesis) Apl. Prof. Dr. Schleyer (thesis) Prof. Dr. Brey (geological mapping) Prof. Dr. Zulauf (geological mapping)	Frankfurt a.M.
Summer Term 2005	Intermediate Diploma at Johann-Wolfgang Goethe University (equal to BSc.)	Frankfurt a.M
Since 1.10.2003	Study of Geology/Palaeontology at Johann-Wolfgang Goethe University	Frankfurt a.M.
1996 – 2003	Kaiserin-Friedrich-Gymnasium (grammar school) Degree: Abitur	Bad Homburg
1994 – 1996	Wilhelm-Hausenstein-Gymnasium (grammar school)	Durmersheim
1991 – 1994	Primary school	Durmersheim
1990 – 1991	Primary school	Karlsruhe

LANGUAGE SKILLS

- German (native)
- English (fluent)

BÄRENSTRASSE 13 • D- 60316 FRANKFURT AM MAIN
TELEFON: +49-69-78086462 • MOBIL: +49-151-40388059 • FAX: +49-6172-944986
E-MAIL: T.LUCHS@GMX.DE

- French (intermediate)
- Spanish (basic knowledge equal to classification A2.1)
- additionally: stays in South Africa and Spain

EMPLOYMENT HISTORY

Since November 2008
Institute for Mineralogy Dept. Petrology & Geochemistry, Frankfurt a.M.:
- Http://www.mineralogie.uni-frankfurt.de/petrologie-geochemie/
- Ph.D. candidate (supervisors: Prof. Dr. Brey and Dr. Gerdes)
- Trace element and isotope geochemistry
- Geochronology and characterization of crustal (U-Pb, Hf) and mantle material (Lu-Hf, Rb-Sr, Sm-Nd) using LA-ICPMS and MC-ICPMS

End of July 2006 – end of October 2006:
Kym L. Morton Consulting Services (KLMCS), Lanseria, South Africa (internship):
- Http://www.klmcs.co.za
- Writing of reports about the hydrogeochemistry of different diamond mines in Botswana for the identification of ground water flow paths including a one week stay at one of the mines
- Drill core logging
- Interpretation of aerial photographs
- Water table measurements
- Ground water sampling

August 2005 – Oktober 2008:
Institute for Mineralogy Dept. Petrology & Geochemistry, Frankfurt a.M.:
- Http://www.mineralogie.uni-frankfurt.de/petrologie-geochemie/
- Student assistant, main area of responsibility: Electron Probe Micro Analysis (EPMA)
- Tasks on mass spectrometer and scanning electron microscope (SEM)
- Miscellaneous duties

October 2004 – July 2005
Senckenberg Museum, Frankfurt a.M.:
- Http://www.senckenberg.de
- Temporary job superintendence

MEMBERSHIPS

- Deutsche Mineralogische Gesellschaft (DMG)
- Geologische Vereinigung (GV)
- Geochemical Society (GS)

BÄRENSTRASSE 13 • D- 60316 FRANKFURT AM MAIN
TELEFON: +49-69-78086462 • MOBIL: +49-151-40388059 • FAX: +49-6172-944986
E-MAIL: T.LUCHS@GMX.DE

LIST OF LITERATURE

Scientific publications (Peer review):

- Luchs, T., Brey, G.P., Gerdes, A., Hoefer, H.E. (submitted). The lithospheric mantle underneath the Gibeon Kimberlite field (Namibia): a mix of old and young components – evidence from Lu-Hf and Sm-Nd isotope systematics. Precambrian Research.

Conference abstracts:

- Luchs, T., Brey, G., Gerdes, A., Hoefer, H.E. (2012). Lu-Hf and Sm-Nd geochronology and geothermobarometry of the lithospheric mantle beneath the Gibeon kimberlite field, Namibia, 10IKC 6. – 11.2., Bangalore India. (Poster presentation)
- Luchs, T., Brey, G., Gerdes, A. (2011). Chronological and thermal history of the lithospheric mantle underneath the Gibeon kimberlite field, Namibia, Goldschmidt Conference 14. – 19.8, Prague Czech Republic. (Oral presentation)
- Luchs, T., G. Brey and A. Gerdes (2010). Insights on the evolution of the lithospheric mantle underneath the Gibeon Kimberlite field, Namibia. Geochimica Et Cosmochimica Acta 74(12): A639-A639. Goldschmidt Conference 13. – 18.6., Knoxville USA. (Poster presentation)
- Luchs, T., Gerdes, A., Brey, G. (2009). U-Pb geochronology of zircons from the South Eastern volcanic Province (SEVP), Spain, DMG Conference, 13. – 16.9, Halle. (Poster presentation)

Upcoming:

- Luchs, T., Brey, G., Gerdes, A. (2012). Archean crust components within the Rehoboth Terrane, Namibia: evidence from xenolith derived zircons in kimberlites and carbonatites, 1st European Mineralogical Conference 2. – 6.9., Frankfurt Germany. (Poster presentation)

BÄRENSTRASSE 13 • D- 60316 FRANKFURT AM MAIN
TELEFON: +49-69-78086462 • MOBIL: +49-151-40388059 • FAX: +49-6172-944986
E-MAIL: T.LUCHS@GMX.DE